AD-A134 719 PAPERS SELECTED FOR PRESENTATION AT THE INTERNATIONAL SYMPOSIUM ON REMOTE..(U) ENVIRONMENTAL RESEARCH INST OF MICHIGAN ANN ARBOR JUN 82 1/6

UNCLASSIFIED F/G 14/5 NL

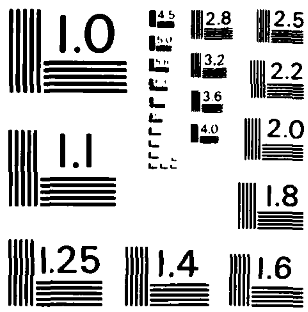

MICROCOPY RESOLUTION TEST CHART
NATIONAL BUREAU OF STANDARDS-1963-A

PAPERS SELECTED for PRESENTATION at the SIXTEENTH INTERNATIONAL SYMPOSIUM ON REMOTE SENSING OF ENVIRONMENT

Volume I

2–9 JUNE 1982

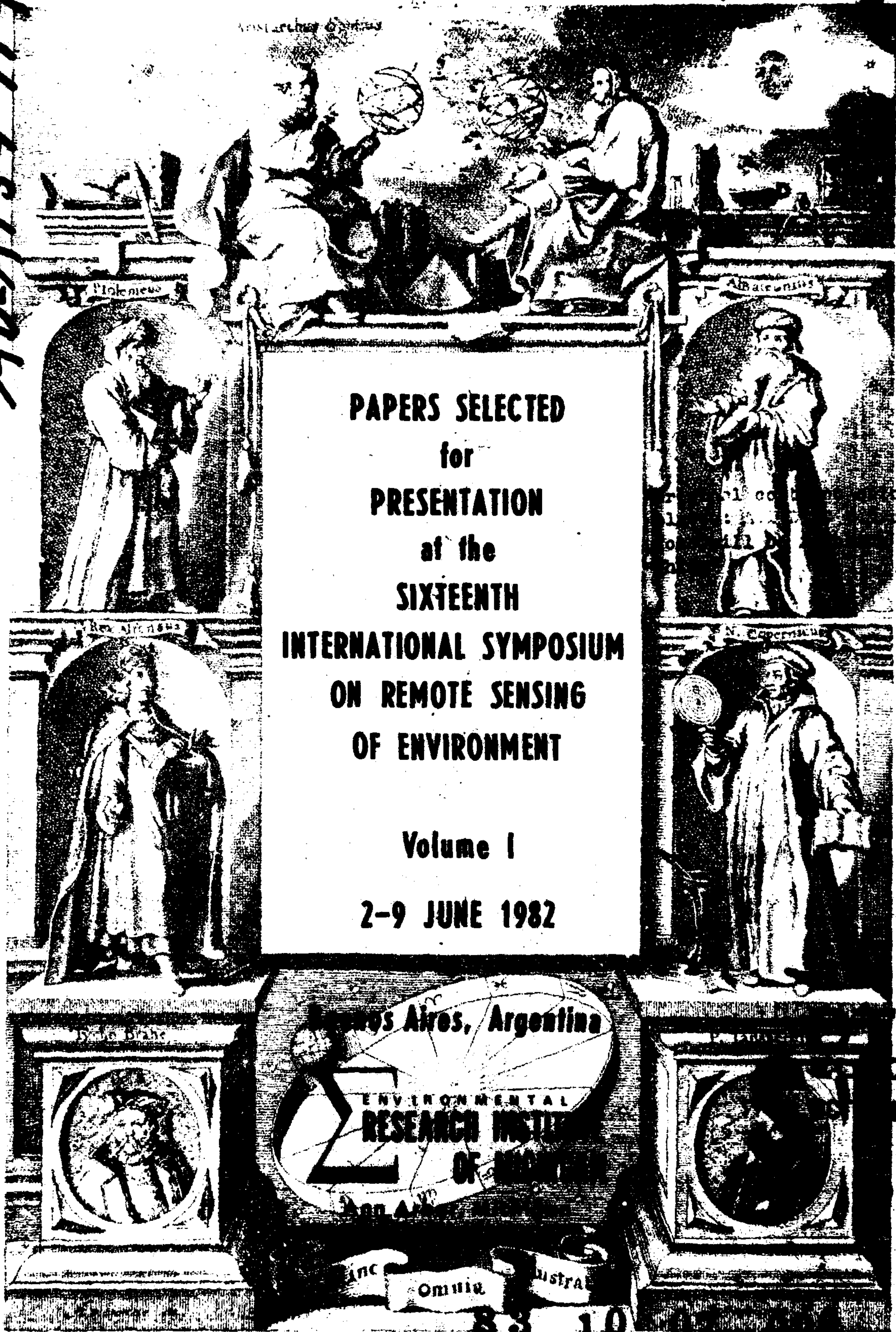

NOTICES

Reproduction Notice. Reproduction in whole or in part is permitted for any purpose of the United States Government. This document has been approved for public release and sale; its distribution is unlimited.

Final Disposition. After this document has served its purpose, it may be destroyed. Please do not return it to the Environmental Research Institute of Michigan.

COMPONENT PART NOTICE

THIS PAPER IS A COMPONENT PART OF THE FOLLOWING COMPILATION REPORT:

(TITLE): Papers Selected for Presentation at the International Symposium on Remote Sensing of Environment (16th) Held at Buenos Aires, Argentina on 2-9 June 1982. Volume 1.

(SOURCE): Environmental Research Inst. of Michigan, Ann Arbor.

TO ORDER THE COMPLETE COMPILATION REPORT USE AD-A134 719.

THE COMPONENT PART IS PROVIDED HERE TO ALLOW USERS ACCESS TO INDIVIDUALLY AUTHORED SECTIONS OF PROCEEDINGS, ANNALS, SYMPOSIA, ETC. HOWEVER, THE COMPONENT SHOULD BE CONSIDERED WITHIN THE CONTEXT OF THE OVERALL COMPILATION REPORT AND NOT AS A STAND-ALONE TECHNICAL REPORT.

THE FOLLOWING COMPONENT PART NUMBERS COMPRISE THE COMPILATION REPORT:

AD#:	TITLE:
P001 987	Remote Sensing Applications in Mexico.
P001 988	Use of LANDSAT Images in Integrated Natural Resource Surveys in Bolivia.
P001 989	Main Advances and Needs in Chilean Remote Sensing Programs.
P001 990	The Colombian Remote Sensing Program.
P001 991	Applications of Satellite Remote Sensing for U.S. Crop Acreage Estimation, 1980-81 Results.
P001 992	Research in Satellite-Aided Crop Forecasting.
P001 993	Soil Loss Prediction in a Geographic Information System Format.
P001 994	Operational Use of Satellite Data in Crop Condition Assessment.
P001 995	Rio Pilcomayo-Banado La Estrella (Argentina): LANDSAT Temporal Analysis of a Riverine Environment.
P001 996	The Use of Satellite Data for Urban Monitoring in the Sao Paulo Metropolitan Area.
P001 997	Application of LANDSAT Data to Geologic Mapping Tropical Jungle Environment: Caroni River Basin, Venezuela.
P001 998	Geobotanical Discrimination of Ultramafic Parent Materials: An Evaluation of Remote Sensing Techniques.
P001 999	Impact of Hydrothermally Altered Soil on Vegetation as a Tool in Geothermal Exploration.
P002 000	Integrated Remote Sensing, Geological and Geophysical Data Processing and Analysis for Hydrocarbon Prospection in the Parana Basin, Brazil.
P002 001	El Nino Observations by Remote Sensing.
P002 002	The ERS-1 (ESA Remote Sensing Satellite) Programme of the European Space Agency: Its Applications to Mineral and Marine Resources, Meteorology, Climatology, and Oceanography.
P002 003	Remote Sensing Input and Feedback for Hydrologic Forecasting and Simulation Models.
P002 004	Recent Advances and Future Prospects for Weather, Climate, and Ocean Space Observations.

COMPONENT PART NOTICE (CON'T)

AD#:	TITLE:
P002 005	Climate Applications of Satellite Remote Sensing.
P002 006	Monitoring Marine Pollution by Airborne Remote Sensing Techniques.
P002 007	A Technique for Mapping Environmental Change Using Digital LANDSAT Data.
P002 008	Using LANDSAT Digital Data to Identify Erosional Zones in the Cuenca Alta del Rio Bogota.
P002 009	An Application of Cluster Analysis for Determining Homogeneous Subregions: The Agroclimatological Point of View.
P002 010	Remote Sensing of Wind Erosion in Croplands.
P002 011	Crop Identification and Area Estimation in the Southern Part of the Province of Buenos Aires, Argentina - Using LANDSAT Data.
P002 012	LANDSAT and Radar Mapping of Intrusive Rocks in SE-Brazil.
P002 013	Preliminary Field Tests with Oil Slicks Using Microprocessor Controlled Microwave Radiometer System.
P002 014	The Measurement of Particle and Chlorophyll Concentration in Water Using the Multi Scattering Model.
P002 015	Severe Convective Storm Detection Based on Satellite Infrared Imagery Analysis.
P002 016	Discrimination between Rangeland Pasture Communities in the North-West of Australia Using LANDSAT Data.
P002 017	Remote Sensing Analysis of Flooding and Salinity Problems in the NW Area of Buenos Aires Province, Argentina.
P002 018	Studies on Some Urban Problems by Using Airborne Remote Sensors in Santiago, Chile.
P002 019	The Use of a Geographic Information System to Combine Land Use Information Derived from LANDSAT with Soils Data to Stratify an Area in Argentina for Crop Forecasting.
P002 020	Biophysical Mapping of the Republic of Haiti through the Use of Enhanced LANDSAT Imagery.
P002 021	Optimum Assessment of Subsurface Water Parameters Using Radiance Measurements from Space.
P002 022	Limnological Study of the Coastal Lagoon 'Coyuca de Benitez, Guerrero' during an Annual Cycle (Summer 1981 - Spring 1982).
P002 023	Cultural and Environmental Effects on Crop Spectral Development Patterns as Viewed by LANDSAT.
P002 024	Assessment of Disease-Induced Yield Reduction in Cotton Using Simulated Satellite Imagery.
P002 025	Optimal LANDSAT Transforms for Forest Applications.
P002 026	Small Grains Area Estimation for Trenque Lauquen Partido Using Digital Image Processing Techniques.
P002 027	LANDSAT-Related Study for the Mali Land Use Inventory in West Africa.
P002 028	Spot Simulations in Bangladesh.
P002 029	Image Registration by Sequential Tests of Hypotheses: Gaussian and Binomial Techniques.

AD:	P002 030	TITLE:	Chesapeake Bay Plume Study (Superflux) Relative to the Biology of the Contiguous Shelf, Fishery Research and Monitoring.
	P002 031		Impacts of Climate on Variations in Summer Ice Cover in the Canadian Arctic.
	P002 032		Vegetation Assessment of the Northern Arabian Shield for Ground-Water Exploration Using Edge-Enhanced MSS (Multispectral Scanner) Images.
	P002 033		Development of Operational Snowmelt Forecasting Model for Very Large Watersheds in Himalayas.
	P002 034		Automatic Interpretation of MSS (Multispectral Scanner)-LANDSAT Data Applied to Coal Refuse Site Studies in Southern Santa Catarina State, Brazil.
	P002 035		Analysis of Multi-Data LANDSAT-GEOPIC for Map[illegible]ng Vinal (Prosopis ruscifolia) and Its Temporal Expansion.

ORGANIZED BY

Comisión Nacional de Investigaciones Espaciales
Buenos Aires, Argentina

Environmental Research Institute of Michigan
Ann Arbor, Michigan, USA

SPONSORED, IN PART, BY

ARGENTINA

Comando en Jefe de la Fuerza Aerea Argentina
Secretaría de Planeamiento de la Presidencia de la Nación
Ministerio de Relaciones Exteriores y Culto
Ministerio de Economía
Ministerio de Salud Pública y Medio Ambiente
Ministerio de Educatión
Ministerio de Obras y Servicios Públicos
Aerolíneas Argentinas
Yacimientos Petrolíferos Fiscales
Consejo Federal de Inversiones
Municipalidad de la Ciudad de Buenos Aires

UNITED STATES

U.S. Geological Survey
U.S. Department of Agriculture
Environmental Research Institute of Michigan
Naval Environmental Prediction Research Facility
National Aeronautics and Space Administration
National Oceanic and Atmospheric Administration

CANADA

Canada Centre for Remote Sensing

EXECUTIVE COMMITTEE

INTERNATIONAL SYMPOSIA ON REMOTE SENSING OF ENVIRONMENT

DR. L.R. BRESLAU
Cold Regions Research and Engineering Laboratory
Hanover, New Hampshire

DR. J.J. COOK (Chairman)
Environmental Research Institute of Michigan
Ann Arbor, Michigan

MR. F.P. DIEMER
U.S. Department of Energy
Washington, DC

DR. F. EL-BAZ
Itek Corporation
Lexington, Massachusetts

DR. F.P. HUDSON
U.S. Department of Energy
Washington, DC

MR. J.W. JARMAN
U.S. Army Corps of Engineers
Fort Belvoir, Virginia

MR. J.F. KOCA
Federal Highway Administration
Washington, DC

DR. A.D. MARMELSTEIN
U.S. Fish and Wildlife Service
Washington, DC

MR. R. McARDLE
U.S. Department of Agriculture
Washington, DC

MR. A. MEER
U.S. Department of State
Washington, DC

DR. R. NAGLE
Naval Environmental Prediction Facility
Monterey, California

DR. C.K. PAUL
U.S. Agency for International Development
Washington, DC

DR. I.M. PIKUS
National Science Foundation
Washington, DC

DR. W. RANEY
National Aeronautics and Space Administration
Washington, DC

MR. E.M. RISLEY
U.S. Geological Survey
Reston, Virginia

MR. W.G. ROHDE
U.S. Geological Survey
Reston, Virginia

DR. W.M. STROME
Canada Centre for Remote Sensing
Ottawa, Ontario, Canada

MR. E.J. WEGMAN
Office of Naval Research
Washington, DC

MR. W.H. WIGTON
U.S. Department of Agriculture
Washington, DC

MR. J. ZIMMERMAN
National Oceanic and Atmospheric Administration
Washington, DC

/

SIXTEENTH

INTERNATIONAL SYMPOSIUM ON

REMOTE SENSING OF ENVIRONMENT

PROGRAM COMMITTEE

BRIG. M. SANCHEZ PENA (Co-Chairman)
Comisión Nacional de Investigaciones Espaciales
Buenos Aires, ARGENTINA

DR. JERALD J. COOK (Co-Chairman)
Environmental Research Institute of Michigan
Ann Arbor, Michigan, USA

MR. PIERRE-MARIE ADRIEN
Inter-American Development Bank
Washington, DC, USA

DR. MAURICIO ARAYA FIGUEROA
Universidad Nacional de Chile
Santiago, CHILE

ING. JUAN MANUEL BEVERINA
Subsecretario de Informatica
Secretaria de Planeamiento
Presidencia de la Nación
Buenos Aires, ARGENTINA

ING. SALVANO BRICENO MATUTE
Ministerio del Medio Ambiente y
Recursos Naturales Renovables
Caracas, VENEZUELA

DR. CARLOS BROCKMANN
LARS/Purdue University
West Lafayette, Indiana, USA

CAP. de NAVIO CONRADO CACERES ESPINOZA
Ministerio de Defensa Nacional
Asunción, PARAGUAY

MR. WILLIAM D. CARTER
U.S. Geological Survey
Reston, Virginia, USA

MR. CHARLES CAUDILL
U.S. Department of Agriculture
Washington, DC, USA

MR. KENNETH B. CRAIB
Resources Development Associates
Diamond Springs, California, USA

PROF. S.S. DHAWAN
Department of Space
Bangalore, INDIA

ING. JOSE DIEZ PEREZ
Secretaria de Agricultura y
Recursos Hidráulicos
Mexico City, MEXICO

DR. EDWARD EPSTEIN
National Oceanic & Atmospheric
Administration
Washington, DC, USA

MY. GEN. JOSE ESPONOZA SALAZAR
Comisión Nacional de Investigación
y Desarrollo Aeroespaciales
Lima, PERU

DR. EDUARDO C. GAGGERO
Centro de Investigacion y Difusion
Aeronáutico y Espacial
Montevideo, URUGUAY

DR. JULIO CESAR GANCEDO
Secretaría de Cultura de la
Presidencia
Buenos Aires, ARGENTINA

ING. JOSE SALVADOR GANDOLFO
Consejo Nacional de Investigaciones
Científicas y Técnicas
Buenos Aires, ARGENTINA

MR. ALAIN GAUBERT
Centre National d'Etudes Spatiales
Paris, FRANCE

ING. AGRON. ENRIQUE GOBBEE
Instituto Nacional de Tecnología
Agropecuaria
Buenos Aires, ARGENTINA

DR. HEINZ HABERLE
Zentral Abteilung Raumflugbetries
der DFVLR
Oberpfaffenhofen, WEST GERMANY

ING. RODOLFO DONATO ORELLANA
Instituto Geográfico Militar
Buenos Aires, ARGENTINA

CNEL (R) CARLOS B. PAJARINO
Consejo Federal de Inversiones
Buenos Aires, ARGENTINA

DR. NELSON DE JESUS PARADA
Instituto de Pesquisas Espaciais
Saò José dos Campos, SP, BRAZIL

DR. A. B. PARK
General Electric Company
Lanham, Maryland, USA

TLE. CNEL MARIO A REMETIN
Subsecretaría de Ciencia y Tecnología
Secretaria de Planeamiento de la
Presidencia de la Nación
Buenos Aires, ARGENTINA

DR. HERNAN RIVERA HERMIDA
Centro Interamericano de
Fotointerpretación
Bogotá, COLOMBIA

DR. CELSO R. ROQUE
Natural Resources Management Center
Quezon City, PHILIPPINES

ING. ALBERTO SEGOVIA
Centro de Levantamientos Integrados
de Recursos Naturales por Sensores
Remotos
Quito, ECUADOR

DR. W. MURRAY STROME
Canada Centre for Remote Sensing
Ottawa, Ontario, CANADA

DR. KARL SZEKIELDA
United Nations
New York, New York, USA

ABSTRACT

These volumes contain papers accepted for presentation at the Sixteenth International Symposium on Remote Sensing of Environment, originally scheduled to be held from 2 to 9 June 1982, in Buenos Aires, Argentina. The program for this symposium was organized jointly by the Environmental Research Institute of Michigan (ERIM) and the Argentine Comision Nacional de Investigaciones Espaciales (CNIE) as a part of a continuing series documenting global activities in the field of remote sensing. These meetings are intended to promote increased international cooperation in research, development, and application of this technology, and to stimulate an exchange of information on all aspects of this multidisciplinary field through the presentation of reports on work planned, in progress, or completed.

Scientific and technical papers contained herein include those concerned with the development of remote sensing techniques and methodology, as well as those dealing primarily with the effective utilization of this technology in various application areas such as agriculture, geology, hydrology, land and cultural resources, meteorology and oceanography.

EDITORIAL NOTE

The Sixteenth International Symposium on Remote Sensing of Environment, organized jointly by the Environmental Research Institute of Michigan (ERIM) and the Argentine Comision Nacional de Investigaciones Espaciales (CNIE), was originally scheduled to be held from 2 to 9 June 1982 in Buenos Aires, Argentina. However, due to circumstances beyond the organizers' control the meeting could not be held on schedule and the comprehensive program, including some 250 scientific and technical papers on all aspects of remote sensing technology, was initially postponed and eventually cancelled.

In response to this unfortunate situation the organizers have attempted to provide for the timely presentation and/or publication of all available papers initially planned for presentation at the 1982-Sixteenth Symposium by:

(a) scheduling as many as possible for presentation at the subsequent 1983 Seventeenth Symposium, held in Ann Arbor, Michigan from 9 to 13 May; and,

(b) including all manuscripts and/or summaries received in time for publication within these volumes of "Papers Accepted for Presentation at the Sixteenth International Symposium on Remote Sensing of Environment, Buenos Aires, Argentina."

In general papers contained in these volumes are included in the order of their proposed presentation in Buenos Aires, while those actually presented in Ann Arbor are so designated by footnotes on the initial page of the appropriate manuscript herein. Manuscripts not received in time to meet publication deadlines are, wherever possible, represented by comprehensive summaries of the presentation, or proposed presentation. All are reproduced here exactly as provided by the authors and all material, information, and conclusions are the responsibility of the specific authors involved and not of ERIM, CNIE, the Executive Committee, the Program Committee, or the sponsoring organizations.

An author index is included as a supplement to the table of contents. All illustrative materials have been reproduced in black and white except where individual authors elected to provide their own color prints and/or defray the additional cost of color reproduction. Readers are requested to contact specific authors where color prints of black and white illustrations are desired. Requests for reprints of individual papers should be directed to the authors, while additional copies of the entire Volumes are available from:

Remote Sensing Center
ERIM
P.O. Box 8618
Ann Arbor, MI, 48107, USA
(313) 994-1200, extension 290

Jerald J. Cook

Jerald J. Cook
ERIM
Ann Arbor, Michigan

CONTENTS

Page

Page

Page

Page

Page

Page

REMOTE SENSING APPLICATIONS IN MEXICO

José A. Díez Pérez

Subdirección de Investigación y Tecnología de Apoyo
Secretaría de Agricultura y Recursos Hidráulicos
Mexico City.

ABSTRACT

Because of the large territory of the country, the applications of Remote Sensing are of great importance in Mexico. The terrestrial - photogrammetry was established in 1926 in the Irrigation Commission (Comisión Nacional de Irrigación~~)~~; this Agency, for dam location and irrigation planning, ~~made~~ yet, ~~Aereal~~ Photography in 1928. In 1932 began operating the first commercial company offering photogrammetry.

Modern Remote Sensing began in 1968, when an important project was conducted in collaboration with NASA (U.S. National Aeronautics and Space Administration). Information was gathered using a multiband ~~aereal~~ platform.

Through the Outer Space Commission (Comisión Nacional del Espacio Exterior), research projects were submited to NASA for the ERTS Investigation. In this field some advances were made demonstrating the utility of Remote Sensing in different fields through pilot studies.

Now some projects are being made for different institutions; a review of them is presented. The advances and setbacks of the application of Remote Sensing in Mexico are described in this paper, with some insight in the reason of difficulties and limitations. This experience can be useful to other developing countries.,

Revising the main problems of the country, the experience of trained people and other facts, a conclusion it is that there is a future in the applications of Remote Sensing in Mexico.

/

1. ANTECEDENTS

1.1 Historical and Geographical Scope

Terrestrial photogrammetry was established in Mexico as early as 1926, at the Irrigation Commission (Comisión Nacional de Irrigación). Aereal photography was establiched in 1928 in the same Agency, which was in charge of dam location and irrigation planning during these years (1).

In 1932 began operating in Mexico the first commercial company offering photogrammetry. This company has been joined by others in an effort to supplying aereal photos and cartographical information to government and private enterprises for the past 50 years.

Early applications in Mexico dealt with water related works; this because located between 14^{o} West and 32^{o} North (Fig. No. 1) more than 2/3 of the country territory are drylands (2). Desert arid 31%, semiarid 36%, humid and subhumid 33%. Current population is more than 70 million people (3), with a rate of increase near 3% annual. This fact stresses the investment to maintain the availability of adequate urban services and an agriculture development that enables meeting the demands of such population increment.

The use of aereal and spatial techniques has been and still is very important for the country: it has a surface near 2,000,000 km^2 and a varied and rough topography. These characteristics made soon aereal photography of widespread use,as road planning construction, mineral and oil geological studies.

1.2 Cartography

Aereal photography was used in the cartography of Mexico, published in the 60's. This included a project by the Defense Ministry (Secretaría de la Defensa Nacional) to elaborate topographical maps 1:500 000 and 1:250 000 scales. At the present 1:100 000 scale topographical maps (4) of the southern portion of the country are being produced.

A recent and more complete cartographical task began in 1968 with the fundation of the Territory and Planning Studies Commission (Comisión de Estudios del Territorio Nacional y Planificación: CETENAP), now Direction of Geography (Dirección General de Geografía del Territorio Nacional: DIGETENAL), which began elaborating Topographical, Geological, Land Use, Soil Taxonomy and Potential Land Use maps, all at 1:50 000 scale. Most of this work has been made using panchromatic photos scale 1:20 000 and 1:70 000. The work at 1:50 000 scale continues,it has been covered 75% of the territory; also there has been completed the national coverage of some cartography at 1:1000 000 and 1:250 000 scales.

2. REMOTE SENSING APPLICATIONS

2.1 Mission 91

Strictly Remote Studies began in Mexico in 1968, through an International Collabora tion Agreement signed between our country and USA.

One of the objectives of the Agreement was the development of the Remote Sensing technique in Mexico. As a result, the US National Aeronautics Space Administration (NASA), coordinated by a national institution , the Outer Space Commission (Comisión Nacional del Espacio Exterior CONEE), flew in Mexico some Test Sites the same year.

The NASA 91 Mission used and Electra airplane equipped with two cartographic cameras carrying color and infrarred film, a pack system of six 70 mm cameras, a Side Looking Radar, an Infrared Radiometer and a Thermal Scanner.

Universities and Government Agencies gathered in a Remote Sensing Commitee proposed porjects in different sites, throughout the country (Fig. No. 1). The main objectives of the mission were:

- Assessment and determination of the extension of mineral deposits (5).
- Geological studies related to Geothermal Fields (6).
- To obtain the identification of flooded areas
- Crop classification and pest identification in farmlands
- Definition of pollution sources
- Assessment of soil and water resources

The studies supplied valuable information dealing with the wide potentials of the new techniques, as well as the strategy of their implementation. The main points in this regards were:

1) Before any Mission in run, it is necessary to conduct a previous investigation about the reliability of it.
2) A careful programming of the flight missions has to be done, as well as the choosing of the instruments to be used, accordingly with the objectives of the study.
3) An adequate Ground Truth has to be carried out simultanously to the mission.
4) A data extraction, careful task, has to be performed. It must be undestood that this work differs sometimes from that made by conventional photointerpretation.

2.2 Remote Sensing Flights

Since 1970 Remote Sensing flights were made in the Ministry of Water Resources (Secretaría de Recursos Hidráulicos: SRH) using small airplanes and a multiband set of 70 mm cameras; some studies were conducted on Land Use and Lagoon Cartography (7). In the same institution studies were done on desease detection using aerial infrared film.

In 1975, the Outer Space Commission (CONEE) acquired a twin engine airplane for domestic missions. Besides the avionics, the equipment of the airplane had the following instrumentation (8):

. A set of 4 cameras for multiband missions
. A infrared 5 radiometer
. An infrared scanner.

The system was offered, to be shared, in a User Missions System, to the Remote Sensing Commitee.

Some missions were made; one of these missions was a water pollution study, conducted in 1975 by SRH over the Acapulco Bay (9). Two flights were performed: at dawn for infrared data gathering purposes and the other one during the morning . Were used 70 mm cameras with black and white, color, color infrared films and the Thermal Scanner: also thermal infrared measurements were made by the Radiometer. Using the photographs an identification and quantification of the oil spots into the Bay could be made.

Infrared film was applied on the citrus inventory in the State of Nuevo León, the main national orange producer. This task performed in 1976 was made as a joint project (10) between the Nuevo León University, the Citrus Insects Center (CIC) of the U.S. Ministry of Agriculture, located in Weslaco, Texas, and the Ministry of Water Resources.

The collaboration of the CIC was very valuable again for the country in 1977. That year a Mediterranean Fly invasion appeared in the border with Guatemala. A Medfly Host Plants inventory was proporsed in South Mexico, as a project of the Ministry of Agriculture and Water Resources (Secretaría de Agricultura y Recursos Hidráulicos: SARH), which resulted from merging both ministries into the mexican goverment in 1977.

Beeing impossible to detect the fly infestation on the tree foliage, a Host Plant Inventroy was set to locate all fruit orchards and isolated trees between the Guatemala border, the Mountain Range and the Ocean (11). Main objective was to gather information to assist *the Direction of Plant Pathology (Dirección General* de Sanidad Vegetal, SARH) to stop the plague.

Some teaching and research in Remote Sensing applied to water quality parametres quantification (12), has been made using photographic film in a Laboratory of the Faculty of Sciences of the University of Mexico (Laboratorio Interdisciplinario, Facultad de Ciencias, UNAM).

2.3 Satellite Investigations

The satellite era began in 1971. Using the same US-Mexico Agreement which allowed the mission 91, NASA made in invitation through the Outer Space Agency (CONEE) to the Commitee of all concerned Agencies. The invitation from NASA was to participate as Principal Investigators to define the utility of the Earth Resources Technological Satellite (ERTS).

Investigators from the Agencies requested for black and white ERTS images, negativest and transparencies, most of them 1:1000 000 scale. Outstanding pilot studies using ERTS images were for mineral exploration in the center of the country and three Test Sites for hydrological studies. The first one was made by the Non Renewal Natural Resources Council (Consejo Nacional de Recursos Naturales no Renovables, now Consejo de Recursos Minerales), the Agency dealing with mineral ore detection and quantification, and the other by the Ministry of Water Resources (SRH) in Mexicali, Los Mochis y Papaloapan Test Sites (13),(14), (15).

Besides the familiarization with the new information and development of utilization technologies, the investigations gave useful data from the different zones, as unnoticed fault trends in the first Test Site (A) and in the next three (B,C,D): Land Use maps, Structural Geological maps, *a classification of coastal areas for pollution prevention purposes,* Hydrographics maps, and mud dispersion patterns in lakes and lagoons. (Fig. No. 1).

In 1974 there was also a national participation, by SRH in the Skylab Principal Investigation (16), this platform took a lot of information photographies, multiespectral images and radiometric data over Mexico, in its three Missions. The high resolution of the

Skylab information permitted the data gathering from seven zones, mainly irrigation districts and lakes.

An interesting pilot project was the assessment of salinity in irrigated lands (19), made at the Ministry of Water Resources (SRH). According to the level of salinity, the soils were classified in three groups using a methodology which consisted in the interpretation of LANDSAT images from four different seasons throughout the year. Resulting map was at a scale 1:100 000. This map, was finished in two weeks, with low cost and a high realiability it is a demonstration of the efficiency of the satellite Remote Sensing.

Using Landsat slides, were also drawn maps representing coastal and lagoon features by the Ministry of Water Resources (18). This was performed in the Sinaloa State Coast.

In some Universities has been demonstrated interest in research and application in the field of Remote Sensing Technology; in the University of Chapingo (19), Universidad Autónoma de Nuevo León, which was mentioned and San Luis Potosí University.

In the field of oil exploration, the Petroleum Institute (Instituto Mexicano del Petróleo0, in the Prospecting Division made some research using Landsat photographic images locating structural traps for oil accumulation.

2.4 Satellite Operational Projects

Two main operational projects emerged using ERTS photographic images:

In 1973, the National Hydraulic Plan (Plan Nacional Hidráulico, SRH) was set up to evaluate and plan the efficient use of the Hydraulic Resources in Mexico. The plan required knowledge of recent land Use information on a nation wide basis, for water and soil integration, also it was evident the need to get it in a short time.

The only way to acquire such information at that pace was using ERTS images.

The production of the Land Use map was completed in less than two years, using mainly 1973-1974 false color transparencies by manual interpretations (2). In some regions of special interest (45 million hectares) also potential Land Use Studies were performed (20). The result of this project was a Land Use National Map scale 1:1 000 000.

Another project was in the Ministry of Agriculture (Secretaría de Agricultura y Ganadería, SAG). Between years 1975-1978 under the name of Synoptic Cartography (Cartografía Sinóptica) a more detailed Actual Land Use map of the country was made: scales went from 1:250 000 to 1:500 000. Interpretation was made using manual methods over 1:500 000 false color paper enlargements. The objetive of this work was to present also areas of the different categories to give useful information for planning.

The National Forestry Inventory (Dirección del Inventario Nacional Forestal, SAG), began using besides aereal photos, Landsat images in their works (21); between 1979-1980 advance was 723,900 hectares, covering several states of the country.

2.5 Computer Interpretations

Of great importance in the Remote Sensing applications is the Automatic Interpretation by means of digital computers, time saving, data resolution , also economy increase, can be obtained in regards the manual methods.

When ERTS images became available, digital informations was requested in the Ministry of Water Resources (SRH). First tapes were received in 1973. The task began immediately, trying to read the NASA compatible tapes. As there was no suitable software package around in those days to meet the needs in the Ministry, it was developed a program, on their own, first on a CDC 3 300 and later of a Cyber, both in batch mode. The name SIADIS (Sistema de Interpretación Automática de Imágenes de Satélite) was given to this

package (22). Now SIADIS, with some improvements is being used in a DEC PDP 11-70 computer of the National Hydraulic Plan (SARH), using a hardware system designed there and composed of equipment made from different suppliers.

In 1975 was founded by IBM in Mexico City the Scientific Center (Centro para América Latina; CIBM), as a non-profit organization to make research and development in computer technics.

In 1975 the IBM Scientific Center began working in agriculture, water resources and soil erosion projects. These were carried out by making use of ERIPS (later renamed ERMAN II). During the last seven years, the experience acquired has enabled the Scientific Center to develop more powerful application programs and at the present joint projects include data bases that overlay LANDSAT and cartographical maps for: Geological exploration, soil types, soil erosion, land productivity and urban studies.

The Research Institute on Biotic Resources (Instituto de Investigaciones sobre Recursos Bióticos: INIREB) has been investigating in tropical vegetation inventories Using Landsat digital information. Work has been done in Veracruz state using SIADIS and ERMAN-II (23), (24).

In the University ofMexico, the Applied Mathematics Institute (Instituto de Investigaciones en Matemáticas Aplicadas y Sistemas: IIMAS, UNAM) was installed a project to develop an interpretations computer system. This system named Remote Sensing,P.R. project , was developed in a B-6700 Borroughs Computer (25).

The P.R. system was transferred later to a DEC PDP 11-34 computer where a joint project was performed with the Electrification commission (Comisión Federal de Electricidad) to identify thermal anomalies in the neighborhood of Cerro Prieto Geothermal Field (26). In the IIMAS has been made also teaching in Remote Sensing computer interpretation data.

Institute of Geophisics of the University of Mexico (Instituto de Geofísica, UNAM) installes in 1978 a system for image processing in a NOVA-3 computer. This system, REMEDYS has been mainly applied to geological and geophysical projects, as to define geothermal fields (27),(28).

In 1979 was installed in DIGETENAL a computer system designed in NASA named SIDAM I. This system is provided with the computer and all peripherals needed for aereal scanner and satellite digital information processing was followed by another one, SIDAM 2 in 1980 (29). Both systems, with a visual five channels scanner mounted in a twin engine jet airplane, are a package also used in the anti-drugs policies.

There have been proposed many projects using the digital systems in Mexico:

. Elaboration of an Actual Land Use Map scale 1:250 000 (30)
. Classification and quantification of eroded zones (31)
. Water quality and Land Use Monitoring (32) (33)
. Vegetation Inventory (34), (35), (36)
. Forestry Inventory (37), (38)
. Geothermal Anomalies and lithological detection (26).

Most projects were developed using Landsat information; using the aereal scanner DIGETENAL has performed in 1981 also Urban Zones Studies (29).

2.6 Recent Developments

The Scientific Center (CCIBM) of IBM provided with a 370-158 IBM computer continues working with advanced research projects such as:

. The instalation of a geographical data base system
. An interactive graphics system for analysis of tropical forest dynamics

. New algorithms for analysis manipulation and display of different image types as Landsat, 3D, medical.

The Petroleum Institute (Instituto del Petróleo) uses LANDSAT information as input to tectonic models, in a joint project with CCIBM.

At the University of Mexico UNAM works in the Remote Sensing field continue:

In the Applied Matemathics Institut (IIMAS), besides research in computer interpretation research is made in Remote Sensing hardware (40).

The Instituto de Geofísica besides research in gathering for Geological information is making now investigations in ore and pollutions detections through identification of soil anomalies.

Work in the Remote Sensing field continues by the Laboratory in the Faculty of Sciences (LIFC) and now some research is being made in the Instrumentation Center (Centro de Instrumentos) of the same University.

The Research Institute on Biotic Resources (Instituto Nacional de Investigaciones sobre Recursos Bióticos) continues researching in Vegetation maping; a computer system for Remote Sensing applications is being installed there.

The Direction of Geography (DIGETENAL) uses the systems (SIDAM 1 and SIDAM 2) in specific projects, as a Desert pilot study. The same institution is working now in the elaboration of the cartography for kelp in the Baja California west coast and study of the Guadalajara and Mexico City urban zones (39), this one using multi-temporal data.

One of the Institutions working out in the field of Remote Sensing is the Ministry of Agriculture and Water Resources (SARH). Following the preliminary research effort, described before more projects are being developed at the Ministry:

The National Inventory of Eroded Zones, one of the main problems encountered in Mexico. This task is performed by Direction of Conservation of Soil and Water (Dirección General de Conservación del Suelo y Agua , at a 1:250 000 Scale (41).

Land use Studies are being made in Hydraulic Plan Comission (Comisión Nacional del Plan Nacional Hidráulico), for specific planning projects in several states of the country. Some projects have been also made in some River Bassins.

Now in their computer is the version 4.0 of the SIADIS system, provided with enhancement, image display and plotting routines(42).

Some research in agroclimatical and Environmental Impact applications is being made in Direction of Water Use and Pollution Control (Dirección General de Usos del Agua y Prevención de la Contaminación). GOES digital information is also being used there (43), (44).

A crop Inventory using mixing techniques is been performed by Direction of Agriculture (Dirección General de Agricultura). The synoptic Cartography continues being made, using Landsat 1:250 000 photographic images.

In the Forestry Institute (Instituto Nacional de Investigaciones Forestales) the forestry inventory task continues and a deforestation detection in tropical zones, made jointly with CCIBM (45).

After some successful pilot studies in Plant Pathology (11), a Remote Sensing Center for Desease Prevention is been installed this year in Metapa, State of Chiapas by Direction of Plant Pathology (Dirección General de Sanidad Vegetal) to monitor and

assess plant pests.

3. MAIN PROBLEMS IN THE DEVELOPMENT IN MEXICO

To accomplish a Remote Sensing job there is a lot of requirements that must be met on time so that a project succeeds. Sometimes all these requirements are hard to fulfill in a developing country, where some goods must be imported. Then a mission may fail for lack of the adequate airplane, spare parts for the photo equipment or difficulties in the photographic processing material availability.

Also, there is a difficulty to get satellite information from the Country lacking its own Ground Station. In Mexico we have not a control to record data about the country transmitted to the U.S. Ground Stations. Besides a delay in receiving data, approximately one fourth of Mexico is out of direct reach from those stations.

This difficulty isgoing to be more critical with the new generations of satellites, as Landsat D, D' which have lower orbits and a smaller area coverage. Long-lasting cloudiness presents additional difficulty in the southeast of the Country, with a stronger need for a continuous data collection.

To preclude this situation, and to permit the development of projects such as crop estimation, and water quality monitoring, some attempts have been made to install a Ground Station in Mexico. The first one was by the now disappeared CONEE and some others from to the Ministry of Agriculture and Water Resurces. The last attempt was made in 1981 by the National Science Council (Consejo Nacional de Ciencia y Tecnologia: CONACYT); this institution proposed to instal aGround Station which was to be located in a radio of [illegible]00 km from Mexico City (46). The project included a Service Center and a Center for Processing and training. From its vantage point position the station, should be able to cover the whole territory of Mexico and a portion of Center America.

Preliminary steps were made, but the project was abandoned because a lack of agreement between the government agencies involved.

The postponement of this project implies that three more years will elapse before having a new proposal made, approved and executed.

4. CONCLUSIONS

Remote Sensing is a useful technique for inventoring natural resources and monitoring environmental parameters; for developing countries there is a further interest in its applications:

. Usually we lack a complet cartography of natural resources, meaning different scales and useful information.

. We have still territories with unknown resources.

Remote Sensing presents a good alternative for applications in Developing Countries which require a cartographic basis for their development programs. It is a method to gather information quickly and economically in order to cope with problems such as Environmental Pollution, the advance of Erosion and Plant Diseases.

Remote Sensing can share a responsability in the monitoring of the former parameters establishing pest and pollution warning systems and also soil and crop inventories and assesgment. The FAO proposal for the establishment of a globe frame to monitor agriculture, intenting to assist goverments in their plans formulates a new international strategy for development.

In developing countries food production is a challenge; as stated by FAO (47) in year 2000 the world population will be 6 billion people, twice the 1960's. As the growth of agriculture in developing countries has been inferior than the population growth and in year 2000 90% of population will be in those countries, then food production shall be one of the most difficult problems to resolve.

But institutions of Third world countries can make the error recently stated by George Zarzycki, president of the American Society of Photogrammetry: "There is a danger in applying Technology for Technology's sake". This is very important statement, more important for developing countries, where costs and results must be more carefully balanced. It is then convenient to install an Agency to perform, or at leat coordinate, the national efforts made in the Remote Sensing field. One of the tasks of this agency should be to define the technology transfer in this field. Technology transfer in general, has not been a sucess: it has not reduced the broad lag between developed and developing countries (48); the transfer must rather be focused as an exchange of knowledge and not as a exportation of technology.

In our country, notwithstanding friendly communication links between the technicians, we lack a National Program. My presentation here is made as the personal opinion of seomeone who has been in the Remote Sensing field since its early days in Mexico.

To my way of thinking the first step in any country should be the establishment of a National Program coordinated by a single institution. Then it is important: to define the objectives of the project and the information needed. To perform the previous analysis: if the data collection is possible by Remote Sensing and which is the adequate sensor. To evaluate if the data resolution can be gathered, and compare the costs of the Remote Sensing approach with those from conventional methods.

The performance of our Remote Sensning development has been presented here, from aereal photography to the establishment of the Remote Sensing project, using airplanes and satellites.

Dificulties have appeared in our development, such as the overselling of the Remote Sensing possibilities.

A mixing of non technical and political interests have slowed down our Program, one of the first Latin American Programs.

The first proposals of Remote Sensing were received with enthusiasm. The test site evaluation was made in a very receptive environment and the mission was finally flown. but what happened concerning to Remote Sensing is that some people expected from the technique more than that it could actually give. At the beginning some of the users attributed to the technique, regarding the results it could deliver, an almost magic potential. At an early stage this caused some expectation among the decision makers in their field of concern, but when definite results from Remote Sensing could not be obtained, a certain mistrust, which lasted several years, was developed towards the new technology.

Then in the following years, the goal of the applications in Mexico was, besides its specific objectives, to convince experts and politicians of the excellency of Remote Sensing.

In Mexico an interesting fact is that, compared to developed countries, all the Remote Sensing work has been effected, and still is by governmental institutions. The private companies have not found a propicious field to develop Remote Sensing branches. This may be due to lack of information in the technical media about the technique itself or to the fact that the market is still scarce. The further efforts by private industry are taking color infrared photography, which has been provided to their customers for interpretation (49).

Notwithstanding those difficulties, the truth is that we have a lot of experience

and expertise stored in a lot of trained people: this is the main asset we have now at our disposal in Remote Sensing, and the future of the applications will be in their hands.

In countries which as Mexico have very large territories the satellite information still supplies low cost information for the development of regional and national projects.

5. REFERENCES

1.- Orozco Portugal I., Comisión de Aguas del Valle de México, SARH, Personal Communication, 1982.

2.- Secretaría de Recursos Hidráulicos, Subsecretaría de Planeación, Plan Nacional Hidráulico, Primera Parte, 1975.

3.- Secretaría de Programación y Presupuesto, "X Censo General de Población", Junio de 1980.

4.- Gómez Estrella, Secretaría de la Defensa Nacional, Personal Communication, 1982.

5.- Acosta C. "Some practical results on sensing over Test Site 701: Oro-Tlalpujahua, México". Consejo de Recursos Naturales no Renovables, 1971.

6.- Gómez, R., J.D. Friedman, S.J. Gawarecki and C.J. Banwell, "Photogeologic and Thermal infrared reconnaissance surveys of the Los Negritos Ixtlán de los Hervores Geothermal area, Michoacán, Méx.", Geothermic special Issue No. 2, 1970.

7.- Secretaría de Recursos Hidráulicos, Dirección General de Estudios, "Fotointerpretación de las lagunas La Joya y Buenavista, Chis.", 1971.

8.- Flores N. "El Programa de Percepción Remota en la Comisión Nacional del Espacio Exterior", I Reunión sobre el aprovechamiento de los datos derivados de los satélites tecnológicos para el estudio de los recursos naturales, Secretaría de Comunicaciones y Transporte, - Comisión Nacional del Espacio Exterior. 1975.

9.- Secretaría de Recursos Hidráulicos, Departamento de Percepción Remota "Estudio de Contaminación de la Bahía de Acapulco mediante Percepción Remota", 1976.

10.- Rangel, R.H., G.R. Mancillas, F. Abarca, E.E. Calles, J.A. Díez "Aplicación de Sensores Remotos en la Citricultura". Seminario Internacional sobre el Uso de los Sensores Remotos en el desarrollo de los países, CCIBM, CCAL-77-06, México, D.F., 1976.

11.- Díez J.A., W. Hart, S. Ingle, R. Davis, S. Rivera, "The use of Remote Sensing in detection of the Host Plant of Mediterranean Fly in Mexico", XIV International Symposium on Remote Sensing of Environment, San José Costa Rica, 1980.

12.- Ruíz P.,L. Lemus, G. Izquierdo "Percepción Remota en la Facultad de Ciencias", Seminario Internacional sobre el uso de los sensores remotos en el desarrollo de los países". CCIBM, CCAL-77-06, México, D.F., 1977.

13.- Secretaría de Recursos Hidráulicos, Mexicali Test Site Report, NASA SR9631/8B, 1974.

14.- Secretaría de Recursos Hidráulicos, Los Mochis Test Site Repot, NASA SR9631/8A, 1974.

15.- Secretaría de Recursos Hidráulicos, Papaloapan Test Site Report, NASA SR9631/8C, 1974.

16.- Secretaría de Recursos Hidráulicos, "General Report on SKYLAB Image Investigation", 1977.

17.- Díez J.A., F. Ramírez, "Un nuevo sistema de detección salina en los distritos de riego mediante imágenes de satélites LANDSAT", Seminario Internacional sobre el Uso de los Sensores Remotos en el Desarrollo de los Países, CCIBM, CC AL-77-06, México, D.F. 1977.

18.- Díez J.A., F. Ramírez, "Estudio de las bahías de Santa María, Ohuira y Topolobampo mediante imágenes Landsat". V Congreso Nacional de Fotogrametría, Fotointerpretación y Geodesia", México, D.F., 1976.

19.- Cerda N.,J. Estrada, C. Ortíz, H. Cuanalo. "El uso de fotografías de satélite en la delimitación fisiográfica del Plan Zacapoaxtla", IV Congreso Nacional de Fotogrametría, Fotointerpretación y Geodesia, México, D.F., 1976.

20.- García, F., H.Luna, "Un inventario a nivel nacional del uso actual del suelo", Congreso Nacional de la Ciencia del Suelo, Veracruz, Ver., 1973.

21.- Moncayo F.- "Algunas Experiencias en el estudio de tipos de vegetación y uso del suelo mediante imágenes de satélite", IV Congreso Nacional de Fotogrametrías, Fotointerpretación y Geodesia, México, D.F., 1976.

22.- Díez J.A., M. Medina, C. Mejía, "Principales ventajas de la aplicación del sistema SIADIS, INTERPRETACION AUTOMATICA DE IMAGENES, desarrollado en la S.R.H.", IV Congreso Nacional de Fotogrametría, Fotointerpretación y Geodesia", México, D.F., 1976.

23.- Mejía C., F. Lozano, M. Soto, J.A. Díez, "Avance en el Inventario de la Vegetación en Veracruz; zona cafetalera de Jalapa-Coatepec", Seminario Internacional sobre el Uso de los Sensores Remotos en el Desarrollo de los Países, CCIBM, CCAL-77-06, México, D.F., 1977.

24.- Soto M., L. Giddings, "The Use of LANDSAT data in Mapping Tropical Vegetation", XIV International Simposium on Remote Sensing of Environment, San Jose, C.R., 1980.

25.- Guzmán, A. "Análisis por computadora de imágenes multiespectrales para conocer nuestros recursos naturales", IV Congreso Nacional de Fotogrametría, Fotointerpretación y Geodesia", México, D.F. 1976.

26.- Jinich A., L. Farah, M. Garza, C. Velarde, R. Méndez, J. Resenbluth, J., "Aplication of Machine Processing of Visible and Thermal Data to the Study of the Geothermal Area of Cerro Prieto, XV International Symposium on Remote Sensing of Environment, Ann Arbor, E.U.A. , 1981.

27.- Instituto de Investigaciones de la Industria Eléctrica, C.F.E. Instituto de Geofísica UNAM, "Percepción Remota en Exploración Geotérmica", 1979.

28.- Del Río L., F. Pascaud, S. Camacho, N. Galván, "Remote Sensing techiques for the identification and evaluation of geothermal areas", XIV International Symposium on Remote Sensing of Environment, San José, Costa Rica, 1980.

29.- Ramírez M.F., A. Botello, "Configuración Física de los Sistemas Digitales de Análisis Multiespectral, SIDAM 1 y SIDAM 2", Secretaría de Programación y Presupuesto, Depto. de Teledetección, 1980.

30.- Díez J.A., M. Medina, S. Rivera, "A methodology for a national converage land use by computer", Symposium on Machine Processing of Remotely Sensed data, Purdue, Lafayette, 1979.

31.- García R., G. González, R. Oliva, A. Bustamante, R. Fontanot, "Detección y Tipificación de Zonas Erosionadas en Imágenes de Satélite", Seminario Internacional sobre el Uso de los Sensores Remotos en el Desarrollo de los Países, CCIBM, CCAL-77-06, 1977.

32.- Hernández M., J.A. Díez, J. Villa, "Estudio de Uso de Suelo en el Estado de Durango mediante Percepción Remota", IBM Scientific Center, México, 1978.

33.- Díez, J., F. Ramírez, M. Medina, "Detección de lirio y cuantificación de la calidad del agua mediante Percepción Remota", IV Congreso Nacional de Hidráulica, Acapulto, 1976.

34.- Soto M., F. Lozano, C. Mejía, J.A. Díez, M. Medina, "Mapping Tropical Vegetation Zones", XII International Simposium on Remote Sensing of Environment, Manila, Philippines, 1978.

35.- Ramos H., "El Uso de Datos Multiespectrales obtenidos en Avión para Identificación de Cultivos", S.P.P., 1981.

36.- Valdes, J.A., S. Arredondo, J. Miranda., "Estudio sobre la aplicación del procesamiento digital de imágenes multiespectrales a la detección y cuantificación de áreas cañeras", Fotogrametría, Fotointerpretación y Geodesia, No. 29, 1981.

37.- Varela, S., "El Uso de Imágenes de Satélite en la Dirección del Inventario Nacional Forestal, Seminario Internacional sobre el Uso de los Sensores Remotos en el Desarrollo de los Países, CCIBM, CCAL-77-06, México, D.F., 1977.

38.- García, R., González G., Oliva R., "Complementación de la Carta Forestal de la República Mexicana por medio de Imágenes de Satélite", V Congreso Nacional de Fotogrametría, Fotointerpretación y Geodesia, México, D.F., 1978.

39.- Ochoa Torres A., DIGETENAL, S.P.P., Personal Communication, 1982.

40.- Rodríguez M., A. Haro, J. Alarcón, A. González, "DIMAS Despliegue de imágenes multiespectrales para su análisis sistemático", Publicación 283 IIMAS, UNAM, 1982.

41.- Benítez Omana A., D. Gral. Conservación de Suelo y Agua, SARH, Personal Communication, 1982.

42.- Guitrón De los Reyes A., Comisión del Plan Nacional Hidráulico, SARH, Personal Communication, 1982.

43.- Aste, J. J.A. Díez, "Parámetros obtenidos del Satélite GOES", II Congreso Panamericano y VII Nacional de Fotogrametría, Fotointerpretación y Geodesia, México, D.F., 1982.

44.- Díez, J.A., "Estudio de Impacto Ambiental en Veracruz mediante Percepción Remota", Subdirección de Investigación y Tecnología de Apoyo, DGUAPC, SARH, México, 1981.

45.- García Mayoral P. I.I. Forestales, SARH, Personal Communication, 1982.

46.- Ramírez Cervera C, CONACYT, Personal Communication, 1982.

47.- FAO, "The year 2000 agriculture, Latin America Problems and Options".

48.- Roll H.U. "Una verdadera colaboración en Oceanografía", Ciencia y Desarrollo, CONACYT, MEXICO, Marzo-Abril 1982.

49.- Carstens Martínez A., Compania Mexicana Aerofoto, Personal Communications, 1982.

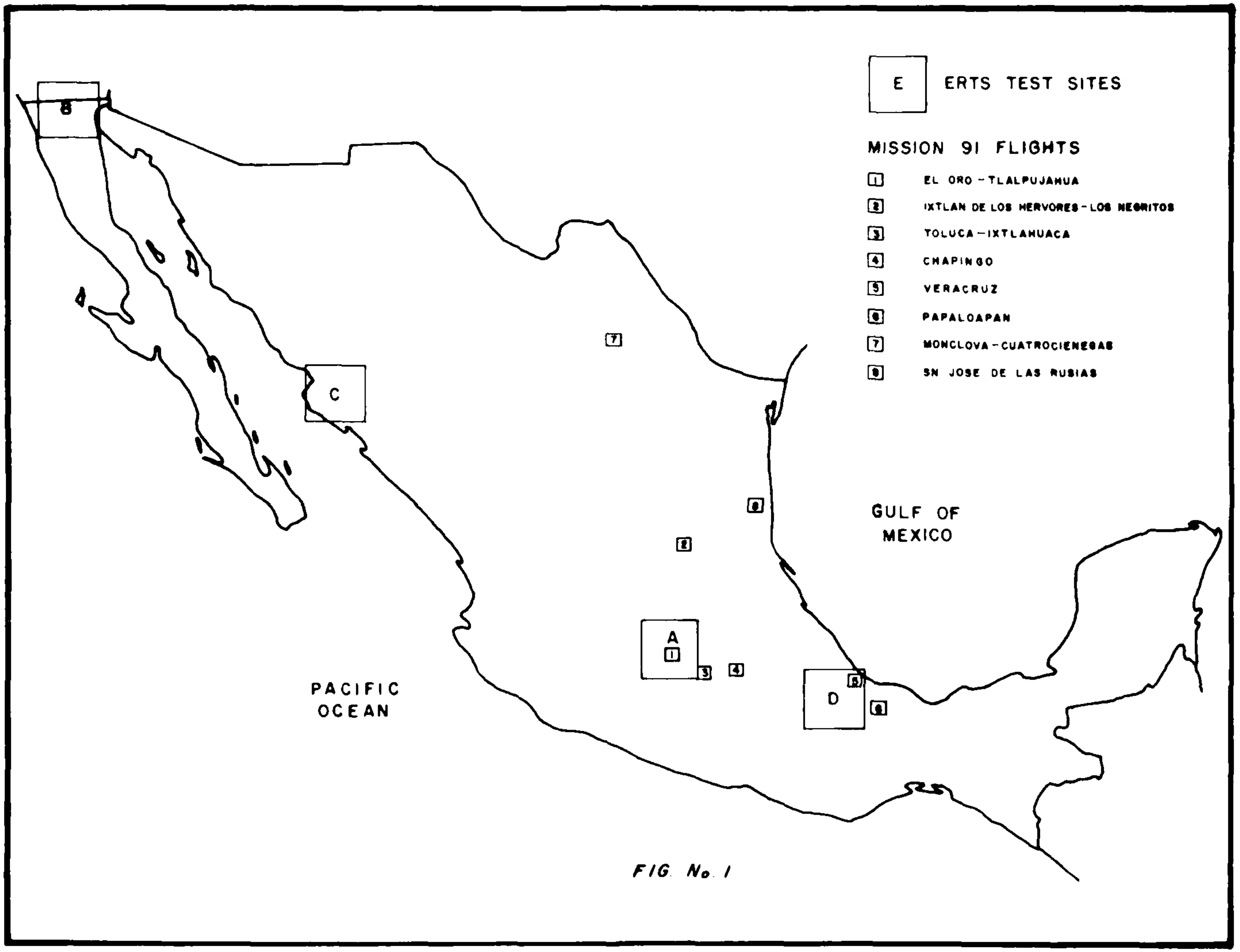
E ERTS TEST SITES
MISSION 91 FLIGHTS
1 EL ORO - TLALPUJAHUA
2 IXTLAN DE LOS HERVORES - LOS NEGRITOS
3 TOLUCA - IXTLAHUACA
4 CHAPINGO
5 VERACRUZ
6 PAPALOAPAN
7 MONCLOVA - CUATROCIENEGAS
8 SN JOSE DE LAS RUSIAS
GULF OF MEXICO
PACIFIC OCEAN
A
B
C
D

FIG. No. 1

USE OF LANDSAT IMAGES IN INTEGRATED NATURAL RESOURCE SURVEYS IN BOLIVIA

PROGRAMA ERTS/BOLIVIA
BY: CAP. ENGR. ANTONIO PEREZ V.

1. INTRODUCTION

Bolivia is a mediterranean landlocked country, located in the central part of South America, with an approximative territorial area of 1.098.000 squa̲re kilometers and a sparse population of five million inhabitants.

Similar to the situatión created in many other undeveloped countries,the natural resources of Bolivia are not still well-studied in an integrated manner; because the inter-action of negative factors. Among them we considered the fo- llows:

a) Tendency of the state-institutions to realize independent studies of several natural resources at different scales, without any planning, that beco- mes so difficult to compile in an integrated way for to get an accurate policy, in order to satisfy the national requirements related to the efficient explora- tion of the land-resources.

b) Lack of coordination in the elaborated survey-works, that were unsui̲table for preparation of the systematic mapping of the country, in order to ob- tain available and integrated data of natural resources and, similary, to prevent the repetition of some another finished studies.

c) Lack of an accurate application of some techniques and methodology used for a more fast and efficient survey of the national resources, in considera̲tion of the great territorial extensión of the country, that shows deficiencies in its national road-system, and wide-territorial extensións are isolated or inac̲cesible for the populated areas.

In 1972 NASA triggered into the sideral-space the ERTS satellite, that was devoted to the research the natural resources of the Earth. Bolivia tooks part of this optimistic project invited by NASA to participate, on experimental way, with applications of ERTS imagery to the systematic study of their natural resources.

Since 1973 the ERTS Program-Bolivia works unceasantly in experimental manner, looking for their potential application in Geology, Geomorphology, Soils Vegetation and Land-use, obtained to the present their most successful results.

Based on that experience, the ERTS Program decided, in 1977, to study the renovable natural resources of the country, in an integrated way, taking in mind the necessity of application of an accurate methodology for make integrated survey, that had been experimented successfully in other areas of the World.

For such purpose, the ERTS-Program selected the methodology provided by the Commonwealth Scientific and Industrial Research Organization (CSIRO), that was suitable and applicable to the geographical conditions of Bolivia.

2. DESCRIPTION OF THE PHYSIOGRAPHIC REGIONS OF THE BOLIVIAN TERRITORY

Before to discuss the way in which the CSIRO methodology was applied in Bolivia, in the following lines we will present a general scheme of the main geographical characteristics of the Bolivian territory:

As it was mentioned above, Bolivia is located in the central part of South America, and it presents some well-defined geographic units, in to their geological features, climatic characteristics, soils, vegetation and fo=rests.

These physiographic units can be classified in two major units:

a) The Andean Block, that is a high-altitude mountain-range and,
b) The lower plains, warm and tropical

Those major units are sub-divided according to their own characteristics such as follows:

ANDEAN BLOCK:

a) Western Cordillera, a volcanic range.
b) Altiplano
c) Eastern Cordillera
d) Sub-andean front

LOWER ORIENTAL PLAINS:

e) Humid lower plains, or tropical humid-sabanas
f) Dry-lower plains, or sub-tropical dry-sabanas.
g) Chiquitos massif.

In a summarized form will be present the main characteristics of them:

a) Western volcanic Cordillera

Between the northern coast of Chile and the Bolivian Altiplano, a volcanic chain is builted-up from volcanic cones, that are mostly extinguished and high-platteaus, located among such volcanoes of Cenozoic age. This volcanic range is formed by a succession of modern lava-flows, tuffs and volcanic activity is observed, except, perhaps, in late-fumaroles and solfatares (i.e;Ollague volcano).

b) Altiplano

Between the main range-slopes of the Cordillera of the Andes is located a high platteau commonly named: the Bolivian Altiplano, which contains its own ridges and some isolated hills.

The Altiplano starts in the northern part of the country and it follows through the peruvian territory towards the Urubamba valley. It reache· an approximative area of 100.000 square kilometers with an average-altitude of 3.500 meters above sea level.

The Bolivian Altiplano contains its interior lakes: Titicaca and Poopó, connected themselves through the Desaguadero river, and the salt-lakes of Uyuni and Coipasa, as the main features.

c) Eastern Cordillera

The Eastern Cordillera of the Andes is a high-mountain complex, located between the Altiplano westwards, towards the sub-andean front, to the East.

It traverses the Bolivian territory describing an arcuate shape, for more than 800 kilometers in lenght, from the peruvian border to the argentinian one. The Eastern Cordillera is rise from a thick-sequence of paleozoic and mesozoic sedimentary rocks, folded and faulted, that could be divided in two-main segments, from a latitude of 17°30' S.

The northern segment of the Cordillera posses some granitic massifs in its core, that rose as beatiful snow-capped peaks, among the elongated and paralleled ranges of the mountain chain.

The Southern part consists of lower ranges and ignimbritic high-platteaus, in which is absent the parallel disposition of the ranges, observed towards the North of the Rod's line. However, a tectonic control exists into the landscape-development of the entire region.

d) Sub-andean Front:

This unit is founded between the eastern slopes of the Eastern Cordillera and the oriental plains (humid and dry-plains) and it is extendend northernwards, from the peruvian border to the argentinian ranges of Salta province, towards the South..

The sub-andean front consists of narrow anticlines and broad synclines of paleozoic to tertiary sedimentary rocks, that conform elongated ranges and deep valleys, respectively.

In this region, the oil-formations were commonly found, inside the faulted anticlines.

e) Lower Humid-plains, or tropical humid-sabanas

At the north of the main chain of the Andes, from the Beni river westwards, towards the brazilian border (the Itenez river), is presented a wide - extended lower plain, that is humid and tropical.

It is a fluviatile plain, consiting of hundreds to thousands of meters of fine accumulated sediments, of tertiary to quaternary age, that were transported through many rivers, that flow from the andean slopes toward the main tributaries of the Amazonian basin.

The landscape of the plain becomes into a truly tropical sabana, divided by gallery-woods, that border the main rivers. These sabanas are mottled by the socalled "islas", that are the higher sites among the plain, where the trees are concentred to form truly "wood-islands", among the main grass-cover of the alluvium, located around them.

At Pando region, an undulate and forest-ground exists, because the presence of outcrops of tertiary sediments slightly folded. This zone is remarkable by their cattle raising and forestal industries.

f) Dry lower-plains, or sub-tropical dry-sabanas

The landscape here is characterized by its xerophyllic vegetation, typical of the dry-regions of South America. Its flora consistes of cactus, acacias, bombaceas, chessnut trees, carob-trees, quebracho and chañar-trees, but especially it contains a sparse vegetation of rickety thorny shrubs and creep-plants, also thorny.

also thorny.

The soil of this region is mostly arenaceous and it is unsuitable for many crops; the underground humidity is sparse and it corresponds to a deep-freatic level. For that reason, the Agriculture is incipient and scarce.

Towards the south of this lower plain, rise some ridges, oriented E-W and also isolated hills of scattered distribution.

g) Chiquitos massif

In the eastern region of Bolivia exists a higher zone, compared to the surrounding humid and dry-lower plains, in which are present some low-mountain ranges, oriented generally northwest-southeast; that form parallel rows, displaced ones against others. The physiographic feature of the chiquitanian chains is their morphology of faulted blocks, with a slight slopes southerward, as can see in the San José and Santiago ranges.

3. METHODOLOGY

The variety of landscapes, their extension and the necessity of new surveys of the existent resources, in a fast and systematic way, of reconaissance needs a methodology that leds to use all field-data, that must be plotted in maps, showing relationships among all factors conforming the landscape, such as: shape, rocks, soil, vegetation, climate, etc.

The suitable methodology that lets to obtain the mentioned objetives was started to use by Christian and Stewart, who applied basically the methodology developed by the División of Land-Research and Regional survey within the Commonwealth Scientific and Industrial Research Organization (CSIRO)as they state:

" A fully integrated resource survey involves an organized effort in which a number of specialist investigators not only collect information in the same area together but, through common objetives, contribute substantially to cach other's work and methods during the various processes of data colection , collation, interpretation, assessment, presentation and the preliminary planning of resource use".

The following aspects are basic in the CSIRO methodology, that were fundamental for the realized surveys in Bolivia:

a) To establish 3 units in the landscape sub-division that are: land-system, land-unit, and site.

b) To divide the area through the land-system, components, which can be related to the pattern observed in aerial-photos.

c) To realize sampling of the Land-system, in places defined both in the aerial photography and on the field, according to the integrated-survey done by the respective pecialists.

To those three aspects ERTS made the following modifications:

- Use of the term: "Land-Complexes" replacing "Land-System", following the geographical sense described above.

- For the definition of the "land-complexes", the landsat multi-temporal images were used, at 1:250.000 scale, applying the same methodology used for the interpretation of aerial-photos.

- For the choice of the sampling-sites were used aerial-photos, at 1:50.000 scale, as complementary work.

- Because the economic situation and the high cost of the projects, all studies were completed with their own socio-economic analysis.

- Based in the searched objetivs in this type of studies the components of the survey were defined as follows:

- Geological - geomorphological studies
- Soil study and their classification
- Vegetation studies and actual use of the land
- Socio-economic study.

Based on these components a multidisciplinary team was formed, that was integrated by the following specialists:

- Geologist-geomorphologist
- Edafologist
- Plant-ecologist
- Geographer
- Hydrologist
- Sociologist

The work was undertaken through the following stages:

a) Pre-Field- work: This stage consisted basically in:

- To collect all existent data
- Preliminarly monoscopic interpretation of the multi-temporal Landsat imagery, at 1:250.000 scale, bands 5 and 7, and color images at the same scale.

- Choice of the sampling areas
- Photo-aerial interpretation of the sampled areas
- Selection of the possible itineraries

b) Field-work: This stage consisted in the sampling on the field and simultaneous interpretation related to the aerial-photos and LANDSAT images; recording, interpretation and systematics of the obtained data from the field bases.

c) Post Field-work: This stage starts with the final interpretation after the field-work; where special importance was paid to the imagery-mosaic obtained.

All data were transferred to the mosaic and the specialists coordinated or defined the land-complexes.

d) Preparation of the Final report: The elaboration of the final report is product of both the final results in each discipline, with special importance paid to the data provided by the land-complexes, that summarize the integrated -survey studies. Moreover, the aditional data can be related to the Geomorphology, Geology, soils, vegetation, Hydrology and socio-economic aspects.

4. REALIZED STUDIES

To the integrated survey-study of the natural resources of the Oriente Boliviano the ERTS Program using the experienced methodology of CSIRO, through a realized study in the Oruro Department (Which produced good results, that were benefical and applicable for the regional development of this area), takes in mind the necessity to promote this kind of studies to another regions of the country; where the accesibility and lack of information required for a more objetive knowledge of their natural resources.

For such purpose, in 1977, was signed an agreement with Instituto Nacional de Colonización (I.N.C.), with which the realization of the integrated survey of the oriental plains region -described above - was conveniently financed. This project was named as: "Estudio Integrado de Recursos Naturales del Oriente Boliviano".

The studied area has an approximate extension of 612.404 square kilometers and it covers the territorial surface of Pando, Beni and Santa Cruz departments.

This survey had as fundamental purpose, to provide the basic information to the authorities of Instituto Nacional de Colonización, about the conditions and features of each region, for their late selection, in more accurate levels, as suitable zones for Colonial settlements.

Integrated -survey of natural resources: Centre-South:

Following the plan preview, to promote the interest of the national authorities in this kind of studies, in July 1979 was signed an agreement with the Secretaría Ejecutiva of PL-480, for corporaciones de Desarrollo of Cochabamba, Potosí, Chuquisaca and Tarija departments, with the purpose to make an integrated survey of the undertaken area of those departments, belonging to the andean region (Western Cordillera, Altiplano and Eastern Cordillera) were described above.

This project had as the main objetive to provide the basic information about the existence of several renovable- natural resources and their possible future planning or development, in each department of Bolivia.

The area covered into the region is approximately 287.996 square kilometers.

5. OBTAINED RESULTS

The final products obtained in both studies (Lower-lands andCentreSouth) are thematic maps, at 1:250.000 scale, of the following disciplines:

- Geological map
- Soils map
- Map of ground types (Low-lands)
- Geomorphological map (Centre-South)
- Vegetation map and actual Use of the Land
- Land -complexes map.

These thematic maps are accompanied of their own technical reports and correspondent socio-economic studies.

The obtained results have been limited amount and details of the provided information, that is represented at different thematic s, because the greatness of the applied scale (Multi-temporal LANDSAT images at 1:250.000).

6. CONCLUSIONS

With respect to the Bolivian experience, in the study of the Natural resource of its territory, appying LANDSAT imagery and CSIRO methodology, suitable to the Bolivian geography, we can show the following conclusions:

- The obtained results can be considered sucessfull, because they to get in April 1982, about 900.400 square kilometers, from a total of 1.098.000 Km^2 that Bolivia has, in other words: approximately 82 percent of the national territory, that leds an accurate settlement, about the potential and distribution of the renovable - natural resources of the country.

- The cost of the two studies: "Oriente Boliviano" and "Centro Sur" implied an estimate contribution of $us. 792.467, that covers a tentative extension of 900.400 square kilometers, with an average-cost of $us. 0.88 by -- each square kilometer.

- If the use of Landsat imagery was the fundamental tool in these works, some limitation related to the identification of some characteristic -- features - important in such cases not were observed, because the greatness of the LANDSAT images used (1:250.000). However, as was quoted above, these limitations were improved in those areas of main interest, with the complementary use of aerial - photos, at 1:50.000 scale, and a more intensive field- sampling.

- This information is the useful-base for further accurate studies, accomplished through more underwent details.

- The introduction of the socio-economic parameter in this kind of studies will increased the possibilities of evaluation, clearly, the economic reality of the country.

- In the study of the integrated-surveys of the Oriente Boliviano project, had been identified 49 units of Land-complexes, inferred by this way, towards the relative homogenity of the whole region.

- About the study of the integrated - surveys of the Central and Southern regions of Bolivia, have been identified 120 units of Land-complexes, - that showed the physiographical complexity of the studied region.

MAIN ADVANCES AND NEEDS IN CHILEAN REMOTE SENSING PROGRAMS

Mauricio Araya F.

Chief Engineer, Remote Sensing Section, Departamento de Geología y Geofísica, Facultad de Ciencias Físicas y Matemáticas, Universidad de Chile. Beauchef 850, Casilla 2777. Santiago, Chile.

ABSTRACT

The efforts performed by several Chilean institutions have allowed to obtain important results to facilitate the operational use of remote sensing techniques in Chile. These results can be classified in terms of data acquisition (spatial, aerial and terrestrial observation levels), data pre-processing (analogic and digital facilities), data interpretation (analogic and digital techniques) and technology transference (outside and inside Chile). Several studies have been successfully developed to evaluate the usefulness of remote sensing techniques in different disciplines (agriculture, geology, hydrology and others). The automatic collection of environmental ground truth data from remote sites by using satellites has been widely experienced in Chile since 1977. Important improvements in digital data processing/interpretation activities will be obtained in the next future. Besides, the new satellites Landsat-D and SPOT will allow to intensify the use of remote sensing techniques in Chile thanks to the combined use of satellite images and aerial remote sensing products.

1. INTRODUCTION

There is not a global national remote sensing program in Chile, as it occurs in other Latin-American countries. However, the combined use of means and efforts deployed by several Chilean institutions has allowed to obtain important results (in terms of professional training and facilities improvements) that are allowing the operational use of remote sensing techniques in Chile. This technology has been considered as a valuable auxiliar tool(such as computing techniques) and in this way its evaluation and operational use has been integrated in the normal activities developed by several Chilean institutions.

This natural but something slow process to integrate remote sensing techniques in the national programs developed by Chilean institutions has its advantages and disadvantages. The main advantages are that remote sensing techniques has been evaluated in different disciplines and their real benefits and limitations have been foreseen by considering the national reality (topographic and environmental conditions, information available through conventional means and possibilities to improve it by using remote sensing techniques, existing infrastructure, needs for technology transference, and other parameters). In this way, all the future investments will really obey to national needs to improve the existing facilities (equipment and technology transference) and so to obtain the maximum benefits of this technology at the lowest price. The main disadvantage, of course, is that a central national program would have allowed the easier and faster obtaintion of the infrastructure to operationally use this technology (however, important risks exist by using this way because it is rather easy to acquire equipment or methodologies that are not quite efficient in Chile). Fortunately, mainly due to the positive results obtained in preliminar experiences, important investments (equipment and technology transference) to improve the existing facilities have been performed during the last time. In this way, it is possible to say that a Chilean Remote Sensing Program is being developed by now.

The main advances and needs in Chilean Remote Sensing Programs will be summarized as follows, in according to the scheme indicated in Figure 1. In this way, different problems will be analyzed: Data Acquisition, Data Pre- Processing, Data Interpretation, Technology Transference.

2. DATA ACQUISITION

This problem will be analyzed in terms of the spatial, aerial and terrestrial observation levels normally used in remote sensing techniques. The main advances and needs can be summarized as follows.

2.1. SPATIAL OBSERVATION LEVEL

Low resolution meteorological images have been received from different satellites since several years ago in Chile. The main users have been the Meteorological Services of Chilean Air Force and Navy. The actual APT (Automatic Picture Transmission) system will be improved in the next future, including Antarctic Peninsula. These images (combined with ground environmental data) allow to prepare the daily meteorologic forecasts for the whole country.

High resolution images (Landsat, TIROS-N, Nimbus CZCS, SPOT) can not be received directly in Chile. It is necessary to acquire these products (negative films or digital tapes) in the existing receiving centers located outside Chile (U. S. A., Brasil, Argentina). Important advances have been obtained, under experimental basis, by NASA Division, Universidad de Chile, to furnish the existing NASA Tracking Station in Chile (about 40 km North from Santiago) to directly receive Landsat images. However, an official decission has not been taken by now, mainly due to economic considerations about the future operational costs of such receiving station. As it is known, the main advantages of having a receiving station are: a) security in satellite access for every desired data acquisition ; b) fastness in data acquisition and processing. However, the installation and continuing operation costs and the cloud coverage problems are the main disadvantages. Anyway, it is hoped that the improved products (in terms of spectral resolution and spatial resolution) of Landsat-D , SPOT and other future satellites will allow to justify the operation of a receiving station in Chile and so to obtain the maximum benefits of these high resolution images.

2.2. AERIAL OBSERVATION LEVEL

The Aerophotogrammetric Service of Chilean Air Force, SAF (Servicio Aerofotogramétrico de la Fuerza Aérea de Chile, SAF) has a wide experience in the use of conventional remote sensors (aerophotogrammetric cammeras equipped with different films, such as B/W, color, B/W near infrared, color near infrared) and during the last years, experience has been obtained in the use of non conventional remote sensors (such as multiband cammera, thermal IR scanner, magnetometer and others). The existing infrastructure can be considerated adequate and different airplanes can be used to obtain the information, in according to the special requirements of every project (i.e. Lear Jet, Twin Otter, King Air and other airplanes). During the last years several projects have been developed by using the existing infrastructure , as it will be seen in Point 6. This data acquisition capability is also accomplished with data pre-processing and data interpretation facilities.

Several improvements are planned or being executing by now, specially related with digital data acquisition, processing and interpretation activities. It is very important to say that this aerial capability has been very useful to facilitate the use of satellite images because, due to the special topographic characteristics of Chile, it is impossible to intend the use of remote sensing techniques by only employing satellite data. Besides, there was a rather good basic information in the country (cartography, land use) at rather detailed scales (1: 50.000 or more in several situations) and so it was necessary to find the real applications of satellite images to improve the existing information. It is hoped that the future Landsat-D and specially SPOT products will allow to intensify the use of remote sensing data by combining aerial and spatial information.

2.3. TERRESTRIAL OBSERVATION LEVEL

Conventional stations to measure different environmental parameters are widely spreaded along the country, in according to the different needs of Chilean institutions. To accomplish this data acquisition capability, important experiences began to be developed by 1977 to test Satellite Data Collection Systems (DCS) to collect environmental ground truth data from remote sites, in an automatic, reliable and practical way by using special sensing stations called Data Collection Platforms (DCPs). These experiences were possible thanks to the valuable cooperation of U. S. Geological Survey (Dr. Richard W. Paulson and Dr. William D. Carter), U. S. NASA and U. S. NOAA. The valuable participation of NASA Division personnel (Universidad de Chile) made possible to modify

the NASA Tracking Station in Chile to directly receive Landsat/DCS and GOES/DCS data. During 1977 to 1980 it was possibly to operate with Landsat/DCS and since 1980/81 it is possible to operationally use GOES/DCS. This technology is being used by several Chilean institutions along the country, including experiences in Antarctic Peninsula (see Point 6.5).

3. DATA PRE-PROCESSING

This problem is related to the preparation of the different remote sensing products to allow its analysis or interpretation by the users. It is necessary to distinguish between analogic or photographic products and digital or computer products.

The analogic or photographic processing facilities can be considered adequate because the Aerophotogrammetric Service of Chilean Air Force (SAF) will be able to operationally use a B/W and color photographic laboratory during the second half of 1982. In this way it will be possible to work with film or paper B/W and color enlargements of aereal and satellite images and photographs.

Digital processing facilities are not available in the country at least to be directly used with satellite or aerial digital tapes. There is an adequate computing infrastruct re along Chile but it would be necessary to perform some modifications to process digital remote sensing data. However, important improvements are hoped for 1982, specially due to the improvements obtained by Servicio Aerofotogramétrico (SAF) and Instituto de Investigación de Recursos Naturales (IREN) and some Chilean universities.

4. DATA INTERPRETATION

This problem is related to the obtention of results through the analysis or interpretation of the different remote sensing products. It is also necessary to distinguish between analogic and digital interpretation techniques.

The existing facilities for analogic, visual or photographic interpretation are rather adequate. However, it could be improved and several efforts are being made or have been made in this sense. As general information, several institutions have conventional photointerpretation devices, additive color multispectral viewer, Diazo developer/printer, digital densitometers and other equipment. Some investments are planned for 1982 and it is hoped to meaningfully improve this capability in the next future.

The situation of digital interpretation capability is rather poor but important improvements are planned for 1982. Some Chilean Universities (Universidad Técnica Federico Santa María, Universidad de Chile, Universidad de Santiago) have obtained some progress in software preparation and it is hopped that when hardware facilities exist in Chile, more advances will be obtained. By now, all the projects that require digital interpretation must be performed outside Chile (U. S. A., Brasil, Canadá, Argentina and other countries). In this sense, NASA Division, Universidad de Chile, has obtained important experience through several experimental projects developed together with other Chilean institutions. The Servicio Aerofotogramétrico (SAF) will contribute to improve this capability in Chile before ending 1982.

5. TECHNOLOGY TRANSFERENCE

This problem is very important and really it is the first step in the use of remote sensing techniques. Without and adequate preparation of the personnel working in national institutions and without a program to assure a continuing technology transference in the country, it is not possible to intend an adequate operational use of remote sensing techniques. It is possible to distinguish between trainig outside and inside the country. Both activities are very important and must be complementary.

In the first step, training was necessarily developed outside Chile because this was a new technology and it was quite necessary to learn about it in the specialized centers located in other countries. However, it is possible by now to combine a preparation in Chile and outside the country, because the institutions having more experience in remote sensing are developing programs to evaluate this technology in different disciplines and also training personnel through these activities. Besides, some specialized institutions (such as the Universities) can offer some courses in remote sensing addressed to students or professionals belonging to other organisms. Of course

many advances are necessary in this sense yet, but the important matter is that this process can already be performed in Chile.

The Facultad de Ciencias Físicas y Matemáticas de la Universidad de Chile (Faculty of Physics and Mathematical Sciences, University of Chile) is a clear example in this sense. Through different experimental projects performed together with several national institutions, the advantages and limitations of remote sensing techniques have been evaluated in different disciplines, besides the obtention of training for the participating personnel. Besides in this Faculty courses on Remote Sensing techniques are prepared for students (engineers and geologists) and professionals belonging to other Chilean institutions. The continuing knowledge updating of the University professors allows to recommend the best choises for operational projects and specialized training outside the country. By now, an important program is being prepared to offer more intensive courses to the future engineers and geologists formed in this Faculty (the more important in the country), to be applied since 1983. The contribution of this Faculty to the remote sensing knowledgement in Chile can be appreciated in some examples summarized in the next section (Point 6). This contribution has been mainly performed through its Remote Sensing Section and NASA Division units.

6. MAIN ASPECTS OF SOME CHILEAN REMOTE SENSING PROJECTS

The next examples summarize the Chilean remote sensing activity in different disciplines. Because of space restrictions in this paper, only the main aspects of these projects are summarized and emphasis has been given to those projects mainly developed by using the national infrastructure (technical and scientific personnel and existing equipment). Anyway these examples will allow to obtain an idea about the Chilean advances and needs in remote sensing.

6.1. AGRICULTURE, FORESTRY AND LAND USE

Several projects have been developed in these disciplines. They have mainly performed by NASA Division/Universidad de Chile (Engs. Heinz Martens and Carlos Pattillo); Instituto de Investigación de Recursos Naturales, IREN (Geologist Arnoldo Ortiz); Dirección General de Aguas, Ministerio de Obras Públicas; Oficina de Planificación Agrícola, ODEPA, del Ministerio de Agricultura (Eng. Rafael Sarroca); Servicio Agrícola y Ganadero, División de Protección de Recursos Naturales, DIPROREN, del Ministerio de Agricultura (Engs. Gastón Sepúlveda and Rodolfo Freres) and other institutions such as COSERREN , a private consulting enterprise (Engs. Carlos Escudero and Guillermo Dalannais). For instance, IREN (Geologist Arnoldo Ortiz) has performed analogic data processing for a natural resources inventory in the North Zone of Chile (about 250,000 km^2, scale 1:250,000) and actually they are working in the Central Zone of Chile (about 300,000 km^2) by using computer enhanced Landsat images, to obtain better accuracy. All the digital processing has been performed outside Chile (INPE, Brasil; EROS, U.S.A.; MDA, Canada); NASA Division/Universidad de Chile has actively participated in several joint programs. Interesting results have been obtained by now but there is a general consensus that Landsat-D and SPOT data will be more useful for these studies (the agricultural valleys in Chile are very small and narrows and a great variety of crops are organized in rather reduced surfaces).

6.2. GEOLOGY AND MINERAL RESOURCES

Several experimental projects have been developed by Instituto de Recursos Naturales, IREN (Geol. Arnoldo Ortiz), Servicio de Minas del Estado, SERMINE (formerly Instituto de Investigaciones Geológicas, IIG; Geologist Gabriel Pérez); Corporación del Cobre, CODELCO (Geologist Enrique Teidy); División NASA/Universidad de Chile (Engs. Carlos Pattillo and Heinz Martens). For instance, IREN has worked in the North Zone of Chile by mainly using Landsat images. It is hoped that the new improved products of Landsat-D and SPOT will also help to develop more accurate experiences. The use of aereal remote sensing has also been experienced (magnetometer, multispectral cammeras) for detailed studies and the future improved capability will allow to perform very important experiences in the next future.

6.3. CARTOGRAPHY

There are three main institutions in Chile related to preparation of the national carto - graphy, at different scales (1: 1.000.000 to 1: 50.000 and more) : Instituto Geográfico Militar, IGM ; Servicio Aerofotogramétrico de la Fuerza Aérea de Chile, SAF (aereal navigation charts mainly); Instituto Hidrográfico de la Armada, IHA (coastal charts mainly). These activities are main-

ly developed by using aerial capability. This aerial capability has been extended iven to Antarctic Peninsula (since 1980) thanks to a landing field operated by Chilean Air Force in King George Island, South Shettland Islands. During the last years (since 1980) the Instituto Geográfico Militar, IGM, has been experiencing the production of controlled charts by using satellite (Landsat) images and ground control points (geodetic points) determined through geodetic satellites (Doppler effect). In this way, a chart over a sector in Antarctic Peninsula will be published soon. However, there are great expectation for the new SPOT products because their improved spatial resolution and stereoscopic capability will allow to use this information in several important national projects.

6.4. OCEANOGRAPHY AND METEOROLOGY

These activities are mainly performed by Instituto Hidrográfico de la Armada, IHA (Com. Patricio Figueroa), Servicio Meteorológico de la Armada (Com. Germán Valdivia), Servicio Meteorológico de la Fuerza Aérea de Chile y Dirección de Aeronáutica (Com. Federico Roll), Instituto de Fomento Pesquero, IFOP (Eng. Rolando Kelly) and other institutions related to water resources, such as Dirección General de Aguas, DGA, del Ministerio de Obras Públicas (Engs. Humberto Peña y Javier Narbona) and Empresa Nacional de Electricidad, ENDESA (Eng. Andrés Benitez and Eng. Francisco Berni). Satellite meteorological images (APT system), conventional ground truth data, aereal photographs and Satellite Data Collection Systems (Landsat and GOES) are being used to perform these studies. It is hoped to intensify the use of remote sensing data in the next future when improved aerial capability (digital data acquisition/interpretation) and satellite digital data interpretation facilities be available. Besides, the use of SPOT data together with Landsat-D and Nimbus CZCS products will allow to perform more important studies yet. The operational use of Satellite Data Collection Systems for the automatic obtention of environmental ground truth data is being evaluated by now by several institutions through joint projects with NASA Division/Universidad de Chile.

6.5. ANTARCTIC RESOURCES AND ENVIRONMENTAL CONDITIONS

An important Antarctic Remote Sensing Program is being developed in Antarctic Peninsula with the sponsoring of Chilean Antarctic Institute (Instituto Antártico Chileno, INACH) and the technical and scientific guidance of Facultad de Ciencias Físicas y Matemáticas, Universidad de Chile (Eng. M. Araya F., Chief of Program). This Program has two main objectives: a) to improve the knowledge of antarctic natural resources ; b) to improve the knowledge of antarctic environmental conditions. To accomplish these objectives remote sensing techniques are being used and the three observation levels (spatial, aerial and terrestrial) have been considered. Because no aerial logistic capability was available until 1980 (through a landing field operated by Chilean Air Force in King George Island) and no capability for direct reception of satellite images in Antarctic and restrictions in digital data processing existed by then, emphasis was given to the deployment of an experimental net of automatic meteorologic stations (Data Collection Platforms) that send their environmental data to Santiago via Landsat and GOES satellites. NASA Station near Santiago receives, processes and distributes the information to INACH and Universidad de Chile(Remote Sensing Section). However, for next summer 1982/83 aerial multispectral photographs and images will be obtained over selected zones in Antarctic Peninsula and satellite images will be also used in a regular way.

The deployment of this experimental net of DCPs began in 1978 and its operational use could begin by now. Most of the problems that have arisen have been solved and actually only some problems with data quality (related to sensors designs) and reliable power supply (a combined system using solar and wind energy, controlled by microprocessor will be used) are being finished by now. For more details on these studies, please see References 6,7,8. As a general result it is possible to say that actually has been obtained a continuous operation of these DCPs along the whole year and the data quality is good when adequate sensors have been used. Figure 2 shows the actual net of DCPs. During summer 1982/83 the final distribution will be : Base O'Higgins, Duse Bay (Weddell Sea Coast), Punta Spring (Hughes Bay) and Bahía South. This environmental information will be very useful for helping navigation in this area because more accurate meteorologic forecasts will be obtained. All these DCPs are unattended along the year. Photos 1 and 2 show the typical aspect of these installations. Finally, Figure 3 shows the operational system to be used in Antarctic Peninsula to collect environmental data via satellite to accomplish the information collected through conventional means. The Antarctic Regional Meteorological Center Presidente Frei (Marsh Base) will be able to distribute this information to all the countries that need it. It is important to say that all these installations have been performed by chilean technical personnel (NASA Division/Universidad de Chile has cooperated very well). The valuable cooperation

of Comando Antártico del Ejército (Antarctic Corp of Chilean Army) has made possible the difficult expeditions and installations of DCPs by crossing hundreths kilometers through snow to reach Duse Bay from O'Higgins Base. Also, the valuable cooperation of Antarctic Corps of Chilean Air Force and Navy has made possible the installation of the other DCPs.

6.6. SNOW-WATER RESOURCES IN LOS ANDES RANGE, CHILE

The study of snow-water resources in Los Andes Range, Central Zone of Chile, is very important to make the snowmelt runoff forecasts because during the dry season (October-April) almost all the available water depends on snowmelting. In this way these forecasts are very important for agriculture, hydroelectric power generation, water supply (potable water, recreation, etc.). There are two institutions that mainly need to make these studies: Dirección General de Aguas, Ministerio de Obras Públicas (DGA) and Empresa Nacional de Electricidad (ENDESA). DGA needs to perform these studies along the whole country and ENDESA only in those areas where hydroelectric dams exist. The use of Satellite Data Collection System is being evaluated by both institutions and DGA has several DCPs installed in pilot basins in the Central-North and North Zones of Chile (Engs. Humberto Peña and Javier Narbona). The use of Landsat images is also being evaluated to study glaciers (Photo 3) and to improve snowmelting runoff forecasts. An agreement stablished between DGA (Engs. Humberto Peña and Javier Narbona) and Remote Sensing Section, Universidad de Chile (Eng. M. Araya F., Chief of Project, and Eng. Alejandro Farías) will allow to evaluate the usefulness of Landsat images for improving snowmelt forecasts. Three pilot basins (Elqui, Maipo and Ñuble Rivers) will be used for these purposes (Figure 4) and the existing Landsat images data bank belonging to DGA will be employed (images obtained once every month since 1977 to 1980). These results will be published by ending 1982. Anyway, the improved products of Landsat-D and SPOT will help very much to these studies, above all the thermal bands of Landsat-D and the high resolution SPOT images that will allow to work at scales 1: 50,000 or more . Besides, the lateral view of SPOT images will allow to obtain valuable information on altitude and it will give more opportunities to obtain images without cloud coverage problems.

6.7. GEOTHERMAL RESOURCES IN LOS ANDES RANGE, CHILE

Important advances have been obtained in the study of geothermal resources in Los Andes Range, Chile, by using remote sensing techniques. These experiences have been performed with the valuable cooperation of Servicio Aerofotogramétrico de la Fuerza Aérea de Chile, SAF (Com. Hernán García, Com. René Fonteneau, Com. Sergio Carrasco, Cnl. Jaime González, Cap. Juan Espinoza, Cap. James Jurica, Sgt. Carlos Velásquez, Sgt. Héctor Garrido); Comité Geotérmico CORFO (Geologist Raymundo Piracés); Universidad de Chile (Eng. Mauricio Araya F., Chief of Project; Eng. Mario Pardo , Prof. Víctor Villanueva) and the partial sponsoring of Servicio de Desarrollo Científico, Universidad de Chile. These studies have been addressed to identification of new geothermal areas (prospection stage) and detailed studies of previously identified geothermal fields (exploration stage). Geothermal energy is widely distributed along Los Andes Range and it can be used for different purposes (electric power generation, tourism and others). Besides it is possible to intend to stablish corralations between regional geology (structural features such as geologic faults and linements), geothermal activity and regional seismicity by considering the Plates Theory for South America. The main results obtained by now can be summarized as follows.

El Tatio geothermal field (Fig. 5) was selected as a pilot area to evaluate the usefulness of airborned remote sensors in the study of geothermal fields already identified (exploration stage). Because this field represented the most advanced geothermal project in Chile (a 30 MW power plant is going to be installed), more than 10 years studied, it would be possible to compare the remote sensing data with the existing conventional information. This was the first study of geothermal fields performed in Chile by using remote sensing techniques (Eng. M. Araya and Geol. R. Piracés, Chiefs of Project) and very promising results were obtained. A twin Otter airplane belonging to S.A.F. remained about one week in the field until all the necessary information was obtained. A portable field photographic laboratory was installed at Calama Airport, the operation center. In this way it was possible to develop the photographs and images in almost real time and so any gap in the photographic coverage or any specially interesting detail could be flown again to obtain the desired additional information. Besides, it was easier to better plan the field verification activities. A multiband camera (Bandsa AMB-1 or blue, 0.4-0.5 μm; AMB-2 or green, 0.5-0.6 μm; AMB-3 or red, 0.6-0.7 μm; AMB-4 or near infrared, 0.7-0.9 μm; approx.) and a thermal infrared scanner (8-12 μm, IFOV 1,5 milirad, RNS 0.25°C) were used to make mosaics covering all the pilot zone. Photo 4 shows an example of multiband photographs and Photo 5 shows some typical thermal images . In

spite of these were analogic products it was possible to obtain enlargements and enhancements (by using color composite techniques and density slicing ones) to obtain results. Anyway, thermal images were considered key elements for these studies. Photo 6 shows a reduced thermal mosaic over El Tatio and Figure 6 represents the main structural features obtained mainly from these thermal images. It was necessary to combine both products because thermal images had a deformation (stretched along cross flight direction); besides, multiband photographs allowed to obtain color composites to enhance certain features such as rocks, vegetation, salty soils and others. As a general conclussion, aerial remote sensing data represents a very valuable auxiliar tool to be used in the first steps of the study of a geothermal field. This information would be very useful to plan the field geologic activities and important savings could be obtained in terms of money and time. Besides, thermal images give valuable information that could not be obtained through conventional means. These products were obtained at typical scales 1: 7,000 to 1: 20,000.

The use of Landsat multispectral and multitemporal images in regional studies (prospection stage) to identify new geothermal fields was successfully essaied in the Central Andes, Chile. A methodology was determined to identify geothermal areas over snowed zones in Los Andes Range, Central Zone of Chile. The pilot area was selected near Del Maule Lagoon (about 300 km S-E from Santiago) and La Invernada Lagoon (Fig. 7). Four Landsat images, belonging to different seasons, were acquired at INPE, Brasil (Sept. 6, 1977; Dec. 9, 1978; Apr. 19, 1978; Feb. 1, 1979). Color composites were used for these studies, at scales 1: 250,000. These products allowed to obtain good spatial resolution and good contrast to identify specific features over snowed areas (vegetation, water bodies, snowmelting areas, etc.). This methodology is based on the correlation of permanent features (geologic faults and linements, volcanic structures, identified geothermal fields, zones of hydrothermal alteration, topography, hydrology) and variable features (temporal snow distribution specially near volcanic structures, variations of water bodies and vegetation over sowed areas). The multitemporal observation is very important in this methodology (Photo 7). Three steps must be followed to obtain results : 1) Compilation of geologic antecedents, through the existing information and also derived from Landsat images (permanent features); 2) Analysis of variable features, specially near volcanic areas (for instance, zones where liquid water remains abnormally uniced during cold season); 3) Integral analysis of the information obtained in steps 1 and 2, to confirm or to discard the forecasted areas of potential geothermal activity (sometimes it is necessary to verify in terrain). In this pilot study all the forecasted zones were successfully confirmed, by using existing data or by terrain activities. Figure 8 summarizes the results obtained in this experience. This methodology does not assure 100% reliability: it mainly allows to identify water springs near volcanic areas and because of their proximity to volcanic structures and the analysis of other parameters, it is possible to forecast potential areas of geo - thermal activity. However this methodology allows to reduce the area to be explored with more detail (through airborne remote sensors). This pilot experience and its successful results allows to think in the feasibility to determine a general methodology to be applied along the whole country. The future improved products of Landsat-D (thermal images) and SPOT (very high resolution images) will allow to improve this methodology yet.

Based on the positive results obtained in pilot experiences , a general methodology valid for the whole country will be determined. Five more pilot zones (Fig. 9, Photo 8) will be studied thanks to the partial sponsoring of Servicio de Desarrollo Científico, Universidad de Chile. The final general objectives of this program are : 1) to stablish a permanent surveillance system on volcanic activity along Chile; 2) to obtain a national cadaster on geothermal resources, scale 1: 250,000 mínimum ; 3) to intend to stablish models to correlate regional geology (mainly faults and linements), volcanism and regional seismicity. Three stages will be followed to accomplish these objectives: a) Experimental Stage or Landsat 1,2,3 data (1980/82) ; b) Semi-Operational Stage or Landsat-D data (1982/84) : thermal images will accomplish the methodology; c) Operational Stage or SPOT and Landsat-D data (since 1985) : very high resolution SPOT images will improve the methodology. Besides, it is supposed that the aerial capability to acquire and to process remote sensing data will be improved with digital acquisition/processing devices (to allow more accurate studies by using only aerial data or combination of aerial and satellite products).

The same products used in snow-water resources and geothermal activity studies along Los Andes Range can be used in the study of regional geological features (specially faults, linements and volcanic structures) to stablish correlations with other gephysic parameters (such as seismic regions along Chile). In the case of Chile, seismicity is mainly related to the tectonic interaction between South America plate and Nazca plate. Collision of these plates gives origin to a subduction zone and a deep oceanic trench parallel to the Chilean coast (Pacific Ocean). Mountains

like Los Andes , volcanic structures and regional geology are associated also with this subduction zone (Fig. 10). Seismic evidences indicate that the downgoing slab has different inclinations, which will produce zones with different seismic and volcanic characteristics. Barazangi and Isacks (1976), using 1700 seismic events between latitudes 0° - 45° S and longitudes between 60° - 85° W, have delimited three major zones between 18° - 45° S for the subducting plate, having different inclinations (Fig. 11). Consequences of these phenomena are different seismicity and earthquake mechanisms for different regions and no volcanic activity in the zone 26° - 33° S (and also, different geomorphology). Seismic and volcanic zonification is very important to evaluate the potential seismic and volcanic hazards in every region (this is very useful in civil engineering designs). Use of remote sensing techniques will be very useful to accomplish this regional zonification by identifying surficial geological parameters and trends related to volcanic activity and seismic active faults. A better understanding about tectonics stress acting at the subduction zone and the associated structures generated by the collision of the plates can be obtained by using remote sensing techniques. Also correlations of earthquakes and geology with volcanic and no-volcanic zones will be intended in the next years. For more details, please see References 9, 10, 11.

6.8. ENVIRONMENTAL POLLUTION, URBAN TRAFFIC AND OTHER PROBLEMS INTERESTING TO CIVIL ENGINEERING DESIGNS

A cooperation agreement stablished between Servicio Aerofotogramétrico, SAF (Aerophotogrammetric Service of Chilean Air Force) and Facultad de Ciencias Físicas y Matemáticas, Universidad de Chile (Remote Sensing Section, Eng. M. Araya, Chief of Project) has allowed to develop several interesting experiences related to some important urban problems in Santiago, Chile. The objectives of these projects were to develop operational methodologies to be employed in future projects. The valuable cooperation of SAF (specially Com. Hernán García, Com. Sergio Carrasco, Com. René Fontenea , Cnl. Jaime González) has made possible to develop these important experiences. Several researchists from Universidad de Chile also cooperated in these experiences (specially Eng. Jaime Gibson, research asssitants Nelly Nussbaum and Rodrigo Fernández).

The use of multiband cammera and thermal infrared scanner, mounted on a SAF Twin Otter airplane, has allowed to determine basic parameters related to environmental pollution. Potential sources of smog (and its relative importance) were clearly identified in thermal images. A thermal map over a pilot zone in Santiago has been developed allowing for real updated view of the different hot sources and its relative contribution to atmospheric pollution. It can be seen that residential areas have several small hot sources (chims, etc.) meanwhile suburbs have a small number of big hot sources (industries). Pollution of water streams can also be clearly identified through thermal images and dramatic examples have been collected over pilot zones in Santiago (Mapocho River). The same technology has showed its potential value to identify problems related building isolation and the related potential energy saving during winter time. Photos 9 and 10 show some examples of these phenomenas. It has also been determined the ability of near infrared spectral band (multiband camera) to penetrate light fog. Both multiband cammera and thermal infrared scanner were very useful in these pilot studies. It is hoped that the future SPOT and Landsat-D products will allow to better combine aerial and spatial data to perform more operational studies. Besides, the future improved capability for aerial acquisition/processing of multispectral data will also help to intensify the use of remote sensing technology in these studies and so to obtain the best use of this capability.

The use of conventional aerial B/W photographs has allowed to obtain very promising results on the identification and quantification of urban traffic flow problems. It has been possible to essay a methodology to evaluate vehicle concentration and its temporal and spatial distribution at peak hours. A pilot circuit (Fig. 12) in downtown Santiago was choosen to evaluate this methodology. This area is specially congested at the typical peak hours (morning, midday and afternoon). Because of light conditions (September 1981) the morning period was selected to perform this experience. A SAF Twin Otter airplane obtained B/W photographs (scale 1: 2,000 but 1: 10,000 could be also useful) since 7:30 to 9:45 A. M. The circuit was repeated every 10-15 minutes and so about 8 photographic sequences were obtained for every street in the circuit. This information was used to build a time-space diagram with vehicle isoconcentration curves. Congestion evolution along a specific street can be evaluated (in time and space) and bottlenecks could be clearly identified. Figs. 13a and 13b show two examples for light vehicles in Avenue Bernardo O'Higgins (East bound direction and West bound direction). The vehicle concentration was measured for every block with signalised junction. The congestion level is given by the number of vehicles/lane/km . In this way, all the isodensity curves having values more than 65 veh/km/lane represent abnormally congested levels. The

maximum congestion level is represented by the isodensity curve 200 (that is 200 veh/km/lane, about 5 km for vehicle). More studies will be developed to evaluate the real potential of this methodology in urban traffic problems. However, these preliminar results allow to think in the future operational use of this technology for solving different problems. For more details on these studies, please see Refernce 12.

7. CONCLUSSIONS

Remote sensing techniques represent a valuable auxiliar tool to develop several studies related to different disciplines in Chile. Spatial, aerial and terrestrial observation levels are being used by now. The main needs are represented by more expedite satellite images acquisition and improved digital devices to process spatial and aerial multispectral data. However, important improvements are planed in this sense for 1982. Aerial observation level is a key element in Chile due to the special topographic conditions of the country. For this reason, the planned improvements will be very important for the intensive operational use of remote sensing technology in Chile. Besides, the new future improved Landsat-D and SPOT data will satisfy almost all the needs for the different studies in the country. The technology transference to be performed by Chilean Universities and other national institutions will also contribute to this progress.

8. REFERENCES

1. Araya M., Main aspects of some remote sensing projects developed at the Facultad de Ciencias Físicas y Matemáticas, Universidad de Chile, II Simposio Brasileiro de Sensoramiento Remoto, INPE, Brasilia, Brasil, May 10-14, 1982.

2. Araya M., Algunas consideraciones sobre avances y necesidades del Programa Chileno de Percepción Remota, Seminar on Latin American Users on Satellite Remote Sensing, INPE/NOAA, Sao José dos Campos, Brasil, November 30-December 2, 1981.

3. Pattillo, C., Informe del Proyecto AEMS, División NASA/Universidad de Chile, IREN, DGA. Santiago, 1980.

4. Ortiz, A., Advance in research and use of remote sensors in natural resources development studies-Chile, XII International Symposium on Remote Sensing of Environment, ERIM, Manila, Philippines, April 20-26, 1978.

5. Ortiz, A., Detección de rasgos indicadores de desertificación en la Región Metropolitana y V Región en imágenes Landsat, Congreso Internacional de Zonas Aridas y Semi-Aridas, Universidad de Chile, La Serena, Chile, Jan . 1980.

6. Araya, M., Main aspects of two Chilean remote sensing projects developed under extreme severe environmental conditions: desertic North and antarctic South, XIII International Symposium on Remote Sensing of Environment, ERIM, Ann Arbor, Michigan, April 1979.

7. Araya M., Rojas R., Vásquez P., Deployment of satellite automatic weather sensing stations in Antarctic Peninsula: logistic problems and solutions, XVII SCAR Reunnion, Symposium on Antarctic Logistics, Leningrado, U. S.S.R., June 28-July 9, 1982.

8. Araya M., Radrigán R., Brante G., Weber I., Use of wind and solar energy as power supply for satellite automatic weather sensing stations in Antarctic, XVII SCAR Reunnion, Symposium on Antarctic Logistics, Leningrado, U. S. S. R., June 28-July 9, 1982.

9. Araya M. and Piracés R., Use of remote sensing techniques to study geothermal resources in arid and semi-arid zones in Chile, First Thematic Conference on Remote Sensing of Arid and Semi-Arid Lands, ERIM, El Cairo, Egypt, January 1982.

10. Araya M., Piracés R., Pardo M., Main advances and needs on the study of geothermal resources in Chile by using remote sensing techniques, Symposium of International Society of Photogrammetry and Remote Sensing, Commission VII, GDTA, Toulouse, France, September 1982.
11. Barazangi M. and Isacks B., Geology 4, page 686 (1976).

12. Araya M., Gibson J., Fernández R., Nussbaum N., Studies on some urban problems by using airborne remote sensors in Santiago, Chile, XVI International Symposium on Remote Sensing of Environment, ERIM/CNIE, Buenos Aires, Argentina, June 2-9, 1982.

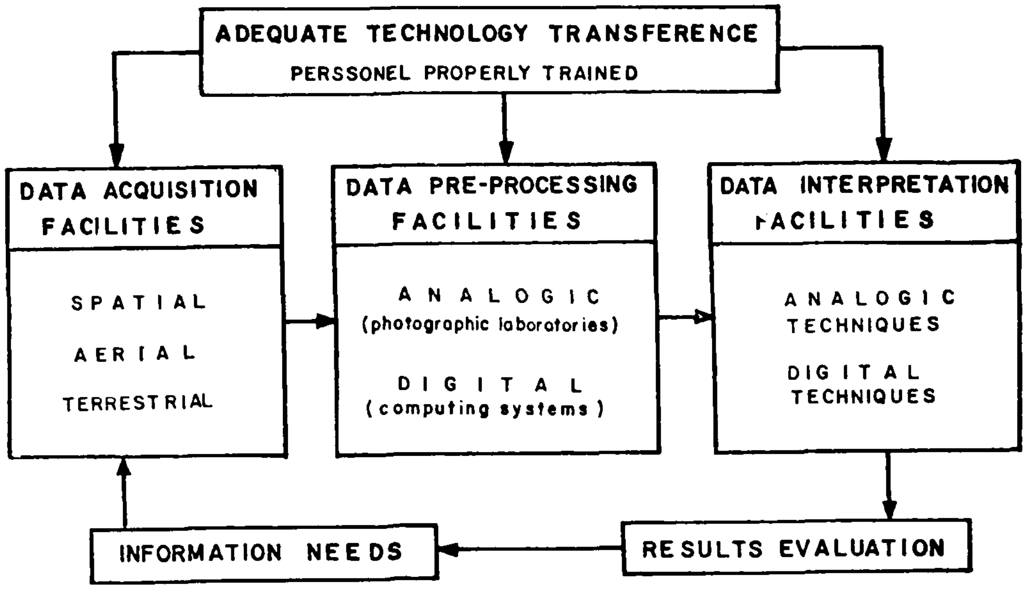

FIG. 1. Basic elements in the use of remote sensing techniques. Almost all these elements are being used in Chilean Remote Sensing Program and important improvements are planned before ending 1982.

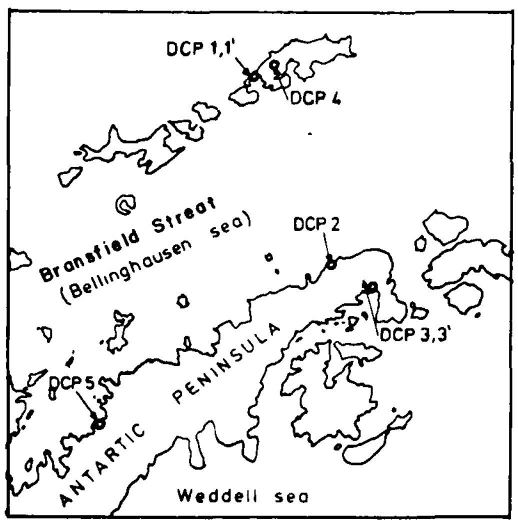

FIG. 2. Scheme of DCPs installations in Antarctic Peninsula (1982).

PHOTO 1a. Typical installation of DCP in Antarctic Peninsula (DCP 3,3'). The mounting tower is fixed on rocks.

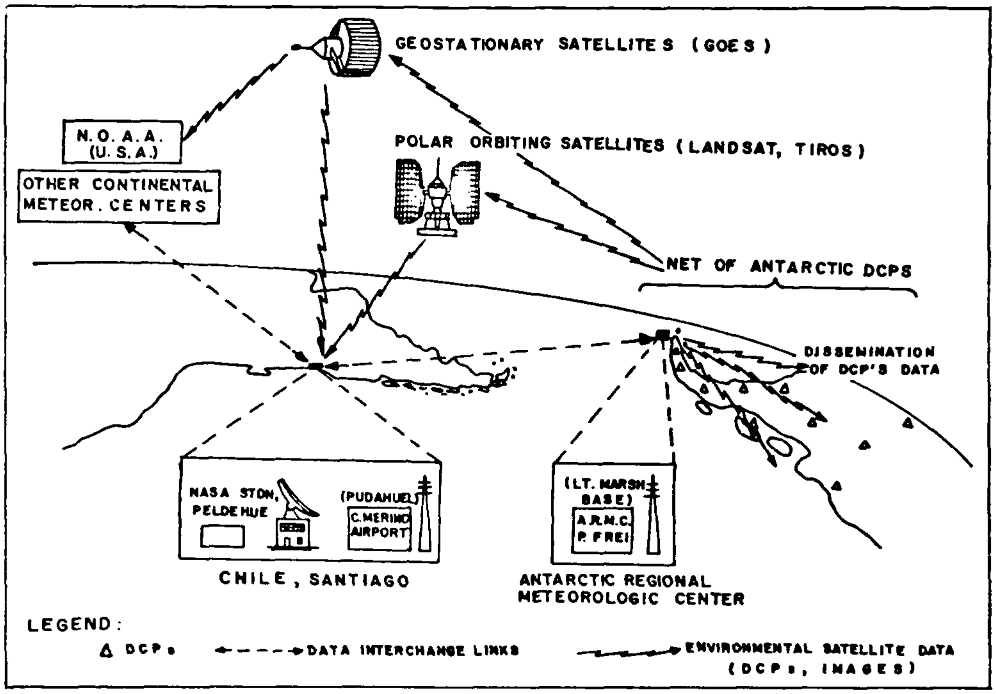

FIG. 3. Operational scheme to collect environmental data from remote sites in Antarctic Peninsula by using Satellite Data Collection Systems (DCS).

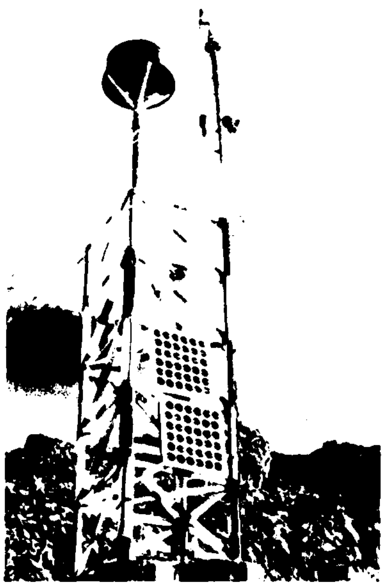

PHOTO 1c. Antarctic scene as seen form the DCP installation site at Duse Bay, Weddell Sea Coast. O'Higgins Base, the exploration starting center, is about 70 km behind the mountains.

PHOTO 1b. Typical DCP installation in Antarctic Peninsula (Duse Bay). The big solar panels are clearly seen, besides Landsat antenna and sensors.

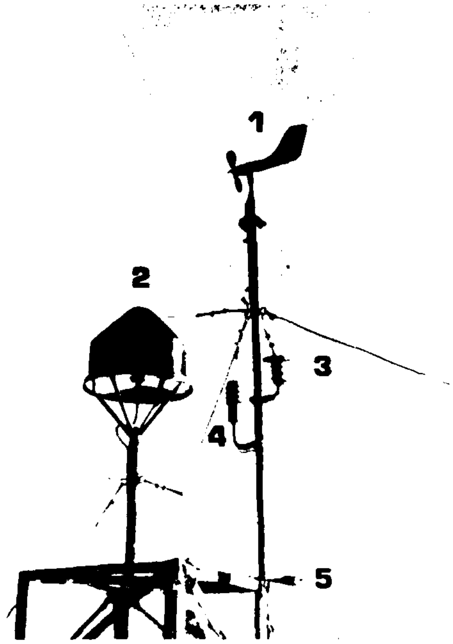

PHOTO 2. DETAIL OF SENSORS FOR TYPICAL DCP. This DCP was installed at Antarctic Peninsula, but similar installations are used by DGA and ENDESA. It is seen: Landsat antenna (2), wind speed/direction sensor (1), air temperature sensor (3), air humidity (4) and solar radiation sensor (5).

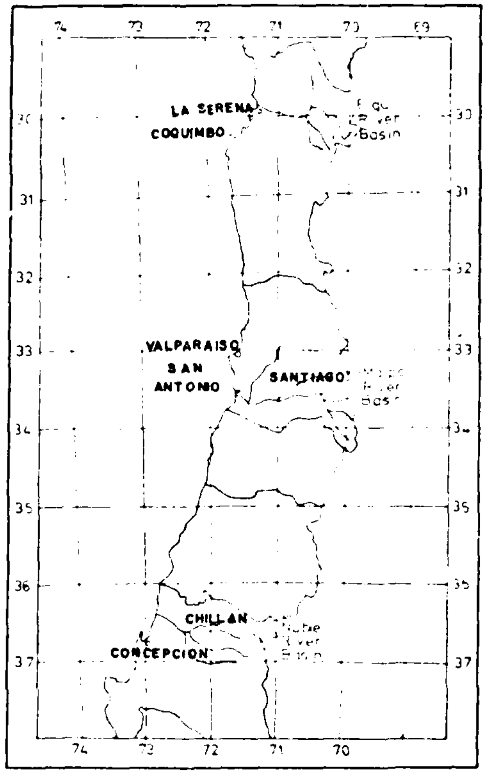

FIG. 4. PILOT BASINS (Elqui, Maipo and Ñuble Rivers) TO BE STUDIED BY USING LANDSAT IMAGES TO IMPROVE SNOWMELTING RUNOFF FORECASTS.

PHOTO 3a. SECTOR OF LANDSAT IMAGE (MSS-5) OVER GLACIERS IN SOUTH ZONE OF CHILE. Water sediments are seen in white tones.

PHOTO 3b. THE SAME LANDSAT IMAGE IN NEAR INFRARED BAND (MSS-7). Lake shape is clearly seen and some glaciers plumes and natural dams(D).

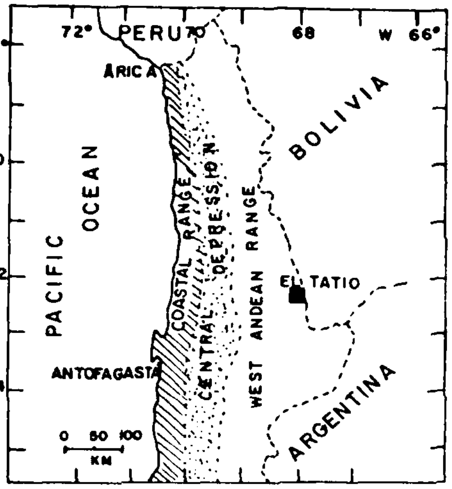

FIG. 5. Location map of El Tatio geothermal field, North of Chile (about 1000 km N-E from Santiago).

PHOTO 5a. THERMAL IMAGE OVER EL TATIO. White tones are associated to higher temperatures. Heat loss is produced here by two phenomenas: hot drainage (upper right corner) and different matterials (lower left corner).

PHOTO 5b. THERMAL IMAGE OVER EL TATIO. Heat loss due to different matterials properties claerly show some geologic linements (black and white contrast).

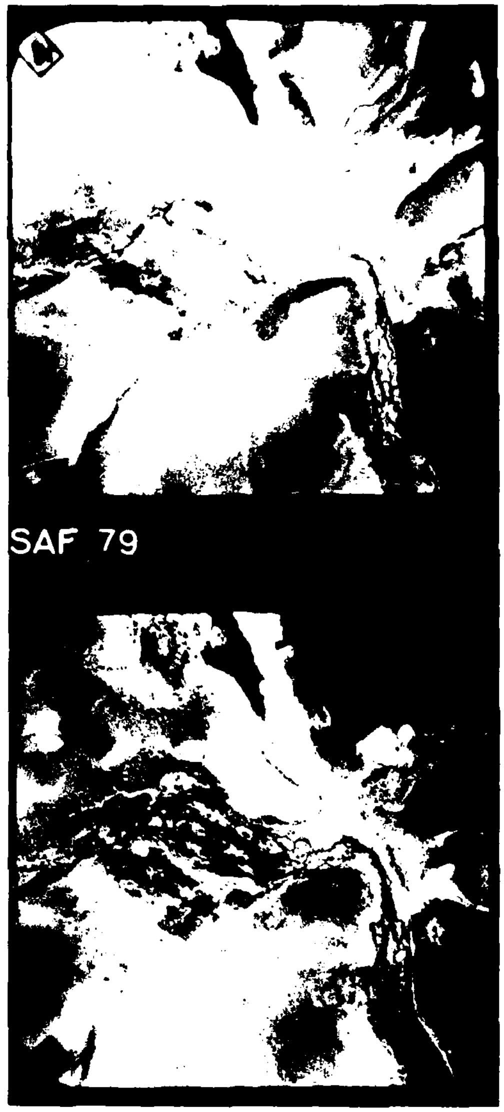

PHOTO 4. HALF MULTIBAND PHOTOGRAPHY OVER EL TATIO. Spectral Bands AMB-1 and AMB-4 are shown here. The four spectral bands used were: AMB-1 or blue (0.4-0.5 µm), AMB-2 or green (0.5-0.6 µm), AMB-3 or red (0.6-0.7 µm) and AMB-4 or near infrared (0.7-0.9 µm), approx. The original B/W product could be processed to produce useful color composites to enhance certain features such as rocks, vegetation, salty soils and others.

PHOTO 6. Thermal mosaic over El Tatio geothermal field (white tones are associated to higher temperatures). Original scale was about 1: 10,000 (actually abo t 1: 70,000). This information about heat loss in the field is very valuable to plan the geologic field activities.

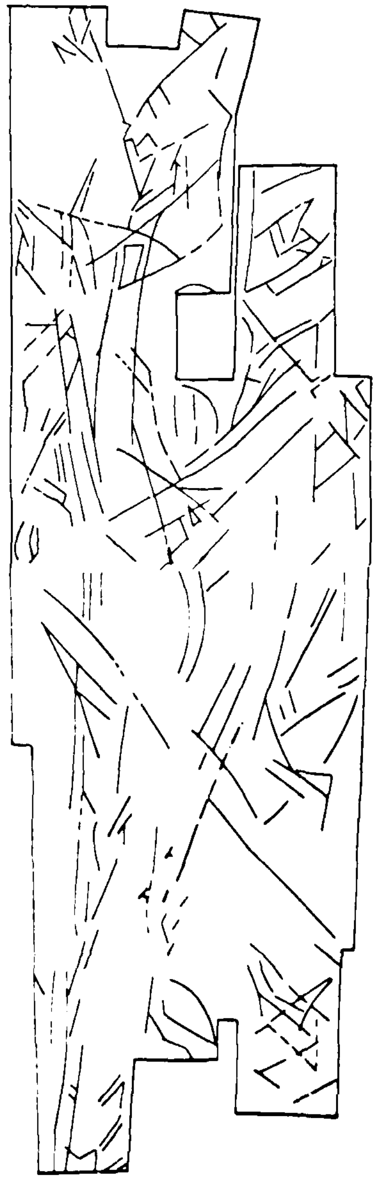

FIG. 6. Main geologic structural features obtained from both multiband photographs and thermal images (mainly). These features were recognized through different heat loss properties of the soil matterials and also through the alinement of hot water springs. These results agree with the existing data.

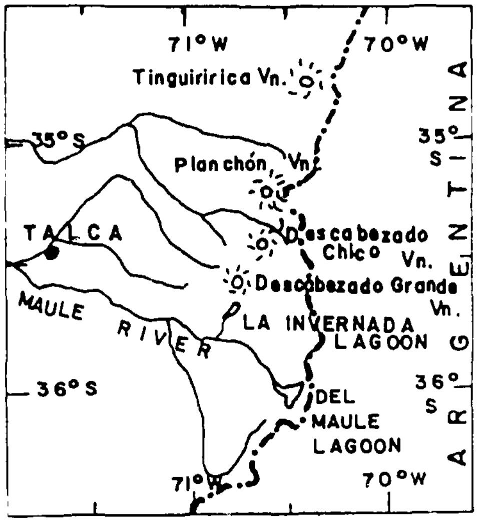

FIG. 7. LOCATION OF DEL MAULE LAGOON AND LA INVERNADA LAGOON, CENTRAL ZONE OF CHILE.

FIG. 8. MAIN RESULTS OBTAINED IN DEL MAULE AND LA INVERNADA LAGOON PILOT AREAS. The potential areas of geothermal activity forecasted (gross lines) were successfully verified.

PHOTO 7a. SECTOR OF LANDSAT IMAGE (Apr. 1978) OVER LA INVERNADA LAGOON ZONE. Water springs are identified through red spots (vegetation); abnormal snowmelting near volcanic areas probably means geothermal activity(black arrows). A,B,C are volcanic areas.

PHOTO 7b. SECTOR OF LANDSAT IMAGE (INPE,BRASIL, Dec. 1978) OVER LA INVERNADA LAGOON ZONE. Some water bodies (black arrows) remain abnormally uniced; these phenomenas near volcanic areas (A, B, C) probably indicates geothermal activity. These forecasts were successfully proved.

PHOTO 8a. LANDSAT IMAGE (MSS-5) OVER VOLCANIC AREAS, SOUTH OF CHILE. *No difference is seen on snowed areas.*

PHOTO 8b. THE SAME LANDSAT IMAGE (MSS-7). *Near infrared band clearly shows the abnormal snow-melting areas near active volcanos(2, 3, 4).*

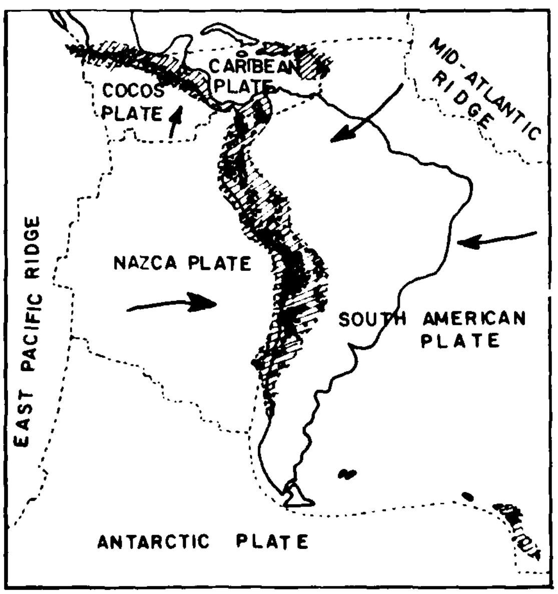

FIG. 10. SOUTH AMERICA AND NAZCA PLATES, AND SEISMIC ACTIVITY ALONG THE ANDES RANGE.

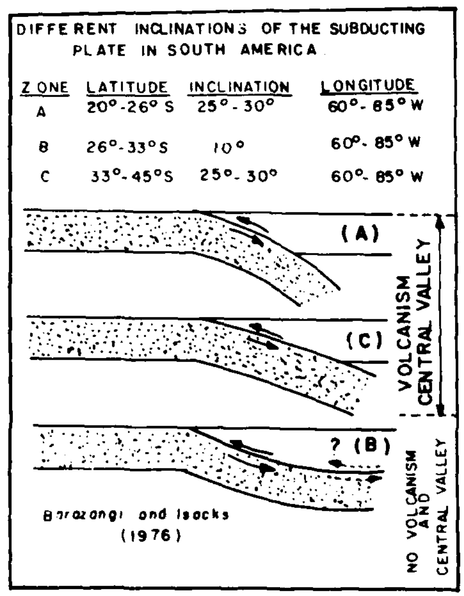

FIG. 11. INCLINATION OF THE DIFFERENT SECTORS OF SUBDUCTING PLATE, SOUTH AMERICA, CHILE.

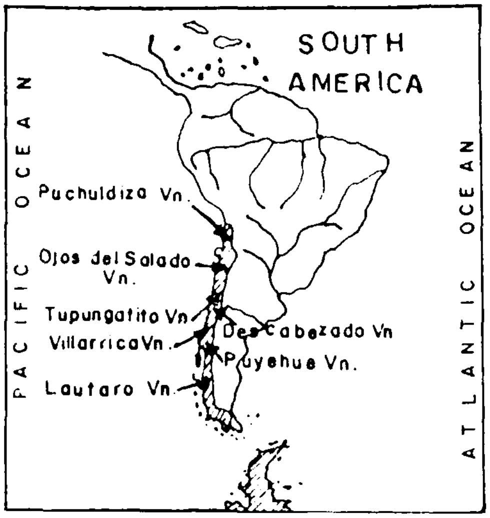

FIG. 9. PILOT VOLCANIC AREAS TO BE STUDIED TO DETERMINE A GENERAL METHODOLOGY FOR THE WHOLE COUNTRY.

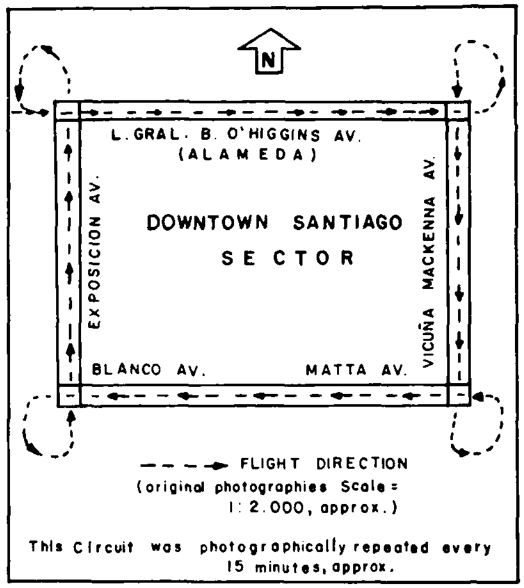

FIG. 12. PILOT CIRCUIT OVER SANTIAGO.
These photographs allowed to draw the iso-density curves showed in Fig. 13.

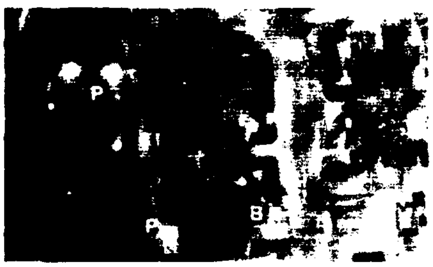

PHOTO 9a. THERMAL IMAGE OVER SANTIAGO. Some potential sources of smog (white points) can be seen in this residential area (P, B).

PHOTO 9b. THERMAL IMAGE OVER SANTIAGO. Building heat loss problems (H) can be seen; ventilation chims of the subway are also identified (S).

PHOTO 10. THERMAL IMAGE OVER MAPOCHO RIVER AREA IN SANTIAGO, CHILE. San Carlos channel (1) is modified by the warming effect of and industry (2) before arriving to Mapocho River (3, [illegible]).

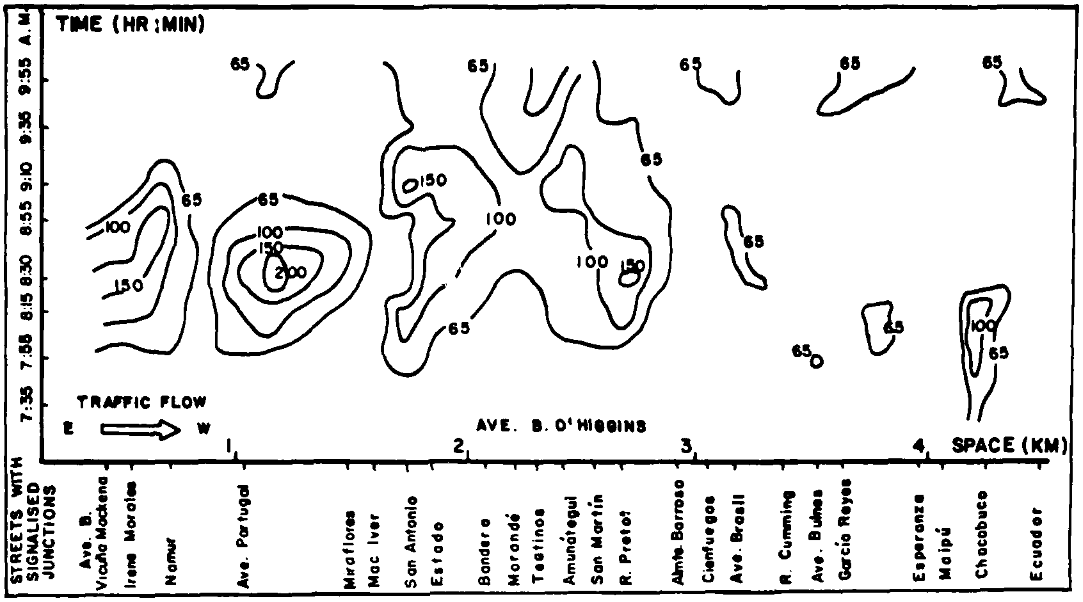

FIGURE 13a. ISO-DENSITY CURVES (VEH/KM-LANE) FOR LIGHT VEHICLES IN BERNARDO O'HIGGINS AVE., WESTBOUND DIRECTION; SANTIAGO, CHILE.

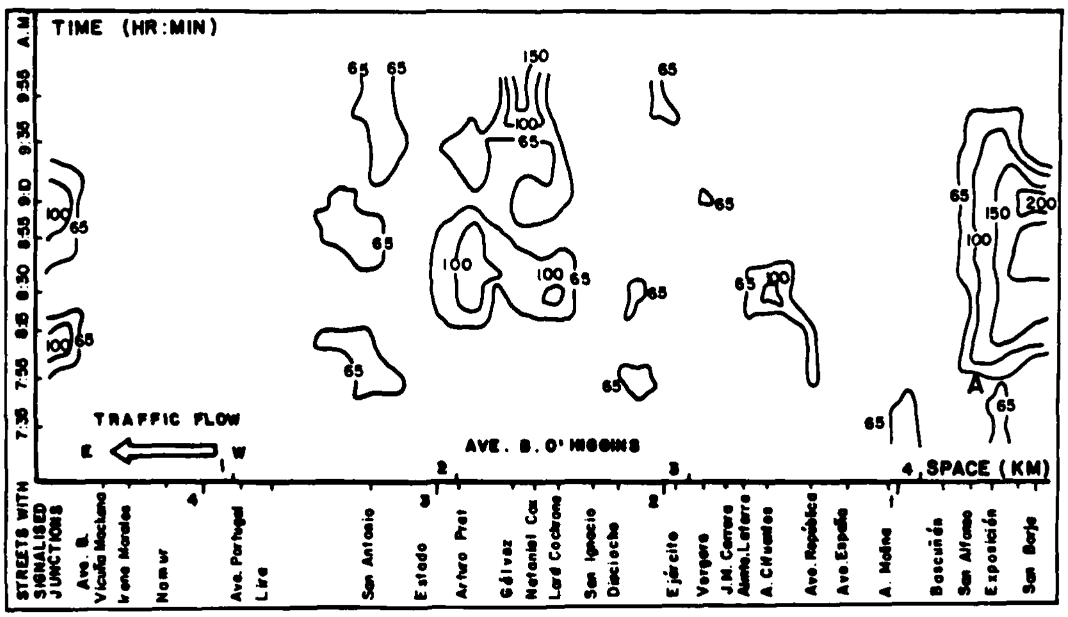

FIGURE 13b. ISO-DENSITY CURVES (VEH/KM-LANE) FOR LIGHT VEHICLES IN BERNARDO O'HIGGINS AVE., EASTBOUND DIRECTION; SANTIAGO, CHILE.

THE COLOMBIAN REMOTE SENSING PROGRAM

Eng. HERNAN RIVERA H.

CENTRO INTERAMERICANO DE FOTOINTERPRETACION, CIAF

Bogota, Colombia

SUMMARY

This report describes the remote sensing activities in the study and evaluation of natural resources in Colombia, and at the same time it summarizes all the information related to these activities, their use and development during the last ten years, indicating the present situation and placing special emphasis upon short range plans and projects.

The first part of this report is focused on making an analysis about the nature of the remote sensing in Colombia and its use, afterwards the experiences and accomplishments of CIAF in this field.are introduced, and then, the relationship of the Colombian Remote Sensing Program vs. other national plans for development is described. The main plans we refer to are: Plan de Integracion Nacional, "PIN", Programa de Desarrollo Rural Integrado, "DRI", Plan Nacional de Alimentacion y Nutricion "PAN" and Politica Nacional de Ciencia y Tecnologia. The goals and organization of the program are presented in the last part of this report, together with the description of those activities deemed necessary for performing them.

1. BACKGROUND OF THE PROJECT

1.1 Introducion

As a result of the activities performed by CIAF for the last fifteen years, in the field of remote sensing training and research, the First Symposium on Remote Sensing was organized in July, 1981 which objectives are presented on the following pages.

In several seminars and meetings at international level, it has been concluded that the techniques of the remote perception are useful in the sectorial and multidisciplinary surveys, and in the monitoring and dynamic processes and their development. Likewise, the establishment of Latin-American Training Centers has been recommended, in order that those centers may provide the double function of advising and promoting information related to the remote

sensing, strenghtening the present capacity and developing it towards Regional Training Centers with financial and technological support of international organizations.

There is also the fact that in all the meetings at a regional level the common aim to recommend the formulation of national plans of remote sensing has been evident, basing same on the training of technical personnel, mainly at those regional centers already in existence and making the Official Entities, i.e. top executives the National Planning Office, and other Decision Making people, well aware of the potential remote sensing techniques offer.

CIAF counts with very highly specialized people for the fulfillment of most of its objectives in the training of personnel at a regional level. This is the reason why the formulation of a plan at a national and regional level becomes essential, so policies at a long, medium and short range may be designed to accomplish program of technical training, advisory and research, hoping positively that by these means the national and regional shortcomings on remote perception may be overcomed, and that through the application of its techniques, the solution of some of the problems of the country may be found.

1.2 Application of the Remote Perception Techniques in Colombia

From the great variety of systems of remote perception existing at present in the world, Colombia mainly uses aerial photography, radar imagery and Landsat imagery. The last two techniques have not obtained in Colombia the usage and importance received from other Latin-American countries, due to the following reasons:

a. The incidence of tropical conditions of the Colombian territory in regards to atmospheric limitations, difficults the coverage of this type of imagery.

b. The limitation in the coverage of the Landsat existing Reception Station. However the antenna located in Brasil covers the Southeast part of Colombia, while the rest of the country is left within far angles which handicaps the obtaining of imagery of good quality. This means that if it is not possible to obtain in real time, imagery of good quality, it could be obtained from NASA "in deferred".

c. The absence of an agreement with NASA, by means of which it could be provided that when the Satellite crosses over Colombia it may register the necessary information, forwarding it to the nearest Reception Station.

d. The availability of basic information on natural resources, which could be compared with that obtainable from the Landsat imagery interpretation, by simple conventional methods.

e. The absence of the appropriate equipment which permits digital processing of the imagery in order to derive satisfactory results.

f. The lack of an adequate information at a level of Decision Making Officers on the possibilities, limitations and the actual potential of remote sensing.

Notwithstanding the foregoing considerations, Colombia has not been behind on the use and research of this new technology. The scientific interest of a group of specialized professionals, the large number of Colombian personnel formed skilfully by CIAF through fourteen years of hard work and the display of its technological proficiency at a world wide level, have given CIAF the opportunity to be asked to take care of some very important jobs of applied research.

/

The technology of the LANDSAT system has generated a lot of interest at a scientific and technological level due to the most recent and important applications of its imagery for the evaluation of agriculture crops, monitoring forestral resources and wild life, definition of limits among vegetable communities, detection of thermal anomalies, environment protection, marine resources and seaside engineering, studies of dynamic processes, etc.

With the cooperation of other local organisms, CIAF organized in July 1981, the First Colombian Symposium on Remote Sensors. The specific objectives of this Symposium were:

a. To present an up-dated information on remote sensors and their technical expectations at a short and medium range.

b. To analize at a world-wide level the present and potential status of the applications of remote sensing.

c. To analize the present status of teaching, research, application and scope of the remote sensing use in Colombia for the study of the environment and natural resources.

d. To present criteria for the selection of technical systems of remote sensing for specific purposes.

e. To suggest integration plans for the interchange of experience and data in order to establish a National Program of Remote Sensing.

The most outstanding recommendation of this Symposium was the "Establishing of a Center for the Image Processing", preferrably within the frame of the existing Colombian institutions.

The development of Colombia depends on a large scale of its natural resources development, such as the agriculture, forestry and cattle. In order to have a better use of these resources, it is necessary to evaluate and to inventory them, and to begin programs for the better handling and use of soils, in order to finally accomplish an improvement on the present yields.

A systematic reliable and opportune information is necessary to develop new resources or to improve the exploitation of those developed at present. Such an information at its different stages of detail may be obtained establishing a national information system about the agriculture and cattle resources. It is very important then, to enforce an intensive use of the different techniques on remote sensing such as aerial photography, infrared photography, radar and satellite imagery.

There is a big gap in the use of remote sensing data, due to technological differences, between the developing countries and developed ones. The formers need to improve their practical knowledge on the use of remote sensing and to apply the experiences and research accomplished by the developed countries, mainly on the surveying of agricultural resources, crop prediction, detection of plagues and other afflictions of the agriculture, farming census, changes in the use of soils, etc.

The determination of homogeneous regions would constitute an important starting point, as it is expected that through the permanent and intensive use of the information derived from an image of satellite, radar or aerial photography, to continue the evaluation of the different resources and their changes is possible, as well as, to make a nimble and actual planning of cattle and agriculture, within each one of those regions already delimited and characterized.

The explosion of world-wide information on remote sensing has led many official institutions and private advisors to request concrete information from CIAF, as to the potential and limitations of the remote sensing on studies of natural resources. The establishment of a National Program on Remote Sensing would come as a logical complement to the Post-Graduate Courses in Photo-interpretation, as at the same time this program is in charge of carrying out a vigorous research plan as to how to apply remote sensing in different disciplines. The results of the research will serve as the basic material for courses in the application of high quality remote sensing at a Master's Degree level, and as a basis to solve inquiries and to make decisions on how to apply this technology in different projects of data collection or research as to the nature and type of the environment.

2. ANTECEDENTS OF THE INSTITUTION

2.1 Legal Background

The Centro Interamericano de Fotointerpretacion, CIAF, was created by Presidential Decree 1113 on June 10, 1967.

2.2 Nature, Objectives, Functions and Structure

CIAF is a public right non-profit organization with autonomous legal solicitorship, administration and budget. A decentralized public institution, branch of the Ministry of Public Works and Transport, operated under methods of business administration.

The objective of CIAF is to carry out plans, programs, academic projects of research and advisory on photogrammetry, interpretation and use of imagery of the earth surface, as to the development of natural resources both renewable and non-renewable and their use in forestry, geology, geography, in the classification and design of agricultural soils and design and construction of civil work and other earth sciences.

In order to carry out the objectives mentioned above, CIAF develops the following functions:

a. To organize and give out courses for graduated personnel, in order to grant them -post-graduate degrees-.

b. To organize and give out courses for people who due to their work, need to acquire photogrammetric knowledge, techniques of interpretation of the earth surface imagery, through the use of both scientific and technological resources, to be applied to the earth sciences.

c. To organize and give out courses and seminars to update professionals or intermediate level personnel, in the use of advanced technology in areas referred to above.

d. To promote and develop, through programs and projects the use and application of photogrammetry earth surface imagery interpretation, to the development of natural resources, both renewable and non-renewable on behalf of the national economy.

e. To design and develop research in the aforementioned fields, both for academic purposes, as well as to take care of legal advisory services for national and foreign entities.

f. To promote information on CIAF research accomplishments on soil studies, and other areas related to its work, to expand cientific service information.

g. To procure the increasing of investments from private and public sectors, or from national or foreign sources, to support the development of programs and projects of research, academical training, implementation of services on areas of CIAF concern.

h. To furnish technical assistance to all those research and development projects requiring the technological and scientific resources of photogrammetry and photointerpretation, on behalf of the economy of Colombia.

The following chart shows the Administrative Internal Structural of CIAF.

2.3 Technical Administrative and Supporting Personnel

CIAF staff is compound by 30 specialized professionals distributed among the Technical Offices and Units, besides those 4 of the Administrative area, and 54 assistants.

2.4 Phisical Resources

CIAF buildings for administration, classrooms, library, laboratories, research and services in general cover an area of 4.000 m^2. In due course an additional 400 m^2 area will be assigned specifically for digital processing of imagery and its relative laboratory.

2.4.1 Equipment

CIAF counts with a modern equipment for photogrammetry and interpretation, in addition to photographic laboratories, however for the National Program on Remote Sensing, and to improve the teaching facilities, CIAF needs to acquire an adequate equipment of digital processing imagery, and relative photographic laboratory. As transportation means CIAF counts with 12 vehicles mostly assigned to the field work of research-experts and students.

2.4.2 Bibliographic Facilities

CIAF Publication and Information Office counts with 15.000 units, formed by books, magazines, bulletins, maps, summaries, etc.

2.5 Institutional Experience

The Centro Interamericano de Fotointerpretacion, CIAF, was developed due to the interest of both Dutch and Colombian Governments to establish an institution that would offer training and advanced courses in the use of aerial photography on the competitive and comparative basis of that of the International Institute for Aerial Surveys and Earth Science, ITC, for professionals, investigators and teachers, working for the development of the Latin American countries natural resources.

The Dutch Government entrusted ITC for the development and operation of the CIAF Project. Accordingly, towards the end of 1967 arrived in Colombia Officers and Professors from ITC, to put into execution the courses organization and the setting up of the technical equipment. During the length of the project all these people were in charge of the initial phase of the

INTERNAL ORGANIZATION FRAME OF CENTRO INTERAMERICANO DE FOTOINTERPRETACION
— C I A F —

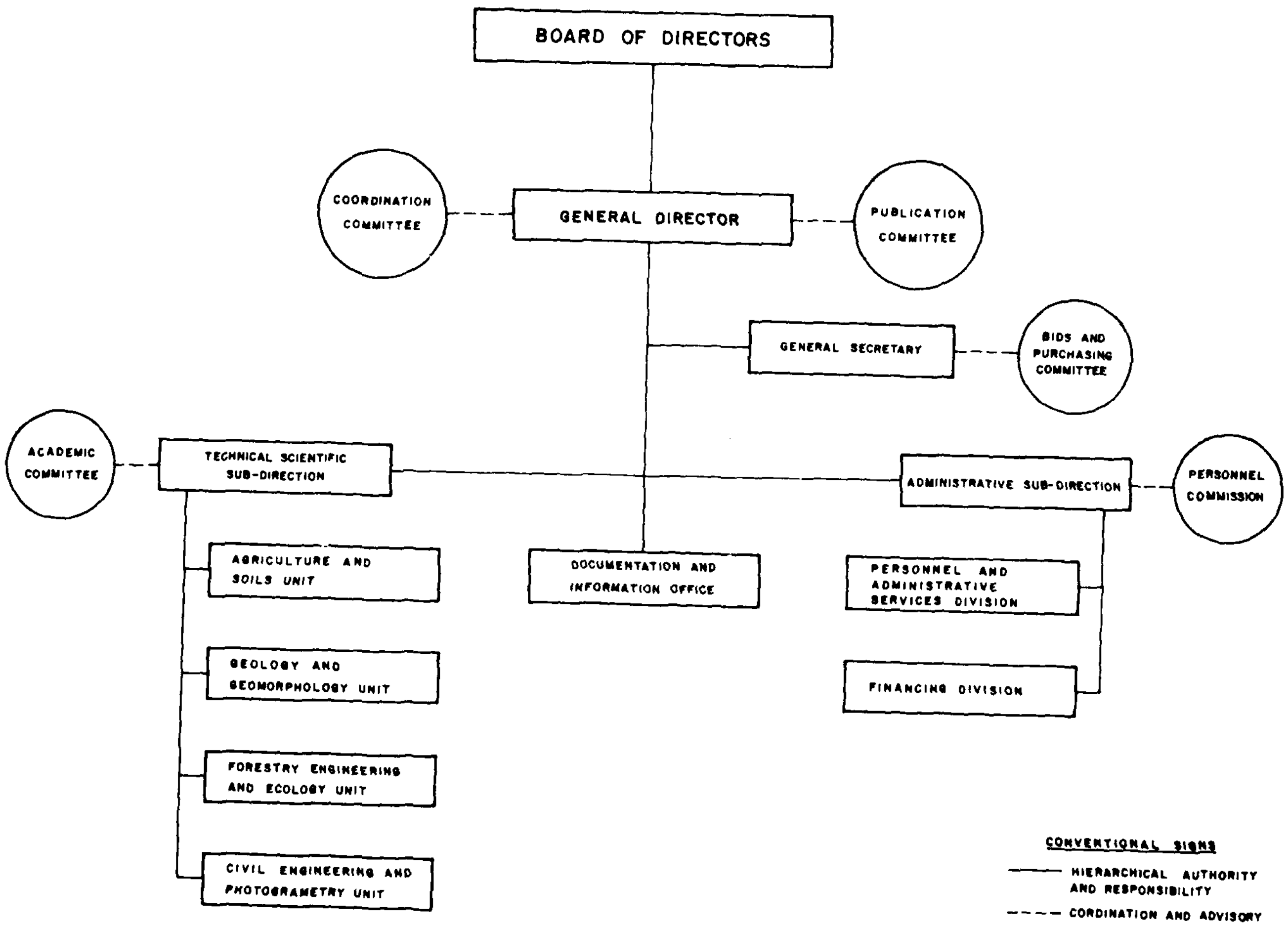

academic work, while the Colombian counterpart personnel attended to the foreseen training courses in Holland. Gradually, as the project got on its way, the Colombian technicians were taking charge of the organization and direction of courses, as well as of other activities closely related to the objectives of the programs. Today CIAF counts with Holland financial assistance for scholarships granted to Latin American and Colombian students, and academical technical assistance of ITC experts for the geology and geomorphology areas.

It is necessary to mention that ITC-CIAF Project did not foresee the establishment of permanent links between the two institutions, after the completion of same, however quite a few events have been performed jointly. At present CIAF-ITC are well aware of the need to re-establish a mutual cooperation by means of a new agreement, that will be settled in 1983 and detailed under numeral 2.7.1

It is important to point out that CIAF is accomplishing an important roll as a regional level institution, and as a link among Latin American countries. About a 65% of the professionals attending CIAF courses, come from other Latin American countries different from Colombia.

2.5.1 Regular Courses

Since 1968 CIAF has offered courses on Photointerpretation and Remote Sensing, applied to Forestry, Engineering, Geology and Soils, with a length of nine months. Since 1972 a course in Photogrammetry and Photointerpretation applied to Civil Engineering has been offered, and since 1981 there is available a program on Photointerpretation and Remote Sensing for Regional Surveys. Over 600 students from 22 countries have attended to CIAF training courses.

2.5.2 Special Courses

CIAF has short term specialized courses to give instruction in the use and application of remote sensing to technicians and professionals, who due to their work, need to up-date their knowledge. Such courses last from one to sixteen weeks and up to now, over 1.400 people have attended to them.

The themes of the specialized courses refer to the following applications: Cadastral Survey, Civil Engineering, Forestry, Geology, Soils, Geomorphology, Archeology, Road Design, Rural and City Problems, Geography, Radargrametry, Radar Imagery Interpretation, Photogrammetry for Technicians in the general use of information on Remote Sensing. All courses offered by CIAF are full time.

2.5.3 Research

Several research jobs have been performed to prove the usefulness of Remote Sensing in studies and surveying of Forestry, Geology, Hydrology, Physiography and Edaphology fields. The results of this work have been published either in CIAF magazine, or in internal bulletins of the institution. Some o. the research data accomplished have been presented in scientific and professional congresses.

2.5.4 Consultancy

CIAF has been giving technical assistance in fields of its specialization, to different national projects and providing with advisory services to other Latin-American countries and international organisms. Due to the policy issued by the Ministry of Public Works and Transport, from 1980 on, CIAF has increased considerably its technical assistance, policy that nevertheless is included

within its objectives and functions. Some of the most important projects developed up to now are:

a. Proyecto Radar del Amazonas, PRORADAM, directed to explore mineral and forestal resources and soils of Colombia Amazonia.

b. For countries members of the PACTO ANDINO, it was developed a methodology for the Survey of Tropical Rain Forest.

c. Instituto Nacional de los Recursos Naturales Renovables y del Ambiente, INDERENA. The supervision for taking aerial photography of the Magdalena Valley, to estimate the volumes of floods and to evaluate physical resources.

d. Ferrocarriles Nacionales de Colombia. Preliminary projects and exploration studies in several railroad lines, through aerial photography.

e. Federacion Nacional de Cafeteros de Colombia. Selection of scales and films, to carry out the national coffee census.

f. Instituto Colombiano de Hidrologia, Meteorologia y Adecuacion de Tierras, HIMAT. Several studies for the project "Plan de Regulacion Fluvial y Defensa contra las Inundaciones". (Plan of Fluvial Regulation and Defense Against Floods).

g. Ministerio de Agricultura (Oficina de Planeamiento del Sector Agropecuario). To characterize homogeneous areas through the use of remote sensing imagery in order to establish the most adequate methodology for the National Agriculture-Cattle Census.

h. Ministerio de Obras Publicas y Transporte. Carrying out studies of road projects, offering advice in the techniques of photogrammetry, photointerpretation and remote sensing.

i. Interconexion Electrica S.A. Consultation on photogrammetry, interpretation and use of imagery of the earth surface for the different types of hydrological and energetic development.

j. Corporaciones Regionales del Cauca, de la Sabana de Bogota, y del Tolima. Physical inventory of the hydrographic basins.

k. Organizacion de los Estados Americanos, OEA. Advisory and technical assistance for soils surveys studies, selection of dam construction sites, infraestructure studies for carrying out geological-mining inventories.

l. Instituto Interamericano de Cooperacion para la Agricultura, IICA. An evaluation of the present condition of the Remote Sensing in Latin America.

There is at present a cooperation, consulting, technical assistance and professional help agreement with the Centro de Levantamientos Integrados de Recursos Naturales por Sensores Remotos (CLIRSEN) for surveying through radar imagery in the Republic of Ecuador.

2.5.5 Publications

CIAF has produced about 300 technical documents distributed among books, technical reports, class notes, summaries, instruction for field work, etc. Some of the books produced by CIAF are being used as texts in several universities and technical institutes. CIAF publishes a yearly scientific magazine,

distributed at a continental level, with articles on remote sensing, photogrammetry and photointerpretation, which serves as a means of communication between CIAF and other Latin American organizations.

2.5.6 Other Activities

CIAF has cooperated and participated in the organization of seminars and scientific meetings at a national and international level, such as the following:

1972 - Seminar on Radar Imagery

1978 - Seminar on Remote Sensing and Photointerpretation offered to Professors of Colombian Universities.

1979 - II International Seminar on Remote Sensing and Decision Making.

1980 - I Seminar on the Quaternary of Colombia

1981 - Meeting of Experts on Erosion Processes of the Northern Andes

1981 - I Colombian Symposium on Remote Sensing.

Likewise, several experts from CIAF have attended to national and international meetings, seminars, presenting and discussing the accomplishments of CIAF methodology and research work.

2.6 Relation of the Program vs. other National Development Plans

2.6.1 Plan de Integracion Nacional "PIN"

(National Integration Plan "PIN")

The specific goals of this plan are:

a. Economic decentralization and regional autonomy.

b. Transportation and communication system development.

c. Development of the mining and energetic sector.

d. Development of a new social strategy.

The general aim is to seek a better rationalization in the resources use, producing favourable conditions for their exploitation by the private sector, through an integral policy, according to the general social interest, and increasing the State action in areas where the marketing mechanisms do not produce the best results.

This strategy will be focused on three main points:

a. Forestry development

b. Fishing and agriculture

c. Better use of hydrographic basins.

2.6.2 Programa de Desarrollo Rural Integrado "DRI"
(Integrated Rural Development Program "DRI")

The main objectives of this program are the following:

a. Improve agriculture and cattle production, specially in massive consumption food, increasing productivity in areas being exploited at present.

b. Increase the small farmers income.

c. Create new sources of productive jobs in the agriculture sub-sector.

d. Expedite access to the marketing of products and services, through construction of roads and improvement of commercial systems.

e. Increase living conditions of small farmers, offering them basic health services, education, nutrition, drinkable water, housing improvement.

f. Promote the organization and community participation on self sustained development, creating users commitees at a level of very small rural communities and towns.

2.6.3 Plan Nacional de Alimentacion y Nutricion "PAN"
(National Food and Nutrition Plan "PAN")

This plan is considered as a strategy for improving the present food and nutrition conditions of the Colombian population, specially the most vulnerable groups, through the coordination of more than 18 State entities, working at present in this project, closely joined by the private production sector and the open participation of those communities being favoured with the plan.

The analysis of the food and nutrition situation of the Colombian population, reveals three areas requiring particular attention:

a. To overcome the so-called "Food Gap" originated by the existing difference between the availability of food and the consumer's demands, particularly in the most affected population level.

b. The improvement of health status and environment conditions of rural and marginal city population, giving particular attention to the children.

c. The permanent and systematic control of food and nutrition situation of Colombian population, establishing an information system to indentify opportunately those situations that might endanger the nutritional condition of the population.

The Plan Nacional de Alimentacion y Nutricion "PAN", which coordination is under the responsibility of Departamento Nacional de Planeacion, integrates and organizes all the activities of the different private and public organisms in those fields identified as of prime importance, in order to fulfill the proposed objectives.

2.6.4 Technology and Science Policy

The general objective of the scientific and technological development policy is the application of science and technology to the strengthening of the productive sector entailed with programs of development designed by the State. Working towards this goal, a solid national investigative capacity will be sought, stimulating an ample process of technological innovation in Colombia. To accomplish this objective a strategy has been designed, including the following:

a. To develop programs directed to the strengthening of the productive sector capacity to evaluate, select and assimilate the technology demanded by this sector.

b. To promote the transference and diffusion of technology, from both foreign and domestic sources, to the productive sector, aiming to expedite the adequation and adaptation of this technology to the needs of the country.

c. To vinculate the scientific technological development programs with the sectorial development of the Plan Nacional de Integracion "PIN" such as the agriculture cattle policy, food system and the energy, education, industry and natural renewable resources sectors.

d. To develop programs directed towards the selective strengthening of the national infra-structure in science and technology, through the promotion of research, the support of institutions that may give a contribution in this field, and the development and improvement of the human resources the country needs for these activities.

2.7 Other Foreign Cooperation

2.7.1 Project CIAF-ITC of Holland

The Government of the Netherlands, through its Minister of Cooperation for Development, on quite a few occasions has confirmed its decisive support to the availability of higher education mainly at institutions like CIAF, located within developing countries. Such a support comes together with a broad transference of the Dutch highly specialized experience and technology.

CIAF has already presented a proposal which perfectly fits within these guidelines:

a. To support and strengthen CIAF education programs in order to reach a level of proficiency compared with those of ITC Holland.

b. To exchange experience not only in the academic aspect but in the criteria to adopt when identifying the users requirements, and at the same time to establish a consistent evaluation of academic and research performance in both institutions. The exchange of experiences should take place as an extension of the seminar foreseen above, for three days allowing the time deemed necessary to prepare the relative documents.

c. To transfer knowledge and technology from ITC to CIAF in order to contribute to the strengthening of CIAF education program which is closely related to the development of Colombia.

d. To design and execute joint research CIAF-ITC programs, seeking their improved applicability on further development and accomplishments of both institutions.

e. To sponsor and support with ITC experts, all advisory work undertaken by CIAF.

f. To reestablish the relationship and cooperation between CIAF-ITC on a permanent and well programmed basis.

2.7.2 Project CIAF-INDERENA-University of North Dakota

INDERENA completed very recently, a very important regional study in the

area of the Magdalena River Delta. A period of five years was necessary to obtain several forms of thematic data, required for INDERENA program of environmental pursuiting and eco-development monitoring.

The employment of modern techniques such as Remote Sensing and Digital Data from Satellite, could have reduced time and expenditure in the obtaining of such data, and even more, the analysis or use of the same could be drastically simplified if this data was introduced to an appropriate Geographic Information System "GIS".

This proposal gives the development, testing and transference of a computer software, necessary for the performance of a GIS system, specially adapted to satisfy INDERENA-CIAF needs. This procedure would include the introduction and use of all data compiled by INDERENA for the region of the Magdalena River under study.

Since the GIS has been developed at University of North Dakota Institute for Remote Sensing, "UNDIRS", the INDERENA thematic data for this study of the Magdalena River will be introduced to that system where it will be immediately utilized for the development of the GIS users testing techniques and methodology.

The main objectives of this project are:

a. To determine to which extent the information from the Landsat may provide thematic data for INDERENA/CIAF.

b. To develop a GIS in order to satisfy INDERENA/CIAF data handling needs such as storing and updating of environmental economic data analysis.

c. To transfer the required technology to INDERENA/CIAF in Bogota, for future use.

2.7.3 Other Projects

Besides the foreign cooperation programs previously described, CIAF maintains research and academic support agreements with the Instituto de Investigaciones Geologico-Mineras "INGEOMINAS", Universidad de Los Andes, Universidad Distrital, Universidad del Cauca and Universidad del Tolima.

3. OBJECTIVES OF THE PROGRAM

The direct objective of the Programa Nacional de Sensores Remotos will be to improve the CIAF efficiency in the field of remote sensing through the following means:

a. Providing training to all personnel necessary for the development of the project.

b. Organizing symposiums, congresses, meetings and other activities on remote sensing.

c. Promoting and developing at a national and international level, short courses on the principles and applications of the remote sensing techniques in different disciplines.

d. Designing, promoting and fulfilling advanced courses, at a national and international level, granting the title of "Master of Science on Remote Sensing" with emphasis on soils, forestry, geology, civil engineering and

regional surveying. The agreements "CIAF-National University", "CIAF-Distrital University", "CIAF-University of North Dakota", will permit the implementation of this program.

e. Strengthening and mainteining the CIAF educative programs to a level of quality and proficiency as those from ITC.

f. Establishing agreements with computing centers and faculties of System Engineering in order to prosecute research and development projects on processing and digitalization of remote sensed imagery as well as on design and implementation of georeferenced data base.

g. Investigating technical and economical feasibility for the establishment of a reception station of remote sensed imagery, placed within a country of the north area of South America.

h. Establishing and operating an advisory center to perform special works, studies and research on natural resources, using remote sensing techniques.

The final objectives of the proposed program, which are the results of conclusions, recommendations, and work experience of this technical cooperation project are:

a. To contribute to the improvement of agriculture production.

b. To contribute to the improvement of techniques to detect and control plagues of the crops.

c. To contribute to the development of fishing and aquiculture.

d. To contribute to the urban and regional development.

e. To produce thematic maping for the development of projects of agriculture sectors, food and natural resources.

f. To develop technological specifications and methodology for analysis, inventories, diagnosis of natural resources renewable and non-renewable.

g. To cooperate with the energy and mining development.

h. To train Colombian and foreign experts and professionals in the basic techniques and methodology for research and evaluation of physical resources through remote sensing.

i. To train Colombian and foreign experts and professionals in the basic methodology and techniques of research and evaluation of non-renewable natural resources.

4. DESCRIPTION OF THE PROGRAM

4.1 Direct Results

4.1.1 Reports

4.1.2 Cartographic Products

4.1.3 Research

4.1.4 Training

4.1.5 Plant Facilities

4.1.6 Bibliographic Resources

4.1.7 Equipment

4.1.8 Materials

4.2 Activities

4.3 Time Table

5. PROGRAM ORGANIZATION

The setting-up, planning, administration and supervision of the activities would be under the responsibility of:

. CIAF General Director

. CIAF Technical-Scientific Sub-Director

. CIAF Remote Sensing Program Coordinator

. BID Representative in Colombia

. Departamento Nacional de Planeacion Representative.

For the development and fulfillment of the research projects and advisory on remote sensing, the following executives will be responsible:

. CIAF Remote Sensing Program Coordinator

. CIAF Professional Technicians

. CIAF Photography Technician

. Equipment Operator.

For the agreements of consultation there will also be technical professionals from the interested parties, who, together with the Coordinator of the Remote Sensing Program, will be responsible for the fulfillment of the different stages included in the agreement. They will submit periodical reports about the project advancement to the General Director of CIAF, to the Technical Sub-Director and to the Representative of the participating firm. The human and physical resources required for the consultation project, available at CIAF but not attached to the National Remote Sensing Program, will be provided and supervised by CIAF own Consultation Office.

Besides the technicians from CIAF, an expert from ITC will participate in the selection of the image digital processing system, and the photographic laboratory. This participation of ITC is very important inasmuch as they count with enough knowledge and experience in this field, while in Colombia a similar equipment does not exist so far.

In regards to reports, publications, bibliographic resources and related activities, the CIAF Office for Information and Publishing will take care of the whole coordination.

The setting-up, planning, development, administration and supervision of the "Master of Science in Remote Sensing Program", with the different specializations, will be under the responsibility of:

. The General Director of CIAF
. The Technical Scientific Sub-Director of CIAF
. The Coordinator of the Remote Sensing Program
. The Coordinator of the Master of Science in Remote Sensing Program
. A Representative from the University or Universities with which the "Specialization Agreement" may be established.
. A Representative from the Instituto Colombiano para el Fomento de la Educación Superior "ICFES".

The final report on the scope and performance of the National Program on Remote Sensing will be introduced to the Departmento Nacional de Planeacion BID, as well as to all other local and foreign institutions participating on it.

7. BUDGET OF THE PROGRAM

The total worth of the project is estimated in US$ 5'000,000. It is expected that the financing of the program may be achieved through international loans, CIAF own resources, and additional contribution from the Colombian Government.

8. JUSTIFICATION OF THE PROGRAM

Through the development of this project CIAF will be able to satisfy the following needs:

a. To have available in a permanent basis a National Program on Remote Sensing, which oriented appropriately by CIAF will permit the coordination of all those activities developed by different national institutions in the field of remote perception, avoiding in that way, duplication of efforts and resources.

b. Training and refreshing courses for the CIAF technical personnel, at different levels and with the participation of all the academical sectors of the institution.

c. Training of foreign and local technicians through a program of studies at a "Master of Science in Remote Sensing" level.

d. Training to former students of CIAF through intensive courses.

e. Participation of technicians in a great number of international events, such as conferences, symposiums, forums, etc. which altogether will allow them the updating of their knowledge in a very aspect of the remote perception field.

f. The scientific research on food production, agriculture, aquiculture, renewable and non-renewable resources, which are areas of essential importance both for Colombia and Latin America.

g. Multiplication and transference at a Latin American level of the innovation process and the promotion of techniques related with the remote sensing and their applications.

h. Integration with different local and foreign entities, allowing the constant interchange of knowledge and experiences.

i. Updating of the library, acquiring a large supply of specialized magazines, books, etc. and by the contribution of the reports and publications originated along the development of the present project.

j. To acquire the appropriate equipment for the processing of imagery and photography.

k. To entail very highly qualified specialists with the Remote Sensing Program.

CIAF demands the essential cooperation of BID because its own available physical, economical and human resources are not enough for the fulfillment of the future needs of the institution and the country in the field of remote sensing.

On the other hand, CIAF considers that the support of BID is actually an investment, because while the project is in force (five years) and after its completion, the multiplicating effects obtained by CIAF at a Latin American level will reduce the costs, due to the experience and accomplishments of unpredictable value, for both Colombia and other countries of the region.

AD P001991

APPLICATIONS OF SATELLITE REMOTE SENSING FOR U.S. CROP ACREAGE ESTIMATION, 1980-81 RESULTS

JAMES W. MERGERSON
GEORGE A. HANUSCHAK
PAUL W. COOK

Remote Sensing Branch
Statistical Research Division
Statistical Reporting Service
U.S. Department of Agriculture
Washington, D. C., USA

ABSTRACT

As part of the AgRISTARS (Agriculture and Resources Inventory Surveys through Aerospace Remote Sensing) DCLC (Domestic Crops and Land Cover) project, the Remote Sensing Branch (RSB) of the Statistical Reporting Service (SRS) is investigating the operational use of LANDSAT data in an applied research mode.

Currently, six States (Kansas, Missouri, Oklahoma, Illinois, Colorado, and Iowa) are participating in the project. The primary objective is to provide timely, more precise crop area estimates for major crops in selected States. The SRS approach is to use ground gathered June Enumerative Survey (JES) data in conjunction with LANDSAT data to improve the precision of crop area estimates.

This paper presents an overview of SRS, the SRS Remote Sensing Environment, project implementation, costs, contributions and project results.

1. THE SRS STRUCTURE 5/

An agricultural producer today is a combination of highly skilled technician and executive who frequently must apply considerable expertise and make demanding decisions such as a manager of a factory or other business would have to do. To operate efficiently, effectively and profitably, farmers, ranchers, and others in agriculture require accurate and timely information, and reliable evaluations concerning production, supplies, prices, exports, weather and other inputs.

SRS provides the channel for the orderly flow of this intelligence about the agricultural economy of the United States of America (USA). This agency is responsible for the National and State crop area estimates and other agricultural statistics as well as the coordination and improvement of the United States Department of Agriculture's (USDA's) statistics program. SRS is also concerned with statistical research and methods to improve gathering, evaluating, and processing information.

The agency also performs technical assignments for other Federal and State agencies in addition to limited services for agriculturally related private firms on a reimbursable or advance payment basis. The services provided consist of surveys and data collection activities. SRS also participates in the Agency for International Development's (AID) foreign visitor training program and provides technical consultation and support to developing countries in implementing agricultural estimating programs.

SRS has served agriculture for over a century under various organizational titles. Tasks and procedures have changed continually over the years to accommodate changing needs. SRS is a broad-based non-policymaking organization headquartered in Washington, DC. The agency consists of a Crop Reporting

Figure 1. U.S. DEPARTMENT OF AGRICULTURE
STATISTICAL REPORTING SERVICE

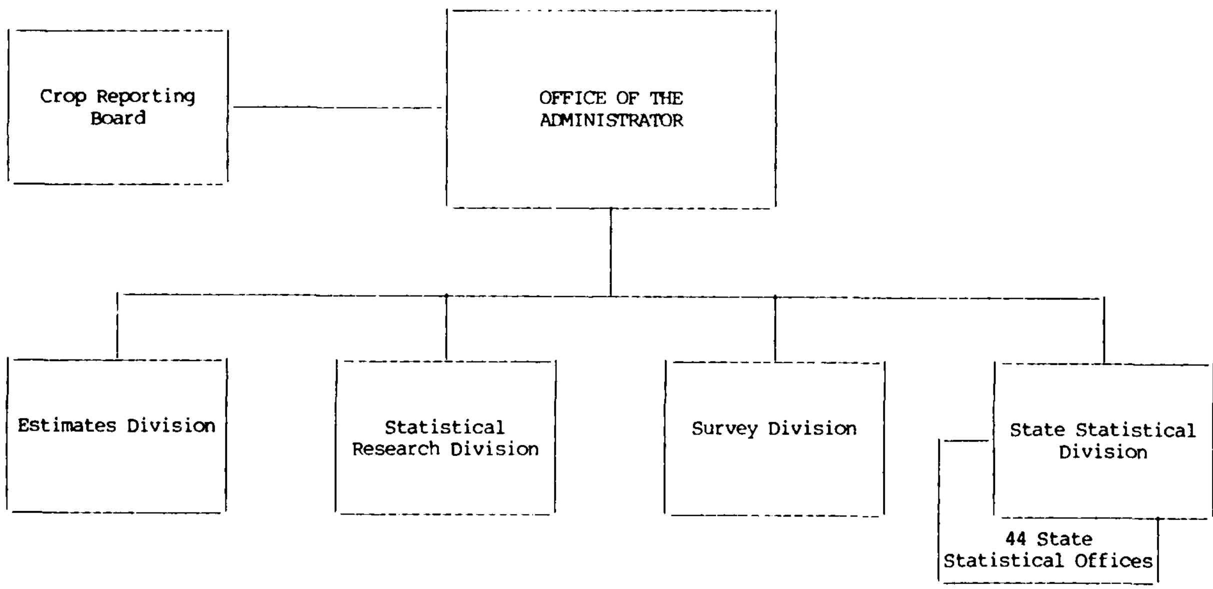

Board, State Statistical Division, Estimates Division, Survey Division, and Statistical Research Division. An organizational chart is shown in Figure 1.

The State Statistical Division consists of 44 State Statistical Offices (SSO's); one office serves the six New England States (Maine, New Hampshire, Vermont, Massachusetts, Connecticut, and Rhode Island) and the Maryland Office also serves Delaware. This decentralized approach for making estimates is based on the assumption that statisticians located in the SSO's can best adapt general procedures to the varied local circumstances and have a far better grasp of regional conditions affecting agriculture.

The SSO's are the primary data collecting, processing, evaluating, estimating, and publishing units of SRS. Following prescribed procedures, they conduct surveys and recommend statistical estimates for their States and counties to the Crop Reporting Board. These estimates are published after Board review and adoption. Other major responsibilities of the SSO's include liaison with the State agricultural sector and maintenance of a corps of voluntary reporters for surveys and a part-time staff of enumerators.

The Crop Reporting Board reviews and adopts official State and national estimates for crops and livestock as required by USDA regulations. The Board includes a Chairman, the SRS Deputy Administrator, a Vice Chairman, the Estimates Division Director, a Secretary, and the Chief of Data Services Branch, Survey Division. In addition to the six permanent members, five or six commodity specialists are selected by the Chairman from the Estimates Division and the SSO's to participate in determining the estimates.

The Estimates Division is the primary source in SRS for agricultural statistics. They analyze and interpret the various sources of data. Their analysis and interpretations are used by the Crop Reporting Board in making estimates and forecasts of the Nation's agriculture. The Division evaluates commodity statistics, determines needs, and implements proper statistical plans in support of the crop and livestock reporting program. Estimates Division also ensures that appropriate methods and procedures are used in all phases of the program.

The Survey Division is responsible for preparing and establishing procedures used by the SSO's in collecting data by mail and enumerative surveys, and for carrying out the objective yield measurement program. The Division designs and tests survey techniques including forms and questionnaires, writes data collection instructions, and conducts training schools for enumerators. The Division processes the data and produces summaries for use by the SSO's and the Crop Reporting Board in setting official estimates. The Division also conducts data collection activities for other USDA and Federal or State Agencies on a reimbursable basis.

The primary functions of the Statistical Research Division are to develop new and improved collecting, estimating, and forecasting methods for Agricultural Statistics and to encourage the use of sound statistical techniques throughout USDA. The Division devises improved sampling techniques and methods of controlling sampling errors, constructs area and list sampling frames, and researches nonsampling errors stemming from questionnaire wording, enumerator's interviews, or other causes. New models for assessing the yield of field and fruit crops are investigated. The potential of remotely sensed data in contributing to the SRS program is also studied quite extensively. The Applications Section of the RSB is currently investigating the operational implementation of remote sensing technology as part of the AgRISTARS DCLC project which is the focus of this paper.

2. THE SRS REMOTE SENSING ENVIRONMENT

AgRISTARS is a joint research program between USDA, the National Aeronautics and Space Administration (NASA), the U.S. Department of Commerce (USDC), the U.S. Department of Interior (USDI), and AID. AgRISTARS was established to investigate the use of remote sensing in agriculture. The Remote Sensing Branch of SRS has assumed the responsibility for implementing the DCLC project.

The DCLC project started in 1980. LANDSAT data are combined with conventional ground gathered data to provide timely, more precise, year-end major crop area estimates in selected States. Kansas and Iowa were chosen as the first two States in 1980. Missouri and Oklahoma were added in 1981. Colorado and Illinois are the new additions for 1982. The primary objective is to obtain major crop area estimates with reduced sampling errors. Major crops to be estimated in each State are shown in Table 1.

Figure 2. AgRISTARS DCLC REMOTE SENSING ENVIRONMENT

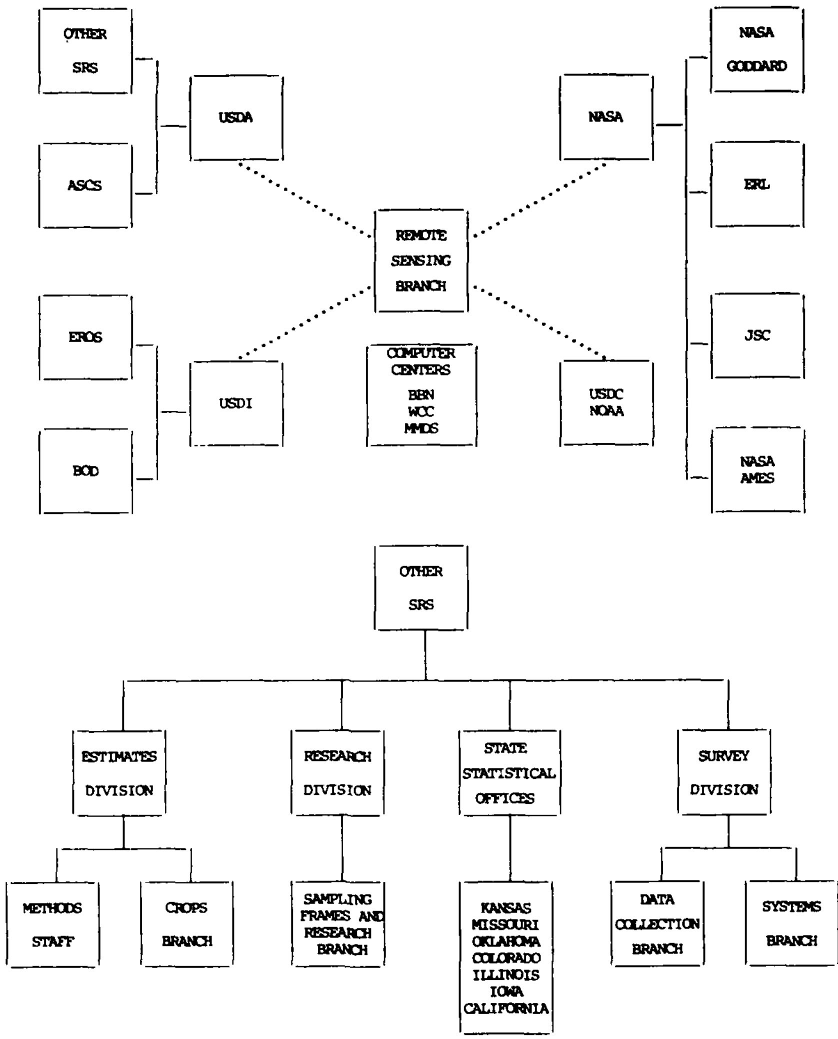

Table 1. Major Crops By State

STATE	MAJOR CROPS
Kansas	Winter Wheat
Oklahoma	Winter Wheat
Colorado	Winter Wheat
Missouri	Corn and Soybeans
Illinois	Corn and Soybeans
Iowa	Corn and Soybeans

Successful completion of the DCLC project requires the cooperation of several U.S. Government agencies as well as input from a number of divisions within USDA's SRS. The SRS Remote Sensing environment is illustrated in figure 2. Although the contributions of each Agency are varied, each serves a vital function in determining the final outcome of each year's project. Besides USDA, the departments represented are the following; NASA, USDC and USDI. There are also two commercial computer centers which are used in processing both the ground data and the LANDSAT data. The following will present in capsule form tasks which each of these governmental and commercial entities perform in providing support to the DCLC project.

NASA launched the LANDSAT series of satellites and has four groups which have continued to support the DCLC project in utilizing the LANDSAT digital data. NASA's Goddard Space Flight Center (GSFC), located in Greenbelt, Maryland, processes the LANDSAT data after it is beamed to Earth. Earth Resource's Laboratory (ERL), located in Bay St. Louis, Mississippi, has assisted with scene registration algorithms and has developed an automated method for shifting segments using computerized routines. Johnson Space Center (JSC), located near Houston, Texas, has provided research support on clustering, classification and estimation procedures. The NASA Ames research complex, located in California, has provided substantial computer facilities for full scene classification. Prior to 1981, the ILLIAC-IV was the main computer, however, it was replaced by a CDC 7600 during 1981. A CRAY-1S computer, provided by NASA Ames, will be used for full scene classification in 1982.

NOAA of the USDC provides satellite imagery from weather satellites. These images aid DCLC investigators in determining cloud-free dates of imagery within a day of acquisition. This permits early identification of potentially useable LANDSAT scenes which are sufficiently cloud-free for use in analysis.

Three computer centers are used in the data processing effort. Two centers are commercial facilities. One center is operated by Bolt, Beranek, and Newman (BBN) in Boston, Massachusetts. Most of the computing is performed at BBN. The other commercial center is Martin Marietta Data Services (MMDS) located in Orlando, Florida. All the ground data update functions are performed on this system and clean data tapes for use at BBN are produced. USDA's Washington Computer Center (WCC), located in Washington, D.C., provides support for reformating LANDSAT computer compatible tapes (CCTs).

USDI provides assistance both through its Earth Resources Observation Service (EROS), located in Sioux Falls, South Dakota, and through its Branch of Distribution (BOD). EROS provides both hard copy photographic copies of the LANDSAT MSS data in transparency and photo format as well as the digital data in the form of CCTs.

A number of divisions within USDA participate in providing support services to the RSB. Within the Statistical Research Division, the Sampling Frames and Survey Research Branch updates county maps with segments rotated into the sample each year and provides framework maps for digitizing strata boundaries on BBN so that estimates can be made for each land use stratum. The Data Collection Branch and Systems Branch of the Survey Division provide JES support for the ground data collection effort. Systems Branch provides programming support by creating computer generated questionnaires for an intentions follow-up survey. The SSO's collect the JES ground data, perform a field level edit and also digitize the segment level field boundaries. The Estimates Division is represented by both Methods Staff and the Crops Branch. The Methods Staff establishes specifications for the JES design and ensures that special requirements for remote sensing use are met. Finally, the Crops Branch accepts DCLC input in establishing estimates for the Annual Crops Summary.

/

3. BACKGROUND AND OBJECTIVES

LANDSAT data are combined with ground-gathered survey data to provide timely, year-end major crop area estimates in selected states. A regression estimator as described in Cochran (Section 17.1-7, third edition) [1] was used. The regression estimator as used by the RSB has been previously described by Hanuschak and others [2].

In 1980, clustering was performed using the LARSYS [6] clustering algorithm. In 1981 the CLASSY[4] clustering algorithm was used. Clustering is a data analysis technique by which one attempts to determine the natural or inherent relationships in a set of observations or data points.

A Gaussian Maximum likelihood classifier was used in both years. Classification is based on discriminant analysis [2]. Discriminant analysis is a process used in attempting to differentiate between two or more populations of interest based on multiviariate measurements.

The SRS objective of providing timely, year-end state and sub-state crop area estimates with reduced sampling errors by using ground gathered data in combination with LANDSAT data, was accomplished in 1981.

In 1981, winter wheat harvested area estimates for Kansas and Oklahoma were provided to the SRS Crops Branch and the SRS SSO's on October 30, 1981. Corn and soybeans planted area estimates were provided to the Crops Branch and the SSO's on December 16, 1981, for Iowa and Missouri. For Missouri, rice and sorghum planted area estimates were also provided to the SSO and the Crops Branch. The data were reviewed by the Crops Branch and SSO's in their final end of season annual Crops Summary.

During 1980, acquisition of quality and timely LANDSAT data was severely impaired. Satellite and LANDSAT preprocessing problems lowered the digital data quality and increased the delivery time necessary for receiving LANDSAT data products. Many of the LANDSAT data quality and timeliness problems encountered during 1980 were due to ground handling complexities at NASA Goddard which were fixed prior to the 1981 DCLC project.

4. STATE STATISTICAL OFFICE CONTRIBUTION

The SSO's played an integral part in the outcome of the DCLC project. Part of their role was to be the primary ground data collectors. In this role the SSO's provided field boundary, acreage, crop and land cover type data for the randomly selected SRS area segments. These data were collected during the June Enumerative Survey (JES) and special follow-up surveys in Iowa and Missouri. The data were used to establish training fields for computer classification of LANDSAT digital data and again for estimation. After collecting the ground data, an intensive field level edit was made by each state followed by digitization and plotting of the segment data.

Prior to FY80 these functions were performed by the RSB staff in Washington, D.C. In view of an expanding program, it was apparent due to efficiency considerations that some tasks would have to be performed in a decentralized fashion. Thus, the field level edit, digitization and plotting functions were successfully transferred to each of the four SSO's.

The field level edit is a labor intensive effort that was performed during a two week period following the JES. Recorded information on photographs, questionnaires and computer records were verified.

Segment digitization is the process of converting segments from fields drawn on aerial photographs or topographic maps to a computer file of coordinates in a geographic coordinate system. This task was performed using a tablet digitizer, in conjunction with an interactive software sub-system (EDITOR). After the segments were digitized, they were plotted and checked for accuracy. In 1981, a much greater amount of time was required for digitization than in previous years. This was due both to problems with a sudden change in the Bolt, Beranek and Newman (BBN) data processing facility operating system as requested by the General Accounting Office (GAO) and to equipment breakdowns in the SSO's and RSB.

The other major role of the SSO's was interpretation of the final state and sub-state level estimates generated at the end of the project.

/

5. LANDSAT DATA ACQUISITION

The following LANDSAT products were used: 1:1,000,000 scale positive black and white transparencies (bands 5 and 7), 1:250,000 scale paper products (bands 5 and 7) and computer compatible tapes (CCTs). Delivery of these products involved two phases. The data were first transmitted from satellite to NASA Goddard where it was processed and sent via DOMSAT to the EROS Data Center (EDC). EDC in turn processed the data, filled the data order, and shipped the products to SRS.

In 1981, while data delivery was improved, the 10-14 day requirement for delivery after acquisition was not met. Delivery times ranged from about 1 week to 20 weeks with an average time of 3 to 4 weeks. As a result of not obtaining some data in a timely manner, a considerable amount of overtime work had to be performed to meet timeliness deadlines. This turnaround time must be improved for the continued expansion of the DCLC program.

6. DATA PROCESSING

Prior to processing the LANDSAT data, analysis districts were determined. Analysis districts consisted of counties partially or completely contained in one or more scenes of the same LANDSAT pass. Areas overlapping two scenes were assigned to a specific scene by looking at cloud cover, data quality, imagery dates, and each scene's containment relative to the other.

Several data processing centers were used in processing the JES and LANDSAT data to calculate regression estimates. The Martin Marrietta Data System (MMDS), Bolt Beranek and Newman (BBN), Washington Computer Center (WCC), and the CDC 7600 computer at NASA Ames were used. The major software package used was EDITOR[3]. EDITOR is a comprehensive interactive data analysis system for processing LANDSAT and JES data. EDITOR runs on a modified DEC System-10 computer and is available at BBN in Cambridge, Massachusetts. Some EDITOR programs are also implemented on CDC 7600 and CRAY-1S computers at NASA Ames. EDITOR was used for digitization, registration and analysis of the JES and LANDSAT data.

A data set containing ground data from the JES was created and edited using a set of SAS programs on the MMDS. The final edited data set was then transferred to BBN. Boundary information for each field of crop data was digitized on BBN and converted to a geographic coordinate system by calibrating the segment photo to U.S. Geological Survey (USGS) maps. The calibration process consisted of locating corresponding points on both the aerial photograph and the USGS map on which the segment could be located. A regression routine then converted the digitizer coordinates to map coordinates by using coefficients calculated from the corresponding points data.

LANDSAT computer compatible data tapes were reformated at WCC and copies of the tapes containing the reformated data were mailed to BBN and to NASA Ames for processing.

Each selected scene was registered to USGS maps in Washington, DC. This process called registration relates LANDSAT row-column coordinates with USGS map latitude-longitude coordinates by means of third order bivariate polynomial equations.

A second step of registration followed the initial scene registration. This step consisted of using grey-scale print-outs and segment plots to shift each segment to a more accurate location based on interpretation of lightness-darkness regions within the print-out.

An EDITOR operation termed "masking" was next used to establish the location of the LANDSAT pixels for each field. The locations were stored in "segment mask" files which were then used to extract LANDSAT pixels corresponding to specific crop types or land uses. Criteria that could also be used in selecting pixels were field boundary information (that is, to include or exclude field boundary pixels), crop conditions, field codes and field size. This extracting process is known as packing and the files are termed "packed" files.

Packed files containing no field boundary pixels were clustered by crop type and land cover. Files containing more than 5000 pixels were sampled before clustering to save computer costs and reduce turnaround time. The statistics describing the clusters generated were saved in "statistics" files which were

combined to form a "combined statistics" file which represented all sampled crop and land covers for the segments represented.

The combined statistics file was then used to classify pixels into a cover type. Counts of the classified pixels were made by cover types within a segment. The classified pixel counts along with the corresponding JES data were then used in making sample level estimates. Full frame classification, aggregation of pixels by stratum and large scale estimation were then performed for each analysis district. Full frame classifications were performed on a CDC 7600 computer at the NASA Ames Research Center in 1981 and on the ILLIAC-IV in 1980. After the data for each states analysis districts were processed, a state level estimate for each crop of interest was obtained using an accumulation program. The accumulation program aggregates all substate estimates to a state total. Area estimates for which LANDSAT data are or aren't available are included in the state total. Direct expansion estimates using only JES segment data were provided for areas where LANDSAT data were unavailable.

In 1981 much work had to be performed outside of regular working hours due to problems associated with the BBN computer system. BBN was forced by an external group to modify their system. This modification placed severe limits on the percentage of the machine's capacity that we could utilize. This problem has been corrected.

7. ESTIMATION RESULTS

LANDSAT regression estimates for 1980 and 1981 are in Table 2. State level relative efficiencies ranged from 1.3 to 1.9 in 1980 and from 1.3 to 2.3 in 1981. Relatives efficiencies at the substate levels ranged from 1.2 to 6.4 in 1980 and from 1.2 to 15.8 in 1981. Relative efficiency measures the degree of improved precision obtained from using the LANDSAT data in addition to the ground data. The figure obtained indicates the factor by which the sample size would have to be increased to equal the precision obtained using LANDSAT data in addition to the randomly selected JES segment data. The 1980 and 1981 results were negatively impacted due to missing data in some areas due to clouds, data quality, and failure to achieve 10 to 14 day delivery of LANDSAT data to SRS from time of acquisition.

Table 2. 1980 and 1981 State Level Estimates

Year	State	Crop	Estimate (Ha)	R.E.
1980	Kansas	Winter Wheat	5,052,500	1.3
1980	Iowa	Corn	5,803,200	1.9
1980	Iowa	Soybeans	3,291,350	1.5
1981	Kansas	Winter Wheat	5,297,900	2.3
1981	Oklahoma	Winter Wheat	2,519,600	1.3
1981	Missouri	Corn	774,600	2.2
1981	Missouri	Soybeans	1,963,700	2.1
1981	Iowa	Corn	5,820,200	1.6
1981	Iowa	Soybeans	3,275,150	1.6

8. PROGRAM COSTS AND CONTRIBUTIONS

Since the AgRISTARS DCLC program has now expanded to six States, there is a renewed interest in the relationship between program costs and contributions. Some historical perspective provides insight into the cost trend associated with SRS's use of LANDSAT data in conjunction with the ground data from the JES.

The first entire State project was conducted from 1975 to 1977 using 1975 data. The study area was Illinois. The cost associated with this project included all research and development efforts including a comprehensive software system (EDITOR). The total project cost was approximately $750,000. The first timely project for an entire State was conducted in 1978 using 1978 data from Iowa. Since most of the methodology and software had already been implemented, the cost decreased to about $300,000. In 1980, the AgRISTARS DCLC project costs for Iowa and Kansas were approximately $200,000 per State. In 1981, the project costs for Iowa, Kansas, Oklahoma, and Missouri were approximately $180,000 per State. There is

an obvious downward trend in the LANDSAT project costs that is expected to continue as the move from research and development to applications continues.

The cost of the JES for the 1981 four State project was approximately $64,000 per State. The estimated overall cost per State associated with estimates from the JES ground data only, and the JES plus LANDSAT regression estimates is shown in Table 3. The cost can be ratioed for various relative efficiencies to determine if the improvement in statistical precision is cost effective relative to the alternative of increasing the JES sample size.

The use of LANDSAT data in conjunction with JES data is cost effective for all relative efficiencies with a corresponding cost ratio less than or equal to one. Using this criterion a relative efficiency of about 2.5 would be the break even point. In future years it is expected that the break even point will be lower. The reason for this expectation is that JES costs per unit probably will rise and JES plus LANDSAT costs per unit will probably decrease. The JES costs per unit will probably increase due to increases in travel and interview costs. More efficient computer data processing and proration of labor costs over large geographic areas should result in lower JES plus LANDSAT costs per State.

Including all full State projects since the first full State project in Illinois in 1975, the majority of relative efficiencies at the sub-state level have easily passed the cost ratio criterion but results have been considerably more mixed at the State level. State level relative efficiencies vary according to the number of satellites available, the amount of cloud cover during the optimum window, and the timeliness and quality of LANDSAT data delivered to SRS.

However, there are several problems associated with the 1981 cost ratio criterion. One problem is that it does not reflect the benefits associated with keeping a staff trained in the technical knowledge of new and vastly improving satellite sensors. Another problem is that it doesn't reflect the benefits to SRS of the improved precision of major items (other than crop area) on the JES questionnaires that would occur if the sample size were increased. This second problem is somewhat diminished in that there exists some serious questions about whether or not it would be feasible to increase the JES sample size by a factor of 2-1/2 or more. With current budget restraints and limitations on both full and part-time staff, and the additional recruitment and training of JES enumerators required to increase the JES sample size, use of LANDSAT data becomes perhaps the only feasible alternative for future expansion of data collection for domestic crop area estimation.

9. SUMMARY

The cooperation of several U.S. government agencies (USDA/SRS, USDA/ASCS, NASA/GODDARD, NASA/ERL, NASA/JSC, NASA/AMES, USDI/BOD, USDI/EROS, and USDC/NOAA) was required to implement the 1980, 1981 and 1982 AgRISTARS DCLC Program. In 1980, more precise crop area estimates were provided using LANDSAT data in conjunction with ground gathered data for two states. Winter wheat harvested area estimates were provided for Kansas. Corn and soybeans planted area estimates were provided for Iowa. In 1981, more precise and timely crop area estimates were provided using LANDSAT data in conjunction with ground gathered data for four States. Winter Wheat harvested area estimates for Kansas and Oklahoma were provided to the SRS Crops Branch and the SSO's on October 30, 1981. Corn and Soybeans planted area estimates were provided to the Crops Branch and the SSO's on December 16, 1981, for Iowa and Missouri.

The SSO's played a key role in both projects. They performed field level edits, digitization, plotting, and both state and substate evaluation of the regression estimates.

Both projects were hampered due to problems in acquiring quality and timely LANDSAT data. In 1981, the project was hampered due to problems with the BBN computer system due to changes in their operating system as requested by the General Accounting Office (GAO).

10. ACKNOWLEDGMENTS

The authors wish to acknowledge the outstanding support provided by SRS's Remote Sensing Branch Support Staff (Sandra Stutson, Tjuana Fisher, George Harrell, Eric Hendry, Lillian Schwartz, Archie Nesbitt,

Pearl Jackson) and Ed Camara. Thanks also go to Robert Slye and Ethel Bauer of the NASA-Ames Research Center. JES cost data were provided by Larry Sivers, Ron Radenz, Jim Ramey and Wayne Gardner of SRS. The support of the Research Section of the Remote Sensing Branch and the four State offices (Kansas, Oklahoma, Iowa, and Missouri) in implementing this project is sincerely appreciated. Members of the following SRS work units also contributed to this project: Sampling Frame Development Section, Methods Staff, Enumerative Survey Section, Crops Branch and Systems Branch The cooperation of USDA/ASCS, NASA/GODDARD, NASA/ERL, NASA/JSC, NASA/AMES, USDI/BOD, USDI/EROS, and USDC/NOAA in implementing this program is appreciated. Special thanks to Yvonne Zamer and Mary Ann Higgs for their word processing efforts. Bob Losa prepared the figures.

11. REFERENCES

1. Cochran, William G. Sampling Techniques. Third edition, John Wiley and Sons, 1977.

2 Hanuschak, G., and others. Obtaining Timely Crop Area Estimates Using Ground-Gathered and LANDSAT Data. Economics, Statistics, and Cooperative Service, US Department of Agriculture, August 1979.

3. Ozga, M., W.E. Donovan, and C.P. Gleason. An Interative System for Agriculture Acreage Estimates Using LANDSAT. Proceedings of the 1977 Symposium on Machine Processing of Remotely Sensed Data, Purdue University, West Lafayette, Indiana.

4. Lennington, R.K., and M.E. Rassbach. Mathematical Description and Program Documentation for CLASSY, An Adaptive Maximum Likelihood Clustering Method. LEC-12177 (JSC-14621), April 1979.

5. "Scope and Methods of the Statistical Reporting Service", Miscellaneous Publication No. 1308, USDA, SRS, July 1975.

6. Swain, P.H. 1972. Pattern Recognition: A Basis for Remote Sensing Data Analysis. Laboratory for Applications of Remote Sensing, Purdue University, West Lafayette, Indiana. Information Note 111572.

TABLE 3. Cost of JES and JES + LANDSAT Comparisons 1/ (Dollars)

Relative Efficiency	1. Cost of JES 2/	2. Cost of JES Plus LANDSAT 3/	Cost Ratio (2 ÷ 1)
1.0	64,000	180,000	2.81
2.0	146,000	180,000	1.23
2.5	187,000	180,000	0.96
3.0	228,000	180,000	0.79
4.0	320,000	180,000	0.58
5.0	392,000	180,000	0.46

TABLE 4. Major Item Costs JES and JES + LANDSAT 1/ (Dollars)

JES Cost/State		JES + LANDSAT Cost (4 States) 3/	
SSO	55,000	SSO	50,000
DC Staff	7,000	DC Staff	210,000
MMDS	2,000	BBN	355,000
Total	64,000	EROS	25,000
		NASA (Ames)	25,000
		Travel	25,000
		Equipment	10,000
		Materials	20,000
		Total	720,000
		Cost/State	180,000

1/ Cost of initial area frame development and current sample size JES drawing is not included. This cost is approximately $80,000/state (1983 Nebraska cost projection).

2/ The cost of additional sampling and materials for relative efficiencies greater than 1.0 is included.

3/ Cost figures represent additional costs.

TABLE 5. JES and JES + LANDSAT Benefits

JES Costs	JES + LANDSAT Costs
$64,000/State and Increasing	$180,000 Additional/State and Decreasing
<u>Benefits</u>	<u>Benefits</u>
Objective Method	Objective Method
National and State Estimates (Multiple items)	Improved National, State and Sub-state Estimates (Major crops only)
Potential to do Land Cover area estimates (State Level)	No Additional Respondent Burden
	Research and Development and Utilization of an Improving Technology (Next Generation of Satellites)
	Public Relations Benefit
	Potential to do Land Cover Estimates (State and Sub-State)
	Procedure Uses <u>ALL</u> Crop Area Information in the JES

A CROP FORECASTING PROGRAM FOR BRAZIL USING EARTH OBSERVATION SATELLITE DATA

N.J. Parada
D.C.M. da Silva
F.C. de Almeida
F.R.D. Velasco
M.N. Barbosa
M.R. Dias
R.A. Novaes

Instituto de Pesquisas Espaciais
Conselho Nacional de Desenvolvimento Científico e Tecnológico
São José dos Campos, SP, Brazil

SUMMARY

It is well known that most of the developing countries, including Brazil, are having difficulties meeting their energy and food needs. As an attempt to deal with such difficulties, Brazil has been making heavy investments in agriculture. In this context, crop forecasting systems play a major role as effective tools for agriculture related policy making.

As a result, INPE (Brazilian Institute for Space Research) is engaged in a program that aims at the development of reliable, accurate and timely forecasting systems for several crops, based on satellite data.

With regard to energy, sugar cane has proved to be extremely important in alcohol production, and that is the reason why INPE has decided to start its program with the development of a sugar cane crop forecasting system. INPE's prior experience in estimating sugar cane acreage in the state of São Paulo, through visual interpretation of LANDSAT images, has encouraged such a decision.

Other crops such as soybeans and corn will be considered in later developments.

The crop production estimation will be attained through the independent estimation of acreage and yield. Satellite data will be extensively used in these systems: LANDSAT (3 and "D") images in the process of estimating crop acreage and, in addition to that, there exists a research effort to use data from meteorological satellite images which are relevant for estimating crop yield.

A description of the system and the results already obtained will be presented.

USE OF LANDSAT IMAGERY AND GROUND TRUTH INFORMATION TO PROVIDE CROP AREA ESTIMATES - THE CANDIAN EXPERIENCE

R.B. Proud

Agriculture Statistics Division
Statistics Canada
Ottawa, Ontario, Canada

SUMMARY

The Agriculture Division of Statistics Canada (Canada's Central Bureau of Statistics) is charged with the responsibility of providing area estimates of all crops grown in Canada. Such estimates are made during the growing season and at harvest time on a national, provincial and sub-provincial basis. These estimates have been based on the quinquennial census of agriculture with estimates for subsequent years derived from mail and enumerative surveys. To improve the timeliness and accuracy of crop estimates, the Agriculture Division in 1976 first examined the possibility of estimating crop areas using satellite remote sensing techniques. Since then projects have been conducted in co-operation with the Canada Centre for Remote Sensing and provincial government. Largely because of the lack of resources initial progress was slow but subsequent to 1980 an expanded program has lead to considerable success in this area.

It is proposed that an illustrated description of this work be presented at the poster session portion of the 16th International Symposium of Remote Sensing of Environment, June 1 - 9, 1982 in Buenos Aires. The subject of the presentation would be "Use of LANDSAT Imagery and Ground Truthing to Provide Crop Area Estimates – the Canadian Experience". The Agriculture Division would be assisted by the Canada Centre for Remote Sensing in the preparation of this presentation. Such a display would concentrate on the experience in New Brunswick where the system is not operational for potato estimates and in British Columbia and Alberta where estimation of rapeseed, grain and summerfallow area is at a preliminary stage. Plans for extension of the project to apples in Quebec and potatoes in Prince Edward Island would also be portrayed.

The main thrust of the presentation would be to demonstrate how ground data obtained by selecting ground segments from an area frame is used, first to train the computer to recognize individual target fields on the satellite imagery, and then to modify the first estimates using regression techniques. How area segments of approximately 700 hectares are outlined on air photographs and the fields of the target crops and confusion crops are identified by enumerators would be illustrated. Comparisons of the use of ratio and regression estimates would be made. Area estimates from remote sensing techniques would be compared with estimates from more conventional means. The presentation would be illustrated by colour photographs, maps and charts and would be in English and French (a requirement for all presentations by departments of the Government of Canada). the person from Statistics Canada attending the symposium and the poster session would be conversant in Spanish.

SPECTRAL SIGNATURE STUDY OF TWO SUBTROPICAL CROPS IN ARGENTINA

Dipl. Eng. Marcelo Campi
Ing. Agr. Luis Guillon

Comision Nacional de Investigaciones Espaciales
Buenos Aires, Argentina

SUMMARY

In order to study and differentiate some perennial crops among them (in the humid subtropical area), a spectral signature study was carried out.

Survey begun by taking aerial photographs at a very representative area, to use them as ground truth. This step is fairly important when surveying small farm areas, to avoid limit confusion.

Next step was crop placement in the LANDSAT image. For that purpose the following steps were carried out:

a) Histogram equalization (contrast stretching) to ease detailed image recognition.

b) Principal components were very useful when making out main typical features of the area, which in turn were used as references.

c) By band ratioing, vegetation was clearly distinguished from what is it not (5/7 band ratio). Even certain degree in vegetation differentiation was achieved. Likewise 5/6 band ratio turned out to be very useful to differentiate jungle from other vegetation types.

Next step consisted on specific crop delimitation, particularly for tea and yerba mate. That goal was achieved by means of clustering, which proved good accuracy in crop delimitation, as well as by training sets that confirmed clusters as statistically reliable.

The last step was supervised classification by maximum likelihood method, which allowed to release the final map at the area, where both crops were separated between them, and also from other classes (jungle, pasture lands, roads, etc.).

This procedure let us know that regarding crop delimitation, computer usually makes out more than one crop class within the same crop (according to different crop stages), which turns the survey more time consuming, but releasing a more accurate output.

RESEARCH IN SATELLITE-AIDED CROP FORECASTING

J. D. Erickson, J. L. Dragg, R. M. Bizzell, and M. C. Trichel
NASA Johnson Space Center/SH
Houston, Texas 77058, USA

ABSTRACT

Developments of efficient and accurate automated procedures for analysis of multitemporal Landsat multispectral scanner data to extract information on crop area and production can provide a greatly improved capability for practical and affordable use, on a global basis, without requiring ground observations. Evaluations of procedures developed specifically to estimate non-U.S. spring small grains area show accuracies of less than 10 percent relative difference to U. S. Department of Agriculture reference statistics for North Dakota in 1978 and good comparison with 9000 square miles of observations over four states (Montana, North Dakota, South Dakota, and Minnesota) and Saskatchewan, Canada during years (1976-79). Processing a 5x6-nautical-mile sample site requires a few minutes manual time and a few minutes central processing unit time on an AS-3000 computer. Evaluations of summer crop, corn, and soybeans area estimates show unbiased summer crops estimates in the U.S. central corn belt but significant bias in 1 of 2 years for area estimates of corn and soybeans. We expect, based on results to date, to achieve a highly automated corn/sorghum/soybean area estimation procedure that is applicable to Argentina.

1. INTRODUCTION

With the launch of Thematic Mapper only 1 month away, research in satellite-aided inventory and monitoring of global crop production continues to improve in current procedures and to make advances toward practical, viable systems capabilities. These capabilities, when added to current agricultural information systems, are expected to provide more timely and accurate non-U.S. crop information than is now available. Argentina is believed to be interested in such capability for its own crop information systems.

While the overall objective of this research[1] is to develop technology for extracting agricultural information of various kinds, the focus is on improved production forecast technology for assessing non-U.S. areas. The new technology will be evaluated by the U.S. Department of Agriculture (USDA) for possible integration into its information systems. More specifically, our objective is to develop procedures for using aerospace remote sensing and related technology at several times during the growing season to provide more objective and reliable crop area forecasts, with improved preharvest production estimates for selected countries and crops. This paper is a summary paper for others in these proceedings which give additional detail on selected topics.

We have adopted four criteria that reflect key characteristics of the technology and guide us in the research. These are timeliness, affordability, general applicability, and accuracy. Timeliness emphasizes the quick extraction of information. Timeliness is associated with early

season estimates, as well as with estimates made throughout the season. Affordability reflects efficiency and inexpensiveness. General applicability includes having suitable techniques in non-U.S. crop regions, as well as having objective and improvable procedures. Accuracy reflects the degree of bias and variance over time and responsiveness to factors affecting departures from average.

2. TECHNICAL APPROACH

The technical approach is to provide satellite-based, objective estimates of area, yield, and production as a set of inputs into a comprehensive, multidata source information system. The conceptual framework involves estimating crop area and yield for specified regions and multiplying the two to obtain production at the regional level. Automatic data processing approaches are considered necessary to provide objective, timely, and reliable estimates. Our research has been focused on the area estimation component; hence, further discussion will be oriented primarily to that component. Our estimation approaches are an extension of previous development[2]. Area estimates for regions are derived by processing statistical samples (called segments) of satellite digital image data (Landsat MSS). The desire is to estimate crop area periodically throughout the season from the time of planting through harvest.

Current approaches in crop area estimation utilize statistical sample survey methodology. Sampling methodology allows reliable estimates to be made by processing only a very small portion of the data. The efficiency of sampling is a function primarily of the variability in the feature to be sampled. Expansion of the sample estimates to a regional estimate is referred to as aggregation and is a statistical process made more complex by missed acquisitions, called non-response (generally because of intervening cloud cover) and partial response (generally when cloud cover only partially limits the level of information obtained).

Since non-U.S. ground data may be available in limited quantities for research studies but would not be available to support an operational system, and because of efficiency and timeliness considerations, our approach to non-U.S. crop forecasting does not require ground observations.

The variability in the crop scene environment among crop regions and countries is quite large. It is also strongly desirable to minimize human interaction for reasons of objectivity, repeatability, and efficiency. Hence, recent approaches have concentrated on the development of robust procedures that are largely self-adaptive in terms of recognizing crops based on their spectral signatures over time and distance. Some adaptation to specific crop regions is still necessary. The foremost challenge in satellite-oriented global crop forecasting is crop estimation without the ground observations that serve to train (adapt) remote sensing procedures which use them.

Technology development has been based on the use of extensive ground observations obtained in the United States where the reliability of the observations is understood. Regions in the United States that are similar to foreign crop regions of interest have been selected as study areas. Since true analogue regions do not exist, these foreign similarity regions in the United States are not completely suitable. Incremental testing over domains of greater variability of independent data sets is required. Even so, testing on such data sets is limited to the variability of available characteristics. However, by using the available data to establish the sensitivity of the methodology to these parameters, simulation techniques can be employed to establish the performance over a wider variety of conditions.

3. DESCRIPTION OF EXPERIMENTS

The objective in our research experiments has been to develop and evaluate state-of-the-art technologies for estimating area of spring small grains, summer crops, corn, and soybeans, in order to obtain an understanding of the limitations in performance so that R&D efforts may be focused on them. These experiments represent the first "independent" subsystem-level sensitivity tests against the adopted performance criteria of timeliness, affordability, applicability, and accuracy.

The technology that we developed for crop area estimation of spring small grains and that for summer crops, corn, and soybeans were at two different stages of maturity. For spring small grains, a technical breakthrough has been achieved (figure 1). A highly efficient state, from a man/machine systems point of view, has been attained by modeling the interpretive intelligence of skilled and expert image analysts in an automated and objective form — simple, artifical intelligence. Area estimation technology for the summer crops, corn, and soybeans, being 4 years later in initiation, was in a less mature stage of development and was less efficient. Thus, two separate experiments (one for spring small grains and one for summer crops, corn, and soybeans) were designed to optimize the evaluations of these technologies.

3.1 SPRING SMALL GRAINS

Area estimation technology available for evaluation produced regional aggregations as well as component crop area proportion estimates within sample segments.

The segment proportion estimation component was represented by two different technical approaches to the same basic identification scheme of determining different spectral crop appearance development over time. Both approaches exhibit an efficiency improvement, through automation, of an order of magnitude when compared to previous analyst intensive procedures (figure 2). The first procedure (SSG3C) is a completely automated modeling[3] of the previous manually intensive, skilled or expert analyst interpretative procedure. The basic functions are: acquisition selection based on meteorological variables and anticipated Landsat spectral responses for spring small grains; a transform of Landsat data to a level of greenness observed; an automatic, multitemporal, pixel-lableing logic based on a hierarchical process; and a proportion estimator based on a systematic sample of the labeled pixels. SSG3B (same technical approach as SSG3C) which allows an analyst override of the automatic acquisition-selection was also developed[3] and evaluated in this experiment.

The second proportion estimation approach (SSG4) was also completely automatic.[3] The basic functional differences between this approach and that of the SSG3 were: the Landsat data were transformed by a mode which "normalizes" color; a "field" finding algorigthm groups the individual pixels into quasi-fields; the quasi-fields were labeled by a multitemporal logic of "green/not-green" sequence; and the proportion estimate was derived from an enumeration of the labeled fields plus an adjustment for estimated omission rates.

A major objective of the experiment was to ascertain if the cost benefits of procedure automation could be achieved with accuracy comparable to that of the analyst-intensive procedures. Historical, analyst-intensive, sample-segment proportion-estimation procedures in the U.S. spring small grain region were traditionally biased (large mean error, generally negative) yet relatively consistent (small variance). It was anticipated that these automatic procedures in their attempt to capture a significant portion of the crop scene variability within the model (i.e., be unbiased estimators) would probably exhibit a larger variance.

The Landsat data used for the small grains experiment consisted of 300 sample segments collected over a 4-year period (1976-1979) covering the U.S. Northern Great Plains (North Dakota, South Dakota, Montana, and Minnesota) and Saskatchewan, Canada. There were 63 segments from 1976, 91 from 1977, 85 from 1978, and 61 from 1979. Only segments that had ground observations for evaluation were analyzed, with the exception of an additional 65 samples from 1978 of North Dakota in which all allocated Landsat segments were included to support aggregation studies.

The 1976 crop year in this region was warmer than average. The crop season was earlier than average, as was the case in 1977, even though the temperature was near average. The 1978 crop year was cooler than average, which gave normal-to-late planting dates. Late planting was experienced in 1979 as well.

Ideally, the data set for this experiment would be completely representative of non-U.S. crop regions. While it is not, it is the most extensive data set ever used in this type of testing, including about 9,000 square miles of ground observations spread through four states and one province over 4 crop years.

AD-A134 719 PAPERS SELECTED FOR PRESENTATION AT THE INTERNATIONAL SYMPOSIUM ON REMOTE..(U) ENVIRONMENTAL RESEARCH INST OF MICHIGAN ANN ARBOR JUN 82

2/6

UNCLASSIFIED F/G 14/5 NL

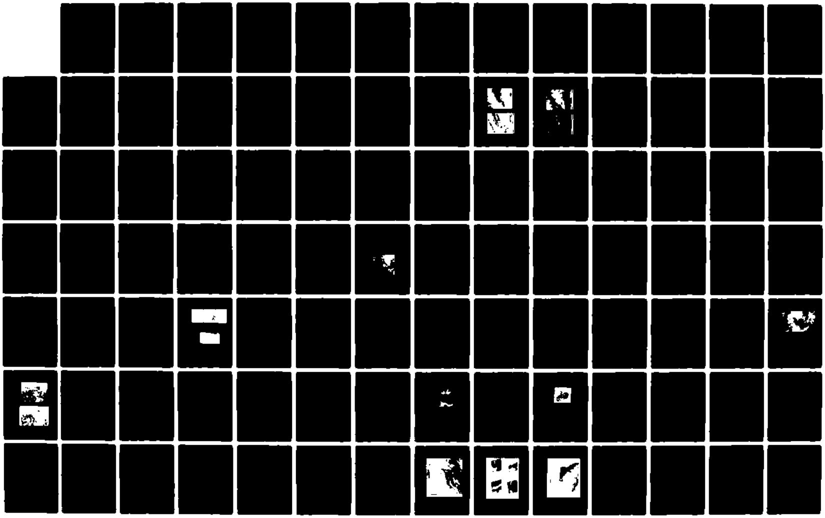

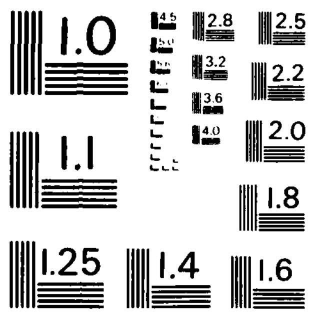

MICROCOPY RESOLUTION TEST CHART
NATIONAL BUREAU OF STANDARDS-1963-A

3.2 SUMMER CROPS

The level of evaluation of summer crops, corn, and soybeans technology was more limited in both scope and purpose due to its less mature state. The results of this experiment would provide identification and quantification of the major subcomponent contributors to the proportion estimation error for future developmental modification prior to the development of an automatic processing approach.

The summer crops, corn, and soybeans proportion estimation technology (called CS-1) performed functions similar to the small grains procedures, such as: Landsat data transformation and feature extraction, target definition and stratification, labeling, within-segment sampling, and proportion estimation. However, the design of the experimental procedure was analyst intensive and structured to allow the tabulation of results at each detailed procedural step for subsequent evaluation and performance analyses.

The Landsat data for the summer crops, corn, and soybeans experiment consisted of 18 sample segments from the 1978 crop year and 10 sample segments from the 1979 crop year. A large data base for evaluation, such as was available for small grains, does not yet exist for corn and soybeans. These segments were drawn from the U.S. Central Corn Belt states of Iowa, Illinois, Indiana, and Missouri.

4. RESULTS

4.1 SPRING SMALL GRAINS EXPERIMENT[4]

4.1.1 North Dakota Aggregations.

The accuracy of these procedures developed specifically to estimate non-U.S. spring small grains area, was performed with data for areas in the United States and Canada (where reliable reference data were available) before attempting adaptation. The results of North Dakota aggregations for 1978 data are (percent relative error and coefficient of variation): +3.5 (C.V. = 4.4), +6.9 (C.V. = 4.3), and -9.2 (C.V. = 4.6) for SSG3B, SSG3C and SSG4 respectively.

The accuracy is expressed relative to the published USDA estimate of the spring small grains acres harvested in North Dakota during 1978 (13.12 million acres).

4.1.2 Subsystem Level Results.

The sample segment proportion estimation accuracy performances are shown in figure 3. The results shown include all segment analyses including machine errors, clerical errors, and otherwise outliers. (These unedited results are also included in the aggregations.) The intent was to identify and quantify all potential contributions to error without regard to producing the best estimate. By not thresholding seemingly obvious outliers, we optimize the probability of isolating the major subcomponent error contributors. Even with this, it was somewhat encouraging that the mean absolute error in most cases was less than 10 percent. Also, the results, when compared to the more labor-intensive historical procedures, verify what was expected, i.e., generally comparable with lower bias and somewhat larger variance.

An indication of the possible performance of the technology for a key foreign region was shown for segments within a previously determined USSR Foreign Similarity Region (FSR) where similar performance to the above was obtained. (See figure 4.)

In general, the automatic procedures currently provide estimates for fewer segments (50 percent to 65 percent processability of total allocated) compared to the historical manual procedures (75 percent).

In terms of the other performance criteria, figure 2 shows a summary of key efficiency parameters related to affordability. Although neither the historical nor the current automated technologies were engineered nor implemented for an operational environment (substantial overhead is necessary in an experimental mode for recording of intermediate output), the

relative improvements exhibited by the automated technologies is obvious. The timeliness in the growing season is some 30 days prior to harvest.

In summary, this first-time evaluation of highly automated, spring-small-grains area-estimation technologies was very encouraging. There was definite improvement in the near-harvest estimation efficiency with modest losses in accuracy as compared to best previous analyst-intensive approaches. For the 1-year, one-state (1978 N.D.) aggregation, no glaring deficiencies were noted. The attractive characteristics of low processing cost, objectivity, repeatability, modularity, and adaptability packaged within an automated framework make the outlook for meaningful advancements very optimistic.

4.2 SUMMER CROPS, CORN, AND SOYBEANS EXPERIMENT[5]

This experiment in summer crops, corn and soybeans proportion estimation technology represents our first attempt to take advantage of an improved systems approach to research. It allowed the effective utilization of the experimental environment for more iterations of development, testing, and feedback to research than heretofore achievable in a given time (such as 6 months).

Figure 5 shows our accuracy results (in terms of mean error and 90-percent confidence limits) for the previously described for crop years 1978 and 1979.

The following are some additional observations:

1. There is a very accurate estimate of crop group (summer crops) with relative mean error (RME) less than 2 percent in both years.

2. For crop type (corn and soybeans) there was a significant bias (corn RME 15 percent, soybeans RME -19 percent) in one of the years (1978).

3. The crop type bias for the other year (1979) was not significant (corn RME 6 percent, soybeans RME 3 percent)

4. The direction of the bias for crop type appears to be consistent between years (corn tends to be overestimated, soybeans tends to be underestimated.

5. The standard deviations for all estimates are relatively consistent and comparable to those achieved in previous "best" spring small grains technologies.

6. Compared to a previous procedure for the 1978 crop years, CS-1 exhibited a significantly lower bias in estimating crop group (summer crop RME -1.5 vs. -16.4 percent) with lower standard deviations for both crop groups and crop types.

In terms of the other preformance criteria the following was observed:

1. Timeliness - processing to crop type is achievable after corn tasseling, which is 30-45 days prior to harvest. This is about the middle of August in the U.S. Corn Belt.

2. The rate of processability of allocated segments with the CS-1 technology was quite high, typically 50 percent to 75 percent.

Quick identification of subcomponent error contributors was achieved. These specific results have led to the earlier-than-planned development of a more-automated summer crop, corn, and soybeans proportion estimation procedure. The process of making the developmental modifications for a new version (CS-1A), conducting a verification test, then designing and implementing a semiautomatic version (CS-1B) has already been accomplished. Results of early verification testing over a sample (10 segments) of the 1978-79 data set show excellent summer crop accuracy[6] and corn and soybeans accuracy of about 10 percent RME and standard deviations of 4 to 6 percent.

The results of this experiment are very encouraging because the developmental time frame (including procedure development, testing, identification of limitations, and procedure improvement) was accomplished in about one-fifth the time of previous research in this area. Additional improvements are expected in this technology.

5. TECHNOLOGY FOR THE ARGENTINE CROP REGION[7]

Significant differences exist between the Argentina Indicator Region[8] (see figure 6) and the U.S. Corn Belt. These differences affect the subcomponents of the technology in such a way as to require adaptation to achieve adequate performance. A milder climate, a more varied crop mix, and distinctly different agronomic practices differentiate the Argentina Indicator Region from the U.S. Corn Belt. The agronomic differences typically include much lower levels of fertilizer consumption and less agricultural mechanization in Argentina.

The following factors have important implications for area estimation techniques as they relate to Argentia:

(a) Planting and harvesting dates can vary considerably. This is due to episodal events such as heavy rains, drought, or a longer growing season.

(b) The area planted to corn in marginally dry areas can be radically affected from year to year, as well as through the season, due to drought. Conversely, soybeans in more humid areas are subject to water stress during and immediately following periods of heavy rains. In the case of both crops, the area harvested can therefore be substantially lower than the area planted, as a result of these events.

(c) Agricultural land-use shifts may be large and made on a real-time basis by farmers, due to sudden changes in market prices.

(d) Sorghum can be a confusion crop for corn, and to a lesser extent, peanuts and soybeans could be confusion crops. The percentage of land devoted to beef cattle pasture, even in the most intensively cultivated areas, is much higher than in the U.S. Corn Belt.

(e) Weed-infested corn and sorghum fields are common. To a lesser degree this is also true of soybeans.

Corn and soybean production is expected to remain a key factor in the Argentine agricultural economy along with wheat and sorghum production. Corn and soybeans continue to be in demand in the world marketplace and Argentina's recently concluded bilateral trade agreements with the Soviet Union, the People's Republic of China, and Mexico, along with export committments to other countries, would seem to guarantee foreign sales of Argentine crops in the foreseeable future. However, inflation, high production costs, and changing market prices must also be faced by Argentine farmers. These factors will ultimately influence the area planted in corn and soybeans, as will environmental conditions.

Such factors must be taken into account in adapting procedures to estimate corn/sorghum/soybeans areas in Argentina.

6. SIGNIFICANCE OF RESULTS

The significance of the present results is threefold:

1. We are able to adequately model the subjective human analyst with an objective process and achieve reasonable accuracies.

2. We were thereby able to develop an information extraction technology which was not prohibitively costly either in terms of manual effort or computational resources. It is affordable within a reasonable standard.

3. If the results reported here could be achieved for foreign regions, substantial improvements in global crop information would result.

This should not suggest that the non-U.S. crop forecasting problem is solved, as several key research problems remain. Briefly, the most critical of these are:

1. Improving the automated selection of acquisitions.

2. Finding methods to estimate crop areas much earlier in the season.

3. Early quantification of the benefits of improved performance of this technology due to the features offered by the Thematic Mapper.

4. Adapting these objective analysis methods to other crops and regions without requiring information which is not available in non-U.S. situations.

5. Finding information extraction methodologies which reduce the quantity and quality of the data required, thus reducing data costs.

6. Doing adequate testing and evaluation to understand the technology performance.

We feel that the present results represent a real break-through both in approach and practicality. We expect, based on results to date, to achieve in the future a highly automated corn/sorghum/soybeans area estimation procedure applicable to Argentina.

ACKNOWLEDGEMENTS

We wish to thank the many professionals of the joint agency and contractor team who have contributed to the research reported here.

REFERENCES

1. AgRISTARS Annual Report for FY81 AP-J2-04225, NASA Johnson Space Center, Houston, Texas, January 1982, pp. 9, 10, 22-30.

2. R. B. MacDonald and F. G. Hall, Science 208, 670 (1980).

3. J. T. Waggoner and D. E. Phinney: Project Procedures Designation and Description Document, Vol. I. FC-L1-00715/JSC-17154, NASA Johnson Space Center, Houston, Texas, June 1981.

4. FCPF Preliminary Technical Results Review/Spring Small Grains, Vol. I., FC-J1-04175/JSC-17433, NASA Johnson Space Center, Houston, Texas, September 28, 1981.

5. FCPF Preliminary Technical Results Review/Corn and Soybeans, Vol. II., FC-J1-04175/JSC-17433, NASA Johnson Space Center, Houston, Texas, September 29, 1981.

6. ITD Semi-Annual Review to Level I, IT-J2-04267/JSC-17830, NASA Johnson Space Center, Houston, Texas, April 15, 1982.

7. D. R. Hicks, "Agronomic Characterization of The Argentina Indicator Region," SR-E2-04222/NAS9-15476, ERIM, Ann Arbor, Mich., January 1982.

8. C. J. Ramirez and C. R. Reed, "Selection of the Argentine Indicator Region," IT-L1-04132-17408, NASA Johnson Space Center, Houston, Texas, March 1982.

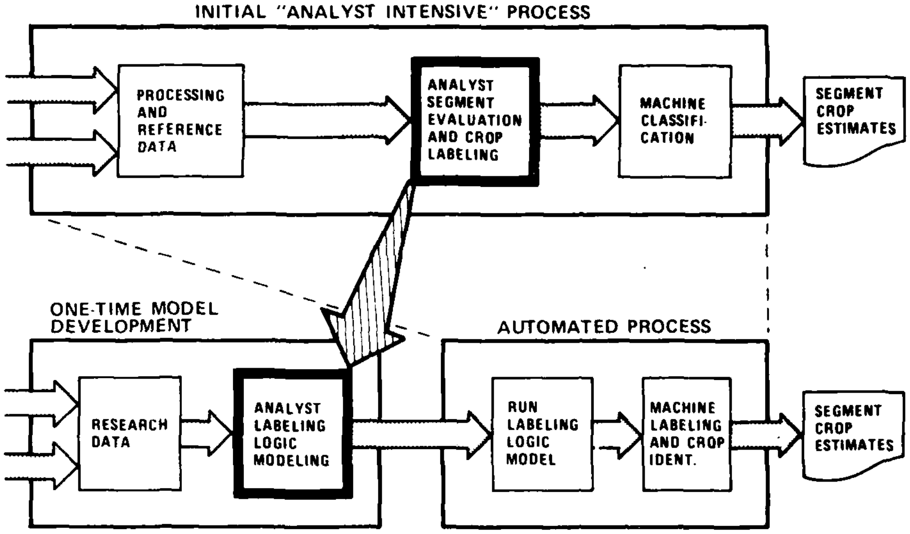

Figure 1. Technical breakthrough (modeling of analyst function enabled automatic processing).

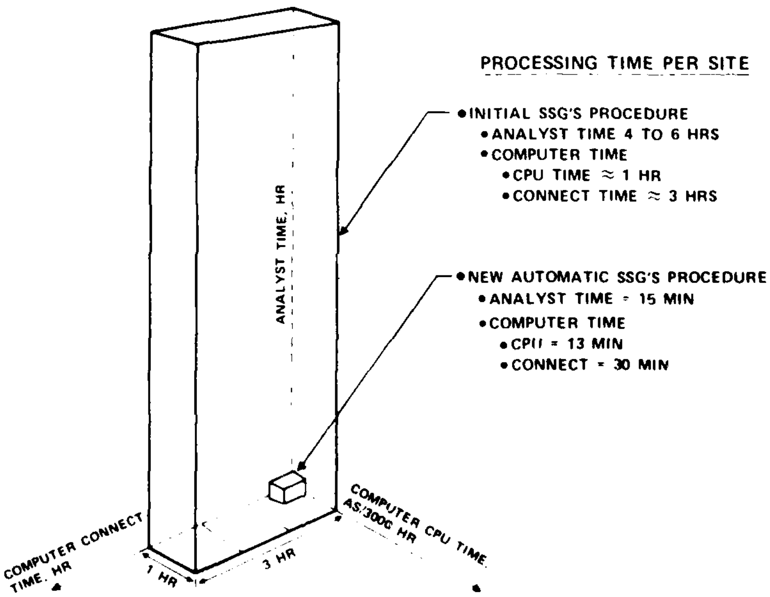

Figure 2. Improved efficiencies of automated information extraction process.

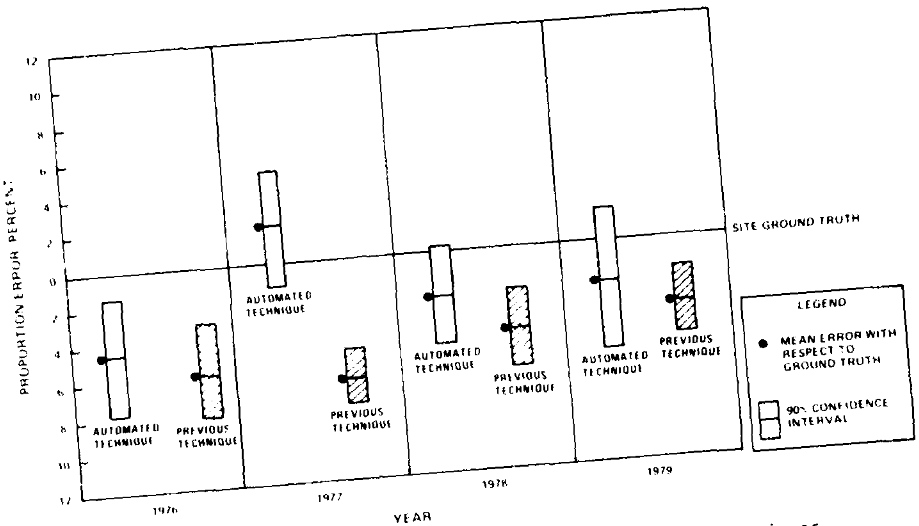

Figure 3. Accuracy comparisons of spring small grains techniques.

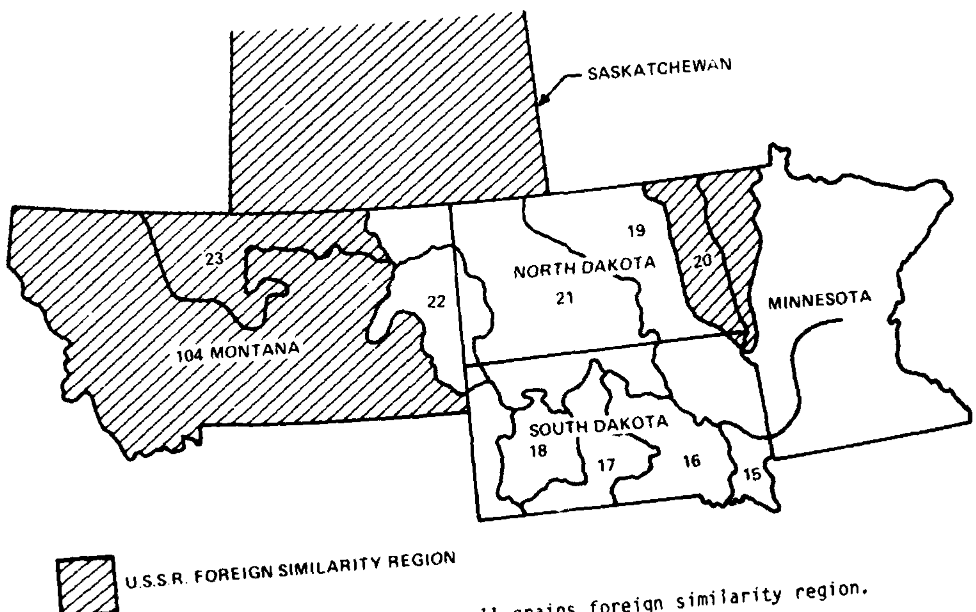

Figure 4. U.S.S.R. spring small grains foreign similarity region.

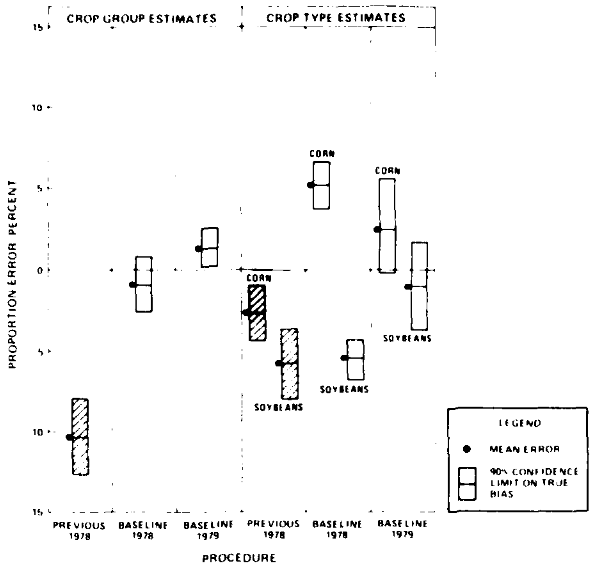

Figure 5. Comparison of corn and soybean baseline subsystem with previous results.

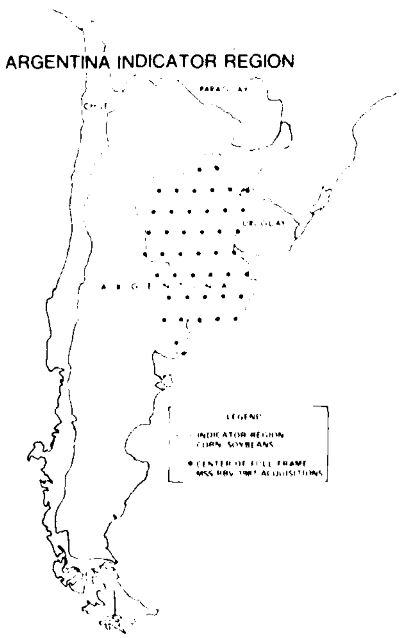

Figure 6. Argentina corn and soybeans indicator region.

ARGENTINE CROP ESTIMATION PROGRAM

Francisco V. Redondo

Comisión Nacional de Investigaciones Espaciales
Buenos Aires, Argentina

SUMMARY

The feasibility of Landsat data analysis for agricultural studies and crop recognition are well known, so crop forecasting can be objective, reliable, time oportune and economic when satellite information is used in conjunction with ground data.

The present official production forecast procedures in Argentina can be improved in some of those characteristics using satellite information. The Argentine crop estimation program using remote sensing techniques was initiated in 1980 with the support of P.N.U.D. and the cooperation of the Secretary of Agriculture and Livestock.

The Pradera Pampeana (the major agricultural area of about half million km^2) was chosen for the development and the implementation of the methodology. Crop production forecast is made by multiplying area estimation times yield prediction.

- Area estimation subsystem: Visual analysis of historical series and present data of Landsat imagery were used for the stratification of the Pradera Pampeana in land use homogeneous areas. A sampling design was done in order to work within homogeneous strata. Digital analysis was carried out on administrative defined pilot areas. Aerial photographs (B&W and CIR) were taken and several field trips took place. Wheat (the main crop) and small grains were studied and area estimated during the crop years 80/81 and 81/82. Summer crops (corn, sunflower and soybean) were analyzed during the last year.

- Yield prediction subsystem: Agrometeorological models were used for yield prediction of the most important crop. A data bank was created with historical meteorological and crop statistic data. The approach included wheat, corn and soybean in the project pilot areas. Several programs were implemented in order to calculate agroclimatic index for crop monitoring. With the same objective satellite information (meteorological and Landsat) is going to be studied to join the present approach in precipitation, cloud cover and growing conditions analysis.

The results are satisfactory; area estimation in pilot areas gave reliable and oportune information compared with final official figures. The agrometeorological models are going to be used in this crop year.

SOIL LOSS PREDICTION IN A GEOGRAPHIC INFORMATION SYSTEM FORMAT*

Michael A. Spanner

Technicolor Government Services Inc.
Ames Research Center
Moffett Field, CA, 94035

Alan H. Strahler

Department of Geology and Geography
Hunter College of City University of New York
New York, New York

John E. Estes

Department of Geography
University of California
Santa Barbara, CA, 93106

ABSTRACT

Soil loss due to erosion from rainfall was accurately predicted for the Santa Paula 7.5 minute quadrangle, Ventura County, California, utilizing the VICAR/IBIS image processing and geographic information system to simulate the Universal Soil Loss Equation (USLE). This work was part of a NASA funded research project investigating methods of incorporating collateral information in Landsat classification and modelling procedures (NSG-2377), performed at the University of California, Santa Barbara. Representing the rainfall, soil erodability, length of slope, slope gradient, crop management and soil loss tolerance coefficients of the USLE were data planes generated from digital Landsat data, USGS Digital Elevation Model topographic data, a digitized NOAA isopluvial map and digitized USDA soil conservation service soil maps. The Pearson product moment correlation coefficient, R, of soil loss predicted from the developed geobased model to a sample of manually derived soil losses was .91 after a log transform, significant to the .0001 level. Estimates of accuracy for the intermediate data planes representing the rainfall, soil erodability, length of slope, slope gradient, crop management and soil loss tolerance ranged from a correlation coefficient, R, of .81 for the length of slope to 100 percent for the rainfall coefficient. The soil loss information system accurately targeted soil loss problem areas for subsequent analysis by Soil Conservation Service personnel.

1. INTRODUCTION

Soil loss due to erosion from rainfall is a serious problem in the United States and the world. The Pacific Southwest Inter-Agency Committee estimated in 1971 that sixty-five percent of the agricultural regions in the United States

*Presented at the Seventeenth International Symposium on Remote Sensing of Environment, Ann Arbor, Michigan, May 9-13, 1983.

require some form of erosion control. The purpose of this paper is to demonstrate the potential of Landsat multispectral scanner data, digitized United States Department of Agriculture Soil Conservation Service (USDA SCS) soil maps, digitized National Oceanic and Atmospheric Administration (NOAA) precipitation-frequency maps, and United States Geological Survey (USGS) Digital Elevation Model (DEM) topographic data in a geographic information system to simulate the Universal Soil Loss Equation.

The Universal Soil Loss Equation, developed by the USDA Soil Conservation Service, predicts sheet and rill erosion due to rainfall in agricultural regions (Wischmeier and Smith, 1965). Variables of the Universal Soil Loss Equation are coefficients of rainfall, soil erodability, length of slope, slope gradient, crop management and conservation practice. The collection of the variables to the USLE is accomplished by Soil Conservation Service personnel on a per site basis. From tables and charts (USDA Science and Education Administration, 1978), as well as measurements obtained in the field, a prediction of soil loss is calculated for an area in terms of tons of soil lost per acre per year. Sites may range from one to ten acres in extent, depending on the homogeneity of the location.

Input of the Universal Soil Loss Equation to the Video Image Communication and Retrieval Image Based Information System (VICAR/IBIS), allowed a more extensive area to be assessed for erosion potential by representing each site on a georeferenced grid. Variables from the USLE for the Santa Paula 7.5 minute quadrangle in southern Ventura County, California (figure 1), were input to VICAR/IBIS; deriving a prediction of soil loss in tons per acre per year for this mixed agricultural and rangeland location.

2. BACKGROUND

The Santa Paula 7.5 minute quadrangle is located in the northeastern portion of the Oxnard Plain, a fertile region of prime agricultural land. Approximately one-half of the quadrangle is composed of the relatively flat Las Posas Valley and Santa Clara River floodplains. Lemon, orange and avocado orchards as well as row crops such as lettuce and celery predominate on the rich soils of the lowlands. The other half of the quadrangle consists of the marine sedimentary sequences of South Mountain. Slopes here exceed 100 percent in some locations. Vegetation on South Mountain is mainly Mediterranean annual grasses and chaparral, with a small oak woodland community.

Increasing accumulations of sediment are being deposited in the drainage ditches, and ultimately in Mugu Lagoon, a terminus of drainage for this watershed. The siltation of Mugu Lagoon is largely due to the poor soil conservation practices, sparse grass cover and frequent fire in the upper portion of the watershed. New avocado orchards are being introduced in the canyons extending into the steeper mountainous areas. The sparse ground cover provided by the immature avocados in conjunction with steeper slopes, have created a potential soil loss problem. Overgrazed Mediterranean annual grasses in the foothills inadequately protect the soil from rainfall induced erosion. Three fires have occurred in the South Mountain area since 1980, removing the natural vegetative cover, and resulting in increased soil erosion rates.

Major planning and construction efforts are necessary to accomodate the increased sediment load. The USDA Soil Conservation Service in Somis, California, as well as the U.S. Army Corps of Engineers, the Ventura County Water Agency and the California Coastal Commission are actively pursuing solutions for the problem of soil loss within the Oxnard Plain drainage. These agencies are concerned with sediment loss reducing crop productivity, as well as the problem of sediment accumulation in the upper watershed and in Mugu Lagoon. A prediction of erosion rates for the watershed will allow the Soil Conservation Service to delineate problem areas and implement appropriate conservation practice techniques.

3. SOIL LOSS PREDICTION

A number of models have been developed to predict erosion and sediment yield, and with few exceptions these models are based on soil, geologic, climatic, topographic, vegetative and land use/land cover information. Musgrave (1947) presented a first quantitative evaluation of factors in sheet erosion, based on soil, crop cover, degree of slope, length of slope and precipitation information. Meeuwig (1971) developed a model that predicted soil stability on high elevation rangeland using soil, vegetative cover, slope and organic matter parameters. Foster and Meyer (1971) developed a mathematical relationship for the continuity-of-mass transport, and an equation relating detachment of sediment by runoff and sediment load. For known soil, precipitation and topographic characteristics, the erosion pattern along a slope was predicted. A practical model for predicting mass wasting events was presented by Swanston et al. (1980) based on a general evaluation of the stability of an area using climatic, topographic, vegetative, geologic and soil characteristics from aerial photographs, maps, field observations and a limited strength-stress analysis. The models described above are not suitable for soil loss prediction within a geographic information system for one or more of the following reasons:

(1) Inappropriate for generating image datasets (Meeuwig, 1971, Foster and Meyer, 1972);

(2) Limited applicability to a mixed agricultural and rangeland region (Meeuwig, 1971, Swanston et al., 1980); and,

(3) Insufficient quantitative verification of the model (Musgrave, 1947, Swanston et al., 1980).

Universal Soil Loss Equation

The Universal Soil Loss Equation developed by the United States Department of Agriculture Soil Conservation Service is appropriate with respect to the three categories previously discussed for geographic information system soil loss modeling. The USLE predicts sheet and rill erosion due to rainfall for agricultural regions in terms of tons of soil loss per acre per year. The Universal Soil Loss Equation was originally developed from 10,000 plot years of runoff and soil loss data collected from forty-seven research stations in twenty-four states. Studies were undertaken which measured the contribution of rainfall, soil properties, slope angle, length of slope, crop management and conservation practice to the loss of soil (Wischmeier and Smith, 1965). A prediction of soil loss was obtained for regions east of the Rocky Mountains. Recent work has extended the USLE to the entire United States, including range and forest lands (USDA Science and Education Administration, 1978).

The basic soil loss equation is:

$$A = R * K * L * S * C * P$$

where:

A = Predicted soil loss in tons/acre/year,
R = Rainfall Factor,
K = Soil Erodability Factor in tons/acre/year,
L = Length of slope Factor,
S = Slope Gradient Factor,
C = Crop Management Factor,
P = Conservation Practice Factor.

R, L, S, C and P are dimensionless coefficients. The product of R, K, L, S, C and P provides an estimate of soil loss measured in tons per acre per year. A soil loss tolerance has also been calculated; the maximum permissible annual soil loss, ranging from one to five tons per acre per year (USDA Agricultural Research Service, 1961). A site has a potential soil loss problem if the

the predicted A value exceeds the T value for that location.

Soil Loss Information System Models

Remotely sensed data have been used to derive specific coefficients of the Universal Soil Loss Equation. Morgan et al. (1979) used color and color infrared 70 mm photography at a scale of 1:60,000 to calculate the crop management (C) factor of the USLE. In a later study, Morgan et al. (1980) used the same imagery to determine the conservation practice (P) factor. Stephens and Cihlar (1981) calculated the correlation between the ratio of the near infrared/red reflectance to the C coefficient of the USLE using simulated SPOT 1, Landsat D and Landsat 1 data in a region composed of pasture, forest and cropland.

Past implementation of the USLE into geographic information systems for soil loss prediction have been subject to the reliance on manual derivation of topographic data and/or varying sources of crop management information. Singer et al. (1976) developed a computer simulation of soil loss using the Universal Soil Loss Equation in which vegetation maps provided the crop management factor and the topographic data were manually derived from topographic sheets for a rangeland site in northern California. Patterson and McAdams (1980) input the USLE to a geographic information system to produce erosion hazard potential maps using Landsat MSS data for the image base and soil maps to derive the slope and length of slope information. Berger and Jensen (1980) modelled flood potential due to urbanization in a humid subtropical southeastern environment. Large scale, 1:6,000 color and black and white photographs provided land cover information; slope and slope length data were obtained from the photographs in conjunction with 7.5 minute topographic maps. An automated data base approach for prediction of deforestation induced mass wassting was accomplished by Logan (1981) through a modification of the Swanston et al. model using Landsat and Defense Mapping Agency (DMA) Digital Terrain Tapes. However, this model is best suited for a forested watershed; it's applicability to a mixed agricultural and rangeland location is questionable. The need exits for development of an automated GIS for soil loss prediction in an agricultural region. The following sections describe such a system.

4. APPROACH

Digital image processing for this soil erosion study was performed on the Video Image Communication and Retrieval Image Based Information System (VICAR/IBIS). Originally created to process image data from planetary exploration programs, VICAR has been expanded to include applications in earth resources, land use, biomedicine and astronomy. IBIS is a geographic information system which allows the conversion of georeferenced data to an image format for use with remotely sensed data. IBIS was built upon VICAR, permitting image to image registration; whereby images of different scale from any number of datasets can be superimposed, allowing corresponding pixels to represent the same geographic location (Bryant and Zobrist, 1976).

Geobased Data

The isopluvial map for the Ventura County area, obtained from the NOAA Precipitation-Frequency Atlas of the Western United States (Millet et al., 1973), was the source of the rainfall coefficient. USDA Soil Conservation Service soil maps at a scale of 1:24,000 and corresponding to the USGS 7.5 minute quadrangle provided the soil erodability and soil loss tolerance information. Digital Elevation Model topographic data obtained from the National Cartographic Information Center provided the slope and length of slope coefficients. DEM are processed to yield one Digital Elevation Model for each 7.5 minute quadrangle, with a spatial resolution of thirty meters and a root mean square (RMS) elevation error of seven meters. DEM are a vast improvement over Defense

Mapping Agency (DMA) Digital Terrain Tapes, which are generated from 1:250,000 scale topographic maps and are sampled to a 225 foot horizontal grid. Digital Landsat Multispectral Scanner (MSS) data from Landsat 2 collected on June 14, 1978 for the Santa Paula area were used to calculate the crop management factor.

Registration of Data Planes

Variables of the Universal Soil Loss Equation were transformed into georeferenced digital data planes generated from these data sources using VICAR/IBIS (figure 2). The raw Landsat data were registered to the Santa Paula 7.5 minute topographic quadrangle through the use of ground control points and a rubber sheeting algorithm. A bilinear resampling of the Landsat data to sixty meter square pixels (0.9 acre), generated a 231 line by 192 sample image. Sixty meter square pixels served as the basic resolution unit for this study because sixty meters is an even multiple of the thirty meter Digital Elevation Model. The rainfall, soil erodability and soil loss tolerance images were generated and registered to the sixty meter square, 231 line by 192 sample grid by IBIS and supplemental digital processing routines which converted digitized vector map boundaries to raster data planes. DEM, the source for the slope and length of slope coefficients was registered to the grid using ground control points and a rubber sheeting algorithm with nearest neighbor resampling. The 231 line by 192 sample sixty meter square grid was outlined on the Santa Paula topographic sheet, facilitating registration and accuracy assessments. Sub-pixel registration accuracy was accomplished for all data planes.

Intermediate Data Plane Processing

Rainfall (R) coefficients were derived from SCS curves relating two-year six-hour precipitation to the rainfall factor (USDA Soil Conservation Service, Davis, 1977). Isopluvials from the NOAA Precipitation-Frequency Atlas were transferred to the Santa Paula 7.5 minute quadrangle, digitized, and then converted to a raster dataset of isopluvial borders. Next, the ispoluvial borders were converted to an image with a unique digital number (DN) assigned to each polygonal rainfall region. Finally, an R coefficient was assigned to each polygon.

The SCS have developed soil erodability (K) coefficients for the soil series and soil phases found in Ventura County (USDA Soil Conservation Service, Ventura County, 1969). Soil boundaries corresponding to the series and phases from the SCS soil maps were digitally encoded and converted to a raster data set. The raster image of soil polygon borders was transformed to an image in which each polygon was represented by a unique DN. Final editing assigned a K coefficient to each of the rasterized polygons.

The length of slope (L) variable is defined by the SCS (Zingg, 1940), as the distance from a point in a watershed to the source of runoff for that point, generally a ridge or a hilltop. An algorithm was developed to compute length of slope from Digital Elevation Model topographic data. The algorithm creates a three by three moving window which follows the direction of steepest slope. The Pythagorean distance between the center cell and the steepest cell surrounding it is calculated, and the cell representing the steepest slope then becomes the origin for the next move of the three by three kernal. The steepest slope from the new origin is determined and the Pythagorean distance is again calculated. This cell becomes the new origin. The window continues its movement until the slope drops off in all directions, indicating that the source of runoff for the initial cell has been located. The sum of the distances for all the previous moves is determined and tallied to the initial cell. Movement of the window is limited to forty-five degrees from the previous move to more closely simulate real runoff conditions. The slope length for each cell was then converted to the L coefficient using the relation: $L = (\lambda/72.6)^{0.5}$, where λ equals the slope length in feet, as defined by the SCS (Wischmeier et al. 1958) (figure 3).

Slope gradient (S) was calculated from the Digital Elevation Model by determining the gradient of a plane tangent to the centerpoint of a three by three window of the DEM. The four nearest neighbors of each cell were used to calculate the slope gradient of the plane in radians, and then converted to percent slope to correspond to the SCS slope factor. For slopes less than nine percent, the relation: $(0.43 + 0.30S + .043S^2) / 6.617$, where S equals percent slope was used to translate the slope gradient to the S factor. For slopes exceeding nine percent, $(S/9)^{1.3}$ defined the S coefficient (USDA Soil Conservation Service, Davis, 1977). By applying the appropriate equation an S value was assigned to each cell.

The crop management (C) factor is based on the type of crop or vegetative cover in a specific area, and the protection it provides against erosion (Wischmeier, 1960). An unsupervised clustering algorithm was applied to the registered raw Landsat data to derive crop management classes. After spectral editing, 100 clusters were retained for input to a multispectral classifier which combined paralellepiped and Bayesian maximum liklihood techniques. A CRT display of the 100 classes in conjunction with 1:32,000 scale color infrared (CIR) photographs, the 7.5 minute quadrangle and field inspection were used to label the classified clusters to their proper crop management class. Ten classes were developed to distinguish the different effects crop management practices have on erosion potential: mature orchard, immature orchard, row crop, river, urban, dense sod, chaparral, grass, oak woodland and barren.

Unfortunately, Landsat spectral data did not provide sufficient information to allow accurate discrimination between orchards and natural vegetation. From examination of the 7.5 minute quadrangle, field inspection and air photo interpretation, it was apparent that few orchards existed above 800 feet or on slopes exceeding ten degrees. Therefore, a binary mask was created using the DEM elevation and slope information identifying all elements greater than 800 feet in elevation and all slopes greater than ten degrees. Cells less than 800 feet in elevation and with a gradient of less than ten degrees retained cluster numbers 1-100. Cells with an elevation exceeding 800 feet and/or with a gradient exceeding ten degrees were renumbered 101-200. The 200 classes were then labelled into the ten crop management classes (figure 4). The stratification accurately separated orchards from natural vegetation. C coefficients were assigned to each of the crop management cover classes according to guidelines set by the SCS.

Conservation practices (P) are defined by the SCS (USDA Science and Education Administration, 1978), as techniques which decrease the loss of soil by reducing the effective slope length. These techniques include such practices as contouring, contour stripcropping and terracing. These practices, however, are not resolvable on Landsat, nor available as collateral data; therefore, the P coefficient was not applied in this experiment. The conservation practice factor was set to one, indicating a lack of erosion control techniques. Soil conservation measures are not prevalent in the Santa Paula area, however, locations where erosion reducing techniques are applied will have lower erosion rates than those predicted here.

The Soil Conservation Service have developed soil loss tolerance (T) coefficients for the soil series and phases in Ventura County. The soil loss tolerance image was generated from the same vector dataset that produced the soil erodability image. The only difference arose in the final labelling of the soil mapping units to soil loss tolerances instead of soil erodabilities. Soil loss tolerances ranged from one to five tons per acre per year.

Predicted Soil Loss

The five data planes representing the R, K, L, S and C coefficients were multiplied together based on the USLE to derive the A coefficient. A predicted

soil loss in tons per acre per year was calculated for each sixty meter square cell in the 231 line by 192 sample grid for the Santa Paula quadrangle (figure 5). The final step was the subtraction of the predicted soil loss image from the soil loss tolerance image. The resultant film writer image displays locations where predicted soil erosion exceeded soil loss tolerances (figure 6).

5. ACCURACY AND ANALYSIS

Accuracy assessments were made for each data plane, and the predicted soil loss from the digital model was tested against the manually derived USLE prediction for a stratified random sample of sites (table 1). Twenty-five random samples from each of the ten classes were obtained from field inspection and air photo analysis from 1:32,000 scale CIR imagery for ground truth to test the classification. From the stratified random sample, 84.3 percent of the pixels were correctly classified; by weighting each class by it representative area, 87.2 percent of the quadrangle was correctly classified. Most of the confusion in the classification was between classes with relatively similar C coefficients, which agrees with Stephens and Cihlar's work relating vegetative cover to the C coefficient of the USLE.

Accuracy assessments for the collateral data were obtained from ten random samples of the original twenty-five samples for each class, excluding the river and urban class. The SCS does not provide guidelines for the calculation of river or urban classes. Therefore, these regions were excluded from further study, comprising approximately fifteen percent of the study area. A subsample of eighty sites remained, ten sites for each of the eight classes of interest. The rainfall, soil erodability and soil loss tolerance images are discrete datasets. Thus, a standard accuracy percentage scheme was devised for accuracy assessment. The slope and length of slope images are continuous datasets, therefore, a Pearson product moment correlation coefficient was calculated to test the topographic variables.

The eighty sites on the digital rainfall image were tested against the isopluvial polygons drawn on the Santa Paula quadrangle. Accuracy of the digital rainfall image was 100 percent. Accuracies of the digital soil erodability and soil loss tolerance images were evaluated against the SCS soil maps utilizing the same eighty site random sample. The accuracy for both the soil loss tolerance and soil erodability images was 96.25 percent. From the 7.5 minute topographic sheet, the slope and length of slope were manually calculated for the eighty site sample. These values were tested against the automated slope and length of slope calculations. The Pearson product moment correlation coefficient, R, for the manual versus digital slope calculation was .93, significant to the .0001 level. The R coefficient for the manual versus digital calculation of slope length was .81, also significant to the .0001 level.

The predicted soil loss calculated by the geobased soil loss model was tested against the manually derived coefficients of the USLE using the same random sample. Coefficients for the manual USLE were obtained from the rainfall map, the SCS soil maps, slope and length of slope from the topographic sheet, and ground truth and air photo analysis of the study area. These coefficients were multiplied together based on the USLE yielding an A value. The geobased derived coefficients were also multiplied together yielding an A value. Because the USLE is a multiplicative function, it is appropriate to transform the geobased and manually based values to their natural logarithms before calculating a correlation coefficient (Li, 1964). The Pearson product moment correlation coefficient, R, of the log transformed A prediction was .91, significant to the .0001 level.

An informal sensitivity analysis performed on the effects of the five coefficients of the final predicted soil loss is presented in table 2. The greatest variability was obtained from the slope and crop management coefficients. The misclassification of chaparral (C = .01) as barren (C = .75) created

an error in the A factor of 7500 percent. However, this error occurred only once in the sample analyzed. Slope is a very sensitive coefficient of the USLE, however, the slope factor depicted by the DEM is fairly accurate, and error within this calculation is unlikely to extend the full range of the S value. The soil and rainfall images are accurate and do not account for much error in the A calculation. Length of slope is the least accurate of the datasets. Fortunately, it has the second lowest sensitivity of the five coefficients, reducing the impact of miscalculation of the L factor on the predicted soil loss.

Several trends are apparent from analysis of the predicted soil loss image:

(1) Soil loss is not a problem on the floodplains and valleys, except for row crops on soils with low soil loss tolerances or on steeper slopes;

(2) Immature avocado orchards display high predicted soil losses in the canyon sites, however, the problem is not extensive; and,

(3) The steeper mountainous areas have serious soil loss problems, especially sites exhibiting a grass canopy.

The predicted soil loss image clearly indicates that sites with steeper slopes and a grass canopy are the major contributing areas for soil lost within the Santa Paula quadrangle. Predicted erosion rates for the grass class exceeds thirty tons per acre per year, and in some locations ranges as high as 200 tons per acre per year for extremely erodable areas. The Soil Conservation Service can implement this information by introducing a more protective plant cover such as chaparral or sod forming grasses on the sensitive sites.

6. CONCLUSION

A geographic information system including Landsat and collateral data can accurately map soil loss using the Universal Soil Loss Equation. This system can inventory large areas for predicted soil loss with a savings in time and money over conventional ground sampling (Hanuschak, 1979). It is best applied as a prescreening mechanism to identify major areas of soil loss, in which a user is concerned with relative amounts and the spatial extent of soil erosion. Prediction of soil erosion for a small site is useful, but the ability to project this prediction to a larger area provides a much greater perspective of soil loss problems to resource managers. This geobased soil loss information system accurately depicted the Universal Soil Loss Equation for a 7.5 minute quadrangle, an agricultural and rangeland region of nearly 100 square miles. The strength of a geographic information system lies in the accuracy of the input data, and the ability of the sytem to process and display the data in a suitable fashion for resource analysis. We believe that the geographic information system soil loss model presented herein succeeded on all counts.

7. REFERENCES

Berger, Z. and J.R. Jensen, 1980, "Modelling Soil Loss and Flood Potential Due to Urbanization in Humid Subtropical Southeastern Environments," Proceedings of the Fourteenth International Symposium on Remote Sensing of Environment, pp. 1057-1068.

Bryant, N.A. and A.A. Zobrist, 1976, "IBIS: A Geographic Information System Based on Digital Image Processing and Image Raster Datatype," Second Annual Symposium on Machine Processing of Remotely Sensed Data: Laboratory for Applications of Remote Sensing, Purdue University, pp. 1A1-1A7.

Foster, G.R. and L.D Meyer, 1972, "Transport of Soil Particles by Shallow Flow," Transactions American Society of Agricultural Engineers, Vol. 15. No.1, pp. 99-1-2.

Hanuschak, G., R. Sigman, M. Craig, M. Ozga, R. Luebbe, P. Cook, D. Kleweno and C. Miller, 1979, "Crop-Area Estimates from Landsat: Transition From Research and Development to Timely Results," Fifth Annual Symposium on Machine Processing of Remotely Sensed Data: Laboratory for Applications of Remote Sensing, Purdue University, pp. 86-94.

Li, C.C., 1964, Introduction to Experimental Statistics, McGraw-Hill Book Company, 460 pp.

Logan, T.L., 1981, "A Data Base Approach For Prediction of Deforestation-Induced Mass Wasting Events," Proceedings American Society of Photogrammetry, pp. 197-211.

Meeuwig, R.O., 1971, "Soil Stability on High Elevation Rangeland in the Intermountain Area," U.S. Department of Agriculture, Forest Service Research Paper INT-94.

Miller, J.F., R.H. Frederick and R.J. Tracey, 1973, Precipitation-Frequency Atlas of the Western United States, National Oceanic and Atmospheric Administration, 71 pp.

Morgan K.M., D.R. Morris-Jones, G.B. Lee, and R.W. Kiefer, 1979, "Cropping Management Using Color and Color Infrared Aerial Photographs," Photogrammetric Engineering and Remote Sensing, Vol. 45. No. 6, pp. 769-774.

Morgan, K.M., D.R. Morris-Jones, G.B. Lee and R.W. Kiefer, 1980, "Airphoto Analysis of Erosion Control Practices," Photogrammetric Engineering and Remote Sensing, Vol. 46, No. 5, pp. 637-642.

Musgrave, G.W., 1947, "The Quantitative Evaluation of Factors in Water Erosion, A First Approximation," Journal of Soil and Water Conservation, Vol. 2, No. 3, pp. 133-138.

Pacific Southwest Inter-Agency Committee, 1971, Comprehensive Framework Study, California Region Watershed Management, Water Resources Council, Appendix VIII, 156 pp.

Patterson, F.A. and P.M. McAdams, 1980, The Use of Landsat MSS Data to Produce Erosion Hazard Potential Maps, NASA National Space Technology Laboratories, 18 pp.

Singer, M.J, G.L. Huntington and H.R. Sketchley, 1976, "Erosion Prediction on California Rangeland: Research Developments and Needs," Soil Erosion Prediction and Control, Proceedings Soil Conservation Society of America, pp. 143-151.

Spanner, M.A., 1982 Soil Loss Prediction in a Geographic Information System Format, Master's Thesis, Department of Geography, University of California, Santa Barbara 97 pp.

Stevens, P.R. and J. Cihlar, 1981, "The Potential of Remote Sensing for Monitoring Soil Erosion on Cropland," Proceedings of the Fifteenth International Symposium on Remote Sensing of Environment, (in press).

Strahler, A.H., J.E. Estes, P.F. Maynard, F.C. Mertz and D.A. Stow, 1980, "Incorporating Collateral Data in Landsat Classification and Modelling Procedures," Proceedings of the Fourteenth International Symposium on Remote Sensing of Environment, pp. 1009-1026.

Swanston, D.N., F.J. Swanson and D Rosgen, 1980, "Soil Mass Movement," An Approach to Water Resources Evaluation Non-Point Sources: Silviculture, USDA/EPA Environmental Research Laboratories, Athens, Georgia.

USDA Agricultural Research Service, 1961, "A Universal Equation for Predicting Rainfall-Erosion Losses," ARS 22-66.

USDA Science and Education Administration, 1978, "Predicting Rainfall Erosion Losses: A Guide to Conservation Planning," Agricultural Handbook #537, 58 pp.

USDA Soil Conservation Service, Davis, California, 1977, Guides for Erosion and Sediment Control, United States Department of Agriculture, 32 pp.

USDA Soil Conservation Service, Ventura County, 1969, Summary of Soil Characteristics and Qualities, Ventura Area, California, United States Department of Agriculture 104 pp.

Wischmeier, W.H., D.D. Smith and R.E. Uhland, 1958, "Evaluation of Factors in the Soil Loss Equation," Agricultural Engineering, Vol. 39, no. 8, pp. 458-462.

Wischmeier, W.H. and D.D. Smith, 1965, "Predicting Rainfall Erosion Losses From Cropland East of the Rocky Mountains," U.S.D.A. Agricultural Research Service, 45 pp.

Zingg, A.W., 1940, "Degree and Length of Slope as it Affects Soil Loss in Runoff," Agricultural Engineering, Vol. 21, No. 2, pp. 59-64.

TABLE 1. COLLATERAL AND PREDICTED SOIL LOSS DATA PLANE ACCURACIES

Dataset	Accuracy
Rainfall	100.00 Percent
Soil Erodability	96.25 Percent
Length of Slope	.81 Correlation
Slope Gradient	.93 Correlation
Crop Management	84.30 Percent
Soil Loss Tolerance	96.25 Percent
Predicted Soil Loss	.91 Correlation

TABLE 2. SENSITIVITY ANALYSIS

Coefficient	Range	Percent Change
R	.50 - .70	140
K	.15 - .43	286
L	1.35 - 2.92	221
S	1.00 -34.10	3412
C	.01 - .75	7500

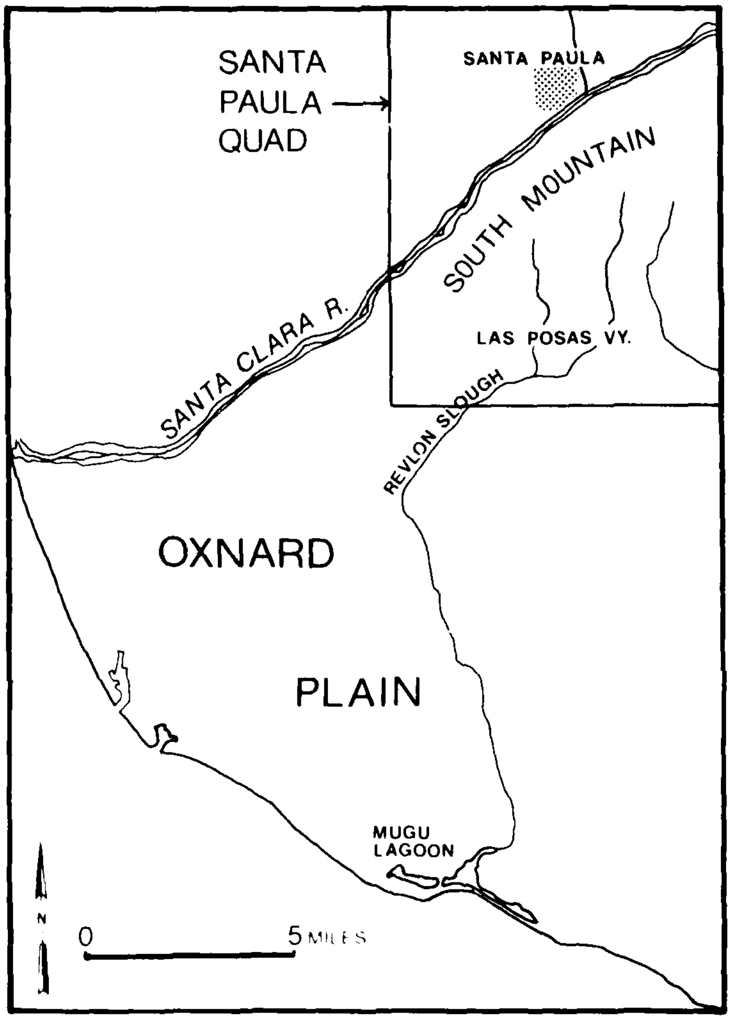

Figure 1. This map shows the location of the major watershed features discussed within the paper.

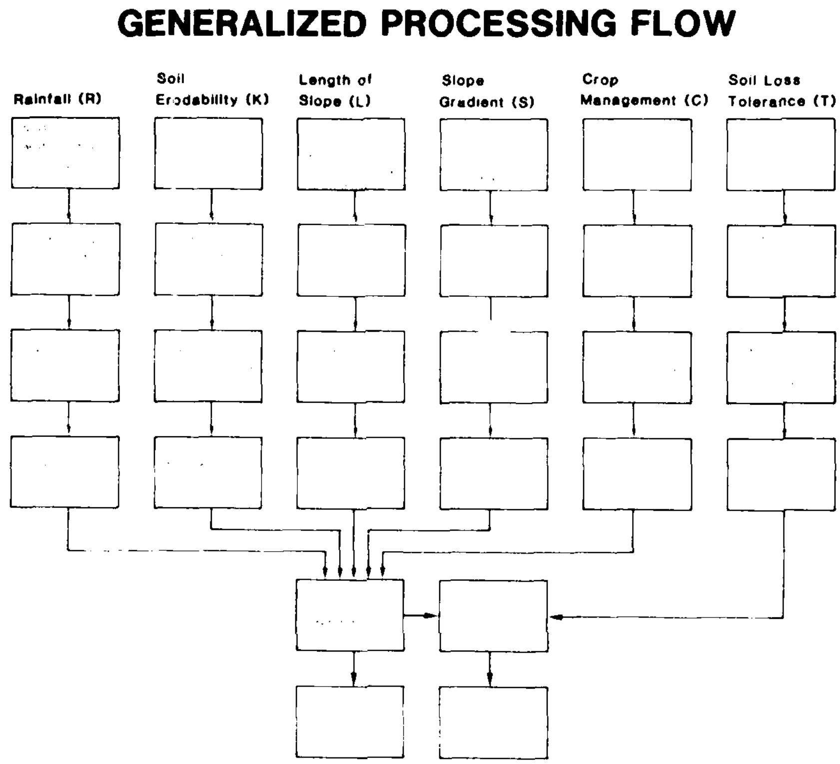

Figure 2. Generalized processing flow for the soil loss information system.

Figure 3. Registered length of slope image generated from DEM. Dark tones represent short slope lengths; light tones represent longer slope lengths.

Figure 4. Registered ten class crop management image generated from Landsat MSS data, and slope and elevation information from DEM.

Figure 5. Registered predicted soil loss image based on GIS inputs to the USLE. Lightest tones depict predicted soil losses less than 5 tons/acre/year. Darkest tones represent predicted soil losses exceeding 30 tons/acre/year.

Figure 6. Registered differenced image of predicted soil loss and soil loss tolerance images. Light tones represent locations where the predicted soil loss is less than the soil loss tolerance. Dark tones represent sites where the predicted soil loss exceeds the soil loss tolerance.

OPERATIONAL USE OF SATELLITE DATA IN CROP CONDITION ASSESSMENT

B. E. Spiers

Foreign Agricultural Service
U.S. Department of Agriculture
Houston, Texas, U.S.A.

ABSTRACT

The purpose of this paper is to describe how the Foreign Agricultural Service (FAS) of the USDA utilizes remotely sensed satellite data in the assessment of crop conditions for selected crops in some areas of the world. The Foreign Crop Condition Assessment Division (FCCAD) is part of the Office of International Agricultural Statistics which has the responsibility within USDA for producing foreign crop production estimates. After five years of developmental work with other government agencies, the FCCAD was established in 1978 to provide FAS with assessments of conditions over selected areas using remotely sensed data as its prime source of data. The FCCAD does not make final production estimates as an end product, but provides reports of assessment that are used as an additional source of information by those that make production estimates.

The Foreign Agricultural Service (FAS) of the United States Department of Agriculture (USDA) maintains a worldwide agricultural intelligence and reporting system to: (1) provide farmers, agribusiness and policy makers with up-to-date information on worldwide agricultural production and trade and (2) support the development and expansion of foreign markets for U.S. farm products. The Foreign Crop Condition Assessment Division (FCCAD) is part of the Office of International Agricultural Statistics (IAS) which has the responsibility within FAS for making foreign crop estimates. The FCCAD does not make final crop production estimates, but provides reports of assessments and conditions to other divisions within IAS that have the responsibility for crop production estimates. The reporting divisions use the FCCAD reports as an additional source of information to be analyzed in making crop production reports.

The FCCAD was established in 1978 after five years of development work with other U.S. governmental agencies. Its charter is to provide assessments of crop conditions in major crop growing areas of selected countries through the use of satellite remotely sensed data, meteorological data and agricultural data.

The FAS established a computer center in Houston, Texas, near the Johnson Space Center to share LANDSAT data and data handling cost and to take advantage of USDA personnel/experience gained while working on the Large Area Crop Inventory Experiment (LACIE).[1]

The FCCAD computer hardware consists of three systems in Houston, Texas, and one system in Washington, D.C. Due to fiscal and policy constraints the equipment for this operation was purchased over a three year period, 1976-1979, with some additional capabilities added since 1979. Management decided to implement the desired capabilities on minicomputers, using competitive bidding for off-the-shelf components. The center currently has (1) a system to extract digital image data from high density "A" or "P" tapes and from 1600 BPI tapes from the National Oceanic and Atmospheric Administration's (NOAA) 6 and 7 satellites, (2) a system that contains a gridded data base with meteorological data, vegetative indices and model results, and (3) a system that drives three analyst stations with digital data manipulation capabilities. The FAS facility in Houston has a fourth system located in Washington, D.C., at FAS headquarters. A direct communications link between the Washington, D.C., system and the data base system was installed for data transmission between the two sites, reporting, and data base query by headquarters analyst.

The FCCAD uses digital data from two series of satellites - MSS data from LANDSAT and Advanced Very High Resolution Radiometer (AVHRR) data from the NOAA. Due to manpower and resource limitations, the 700 plus scenes of LANDSAT data taken during an 18 day period have to be screened and/or processed in such a manner that six or seven analysts could extract the most useful information possible in the shortest amount of time. We found that by sampling the full frames and retaining subscenes[2] of every fifth pixel on every fifth line that we got a representative image containing sufficient data to monitor crop conditions. When an in-depth analysis is needed, full resolution images are extracted in varying sizes up to 90 x 90 kilometers.

During 1981 we added NOAA's AVHRR data to supplement the LANDSAT data. Channels one and two of the AVHRR data are somewhat spectrally similar to bands five and seven of the LANDSAT MSS. We have developed a software package[3] to extract and frame these data in 1020 pixels by 510 lines that cover approximately 500 by 1000 kilometers. AVHRR satellite coverage is received every five to nine days compared to 18 days for LANDSAT. These data are highly complimentary to the LANDSAT. The area covered by the 700 plus LANDSAT scenes can be covered by less than 100 AVHRR frames. The data received from these two satellite series are extracted and loaded onto imagery packs by country or regional designations for analysis by the designated country analyst.

One of the unique features of the FCCAD operational system is the User Information System (UIS) Data Base. The data base is designed around the one-fourth mesh I,J grid with point locations for meteorological stations. A geographical hierachical structure is used to store and retrieve data elements. The data base has been designed to accept the following data elements at the cell quardant level - hierachy, soils, agrophysical unit and cropland intensity. At the cell and/or station level, historical norms for temperature and precipitation, daily minimum and maximum temperatures, daily precipitation, snow cover, and evapotranspiration (ETP) are stored. As the gridded or station meteorological data are being loaded, several models are run and the results of these models are also stored in the grid cell or station record. These consist of soil moisture,[4] crop calendar,[5] winterkill,[6] and crop stress model results.[7,8] As the digital data are loaded to the imagery packs for the analyst, several vegetative index numbers are calculated on both MSS and AVHRR data for the grid cells and loaded to the data base. We also store historical area, yield, and production data for each country being worked at the smallest political level available.

The Analyst Terminal System (ATS) consists of three analysts stations using operational software designed by the Ford Aerospace Corporation in 1977. The Integrated Multivariate Data Analysis and Classification System (IMDACS) is a highly versatile interactive software system used for analysis of digital imagery. The IMDACS is installed on a DEC PDP-11/70 and uses image display and manipulation systems manufactured by the International Imagery Systems (I^2S) of

Stanford Technology Corporation. The software system has several processors that assist an analyst or researcher in displaying digital imagery, both satellite and aircraft, on video monitors. Image data in the I^2S refresh memories can be redisplayed by using breakpoint mapping of intensity pairs or by using the interactive trackball controlled cursor.

The IMDACS has the capability to cluster and classify[9] digital data into specially meaningful groups of pixels. Both interactive and adaptive clustering can be used for this purpose in both a supervised and unsupervised mode. Statistics from clustering or training fields can be used for maximum likelihood classification.

Both clustering and classification use a Floating Point AP-120B array processor to rapidly segment the digital data. Another IMDACS processor allows the analyst to interrogate cluster/classification maps for crop or signature identification and labeling. Other processors provide cartographic and manual image registration functions.

Since the initial IMDACS several major capabilities have been added to enhance its operational system.

- Rapid Image Display[10] - to reduce the amount of console interaction when displaying images.
- Vegetative Index Processor[11] - to calculate the intensity and dispersion of green vegetation at the grid cell or scene level of masked or unmasked areas.
- Grid Cell Overlay[12] - to superimpose the I,J grid over an image with annotation of I,J identification at selected junctures.
- Image Transfer System[13] - to reformat eight byte data into four byte data and transmit color infrared images to Washington, D.C., over communication lines for joint analysis with FAS analysts.

The Terminal Support System (TSS) is located in the Washington, D.C., office of FAS and serves as a link between the two locations. This system is used to query data from the UIS in Houston and as a communications link to transfer meteorological data to Houston and imagery data to Washington, D.C. In addition, the TSS is part of a worldwide network that allows Agricultural Officers in some foreign post to issue abnormal event alerts or queries to FCCAD and have FCCAD generate crop condition assessment reports in response.

The key ingredient to the FCCAD crop condition assessment activities is the country analyst. The analysts are assigned to specific countries or areas of the world for which crop assessments are to be made. The crop analysts are country experts as well as knowledgeable remote sensing analysts. They must have detailed knowledge about all aspects of agriculture in their assigned area. These include cultural practices, cropping areas, soils, historical production, agricultural trends, government agricultural policy, transportation networks, export/import facilities and capabilities, and the interrelationship of the agricultural economy as it relates to the overall economy. The backgrounds of our current analysts consist of formal education in economics, soils science, agronomy or geography as well as being trained in remote sensing. One common element of all our analysts is a rural or farm background.

The following two scenarios are fairly representative of the operational capabilities of the FCCAD. The data base for all countries is at different levels of completeness depending on how many years we have worked the country. The discussion that follows is not applicable on a worldwide basis.

Scenario I

The analyst follows crops throughout the year as they are planted, mature and harvested using visual inspection of the imagery as well as results from the data base. Our current technique consists of determining the condition of the current year's crops in comparison with a base or past year. He/she reviews the data that are available for his/her area;[14] i.e., vegetative indices at the cell level, soil moisture model calculations, winterkill model results, daily station and/or grid precipitation and temperature in conjunction with the visual analysis of the LANDSAT and NOAA imagery. The analyst then makes a determination on the condition of the crop by comparing the available data against data from the base year or against data acquired earlier in the crop year. Using this method he/she makes conclusions - the crop is better or worse than the base year, the crop is suffering from abnormal moisture or temperature stress, the area devoted to a group of crops is more than or less than the base year, or the crop is ahead or behind the normal season. Depending on the experience of the analyst and the country being worked, it is possible to determine a percentage range for the increase or decrease of area or production with a modest degree of accuracy. Quantifiable estimates for these factors are pending development of acceptable yield models and area change determination schemes.

Scenario II

The Division receives an alert from our Agriculture Officer at a foreign post. He/she reports the possible shortage of water for irrigation due to a period of drought and the location of 12 of 15 key reservoirs that he/she would like for us to monitor. LANDSAT imagery for these areas is extracted from historical data as well as current data, and the surface area of the lakes is determined with our IMDACS classification capability. The results for each pass are compared to determine if the available water is increasing or decreasing. The analyst determines the crop area being irrigated by each reservoir and assesses the crop condition with the same tools discussed in Scenario I. Reports are furnished back to the foreign post, as well as to the Washington, D.C., office.

The FCCAD does not make crop condition or production reports for publication. All the reports made by the Division are made to the Office of International Agricultural Statistics at FAS headquarters which uses the information as an additional source of data to be combined with its other information in making USDA foreign crop production estimates.

The capabilities discussed in this paper and other capabilities currently being used by the Division fall short of our desired goals. In order to reach our long range goals of a complete crop production estimation system new models, data handling techniques, etc., being developed and tested by the research and development community which are applicable to FAS requirements will be implemented on our systems as resources are made available.

REFERENCES

1. "Proceedings of Plenary Session, The LACIE Symposium", October 1978. NASA/JSC-14551.

2. Aaronson, A.C., 1980. "The Effect Systematic Stratified Sampling has on the Computation of Vegetative Index Numbers." TM No. 12. USDA/FAS/FCCAD, Houston, Texas.

3. "FCCAD METSAT Data Scene Processor User's Guide," 10-OP, July 15, 1981. USDA/FAS/FCCAD, Houston, Texas.

4. "Two-Layer Soil Moisture Model, Early Warning (EW), Data Base Interface Driver User's Manual," November 1981. AgRISTARS, EW-LI-00734.

5. Robertson, G.W., 1968. "A Biometeorological Time Scale for a Cereal Crop Involving Day and Night Temperatures and Photoperiod." International Journal of Biometeorology. 12:191-223.

6. Ravet, F.W., and G. W. May, 1979. "A Meteorological Model to Aid in the Detection of Winterkill," TM No. 5. USDA/FAS/FCCAD, Houston, Texas.

7. Ravet, F.W., and J. R. Hickman, 1979. "A Meteorologically Driven Wheat Stress Indicator Model," TM No. 8. USDA/FAS/FCCAD, Houston, Texas.

8. "Wheat Stress Indicator Model, Early Warning (EW), Data Base Interface Driver User's Manual," November 1981. AgRISTARS, EW-LI-00732.

9. "LANDSAT Image Classification Procedures," 3-OP(CL), Rev. 1, dated August 3, 1979. USDA/FAS/FCCAD, Houston, Texas.

10. "The Rapid Image Display (RID) Processor," Lockheed - LEMSCO-15306, dated November 18, 1980.

11. Dario, E.R., "Computer Program Overview, User Run Instructions, VI Programs," dated June 1, 1980, rev'd August 1, 1980, and October 1, 1981. USDA/FAS/FCCAD, Houston, Texas.

12. "Grid Cell Overlay Processor User's Guide," Lockheed - LEMSCO-15601, dated September 26, 1980.

13. "Total Image Transfer System (TIX Processor) User's Guide," Preliminary. USDA/FAS/FCCAD, Houston, Texas.

14. Evans, S.M., "Agriculture Information Display System (AIDS) User's Guide," 6-OP, rev. July 6, 1981. "Geographic User's System (GUS) User's Guide," 9-OP, rev. October 28, 1981. USDA/FAS/FCCAD, Houston, Texas.

LANDSAT AND SPACE RADAR CONTRIBUTIONS TO THE U.S. JUNE ENUMERATIVE SURVEY OF AGRICULTURE: ATMOSPHERIC EFFECTS ON THE PRECISION OF ESTIMATES

David S. Simonett
Edward M. Irvin
Lee F. Johnson

University of California
Santa Barbara, California

SUMMARY

The U.S. Department of Agriculture (USDA) conducts a series of annual surveys to estimate crop acreage, yield, production, and numerous other facets of the agricultural economy. This information helps the U.S. agricltural community operate efficiently and profitably.

The USDA uses probability surveys based upon area frame sampling to prepare crop estimates. The 48 conterminous States are stratified according to agricultural intensity, and the strata are further subdivided into discrete land segments. Crop enumerators visit a stratified random sample of segments, and completely account for the land use in each. Unbiased direct expansion State and national crop estimates are made by multiplying each segment total by the reciprocal of the probability of sample selection, and summing over all strata.

The June Enumerative Survey (JES) is the major acreage survey for spring-planted crops. It is based on a sample of about 16,000 segments throughout the 48 states. Acreage estimates usually remain unchanged during the growing season, and form the basis for ensuing crop production forecasts.

Commodity information serves to lessen market fluctuations by improving inventory adjustments, production schedules, and resource planning and allocation decisions. Thus, it is imperative to explore methods of reducing the error of crop estimates. We intend to assess the abilities of LANDSAT and a hypothetical active microwave sensor to provide timely data for inclusion in the June Enumerative Survey.

Recent studies show improved precision of crop acreage estimates by using LANDSAT together with JES field statistics to derive a regression estimator. It is possible to enlarge the effective sample size by using classified LANDSAT data with a known relationship to field data. However, information loss due to cloud cover limits the value of the LANDSAT contribution to USDA forecasts.

An orbital radar sensor would avoid the cloud cover constraint placed upon optical systems. The only real source of atmospheric degradation of radar imagery is precipitation intensity on the order of .5 centimeters per hour.

We estimated a data base of LANDSAT image cloud cover statistics and ground-observed precipitation statistics to assess the probability of obtaining single- and multi-date coverage in the month preceding the JES. LANDSAT has mean probabilities of .68, .48, and .35 of acquiring 1, 2, and 3 images of a path-row position, respectively, with less than 30 percent cloud cover. In contrast, radar would be able to provide 1, 2, or 3 non-degraded images with probabilities very near 1.0. We found expected cloud degradation of a given LANDSAT image between 40 and 50 percent in major grain-producing regions. By comparison, the exected degradation of a given radar image is only about 1 percent.

We used a computer simulation which considered cloud amount, size, and spatial distribution in calculating the proportion of crop area imaged at least once during the month preceding the June Enumerative Survey. Results showed approximately 80 percent of a crop area will be imaged at least once after three looks at all path-row locations with the state.

Ground-based and airborne radar studies have provided positive indications of radar's crop identification ability. Further research is needed to clearly define the agricultural monitoring potential of an orbital system.

Following this, thorough consideration of satellite input to crop surveys must be undertaken. The figures presented formulate expectations regarding the data delivery capabilities of the two systems, operating within the time constraints of an operational crop monitoring project. The imaging time available to radar far exceeds that available to LANDSAT.

A complementary LANDSAT and radar system would be a powerful data collection tool. Radar might play an auxiliary role in arid climates, increasing the dimensionality of the orbital data set. In more humid climates, radar would assume primary importance, with LANDSAT providing supplemental coverage when available. An all-weather radar system may be a highly effective sensor in the context of a well-designed agricultural sampling frame, simply because it is able to image the target area independently of cloud cover conditions.

RIO PILCOMAYO-BAÑADO LA ESTRELLA (ARGENTINA): LANDSAT TEMPORAL ANALYSIS OF A RIVERINE ENVIRONMENT

Alberto B. Viola and Carlos M. Viola Binaghi
Aeroterra S.A., Buenos Aires, Argentina

and

William G. Brooner and Donald Garofalo
Earth Satellite Corporation, Chevy Chase, Maryland, USA

ABSTRACT

The Rio Pilcomayo-Bañado La Estrella project focused on areas in Argentina and Paraguay where the Rio Pilcomayo is actively depositing sediments, frequently in excess of 100 million tons annually. Interventions in the river's course, through both mechanized channelization, and by seasonal overbank flow and varying depositional processes, continually alter the landscape.

The principal objective of the project was to study temporal hydrological changes, physiography and land cover in the project area using multi-date digitally processed Landsat data, as well as climatological, hydrological and ground collected data.

Multidate Landsat images were useful for identifying and mapping surface hydrological features, their spatial distribution, and river channel changes resulting from both normal flow processes as well as artificial diversions.

A Landsat multispectral classification involving a combined unsupervised/supervised technique was used to "map" twelve (12) land cover categories in an area of 1,531,360 hectares. A digital temporal change analysis provided quantitative data of different surface hydrology conditions over three Landsat image dates, 1972-1978-1980.

1. INTRODUCTION

The Rio Pilcomayo flows out of the Bolivian Andes across the Gran Chaco of Argentina and Paraguay. In northwestern Formosa Province (Argentina), the river forms part of the international boundary between Argentina and Paraguay.

Bañado La Estrella lies south of the Rio Pilcomayo channel and is approximately 400 km northwest of the provincial capital city of Formosa (Argentina) and 450 km west of Asuncion (Paraguay).

The physiographic and hydrological characteristics of the Bañado La Estrella result from the dynamics of the Rio Pilcomayo. Water in the Bañado La Estrella results from overland and shallow channel flow of seasonal floodwaters originating from the Rio Pilcomayo. During the past decade additional waters, fed into the Bañado through several canals connected to the river channel, have both expanded the areal extent of inundation in the Bañado and lengthened the period of inundation.

In the present studies, Landsat digitally enhanced imagery, along with climatological and hydrological records and field survey data, were used to prepare a series of map products and analyses on the land cover, surface hydrology, temporal hydrologic dynamics, and physiography for a 17,000 km^2 area centered on the Rio Pilcomayo and adjacent Bañado La Estrella.

2. OBJECTIVES

The principal objective of the project was to study temporal hydrological changes, physiography and land cover in the project area using multi-date digitally processed Landsat data, as well as climatological, hydrological, and ground collected data. A series of Landsat overlay map products were prepared at 1:100,000 scale to illustrate these changes and features. Specific analyses and resulting products include:

- A color Landsat photomap series at 1:100,000 scale showing the Rio Pilcomayo-Ba ado La Estrella and adjacent regions, covering an area of approximately 38,000 km^2.

- Analyses and maps of temporal dynamics of the surface hydrology, and changes occurring between 1972-1981 in the project area comprising 17,500 km^2.

- Analyses and maps of physiographic features were prepared at 1:100,000 scale for the project area.

- Landsat multispectral classification procedures were used in the GEOPIC Interact System to produce a land cover analysis using the November 1980 Landsat scene. The classification used a unique approach involving combined unsupervised and supervised techniques to "map" twelve (12) categories in an area of 1,531,360 hectares. These land cover categories relate to ecological environments, incorporating soils, landform and climatic variations. Results were shown both cartographically (1:100,000 scale) and in tabular format.

3. STUDY AREA

The Rio Pilcomayo-Ba ado La Estrella study area contains approximately 38,000 km^2 which includes a portion of the Pilcomayo River and its adjacent areas. Located within this zone of influence is the Ba ado La Estrella, south of the main river channel. Landsat images were processed to provide complete coverage of the 38,000 km^2 area. Analyses of the land cover, surface hydrology and physiography were conducted for a 17,000 km^2 area centered in the region of the river channel and adjacent Ba ado La Estrella.

The study area consists of portions of four Landsat image locations, defined by the following path/row identifiers: 244/77, 245/76, 245/77 and 246/76. The processing of individual scenes at 1:100,000 scale, and the temporal hydrology, physiography and land cover analyses, were conducted for a study area of approximately 17,000 km^2, defined by the lower one-half of the Landsat images for Path 245/Row 76. In addition, selected image products were prepared at 1:100,000 scale for the northeast quadrangle for Landsat image Path 246/Row 76.

Formosa Province lies between approximately 22.5° and 27° south latitude and 57.5° west longitude. The capital of the Province is the city of Formosa located in the easternmost part of the Province. The northern border of the Province is also the international boundary between Argentina and Paraguay. The eastern border of the Province is the Paraguay River, also an international border between Argentina and Paraguay. The Province is bordered in the south by Chaco Province and in the west by Salta Province.

The study area is rural and sparsely settled. Just south of the Rio Pilcomayo are scattered agricultural fields and pastures of 4 to 10 km^2 in area, surrounding small settlements.

The climate is semiarid, and vegetation is characterized by two main types: xerophilic in areas not subject to regular flooding, and hydrophilic in areas flooded yearly the Rio Pilcomayo system. Past and present floodplains, built by sedimentation over the past two to three million years, dominate the landsape.

Rio Pilcomayo flows northwest to southeast, over a slight gradient of about 0.2 meters/km. It is actively depositing sediments, frequently in excess of 100 million tons annually. Interventions in the river's course, through both mechanized channelization, and by seasonal overbank flow and varying depositional processes, continually alter the landscape.

Precipitation decreases from east to west in the Province of Formosa. The wettest months of the year within the project area are October through May with monthly rainfall ranging between 30 and 135 mm; in the dry season, June to September, monthly rainfall ranges between 5 and 30 mm. This is in contrast with the eastern part of the Province which has monthly rainfall for the wet months ranging between 115 and 165 mm, and for the dry months between 40 and 80 mm. Average annual precipitation in Formosa is 1,370 mm, while the project area has 500-700 mm of annual rainfall. Estimated potential annual evaporation from the region is on the order of 2,000 mm.

4. RECONNAISSANCE FIELD SURVEYS

Collection of field data, or "ground truth" on soils, vegetation, landforms, cultural features, etc., is commonly imperative to extraction of accurate information from Landsat imagery. Preliminary interpretation of Landsat images without benefit of ground truth information normally results in generation of many questions regarding the natural and man-made features within a project area. Further, the value of Landsat as a tool in planning field surveys cannot be overstated. Even an experienced image interpreter who has some knowledge of the area is certain to identify on Landsat images, features and/or subtle tonal differences whose significance must be resolved by an on-the-ground visit or low-altitude aircraft overflight of the area in question.

After preparation of GEOPIC enhanced Landsat images, Aeroterra/EarthSat conducted field surveys in the area in June 1981. These surveys included correlation of field observations with Landsat GEOPIC images and documentation of field characteristics relevant to the analyses for: temporal hydrological changes, physiographic study and land cover classification.

Tonal and texture changes on the Landsat scenes, suggestive of differing land use/land cover types along a transect, were selected as field check sites.

Upon completion of the reconnaissance ground and aerial surveys, all collected field and office data (including hydrological and climatological records) were synthesized and organized to facilitate correlation with data acquired during the subsequent Landsat analyses.

5. SELECTION AND PREPARATION OF LANDSAT DATA

Fourteen (14) Landsat scenes were selected and acquired, of which ten (10) were digitally processed in EarthSat's GEOPIC system and used in the study. Seven (7) of these Landsat GEOPIC images cover the primary Rio Pilcomayo-Ba·ado La Estrella study area (Path 245/Row 76). These images cover the period between September 1972 and March 1981, involved three Landsat satellites (Landsats 1, 2 and 3) and three ground receiving stations: NASA GSFC (USA), CNIE (Argentina), and INPE (Brazil). GEOPIC images were produced for analysis at 1:250,000 and 1:100,000 scale.

6. PREPARATION OF LANDSAT PHOTOMAPS

Landsat GEOPIC images were mosaicked to prepare a color Landsat photomap series at 1:100,000 scale, covering an area of approximately 38,000 km^2 including the Rio Pilcomayo-Ba·ado La Estrella study area and adjacent areas.

The Landsat photomaps provide a broad geographical overview of the physical resources and infrastructure of northwest Formosa Province for regional mapping, geographical and natural resource studies, planning and multiple resource applications. The Landsat photomap series consisted of four (4) Landsat map sheets, compiled from portions of four digitally processed Landsat images.

The Landsat photomap task involved the following activities:

1. Selection and acquisition of Landsat digital tapes.

2. Digital image processing of each Landsat scene.

3. Mosaicking of four images, best fit to available cartographic

controls and adjacent images.

4. Cartographic compilation of four map sections covering the project area at 1:100,000 scale.

7. TEMPORAL ANALYSIS OF SURFACE HYDROLOGY 1972-1980

Significant hydrologic features found in the Rio Pilcomayo-Bañado La Estrella study area include: the active channel of the Rio Pilcomayo; through-flowing water in sheets in "bañados" during flood periods; semipermanent lakes with open water in oxbows and in depressions; "esteros" depressions which temporarily hold shallow water bodies; unfilled (dry) segments of linear channels; and "cañadas", ancient sediment-filled channels, serpentine in outline. The only through-flowing stream in the study area is the Rio Pilcomayo, and permanently flowing tributaries to the Pilcomayo River occur in the segment studied. Within the river's floodplain, two important hydrologic features are "esteros" and "bañados".

Esteros are areas of shallow depression with no external drainage, and with little or no arboreal vegetation, containing standing water for prolonged periods, and slow vertical accretion. They may show open water, be covered by floating acquatic vegetation, or have lesser or greater amounts of hydrofillic sedges and reeds. Water in esteros may be derived either from precipitation or from overflow of the river; in the latter case the estero may become temporarily part of a larger bañado. However, when the through-flow stops as the flood recedes, the estero still holds water subject to evaporation processes.

Bañados are depression areas containing overflow with external drainage downstream. Water in a bañado is primarily derived from rivers, not local precipitation.

Features found on the upper surfaces include abandoned channels and cañadas. Water flow and ponding follow and outline subtle variations in relief which are in many instances imperceptible to an observer in the field. The differential distribution of water during the rainy season still reflects the original landscape and enhances the inherited subtle relief, causing the formation of bands of soil with different moisture content and pedologic development. These variations in turn, control the relative vigor and even the species of plants which grow on these features. Within the limits of the study area, gross variations in vegetation appear to be related more closely to the yearly range in near surface moisture content than to the texture or age of the soils.

The changes in hydrologic features of the floodplain which occurred between 1972 and 1980 were presented in colors corresponding to dates of interpreted Landsat GEOPIC images acquired in September 1972, March 1976, February 1978, and November 1980, over a background of the November 1980, MSS-7 image. Upstream the river has shifted its channel in places by normal down-valley sweep and migration of meanders and bends. The length of the Pilcomayo River within the Landsat scene was approximately 184 km in 1972, but only 76 km in 1980 as a result of diversions of its discharge into Argentina and Paraguay.

8. ANALYSES OF SEASONAL WATER LEVEL CHANGES

Repetitive satellite-gathered information is uniquely suited to monitoring temporal changes in surface phenomena, such as floods and land cover or land use variations. A demonstration of digital analyses of Landsat temporal data for evaluating variations in hydrologic features was conducted by comparing September 1, 1972, February 11, 1978 and November 15, 1980 images. The development of these digital processing techniques for mapping land cover and landscape changes has greatly increased the value of Landsat's temporal characteristics for many land planning and resource management applications.

The objectives of the Temporal Analysis of Water Level Change were to analyze different surface hydrology conditions using Landsat data. A variety of data combinations were considered, including high and low water level differences, but the available data were inadequate for such investigation.

The most significant event occurring within the project study area during the eight-year period (1972-1980) was the construction of canals to divert flow from the Rio Pilcomayo into

the Bañado La Estrella upstream from normal overflow points. These canals were constructed in the mid-1970's. Available Landsat imagery clearly shows the pre-canal hydrological pattern (1972 scene) and the post-canal hydrological pattern (1980 scene), contrasted over a period of eight years.

Hence, the resulting objective of the Landsat temporal change analysis was to analyze different surface hydrology conditioned resulting from the construction of diversion canals. Spatial impacts of cultural diversions to the Rio Pilcomayo leading to extensive changes in the Bañado La Estrella system were documented on a color multi-temporal image at 1:100,000 scale.

Digital processing for temporal surface hydrology analyzed from multi-date Landsat images in the Rio Pilcomayo-Bañado La Estrella project consisted of the following steps:

1. Digital processing of the three Landsat scenes.

2. Visual evaluation of Landsat scenes.

3. Classification of surface hydrology features on each of the three Landsat scenes.

4. Multi-date image registration.

5. Differencing of the registered classification features.

6. Conversion of digital data to film and film processing.

7. Evaluation and analysis of temporal change results.

Surface hydrology features considered in this analysis include both open water and inundated marshes or areas of aquatic vegetation. Both of these features included a variety of spectral signatures on the Landsat images.

Each of these temporal landscape features were assigned discrete colors by the computer, and combined with band 5 of the 1980 Landsat scene which provided spatial orientation to the displayed data.

The November 15, 1980 Landsat image shows less surface water than the September 1, 1972 Landsat image, in addition to changes in the location of flow resulting from diversion structures. The total 1980 area was 30,612 hectares, in 1978, 34,960 hectares, and the total 1972 was 41,507 hectares, within a total area of analysis of 1,306,160 hectares.

The approximate area of the present floodplains and seasonal inundation zones was shown by combining the riverine vegetation class and the 1980 surface hydrology features. This area is approximately 157,149.4 hectares.

9. LANDSAT ANALYSIS OF LAND COVER FEATURES

Another objective of the Rio Pilcomayo-Bañado La Estrella project was to conduct a Landsat classification to provide cartographic and quantitative data on the distribution of land cover types, including vegetation, water and bare soil features, in the Bañado La Estrella zone.

To achieve this objective, information obtained during field surveys, and analyses of aerial and ground photos were used and correlated with analyses of the November 15, 1980 scene.

Procedures of classification used in this project consisted in a combination of supervised and non-supervised classification techniques. A non-aligned non-supervised euclidean distance algorithm was used in order to make the initial pixel arrays within the training area. The result of this array was used for "training" a maximum likelihood classification.

A maximum likelihood algorithm used training area statistics to estimate the multivariable probability densities of each spectral class. The euclidean distance classification generated 30 spectral classes which were used to define the 30 maximum likelihood classes which were then extrapolated over the complete study area.

The spectral classes were grouped in twelve (12) categories of land cover based on the training area data derived from field surveys and collateral data sources. Results included both cartographic and tabular statistical products.

The land cover classification map covers an area of approximately 85 km X 180 km (totaling 1,531,360 hectares) at 1:100,000 scale. The twelve (12) categories, each color coded, included the following types and areal extent.

Color	Land Cover Category	Hectares	
Blue	Clear water	977.6	0.0
Light Blue	Turbid water	7,268.8	0.5
Tan	Bare soil (dry)	19,928.8	1.3
Gray	Moist/wet soil	161,630.8	10.5
Yellow	Grasses, sparse	278,758.0	18.2
Cyan	Marsh/swamp	81,808.8	5.3
Green	Forest-low open	199,706.0	13.0
Dark Green	Forest-open low/high	125,536.8	8.2
Orange	Forest-closed high	28,863.2	1.9
Dark Red	Forest-closed low/high	420,677.6	27.5
Red	Forest-riverine, dense	128,551.6	8.4
White	Unclassified	70,012.0	5.1
	Total	1,531,360.0	99.9

10. CONCLUSIONS AND RECOMMENDATIONS

The present investigations focused on demonstrating applications of modern satellite imaging technologies to analyzing the Rio Pilcomayo-Bañado La Estrella area landscape and its temporal dynamics. The investigations included original and unique applications of Landsat imagery, and successfully met the specified objectives.

The present investigations were the first application of temporal Landsat data to the synoptic analysis of the Rio Pilcomayo-Bañado La Estrella area. All of the Landsat images were processed in the GEOPIC system.

The Landsat photomaps of the project area provide a broad geographical overview of the physical resources and infrastructure of northwest Formosa Province for regional mapping, geographical and natural studies, planning and multiple resource applications.

Reconnaissance field surveys acquired data on land cover, soils, climate, geomorphic processes and recent hydrology which enabled project scientists to correlate features on the Landsat imagery with the characteristics and distribution of landscape features observed in the field. The reconnaissance field surveys were an essential element to the successful completion of the study and results obtained.

Changes observed on multi-date Landsat imagery included normal processes such as river channel shifts and changes due to artificial diversions. A map produced at 1:100,000 scale shows flow and channel features interpreted from sequential Landsat images for 1972, 1976, 1978, and 1980; data for each year is shown in distinct colors over a background of the November 1980, MSS-7 image.

A digital temporal change study provided a quantitative analysis of different surface hydrology conditions over three Landsat image dates, 1972-1978-1980. The spatial extent of surface water in each period (or combination of periods) was classified and color coded over a background of the 1980 image. In 1972, water covered 41,507 hectares; in 1978, 34,960 hectares; and in 1980, 30,612 hectares within a total area of 1,306,160 hectares. The

variations are both locational as well as areal, and result from combined natural landscape processes, cultural landscape modifications, and seasonal/annual discharge fluctuations.

The incompleteness of Landsat temporal data covering consecutive wet and dry seasons made annual and seasonal variations in water level difficult to evaluate. A more precise evaluation of seasonal water level changes could be conducted using Landsat images acquired at various dates throughout a single year. It is recommended that future investigations use this approach, and compare two types of years, wet and dry. Thus, a comparison of the dynamics of the river and floodplain systems for the extremes in flood ranges could be made.

A land cover classification map was produced using the November 15, 1980 Landsat scene. The classification used a unique approach involving combined unsupervised and supervised techniques to map twelve (12) categories of land cover in an area of approximately 1,530,000 hectares. The categories represent land cover and can generally be related to ecological environments, incorporating soils, landform and climate variations in the project area. Results were shown both cartographically in a color classification image (1:100,000 scale) and in tabular format.

Within the project area, gross variations in vegetation appear to be related more closely to yearly ranges in near-surface soil moisture content than to soil texture or age. Changes in soil moisture caused by stream divagation and frequency can affect markedly the existing vegetation. The time required to establish xerophilic hardwood vegetation on abandoned levees appears to take hundreds of years after the ground is left bare by the disappearance of hydrophilic vegetation. Invasion rates of preferred woody forest species, adapted to semiarid conditions characteristics of older uplands, are very slow. In the meantime, baren areas are susceptible to rapid invasion of undersirable species, such as Vinal (Prosopis ruscifolia). This should be kept in mind in planning land use or future modifications of the Pilcomayo; resultant ecological impacts may be undesirable and require decades to reverse.

A combination of existing data, effective field survey techniques, synoptic Landsat imagery, and GEOPIC processing and analysis techniques provided new information on the hydrologic dynamics and morphological processes of the Rio Pilcomayo-Ba ado La Estrella system. Such information is essential to resource management and development planning in Formosa Province.

The success of a resource evaluation and analysis, such as the Rio Pilcomayo-Ba ado La Estrella investigation, and a resource development program using remotely sensed data, requires a variety of professional skills and experience if the program is to result in useful information for planning and management. It is our belief, that the principal skills and professional experience required lie in three areas: resource inventory and mapping, resource development planning and implementation, and remote sensing technologies. The Rio Pilcomayo-Ba ado La Estrella investigation team, including professional participa[illegible] of Aeroterra, EarthSat, and the Secretariate of Planning and Development, Formosa Province, completely and expertly met these requirements.

AD P001996

THE USE OF SATELLITE DATA FOR URBAN MONITORING IN THE SÃO PAULO METROPOLITAN AREA

Magda Adelaide Lombardo
Gilberto Camara
Antonio Eduardo Costa Pereira

Instituto de Pesquisas Espaciais - INPE
Conselho Nacional de Desenvolvimento Científico e Tecnológico - CNPq
Caixa Postal 515 12200 São José dos Campos SP BRAZIL

and

José Roberto Tarifa

Universidade de São Paulo, São Paulo, SP BRAZIL

ABSTRACT

Researchers from INPE and USP have been working in monitoring urban São Paulo for some time. The main projects involve the monitoring the urban growth and the study of the urban heat island of metropolitan São Paulo. In this paper we are going to describe the two projects without going into details, which can be gotten in two other papers included in these proceedings. These papers are "The Use of Landsat Data to Monitor the Urban Growth of São Paulo Metropolitan Area" by Niero et al. and "Use of Infrared Images in the Delimitation of São Paulo's Heat Island" by Lombardo et al.

1. USE OF METEOROLOGICAL SATELLITES IN THE STUDY OF SÃO PAULO'S HEAT ISLAND

It is important to try to understand the relationship between the type of urban land use and the urban heat island as well as between the heat island and pollution. The understanding of these relationship could lead to a better control of urban land use and, in consequence, to better urban climates and quality of life. It could also lead to better projects of artificial towns, which are so common in fast growing countries like Brazil. Of course, to understand the relatioship between the heat island and land use, it is necessary to study the physics of the heat island. It is also necessary to study the heat island in places where it exists; this kind of study could help the meteorologists in constructing better models of the island and pinpointing its causes. This was the reason for starting the heat island project in INPE.

In the study of the heat island, meteorological measurements may be taken in situ. This kind of in situ measurements has been performed by many researchers in the Northern Hemisphere. It is possible to refer, among others, to Chandler (CHANDLER, 1965) and Shitara (SHITARA, 1964).

The in situ measurements can become very expensive and time consuming in the case of monitoring the heat island for long periods of time or in large areas. This was probably the reason which lead some researchers to use airplanes and satellites in this kind of monitoring. A paper about the use of satellites is that of Matson et al. (MATSON et al., 1978). The satellite images overcome some of the limitations of in situ measurements since they are widely available, inexpensive and are taken during all the year. Of course they have their own limitations; the values of temperatures obtained are less precise due to atmospheric effects and to the difficulties of determining certain parameters like emissivity; atmospheric effects, in particular, can, under certain conditions, make it absolutely impossible to get any usefull information from infrared images alone.

In the beginning of the project to study São Paulo's heat island, the researchers involved though of using in situ measurements. Afterwards it was decided to switch to satellite images due to the difficulties enumerated above. In the present study it was used as much ground truth as possible. The satellite radiometers, for example, are calibrated using surface reference temperatures (instead of the on board references). The reference temperatures are chosen in areas easily identifiable in the images and where the temperatures are homogeneous. Besides the reference temperatures, other temperatures measured in sity are used to check whether the results are good or not. The correction of atmospheric effects is made with the help of radiosondes. The general procedure to get a temperature image is similar to the one given by Chahine (CHAHINE, 1980) and is described in Lombardo et al. in these proceedings.

To perform studies of heat island one must first obtain temperature images from the count images received from the satellite. Putting these images in a graphical terminal and positioning the cursor in a point of the image, one can get the temperature of the point with a certain precision (0.5º C). In the delimitation of the heat island, we also use images of intervals of 1º C.

The result of our study is that there is a big heat island in the center of the city and smaller islands in industrial areas and secondary centers. It was noticed that the land use characteristis of the secondary centers are similar to the characteristics of the main center. The difference between the temperatures in the heat island and in the skirts of the city is of about 5º C. The temperature of urban parks is lower than in the areas surrounding the park. For more details, the reader is refered to Lombardo et al. in these proceedings.

2. MONITORING OF URBAN GROWTH IN METROPOLITAN SÃO PAULO

The monitoring of urban growth in São Paulo presents problems which are similar to the ones presented by the study of the urban heat island. One can make the monitoring by in situ observations, but these observations are expensive and time consuming. For this reason, researchers in INPE decided to study how good LANDSAT images are to monitor urban growth in São Paulo. Their results are encouraging and are presented by Niero et al. in these proceedings. The greatest problem found by Niero et al. was to separate urban from rural areas in the rural-urban fringe. This problem can be solved by studying many images at different periods, bearing in mind that rural areas present greater temporal variation than urban areas.

3. CONCLUSION

It is hoped that both the heat island and the urban growth projects associated with studies of urban land use will be useful to urban planners working with metropolitan São Paulo. The study of urban growth in a city like São Paulo is important, for example, to help in the control of growth toward protected areas (like parks, sanctuaries, reservoirs, etc.). The heat island project may be useful in allocation of urban space, specially if associated with studies of pollution.

BIBLIOGRAPHY

1. CHAHINE, M.T. "Infrared Remote Sensing of Sea Surface Temperature" in "Remote Sensing of Atmospheres and Oceans" edited by Adarsh Deepak, Academic Press, 1980.
2. CHANDLER, J. The Climate of London. London, Hutchinson University Library Publishers, 1965, 292p.

3. SHITARA, H. An Analysis of the distribution of the nocturnal air temperature in a coastal area Tokyo Journal of Climatology, 1(2): 84-85, 1964.

4. MATSON, M.; Mc CLAIN, E.P.; Mc GINNIS, D.F. & PRITCHARD, J.A. "Satellite detection of urban heat islands". Monthly Weather Review, 106(2): 1725-1734, 1978.

APPLICATION OF LANDSAT DATA TO GEOLOGIC MAPPING TROPICAL JUNGLE ENVIRONMENT: CARONI RIVER BASIN, VENEZUELA

Henry Briceño
Colorado School of Mines, Golden, Colorado, U.S.A.
Universidad Central de Venezuela, Caracas, Venezuela

Keenan Lee
Colorado School of Mines, Golden, Colorado, U.S.A.

ABSTRACT

Vegetation spectral information from LANDSAT and SLAR images, combined with landform analysis have been successfully applied to the detection of diamond-bearing placers in the jungle-covered mid-section of the Caroni River, Venezuela. Six targets were selected for exploration from the photogeologic interpretation; three out of four field-checked targets have proved to be diamondiferous. The remaining are also alluvial areas, but their diamond potentials await for exploration. Photogeologic maps from these images satisfactorily correspond with the regional geologic features in the area. Mapping and statistical analysis of over 9,000 linear features from SLAR and LANDSAT images show that illumination direction affects the data to the point of rendering it almost useless if not corrected for such effects. We have developed mathematical functions to correct for these illumination direction effects in SLAR and LANDSAT linear feature data.

1. INTRODUCTION

In the present study, photogeologic interpretation of the mid-section of the Caroni River basin, Venezuela (Fig. 1), was performed as the initial stage of a larger program for diamond placer exploration for the Ministry of Energy and Mines of Venezuela. The most outstanding obstacles facing the program were, among others, remoteness of the area, lack of access, thick jungle cover, extremely humid climate and poorly known geology. LANDSAT image No. E-21446-13324 and SLAR photomosaics No. NB-20-7, 8, 11 and 12 (Catogafia Nacional de Venezuela), and black-and-white aerial photography were selected for a systematic photogeologic analysis encompassing drainage maps, photogeologic maps, lineament maps, and finally, placer target selection. Thick and continuous vegetation cover, usually considered a constraint for geologic mapping with remote sensors, was used as the main source of data for the interpretation. The underlying rationale is that spatial changes in the spectral domain can be considered as a function of changes in vegetation type, density, stress, etc., which are functions of the soil physicochemical properties. The latter, in turn, are dependent upon the rock types from which the soil was developed. In short, the vegetation cover reflects the underlying bedrock. This simplistic approach, combined with landform analysis gave satisfactory results.

Mapping and statistical analysis of over 9,000 linear features from LANDSAT and SLAR images show that illumination direction (either sun azimuth or antenna look direction) affects the data so strongly, that it renders such uncorrected data almost useless for tectonic interpretation. During the

lineament analysis stage of this study, we have developed Modulation Transfer Functions (MTF) for LANDSAT and SLAR to correct for these illumination direction effects.

2. LANDSAT

Four types of LANDSAT images at 1:250,000 scale were used in this study, (1) black-and-white MSS-7 standard product from EROS; (2) false color composite (FCC) from MSS-4 (blue), MSS-6 (green) and MSS-7 (red); (3) color ratio composite (CRC) from MSS-4/MSS-5 (red), MSS-4/MSS-6 (blue) and MSS-6/MSS-7 (green); and (4) color ratio image (5/6 R) from three different stretchings of the MSS-5/MSS-6 relation, as described by Raines and others (1979). The color images were kindly processed at the U.S.G.S. Remote Sensing Branch at Denver by Don Sawatsky and Dan Knepper.

2.1 Geomorphology

The geomorphological analysis began with the delineation of drainage patterns, for which LANDSAT MSS-7 (Fig. 2) proved to be the best choice. Drainage mapping at a scale of 1:250,000 highlights the anomalous patterns of the Caroni River and its tributaries by showing abundant barbed junctions, rapids and deranged areas (Fig. 3). These features suggest captures and channel diversions in recent times. The works of van der Hammen (1972), Barbosa and Ramos (1961), and Garner (1967), indicating that climatic changes in the last few thousand years have periodically stripped the jungle cover in the Amazon region, partially explain these drainage anomalies. Field observations during this study have detected the existence of a thin veneer of fine-to-very-fine grained sands carpeting most of the erosional surface at 400 m.a.s.l.; furthermore, old dunes covered with bushy vegetation have been located west of Canaima (Fig. 3). These features indicate a dry period when wind-blown sediments were spread over the region. Radiocarbon dating of fluvial sediment immediately underlying these fine sediments gave an age of 8,030 ± 110 years B.P.; the fine grained sediments, of probable eolian origin, show a depositional break at their mid-section that has been dated as 6,470 ± 340 years B.P. From these geomorphological and radiocarbon dating data, we postulate that the climate in the region changed from very humid (woodland forest) to dry (open savanna) about 8,000 years ago, and the dry period extended until about 6,000 years ago, when humid conditions resumed. A second climatic cycle seems to follow, with a period of aridity preceding the present conditions of humid jungle.

A feature common to both the Caroni and Paragua rivers, is the presence of wide valleys west of their narrow, structurally controlled channels. These wide valleys seem to be the natural courses of the proto-Caroni and proto-Paragua rivers; furthermore, the Caroni in its mid-section is an "overfit stream", meaning that it carries too much water for such a narrow valley. These evidences point toward a northeast tilting of the northern part of the Guayana Shield during the Holocene, causing the river channels to migrate eastward and to lean against the east margin of their proto-valleys.

Four major planation surfaces have been documented: (1) the top of the Auyantepuy, lying at about 2,600 m.a.s.l., characterized by an unique example of karst topography developed on silicified sandstones, correlated with the Pakaraima Surface of Guyana (McConnell, 1969); (2) the continuation of the Gran Sabana Surface at about 1,200 m.a.s.l. south of the Auyantepuy plateau; (3) scattered renments of a planation surface at 500-600 m.a.s.l. that may be correlated with the Kopinang Surface of Surinam and Brazil of Late Cretaceous to early Tertiary age (McConnell, 1969); and (4) the floor of the central valley at about 400 m.a.s.l., which probably correlates with the Kaieteur Surface of mid Tertiary age (McConnell, 1969).

The three lower planation surfaces are covered with persistent laterite profiles. The 400 m surface is of special importance in the present study because the major diamond placers in the region occur on it, or in topographic lows developed by erosion of the laterite.

2.2 Rock-unit map

By mapping on MSS-7 (Fig. 2), combining spectral and landform data, we have obtained a land cover map that closely resembles the geographical distribution of the lithologic units (Fig. 4). The major rock units in the area, the Cuchivero Group metamorphic rocks, the Roraima Group sedimentary rocks and a suite of intrusives have been accurately delineated. Although only subdivision at the formation level are presented in this paper, a more detailed subdivision, down to member rank, has been performed in the study.

The Cuchivero metamorphic rocks occupy the central and south parts of the area, and display minor topographic relief as rolling hills and scattered mountains above the level of the flat central valley (Figs. 3, 4). The low relief areas correspond to the location of the metavolcanic and metasedimentary rocks (P€_{cm}) covered with the thickest vegetation, and the higher mountains in the southern part of the central valley are developed on massive and resistant units of probable intrusive origin (P€_{cq}), supporting lighter vegetation

The Roraima sedimentary rocks (P€_{r}) and associated diabase sills are easily interpreted by their layered appearance and cliff-forming nature. These sedimentary rocks, except for the shales, support less vegetation than the Cuchivero rocks. The diabases support very lush vegetation except at the mountain tops where lateritic profiles are thick. In the northern part of the central valley is a section of sedimentary rocks (P€_{s}), which underlies the Roraima Group, and has not been previously described in the literature.

Finally, the apparently unmetamorphosed intrusive rocks (P€_{I}) crop out south of the Guaiquinima Plateau as massive, circular, high relief features above the Paragua River valley. They are covered with vegetation as dense as that on the Cuchivero metamorphosed intrusives, and with similar spectral properties, suggesting similar intermediate-to-felsic composition.

3. SLAR AND AERIAL PHOTOGRAPHY

SLAR photomosaics were used for lineament mapping and for gathering textural and topographic information to complement the LANDSAT interpretation. The combination of the high spatial resolution of SLAR (14 m) and the spectral information from LANDSAT proved to be complementary for mapping in this environment. Textural differences on the vegetation seen in SLAR are generally expressed as either tonal or color differences in LANDSAT images.

Black-and-white aerial photography at scales ranging from 1:120,000 to 1:25,000 were used at the end of the interpretation stage to map structural details not observable in the LANDSAT and SLAR images. The full potential of these photographs has not been exploited.

4. LINEAMENT ANALYSIS

The approach taken to lineament mapping in the present study was a slightly selective one, in which all linear features were mapped except bedding planes, obvious cultural features, or sensor artifacts. Linear feature maps were interpreted from LANDSAT black-and-white MSS-7 and from SLAR mosaics, both at a scale of 1:250,000.

A total of 9,478 linear features were mapped; 4,349 were LANDSAT linear features and 5,125 SLAR linear features. Serious discrepancies are observed between LANDSAT and SLAR distribution and even between SLAR distributions mapped in the Roraima Group north and south of 6^{o} North Latitude (Fig. 5). These discrepancies arise because the area north of 6^{o} North Latitude (Area A) was imaged with SLAR under illumination from the east, the area to the south (Area B) under illumination from the north, and finally, the sun azimuth for LANDSAT was 126 degrees.

The works of Wise (1969), Sawatsky and Lee (1974) and Eppes and Rouse (1974) have shown that the detectability of any given linear feature is a function, among other factors, of the deviation angle (δ) and the relationship between the depression angle (or solar angle) and the slope angle. For an actual distribution of linear features (X_a) in a given area, the relationship with the observed (mapped) distribution of linear features (X_o) is as follows:

$$X_o = X_a * MTF \tag{1}$$

where MTF is the Modulation Transfer Function for the sensor system applied (e.g., MTF_s is the MTF for SLAR).

<u>4.1 SLAR Modulation Transfer Function</u>

Considering the ROraima Group SLAR distributions in areas A and B,

$$X_{o,A} = X_{a,A} * MTF_{S,A} \text{ and } X_{o,B} = X_{a,B} * MTF_{S,B} \tag{2}$$

and $$MTF_{S,A} = (MTF_{S,B})^{-1} \tag{3}$$

where equation (3) should hold because the same sensor (SLAR) was used, but the illumination direction differed by 90^{o}. Also, because the areas A and B have about the same linear feature distributions as seen from LANDSAT data (Fig. 5c, d), then,

$$X_{a,A} \simeq X_{a,B} \tag{4}$$

From equations (2), (3) and (4), the actual frequency of linear features in the overall area (A + B), is obtained,

$$X_{a,(A+B)} = \sqrt{X_{o,A} * X_{o,B}} \tag{5}$$

and for each azimuth direction θ, the relationship is:

$$x_{a,(A+B),\theta} = \sqrt{x_{o,A,\theta} * x_{o,B,\theta}} \tag{6}$$

finally, the amplitude of the MTS_s at each azimuth direction θ is given by,

$$\text{Amp. } MTF_{s,\theta} = \sqrt{x_{o,B,\theta}/x_{o,A,\theta}} \tag{7}$$

The discrete nature of the linear feature distributions complicates the derivation of the MTF_s with equation (7), so computer modelling of the MTF_s was carried out using non-recursive filters. The best result was obtained with a function similar to the one suggested by Eppes and others (1974). The function is shown in Fig. 6, and has the form of,

$$\text{Amp. } MTF_{S,\delta} = \sqrt{\frac{1. - \text{Cos } 2\delta}{2}} + .1511 \tag{8}$$

where δ = deviation angle (angle between the illumination direction and the linear feature). This function is graphically shown in Fig. 6.

The Roraima Group SLAR data from areas A and B were corrected with their respective MTF^{-1} and the average of these two corrected distributions was calculated to represent the corrected frequency distribution in the overall

area. This average distribution is plotted in Fig. 7, together with the distribution obtained from equation (6). The high correlation between these two distributions indicates that either is representative of the actual frequency distribution of linear features in the Roraima Group rocks, and furthermore, it confirms the assumption that there is no significant difference in tectonic style between the north and south areas (areas A and B).

4.2 LANDSAT Modulation Transfer Function

Once the actual distribution of lineaments in the Roraima was obtained, the derivation of the MTF_L for LANDSAT was tackled, and so far, the best approximation has the following form,

$$\text{Amp. } MTF_{L,\delta} = \frac{1.03 - \cos 2\delta}{9.21 - 7.\ \cos 2\delta} \qquad (9)$$

This function is shown graphically in Fig. 8.

4.3 Significant trends in linear features

The significant maxima and minima (Knepper, 1974) were calculated for each corrected linear feature distribution and are shown in Fig. 9. They are very similar for the Cuchivero Group and the Roraima Group, but the intrusive rocks show low correlation between sensors, perhaps due to the small sample population considered. In the Cuchivero Group the NW linear feature trends are related mostly to foliation, although some faulting and jointing of secondary importance occur. The NE linear features represent fracturing, either along right-lateral shear zones of considerable extent (tens of kilometers) or joints. In the Roraima Group rocks, the NW trend represents joints and normal faulting associated with the gentle folding of the sedimentary section. Major faults (tens of km) parallel the fold axial planes in many instances. The NE lineament trends in the Roraima are associated with faults (some up to 80 km long), dikes, and joints. The intrusives show a persistent NE trend of long fractures (tens of km), probably faults, and north-trending linear features of secondary importance. The NW trend is due mostly to joints.

Finally, the frequency distributions for each rock groups were compared by using ternary diagrams (Fig. 10). In these diagrams, the azimuth axis is perpendicular to the plane of the triangle, and a given point in the plot represents the relationship among the frequencies of linear features in the three rock types, at a specific azimuth direction. As an example, for a given azimuth direction δ, the Roraima coordinate (R_C) is obtained as follows:

$$R_C = (x_{R,\delta} / (x_{R,\delta} + x_{C,\delta} + x_{I,\delta})) * 100.$$

where,

$x_{R,\delta}$ = frequency of linear features in Roraima rocks at azimuth δ

$x_{C,\delta}$ = frequency of linear features in Cuchivero rocks at azimuth δ

$x_{I,\delta}$ = frequency of linear features in Intrusive rocks at azimuth δ

A large subset of data falls along the Cuchivero-Roraima axis, denoting linear features common to these two rock groups and suggesting that the emplacement of the intrusives postdates major fracturing of the Roraima Group rocks. Because the Roraima has been dated as 1.8 b.y. old (Snelling and McConnell, 1969), the intrusives probably belong to the widely documented thermal event that took place 1.5 b.y. ago.

/

5. EXPLORATION TARGET SELECTION

The most important criteria used for selecting potential diamond bearing placers are:

I-Geographic-geomorphic criteria
1.-Large, structureless (flat) areas at about 400 m.a.s.l.;
2.-Close spatial association to the Lower Roraima rocks, believed to be the immediate source of diamonds;
3.-Areas located along the postulated proto-Caroni valley;
4.-Areas lacking the linear features prevailing in the surrounding rocks; and
5.-Elongated areas whose general pattern is unrelated to the local trend of the rock units.

II-Spectral criteria
1.-Uniform tone of medium-to-dark gray in the MSS-7 image;
2.-Dark reddish-gray color in the FCC image; and
3.-Light blue areas in the 5/6 R image.

Results

By using these criteria, six major targets were selected (Fig. 4) for further exploration. Four targets have been field-checked at the time of this writing, and three of them were diamond-bearing placers. The remaining targets also are alluvial areas, but assessment of their diamond potential awaits exploration.

6. CONCLUSIONS

The conclusions of our work can be summarized as follows:

1. The use of vegetation as the primary source of spectral data, combined with landform analysis, for discrimination of geologic units is a powerful tool for regional geologic mapping in tropical jungle.
2. Drastic climatic changes, together with northwastward tilting of the northern part of the Guayana Shield, have developed the abnormal drainage pattern of the Caroni River basin.
3. Linear feature data, interpreted from a single image from either LANDSAT or SLAR, are NOT representative of the linear feature population in the imaged area. If only one illumination-source image is used for interpretaion of linear features, it MUST be corrected for illumination direction effects before any geologic interpretation from these features is performed. The inverse of the MTF's presented here (Figs. 6 and 8) are suggested corrections.

7. REFERENCES

Barbosa, O. and Ramos, J., 1961, Principal aspects of the geomorphology and geology in the Territory of Rio Branco, Brazil: Proc. 5th Inter-Guiana Geol. Conf., Georgetown, British Guiana, p. 33-36.

Eppes, T. and Rouse, J., 1974, Viewing-angle effects in radar images: Photog. Eng., v. 40, p. 169-173.

Garner, H., 1967, Rivers in the making: Sci. Amer., v. 216, p. 84-94.

Knepper, D. (Editor), 1974, Geological and mineral and water resources investigations in western Colorado using ERTS-1 data: Final Report: Colorado Sch. Mines, Rem. Sen. Rept. 75-1, p. 130-134.

McConnell, R., 1969, The succession of erosion bevels in Guyana: Geol. Surv. Guy. Rec., v. VI, p. VIII-1-16.

Raines, G., Offield, T. and Santos, E., 1978, Remote sensing and subsurface definition of facies and structure related to uranium deposits, Powder River Basin, Wyoming: Econ. Geol., v. 73, p. 1706-1723.

Sawatsky, D. and Lee, K., 1974, New uses of shadow enhancement: Colorado Sch. Mines, Rem. Sen. Rept. 74-5, 20 p.

Snelling, N. and McConnell, R., 1969, The geochronology of Guyana: Geol. Mijn., v. 48, p. 201-213.

van der Hammen, Th., 1972, Changes in vegetation and climate in the Amazon Basin and surrounding areas during the Pleistocene: Geol. Mijn., v. 51, p. 641-643.

Wise, D., 1969, Pseudo-radar topographic shadowing for detection of sub-continental sized fracture systems: Proc. VI Int. Sym. Rem. Sen. Env., v. 1, p. 603-615.

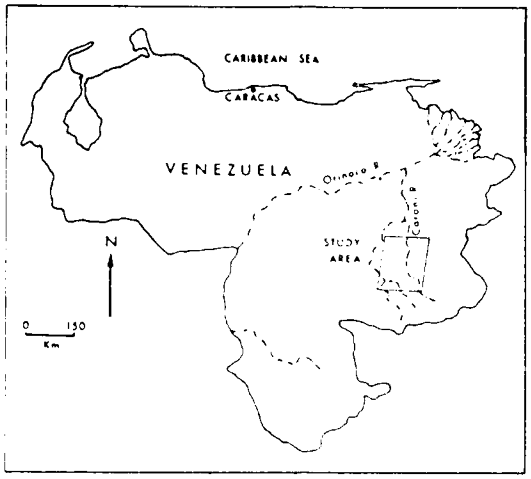

Fig. 1 Location Map

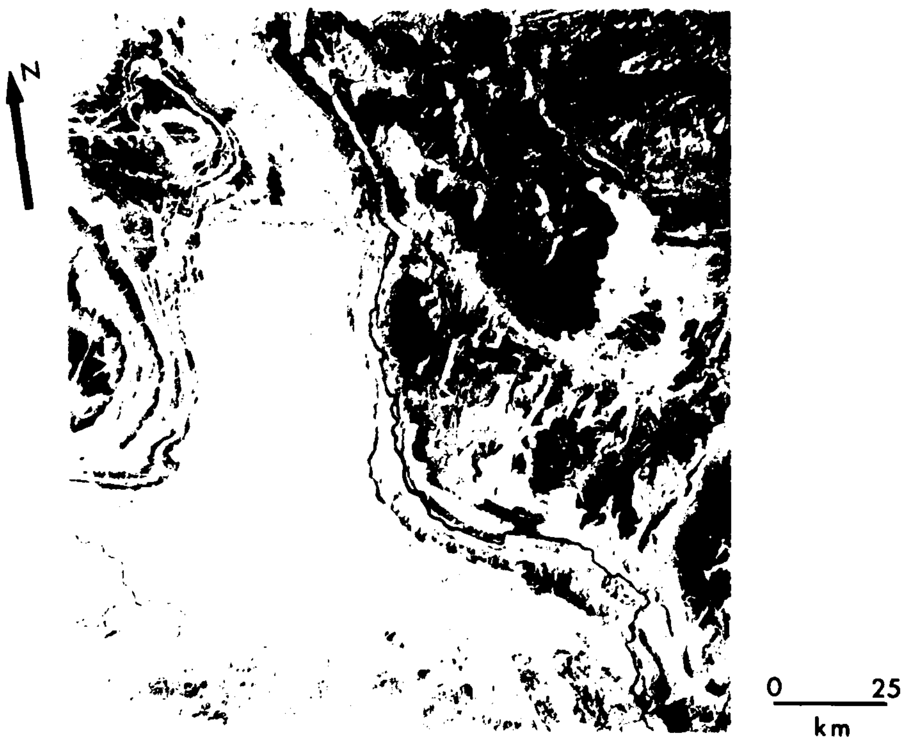

Fig. 2 LANDSAT MSS-7

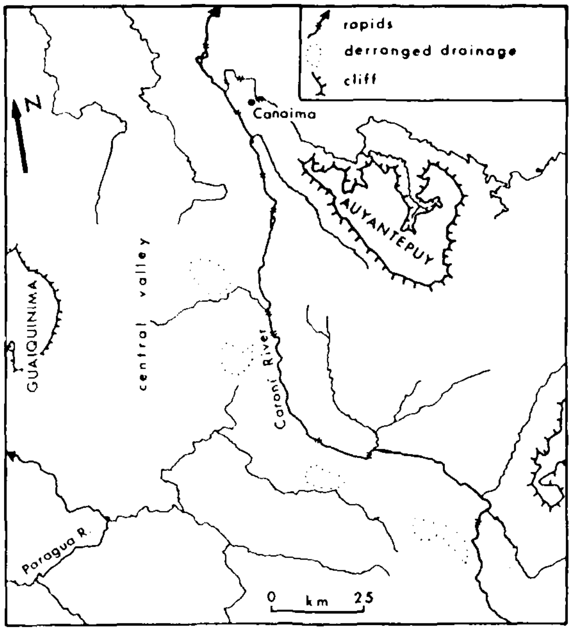

Fig. 3
Generalized
drainage map

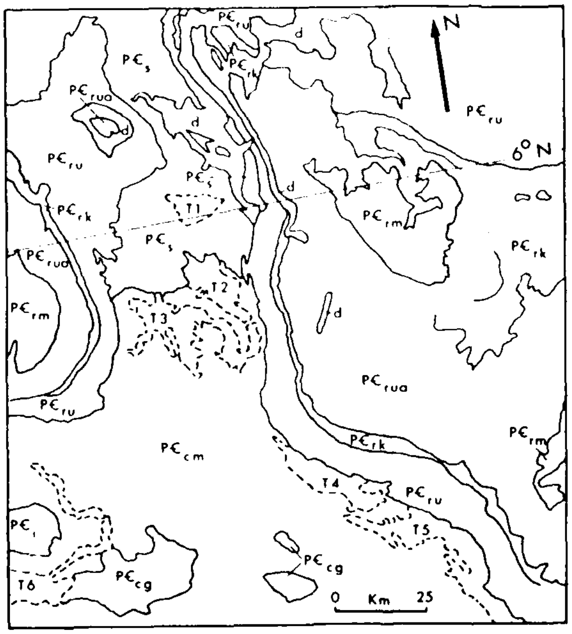

Fig. 4
Generalized Photogeologic
Interpretation

T3	Exploration Target		
$P\mathcal{E}_i$	Intrusives		
d	diabase		
$P\mathcal{E}_{rm}$	Mataui Fm.		Roraima Gp.
$P\mathcal{E}_{rua}$	Uaimapué Fm.		Roraima Gp.
$P\mathcal{E}_{rk}$	Kukenan Fm.		Roraima Gp.
$P\mathcal{E}_{ru}$	Uairén Fm.		Roraima Gp.
$P\mathcal{E}_s$	pre-Roraima sediments		
$P\mathcal{E}_{cg}$	meta-intrusives		Cuchivero Gp
$P\mathcal{E}_{cm}$	metavolcanics		Cuchivero Gp

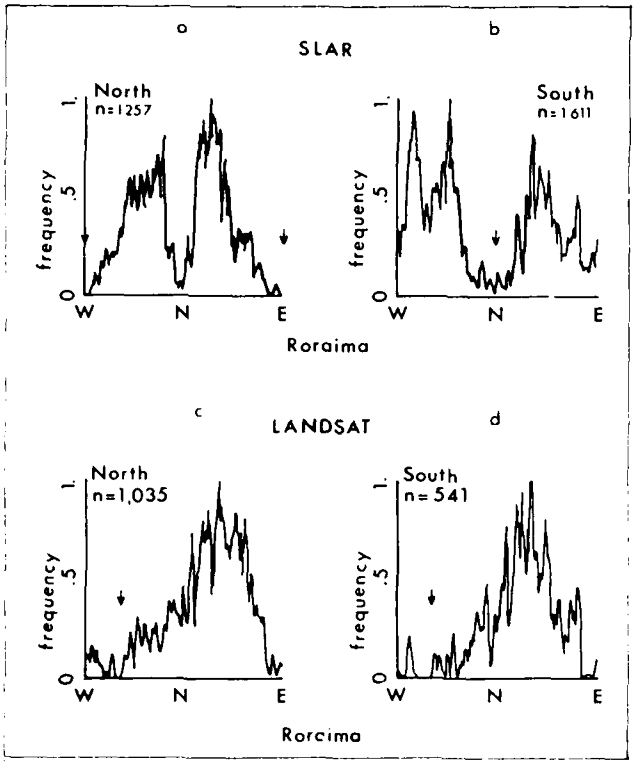

Fig. 5 Linear feature distributions north and south of 6° N Latitude
(↓ illumination direction)

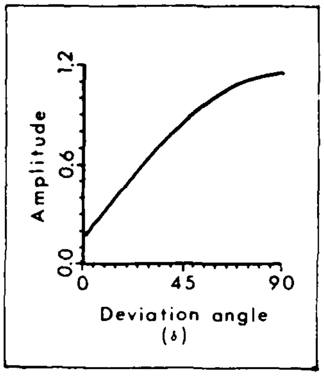

Fig. 6 SLAR Modulation Transfer Function

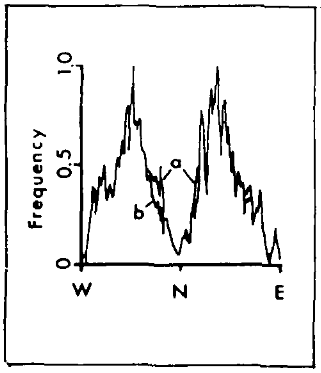

Fig. 7 Roraima SLAR distributions
a = corrected and averaged
b = from Equation 6

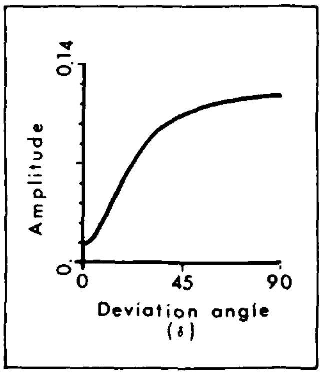

Fig. 8 LANDSAT Modulation Transfer Function

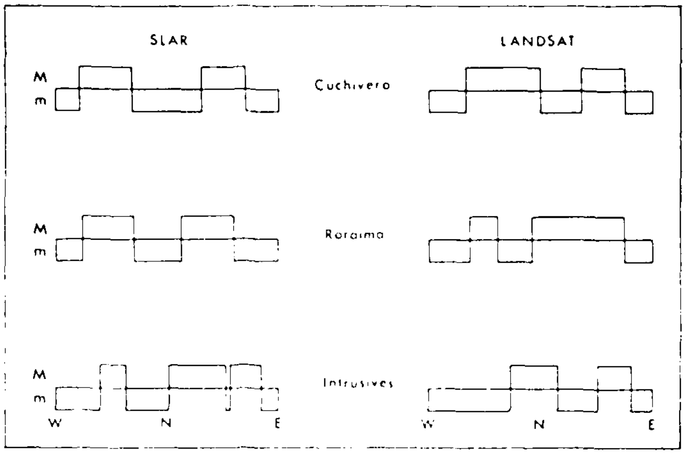

Fig. 9 Significant maxima (M) and minima (m)

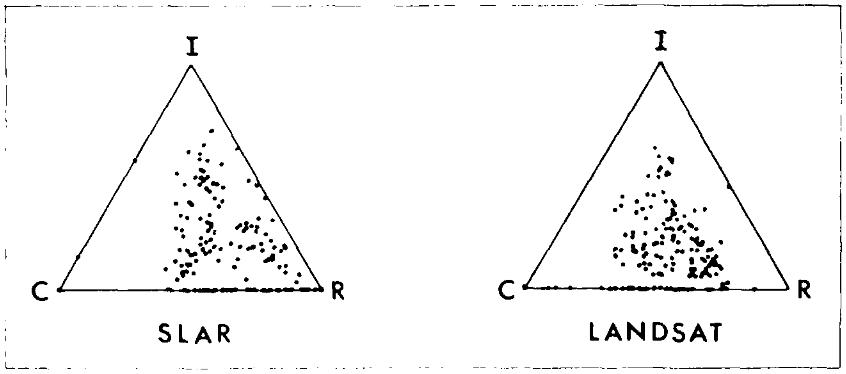

Fig. 10 Ternary diagrams for linear feature frequencies
(C = Cuchivero; R = Roraima; I = Intrusives)

GEOBOTANICAL DISCRIMINATION OF ULTRAMAFIC PARENT MATERIALS: AN EVALUATION OF REMOTE SENSING TECHNIQUES*

D. A. Mouat

NASA Ames Research Center
Moffett Field, California, U.S.A.

L. A. Morrissey
E. M. Horn

Technicolor Government Services, Inc.
NASA Ames Research Center
Moffett Field, California, U.S.A.

ABSTRACT

Color and color infrared aerial photography and imagery acquired from a Daedalus DEI-1260 multispectral airborne scanner were employed in an investigation to discriminate ultramafic rock types in a test site in southwest Oregon. An analysis of the relationships between vegetation characteristics and parent materials was performed using a vegetation classification and map developed for the project, lithologic information derived from published geologic maps of the region, and terrain information gathered in the field.

Several analytical methods including visual image analysis, band ratioing, principal components analysis, and contrast enhancement and subsequent color composite generation were used in the investigation. There was a close correspondence between vegetation types and major rock types. These were readily discriminated by the remote sensing techniques. It was found that ultramafic rock types were separable from non-ultramafic rock types and serpentine was distinguishable from non-serpentinized peridotite. Further investigations involving spectroradiometric and digital classification techniques are being performed to further identify rock types and to discriminate chromium and nickel-bearing rock types.

1. INTRODUCTION

Most techniques for rock type discrimination involve a direct analysis of some set or sets of attributes or characteristics of the rock types themselves.

*Presented at the Seventeenth International Symposium on Remote Sensing of Environment, Ann Arbor, Michigan, May 9-13, 1983.

Remote sensing techniques for rock type discrimination are highly oriented toward the surface materials. Most systems in use are oriented toward these same surface materials. As such, remote sensing-based strategies in areas of high vegetation cover are precluded from making direct observations of the soil and rock surface. The use of remote sensing in these areas is often restricted to structural analysis; vegetation is frequently ignored. That vegetation is often associated with geologic parameters has long been known.[1,2] These references report on research showing close correlations among vegetation characteristics and geological parameters. Those vegetation characteristics can be used to derive geologic information and to discriminate parent materials. This strategy forms the basis of geobotany.

Remote sensing-based geobotanical investigations center on the manner in which vegetation parameters interact with electromagnetic radiation and frequently include ancillary information such as terrain factors. That interaction is used to describe differences in the geologic landscape. The remote sensing techniques rely upon a careful consideration of those vegetation parameters which correlate with parent materials and which can also be readily detectable.

2. STUDY AREA

A study area was selected in southwestern Oregon within the Siskiyou Mountains (Figure 1). This region is known for its unique vegetation and geology. A wide diversity of vegetation types has been recognized[3] as occurring in relation to the steep climatic gradients and diverse parent materials of the area.

A test site of approximately 25 square kilometers was selected from within the larger study area in order to establish vegetation-parent material relationships and to develop and test remote sensing techniques for discriminating the geobotanical associations. The test site is representative of the larger area in that it traverses a diverse assemblage of rock types (including ultramafics) and vegetation. It is located in southwest Josephine County (Figure 1) and is characterized by rugged topography with elevations ranging from approximately 400 meters along the Illinois River to nearly 1500 meters near Fiddler Mountain. Cave Junction, with a population of approximately 1,000, is located eight kilometers to the south.

The location of the study area dictates a wide range of climatic conditions dependent upon elevation, aspect, and position. The climate adjacent to and west of the study area is strongly influenced by maritime air from the Pacific Ocean. Summers are mild, with mean temperatures of 20 degrees C., and precipitation is scant. Winters are cool with mean temperatures averaging near 5 degrees C., and precipitation is heavy. Most of the precipitation occurs during the late Fall, Winter, and early Spring and usually exceeds 200 cm. Further east, the maritime influence decreases. Fog and humidity are decreased and temperatures are a bit more extreme than on the west side of the ranges. Precipitation is also less, averaging between 100 and 200 cm. Within the study area, snow rarely exceeds one meter below an elevation of 1,000 meters (climate data is from Meyer and Amaranthus[4]). As might be expected, both temperature and snow accumulation are greatly affected by elevation as well as by aspect. The effect on the vegetation is often dramatic.

3. GEOLOGY AND VEGETATION

3.1 GEOLOGY

The study area occurs within the Klamath Mountains geomorphic province of northern California and southwestern Oregon. These mountains consist of four north-trending arcuate belts of rocks which are convex to the west[5]. The two western belts, the Western Paleozoic and Triassic Belt and the Western

Jurassic Belt go through Josephine County. The study area occurs primarily within the Western Jurassic which includes the Galice and Rogue Formations and associated ultramafic rocks. The rock units dip steeply to the east and include several thrust faults.

The Galice Formation consists primarily of metasedimentary and metavolcanic rocks. The former include slaty shales and slaty siltstones along with poorly sorted shale, siltstones, and sandstones of mixed origin. The metavolcanics consist primarily of thick breccias and tuffs as well as andesitic flow rocks.

Ultramafic rocks, apparently injected into the metavolcanics and metasediments in a solid mass, occur as narrow lenses and stringers within the Galice and Rogue Formations. They also occur as massive plates or sheets, one of which extends through the test site. The ultramafic rock types include peridotite, serpentinite, and serpentinized peridotites varying in composition from dunite to pyroxenite. Some of these rock types (e.g. dunite) are almost emtirely olivine $(Mg, Fe)_2 SiO_4$) and, as such, may have extremely low calcium/magnesium (Ca/Mg) ratios. This chemical composition may have profound implications for the associated vegetation assemblages which occur within the region.

3.2 VEGETATION

The vegetation of the study area region is one which combines elements of the California, coastal Oregon and eastern Oregon floras with a large number of species indigenous only to the Klamath Mountains region.[6] It results from a complex interaction of cultural, climatic, geologic, and topographic factors.

The study area region's vegetation follows the distribution of vegetation zones as described by Franklin and Dyrness (1973).[6] The zonal outline follows:

Zone	Dominant species or genera
Interior Valley Zone	Pine, Oak, Douglas fir
Mixed - Evergreen Zone	Douglas fir - Sclerophyll shrubs
Mixed Conifer Zone	Douglas fir, Pine, Incense cedar
White fir Zone	White fir

These types are greatly modified by fire and logging practices. Whittaker described changes in vegetation according to a variety of environmental gradients (primarily aspect, elevation, moisture, and rock type).[3] He described the vegetation for three representative rock types: diorite, gabbro, and serpentine. Low elevation diorite vegetation gradates from Port Orford cedar - Douglas fir forests in mesic sites through Douglas fir forests with sclerophyll trees in intermediate sites, to sclerophyll forest with scattered Douglas fir in xeric sites. Low elevation gabbro vegetation gradates from more open Port Orford cedar - Douglas fir stands, through more open sclerophyll - Douglas fir stands, to open, xeric pine - Douglas fir - oak - manzanita stands. Low elevation serpentine vegetation gradates from still more open Port Orford cedar - western white pine - Douglas fir mesic stands, through very distinctive forest-shrub stands with several conifers and two-phase undergrowth of sclerophyll shrubs and grasses, to Jeffrey pine woodlands. Toward higher elevations on diorite, the forests of Douglas fir and sclerophylls gradate into montane forests dominated by Douglas fir and white fir above 1200 m. Higher elevation vegetation on gabbro and on serpentine consists of an expansion of the types mentioned for their lower elevation counterparts with the mesic types expanding toward the xeric sites. The higher elevation

vegetation on gabbro is also characterized by an increasing abundance of true firs (Abies spp.) and by the presence of Brewer's spruce (Picea brewerana).

4. METHODS

Methods were developed to correlate vegetation factors with lithologic and terrain factors and then to discriminate those relevant vegetation parameters with the use of remote sensing techniques.

A preliminary vegetation classification was developed for the test site and was subsequently used to correlate that vegetation with topographic and lithologic factors. The test site was first stratified by general rock type[7] and then by homogeneous image type as interpreted from the analysis of available color and color infrared photography at several scales (1:15,840, 1:24,000, 1:48,000, and 1:130,000). Sample sites were randomly selected within the constraints of access to transportation routes. During the Fall of 1981, data were collected on species composition (of the tree and shrub layers), species dominance and cover, total vegetation cover, slope angle, aspect, elevation, and rock type. The field vegetation information was combined with published and unpublished research on the Siskiyou Mountains vegetation in order to provide a vegetation classification framework within which the types of the test site could be placed. Table 1 illustrates the preliminary hierarchical physiognomic vegetation classification developed for the project. Those types which occur within the test site are marked by an asterisk (*).

The vegetation information was integrated with the lithologic and terrain information on an ESL Interactive Digital Image Manipulation System (IDIMS) by recording values of those parameters to areas covered by pixels acquired from two overflights of the study area with a U-2 aircraft carrying a Daedalus DEI-1260 airborne scanner. Imagery was acquired on September 11, 1981 and on July 15, 1982. The 1.25mrad IFOV resulted in a spatial resolution of approximately 25m over the study area region. Each flight had a somewhat different spectral configuration (Table 2).

Both sets of imagery were first processed to simulate color infrared photography. A false color composite (FCC) was generated from channels 7, 5, and 3 (red, green, and blue were assigned to those channels, respectively) of the July 1982 imagery. A subsequent composite from the same imagery was generated from the ratios of channels 7:5, 5:3, and 10:9 (red, green, and blue were assigned to those ratios, respectively). Along with similar composites from the previous data set, these were the primary images used in subsequent analyses. Channel 10 of the September 1981 imagery (2.05 - 2.35um) was contrast enhanced for use in direct rock type discrimination. A principal components analysis (A Karhunen-Loeve transformation) was performed on both sets of imagery (figure 2). Landsat MSS FCC imagery from September 11, 1979 (scene id. # 21693-18111) was acquired for subsequent analysis.

5.0 RESULTS

Ground information collected from the field sites was used to correlate landscape attributes and to identify and evaluate the spectral data sets. Contingency tables comparing the ground information with the landscape attributes were computed to correlate vegetation types with parent materials and soils. These tables were analyzed to determine significant vegetation-terrain relationships. This analysis provided the basis for a statistical description of the distribution of each vegetation type in terms of the other landscape variables. This same ground information was also compared with the digital information to identify spectral classes. Results from those two sets of contingency tables were then used in a comparative evaluation of the various data sets generated in the analysis.

A number of results can be extracted from the contingency tables which

were generated with an IDIMS software package:

1. Several vegetation types occur on ultramafic parent materials and are completely absent on non-ultramafic parent materials. Included are both of the Jeffrey pine dominated conifer forest types (Do and Dc in the classification), the open Douglas fir - mixed oak forest type (Lo), the open Douglas fir - tanoak type (No), the open shrubby California laurel type (So), and the open grass type (Uo).

2. Two types occurred only on metavolcanic and/or on metasedimentary rock types. These were the closed Douglas fir - tanoak forest type (Nc) and the open manzanita - ceanothus type (Po).

3. The remaining types occurred on several rock types.

4. The near IR to red (channels 7 and 5; July 1982 imagery) ratio was able to separate these groups. The other ratios were less successful.

The Landsat MSS FCC imagery was poorly suited for separating the rock types on account of poor scale (resolution) and poor color differentiation. The principal components analysis showed that the first component, probably related to brightness, was poorly suited for separating the rock types, while the second component, probably related to greenness, was more successful. This would seem to indicate the importance of vegetation information in separating rock types in this region. The third principal component was completely speckled and was probably due to poor data acquired for two of the channels. The fourth component appeared to be related to terrain texture and was not directly useful in the geobotanical analysis although it may prove useful for providing information on rock structure. Figure 2 illustrates principal components 1, 2, and 4 for most of the test site. The enhanced channel 10 appeared to be highly useful in separating areas of serpentine. Both the color and color infrared aerial photography were useful for identifying the general vegetation types which were correlated with the rock types.

6. DISCUSSION

Relationships between vegetation characteristics and rock type in the Siskiyou Mountains have been described by several researchers. This study substantiates a number of their hypotheses and suggests areas for continued study especially with the use of remote sensing techniques.

Vegetation on ultramafic rock types is much more open and the tree layer is much sparser than on neighboring non-ultramafic rock types having similar environmental characteristics (Figure 3). Ultramafic rock types are characterized by a much greater percentage of conifer species in the tree canopy than do non-ultramafic rock types. Several broadleaf species which occur on non-ultramafic rock types in the tree form are very common, and often dominate, in ultramafic rock types in a shrubby form (these include California laurel, canyon live oak, tanoak, and chinkapin). This study not only shows that vegetation type differs with rock type, but also that vegetation density changes as well.

One hypothesis suggests that ultramafic rock types result in early seral vegetation types. Whittaker[8] suggests the following evidence to refute this theory: seedling data show that the dominant trees are reproducing; soil data show that serpentine soils are just as mature as diorite soils; islands of ultramafic rock types within non-ultramafic rock types have the same kinds of vegetation which occur in much larger areas of ultramafics. While fire is of major influence, it probably does not differentially affect ultramafic rock types.

Whittaker[3,8], White[9], and Kruckeberg[10] show that low calcium levels and a low Ca/Mg ratio result in calcium nutrient deficiencies in some instances and magnesium toxicity in other cases. Whittaker[3,8] further adds that xeromorphism is a characteristic effect of serpentine soils on the vegetation. White[9] has discussed the toxicity of chromium, nickel, and cobalt.

Thus the vegetation which develops in the region is one which is differentially affected by xericity, nutrient, deficiencies, magnesium and possibly chromium, nickel, and cobalt toxicity. The esponse in the vegetation is dramatic.

Remote sensing techniques which can discriminate the resultant differences in vegetation type and density can be used to separate rock type. Differentiation of rock types within ultramafic units and isolation of anomalous deposits of several minerals (including Cr, Ni, and Co) may further affect floristic and physiognomic characteristics of the vegetation and may affect their spectral distribution.

7. CONCLUSIONS

The following conclusions are drawn from the results of this on-going investigation:

1. There exists a number of close relationships between vegetation characteristics and lithologic factors in areas containing ultramafic rock types in southweast Oregon.

2. Vegetation type and density is often quite different on ultramafic rock types as compared with non-ultramafic rock types. These can often be used to discriminate those rock types.

3. Image processing of airborne multispectral scanner data can be used to differentiate those vegetation factors which correlate with ultramafic rock type.

4. Ultramafic rock types can be differentiated from other rock types by the use of these techniques.

8. REFERENCES

1. Brooks, R. R. 1972. Geobotany and biogeochemistry in mineral prospecting. New York, Harper and Row, 290p.

2. Mouat, D. A. 1974. Relationships between vegetation and terrain variables in southeastern Arizona. Ph. D. dissertation, Oregon State University, Corvallis, 242p.

3. Whittaker, R. H. 1960. Vegetation of the Siskiyou Mountains, Oregon and California. Ecological Monographs, 30:279-338

4. Meyer, L. C. and M. P. Amaranthus. 1979. Siskiyou National Forest Soil Resource Inventory. U.S.D.A. Forest Service, Pacific Northwest Region, 258p.

5. Hutz, P. E. 1971. Plutonic rocks of the Klamath Mountains, California and Oregon. U.S. Geological Survey Prof. Paper 684-B, 20p.

6. Franklin, J. F. and C. T Dyrness. 1973. Natural vegetation of Oregon and Washington. U.S.D.A. Forest Service, Pacific Northwest Forest and Range Exp. Station General Tech Report PNW-8, 417p.

7. Ramp, L. and N. V. Peterson. 1979. Geology and Mineral Resources of Josephine County, Oregon. State of Oregon Dept. of Geology and Mineral Industries Bulletin 100, 45p. with map

8. Whittaker, R. H. 1954. The ecology of serpentine soils: a Symposium. IV. The vegetational response to serpentine soils. Ecology 35:275-288.

9. White, C. D. 1971. Vegetation-soil chemistry correlations in serpentine ecosystems. Ph.D. dissertation, Oregon State University, Corvallis, 274p.

10. Kruckeberg, A. R. 1969. Plant life on serpentinite and other Ferro-magnesian rocks in northwestern North America. Syesis Vol. 2, parts 1 and 2, pp15-119.

11. Wells, F. G. and D. C. Peck. 1961. Geologic map of Oregon west of the 121st meridian. State of Oregon Dept. of Geology and Mineral Industries Misc. Geological Investigations Map I-325 (1:500,000).

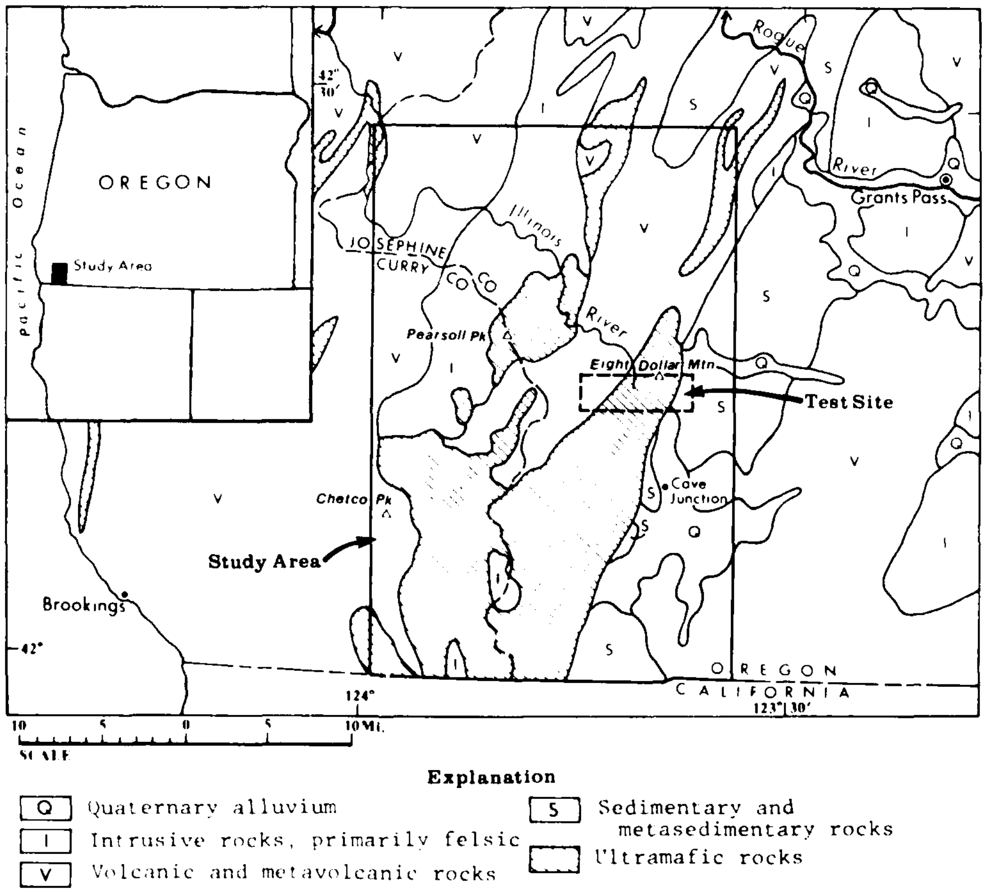

Figure 1. Location of the study area and test site (Geology after Wells & Peck).

Figure 2. Karhunen-Loeve Transformations components 1, 2, and 4. Eight Dollar Mountain is at the right edge of each image. (Imagery of 9/11/81)

Figure 3. Vegetation on ultramafic rock type (right) and non-ultramafic rock type (left). The ultramafic vegetation is characterized by an open California laurel, California coffeeberry, box-leaved garrya shrub type (So in classification) with sparse Jeffrey pine and scattered grass understory while the non-ultramafic vegetation is characterized by a closed Douglas fir - tanoak mixed conifer broadleaf forest (Nc).

Table I.

Preliminary Classification of Vegetation Cover for the Central Siskiyou Mountains (vegetation classification produced by R. Frenkel and C. Kiilsgaard, Oregon State University, 1982)

Class	Subclass	Vegetation type	Symbol open	Symbol closed
Forest (greater than 15% tree cover)	Conifer	Douglas fir	Ao*	Ac*
		true fir, mtn. hemlock	Bo	Bc
		knobcone pine	Co	Cc
		Jeffrey and ponderosa pine, incense cedar, Douglas fir	Do*	Dc*
		Douglas fir, western hemlock, Port Orford cedar	Eo	Ec
		Douglas fir, white and sugar pine	Fo	Fc
	Broadleaf Evergreen	chinkapin, tanoak, madrone canyon live oak	Go*	Gc*
	Broadleaf Deciduous	Oregon white oak, Calif. black oak	Ho*	Hc*
		bigleaf maple, red alder	Jo	Jc*
	Mixed Conifer Broadleaf	Douglas fir, chinkapin tanoak, madrone	Ko*	Kc*
		Douglas fir, canyon live oak, Oregon white oak, Calif. black oak	Lo*	Lc*
		Douglas fir, tanoak	No*	Nc*
		Douglas fir, canyon live oak	Oo	Oc
Shrub (less than 15% tree cover, over 15% shrub cover)		Green Manzanita, ceanothus	Po*	Pc*
		Tanoak, blackberry, vine maple, canyon live oak (seral)	Ro*	Rc*
		Calif. laurel, Calif coffee-berry, box-leaved garrya	So*	Sc*
		rhododendron, azalea, kalmiopsis	To	Tc
Graminoid		grasses (fescue, brome, etc.)	Uo	Uc
		beargrass	Vo	Vc

*occurs within test site

Table II.

Spectral Characteristics of the Daedalus DEI-1260 Scanner

Configuration A

Channel #	Bandwidth
-*	0.38 - 0.42um
1	0.42 - 0.45um
2	0.45 - 0.50um
3	0.50 - 0.55um
4	0.55 - 0.60um
5	0.60 - 0.65um
6	0.65 - 0.69um
7	0.70 - 0.79um
8	0.80 - 0.89um
9	0.90 - 1.10um
10	2.05 - 2.35um

Imagery acquired on 9/11/81

* not recorded

Configuration B

Channel #	Bandwidth
1	0.42 - 0.45um
2**	0.45 - 0.52um
3**	0.52 - 0.60um
4	0.60 - 0.62um
5**	0.63 - 0.69um
6	0.68 - 0.75um
7**	0.76 - 0.90um
8	0.91 - 1.05um
9**	1.55 - 1.75um
10**	2.08 - 2.35um
11**	10.40 - 12.50um

Imagery acquired on 7/15/82

** these channels approximate the characteristics of the Thematic Mapper sensor on Landsat 4.

AD P001999

IMPACT OF HYDROTHERMALLY ALTERED SOIL ON VEGETATION AS A TOOL IN GEOTHERMAL EXPLORATION

S. Camacho, L. del Rio, L. Sanchez
Instituto de Geofisica, UNAM
04510 Mexico, Mexico

and

J. Gonzalez
Centro Cientifico, IBM de Mexico
Cantil #150, Pedregal
01900 Mexico, Mexico

ABSTRACT

The spectral reflectance of vegetation over the Caldera of Los Humeros is used to locate potential geothermal areas. The ratio of Landsat band 7 to band 5 is found to be an excelent discriminant between anomalous and background trees. A maximum likelihood classification outlines the anomalous vegetation. This is coupled with a criterion to account for bare spot, mud ponds, fumaroles and other surface manifestations. The result is an outline of the area with highest level of geothermal activity.

1. INTRODUCTION

The Mexican Volcanic Belt (MVB) covers an extension of 176,000 Km^2, crossing the central part of Mexico from the Pacific Ocean to the Gulf of Mexico. There are hundreds of zones within this belt which present favorable characteristics for the existance of geothermal areas. These characteristics are recent vulcanism, high density of faulting and appropiate drainage. A methodology has been developed for a first selection of the most promising zones. This methodology is described in detail elsewhere (Del Rio, 1982,a,b,) Essentially the method consists of a statistical analysis of maps, Landsat images and aerial photograph interpretation carried out in two stages.

First, a window of 6° bc 6° (approximately 100,000 Km^2) at $20^{\circ}N$, was interpreted on Landsat images and divided into zones of $.5^{\circ}$ by $.5^{\circ}$; each covering approximately 1,400 Km^2. Some of the most important parameters considered for each zone are: density and principal directions of faults, density, dimensions and alignment of eruption centers, lithology, topographic emplacement, hidrology and soil alteration. These data are the elements of a small population nearly normally distributed. The analysis consists of determining mean and standard deviation for each parameter and selecting for the next step only those zones with favorable characteristics; that is, parameter

values greater than the mean plus standard deviation.

The final stage is an extension of the same algorithm but applied to a selected area at a greater scale. The end product consists of areas, 75 Km^2 whose characteristics are the most favorable over the whole region. Since the number of these smaller areas is still considerable another criterion for discrimination is needed.

With more than 70% of the MVB covered with moderate to heavy vegetation, geobotany should offer further discrimination criteria. Although it has been known for several hundred years that plants serve as indicators of the presence of certain minerals, in the last 15 years an intensive effort by several researchers (Canney, 1969; Yost and Wenderoth, 1971; Howard et al, 1971; Press, 1974) has established that anomalies in soil chemistry are highly correlated with vegetation changes in spectral reflectance, density and morphology. Unfortunately there is very little else which may be said conclusively regarding trends. The only conclussions that can be gathered are that chlorophyll content is best seen in the 500-600 nm region exhibiting a higher reflectance for a higher content of chlorophyll and that the relative vegetation cover vs soil is shown by the IR (700-1100 nm) reflectance. Whether the IR reflectance for anomalous trees is higher or lower than for background trees, depends on the degree to which trees have been affected and on the relative IR reflectance of the soil with respect to the trees. In spite of the complexities involved in the relationship between vegetation and soil, the cumulative results obtained indicate that the anomalous tree-soil unit has a different reflectance compared to a background tree-soil unit. One of the goals of this work has been to evaluate the discriminability of tree-soil units present in a geothermal area from their background counterpart.

2. BACKGROUND

It has now been accepted that the effect of an anomalously mineralized soil on the vegetation which grows over it can be of three types.

1) The area may have absence of non-stress tolerant vegetation or the presence of stress tolerant plants.

2) The vegetation on the anomalous area may have a different morphology due to giantism, dwarfism or orientation of branches and leaves.

3) In the spectral region covered by Landsat, reflectance is determined primarily by chlorophyll pigmentation (500-700 nm), and by cell structure and internal refractive index discontinuities due to water content in the leaves (700-1100 nm).

All of these are altered when the nutrient uptake of the plant is modified by thermal fluids that carry altered minerals. The fluids work their way up through the faults, where minerals are deposited on the surface along the faults. Through a process of erosion, the minerals are transported to cover a much larger area. Rain water then carries them to horizon A and horizon B where they are absorbed by the roots.

While isolating the contributions of each effect on the spectral signature of the combination trees-plus-soil is a complex task, this spectral signature of the combination can be analyzed throughout the target area for heterogeneities. The search would then be for areas in which the vegetation, regardless of cause (bare spots, reflectance or morphology), has a different signature than that in its surroundings. The validity of this approach is based on the fact that the target area has already been singled out as

having a high probability for geothermal presence. Then any subarea for which its vegetation indicates an anomalously mineralized soil has a higher probabilitiy of being a potential geothermal zone.

3. DESCRIPTION OF THE CALDERA LOS HUMEROS

The Caldera Los Humeros is situated on the eastern end of the MVB, figures 1 and 2. In this region the MVB overlaps the Sierra Madre Oriental. The caldera is a truncated cone with a base radius of 12 ± 2 Km, a height of 400 m and a crater radius of 6 km; its volume is 110 ± 22 km^2 while its extension is 500 km^2. The top of the structure has an altitude of 2,850 m. The mean annual temperature of the caldera is 10°C and its mean annual precipitation, averaged over the area, is 650 mm. The climate is temperate, isothermal with a long cool and rainy summer; its temperature changes are of the ganges kind.

Because of its geographic emplacement, the Caldera is a barrier to the wind. The predominant winds blow from the Gulf of Mexico with a N and NE direction. These winds have a high moisture content which condenses and precipitates on the N and NE flanks of the structure. In this region (Tepoztlan) the mean annual temperature is 15.8°C and the mean annual precipitation is 1763 mm while on the S and SW flanks (Caltona, the precolombian city of the sun) they are 17.6°C and 577 mm respectively.

On the N, NE side these conditions produced a mixed woodland under a frequently covered sky. Pine, grass and yucca grow on top of the Caldera while on the S, SW portion of it, only grass, yucca and nopal grow.

The Caldera Los Humeros rests over 3.5 to 5 My rhyolites; it is made up of basalts, andesites and rhyolites with predominance of the second. The crater is filled with a 70 m pumice bed. The youngest flow found in this area is less than 1 My old.

This volcanic structure is dissected by three main faults: Monte Nuevo, N65°E: which is the youngest; Zaragoza, N35°W, and Los Humeros, NS, the oldest of the system.

Within 3 Km from the rim there are 86 small volcanic buildings. These volcanos are clustered in aligmments and distributed on a 6 Km radius ring; the alignments point to the center of the crater. It can be said that this volcanism followed the radial and concentric faults produced by the development of the structure.

Although the volcanic centers on the Caldera are aligned mainly in the direction of the youngest fault system, N65°E, the geothermal alteration and manifestations are along the oldest system, Los Humeros Fault.

There are four mayor plant communities inside the Caldera; grass, crops, izotal and woodlands. Only the dominant species of each community were classified.

The crops are mainly _Bideus sp_ and _Argemiore sp_ and are limited to the flat lands where they are found on altered soil as well as on normal soil. Secondary vegetation is found everywhere throughout the Caldera. Grasslands are communities of vegetation that grow after natural vegetation has been striped or where crops have been cut; dominant spp are _Poa villaroel_ and _Stipa icha_. Woodlands are pine-oak forests and are well delimited, they are usually on badlands. Izotal includes communities with predominance of _Nolina_ and _Yucca_. The last community is the only one that shows a dominance gradient with the grasses. The changes are well delimited since these communities develop on hills where, according to the dominant wind, they present or lack predominance.

4. IMAGE ANALYSIS AND PROCESSING

The Landsat image used corresponds to the month of May 1976. This image is of good quality and cloud free over the Caldera although band 7 presents stripping. For the purpose of this study, the area was limited to the Caldera and its immediate surroundings. This area was chosen because of the prior knowledge of the existance of a thermal reservoir within the Caldera which was reached by an exploratory well. Four other wells have been drilled since, each reaching the reservoir at an approximate depth of 1700 m. The temperature of the dry steam of these wells is around 260^{o}C. Also, from the first area selection criterion outlined previously, three of the 75 km^2 circles, fell partly inside and partly outside the Caldera. The wells mentioned are located within these circles, (see figure 1).

If the target area happens to be a geothermal area, as is the case, then it will have a number of surface manifestations such as bare spots, kaolin deposits, fumaroles, mud ponds etc. All of these manifestations are too small (tens of square meters at most) to be "seen" by Landsat. However, their combined effect is to make the area different from its surroundings by giving it a "patchy" appearance, as seen for instance in aerial photography. In order to use this fact as additional information, a concept of "disimilarity of the area" was developed. This involved a quick comparison of 1 km^2 squares, each, with its eight neighbors, to determine those which are most disimilar to the rest.

To this end, the study area in the image was subdivided into seven parallel strips alligned with Los Humeros fault. Each strip is 1 Km wide by 13 Km long and partitioned into 1 Km^2 squares. The third strip contains a high density of surface manifestations. The strips on each side help to account for variations in the reflectance of vegetation due to its topographic emplacement.

The similarity of a square with respect to its neighbors was tested using an algorithm whose logic consists of:

1) Calculation of mean and standard deviation, for each Landsat band, of the pixels corresponding to each area (square).

2) Calculating the average of the eight means of the surrounding areas and subtracting it from the central mean.

3) The magnitude of this difference vector is subtracted from the magnitude of the central standard deviation.

4) The sign and magnitude of this residue is an indirect measure of the similarity of the central area with respect to its neighbors; if the residue is positive then it indicates that the central area is different, by more than one standard deviation, from its neighbors.

The results were scaled and normalized for display on a color monitor. Each square was labeled with a number (0-15) resulting from the analysis. The higher values correspond to the areas which are most disimilar to their neighbors.

Training fields for a maximum likelihood classification were chosen based on extensive ground truth coverage of the Caldera. Nine different vegetation classes were assigned, covering dense (6.7 per 100 m^2) pine trees located far, (more than 4 Km) away from the known geothermal area and dense pine trees located close (one, two and three Km) to the manifestations. The fields

represented sparse coverage (1.2 per 100 m^2) located both far and close as well as trees growing on basalt flows and soil of pumice origin. Other training fields, such as bare soil, agricultural etc, were also given to improve the quality of the overall classification.

Table I shows mean and standard deviation for each of the nine classes of vegetation training fields. The symbol next to the class represents the anomalous (A) or background (B) category depending on their nearness to hydrothermally altered soil. Figure 3 shows the relative brightness value of each of the four bands for the training statistics corresponding to two anomalous and two background fields. The fifth band shown corresponds to the 7/5 ratio for the nine vegetation classes. The outstanding result is that the anomalous vegetation has a distinguishably lower IR/RED (7/5) ratio. A similar behavior had been observed on the geothermal field of Los Azufres, Michoacan (Del rio et. al, 1980).

Figure 4 shows the result of a maximum likelihood classification performed on the image. Vegetation was classified as either background or anomalous; the latter is shown in two colors (tones). The superimposed grid shows the 1 Km^2 squares which were analyzed for disimilarity. Figure 5 shows the classification (smoothed with a 5 x 5 window) with an overlay of the most disimilar squares. A contour indicates the vegetation with an anomalous spectral signature. The impacted vegetation is located S, SW of Los Humeros fault and is contained within two of the circles shown in figure 1. The union of the areas of anomalous vegetation with the most disimilar squares then outlines the area of potential geothermal activity as manifested on the surface. The intersection of the two criteria should outline those areas of highest interest for conventional geophysical prospecting.

5. CONCLUSSIONS

When this work started, only one exploratory well had been drilled. Parallel to this study, the rest of the wells shown were drilled. All five wells are located within the two circles of highest probability as is the anomalous vegetation found from the classification procedure. The disimilar squares have a marked NS trend aligned with Los Humeros fault and the bulk of surface manifestations. When integrated, all this information gives a good indication of the limits of the area which should first be explored on the ground. In the future, geochemical analysis should be done to quantify the degree to which the vegetation reflects the altered soil. Also, the disimilar-square test should be extended to cover the entire study area.

REFERENCES

1. Canney, F.C., 1969 - Remote Detection of Geochemical Soil Anomalies; Second Annual Earth Resources Prog. Status Rev. (N2); NASA; Houston, Tex. pp 7-1

2. Del Rio, L,P. Pascaud, S. Camacho and N. Galvan, 1980 Remote Sensing Techniques for Identification and Evaluation of Geothermal Areas. Proc. Fourteenth International Symp. on Rem. Sens. of Env.; San Jose, Costa Rica, Vol. I pp 731-742

3. Del Rio, L. 1982, a. - Metodo para Seleccionar Areas con Alto o Bajo Tectonismo (I). Geofisica Internacional, in press.

4. Del Rio, L. 1982. b. - Metodo para Seleccionar Areas con Alto o Bajo Tectonismo (II). Aplicacion a la geotermia: Caldera Los Humeros. Geofisica Internacional, in press.

5. Howard, J. A., R. D. Watson, T.D. Hessin, 1971
Spectral Reflectance Properties of Pinus ponderosa in relation to Copper Content of the Soil:Malachite mine, Jefferson County Colorado.
Proc. Seventh International Symp. on Rem. Sens. of Env.; Ann Arbor, Michigan, Vol. I, pp 285-298

6. Press, N.P., 1974 - Remote Sensing to Detect the Toxic Effects of Metal on Vegetation for Mineral Exploration.
Proc. Ninth International Symp. on Rem. Sens. of Env.; Ann Arbor, Michigan Vol. III pp 2027

7. Yost, E. and S. Wenderoth, 1971
The Reflectance Spectra of Mineralized Trees;
Proc. Seventh International Symp. con Rem. Sens. of Env.; Ann Arbor, Michigan
Vol. I pp 269-284

Table I: Training fields statistics for anomalous (A) and background (B) vegetation.

Fields	B4	B5	B6	B7	B7/5
PM8 (A)	29.83/1.65	26.75/1.57	32.02/1.57	31.84/1.70	22.77/3.23
PM7 (A)	30.63/2.21	27.62/2.28	30.63/1.26	30.88/2.16	19.83/3.76
PA3 (A)	32.91/2.89	33.25/4.51	40.14/3.76	41.92/3.40	26.76/4.51
PM1 (A)	28.53/1.17	25.15/1.61	30.26/1.16	30.38/1.80	23.50/3.57
PM9 (A)	27.93/1.13	24.34/1.63	29.61/1.25	30.42/1.96	25.24/4.65
PB1 (B)	25.92/.98	21.60/1.06	31.35/1.32	34.48/1.66	40.30/4.58
PD1 (B)	24.85/2.13	20.20/2.96	34.48/3.26	39.42/4.34	56.74/9.48
PD4 (B)	25.88/1.81	22.44/2.39	35.21/2.14	39.98/3.02	49.57/10.67
PR2 (B)	24.38/1.77	20.03/2.22	32.11/2.01	37.08/2.84	52.38/11.29

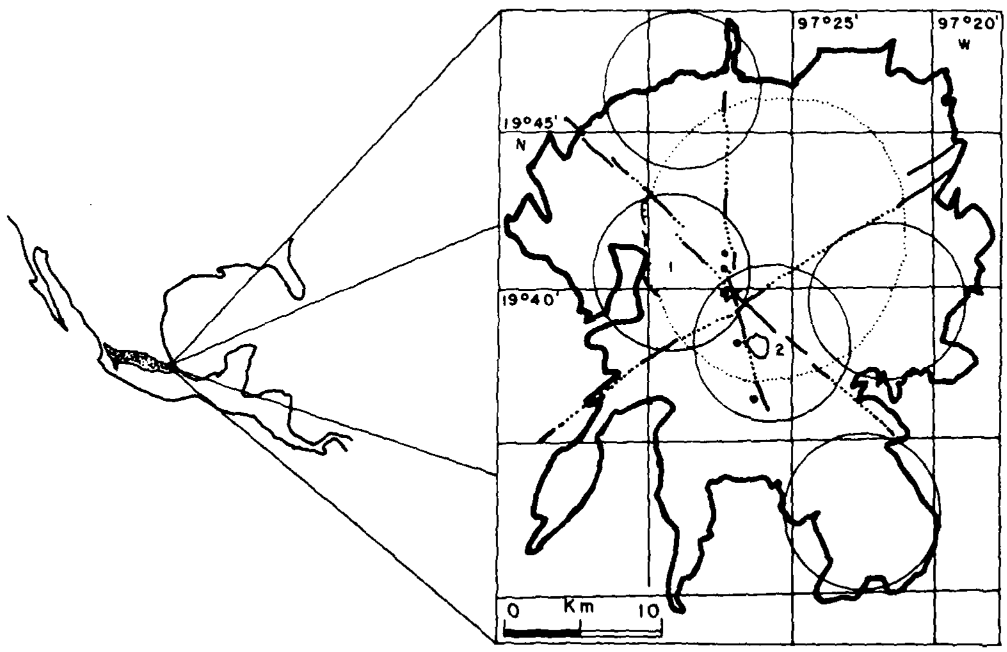

Figure 1: Los Humeros Caldera, (Lines are principal faults, dots are wells, circles 1 and 2 are the most favorable areas)

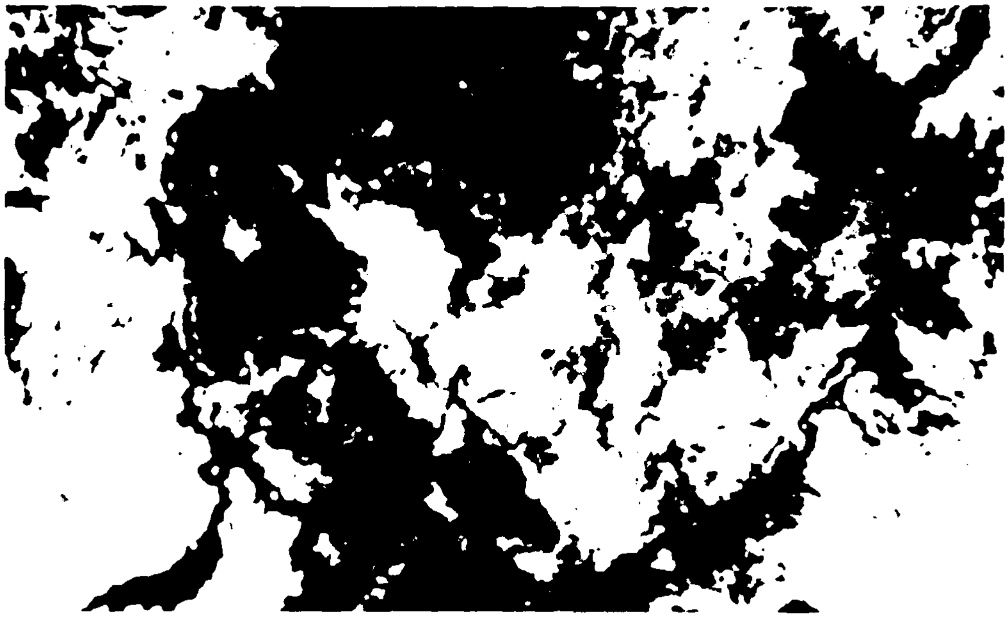

Figure 2: Los Humeros Caldera as seen on band 5 (500-600 nm)

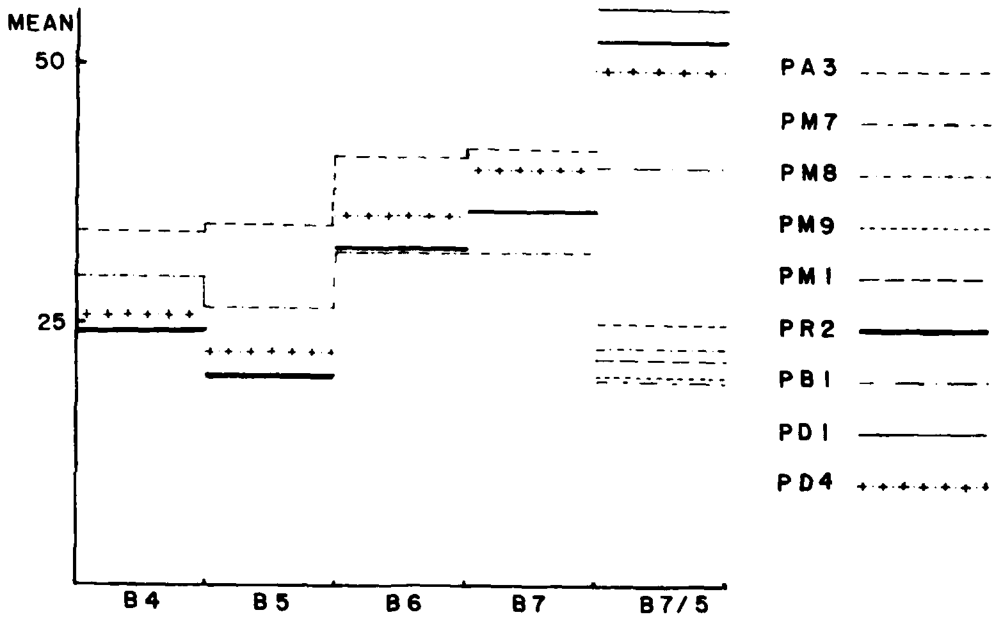

Figure 3: Relative brightness of altered and background vegetation (mean/standard deviation)

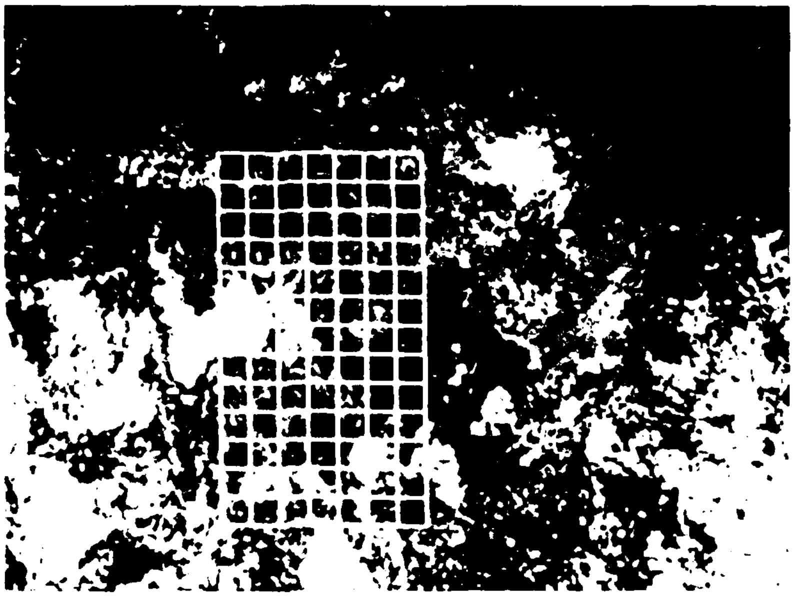

Figure 4: Maximum likelihood classification

Figure 5: Classified image with "most disimilar" squares.

INTEGRATED REMOTE SENSING, GEOLOGICAL AND GEOPHYSICAL DATA PROCESSING AND ANALYSIS FOR HYDROCARBON PROSPECTION IN THE PARANÁ BASIN, BRAZIL (*)

G. Amaral

INSTITUTO DE GEOCIÊNCIAS - UNIVERSIDADE DE SÃO PAULO
Consultant to THEMAG ENGENHARIA LTDA.
São Paulo - SP, Brazil

A. Paiva Filho and A. P. Crosta

THEMAG ENGENHARIA LTDA.
São Paulo - SP, Brazil

ABSTRACT

The extensive basaltic lava flows of the Serra Geral Formation (Lower Cretaceous), in the upper portions of the Paraná sedimentary basin, are a severe obstacle for hydrocarbon prospection. Its thickness and physical characteristics makes difficult the general application of conventional geophysical methods. In order to overcome this problem a research program was developed for PETROBRÁS in order to obtain the maximum geological information from remote sensing data and integrate it with field and geophysical data. Automatic analysis of LANDSAT data with visual inspection of LANDSAT and SLAR imagery resulted in a large amount of lithological and structural information, which were integrated with geological and geophysical data for the selection of target areas for future investigation.

1. INTRODUCTION

This report is part of a larger program with the objective to test the performance of remote sensing data for PETROBRÁS hydrocarbon exploration activities at the Paraná basin.

The author's (AMARAL et al., 1981) presented a preliminary report dealing with the data processing aspects of the above mentioned program.

Figure 1 shows schematically the location and geological setting of the Paraná basin, and the boundaries of the studied area. This basin is

---

(*) This paper reports some results obtained from a program carried out for PETROBRÁS - Petróleo Brasileiro S.A., which authorized its divulgation.

about 2000 km long in the north-south direction and 1000 km wide, covering an area of 1.6 million sq. km. It is filled with up to 5000 of Paleozoic and Mesozoic sediments which are covered by the volcanic rocks of the Serra Geral Formation of Lower Cretaceous Age (± 120 m.y. after AMARAL et al., 1966). This unit covers an area of about 1.4 million sq. km and has an average thickness of 400 m (reaching 1700 m in the Paraná river valley). Its physical characteristics (magnetic, gravity, electrical and mechanical) are a severe constraint for the general application of conventional geophysical exploration techniques (TESSIS, 1979).

Since the oil and gas exploratory targets are located mainly within the Paleozoic sequence (SCHNEIDER, 1979), the Serra Geral Formation is the most important obstacle for the prospection activities. Due to that they were concentrated at the basin's borders where the basalt influence is less important. However, a large number of reports (ALMEIDA, 1981; HAMZA et al., 1978; MEISTER, 1973; OLIVEIRA, 1971; SCHNEIDER, 1979, among others) indicate that better conditions for hydrocarbon generation and accumulation should exist at the central portions of this basin. Owing to that, a number of exploratory wells were drilled more or less randomly to obtain geological information in such areas. Moreover, similar basins in the Siberian Platform (MURATOV, 1974; SOKOLOV and MAZOR, 1980) present oil and gas deposits associated with reactivated basement structures and developed in association with higher thermal flow during basaltic activity.

For those motives our study was conducted in order to obtain the maximum possible amount of information for a better well location. The main objective was the identification of positive structures and its corresponding lows. As secondary objective an attempt was made for the identification and mapping of lithological differentiations within the Serra Geral Formation. The studied area was about 70000 sq. km, corresponding to two LANDSAT frames (WRS path 238, rows 78 and 79), enclosing portions of Paraná, Santa Catarina and Rio Grande do Sul states.

2. METHODOLOGICAL APPROACH

Figure 2 shows, as a flow diagram, the methodology employed in the present work. Most of the data was extracted from LANDSAT and SLAR imagery. LANDSAT photographic products were excellent for visual discrimination of homologous zones (zones of similar texture pattern) corresponding to lithological differences. Band 7 images enhanced topographical features and, consequently, structural features. However, due to solar ilumination azimuth (57^{o}), lines around this direction were not enhanced. SLAR images were excellent for structural analysis, but very poor for lithological discrimination. The viewing angle (E-W) eliminated all lines in that direction. It is important to point out here that also N-S lines were not enhanced contrary to expectations, a fact which are being observed in other programs in our country. Circular histograms for lineaments extracted from both types of image show clearly those differences (Figure 3). Comparison with field data indicated, however, that LANDSAT images yielded two of the three main directions and SLAR mosaics disclosed only one.

An experiment was made for the digital filtering of LANDSAT data following the methodology proposed by PARADELLA and DUTRA (1980), in order to enhance lineaments. The results were excellent but the treatment was restricted for a small area.

As a result of the visual analysis of LANDSAT and SLAR images, three maps were obtained:

- integrated photogeologic map (structure and lithology) (Figue 4);
- LANDSAT lineament map;
- SLAR lineament map.

An arbitrary coordinate system was attributed to the last two maps and the lineaments were digitalized and processed in order to obtain circular histograms, mean azimuth over a uniform grid, dispersion from mean azimuth maps and fracture density maps.

LANDSAT CCT were analysis at the Brazilian Space Research Institute (INPE), using the Image-100 system. Two kinds of processing were performed:

- Image enhancement - noise removal, correction of atmospheric effects, edge enhancement, enlargement and color composition;
- Image classification - using the unsupervised K-means algorithm (HARTIGAN, 1975) on the corrected data for discrimination of spectral classes (Figure 5).

Surface and subsurface data were used for construction of isopach and structural contour maps. Aeromagnetic data were processed in order to remove regional gradients and produce residual maps.

3. RESULTS

Application of the above discussed methodology resulted in the most detailed geological map available for the region. Acidic differentiates (rhyodacite and granophyre) within the Serra Geral Formation were mapped and used as guide-horizons for the structural analysis of the region.

The geological map of Figure 4 sumarizes these results which, in conjuction with regional studies (ALMEIDA, 1981; FERREIRA et al., 1981; HARALYI, 1981; REDMOND, 1979), allowed a new interpretation for the structural development of the area. According to this interpretation, the region was subject to compressional stress associated to the uplift of the Rio Grande do Sul and Ponta Grossa archs, with the resulting development of large flexures. After the volcanic events, the region was submitted to tensional stress which reactivated older fractures and resulted in normal faulting and block tilting. As a result, several favourable structures for hydrocarbon traping developed. Moreover, the acidic differentiates are associated with crustal contamination (CORDANI et al, 1980) indicating periods of higher thermal flow. Due to that, the conditions and timing of hydrocarbon generation were controlled by the volcanic activity in a manner very similar to that of the Tunguska basin in the Siberian Platform, reported by SOKOLOV and MAZOR (1980).

4. CONCLUSION

The achievements of the present program are stronly suggestive for the application of similar approaches for other portions of the Paranã basin, and even for other basins with similar problems.

5. REFERENCES

ALMEIDA, F.F.M. de - 1981 - Síntese sobre a tectônica da Bacia do Paranã. Atas 3º Simp. Reg. Geol. SBG-SP, 1:1-20.

AMARAL, G.; CORDANI, U.G.; KAWASHITA, K. and REYNOLDS, J.H. - 1966 - Potassium-Argon age dates of basaltic rocks of southern Brazil. Geoch. Cosmoch. Acta 30:159-189.

AMARAL, G.; PAIVA Fº, A. and CROSTA, A.P. - 1981 - Integrated remote sensing, geological and geophysical data processing and analysis for hydrocarbon prospection in the Paranã Basin, Brazil. COGEODATA-IAMG Regional Meeting, Rio de Janeiro (In press).

CORDANI, U.G.; SARTORI, L.P. and KAWASHITA, K. - 1980 - Geoquímica dos isótopos de estrôncio e a evolução da atividade vulcânica na Bacia do Paraná (Sul do Brasil) durante o Cretáceo. An. Acad. Bras. Ciênc. 52 (4):811-818.

FERREIRA, F.J.F.; MORAES, R.A.V.; FERRARI, M.P. e VIANNA, R.B. - 1981 - Contribuição ao estudo do alinhamento estrutural do Guapiara. Atas 3º Simp. Reg. Geol. SBG-SP, 1:226-240.

HAMZA, V.M.; ESTON, S.M. and ARAUJO, R.L.C. - 1978 - Geothermal energy prospects in Brazil: A preliminary analysis. Pure and Applied Geoph. 117 (1/2):180-195.

HARALYI, N.L.E. - 1981 - O significado tectônico das anomalias de gravidade na Bacia do Paraná. Atas 3º Simp. Reg. Geol. SBG-SP, 1:274-281.

HARTIGAN, J.A. - 1975 - Clustering Algorithms. John Wiley & Sons, N. York. 351 pp..

MEISTER, E.M. - 1973 - Gradientes geotérmicos nas bacias sedimentares brasileiras. Bol. Tecn. PETROBRÁS 16 (4):221-232.

MURATOV, M.V. - 1974 - Principal types of basins of ancient platforms and the problem of their origin. Int. Geol. Rev. 16 (2):125-132.

OLIVEIRA, M.A.M. - 1971 - Possibilidades de geração e migração tardias de petróleo na Bacia do Paraná. Anais 25º Congr. Bras. Geol. 3:139-157.

PAIVA Fº, A.; CROSTA, A.P. e AMARAL, G. - 1982 - Utilização de dados de sensoriamento remoto no estudo estratigráfico e estrutural da Formação Serra Geral. II Simp. Bras. Sensoriamento Remoto (in press).

PARADELLA, W.R. e DUTRA, L.V. - 1980 - Filtragens digitais de imagens LANDSAT como técnica de auxílio visual na fotointerpretação geológica. Anais 31º Congr. Bras. Geol. 5:2959-2964.

QUADROS, L.P. - 1976 - Efeito das intrusões de diabásio em rochas sedimentares do leste e sul da Bacia do Paraná. Bol. Tecn. PETROBRÁS 19 (3):139-155.

QUADROS, L.P. e SANTOS, A.S. - 1980 - Efeito das intrusões de diabásio sobre o conteúdo orgânico das rochas sedimentares. Anais 31º Congr. Bras. Geol. 1:410-422.

REDMOND, J.L. - 1979 - Paraná Basin, Paraguay: Tectoniques and hydrocarbon potencial. 4th Latin American Geolog. Congr., Trinidad & Tobago.

SCHNEIDER, R.L. - 1979 - Prospectividade petrolífera da Bacia do Paraná. Atas da Meda Redonda: Geologia e Potencialidades Petrolíferas da Bacia do Paraná no Estado de São Paulo. SBG-SP:56-62.

SOKOLOV, B.A. and MAZOR, Yu. R. - 1980 - Oil and gas content of basins of ancient platforms and trap magmatism. Moscow Univ. Geol. Bull. 35 (6): :45-50.

TESSIS, J. - 1979 - Problemas exploratórios da Bacia do Paraná. Atas da Mesa Redonda: Geologia e Potencialidades petrolíferas da Bacia do Paraná no Estado de São Paulo. SBG-SP:73-103.

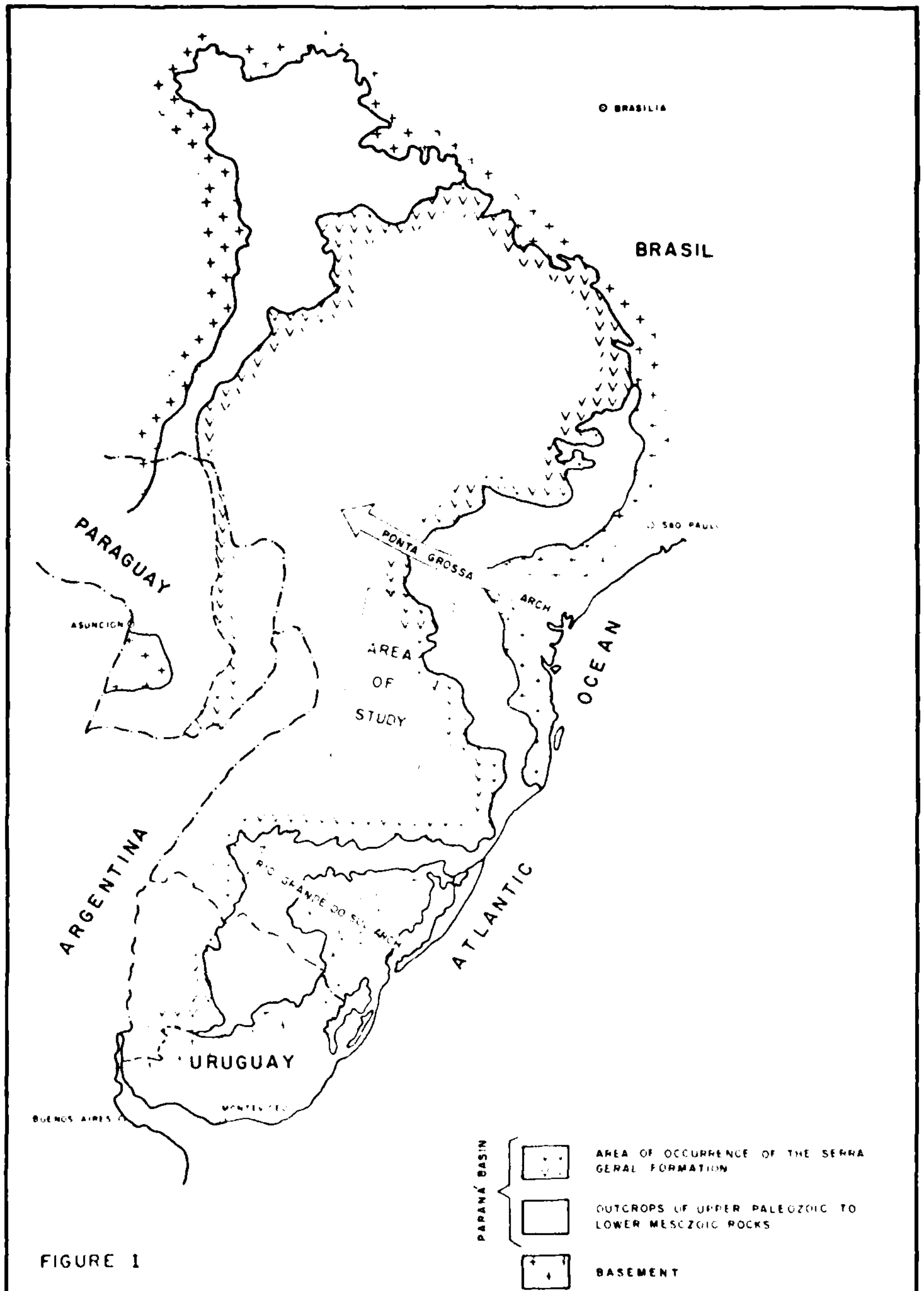

FIGURE 1

SITUATION MAP OF THE PARANA BASIN AND LOCATION OF THE STUDIED AREA

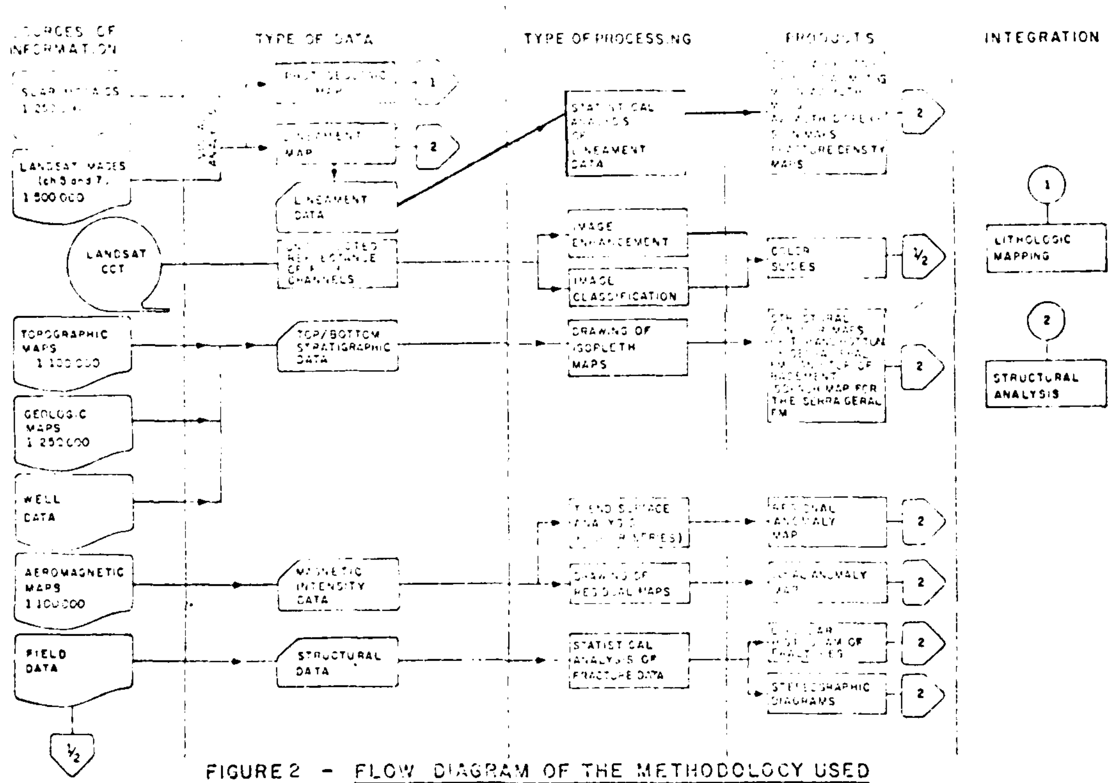

FIGURE 2 - FLOW DIAGRAM OF THE METHODOLOGY USED

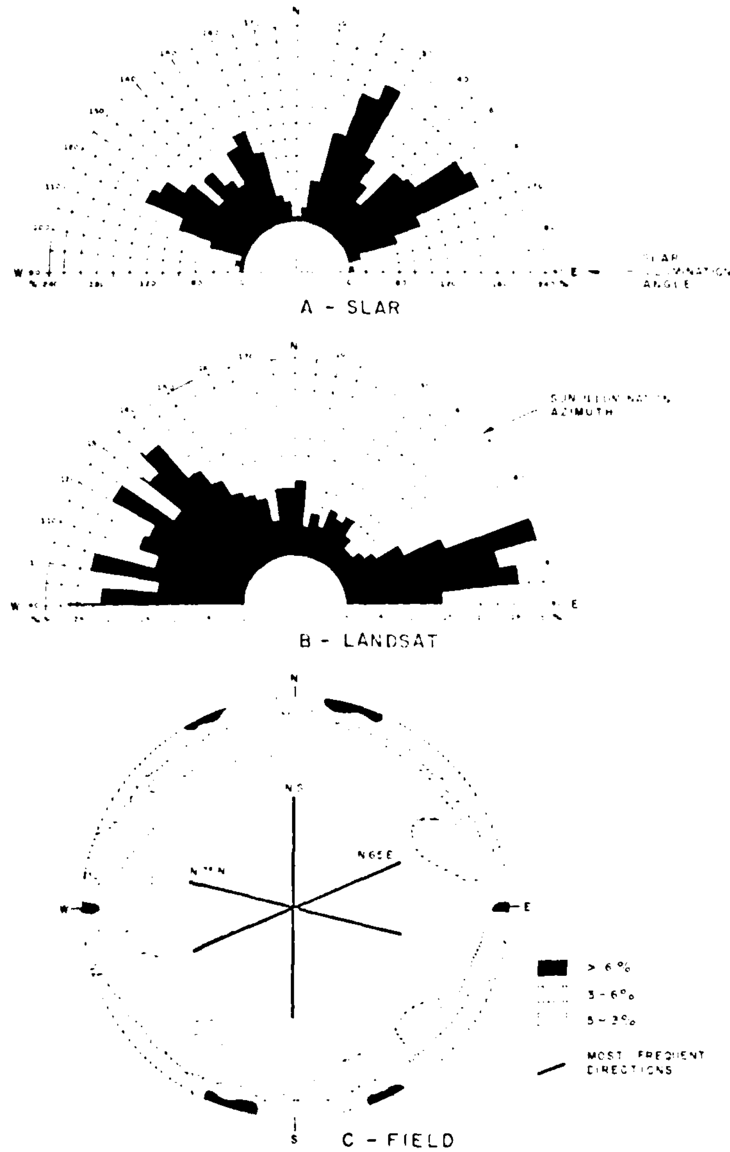

FIGURE 3 – COMPARATIVE LINEAMENT / FRACTURE DENSITY DIAGRAMS A) OBTAINED FROM SLAR MOSAICS, B) OBTAINED FROM LANDSAT, C) MEASURED IN THE FIELD. NOTE THE LACK OF LINES PARALLEL TO THE ILLUMINATION AZIMUTHS. NOTE ALSO, THE LOW FREQUENCY OF LINES IN THE NORMAL DIRECTION, IN THE CASE OF SLAR DATA.

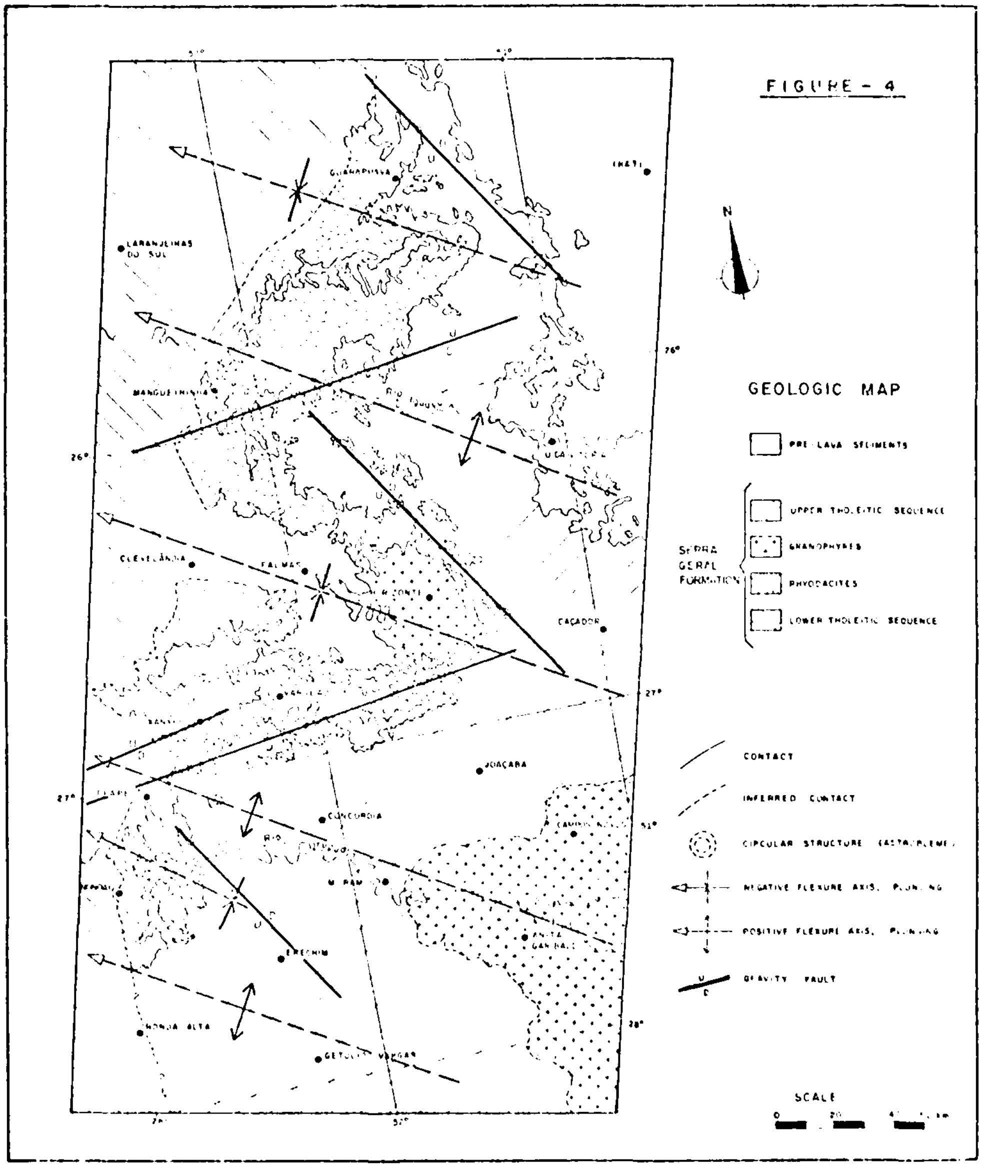
GEOLOGIC MAP
PRE-LAVA SEDIMENTS
SERRA GERAL FORMATION
UPPER THOLEIITIC SEQUENCE
GRANOPHYRES
LOWER THOLEIITIC SEQUENCE
CONTACT
INFERRED CONTACT
GRAVITY FAULT
SCALE
N
ERECHIM
JOAÇABA
CAÇADOR
PALMAS
CONCORDIA

FIGURE - 4

Figure 5 - Acidic rocks classified by the K-means algorithm.
(Original figure in color)

INTEGRATION OF GEOPHYSICAL DATA WITH REMOTE SENSING IMAGES IN GEOLOGY

G. Rochon

Department of Photogrammetry
Laval University
Quebec, Canada

D. Brisebois

Department of Energy and Resources
Province of Quebec

SUMMARY

Even if the techniques associated with geophysical surveys are quite similar in approaches with those used in remote sensing, the data gathered from both sources are very rarely mixed or analyzed simultaneously by a computer.

This study shows that by combining satellite images with topographic data and geophysical data, the resulting images give to the photo-interpreter, a much better perception of the information contained in each of those sources individually. For example, contour lines of magnetic maps (total magnetic field, near surface magnetic component, regional magnetic component, and downward continued regional magnetic component) are digitally processed to create images of those parameters by linear interpolation of the contour lines on a 50 meter UTM grid. A DEM (digital elevation model) was also produced with the same technique and linked to a geometrically corrected Landsat image.

The images of the various magnetic fields, and of the topography, were then transformed as if they were artificially illuminated by a point source, according to the following simple relation:

$$A = k\, A_i \cos^{[illegible]} [illegible]$$

where A_i is the input value of the parameter for a given pixel

[illegible] is the angle between the normal of each pixel, if the image was to be seen as the surface of the earth, and the simulated incident illumination

[illegible] and [illegible] are the constants, positive or negative

A is the output value of the same parameter

Each new image was then combined with the Landsat image and transformed through a Hotelling (or K-L) algorithm. The first three components were finally colour enhanced. This procedure has the advantage of giving a total perception of all the input data, even if some confusion exist on the origin of the "anomalies" or structures seen on the screen. When located these features may be seen individually or in combination for each parameter, on the video display.

This procedure as applied to an area covering a full 1:50,000 topographic map, lead to a much better understanding of the geologic structure of the area under study, as compared to the usual interpretation of the various sources of data.

Other sources of data, including electromagnetic and gravimetric surveys, are presently analyzed with the previous data. The preliminary results will be presented at the symposium.

GLOBAL SATELLITE REMOTE SENSING FOR ENERGY, MINERALS AND OTHER RESOURCES

Frederick B. Henderson III

The Geosat Committee
San Francisco, California

SUMMARY

During the 1970's, the development of civilian satellite remote sensing began on a global scale with the introduction of the U.S. Landsat satellites in 1972. These satellites were designed principally for agriculture, hydrology and land use planning. Applications have demonstrated the value of synoptic perspective, global satellite coverage, and increased efficiency of reconnaissance geology in mapping from space to the energy and mineral resource industries.

The international industrial geological community represented by the Geosat Committee has worked with NASA, JPL and others to demonstrate the potential benefits of the Landsat system and additional satellite capabilities to be realized in the 1980's to the energy and mineral exploration community. Capabilities added to current Landsat systems should include fixed and pointable stereoscopic coverage, increased resolution (to 10 meters IFOV), additional rock/soil sensitive bands, Synthetic Aperture Radar (SAR), and corresponding ground segment systems for digital data processing and applications. The exploration and engineering value of these capabilities have been demonstrated in the joint Geosat-NASA/JPL Test Case Program for oil/gas, uranium, and copper deposits.

Several international satellite systems in various stages of proposal/development may include the U.S. LANDSAT D and D', with both the 4-band multispectral scanner and the 7-band Thematic Mapper scanner. In France, there is the SPOT system (1985); in Japan, MOS (Marine Observation Satellite, mid-80's) and ERS (Earth Resources Satellite, 1987). The European Space Agency (ESA) proposes a marine/land observation system (ERS) late in the 1980's. All these developing satellite systems recognize the necessity of international cooperation, primarily because of the commonly held view of preserving the "Open Skies" policy (mutual accessibility and availability of data) in civilian satellite remote sensing.

The success of the various national developing civilian satellite remote sensing systems will in large measure depend on international cooperation and exchange of data, which will inherently lead to the eventual industrialization of these operational systems. Such industrialization will occur in those areas where industry can more efficiently supply the user community with the required data than can government agencies.

Because of the high cost of obtaining, processing, distributing and preserving the data produced by these future civilian satellite remote sensing systems and because of the high potential value in future exploration and development of non-renewable resources utilizing the satellite data, all national systems are encouraged to move towards internationalization and industrialization of complementary and compatible systems in the 1980's for the benefit of all mankind.

APPLICATION OF LANDSAT DIGITAL ANALYSIS TO MINERAL EXPLORATION IN A FORESTED GRANITIC ENVIRONMENT

B. Bruce

Canada Centre for Remote Sensing
Ottawa, Ontario, Canada

G. Stevens

Acadia University
Wolfville, Nova Scotia, Canada

V. Singhroy

Ontario Centre for Remote Sensing
Toronto, Ontario, Canada

SUMMARY

An active geologic exploration program is vital to any nation which is reliant on revenues from primary resource development. Exploration programs are, however, capital intensive. They are thus often difficult to support under current economic conditions. Any sources of information which can aid in the timely and efficient assessment, planning and management of exploration projects must therefore be seriously considered.

The geologic value of the LANDSAT data source has been well documented under arid and semi-arid conditions. Many areas of current exploration interest are more heavily vegetated, however. This problem has been the subject of several cooperative studies between the Canada Centre for Remote Sensing and the Canadian mining and exploration industry. This paper presents specific results from one such exploration study in a forested granitic region of Eastern Canada.

The study demonstrates methods which have permitted LANDSAT analysis to make a significant contribution to the geologic understanding of the region and to the development of an appropriate exploration strategy. A methodology is outlined in which LANDSAT image analysis facilitates the interpretation of geochemical, geophysical and ground-based geologic observations in a forested region of Devonian granitic intrusions. This case study confirms the clear, critical and continuing role of the experienced geologist in the successful integration of LANDSAT technology in mineral exploration programs.

/

GEOLINEAMENTS AS A TOOL FOR ZONE DIFFERENTIATION IN REGIONAL GEOLOGICAL STUDIES THE APPLICATION OF LANDSAT IMAGE ANALYSIS IN SIERRAS DE CORDOBA, ARGENTINA

Jorge F. Kimsa
Ernesto G. Abril

Comision Nacional de Investigaciones Espaciales
San Miguel, Buenos Aires, Argentina

SUMMARY

This paper presents a method for the study of large areas, especially those that have not been the subject of a thorough geological study. It enables the differentiation of potentially interesting areas to begin a regional survey.

It is based on the nature of the relationship structure deposit, be it genetic or conditioning of mineralization.

Geolineaments are detected in satellite images; they can thus be grouped in smaller areas which show zones whose characteristics differentiate them from their regional context, and subsequently studies. The stages leading to this typification are:

(a) Identification of geolineaments; it is performed visually from Landsat images, using bands 4, 5, 6 and 7 and standard false color composites of periods when the solar angle and the state of vegetation enable a better definition of geolineaments. In the 1:1,000,000 scale remarkable features are located and the 1:250,000 scale is useful for detailed analysis, each interpretation is given in 1:500,000.

(b) Determination of the main bearings.

(c) Distribution depending on longitude.

(d) Determination of the minimum surfaces for identification of anomalies: the region under study is divided with a grill of minimum-side squares in relation to the total work area, its characteristics and the number of geolineaments detected. In order to get more data for statistical analysis, the grill is overlaped with successive shifts.

(e) Obtaining data on each "minimum surface": number of geolineaments included in each grid square, their bearings, the sum of their longitudes, the number of times they intersect, intersection angle and bearing of its bisector.

In addition, the mean longitude is computed as well as the ratio "number of intersections/ numbers of geolineaments".

(f) Statistical analysis: the values obtained are considered sampling data; individual distributions and existing correlations between data pairs are analyzed.

(g) Plotting of results: in the center of each square of the grid with which the region under study has been subdivided, each one of the data is plotted according to the statistical fit previously performed, and the corresponding 1:500,000 scale maps showing the differentiated areas are obtained.

(h) Evaluation: each one of the maps is analyzed individually and later grouped into one representing the most repeatedly differentiated areas. And this is then compaired to the lithological, morphological data as well as to any other data that may be obtained from the images and the pre-existing studies of the region. In this way, the differentiated areas are characterized primarily.

The method is applied to the Sierras de Cordoba, Argentina, a region situated in the "Sierras Pampeanas" geological province.

/

DEVELOPMENT OF A DIGITAL IMAGE PROCESSING MICROSYSTEM

Carlos Ilarregui
Serverino Fernandez
Marcelo Campi

Comision Nacional De Investigaciones Espaciales
Buenos Aires, Argentina

SUMMARY

The Digital Image Processing Microsystem is being developed at CNIE for users with small budgets and low throughput requirements.

It's based on a low-cost home microcomputer with standard printer and minifloppy disk drive.

In order to visualize image data, a special board with the display subsystem, currently being constructed, is required to be connected to a standard color TV set.

This board has dynamic RAM refresh memory, display timing controller and serial I/O port, with electronic pencil as interactive input.

The screen has a resolution of 128 pixel per line, 128 lines, with four images in memory.

User can select video output in b-w 256 levels or color in 8-8-4 levels.

In a second stage, a 256 x 256 video board will be developed.

For mass data storage, the user can select three different media:

- Minifloppy; 8 video screen areas each
- Audio Cassette; half Landsat scene, low cost, low speed
- Video Cassette; high speed, high capacity

For the last two media, special interface will be designed and constructed.

Using the printer as a hardcopy output element, image print-outs are available in true graphics gray scale characters.

The system will not allow either high-speed or sophisticated processing. Software is being implemented in conversational form, for simple use and training, as the nonspecialized user needs.

Processing programs will be a restricted subset of PI Processing System, developed by CNIE.

The aim of this work is to develop a highly portable and extremely low cost system, accessible to a broad range of users with limited resources.

STATUS OF U.S. REMOTE SENSING OCEANOLOGY

John W. Sherman, III

National Earth Satellite Service
National Oceanic & Atmospheric Administration
Washington, DC

SUMMARY

The major developments in remote sensing applications to oceanography stem from the 1978 launches of Seasat, TIROS-N, and Nimbus-7. Each of these NASA satellites provided unique observational techniques to advance both oceanic science and marine operations. The demonstration of concept, or improvements in existing techniques for the remote measurement of surface winds, temperature, waves, ice, ocean color, currents, circulation, have been accomplished in the ensuing years.

Presently, the NOAA satellites now provide global sea surface temperatures with a bias of 0.02°C and an rms accuracy of 0.75°C. In 1984, the U.S. Department of Defense will launch a satellite designated GEOSAT, with the potential to provide global waves and windspeed. Later this year Landsat-D with an improved multi-spectral scanner will enhance bathymetric observations from space.

This review paper summarizes the results of the 1978 oceanic sensors developments which have subsequently evolved.

EL NIÑO OBSERVATIONS BY REMOTE SENSING*

Alan E. Strong

NOAA, National Environmental Satellite,
Data, and Information Service
Suitland, Maryland 20233, USA

ABSTRACT

Several excellent NOAA-7 images have enabled delineation of surface thermal patterns off the South American coast. Comparison with drifting buoys on an interactive processing system show excellent agreement with the new multichannel sea surface temperature (MCSST) algorithms now being used operationally by NOAA. Compositing data over several days allows one to further remove clouds bringing out SST structure over large areas revealing major features in both the Peru Current and the eastern South Equatorial Current of the Pacific Ocean.

1. INTRODUCTION

New spaceborne sensors and improved technology have made it possible to monitor more adequately the region of the South Pacific Ocean influenced by the Peru Current. This upwelling, nutrient-rich current system is believed to be an extremely important ocean variable, one that is directly related to, if not responsible for, many of the variations in the entire air-sea climate system. The most noteworthy extreme of the Peru Current is commonly referred to as the "El Niño" condition. This phenomenon is the result of weakened coastal upwelling and invasion of warmer equatorial waters from the north into the coastal region, upsetting not only normal physical conditions but their biological counterparts as well.

During 1981 NOAA's National Environmental Satellite, Data, and Information Service (NESDIS) drastically revised the method used to calculate sea surface temperatures (SST) from NOAA satellite data (McClain et. al., 1983). The new technique was implemented in November 1981. It uses multichannel Advanced Very High Resolution Radiometer (AVHRR) data to derive atmosphere-corrected SSTs. The correction for atmospheric attenuation by moisture can be applied on a pixel-by pixel basis. Statistics using fixed buoys and drifting buoys have been showing excellent results (Strong and McClain, 1983). The best of these comparisons is coming from drifting buoys. One array of drifting buoys was in the Peru Current during March 1982, being part of the Equatorial Pacific Ocean Climate Study (EPOCS). Results from these buoy/satellite comparisons are presented in this paper.

2. MONITORING EL NIÑO

During the ten years prior to the introduction of the multichannel SST (MCSST) procedure, satellite-derived SSTs typically have been sparse off South American in the Peru Current area. Stratus cloud cover typically obsures this cool upwelling current. Even those scattered retrievals that did managed to survive all the cloud checks had a tendency to be biased slightly negatively, indicating clouds could still be contaminating the field of view.

---

*Presented at the Seventeenth International Symposium on Remote Sensing of Environment, Ann Arbor, Michigan, May 9-13, 1983.

With MCSST procedures becoming operational in late 1981 the Peru coast was selected as a priority area for conducting extensive validations; quality "surface truth" from EPOCS being available for comparison there. February and March 1982 were selected as candidate monitoring months; cloud cover historically being least during that period. Although no "El Niño" had visited the region since 1976, sea surface conditions were still slightly warmer than normal (0.5°C), having never quite returned to normal since 1976. The 1982/83 "El Niño" began developing over the Central Equatorial Pacific during June and July 1982, but did not reach the South America coast until September 1982. Our March 1982 measurements were taken immediately prior to the onset of this El Niño - which has become one of the best developed warm water episodes of modern record.

3. THE MARCH 1982 FIELD STUDY

During February 1982 several cloud-free satellite scenes along the Peruvian coast showed numerous thermal features. Fig. 1 is an example of such detail on February 8, 1982. A special sampling of full resolution AVHRR (Large Area Coverage--LAC) was initiated. A week-long period of clear or nearly cloud-free scenes in middle and late March was selected for further processing on NASA image processing equipment at the Goddard Space Flight Center. Although LAC data at 1-km resolution was not available on all days, coarser 4-km resolution data (Global Area Coverage--GAC) was obtained from NESDIS for a compositing experiment.

The March 22 data, shown in Figure 2 (a-d), shows a black and white version of the color image used in the poster session and is derived from the LAC daytime pass on that day (approx. 1430 local time). Channel 2 (Fig. 2a) (0.725-1.1μm) illustrates how the sunglint contaminates much of the western portion of the scene, while Channels 4 and 5 (10.3-11.3μm and 11.5-12.5μm, respectively) are unaffected by the glint and reveal some evidence of a coastal thermal pattern. After correction for atmospheric water vapor (Figure 2d) these features sharpen noticeably. Areas of the image where Channel 2 reflectances exceed 15% are not processed (displayed as black), as they represent obvious clouds or land targets.

Imbedded in the image of Fig. 2 are the locations of seven (7) small drifting buoys equipped with SST probes. Information from these drifters were supplied by NOAA's AOML (Hansen, 1982) from an EPOCS data set with assistance from Peru's Marine Institute (IMARPE). Table 1 shows satellite/buoy comparisons and location of these drifters on March 22. The outlier (#2197) is the buoy farthest south where the cloud filtering was evidently ineffective. The other drifters tend to show a slightly negative satellite bias but all are within 0.6°C.

On the HP-1000 Interactive System at NASA/GSFC it was possible to composite an entire week of GAC AVHRR from NOAA-7 after the SST daytime algorithm had been run and the data mapped. In forming the composite SST field over this seven day period (19-25 March), wherever more than one SST accumulated at any pixel the highest value was selected for the final composite image. Taking the highest SST, rather than the mean value, helps remove residual cloud contamination.

Figure 3 is the final product, March 19-25. Again, this version is a black and white rendition of the color poster illustration. Buoy locations are included on this Figure for most days and indicate current movement at each drifter location. Structure along the Peru-Ecuador coastline is well portrayed, as is the cooler water of the Equatorial Current through the Galapagos Islands. The wave-like form of the Pacific Equatorial Current front shows up dramatically as three cusp-like features. They are a portion of a series of equatorial long-waves extending westward along on the north side of this cool upwelling current (Legeckis et. al. 1983). These waves typically progress westward with a phase velocity of nearly one wavelength per month.

4. THE 1982/83 EL NIÑO

Data from satellites, buoys, and ships have been used jointly in defining the evolution of the strong 1982/83 El Niño. Figure 4 shows the SST anomalies for June 1982 (a), September 1982(b), December, 1982(c) and March 1983(d) as derived by satellite. Although some stratospheric aerosol from El Chichôn (see earlier paper in these proceedings: Strong, et. al, 1983) removed a degree or two from the associated anomaly pattern, the feature and its evolutuion are well defined from satellite data alone.

5. CONCLUSIONS

Several excellent NOAA-7 AVHRR images have enabled delineation of surface thermal patterns off the South American coast. Comparisons with buoys showed excellent agreement, illustrating how well the new MCSST algorithms are working. Compositing data over several days allows one to further remove clouds and bring out SST structure over large areas, revealing major current features.

The region of Peru Current is an important oceanographic and climatic area. The El Niño of 1982/83 is being monitored by satellites, buoys, and ships more successfully than any previous El Niño, and it appears that this El Niño may be the most significant of the century.

6. ACKNOWLEDGEMENTS

The author is greatly indebted to the assistance of J. Gatlin and D. Endres, NASA/GSFC, who provided support for this project on their HP-1000 Interactive System. The careful review by P. McClain and text preparation by M. Bowman are also deeply appreciated.

7. REFERENCES

Hansen, D. (1983), personal communication.

Legeckis, R., Pichel, W., and G. Nesterczuk (1983), "Equatorial Long Waves in Geostationary Satellite Observations and in a Multichannel Sea Surface Temperature Analysis," Bull. Am. Met. Soc., Vol. 64, No. 2, (Feb. 83), pp.133-139.

McClain, E.P., Pichel, W.G, Walton, C.C, and A.E. Strong (1983), "Ocean Surface Temperatures from Space--A Multispectral Approach," Submitted for publication.

Strong, A.E. (1983), "Using the NOAA AVHRR Data to Monitor El Chichon Aerosol Evolution and Subsequent Sea Surface Temperature Anomalies," In These Proceedings.

Strong, A.E. and E.P. McClain (1983), "Ocean Surface Temperatures from Space--Comparisons with Drifting Buoys," Submitted for publication.

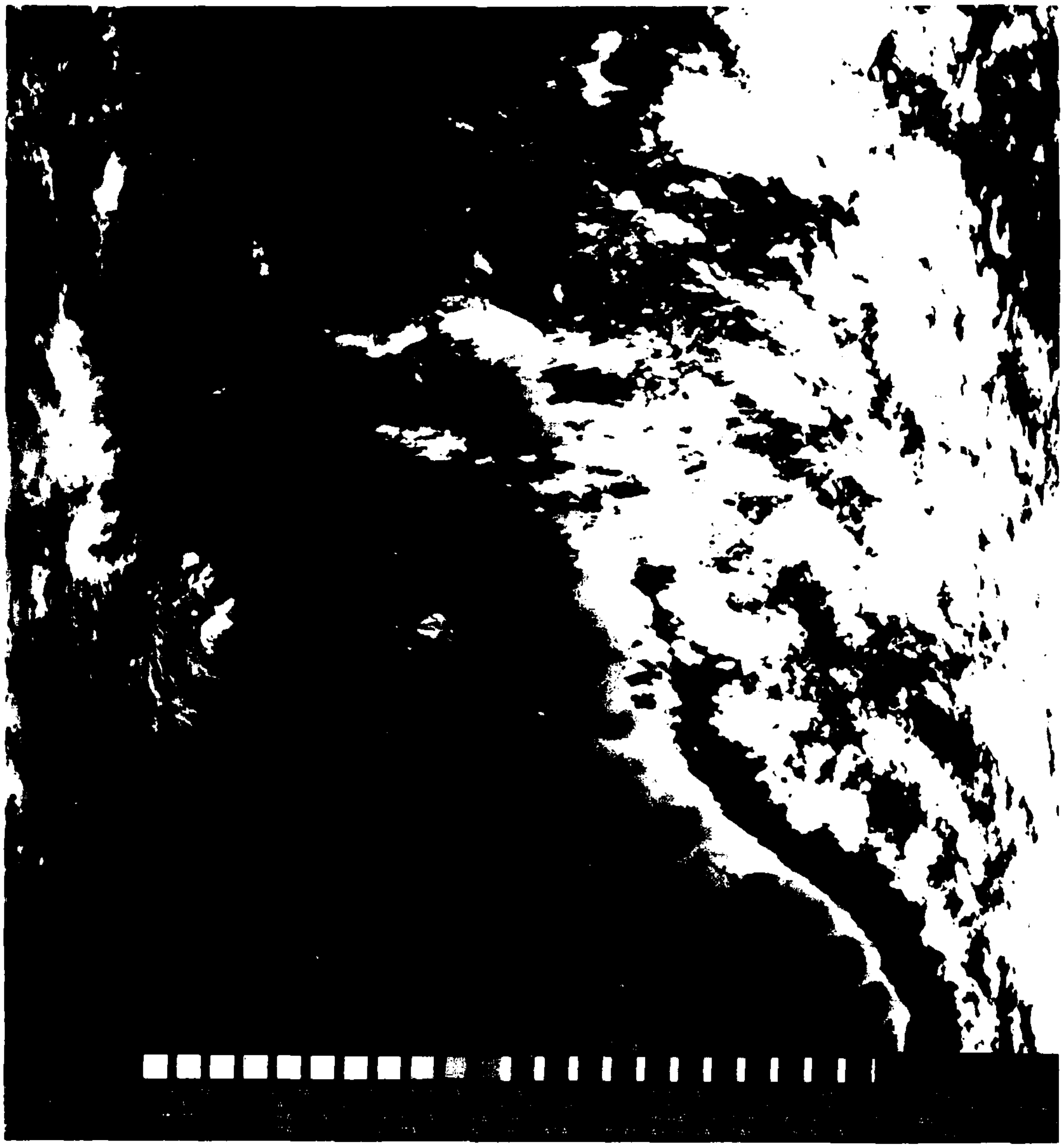

Figure 1. Upwelling Along Peru Coast.

NOAA-7 AVHRR Channel 3 (3.55 to 3.93 μm) for 8 February 1982 at approximately 1130 local time and 1-km resolution. Note: Reflected solar radiation in this particular thermal channel causes some low level clouds to turn black due to higher apparent blackbody temperatures.

Figure 2. Machine Processed and Mapped AVHRR Data.

NOAA-7 AVHRR Channel 2(a), 4(b), 5(c), and MCSST(d) for 22 March 1982 at approximately 1430 local time and 1-km resolution. Notes: (a) MCSST removes moisture and sharpen features in ocean (d) buoy locations (*) used for validations discussed in text.

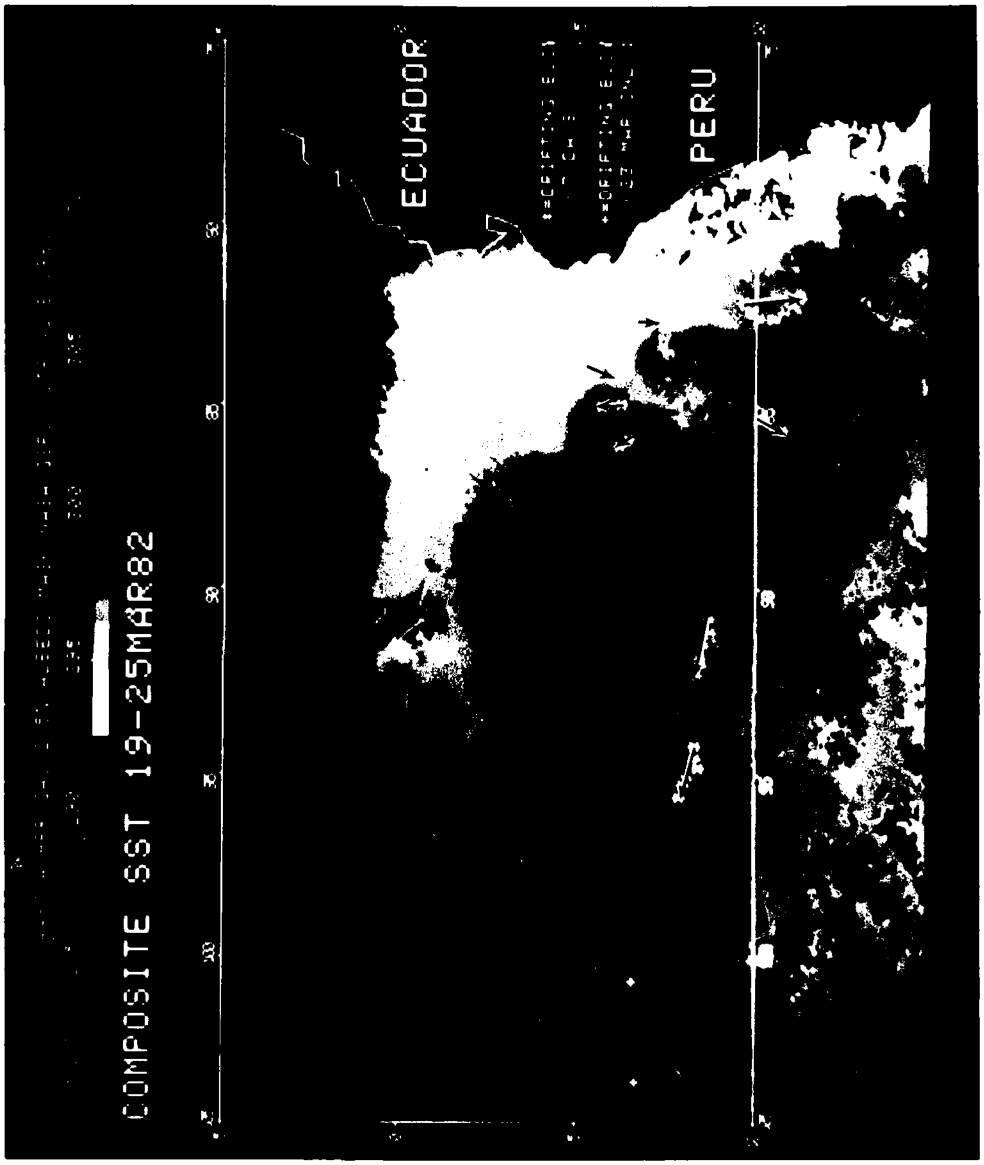

Figure 3. Seven-day Composite AVHRR Data.

NOAA-7 AVHRR GAC (Global area coverage) 4-km resolution data have been analyzed for SST for seven days: 19-25 March 1982 and composited. This removes cloud cover from most areas of the analysis. Buoys (*) are located as they moved through the period (arrows).

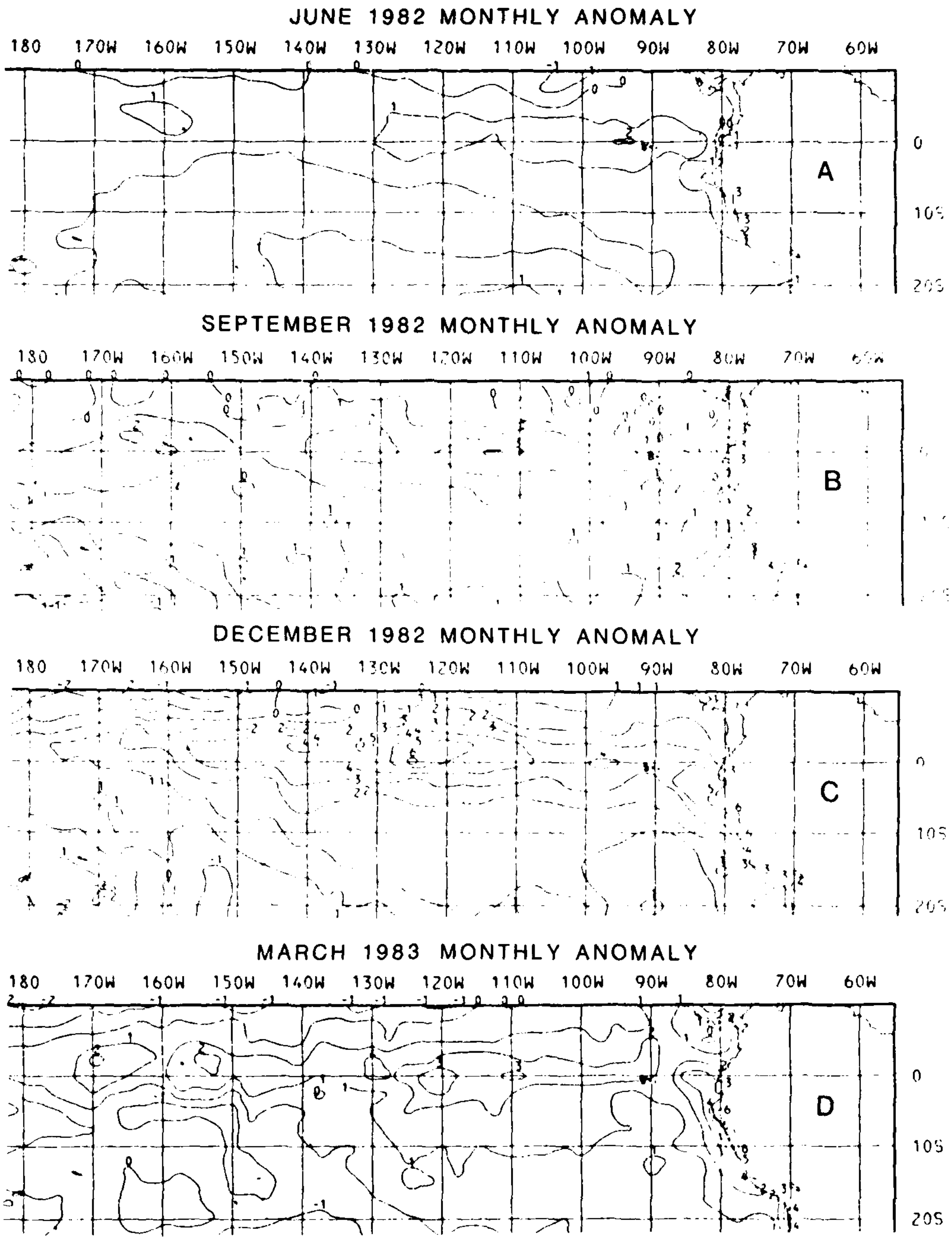

Figure 4. Satellite-derived Monthly Mean SST Anomalies during 1982/83 El Nino

22 MARCH 1982

PERU COAST NOAA-7

DRIFTER I.D.	LOCATION	BUOY SST	MCSST	DIFF.
2162	10.474S 85.407W	26.4°C	25.8°C	−0.6°C
2176	6.885S 82.573W	22.5°C	22.4°C	−0.1°C
2183	6.210S 86.038W	27.0°C	26.7°C	−0.3°C
2188	5.769S 84.946W	25.6°C	25.6°C	0.0°C
2197	10.684S 82.447W	26.6°C	24.4°C*	−2.2°C*
2198	5.858S 84.088W	24.6°C	24.3°C	−0.3°C
2200	10.394S 79.859W	24.1°C	24.1°C	0.0°C

Table 1. Buoy Satellite Validation for 22 March 1982.

THE ERS-1 PROGRAMME OF THE EUROPEAN SPACE AGENCY: ITS APPLICATIONS TO MINERAL AND MARINE RESOURCES, METEOROLOGY, CLIMATOLOGY, AND OCEANOGRAPHY

by C. HONVAULT

European Space Agency
Directorate of Applications Programmes
18, avenue E. Belin, 31055 TOULOUSE Cedex, France

ABSTRACT

In October 1981, the Member States of the European Space Agency decided to initiate the first ESA Remote Sensing Satellite (ERS-1) Programme. The first mission is oriented towards ice and ocean monitoring and the main mission objectives are of both scientific and economic nature;

- to increase the scientific understanding of coastal zones and ocean processes;
- to develop and promote economic applications related to a better knowledge of ocean parameters and sea-state conditions.

The payload of ERS-1 is composed of:

- an Active Microwave Instrumentation (AMI), combining the functions of a Synthetic Aperture Radar (SAR), a Wave Scatterometer and a Wind Scatterometer, primarily for the measurement of wind field and wave-spectra and for all-weather imagin
- a Radar Altimete A), primarily for the measurement of significant wav eights and of major ocean currents;
- an additional instrument to be selected as a result of an Announcement of Opportunity issued in the scientific community of the participating States.

The paper presents the different parameters to be extracted from the system and their potential contributions to the effective utilisation of remote sensing techniques in the fields of petroleum and mineral resources, meteorology, climatology, oceanography and marine resources.

1. INTRODUCTION

Since the early 1970's, a number of remote sensing satellites have been launched, mainly by the USA, and a large number of experiments carried out to asses the value of this new space technology for a wide range of applications. Since 1976 the European Space Agency, assisted by various groups of European Experts, has studied the mission objectives with a view to identifying European needs and eventual contributions to remote sensing satellite programmes.

These activities resulted in a recommendation for the development of two satellite systems: one oriented towards the monitoring of coastal zones and open oceans, and the other oriented towards land applications. A further recommendation was to consider not only the optical instruments for the payloads, but also microwave imaging sensors, e.g. Synthetic Aperture Radar (SAR) providing an all-weather capability. In early 1980, the ESA Member States decided that the first priority should be given to an oceanic mission which could also perform the monitoring of polar regions. The following sections provide a brief description of the parameters measured by ERS-1, and of their use for scientific and application objectives.

2. THE ERS-1 SATELLITE

The priority in the payload has been given to a comprehensive set of active microwave instruments able to observe as completely as possible the surface and wave structure over the oceans. The set of instruments consists of a Wind Scatterometer, the SAR employed as a Wave Scatterometer, and the Radar Altimeter. Results from SEASAT have demonstrated the ability of the Wind Scatterometer to provide wind speeds to an accuracy of 10-20%, and wind directions to within about 20°, and of the Radar Altimeter to provide significant wave heights to about 10 accuracy. Further, the SAR on SEASAT was successful in imaging waves yielding, in most cases, the directions and wavelengths of the dominant waves and potentially the full two-dimensional wave energy spectrum.

In the selected ERS-1 configuration, SAR small-scene wave images will be interleaved with scatterometer data of the same microwave wavelength in a global sampling scheme, thereby enabling the development of algorithms including the important coupling between the wind. the short back-scattering ripples and the longer modulating waves. The simultaneous global sampling of wind and wave fields will furthermore enable the application of mutually supportive objective analysis schemes in which the wind and wave fields are estimated jointly through the application of a dynamic wave model.

For ERS-1, the Wind Scatterometer, Wave Scatterometer, and SAR will be combined as an Active Microwave Instrumentation (AMI). This approach leads to a reduction of the required mass, volume and cost by sharing common hardware.

To summarize, therefore, the ERS-1 baseline payload will consist of the following instruments:

- an Active Microwave Instrumentation (AMI) operating at C-band (5.3 GHz), combining the functions of a Synthetic Aperture Radar (SAR), a Wave Scatterometer and a Wind Scatterometer, primarily for the measurement of wind fields and wave image spectrum, and for high-resolution all-weather imaging over coastal zones, ice areas and land.
- a Ku-band (13.56 GHz) Radar Altimeter (RA) for the measurement of significant wave heights and of major currents over oceans, and of ice profiles.
- an Along-Track Scanning Radiometer (ATSR), as a result of an Announcement of Opportunity (AOP) issued by ESA within the scientific community of the participating States. This is a 3-channel infra-red radiometer, primarily for accurate measurement of sea surface temperature. The possibility is being studied of completing the ATSR with a 2- frequency microwave nadir sounder for measurement of water vapour content in support of the Radar Altimeter.
- a Precise Range & Range Rate Experiment (PRARE) as a result of the same AOP.
- Laser Retroreflectors to provide accurate tracking capability.

AD-A134 719 PAPERS SELECTED FOR PRESENTATION AT THE INTERNATIONAL SYMPOSIUM ON REMOTE..(U) ENVIRONMENTAL RESEARCH INST OF MICHIGAN ANN ARBOR JUN 82

3/6

UNCLASSIFIED F/G 14/5 NL

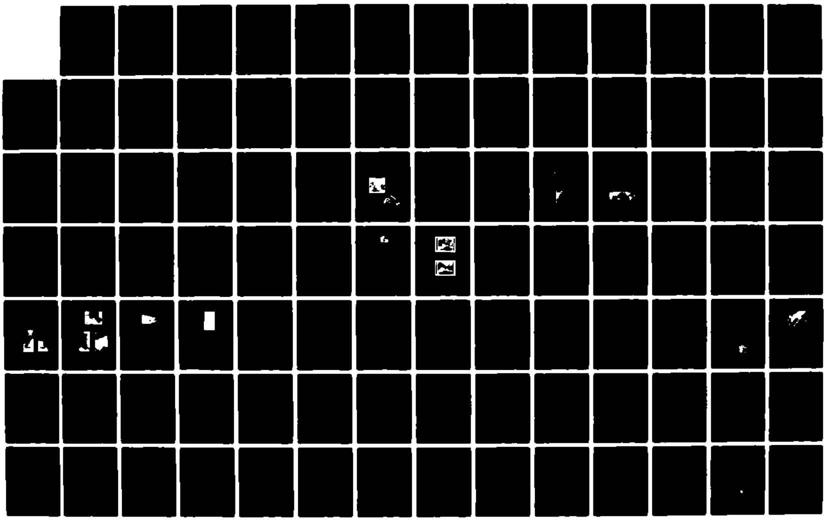

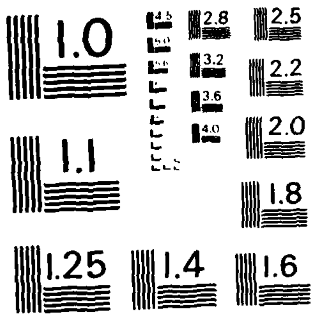

MICROCOPY RESOLUTION TEST CHART
NATIONAL BUREAU OF STANDARDS-1963-A

The data from the payload instruments are collected and formatted within the instrument Data Handling Subsystem before transmission to the ground.

Two channels are foreseen:

Channel 1 . for raw data from the AMI, either in the sampling mode or in the wade mode

Channel 2 . for low bit rate data (Wind Scatterometer data, RA, additional instruments)

. for playback of low bit rate data (data rate about 6 Mbps).

ERS 1 will use the Multimission Platform (PEM) developed within the framework of the French SPOT Programme and will be launched by ARIANE (2 or 3).

The total mass of the satellite in orbit will be about 2,200 kg.

The launch date is expected to be around end 1987 and the target lifetime is 3 years.

3. THE ERS 1 ORBIT

Considering, inter alia, the need:

- to observe high latitude areas including polar caps,
- to simplify the technical requirements for the satellite (thermal control and power generation),
- to ease the interpretation of imaging SAR data,

a sun synchronous, circular orbit with an altitude range of 650 to 700 km had been selected for ERS 1. However, a possible alternative around 775 km is under consideration in order to satisfy a requirement on ground track repetitivity better than 1 km, which is of importance for a number of objectives in physical oceanography (e.g. ocean circulation).

Minor changes of a few km of the orbit altitude will permit major increases in the ground coverage, at the expense of the repetitivity. The flexibility in the tuning of the orbit provides the possibility, for instance, to achieve a full coverage of Canada and Europe with the all-weather imaging instrument within a few days, or a global coverage of the Atlantic Ocean with the wind and wave instruments.

4. THE DATA REQUIREMENTS

4.1 *Coverage*

ERS 1 is intended to allow world-wide coverage, compatible with the duty cycles of its payload instruments. The Agency will accordingly ensure real time transmission from the satellite and effect any necessary coordination with national facilities for data acquisition.

Furthermore, the on board tape recorders will give access to data from any part of the world via the playback data acquisition facility, provided that the global amount of data recorded per recording period has an upper limit of around 5 Gbits.

4.2 Instrument Duty Cycles and Data Transmission

High Bit Rate Mode

Because of the high bit rate (100 Mbps), on-board recording cannot take place and, therefore data acquisition is only possible from areas in the coverage of available stations. The SAR will operate in duty cycle of about 10%.

Low Bit Rate Mode

During the low bit rate mode, the following sensors operate with a duty cycle of 40 to 100%:

Altimeter	:	10 Kbps
Wind Scatterometer	:	1 Kbps
AMI Wave Mode	:	600 Kbps
ATSR	:	100 Kbps.

Combined Modes

The following activities can take place in parallel: AMI imaging mode in real-time transmission plus real-time transmission of low bit rate data plus playback of low bit rate data.

4.3 Measurements

The main physical parameters which will be obtained are summarised in the attached Table 1.

5. THE ERS-1 GROUND SEGMENT

The problem of remote sensing data acquisition, processing and dissemination has been identified as a key aspect when in the near future both European and non-European spacecraft will be in orbit and generating very high data rates for experimental and operational users. In the particular case of oceanic missions for the monitoring of rapidly changing dynamic phenomena, requirements are specially severe and delivery of the information to end users must be performed within a few hours. A figure of 3-6 hours is currently admitted. In addition, many of the potential applications of data coming from ERS-1, which are at present considered experimental, will in fact become nearly operational at the time of the mission and could be put into quasi-operational use after launch, provided facilities for processing and distribution of data in near real-time are in place.

Therefore, when designing the ERS-1 Ground Segment, it is essential to consider the complete end-to-end data system irrespective of which entities will be in charge of some parts of this system. The end-to-end data system includes all activities (both software and hardware) starting from the acquisition and recording of the raw data at the ground station until delivery of the requested information/data to the end-users. This involves a number of activities or functions such as:

- recording of raw data,
- data preprocessing and processing (including algorithm development),
- storage/archiving and handling of archives,
- setting up of catalogues and handling,
- generation of products,
- data/products transmission, distribution and quality control,
- mission control and management.

For this purpose, the ERS-1 Ground Segment will include:

- the mission management and control facilities located at ESOC (Darmstadt, Germany), and combined in the MMCC (Mission Management & Control Centre),

- one station located in Kiruna (Sweden) for coverage reasons, for:
  . acquisition of all payload data (DAF, Data Acquisition Facility),
  . telemetry, telecommand and tracking,
  . provision of near real-time products (RTPF, Real-Time Processing Facility) of a global nature.

For the distribution of the near real-time data to users, two possibilities will be investigated:

- transmission via land lines to regional hubs (WMO solution),
- transmission via satellites such as SIRIO-2/MDD or ECS/ESS.

The inclusion of the Fucino (Italy) and Maspalomas (Canary Islands) stations for acquisition and quick-look processing of SAR data will be studied during the detailed Definition Phase. Other facilities of regional interest, real-time data acquisition facilities, and processing and archiving facilities, which are not necessarily ERS-1 dedicated, but participate in the end-to-end data system, should be elements of the Earthnet Programme or national facilities coordinated by the Earthnet Programme Office.

6. OVERALL MISSION CAPABILITIES

The main capabilities are of both scientific and economic nature and aim at:

- increasing the scientific understanding of coastal zones and global ocean processes which, together with the monitoring of polar regions, will provide a major contribution to the World Climate Research Programme. ERS data used alone, or more commonly used in conjunction with complementary data from buoys, radio-sondes, research vessels, other near-surface platforms and other satellites in pre-arranged global or regional experiments, will enable significant advances to be made in physical oceanography, glaciology and climatology;

- developing and promoting economic/commercial applications related to a better knowledge of ocean parameters and sea-state conditions.

This is of importance in view of the increasing development of coastal and offshore activities and the adoption by more and more countries of the 200 nautical mile economic zone. In addition, monitoring of sea-ice and icebergs will be of importance for industrial activities performed at high latitudes.

7. APPLICATIONS OF ERS-1

Benefits to be expected from a mission such as ERS-1 result essentially from the possibility of generating short-term and medium-term forecasts of weather and ocean conditions on a local or global basis for the continuous and reliable monitoring of the ocean surface. It should be borne in mind that as most of the applications envisaged require that the data be processed and delivered to the end-users within a few hours, the ground segment should be sized accordingly.

The major limitation of current ocean and atmospheric forecasts is the lack of data over the open ocean. Numerical experiments in the USA using SEASAT data, and in Europe by the European Centre for Medium Range Forecasts, have

shown that the inclusion of such data in the models provides more accurate forecasts, valid for longer periods of time. The main inputs required are surface wind field measurements, supplemented by measurements of the surface wave energy spectrum and by direct measurements of wave height, all these parameters being measured by ERS-1 with the necessary accuracy.

All this information can be used in marine industries to improve weather or sea-state dependent operations, to supply better warning of severe wind and wave conditions, to provide a way to improve and manage the resource yield, to permit a better understanding of the ocean and its dynamics.

7.1 Applications to mineral and marine resources

The increased ocean forecast accuracy will have a strong influence on

- exploration operations such as seismic surveys, drill ships, towout operations;
- offshore oil and gas production operation
  . crew scheduling and platform safety
  . installation of pipelines on sea bed;
- development of platforms: wave measurements with the Altimeter will be used for optimisation of platform design criteria;
- deep ocean mining operations;
- marine fisheries: by increasing the efficiency of search effort and gear operations and the safety of the crew and vessel. Sea surface temperature determination is of primary importance for pelagic species fisheries;
- the same measurements, taken in combination with meteorological information, will provide model inputs for predicting the trajectory of pollutants and their potential threat to sensitive shore areas.

7.2 Applications to Marine Transportation

The same measurements will optimize ship routing by

- reducing the time on trade routes and consequently reducing total fuel consumption. Reliable sea-state analysis and prediction can reduce transit time by up to 10 ;
- improving the safety by reduction in hull damage, cargo damage, marine insurance costs, catastrophic ship losses, etc.

In addition, monitoring of sea-ice with the high-resolution all-weather radar imagery will be of direct interest to ship routing in high latitude areas such as the Gulf of Botnia, Artic region, Greenland waters and Canada.

7.3 Applications to Oceanography

- Establishment of models

  Phenomenological and analytical techniques and models play important roles in providing descriptions, and also represent a highly useful and valid approach to the physical understanding of many important oceanic processes. Numerical models of various types are becoming a powerful tool by which diverse observations of the ocean are tied together to form a coherent picture of the state of the ocean and the processes at work.

  For general circulation models, the surface stress measured by the Wind Scatterometer is a significant input, such as time-averaged surface

temperatures provided by the ATSR.

ERS-1 measurements made continuously over several years will supply a great part of the coherent data sets needed for many research problems and for test and tuning of models. Such data sets, if continued operationally, for the basis of extraction of indices for long-term monitoring of variability. The existence of such data sets is of paramount importance for atmospheric and oceanic research, in particular for modelling of the seasonal and interannual variations in the ocean circulation.

- Mesoscale variability

The most energetic mesocale oceanic eddies are formed in the vicinity of strong currents. Recent studies have concluded that these eddies could be attributed to direct forcing by variable winds. Scatterometer, Altimeter and ATSR data will provide data in order to verify the assumptions.

- Storm surge and wave forecasts

These oceanic features are locally related to the wind, and work will be needed in this area to make effective use of Scatterometer and Altimeter data.

- Ocean surface variability

The main contribution to the study of this phenomenon is provided by the Altimeter, which is able to provide important and reliable information on the statistics of ocean waves, in particular the significant wave height H 1/3. This ocean surface variable is very important for marine operations and also for the study of the development, propagation, and effects, of such ocean events as major storm surges. In order to take as much benefit as possible of the capabilities of this instrument, the Agency is contemplating the possibility, as mentioned above, of changing the altitude of the nominal orbit from 675 km to 777 km, in order to decrease the drag effect and perform a track repetitivity on the ground better than 1 km, condition for the provision of useful information on major currents and eddies and on topography of the great continental ice sheets, such as Greenland and Antarctica.

- Internal waves

SAR imagery from SEASAT demonstrated that the images can provide important information on such an oceanic feature. High resolution by SAR observations provided by ERS-1 can be applied to studies of surface current and density structure, which would be inferred from observations of shear instability and internal wave packet spacing. In certain circumstances, SAR images are well correlated with bottom topography down to water depths of 30 to 40 m.

7.4 Contributions to Meteorology and Climatology

- For numerical weather prediction, the surface wind as provided by the Scatterometer will be of primary importance.

- The sea surface temperature provided with a very high accuracy by the Along-Track Scanning Radiometer is one of the important physical factors that determine the exchange of heat energy between the atmosphere and ocean. Patterns of sea surface temperature distribution are very useful to study the time and space variability of many features manifested by temperature gradients. The microwave channels which are likely to be added on the ATSR will permit the elimination of the water vapour influence.

- The mapping of polar ice caps and monitoring of sea-ice boundaries by the SAR and the Altimeter contributes also to research in climatology.

8. PROGRAMME DEVELOPMENT

Most of the applications based on the data provided by ERS-1 are still in a building stage and a lot of preparatory work, both theoretical and experimental, is still necessary. This will require a number of activities before and after launch which are very important for the success of the mission, such as:

- simulation and optimisation of sensor performances (airborne testing),
- development and testing of algorithms and models,
- setting up and testing of data and products,
- definition of distribution networks to meet user requirements,
- development of pilot-projects (small scale) and demonstration missions (large scale),
- continuation of research and development to optimise the use and value of the data provided by the satellite system.

In order to assist the European Space Agency in these activities, teams of external experts (AMI team, Altimeter team, Data team) have been set up.

In conclusion, the experimental/pre-operational phase now proposed for ERS-1 should be used to evaluate the means of reaching a fully operational system. In this context, Europe will be prepared to contribute to a multi-satellite system for global monitoring.

References

Oceanus, Volume 24, Number 3, Fall 1981
NCAR/TN-185, November 1981

[illegible] Geophysical Parameter	Range	Accuracy	Width	Spatial Resolution	Spatial Sampling	Earth Localization	Coverage Repeat Cycle	Delay	[illegible]
WIND FIELD									
Velocity	[illegible] m/s whichever is greater	[illegible] m/s or [illegible] whichever is greater	[illegible]	[illegible] km²	[illegible] km	[illegible] km	Global [illegible] days	[illegible] hrs	[illegible]
Direction	[illegible] 360°	[illegible]	"	"	"	"	"	[illegible]	[illegible]
WAVE FIELD [illegible]	[illegible]	[illegible] whichever is greater	NA	[illegible]	[illegible]	[illegible]	[illegible]	[illegible]	[illegible]
[illegible]	[illegible]	[illegible]	NA	[illegible] km²	[illegible]	[illegible]	"	[illegible] hrs	[illegible]
[illegible]	[illegible]	[illegible]	NA	"	[illegible]	[illegible]			
[illegible]	[illegible]	[illegible]	NA	"	[illegible]				
[illegible]							[illegible] days [illegible]		
[illegible] data			NA	[illegible]		[illegible]	[illegible]	[illegible]	[illegible]
[illegible] quality [illegible]	[illegible] dB [illegible]	[illegible] dB at [illegible] dB [illegible] dB at [illegible] dB	NA	[illegible]	[illegible]	[illegible]	[illegible] storage facility.	[illegible]	
ALTIMETER MEASUREMENTS							Ground track distance [illegible] km Equator for [illegible] day repeat cycle		
Altitude	[illegible] km [illegible]	[illegible] relative [illegible]	NA		[illegible]	[illegible]		[illegible]	[illegible]
[illegible]					"	[illegible]		"	"
[illegible]					[illegible]			"	"
[illegible]		[illegible]	[illegible]	[illegible]		[illegible]	[illegible]	[illegible] hrs	[illegible]
[illegible]		[illegible]							[illegible]

AD P002003

REMOTE SENSING INPUT AND FEEDBACK FOR HYDROLOGIC FORECASTING AND SIMULATION MODELS

E. T. Engman
U.S. Department of Agriculture
ARS-Hydrology Laboratory
Beltsville, Maryland, U.S.A.

ABSTRACT

New methods of remote sensing, such as microwave and thermal infrared, can give us information on the moisture status and temperature of the earth's surface. With the present technology available to us, this type of new information cannot be used effectively for hydrologic forecasting. However, it appears that, coupled with adequate simulation models, these remote sensing data have the potential to greatly improve hydrologic forecasting and simulation accuracies. This paper discusses different forms of remote sensing, the status of current models to use these data, and what changes must be made to incorporate this promising new form of data.

1. INTRODUCTION

Remote sensing technology is advancing very rapidly. In doing so it is beginning to provide information from data that has the potential for a breakthrough in applied hydrology. Infrared and microwave remote sensing provides more than 'air photo' types of cartographic information. Information from these longer wavelengths can tell us a great deal about the state of the watershed; i.e., how wet or dry and how cold or hot it is. This information, coupled with adequate simulation models, should improve forecasting and simulation accuracies. This paper addresses the potential for using these remote sensing data, with an emphasis on soil moisture, and identifies areas where research and development must be done.

2. CURRENT USE OF REMOTE SENSING IN HYDROLOGIC MODELS

Remote sensing is beginning to be used in hydrologic models but, for the most part, these applications are cartographic in nature. About the only areas that remote sensing has made an impact on hydrologic modeling has been in the areas of land use (including impervious area) and snow cover area.

2.2 LAND USE

Jackson et al. (1977) demonstrated that land cover (particularly percent imperviousness) could be used effectively in the STORM model (USACE, 1976). Slack and Welch (1980) demonstrated that Soil Conservation Service (SCS) Runoff Curve Numbers (RCN) could be developed in a cost effective manner for an agricultural watershed in Georgia. Ragan and Jackson (1980) modified the land cover requirements for the SCS procedure for suburban areas so that Landsat data could be used. The RCN's developed from the Landsat data closely matched those obtained from a conventional approach based on air photo analysis. Synthetic flood frequencies developed from the two procedures are essentially identical. The Hydrologic Engineering Center of the Corps of Engineers (USACE, 1979) also had very good results from developing synthetic flood frequency curves from Landsat. Bondelid et al. (1981) developed a software package and users manual to efficiently estimate RCN's from Landsat data.

2.3 SNOW

A NASA Applications Systems Verification and Transfer (ASVT) project on the Operational Applications of Satellite Snow Cover Observations (Rango, 1981) was begun in 1975 and completed in 1979 in cooperation with nine operational water management agencies. Both Landsat and NOAA satellite data were supplied to these agencies for use in improving snowmelt runoff forecasts. When satellite snow cover data were tested in both empirical seasonal runoff estimation and short-term modeling approaches, a definite potential for reducing forecast error was demonstrated. The snow mapping ASVT has proven that satellite snow cover data can be used to reduce snowmelt runoff forecast error in a cost effective manner once all operational satellite data are available within 72 hours after acquisition.

3. REMOTE SENSING METHODS

Remote sensing methods take advantage of specific characteristics or responses from regions of the electromagnetic spectrum. Initially, remote sensing concentrated on areal photography and the visible region of the spectrum. More recently, remote sensing has begun to work with regions of the spectrum with both longer and shorter wave lengths. The following reviews the status of research in some regions outside of the visible spectrum and discusses their potential for applied hydrology.

3.2 MULTISPECTRAL REMOTE SENSING

A long period of experience with Landsat and other multispectral scanner data, which generally includes the visible and near infrared regions of the spectrum, has helped develop user capability. These types of data can be used for estimating land use, snow cover, and vegetation biomass. Current uses have been discussed under the previous section addressing current use of remote sensing in hydrologic models.

3.3 MICROWAVE REMOTE SENSING

Microwave technology is one form of remote sensing that currently shows great promise in providing new information to the hydrologist. The strong dependence of the dielectric properties of the earth's surface layer, soil or snow, on their moisture content at the microwave wavelengths affects the reflectivity and emissivity. These quantities can be remotely sensed with active microwave (radar) and passive microwave (radiometry) systems. In addition to being able to measure the state of the surface through its dielectric constant, microwave systems are not affected by cloud cover and thus, are all-weather instruments.

Microwave technology is useful for measuring near-surface soil moisture. The soil moisture content has a direct effect on the dielectric constant, which can be measured by microwave technology (Schmugge et al. 1980). These systems measure the average soil moisture directly and can be implemented on an airborne platform for rapid large area coverage, thus alleviating the problems of direct measurement encountered using conventional techniques. Microwave approaches also have the capability of sensing the soil through a moderate amount of vegetative cover (Jackson et al. 1981), which extends their utility. Numerous experiments have shown the responses of these sensors to be strongly correlated with the moisture in a layer about 5 cm thick.

Microwave remote sensing can differentiate between frozen and unfrozen soils. For a given soil moisture, the dielectric constant will change considerably when soil water changes from a frozen to a liquid state. Thus there is the potential for remotely determining whether a soil is frozen or unfrozen. This should greatly benefit those people responsible for flood forecasting, particularly in the upper midwestern United States.

Successful applications of satellite observations of snow cover area for snowmelt and water supply forecasting were discussed in the previous section. Although promising, there are also limitations to the snow cover area approach. These include lack of direct information on depth, water equivalent, ripeness, and other fundamental snow pack properties. However, like soil moisture and other hydrologic applications, the microwave region of the spectrum offers the snow hydrologist a potentially powerful tool. Not only would a microwave sensor be an all-weather instrument because it can penetrate cloud cover, but it can also penetrate the snow pack which presents one with the opportunity of inferring many of the properties of the snow pack. These include depth and water content as well as the degree of ripeness, crystal size, and the presence of liquid water in a melting snow pack. Experimental work done at the University of Kansas has shown how the microwave response varies with snow water content (Ulaby and Stiles, 1979) and snow wetness (Ulaby et al., 1978).

3.4 THERMAL INFRARED REMOTE SENSING

In a way analogous to the microwave technology, thermal infrared remote sensing also can measure a state of the earth's surface. In this case the state variable is temperature. According to Price (1981), analysis of satellite acquired thermal infrared data illustrates the feasibility of developing maps of environmental conditions at the earth's surface. These maps would describe the interaction between conventionally mapped surface quantities (e.g., topography, surface cover, soil and rock type) and climatological variables (e.g., air temperature and windspeed) which are presently inferred only through temporal averaging and spatial interpolation of meteorological observations.

Most hydrologic models use point ground level meteorological measurements to determine inputs of precipitation and potential evapotranspiration. Remote sensing observations of surface temperature may represent the actual state of the watershed surface better than the meteorological measurement of air temperature at a point and which can vary dramatically over short distances. Remotely sensed data can also be used as an aid to interpolate between point measurements and to describe environmental variables in a spatial format. This type of information should provide better data for hydrologic models than is currently used. However, the models must be modified to use these data if they are to be effective.

3.5 GAMMA RADIATION REMOTE SENSING

Since 1978 the National Weather Service has been using an airborne gamma radiation snow survey program to gather snow water equivalent data for their river forecast centers (Carroll, 1981). This technique relies on the attenuation of natural gamma radiation from the soil as a measure of the snow water content. The gamma radiation attenuation technique can be used to make airborne soil moisture measurements for the upper eight inches. The National Weather Service program has demonstrated that remotely sensed soil moisture and snow water content are useful for hydrologic forecasting. However, because of atmospheric attenuation of the natural gamma energy, this procedure is limited to relatively low level flights (about 300 m).

4. HYDROLOGIC MODELS

4.2 HYDROLOGIC FORECASTING

Several governmental agencies require timely and reliable hydrologic forecasts to perform their emergency operations functions during times of potential or actual flooding, and for effective water resource management. These forecasts include prediction and assessment of hydrologic drought conditions. The current hydrologic forecast models use as inputs only rainfall (or snow melt) and, in some cases, an estimate of potential evapotranspiration.

Most of the comprehensive hydrologic models have a computation step that involves soil moisture. This value or system state must be initiated and then, timewise, it is constantly recomputed, increased according to added rainfall or decreased by evapotranspiration or drainage. Soil moisture controls the infiltration computation in that it regulates the partition between infiltrated water and storm runoff. Studies by Wilkening (1981) have shown that antecedent soil moisture is a very sensitive variable for calculating infiltration (Figure 1). The success of the prediction (overprediction, underprediction, or an accurate prediction) depends to some extent on the soil moisture state that the hydrologic model is working with.

Since the hydrologic models are designed and calibrated for point measurements, actual measure of the "true" areal values of soil moisture have had only very limited value. The state of moisture conditions conceptually indicated by the models may not relate to the actual field conditions. Thus, with present models, improved measurement of actual conditions may provide very little improvement in the accuracy of timeliness of the hydrologic forecasts. In order to use measurements of soil moisture for forecasts, the models will have to be modified or new models developed to use soil moisture as input data and as feedback to check on predictions.

4.3 SUITABILITY FOR REMOTE SENSING DATA

Peck et al. (1981) conducted a detailed study on the suitability of hydrologic forecasting and simulation models to use remote sensing data. Seven hydrologic models were reviewed. In general, they concluded that remote sensing has limited usefulness for these models in their present form. Their study evaluated possible remote sensing capabilities in addition to land use and snow cover area. These included soil moisture, frozen ground, and snow water content. These three characteristics are currently not used as input data to any of the models studied. However, because of their importance in determining runoff rates and volumes, it appears that demonstrable improvements in forecast accuracy may be achieved if these quantities could be measured for input data.

Two common forecasting models will be discussed in the following sections. In general, the comments made regarding these models will be applicable to most comprehensive hydrologic models.

4.4 NATIONAL WEATHER SERVICE RIVER FORECAST SYSTEM MODEL

The National Weather Service River Forecast System (NWSRFS) is a comprehensive hydrologic model for predicting flood flows and stream flow. The NWSRFS is a modification of the Stanford Watershed Model IV. The soil moisture accounting procedure proposed by Burnash et al. (1973) has replaced the Stanford procedures. A schematic of this model is shown in Figure 2. Inputs to the model are precipitation and potential evapotranspiration.

Six system states were identified by Peck et al. (1981); five of these are related to soil moisture and the sixth to impervious surface area. Soil moisture is treated in upper and lower zones and soil moisture is defined as being either tension water or free water in each zone. Water accretion in the lower zone occurs through percolation from the upper zone. Sixteen parameters are used in the soil moisture accounting portion of the model. These must be determined by calibration with a historical climatological and streamflow data set. These parameters have little or no relationships to soils or the soil water characteristics. Independent measurement of these parameters is not possible. Remotely sensed soil moisture could be used to update and calibrate some of the soil moisture related parameters (Peck el al. 1981) with only a minor modification or adaptation of the model. However, the model would need to be significantly modified to use soil moisture as input data.

4.5 STREAMFLOW SYNTHESIS AND RESERVOIR REGULATION MODEL

The North Pacific Division of the Corps of Engineers has developed the Streamflow Synthesis and Reservoir Regulation (SSARR) model for design, planning, and regulation of water control works. The SSARR model has three basic parts: (1) a reservoir regulation model, (2) a river routing model, and (3) a watershed model. The watershed model, which simulates runoff, will be the focus of discussion in this paper. A schematic of the SSARR model is shown in Figure 3.

Like the NWSFS, the SSARR model has an upper zone and a lower zone to account for soil moisture. A percolation procedure connects the two. There are five model states, four of which are related to runoff (surface and subsurface) and a soil moisture index. The quantity of soil moisture in the upper zone is determined by the soil moisture index. The soil moisture index is adjusted by a seasonal curve or by daily observed pan evaporation. The SSARR model has 13 parameters, most of which deal with the runoff portions of the model. The soil moisture index is affected directly by two parameters and indirectly by one.

5. REVISION OF MODELS

None of the models reviewed by Peck et al. (1981) can use remotely sensed soil moisture input data without major modification to the models. Most could use soil moisture for updating the state or parameters and for calibrating parameters with minor modifications to the model. In general, the models have represented the soil in a way to make the model work and have not considered the possibility of independent determination of soil moisture or soil parameters. For the most part, this approach is justified because soil moisture data would not be available and hydrologists have not been able to handle the spatial variability of soils.

The possibility of using soil moisture as input data would allow the hydrologists to redesign the models so that the soil zone, subsurface flow to groundwater interflow or baseflow, can be conceptualized in a more physically realistic manner. The determination of surface runoff could be accomplished with an infiltration approach whose parameters could be determined independently or could be calibrated. Likewise, subsurface water transport could be modeled using procedures based on our knowledge of flow in porous media.

Figures 4 and 5 illustrate one possible approach to modifying the NWSRFS and SSARR models. In both these cases, soil moisture is treated as input to the model and it affects only the upper zone of soil moisture. Major modifications would be necessary to adapt the models to separate the rainfall input into runoff, percolation, and stored water. It would appear that some form of infiltration approach dependent upon soil moisture would be feasible. The schematics shown in Figures 4 and 5 show this approach. It would be hoped that this type of modification could be made with no affects on the rest of the model. In many cases, interdependency among model parameters that is not fully understood prevents one from a simple replacement of model components, as shown in the schematics.

5.2 FEEDBACK FOR SIMULATION MODELS

Hydrologists have built a large number and variety of continuous simulation models. Most are mass balance-type models, taking rainfall (or snowmelt) as input and routing it to stream flow; often a portion is temporarily stored. The stored water defines the state of the system and, as such, controls the rate of sequential processes and events. Errors in the predicted output often get larger with time, since each successive computation is based on the previous state of the system. How well could we improve our prediction if we could check our system periodically and update our predictions? Repetitive measures of soil moisture used as feedback to the model could do this.

A recent study by Jackson et al. (1980) demonstrated how possible applications of repetitive, remotely measured soil moisture might be used. They discussed how these areal data may be used to calibrate soil and vegetation parameters and to correct errors resulting from point measurements of precipitation. In the study they demonstrated how soil moisture observations are useful in calibration and updating the state of the system. However, it was also pointed out that the model structure itself may preclude a valid analysis of the value of soil moisture measurements or the frequency needed to improve the simulations. If some of the parameters in the model were related and the measured soil moisture and computations were based on soil moisture data as input, a feedback loop would be built into the model to periodically update the moisture state. Figure 6 is a sketch that shows how soil moisture updating could result in improved forecasts and how, without it, progressively larger errors could result.

6. AIRCRAFT EXPERIMENTS

An experiment is underway to test the applicability of soil moisture measurements for hydrologic forecasting. Remotely measured data will be taken in an area where conventional forecasting is now used. Forecasts made with the addition of soil moisture data either as input or feedback will be compared to forecasts with conventional techniques.

Flightlines will be established to sample the major physiographic and land uses of the test basin. Flights will also be made at several elevations to obtain data with varying spatial resolutions. The plan will be to collect data before and after several runoff producing storms and during at least one drying period. The drying period flights will consist of several flights 3 to 5 days apart during a period when the soil will be drying and streamflow will be all base flow. A major need anticipated for these application experiments is a long time series of soil moisture measurements over the same flight lines. These types of data have not been available previously. We anticipate that the frequent, repetitive measurements will enable us to minimize the effects of surface roughness, vegetation, slopes, and other target characteristics on the measurements. They will also help us infer deeper soil moisture conditions than those that can be measured directly.

7. SUMMARY

This paper has discussed the current status of remote sensing in hydrology and the potential for using thermal infrared, microwave and gamma remote sensing for future applications. Two commonly used forecast models are discussed and examples proposed as to how they may be changed to use remotely sensed soil moisture for input data. The use and benefits of using remotely sensed soil moisture as feedback is also discussed. Although the emphasis of this paper is on use of soil moisture, other forms of remote sensing also have the potential for significantly improving forecast models. This information that describes the state of the basin and the spatial variability of moisture and temperature within it has the potential for a breakthrough in applied hydrology.

8. REFERENCES

Bondelid, T. R., T. J. Jackson, and R. H. McCuen. 1981. A Computer Based Approach for Estimating Runoff Curve Numbers Using Landsat Data. AgRISTARS Conservation and Pollution Technical Report CR-R1-04040, 99 pp.

Burnash, R. J. C., R. L. Ferral, and R. A. McGuire. 1973. A Generalized Streamflow Simulation System; Conceptual Modeling for Digital Computers. U.S. Department of Commerce, National Weather Service, and the State of California Department of Water Resources, Sacramento, 204 pp.

Carroll, T. R. 1981. Airborne Soil Moisture Measu. ɹ³nt Using Natural Terrestrial Gamma Radiation. Soil Science, 32(5):358-366.

Jackson, T. J., T. J. Schmugge, and R. R. Wang. 1981. Effects of Vegetation on Passive Microwave Estimates of Soil Moisture. Proceedings, International Geoscience and Remote Sensing Symposium, IEEE Catalog No. 81CH1656-8, pp. 375-387.

Jackson, T. J., T. J. Schmugge, A. D. Nicks, G. A. Coleman, and E. T. Engman. 1981. Soil Moisture Updating and Microwave Remote Sensing for Hydrologic Simulation. Hydrological Sciences Bulletin, 26(3):305-319.

Jackson, T. J., R. M. Ragan, and W. N. Fitch. 1977. Test of Landsat-based Urban Hydrologic Modeling. Journal of the Water Resources Planning and Management Division, ASCE, 103(WR1):141-158.

Peck, E. L., T. N. Keefer, and E. R. Johnson. 1981. Strategies for Using Remotely Sensed Data in Hydrologic Models. NASA Report #CR-66729, Goddard Space Flight Center, Greenbelt, Maryland, 52 pp.

Price, J. C. 1981. Use of Remotely Sensed Infrared Data for Inferring Environmental Conditions from Surface Characteristics and Regional Scale Meteorology. Proceedings, 1981 International Geoscience and Remote Sensing Symposium, Washington, IEEE Catalog No. 81CH1656-8, pp. 1195-1201.

Ragan, R. M., and T. J. Jackson. 1980. Runoff Synthesis Using Landsat and the SCS Model. Journal of the Hydraulics Division, Proceedings, ASCE, 106(HY5)·667-678.

Rango, A. 1981. Applications, Systems Verification and Transfer Project. NASA Technical Paper 1822, Vol. I, Operational Applications of Satellite Snow-Cover Observations-Executive Summary, 81 pp.

Slack, R. B., and R. Welch. 1980. Soil Conservation Service Runoff Curve Number Estimates from Landsat Data. Water Resources Bulletin, 16(5):887-893.

Schmugge, T. J., T. J. Jackson, and H. L. McKim. 1980. Methods for Soil Moisture Determination. Water Resources Research, 16(6):961-979.

Ulaby, F. T., and W. H. Stiles. 1979. The Active and Passive Microwave Response to Snow Parameters, Part II: Water Equivalent of Dry Snow. Journal of Geophysical Research.

Ulaby, F. T., A. K. Fung, and W. H. Stiles. 1978. Backscatter and Emission of Snow: Literature Review and Recommendations for Future Investigations, R. S. L. Technical Report 369-1, University of Kansas Center for Research, Lawrence.

U.S. Army Corps of Engineers. 1979. Determination of Land Use from LANDSAT Imagery: Applications to Hydrologic Modeling. Research Note No. 7, Hydrologic Engineering Center, U.S. Army Corps of Engineers.

U.S. Army Corps of Engineers. 1976. Urban Storm Water Runoff "STORM." Computer Program 723-58-L2520, Hydrologic Engineering Center, Davis, California.

Wilkening, H. A. 1981. Sensitivity of Rainfall Excess to Antecedent Soil Moisture and Soil Hydraulic Properties. Thesis, M. S., Department of Civil Engineering, University of Maryland, College Park, 169 pp.

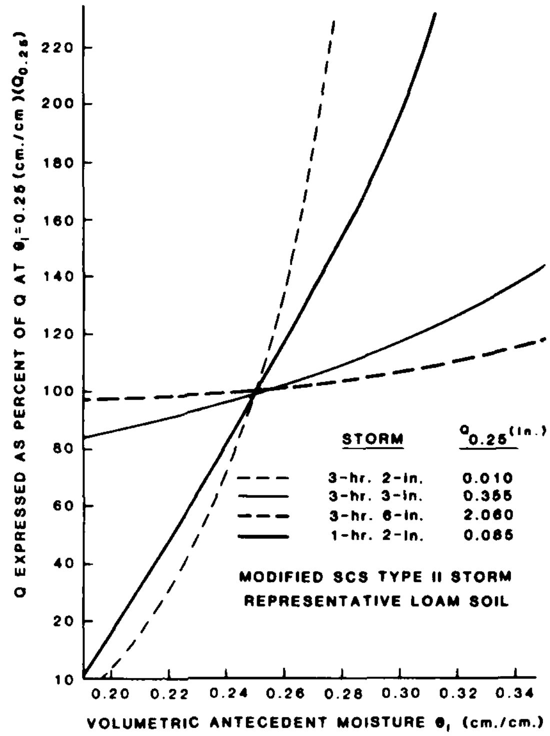

Figure 1. Sensitivity of antecedent soil moisture on runoff calculations using an infiltration equation. (From Wilkening, 1981)

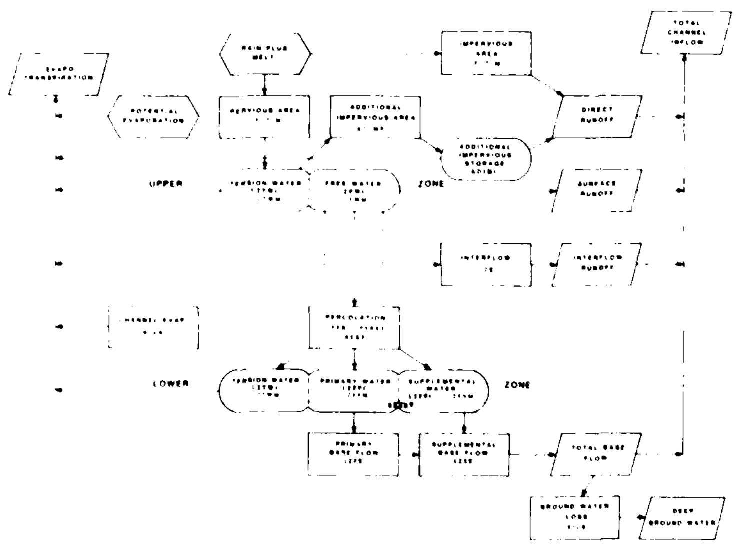

Figure 2. Schematic diagram of the National Weather Service River Forecast System (NWSRFS). (From Peck et al. 1981)

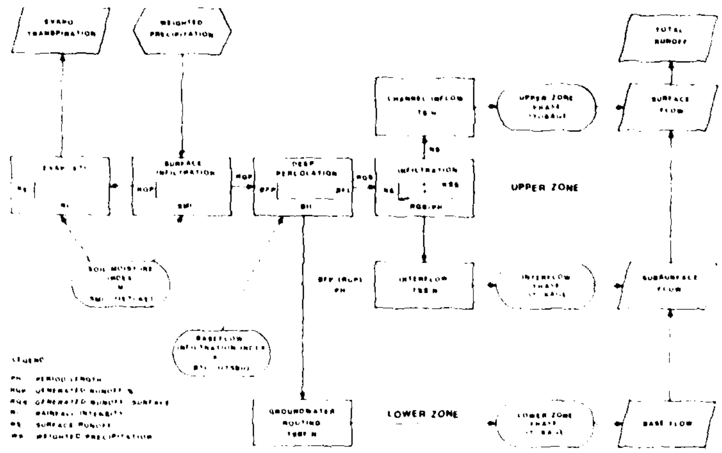

Figure 3. Schematic diagram of the Streamflow Synthesis and Reservoir Regulation (SSARR) Model. (From Peck et al. 1981)

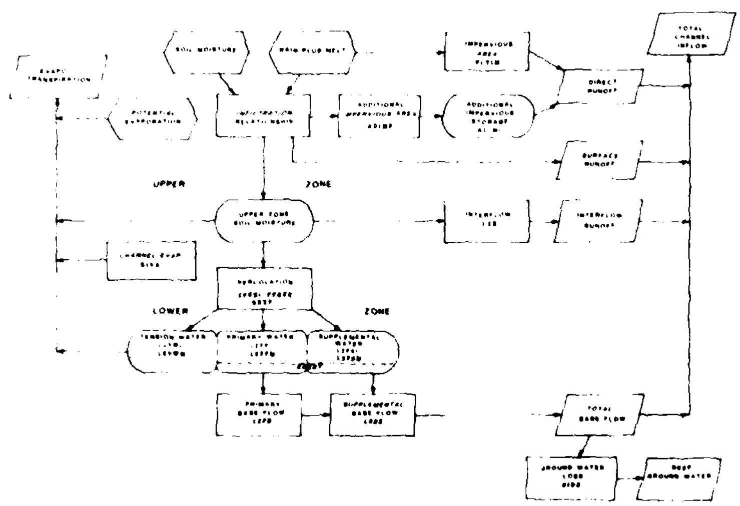

Figure 4. Schematic of NWSRFS Model illustrating how soil moisture input could be used to modify model without changing other parts of the system. Compare this to Figure 2.

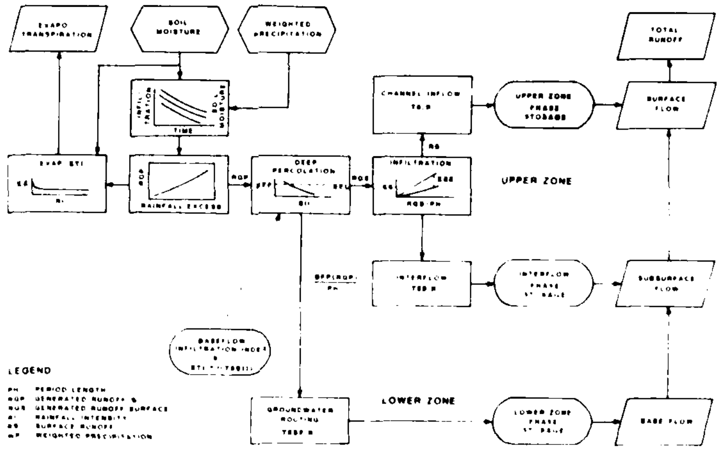

Figure 5. Schematic of SSARR model illustrating how soil moisture input could be used to modify the model without changing other parts of the system. Compare this to Figure 3.

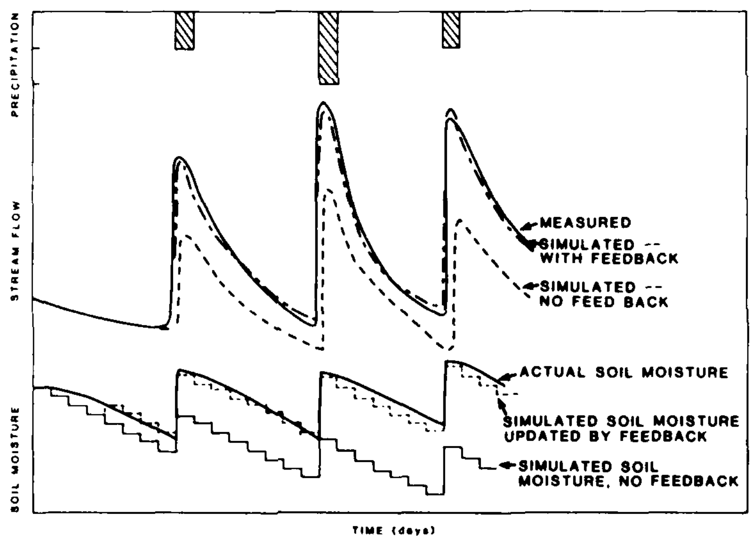

Figure 6. Hypothetical simulations showing how soil moisture used as feedback could be used to correct soil moisture simulations and improve the simulation.

DESERTIFICATION: CAUSES, EFFECTS AND TREND DETERMINATION

J. Eleonora Sabadell

McLean, Virginia

SUMMARY

The definition of desertification adopted by the U.S. National Assessment conducted by the Department of the Interior from 1979 to 1981 was the following:

"The sustained decline and/or destruction of the biological productivity of arid and semiarid lands caused by man-made stresses sometimes in conjunction with extreme events. Such stresses, if continued or unchecked, over the long term may lead to ecological degradation and ultimately to desert-like conditions."

Land uses per se are not causative of desertification, but maximized single or multiple use of the natural resources may produce it. Dry and irrigated farming, grazing, mining, industrialization, urbanization, recreation can initiate and sustain the desertification processes. These processes are manifested by the loss of vegetation and of plant variety; by brush invasion; by the loss of native or introduced animal population; by water and wind erosion, the loss of soil nutrients, the compaction and crusting, and salinization of soils, and the loss/reduction of permeability; and by the water resources salinity builtup and increased sediment load. The dynamics of the processes and the feed-back mechanisms will be illustrated by presenting some case-studies.

The changes in the quality of the resource base due to natural and human-induced causes can be observed, measured, and assessed. To this end baseline data is necessary by which the description and evaluation of the resources and the characteristics of the area in question are known before any major change occurs. This must be followed by monitoring the environmental alterations, if any, and the trends of increased or decreased biological productivity. Remote sensing and rapid data management make possible repetitive surveillance of drylands in a cost-effective manner. A comprehensive system of inventoring and monitoring will enhance development planning and will help in avoiding unanticipated or unwanted consequences of land uses and resources management.

AD P002004

RECENT ADVANCES AND FUTURE PROSPECTS FOR WEATHER, CLIMATE, AND OCEAN SPACE OBSERVATIONS

William R. Bandeen and David Atlas

Laboratory for Atmospheric Sciences
NASA/Goddard Space Flight Center
Greenbelt, Maryland, USA

ABSTRACT

Recently significant advances have been made in the application of space observations to weather, climate, and ocean phenomena. Initial results from the Global Weather Experiment indicate a positive satellite impact on synoptic-scale forecast skill. New atmospheric and surface parameters have been retrieved from the TIROS-N sounding system in addition to profiles of temperature and moisture. At the scales of regional and mesoscale weather, new developments have included stereo topography, using observations from two geostationary satellites, and high temporal resolution sounding and imaging of atmospheric temperature and moisture structure from recent Geostationary Operational Environmental Satellites (GOES). Some exciting General Circulation Model (GCM) experiments have indicated roles of sea surface temperature and soil moisture anomalies in controlling monthly-to seasonal climate. In oceanography, a method has been developed to estimate ocean-atmosphere heat fluxes from satellites, and marked progress has been made in developing techniques for the remote sensing of directional ocean wave spectra. Seasat radar altimeter data have revealed new information on the dynamic topography of the oceans, and Seasat scatterometer winds have been shown to enhance forecast skill. Future prospects include continued improvements in these areas of research and emphasis on the development of active optical (lidar) and microwave (radar) systems for the remote sensing of the atmosphere and oceans.

1. INTRODUCTION

This paper presents some highlights of recent advances in the realms of global weather, mesometeorology and severe storms, climate, and oceanography with the aid of space observations. While the examples are drawn largely from the work of the Goddard Laboratory for Atmospheric Sciences, they are representative of progress being made on the national and international scenes.

2. GLOBAL WEATHER

The Global Weather Experiment

Recent Global Weather research has focussed on the extent to which the

global observing system of the GWE[2] has improved the inference of the horizontal and vertical structure of the mass and motion fields in the tropical and extratropical data-sparse regions. Related to this question is whether more accurate atmospheric states in these regions can result in improved medium-range weather forecasts and thereby extend the limits of useful predictability, a major objective of GARP. The Global Observing System during GARP is depicted in Fig. 1. In addition to conventional observations, this system provided more than 7000 satellite temperature soundings and 6000 cloud-tracked winds daily.

A series of data assimilation experiments was performed with the GLAS analysis/forecast system (Halem et al., 1982) to assess the influence of the FGGE satellite observing system during SOP-1. Three different configurations of the FGGE observing system were analyzed: (a) the full FGGE system, (b) a non-satellite observing system that utilized only the conventional surface data, rawinsondes, pilot balloons, and aircraft, and (c) a surface, aircraft, and satellite-only upper-air system without rawinsondes and pilot balloons. The acronyms for these configurations are FGGE, NOSAT, and NORAOB, respectively.

A series of five-day forecasts was made from initial conditions taken every fourth day from 9 January through 2 March 1979 from each of the three analysis cycles. Figs. 2a and 2b show the S_1 skill score impact results of three-day forecasts evaluated relative to the NMC analysis over North America, Europe, and Australia for the sea level pressure and 500 mb geopotential height fields, respectively. The improvement over Australia with the FGGE data is more consistent and significant in the sea level pressure and 500 mb geopotential height than over the Northern Hemisphere. A smaller positive impact occurs over Europe. The sea level pressure impact over North America is negligible, while at 500 mb the impact is less consistent than over Europe but still positive. The dotted curve in Fig. 2 represents the S_1 skill score for the forecasts from the NORAOB experiment. Over Australia, the accuracy of the three-day NORAOB forecast is better than that of the NOSAT system at both sea level and 500 mb. Over Europe and North America, the NORAOB forecasts are, in general, poorer by about 24 hours.

Figs. 3a and 3b present the ensemble forecast skill as a function of forecast day. The forecasts from the FGGE and NOSAT systems are verified separately over North America and Europe. The forecasts are considered to be different if the S_1 scores differ by more than 2 points, and only those cases for which at least one of the two forecasts retains useful skill (defined as $S_1 < 80$ for sea level pressure and <60 for 500 mb geopotential height) are counted. Forecasts having the same skill indicate no influence of the satellite data. The results show that the dependence of the forecast skill on satellite data increases with the length of the forecast during the first four or five days. After one day, most of the FGGE and NOSAT forecasts have the same skill, whereas beyond three days there is a large number of forecasts whose skill has been increased by the use of satellite data. Only 5 of the 14 forecasts still show significant skill at the end of five days over North America. Of these, the most skillful are from initial conditions provided by the FGGE analysis on January 29 and February 10, 1979. For this reason, and in view of the significant errors that the coarse 4° by 5° resolution can introduce after five days, it was decided to perform a 10-day integration with the 2.5° latitude by 3° longitude GLAS model. Both of these forecasts show remarkable skill over North America during the first eight days of the forecast. Figs. 4a and 4b illustrate the eight-day sea level pressure forecast from 0000 GMT 29 January for the western half of the northern hemisphere and the verifying FGGE sea level pressure analysis for 0000 GMT 6

---

[2]A list of acronyms is given at the end of the paper.

February, respectively. The position and intensity of most of the weather features have been accurately forecast.

Retrieval of Various Parameters from the TIROS-N Sounder

GLAS has developed a method of analysis of HIRS2/MSU sounding data on TIROS-N to produce not only atmospheric temperature profiles, but also sea or land surface temperature, fractional cloud cover, cloud top temperature, and surface emissivity at 51.3 GHz from which estimates of sea-ice and snow cover over land can be obtained (Susskind and Rosenfield, 1980; Susskind et al., 1982). The method involves direct physical inversion of the multispectral radiative transfer equations represented by the HIRS2/MSU observations. No regression is used in the analysis. Global retrievals have been run for the period January 5-February 24, 1979 at a resolution of 125 KM.

Fig. 5 shows monthly mean sea surface temperatures derived from an analysis of the HIRS2/MSU system. The main information comes from channels 18 and 19 on HIRS2 at 4.0 and 3.7μm, respectively. Although at least partially clear fields of view are needed, completely clear spots are not necessary and clouds are accounted for as part of the processing system. Retrievals are done during both day and night; otherwise the retrievals shown have been averaged in a $4^\circ \times 5^\circ$ grid but have not been smoothed.

Fig. 6 shows the sea-surface temperature anomaly field as determined by the HIRS2/MSU retrievals. The anomalies are between 0 and 2° and show a coherent pattern. Also shown in the figure is the anomaly field obtained from ships and buoy measurements during the same period. The main features of both fields show excellent agreement, especially in the Northern Hemisphere where the ship and buoy measurements are well distributed. The RMS difference of the two fields is 0.4°C in the North Atlantic Ocean and 0.5° in the North Pacific.

Fig. 7 shows sea ice extent as determined from the GLAS retrieval for January 1979 and from SMMR on the Nimbus-7 satellite. The sea ice line in the GLAS retrievals is taken as the 0.7 emissivity contour. Surface emissivity is obtained primarily from the 50.3 GHz channel on MSU. The surface emissivity is also indicative of snow cover over land and is a measure of boundary layer wind speed over the ocean.

3. MESOMETEOROLOGY AND SEVERE STORMS

Satellite Stereo Topography

A dramatic recent development in this realm is rapid repeat cycle stereography from two geosynchronous satellites developed by Hasler (1981) and his colleagues. Fig. 8 shows a stereographically produced contour map of a line of tornado producing storms on 3 May 1979. The tallest turret (16.8 km) corresponds to the Mulhall, Oklahoma, tornado. Associated studies show that the severity of a storm and its probability of producing a tornado are related to its rate of rise and its depth of penetration into the stratosphere (Adler and Fenn, 1979). Hasler (1981) has also stereo mapped the topography of hurricanes with dramatic results. Satellite stereography has a variety of important other applications throughout weather and climate, most notably for correctly assigning th true heights of cloud track winds for use in both GCM and mesoscale models, and for developing a 3-dimensional global cloud climatology, since the effects which clouds have on the radiation balance is sensitive to their height.

VISSR Atmospheric Sounder on GOES

Another exciting new development in this area permits the sounding and imaging of atmospheric temperature and moisture structure from the VAS

instruments on GOES-4 and GOES-5 launched in late 1980 and early 1981. These instruments greatly expand the capabilities of previous *geosynchronous* satellites. As with the former satellites, visible pictures of cloud cover over a constant geographical area are taken during daylight hours over the west and east coasts of North and South America. However, unlike sensors on previous geosynchronous satellites, the VAS includes eleven new infrared detectors (totalling twelve including the original window channel) designed specifically to determine the temperature and moisture content of the atmosphere. The modifications to the earlier GOES, which carried only the VISSR, are shown in Fig. 9.

The use of the VAS data has been described by Petersen et al. (1982), Uccellini et al. (1982), Chesters et al. (1982), and Smith, et al. (1981). These observations can be used by meteorologists in many ways. For example, images of water vapor content observed by one of the new detectors can provide a view of atmospheric motion in cloud-free regions. In addition, the location of the jet stream can be related to regions of low and mid-level moisture content, and severe thunderstorms have been observed to form along boundaries of moist and dry air in the middle atmosphere. A combination of two low-level sensing channels can also be used to obtain pictoral representations of the amount of water vapor present near the earth's surface, another factor important to the development of severe thunderstorms.

A depiction of low level moisture (e.g., from the surface to approximately 850 mb) inferred from an analysis of multispectral radiation in the 11-13 μm window is shown in Fig. 10. The method of analysis described by Chesters et al. (1982) utilizes two "split-window" channels, with one centered at 11.2 μm (a clean window) and the other centered at 12.7 μm (a "dirty" window, with moderate absorption due to water vapor). Solid black areas are regions of obvious cloud cover which have been eliminated. Dry areas are shaded dark and moist areas are bright. The histogram (white) at the bottom indicates the frequency of occurrence of precipitable water amounts in the total measurement population. Fig. 11 is an image of radiation received by the 6.8 μm channel and, because of the strong water vapor absorption at this wavelength, depicts mid-level moisture (e.g., approximately 300 to 600 mb) with dark areas indicating dryness and bright areas indicating moisture. White areas are cloud covered. A band of very dry air, poleward of the jet stream, is observed north of the Great Lakes.

The ability to monitor situations where narrow bands of dry air are detected above regions of low-level moisture, thus indicating the potential for convective instability, should provide an important tool to operational forecasters. Such a possibility is illustrated in Figs. 10 and 11 where low level moisture in eastern Iowa (Fig. 10, bright) coupled with mid-level dryness (Fig. 11, dark) preceded severe thunderstorms with 16.8 km tops which developed in less than two hours in an area devoid of any particularly strong dynamical forcing.

The soundings derived from the combined measurements of temperature and moisture throughout the atmosphere obtained from all 12 infrared detectors,in addition to the winds and cloud heights noted earlier, have the potential to revolutionize a meteorologist's ability to forecast severe thunderstorms and tornadoes. Although most severe weather events occur between 2:00 p.m. and 5:00 p.m. local time, the previous data base has been limited to conventional balloon observations of temperature, moisture, and winds taken at only about 70 locations over the US and only at 7:00 a.m. and 7:00 p.m. EST. Measurements from VAS taken in the time/space gaps between the conventional soundings hold great promise for more timely and accurate storm warnings and predictions. In particular, the incorporation of such high temporal and spatial resolution temperature, moisture, and wind soundings into numerical models should advance significantly our knowledge of mesoscale phenomena.

Research is now under way to develop variational analysis techniques to analyze VAS data sets and insert the data into mesoscale models.

4. CLIMATE

The boundary forcings due to anomalies of sea surface temperature (SST), soil moisture, sea ice, and snow change slowly compared to the atmospheric anomalies, and, therefore, they can be potential predictors for monthly and seasonal mean climate. There are several observational and numerical studies which support this hypothesis. Changes in the boundary forcings produce changes in the location and intensity of diabatic heat sources which can produce changes in large scale atmospheric circulation (the Hadley, Walker, and monsoon circulations in the tropics, and quasi-stationary planetary waves in the middle latitudes). Here we describe briefly the results of two numerical experiments with the GLAS climate model to study the sensitivity of sea surface temperature and soil moisture.

Sea Surface Temperature Experiment

Moura and Shukla (1981) have conducted a numerical experiment with the GLAS climate model which shows that a possible mechanism for the occurrence of severe droughts over northeastern Brazil is the northward displacement of the ITCZ associated with anomalously warm SST's in the N. Atlantic and/or anomalously cold SST's in the S. Atlantic. Because of the persistence of such anomalies, the findings have predictive value. In the experiment the model was first integrated for 90 days with climatological SST's (control run), and then integrated again for 90 days after introducing the SST anomalies shown in Fig. 12. Fig. 13 shows 15-day running mean time series of daily rainfall averaged over the areas A and B of Fig. 12 for control and anomaly runs. The results of the anomaly run show that a drought has occurred in area B (including northeastern Brazil) whereas higher-than-average precipitation has occurred in area A.

Soil Moisture Experiment

Globally and annually averaged run-off (266 mm) from the continents is only about 35% of annual mean precipitation (764 mm) over the continents and, therefore, annual evaporation from the global land surfaces is about 60-70% of the rainfall over the global land surfaces. For certain regions and seasons, the mean evaporation from the land is greater than precipitation because water stored in the root zone is evaporated by radiation energy. This would suggest that the evaporation from the land must be one of the important components of the global hydrological cycle. The amount of soil moisture influences the hydrological cycle and atmospheric circulation in two ways. Firstly, it influences the rate of evaporation and therefore determines the available moisture for convection and precipitation. Secondly, it determines the partition of incoming net radiative energy into sensible heat and latent heat components. If the land surface is wet, most of the energy (net short wave and long wave radiation) is utilized for evaporating water, whereas if the land surface is dry, most of the energy goes into sensible heating of the atmosphere. This, in turn, can produce low pressure areas and large scale convergence. The effects of persistent anomalies of soil moisture will, therefore, also depend upon the geographical location with respect to oceans, the prevailing motion field, and the nature of the boundary layer and convection in the area.

Shukla and Mintz (1982) have conducted two numerical experiments with the GLAS climate model: (A) no evaporation from the land surfaces (dry-soil case), and (B) potential evapotranspiration from the land surfaces (wet-soil case). The ocean SST is identical in both numerical experiments. Fig. 14 ((a), (b), and (c)) shows the difference map (A-B) for ground temperature, sea level pressure, and rainfall, respectively. In the dry-soil case, the land

surface is hotter by 20-30^{o}, the sea level pressure over land is lower by 15-20 mb, and the oceanic high pressure centers are stronger. The resulting flow field is very different, and the rainfall over most of the land surfaces reduces by 40-50% with a remarkable exception of three monsoonal areas. For example, over the Indian monsoon regions, the absence of evaporation from the land is more than compensated by the enhanced moisture flux convergence from the surrounding oceans, which is due to a more intense monsoon low over India.

This idealized experiment suggests that persistent anomalies of soil moisture can be one of the important determinants of monthly and seasonal atmospheric anomalies, especially in summer months. More observational and numerical studies are needed to understand the role of these physical processes quantitatively. These results also suggest that the effects of large scale modifications of land surfaces (viz. deforestation, aforestation, large scale irrigation, etc.) strongly depend upon the geographical location of the area and the prevailing dynamical circulation of the atmosphere.

The above experiments also provide insight into the nature and accuracy of observations required from space. The need for measurements of SST and soil moisture is evident.

5. OCEANOGRAPHY

Estimating Ocean-Atmosphere Heat Fluxes During Cold Outbreaks

A method has been developed to estimate ocean-atmosphere heat fluxes during cold outbreaks over the eastern boundary currents (Chou and Atlas, 1981; Atlas and Chou, 1982). Mean sensible heating of the cloud-free region is related to the difference between surface land air and sea temperatures and the distance from shore to the edge of the cloud streets. Mean latent heating is related to the difference between surface land air and sea specific humidities and the distance from shore to the edge of the cloud streets. Nomograms of mean column heating due to these two fluxes have been developed.

Radar Ocean Wave Directional Spectrometer

Marked progress has been made in developing techniques for the remote sensing of directional ocean wave spectra. A microwave radar technique for measuring the vector wavenumber spectrum of the ocean surface has been validated at 10 km aircraft altitudes where excellent agreement between buoy and radar-inferred absolute wave height spectra was found (Jackson, 1981; Jackson et al., 1981). The technique is suitable for satellite application, and we are pursuing an orbital test of such a radar on a future space shuttle mission. One possible satellite configuration is shown in Fig. 15. An example of a directional modulation spectrum $P_m(K,\phi)$ obtained from an aircraft experiment is shown in Fig. 16 where K is wavenumber and ϕ is azimuth. The corresponding nondirectional spectrum (obtained by integrating $P_m(K,\phi)$ over all azimuths) appears in Fig. 17 showing excellent agreement with a colocated buoy.

Seasat Radar Altimeter

Much progress has also been made in the analysis of Seasat radar altimeter data to show the relationship of the dynamic height of the ocean (of about 10 cm accuracy) to the speed of the Gulf Stream and in detecting the 40-to-60 cm deep, 200-to-300 km wide cold core eddies (Cheney and Marsh, 1981; Cheney et al., 1982). Fig. 18 shows all available oceanographic observations obtained during a 2-week period. Heavy dashed and solid lines represent frontal boundaries of the Gulf Stream observed in NOAA-5 infrared imagery during the first and second weeks, respectively. Dots are XBT's converted to dynamic height (0/3000 dbar) and contoured at 10-cm intervals. Concurrent Seasat tracks from which altimeter data are available are superimposed. Fig.

19 shows altimeter residuals for eight collinear passes obtained over a 3-week period. Cold ring 4 was centered 20 km west of the ground track on September 17 but by October 8 had moved further westward from the track (see Fig. 18). Hence, its sea surface height shrinks correspondingly.

A global mesoscale sea height variability map was produced from altimeter measurements made during the last 25 days of the Seasat mission, 15 September-10 October 1978 (Fig. 20). This map was constructed from 125,000 globally distributed variability values determined every 7 km along the ground track. Maximum values of 20-40 cm RMS variability are generated by meanders and eddies of five major current systems: the Gulf Stream, Kuroshio, Agulhas, Antarctic Circumpolar, and Falkland/Brazil confluence. This map reveals a strikingly realistic view of the mesoscale energetics of the oceans.

Seasat Scatterometer

Another instrument flown on Seasat was a scatterometer for determining surface wind speeds. Seasat scatterometer winds have been found to be accurate to ±2 $msec^{-1}$ (Lame and Born, 1982). An objective method which exploits atmospheric GCM's has been developed to eliminate directional ambiguities. GCM prediction simulations show the great value of scatterometer winds in enhancing forecast skill. Ocean model studies show that both the surface wind stress and the ocean topography are needed to define the ocean circulation adequately (Cane et al., 1981).

6. FUTURE PROSPECTS

Future prospects include continued improvements in the aforementioned areas of research and emphasis on the development of active optical (lidar) and microwave (radar) systems for the remote sensing of the atmosphere and the oceans. Current studies indicate that lidar techniques are feasible for the remote sensing from space, with significant improvements in accuracies, of such key meteorological parameters as profiles of temperature, pressure, moisture, and winds, and the height of the planetary boundary layer. A dual frequency Differential Absorption Lidar (DIAL) is being developed for integrated path and differential ranging measurements (Korb et al., 1979; Atlas and Korb, 1981). One frequency is chosen on a portion of the resonant absorption feature that is to be measured (i.e., on-line). A second nearby frequency, which suffers minimal resonant absorption but which has nearly identical attenuation due to various scattering and continuum absorption processes, is used as the reference. The ratio of the signal returns from a given range at the on-line and off-line frequencies may be formulated to yield the integrated optical depth. The DIAL approach may be used for pressure, temperature, and moisture profiling. From a spacecraft at 200 km altitude, pressure profiling at 1 km vertical resolution is expected to be accurate to about ±0.3% from the surface to 6 km with a horizontal resolution of 250 km. Expected accuracies for temperature sensing are approximately ±1°C RMS at 2 km vertical resolution through the troposphere with the same horizontal resolution. Water vapor profiling is expected to provide measurements with better than 20% accuracy through the troposphere. Improved accuracies in these measurements would permit a more accurate specification of the initial state parameters for a numerical model, resulting in more accurate and extended weather predictions.

Similarly, radar systems, in conjunction with passive microwave, infrared, and visible radiometers, appear to hold the key to improvements in the remote sensing of such key parameters as precipitation, soil moisture, and surface winds over the ocean, in addition to the directional wave spectra previously mentioned.

Initial results from the VAS instruments on the spin-stabilized GOES, exciting as they are, point up the substantial improvements that could be

provided by a 3-axis-stabilized platform in a geosynchronous orbit carrying a multispectral visible/infrared imager, a separate infrared sounder, and a microwave sounder/imager. A radiometer with a 1-meter diameter optic appears feasible and would provide a resolution of 1 km at 11 μm, a dramatic improvement over the current 7 km resolution of the GOES imager. An interferometric infrared sounder is being studied for a 3-axis-stabilized geosynchronous satellite. The instrument would be capable of measuring vertical temperature and moisture profiles with increased accuracies and spatial and temporal resolutions required for substantial improvements in mesoscale applications to severe weather problems. A microwave sounder employing a real antenna aperture of 4 meters has been studied for a geosynchronous platform. Operating in the oxygen absorption band at 118 GHz, this instrument could sound at a resolution of 30 km in cloudy areas where infrared techniques are ineffective. An advanced concept currently under study for microwave sounding and imaging from a geosynchronous platform would employ an aperture synthesis approach. Initial results indicate that this approach is promising.

The mass of data continuously transmitted by satellites has often overwhelmed the capability of ground processing facilities to keep up with the flow. With modern advances in microprocessor technology, the possibilities of extensive on-board data processing now are becoming very attractive. Algorithms for extracting desired parameters could be invoked on the satellite, thus speeding up the data handling process and reducing the flood of data currently reaching the ground. An interactive mode permitting reprogramming of the satellite from the ground would provide the necessary flexibility for optimized data handling.

Many important advances have been made in recent years in our ability to observe the atmosphere and oceans from space. The prospects for new advances in the future are challenging, but promising, and should lead to an improved understanding of our environment and an ability to predict changes, due to either natural or man-made causes. The prospects to monitor both the small and large-scale characteristics of the atmosphere and the oceans, to detect and warn of dangerous local and tropical storms and wave conditions and predict their occurrence in advance through the combination of models and satellite observations, to enhance the skill and range of global weather forecasts, and to provide the beginnings of useful climate predictions are all exciting and should contribute greatly to the safety and comfort in which man can live and cope with his natural surroundings.

7. REFERENCES

Adler, R. F. and D. D. Fenn, 1979: Thunderstorm intensity as determined from satellite data. J. Appl. Meteorol., 18, 502-517.

Atlas, David and C. Laurence Korb, 1981: Weather and climate needs for lidar observations from space and concepts for their realization. Bull. Am. Meteorol. Soc., 62, 1270-1285.

Atlas, David and Shu-Hsien Chou, 1982: Coast-ocean-atmosphere-ocean mesoscale interaction. NASA Technical Memorandum 83903, NASA/GSFC, Greenbelt, Md., 29 pp.

Cane, M. A., V. J. Cardone, M. Halem, and I. Halberstam, 1981: On the sensitivity of numerical weather prediction to remotely sensed marine surface wind and temperature data: A simulation study. J. Geophys. Res., 86, 8093-8106.

Cheney, Robert E. and James G. Marsh, 1981: Seasat altimeter observations of dynamic topography in the Gulf Stream region. J. Geophys. Res., 86, 473-483.

Cheney, Robert E., James G. Marsh, and Brian D. Beckley, 1982: Global mesoscale variability from repeat tracks of Seasat altimeter data. (Submitted to J. Geophys. Res.).

Chesters, D., L. W. Uccellini, and W. Robinson, 1982: Low-level moisture images from the VISSR Atmospheric Sounder (VAS) "split-window" channels at 11 and 12 microns. (Submitted to Bull. Am. Meteorol. Soc.).

Chou, Shu-Hsien and David Atlas, 1981: Estimating ocean-air heat fluxes during cold air outbreaks by satellite. NASA Technical Memorandum 83854, NASA/GSFC, Greenbelt, Md., 48 pp.

Halem, M., E. Kalnay, W. E. Baker, and R. Atlas, 1982: An assessment of the FGGE satellite observing system during SOP-1. Bull. Am. Meteorol. Soc., 63, (In press).

Hasler, A. F., 1981: Stereographic observations from geosynchronous satellites: An important new tool for the atmospheric sciences. Bull. Am. Meteorol. Soc., 62, 194-212.

Jackson, Frederick C., 1981: An analysis of short pulse and dual frequency radar techniques for measuring ocean wave spectra from satellites. Radio Science, 16, 1385-1400.

Jackson, F. C., W. T. Walton, and P. L. Baker, 1981: Directional spectra from air - and spaceborne radars. Proceedings of the American Society of Civil Engineers & Engineering Council on Oceanic Resources Symposium on Directional Wave Spectra Applications '81 (Berkely, CA). ASCE, New York, NY, pp [illegible].

Korb, C. L., J. E. Kalshoven, and C. Y. Weng, 1979: A lidar technique for the measurement of atmospheric pressure profiles. Trans. Am. Geophys. Union, 60, [illegible].

Lame, D. B. and G. H. Born, 1982: SEASAT measurement system evaluation: Achievements and limitations. J. Geophys. Res., 87, 3175-3178.

Moura, Antonio D. and Jagadish Shukla, 1981: On the dynamics of droughts in northeast Brazil: Observations, theory, and numerical experiments with a general circulation model. J. Atmos. Sci., 38, 2653-2675.

Petersen, Ralph A., Louis W. Uccellini, Dennis Chesters, Anthony Mostek, and Dennis Keyser, 1982: The use of VAS satellite data in weather analysis, prediction and diagnosis. Preprints Ninth conference on Weather Forecasting and Analysis (Seattle), AMS, Boston, (In press).

Shukla, J. and Y. Mintz, 1982: Influence of land-surface evapotranspiration on the earth's climate. Science, 215, 1498-1501.

Smith, W. L., V. E. Suomi, W. P. Menzel, H. M. Woolf, L. A. Sromovsky, H. E. Rivercomb, C. M. Hayden, D. N. Erickson, and F. R. Mosher, 1981: First sounding results from VAS-D. Bull. Am. Meteorol. Soc., 62, 232-236.

Susskind, Joel and Joan Rosenfield, 1980: The GLAS physical inversion method for analysis of TIROS-N data. NASA Conference Publication 2157, Proceedings of a satellite sounding workshop held July 15, 1980, NASA/GSFC, Greenbelt, Md., pp. 41-55.

Susskind, J., J. Rosenfield, and M. T. Chahine, 1982: Remote sensing of weather and climate parameters from the operational HIRS2/MSU sounders. (Submitted to Mo. Wea. Rev.).

Uccellini, Louis W., Dennis Chesters, and Anthony Mostek, 1982: The application of the VISSR Atmospheric Sounder (VAS) to the study of severe convective storms. Preprints, 12th Conference on Severe Local Storms (San Antonio), AMS, Boston, pp. 471-474.

LIST OF ACRONYMS

DIAL	Differential Absorption Lidar
FGGE	First GARP Global Experiment (1 December 1978-30 November 1979). Also known as the Global Weather Experiment (GWE).
GARP	Global Atmospheric Research Program
GCM	General Circulation Model
GLAS	Goddard Laboratory for Atmospheric Sciences
GOES	Geostationary Operational Environmental Satellite
GWE	Global Weather Experiment (1 December 1978-30 November 1979). Also known as the First GARP Global Experiment (FGGE).
HIRS2/MSU	High resolution Infrared Radiation Sounder - model 2/ Microwave Sounding Unit (flown on TIROS-N/NOAA operational satellites).
ITCZ	Intertropical Convergence Zone
NMC	National Meteorological Center, NOAA
NOAA	National Oceanic and Atmospheric Administration
SMMR	Scanning Multichannel Microwave Radiometer flown on the Nimbus-7 satellite.
SOP-1	First Special Observing Period of FGGE (5 January-5 March 1979)
SST	Sea Surface Temperature
TIROS-N	Television Infra-Red Observation Satellite - model N (prototype of NOAA operational satellites).
VAS	VISSR Atmospheric Sounder (flown on GOES-4 and GOES-5).
VISSR	Visible and Infrared Spin Scan Radiometer (flown on earlier GOES).
XBT	Expendable Bathythermograph

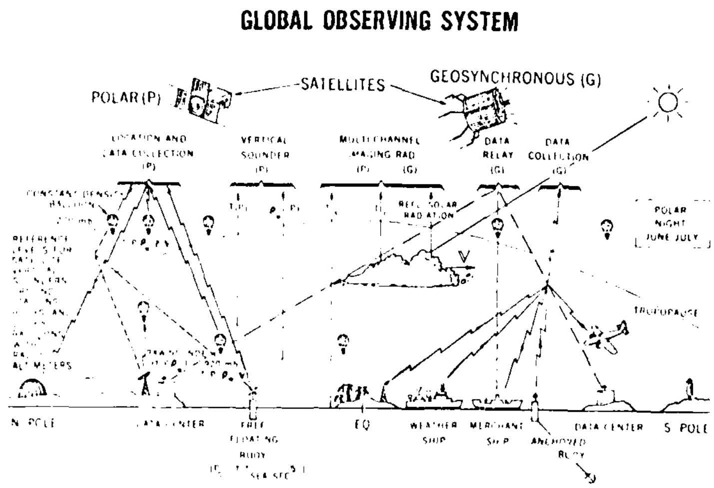

Fig. 1. Schematic of the Global Observing System. (P) refers to polar and (G) to geostationary satellites. Other symbols are: T - air temperature, P - pressure, ρ_w - water vapor, Z - geometric height, **V** - wind vector, T_s - surface temperature, T_c - cloud top temperature, and P_s - surface pressure. Constant density balloons are used only for special observations.

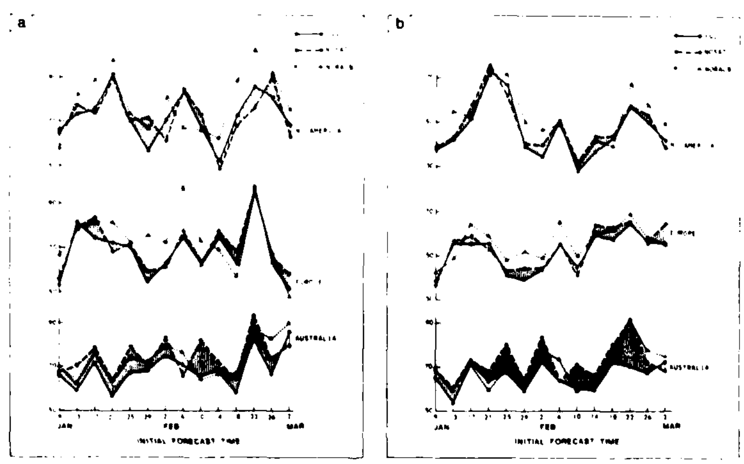

Fig. 2. S_1 skill scores of three-day forecasts evaluated relative to the NMC analysis for (a) sea level pressure and (b) 500 mb.

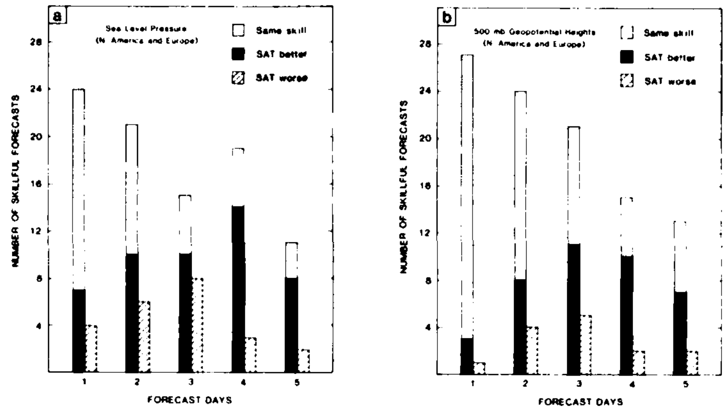

Fig. 3. Ensemble forecast skill as a function of forecast day for (a) sea level pressure and (b) 500 mb.

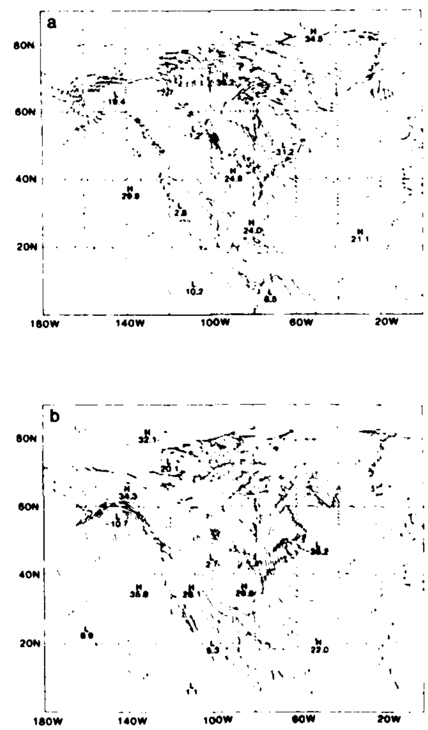

Fig. 4.(a) Eight-day sea level pressure forecast from 0000 GMT 29 January 1979;
(b) Verifying FGGE sea level analysis for 0000 GMT 6 February 1979 (millibars - 1000).

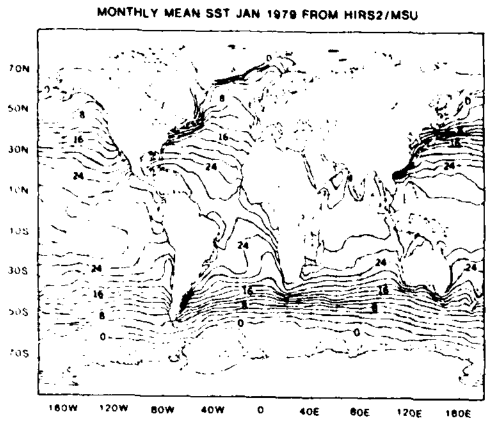

Fig. 5. Monthly mean SST (January 1979) from HIRS2/MSU(°C).

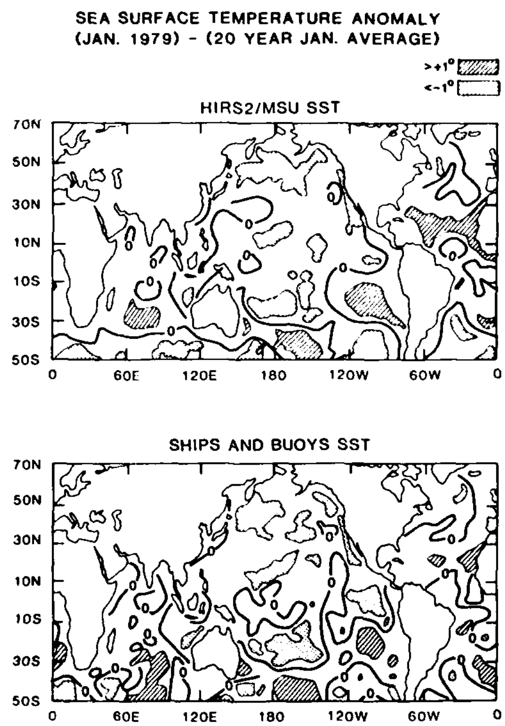

Fig. 6. SST anomaly (January 1979 vs. 20 year January average). Top, HIRS2/MSU; bottom, ships and buoys (°C).

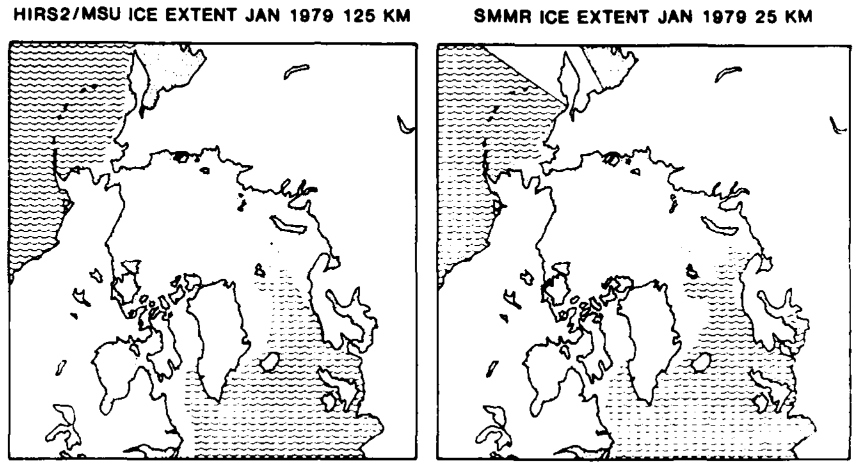

Fig. 7. HIRS2/MSU sea ice extent (left) vs. Nimbus-7 SMMR ice extent (right), January 1979 (ice is stippled).

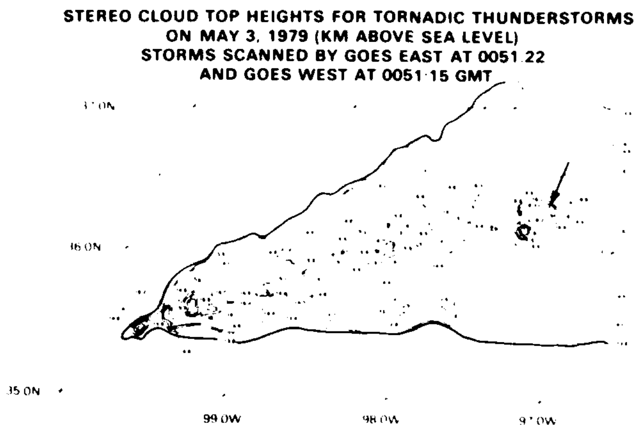

Fig. 8. Stereo cloud top height contour analysis (kilometers above sea level) made from a stereo image pair of an Oklahoma tornadic thunderstorm complex at 0051 GMT 3 May 1979. The tall tropopause-penetrating tops near 16.8 km (arrow) are coincident with a tornado that occurred in the town of Mulhall at nearly the same time.

VAS: VISSR ATMOSPHERIC SOUNDER

- MODIFICATION OF THE OPERATIONAL GOES

1) 11 ADDITIONAL CHANNELS

   7 CO_2 CHANNELS FOR TEMPERATURE
   3 H_2O CHANNELS FOR MOISTURE
   1 WINDOW CHANNEL

2) TWO MODES OF OPERATION IMAGERY, SOUNDING

3) INTERACTIVE SATELLITE CONTROL SELECT (WHERE, WHEN, HOW) FOR SOUNDING OR IMAGING MODES

Fig. 9. VAS modification of the operational GOES.

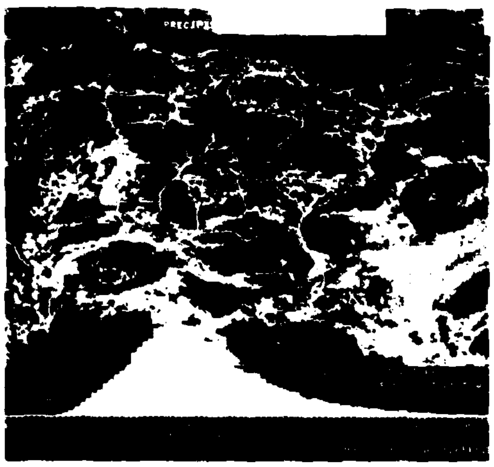

Fig. 10. GOES-5 VAS 11.2/12.7 μm "split window" low level moisture estimates, 2300 GMT, 23 July 1981.

Fig. 11. GOES-5 VAS 6.8 μm mid-level moisture, 2300 GMT, 13 July 1981.

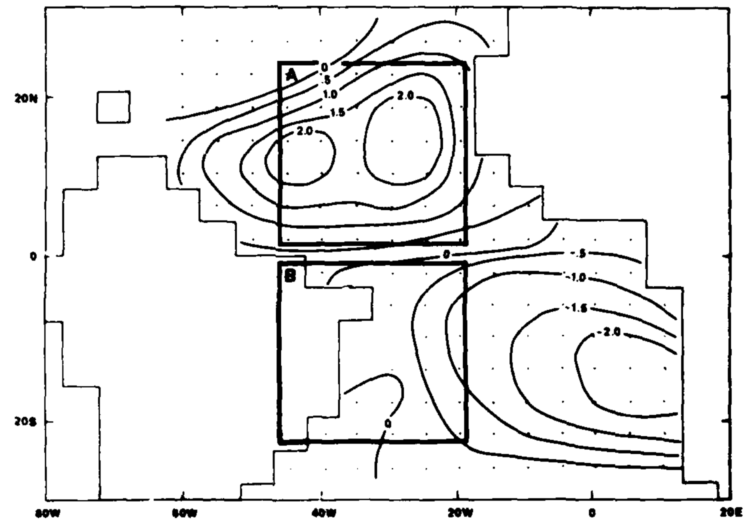

Fig. 12. SST anomaly (^{o}C) for the anomaly run. Thick lines enclose area A (upper) and area B (lower).

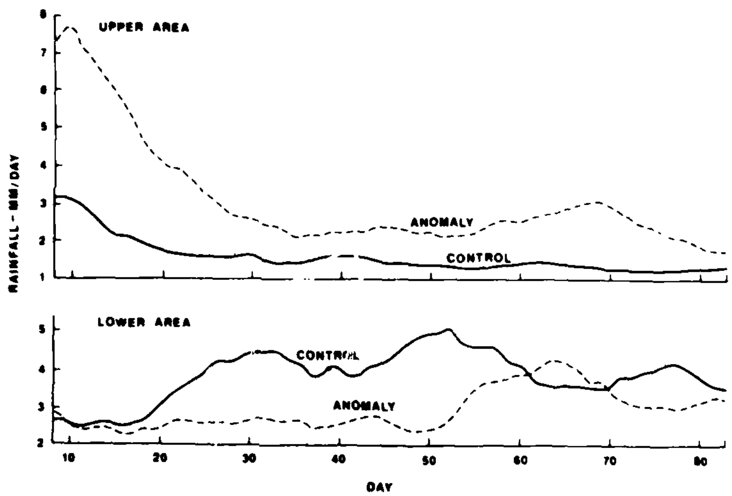

Fig. 13. 15-day running mean of daily rainfall (mm day^{-1}) for upper (A) and lower (B) areas in Fig. 12.

Fig. 14. (RIGHT). Differences (dry-soil case minus wet-soil case) between two model simulations for (a) ground temperature (^{o}C), (b) sea level pressure (mb), and (c) rainfall (mm/day).

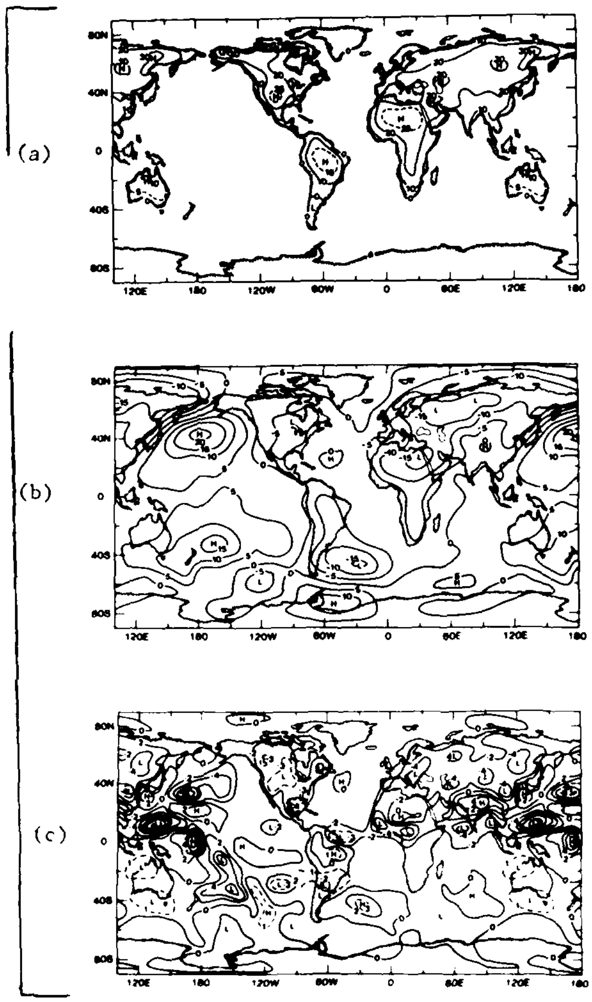

Fig. 15. (BELOW). Radar Ocean Wave Directional Spectrometer: (a) satellite measurement geometry; (b) scan pattern on ocean surface for 700 km altitude, $\theta = 10^{o}$, and 3 rpm scan rate.

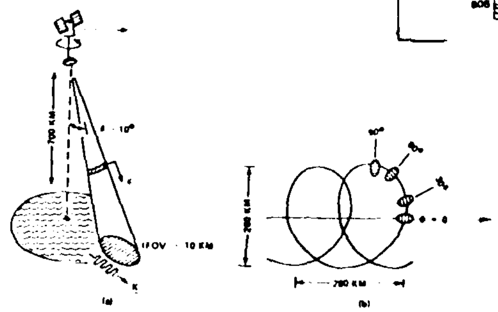

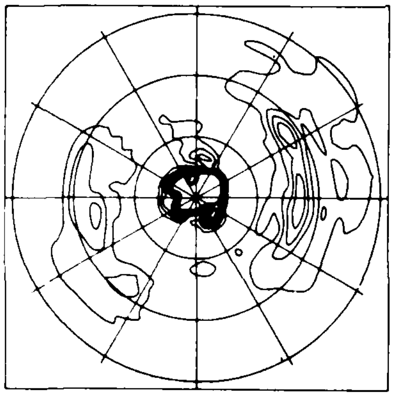

Fig. 16. Example of directional modulation spectrum $P_m(K,\phi)$. Wavenumber rings are spaced at 0.005 cpm (200, 100, 67 meters) and contours are equally spaced.

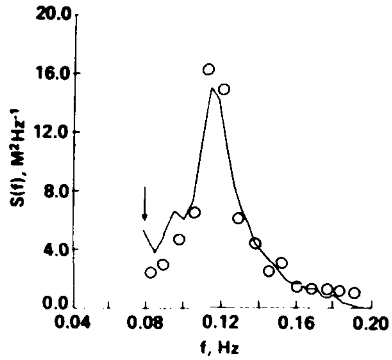

Fig. 17. Comparison of radar-inferred (solid line) and buoy (circles) high frequency spectra in absolute units. The arrow indicates the cut-off frequency in order to avoid effects of the antenna pattern at low frequencies. This nondirectional spectrum corresponds to the directional spectrum in Fig. 16.

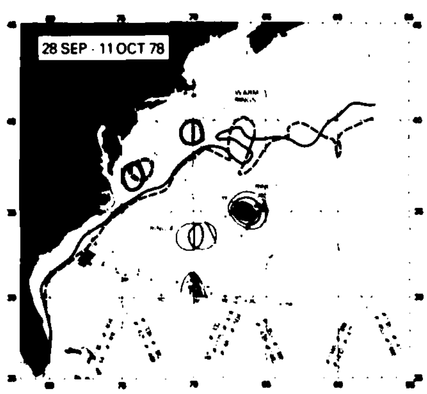

Fig. 18. Oceanographic observations obtained during 2-week period. Heavy dashed and solid lines represent frontal boundaries observed in NOAA-5 satellite infrared imagery during the first and second weeks, respectively. Dots are XBT's converted to dynamic height (0/3000 dbar) and contoured at 10-cm intervals. Concurrent Seasat tracks from which altimeter data are available are superimposed.

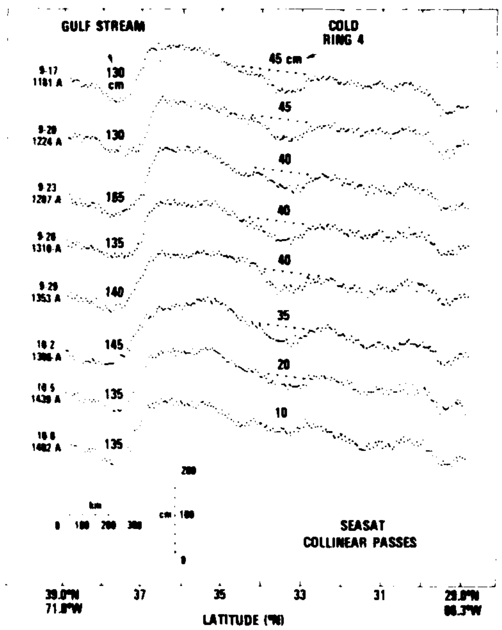

Fig. 19. Altimeter residuals for eight collinear passes obtained over a 3-week period. Cold ring 4 is moving out from beneath the Seasat track during this period (cf. Fig. 18).

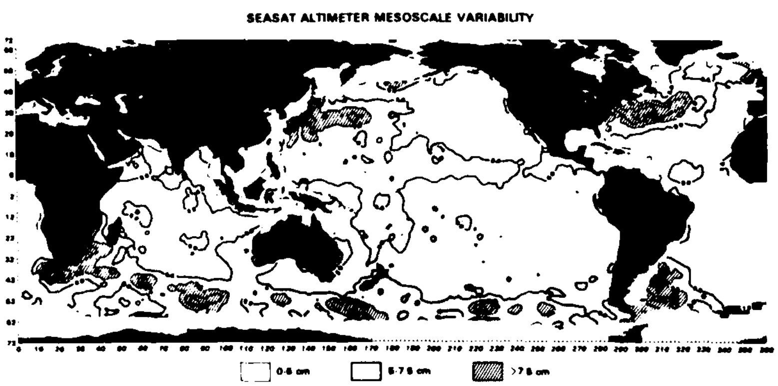

Fig. 20. Global mesoscale sea height variability measured by the Seasat altimeter, 15 September to 10 October 1978. Maxima due to five major current systems are seen: the Gulf Stream, Kuroshio, Agulhas, Antarctic Circumpolar, and Falkland/Brazil confluence.

CLIMATE APPLICATIONS OF SATELLITE REMOTE SENSING

Edward S. Epstein

Earth Sciences Laboratory, National Earth Satellite Service, NOAA
Washington, D.C. U.S.A.

ABSTRACT

Meteorological satellites provide a wide range of valuable climate information. Applications range from systematic monitoring of the earth's radiation budget -- measuring the energy differences that are controlling factors for the global climate systems -- to studying specifics of the local surface climatology. Examples are presented of the use of remotely-sensed data to provide important insights into the validation of climate theories and the factors that influence climage change. Other interpretations of the data allow us to deduce details of local surface climate differences and the seasonal progression of climatic elements, like precipitation and temperature, that are particularly to agriculture.

To some the term climatology implies some system of classification of the collective weather a location experiences over extended periods of time. To others, particularly research scientists, climate is a subject that involves the physical basis of the earth's average weather and models, whether relatively simple or highly complex, that can account for climate as we know it and as it might vary in the response to changes, say, in solar illumination, or volcanic dust, or atmospheric composition. Climate prediction means monthly outlooks to some, and to others it means concern about the next decade or the next millenium. Climate also conjures up the set of local climatic variables, like the accumulation of insolation or precipitation, or the chances of freezes, that are of such crucial importance to agriculture but have many other industrial and other economic applications.

We will not try here to settle on any single definition of climate, but will just note that they all refer to useful and significant aspects of collective weather events. As diverse as these different implications of the term climate may be, moreover, satellite remote sensing has been proven to have something to offer in all these contexts. The satellite enables us to measure and monitor some of the most salient parameters of the climate system, some that help us to understand how the system works, and some that help us to detect the effects of climate. There are many parameters we would like to be able to measure more accurately and more regularly than we are now able to do, parameters like insolation, soil moisture, precipitation, even cloudiness -- but considerable progress has been made. It is this progress -- what we are not able to do -- that I will try to describe. It is remarkable progress, I believe, when one realizes that none of the satellite instruments whose uses I will describe were designed to meet climate needs. Most were designed to provide meteorological data, and this is not quite the same thing.

The climate system is driven by radiation from the sun. The earth reradiates to space an equal amount of energy, to maintain its thermal balance over long periods of time, but the geographical and temporal distribution of the reradiated energy is distinctly different from that of the incoming solar energy. The satellite makes it possible to measure the various components of the earth's radiation budget. Some very critical assumptions are needed to infer the radiation budget from available operational measurements, but to all appearance, these assumptions have been wisely chosen.

One important aspect of the radiation budget is the albedo, or the reflectivity. The visible channels, first of the Scanning Radiometers (SR), and more recently of the AVHRR instruments on the NOAA polar orbiting satellites, allow us to measure, with reasonably good relative accuracy, the solar energy returned in a relatively narrow portion of the visible spectrum and in the specific direction of the satellite, over all parts of the earth at approximately the same local time. One would prefer to make reliable absolute measurements, over the entire spectrum, of the integrated energy scattered in all directions, and to be able to average these over all hours of the day. In fact the results which I am about to illustrate assume a constant solar constant (whose value and variations we are only now measuring with sufficient accuracy as the result of instruments on the NIMBUS-6 and -7 and SMM research satellites), ignore diurnal variations, make somewhat faulty assumptions concerning the angular distribution of scattered light, and use an approximate statistical relationship to estimate the broad-band flux from the narrow-band measurements. In all of these aspects of the measurements, carefully designed experiments on the NIMBUS-6 and NIMBUS-7 satellites and a forthcoming Earth Radiation Budget Experiment are providing the needed data to test and evaluate the various assumptions, and to make improvement to the operationally produced radiation budget estimates. Evidence to date is that the modifications to the data reduction procedures need only be relatively minor, and the extensive data that has been accumulated (Winston et al., 1979; Gruber and Winston, 1978) are a very valuable and useful set. I have mentioned these details to illustrate the problems that are associated with trying to obtain valid climatological data from measurements designed for other purposes.

Figure 1a is the multi-year mean albedo, taken from Winston et al. (1979), for the summer in the Northern Hemisphere and winter in the Southern Hemisphere. Relatively high albedos can be associated with areas of persistent cloudiness in some stormy middle latitude areas, in the vicinity of the intertropical convergence zone, or in areas of persistent low stratus clouds such as off the west coast of Peru), persistent ice and snow cover, or arid zones like the Sahara. The lowest albedos are associated with persistently clear oceanic regions, especially in the subtropics. In such regions a great deal of solar energy is absorbed by the oceans.

A second component of the radiation budget is the emitted terrestrial radiation, also measured by the SR and AVHRR instruments. Figure 1B shows the mean emitted radiation corresponding to Figure 1a. Some of the areas of high albedo, like the belts of tropical cloudiness, are areas of minimum emitted energy. On the other hand, the areas of low clouds off Peru and California have high albedos but also emit large amounts of energy.

Multiplying the albedo by the appropriate value for the solar intensity as a function of latitude and time of year (which also includes the effects of variations in the earth-sun distance) gives the absorbed solar radiation. Subtracting from this the emitted radiation gives the net radiation, as shown in Figure 1c for the mean Southern Hemisphere winter. The pattern is largely zonal, with deficits occurring in the high latitudes of the winter hemisphere and surpluses in the summer hemisphere except quite close to the pole. But there are significant departures from the symmetry, especially in the Northern Hemisphere, where radiation net deficits occur in the subtropics.

Charts similar to these a[illegible] prepared monthly and various summary statistics are regularly computed. There are of course [illegible]gnificant differences from year to year and from month to month, many of which are of particular interest to those who attempt to make predictions of the climate of subsequent months. Although the normal behavior of the radiation budget is dominated by geographically fixed and seasonally oriented patterns such as the ones we have pointed out, it may well be the departures from these normal patterns that warrant attention. As yet, however, with so few years of record, it is still difficult to distinguish the important anomaly from the normal signal.

The statistics of the globally averaged, seasonally varying cycles of the various components of the radiation budget are stable and, for the most part, unders[illegible]dable. Figure 2 shows the annual cycles of albedo, outgoing longwave, absorbed solar, and net radiation for the 45-month period of the atlas of Winston et al. The albedo has a distinct annual cycle, with a maximum in the Northern Hemisphere winter (Southern summer), reflecting primarily a pattern of the Northern Hemisphere. Because of its continentality, the Northern Hemisphere exhibits much more seasonality than the Southern Hemisphere, and the albedo [illegible]ation is

is related to the greater storminess, and clouds in winter, and the significant increase in ice and snow cover.

The annual variation in absorbed solar radiation shows less of a seasonal change than would be implied by the albedo cycle. This is because the earth is farthest from the sun in July and the slightly less intense (3.4%) solar radiation almost compensates for the smaller global albedo at this time of year.

The outgoing longwave radiation is out of phase with the absorbed solar radiation, and has a larger amplitude, reaching its maximum in the Northern Hemisphere summer. The greater cloudiness in the winter, and the large seasonal temperature range of the continental Northern Hemisphere combine to produce this effect. The net radiation responds largely to the pattern of the larger amplitude outgoing radiation cycle, implying that the earth as a whole gains energy during the Southern Hemisphere summer, when the earth is furthest from the sun, and loses it in the period surrounding perihelion.

Figure 2 shows the net radiation negative in all months. This, of course, cannot be the case in the long-term mean, and is probably not the case in any given year. The specific cause of this deficiency is not known, although it is not surprising that one occurs. There is no absolute calibration of the visible channels of the radiometer, and many assumptions are involved in the calculations. Likely, part of the discrepancy is due to the value assumed for the solar constant; part may be a bias in the determination of the longwave fluxes.

The data on the earth's radiation budget has several important applications. It is being used in diagnostic studies of the initiation and evolution of short-term anomalies. It is being used to evaluate critical parameters theoretically related to the sensitivity of the climate system to changes imposed from outside the system as by solar variations or changes in atmospheric composition. It is being used to validate climate models. I also can be used to represent the way in which the annual march of local climates may be viewed from space. I will illustrate, very briefly, each of these applications.

Figure 3 is an example of the importance of the radiation components in the diagnosis of climate. It illustrates how well the emitted longwave radiation over a small section of the tropical Pacific mimics one of the principle indices of the Southern Oscillation. The lower curve is a good index of the fluctuations of the South Pacific Convergence Zone and the Equatorial Pacific dry zone. When the index is high the dry zone extends well west of the dateline and the South Pacific Convergence is located to the south of New Guinea. When the index is low the dry zone has receded to the east and the South Pacific convergence is located northeast of its normal position. In recent years this very large scale atmospheric vascillation has been shown to have a large coherent pattern of behavior that relates to seasonal weather anomalies over large portions of the globe -- including for example the Indian monsoon and winter temperatures over North America. It also involves ocean currents and temperatures -- the El Nino -- off the northwest coast of South America with profound effects on fisheries' resources.

The response of the climate system to external influences (changes in solar output. CO_2, volcanoes) depends strongly, according to most models and theoretical studies, on the way in which cloudiness will change and alter either the albedo (generally a negative feedback), or the emitted radiation (generally a positive feedback, or both. Ohring et al. (1981) have tried to estimate these cloudiness effects by analyzing satellite radiation budget data. Figure 4 is the result of one of their calculations, showing much more of a negative feedback than many others have supposed. This result warrants further searching because it has profound implications for our ideas about climate sensitivity.

Ohring and his collaborators have also applied the radiation budget data to the validation of a model Ohring and Adler (1978) developed for describing the seasonal march of climate. In Figure 5 is a comparison of observed and model-generated longwave fluxes. In this case the biases are not very large, but the pattern of the differences helps us to judge the adequacy of the model and to interpret its output.

Figures 6, 7, and 8 from Ohring and Gruber (1982) are "space climatographs", satellite-derived analogs of more conventional presentations of the radiation budget at the ground for

specific locations. Each shows the seasonal progression of the several components that contribute to the radiation budget over a particular location. Shown in the figures are charts for two equatorial locations (one in South America and one in Southeast Asia) and one middle latitude Asiatic site. The insolation, which has two maxima during the year at low latitudes, is of course a major factor, but the influence of cloudiness, which has strong regional variations, is also very significant. Note that cloudiness does not bear a unique relationship to either albedo or the emitted radiation, but it strongly influences both. The nature and extent of the cloudiness, for a given latitude, are major determinants of the climate.

Most of our interest in climate arises from concern for conditions at or near the surface. For applications to agriculture and energy, for example, the solar radiation reaching the ground is of great interest. The satellite does not allow us to observe that directly -- but it does allow us to infer the insolation (Tarpley, 1981 (Figure 9) within limits that, for some applications, are quite satisfactory.

We also have not yet learned how to monitor precipitation from space, especially over land. But the clouds that produce the rain can be observed, and by observing their characteristics and following their development useful inferences can be made about precipitation. Figure 12 (Scofield, 1981) is a map of 24-hour precipitation estimates over a portion of Texas derived from satellite images. These methods are still crude and of limited accuracy, but are particularly valuable when results are aggregated over some periods of time.

Precipitation also falls in the form of snow. Snow is of interest on the one hand because of its importance to water resources through spring melt and runoff, and on the other hand because its high albedo is an important factor in the overall radiation balance. Weekly snow-cover data for the Northern Hemisphere have been analyzed and processed for the last 15 years, allowing one to discern both seasonal trends and large interannual variations. Figure 13 represents the snow cover over North America for a single month of last winter.

One of the basic meteorological applications of satellite data is the estimation of atmospheric temperatures. Satellite soundings are used routinely for meteorological forecasts around the world. For climate applications, however, it is the surface temperature that is generally of primary interest, and determination of accurate surface temperatures is complicated by atmospheric absorption and emission, by cloudiness, and by variations in the surface characteristics. Over oceans good surface temperatures are attainable (McClain, 1981), but success has been more limited over land. One very practical use of geostationary satellite imagery for surface temperature measurements has been the work of Ellen Chen (1982) in examining the development of freezing conditions over the Florida peninsula. Dr. Chen was not only able to trace the evolution of the freeze conditions on individual nights, but she was also able to identify small scale thermal patterns that persisted from night to night and to a significant extent from year to year. Differences were largely due to surface conditions (soil, soil drainage class, soil thermal properties, land use) and sometimes exceeded 3°C. Thus the geostationary satellite data can be used both to improve prediction of freezing conditions and to differentiate amoung otherwise very similar climate zones.

I will address one final agriclimatological use of the polar orbiting meteorological satellite. In this application the meteorological satellite plays the role of an earth resources satellite. The AVHRR on the NOAA satellites, like the LANDSAT. MSS, is a multspectral imager, although the resolution of the NOAA satellite cannot compare to that of LANDSAT. The two shortwave channels on the NOAA satellite both view the earth in reflected sunlight, but one, in the visible, sees the surface in wavelengths in which vegetation absorbs the solar radiation, while the other, in the near infrared, uses wavelengths in which vegetation does not strongly absorb. Thus a comparison of the apparent brightness of the surface in the two channels is an indicator of the extent of vegetative cover -- a vegetative index. Figures 14 and 15 illustrate such a sahelian vegetative index from AVHRR Channels 1 and 2 [(2) - (1)]/[(2) + (1)] over West Africa approximately one month apart -- Sept. 3 and Sept. 30, 1981. The area of blue hues show minimal vegetative growth ranging to bare ground. Green and reds are quite vigorous grass cover, shading into the lavender that indicates much more lush vegetation. Note the marked changes that accompanied seasonal rains, especially in Mauritania and Senegal, on either side of the Senegal River, within the first 200 km or so of the coast.

Operational satellites are thus providing now a wealth of climate information, with both research and practical implications, that we are only beginning to explore. Undoubtedly new instruments yet to be flown will provide data of more specific climatological value, but climatologists can be kept well occupied extracting and applying information from current operational satellites. The World Climate Program, with the leadership of the World Meteorological Organization, and also the various national and private efforts to extract climate information, are able to move ahead dramatically because of the meteorological satellites.

REFERENCES

Chen, E., 1982: The Development of Nocturnal GOES Infrared Data as a Source of Climate Information. National Climate Program Office, NOAA, Department of Commerce.

Gruber, A. and J.S. Winston, 1978P Earth-atmospheric radiative heating based on NOAA scanning radiometer measurement. Bull. Amer. Meteor. Soc., 59, 1570-1573.

McClain, E.P., 1981: Multiple Atmospheric-Window Techniques for Satellite-Derived Sea Surface Temperatures. Oceanography from Space, Plenum, 73-85.

Ohring, G. and S. Adler, 1978: Some experiments with a zonally averaged climate model. J. Atmos. Sci., 186-205.

Ohring, G., P.F. Clapp, T.R. Heddinghaus, and A.F. Krueger, 1981: The quasi-global distribution of the sensitivity of the Earth-atmosphere radiation budget to clouds. J. Atmos. Sci., 38, 2539-2541.

Ohring, G. and A. Gruber, 1982: Satellite radiation observations and climate theory. Advances in Geophysics (in press).

Scofield, R., 1981: Visible and Infrared Techniques for Flash Flood Hydrological and Agriculture Application. Published in Precipitation Measurements from Space, Workshop Report, David Atlas and Otto W. Thiele, editors, Oct. 1981. Held at Goddard Laboratory for Atmospheric Sciences, Goddard Space Flight Center, Greenbelt, Md., April 28-May 1, 1981, pages D145-D153.

Tarpley, J.D., 1981: Satellite-derived insolation for agriculture: An update of the NESS program. Published in Satellites and Forecasting of Solar Radiation, Proceedings of the First Workshop on Terrestrial Solar Resource Forecasting and on the use of Satellites for Terrestrial Solar Resource Assessment, February 2-5, 1981, Washington, D.C.

Winston, J., A. Gruber, T.I. Gray, Jr., M.S. Varnadore, C.L. Ernest, and L.P. Mannello, 1979: Earth-Atmosphere Radiation Budget Analyses derived from NOAA Satellite Data June 1974-February 1978. Vols. 1 and 2, U.S. Department of Commerce, Washington, D.C., 8 pp. + charts.

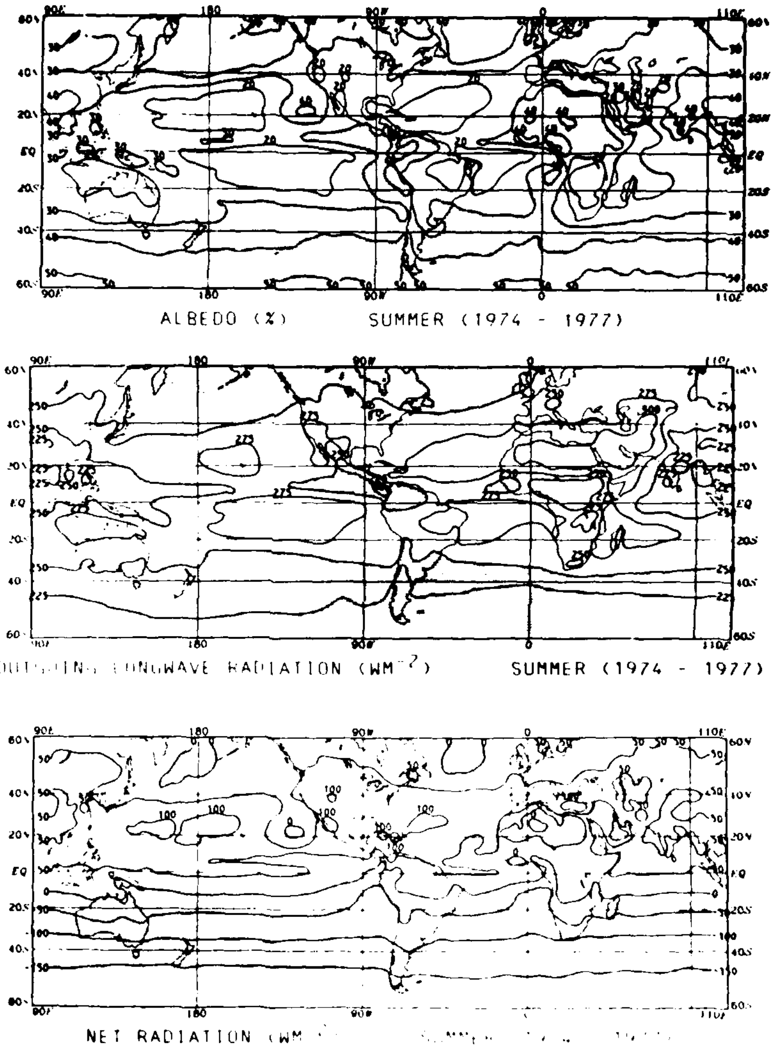

Figure 1

Average summer (NH) (June, July, and August) radiation budget maps. a) albedo (%), b) outgoing longwave radiation (W m^{-2}), and c) net radiation (W m^{-2}).

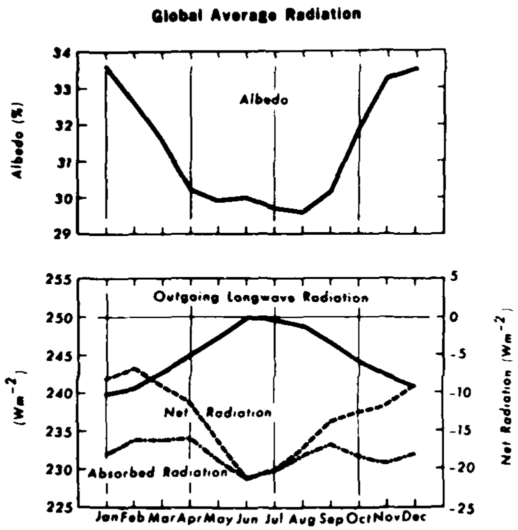

Figure 2

Annual cycle of albedo (%), outgoing longwave radiation (W m^{-2}) absorbed solar radiation (W m^{-2}) and the net radiation (W m^{-2}), based on 45-month SR data set.

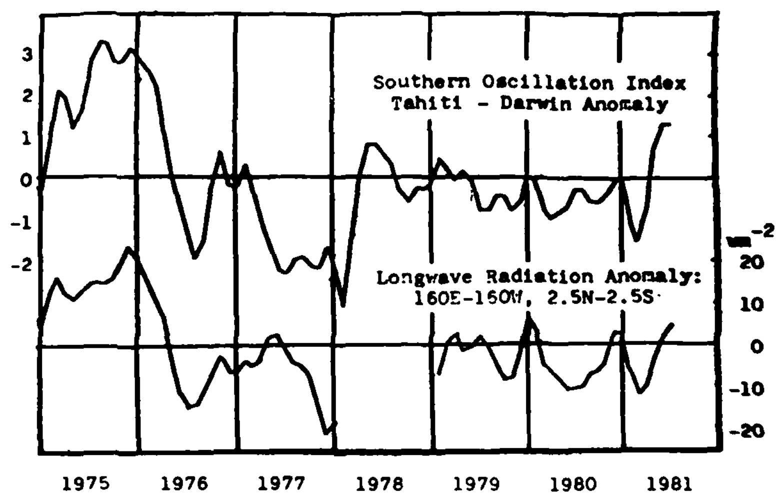

Figure 3

Upper time series: Southern Oscillation Index. Tahiti minus Darwin pressure difference anomaly (Standardized units).

Lower time series: Satellite-derived Longwave Index. This is the longwave cooling anomaly for an area 5°N and S of the equator and 20°E and W of the International dateline. (Courtesy of A.F. Krueger, Climate Analysis Center, National Weather Service, NOAA)

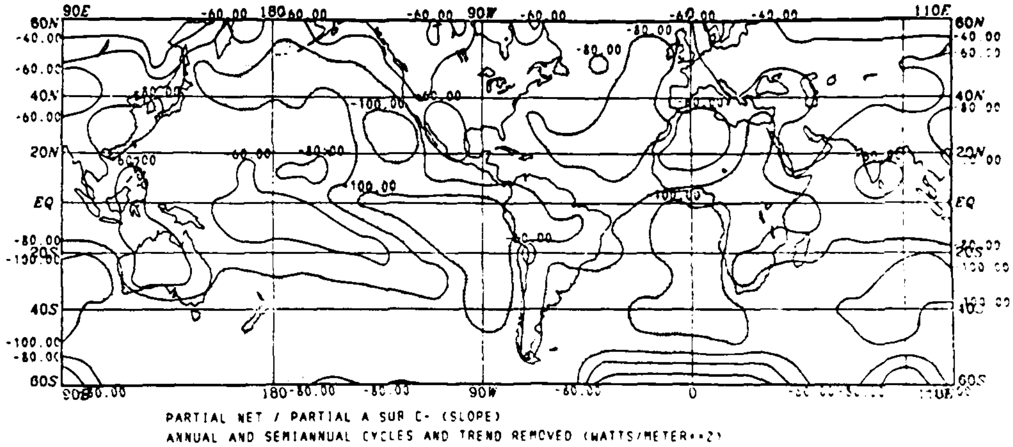

Figure 4

Quasi-global distributions of sensitivity of net radiation at top of Earth-atmosphere system to cloud amount, $\partial Net/\partial A_c$ (W m^{-2}). Values less than -80 W m^{-2} are stipled. (After Ohring et al., 1981).

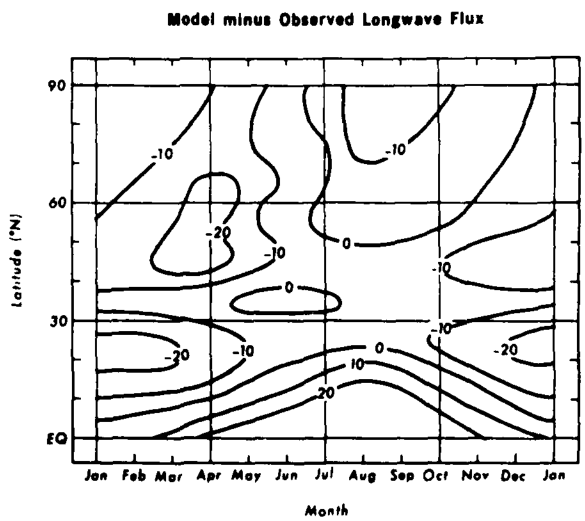

Figure 5

Latitude-month cross section of model minus observed (Gruber and Winston, 1978) longwave radiation fluxes (W m^{-2}). 10 W m^{-2} has been subtracted from the observed fluxes to correct for an apparent positive bias (see text).

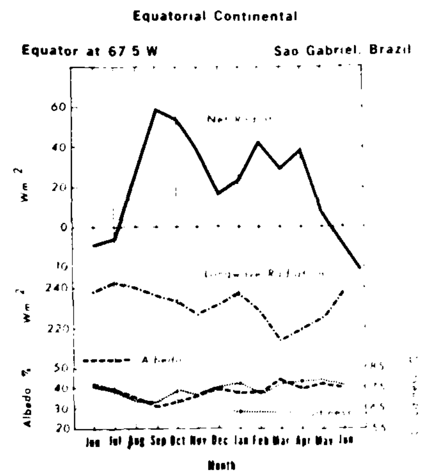

Figure 6

The annual variation of the Earth-atmosphere system radiation budget and cloudiness for an equatorial continental location (Equator, 67.5°W-Sao Gabriel, Brazil) (Ohring and Gruber, 1982).

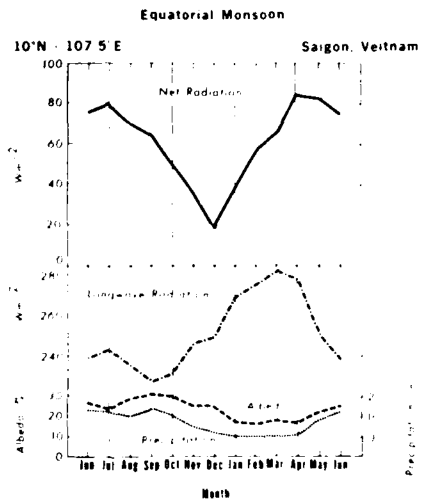

Figure 7

The annual variation of the Earth-atmosphere system radiation budget and precipitation for an equatorial monsoon location (10°N, 107 5°E-Saigon, Vietnam) (Ohring and Gr ber, 1982).

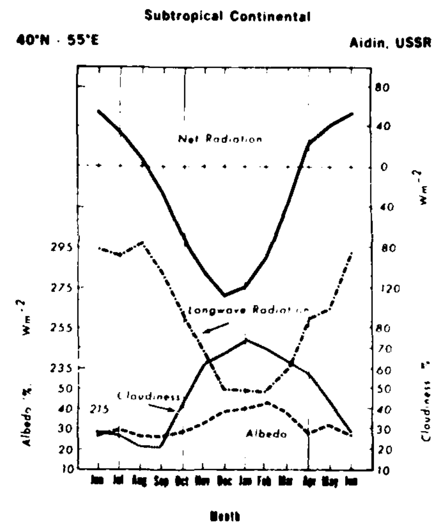

Figure 8

The annual variation of the Earth-atmosphere system radiation budget and cloudiness for a middle latitude continental location (40°N, 55°E-Aidin, USSR) (Ohring and Gruber, 1982).

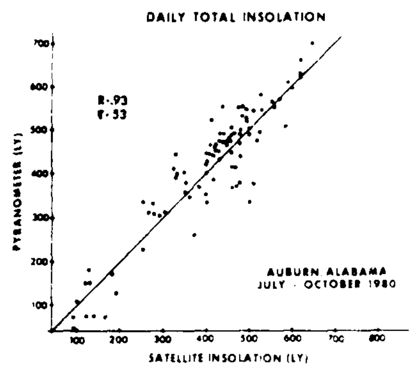

Figure 9

Comparisons of satellite-derived insolation estimates with pyranometer observations at Auburn, Alabama (32.6°N, 85.5°W). Satellite estimates have been interpolated between nearest grid points. (After Tarpley, 1981)

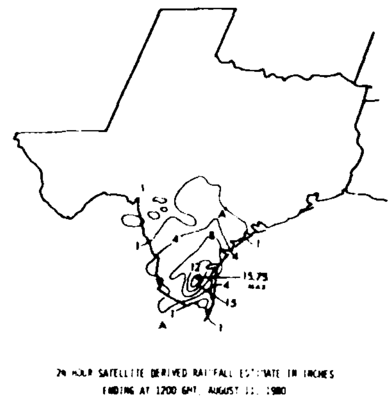

Figure 10

Twenty-four hour satellite-derived rainfall estimate in inches ending at 1200 GMT. (After Scofield, 1981)

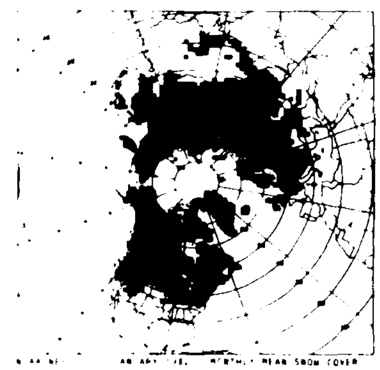

Figure 11

January 1982 digitized monthly mean snow cover prepared from the NOAA/NESS Northern Hemisphere Weekly Snow and Ice Cover Charts.

Figure 12

Vegetative index based on NOAA AVHRR, over Sahelian West Africa, for Sept. 3, 1981. (Courtesy of C.P. Tucker, NASA/Goddard Space Flight Center).

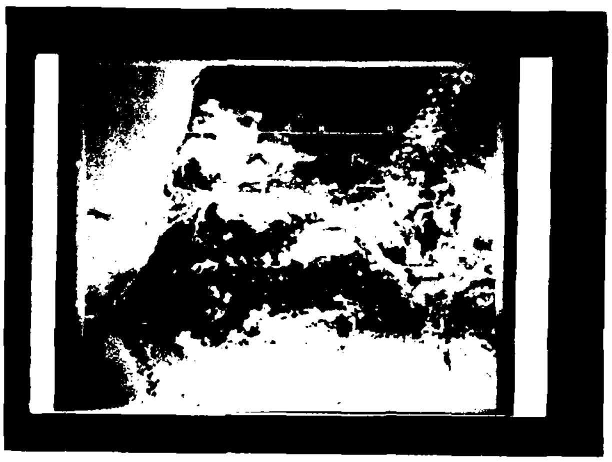

Figure 13

Same as Figure 14, but for Sept. 30, 1981. (Also courtesy C.P. Tucker).

Original figures in color

MONITORING MARINE POLLUTION BY AIRBORNE REMOTE SENSING TECHNIQUES

Shun Yuanfu and Zheng Quanan

The First Institute of Oceanography,
National Bureau of Oceanography,
Qingdao, China.

Teng Xuyan

Changchun Institute of Physics, Academia Sinica.
Changchun, China.

ABSTRACT

In order to harness the marine pollution and make a research on the principles and methods for monitoring the marine pollution by airborne remote sensing techniques, some comprehensive tests of airborne remote sensing, involving monitoring marine oil pollution, were performed respectively at several bay areas of China. This paper presents some typical results of monitoring marine oil pollution. The features associated with the EM spectrum (visible, thermal infrared, and microwave) response of marine oil spills is briefly analysed. It has been verified that the airborne oil surveillance systems manifested their advantages for monitoring the oil pollution of bay environment.

1. INTRODUCTION

Over the past three decades, a great quantity of sewage, waste materials, petroleum and poisonous substances have got into the ocean, which go beyond the self-purification capability of the ocean. Of all of the marine pollutions, the oil occupies a first position. More than ten million tons of petroleum got into the sea per annum in 1970's because of the human's activities. (Report of the Secretary-General.) In general, the oil pollution of bay environment becomes even more serious due to increase of cities, ports and industrial areas. Therefore the oil pollution of bay environment ought to be controlled and tackled in the first place and, without a doubt, it should be attached primary importance to establish effective systems for monitoring marine oil pollution. The traditional surveillance techniques for marine oil pollution have undergone a essential revolution because of the application of remote sensing. A vast amount of researches have been carried out so far for monitoring marine oil pollution by remote sensing techniques (Johe E. Estes, 1972), and more than 60 papers were published up to the 13th International Symposium on Remote Sensing of Environment. Since the beginning of 1970's, as a powerful tool for monitoring marine

oil pollution, the airborne remote sensing systems have come into operation, a typical example of which is the Airborne Oil Surveillance Systems of U.S. Coast Guard (Maurer A.T., 1977). At present, the airborne remote sensing techniques and Landsat data are used in a lot of countries, with the aim of monitoring and analysing the dynamic variations of marine pollution.

The coastal areas of China also suffered from pollution in varying degrees. As a result of the rapid development of industries and sea transportations, rather serious pollution occured in the bay areas adjacent to some industrial cities. Since 1972, a large-scale comprehensive investigation on the marine pollution has been carrying out from the north to south China. A belt-shape area of pollution along the coastal sea of China has been found out and the marine oil pollution has taken a turn for the better through tackling in a comprehensive way since 1976. In order to develop an advanced techniques of monitoring the marine oil pollution, in the past four years, some flight tests of airborne remote sensing were performed successively in Jiaozhou Bay, Dalian Bay, Bohai Bay and Hangzhou Bay. At the same time, the investigations of sea surface truth were conducted. The results indicate that the airborne remote sensing systems are capable of monitoring marine oil pollution within a wide scope and have the advantages of maneuverability, high-speed and synchronism. The data obtained from the new systems, combined with that from the traditional surveillance techniques, can provide a scientific basis for the quality assissment of marine environment, so as to bring the marine oil pollution under control in a comprehensive way.

2. SOME TYPICAL TEST RESULTS AND ANALYSIS

The first test of airborne remote sensing over the coastal sea areas was conducted in September, 1979, at Jiaozhou Bay, Qingdao, organized by the First Institute of Oceanography, National Bureau of Oceanography. The main purpose was, on the basis of laboratory and ground experiments, to research the response of several sensors to marine oil spills, and to test the methods and effectiveness of recording, measuring and monitoring by means of the available sensors, so as to accumulate some practical experience for establishing the marine oil surveillance systems. The subjects above-mentioned were further continued in the next year in an other test located at Bohai Bay near by Tianjin.

a). Observations of the oil slick spreading

The major components of oil pollutants in the bay areas are crude oil and bunker fuel oil. We first observed the rule of spreading and the rate of drifting of different kind of slicks so as to determine the pollution sources and to distinguish the composition of oil in terms of the remote sensing data.

In situ observations showed that the oil spills float on water and spread into smooth slick as soon as they are emptied into the sea. The rate of spreading, the range of expanding and the thickness of slick depend on the property of oil, the temperature of seawater, the sea conditions and the physicochemical property of seawater such as surface tension. In general cases, the oil slick originally is fairly thick and appears a dark brown or black, but it readily spreads into a thin flim and turns to bright colors as like the rainbow tones. As the slick gets even more thinner, the rate of spreading slows down and appears silvery white up to beyond recognition. The spreading rate of crude slick is measured as shown in Fig. 1, on the order of 200 m/h.

In terms of the drifting direction, shape, grey level of marine oil slick combined with the ambient informations and hydro-meteorologic materials, the pollution sources can be determinated. The drifting rate and directions depend on the effects of both tidal current and wind. It is stated that the slick drifts 2.5 to 4.2% as fast as the wind speeds, in case of no effect of the

currents (A.N. Smith, 1970). With a wind speed of 4.3 m/s, we found at Jiaozhou Bay that the drifting rate of oil slick is of the order of 0.3 m/s, involving the effect of the currents. The slicks may exist as films of large areas, spots or strips, depending upon the kind of oil and the environmental factors. To the accompaniment of oil spreading, the phenomena of volatilization, dissolution, oxidation, emulsification and sediment occur continuously.

b). The reflectance spectral characteristics of the oil slick

There exist different reflectance spectral characteristics between the sea surface covered with oil spills and that which is clean. Fig. 2 shows three curves of the reflectance spectral characteristics measured in a water tank of laboratory. It is clear that the reflectivity of oil slick is higher than that of seawater. In the near infrared portion of the spectrum, the reflectivity is lower, and in the blue-green portion of the visible spectrum, however, it is relatively higher. As reported by most researchers, the blue-green bands is entirely satisfactory for the imaging of slick areas.

The density difference on the multispectral films, belween the oil slick and the background seawater, have been measured using a densimeter. It is also evidence that the reflectance spectral characteristics of oil slick vary with the bands. Some values of the density difference are listed in table I.

Table I. The Density Difference Between the Oil Slick and the Background Seawater on the Films.

	blue	green	red
Heavy diesel oil	0.12	0.02	0.01
Crude oil	0.15	0.04	0.03

c). Multispectral remote sensing for marine oil spills

As is well known, the remote sensing of the marine oil spills depends on the sensor's capacities of recording, displaying and measuring the electromagnetic energy emitted, reflected and scatterred by marine oil spills. In view of the highest resolution, the multispectral photographic techniques were first to monitor the actual oil pollution of the bay environment after the simulating tests. The results showed that either the crude oil slick or the heavy diesel oil slick, formed not long after, was able to be imaged in various bands at the low light level, while the ultraviolet-blue bands were best for the formation of distinct images. On the other hand, the thin film regions within both kinds of the oil slick were able to be detected only by relying on the ultraviolet-blue bands. So it can be found that the contrast of tones between the thin film and the thicker one is different owing to the fact that the bands adopted are not alike. For concreteness, the highest contrast is yielded in the blue bands, the less high in the green bands and the least high in the red bands. However, the red bands are most sensitive to reflectance of suspended sediments in water and the wakes.

Fig. 3 shows that two multispectral photographs of different bands, taken in the Bohai Bay near the Haihe River mouth from an altitude of 1,000m, were obtained by a multibands camera made by our own institute. In blue bands (0.40

to 0.48 μm), the imagery of the oil slick of which appears as a continuous strip is more distinct, while in red bands (0.60 to 0.70 μm), that of the turbid water bodies can be seen in addition. The oil slick can be confirmed through comparison. A color photograph taken synchronously yields additional informations: the central region of the slick appears light yellow, the boundary is surrounded with interference rings of all the colors of rainbow. In situ investigation indicated that this slick was bunker fuel oil. Fig. 4 gives a colored density segmental image made from a multispectral photograph taken at the outlet of a port in Qingdao. In the colored image, the thick oil slick appears brown, and the thin one appears pink. The ground truth showed that the pollution regions were covered with a great deal of mixed waste oil discarded by vessels. The oil spills were drifting to depart from the port, being effected of the ebb tide and the wind. The case of unlawful oil drainage by vessels have been monitored as shown in Fig. 5(a), taken in the Bohai Bay. Fig. 5(b) is colored density segmental image of Fig. 5(a), where the light violet shows the major parts of oil spills. It is clear that the imagrey of oil spills has been enhanced obviously. There are oil spills surrounding the marine platform of oil extraction. The ground truth data indicates that this spill is too thin to be observed by naked eye. The ultraviolet bands is very effective for imaging the thin films, as seen in Fig.6. The lighter tone shows the thin oil films spreading into the open ocean.

d). Thermal infrared and microwave remote sensing for marine oil spills

During the tests over Jiaozhou Bay, the flight tests for experimental verification were performed by means of airborne thermal infrared and microwave sensors.

Table II gives the difference of radiometric temperature ΔT between the background seawater and the oil spills by using a infrared radiometer (8 to 12 μm).

Table II. The Difference of Radiometric Temperature ΔT Between The Background Seawater and The Oil Spills.

Oil type	cloudage	Temperature of seawater(°C)	ΔT(K)
Crude oil	0	24.7	1.55 ± 0.05
	7	24.0	0.60 ± 0.10
Heavy diesel oil	0	24.7	1.1 ± 0.00

Fig. 7 is the infrared radiometric curve of heavy diesel oil spills. As shown in Table II, in the overcast sky conditions, there is a marked drop in the ΔT between the seawater and the crude oil spills. A possible reason for that is the higher infrared reflectivity of the oil spills, which reflect the incidence quantity stemming from clouds as a infrared radiation source. So, the ΔT is offseted to some extent. It should be noted that the infrared emissivity of oil spills is different due to the type and thickness. Following the tests over Jiaozhou Bay, thermal infrared systems operating in a scanning mode also acquired many images of oil spills and industrial pollutants over some other bay areas. The results show that the value of ΔT is within 0.86K to 1.7K, while the theoretical value is 1.6K (Buettner and Kern, 1965.).

So far as the microwave radiation of oil-covered water is concerned,the oil film behaves in a manner that causes two separate and distinct effects (J.C. Aukland, 1969), i.e., smoothing effect and radiation effect. Based on the latter effect, the 3cm bands scanning microwave radiometer detected the oil slicks under calm sea conditions. A numerical image of an oil slick acquired at night is given in Fig. 8, where "2" shows sea water, "3" to "5" show the oil slick, and the oil type is crude oil. The experimental values of brightness temperature increment compared with the background seawater indicated that it was about 10K to 30K for thick slicks.

3. CONCLUSIONS

From the results of the remote sensing tests the following conclusions may be drawn.

a). On the basis of an analysis of the multispectral imagery it is concluded that the ultraviolet bands occupies first place for the detection of thin oil slicks, while the blue-green bands comes second, and the red bands is more effective for imaging thicker oil slicks, but the near-infrared bands generally does not yield good results.

b). For utilizing multispectral photography, the sky conditions greatly influence the contrast between oil and seawater. The highest contrast ratios is observed on photograph obtained during periods of overcast sky conditions.

c). The color photography is an effective tool for detecting oil spills. It can provide the important colored tonal signatures of various conditions of an oil slick, though there is poor contrast between oil and seawater.

d). The imagery interpretations show that the marine oil spills are readily distinguished from the wake and turbid water bodies by the method of comparison. It is satisfactory for delineating the oil-water boundary and determining the distribution of oil slicks of various thickness, as well as for drawing the time-spatial pattern of pollution over the bay areas, by means of the colored density segmental imagery and the false-color composites imagery. Then, it is possible to estimate the extent of pollution quantitatively. Especially, the thick region of oil slick is of great value to estimate the spills volume, because the thick region contained more than 90 percent of the oil in less than 10 percent of the area of the visible slick (J.P. Hollinger, 1974.).

e). At present no airborne sensors is capable of providing accurate information on the type or real-time data on the thickness of an oil slick. According to the limit of thickness detectability of various sensors and the colored tonal signatures of oil slick, we have attempted to estimate the oil slick thickness roughly. Further research of estimating the oil slick thickness is in progress in our laboratory.

f). Thermal infrared remote sensing and microwave radiometry offer both day and night surveillance capabilities. It is also possible to determine oil slick thickness and volume if the precision of microwave radiometer can be improved and proper frequency applied to detect oil spills can be adopted.

Finally, the home-made sensors, which constitute the major parts of the airborne oil surveillance systems, are effective, reliable and of low-cost. It is important to pay attention to realization of returns on an investment for developing countries.

4. ACKNOWLEDGMENTS

The authors wish to express their thanks to Associate Scientist Chen Zeshi and Zhang Junrong for their advice and assistance, Mr. Wang Jianwen, Jing Jiyi,

Ding Yongyao, Shi Yuanxun, Shi Changqing, Wang Gengyou for their help in our research work.

5. REFERENCES

Report of the Secretary-General, The Sea Prevention and Control of Marine Pollution, United Nations Economic and Social, Fifty-first Session, 1971.

Estes, J.E and L.W. Senger, The Multispectral Concept as Applied to Marine Oil Spills, Remote Sensing of Environment, 2, 141-163, 1972.

Maurer A.T., U.S. Coast Guard Airborne Oil Surveillance Systems Status Report, Proceedings of the 11th International Symposium on Remote Sensing of Environment, 1639-1640, 1977.

Smith, A.N., The Problem of Oil Pollution of the Sea, Advances in Marine Biology, Vol. 8, London and New York, 1970.

Buettner, J.K. and C.D. Kern, The Determination of Infrared Emissivity of Terrestrial Surface, J. Geophys. Res. 70, 1329-1337 (1965).

Aukland, J.C. and W.H. Gomway, Detection of Oil Slick Pollution on Water Surface with Microwave Radiometer Systems. Proceedings of the 6th International Symposium on Remote Sensing of Environment. 789-796, 1969.

Hollinger J.P., Passive Microwave Sensing of Oil Slicks, Proceedings of the 9th International Symposium on Remote Sensing of Environment, 1761-1762, 1974.

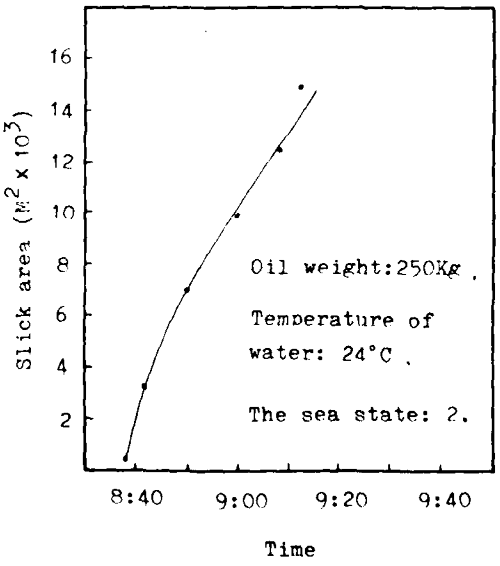

Fig. 1. The spreading rate of crude oil slick.

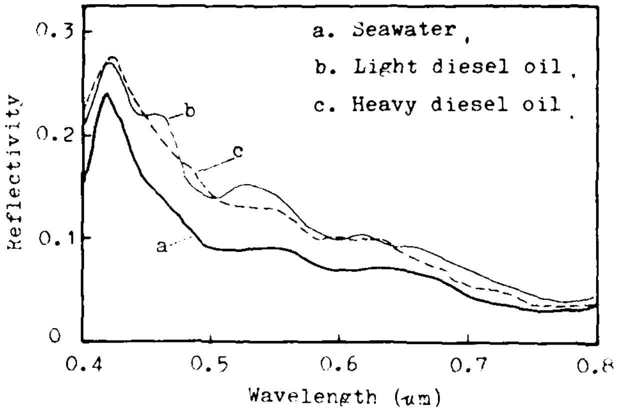

Fig. 2. The curves of reflectance spectral characteristics for seawater, light diesel oil and heavy diesel oil.

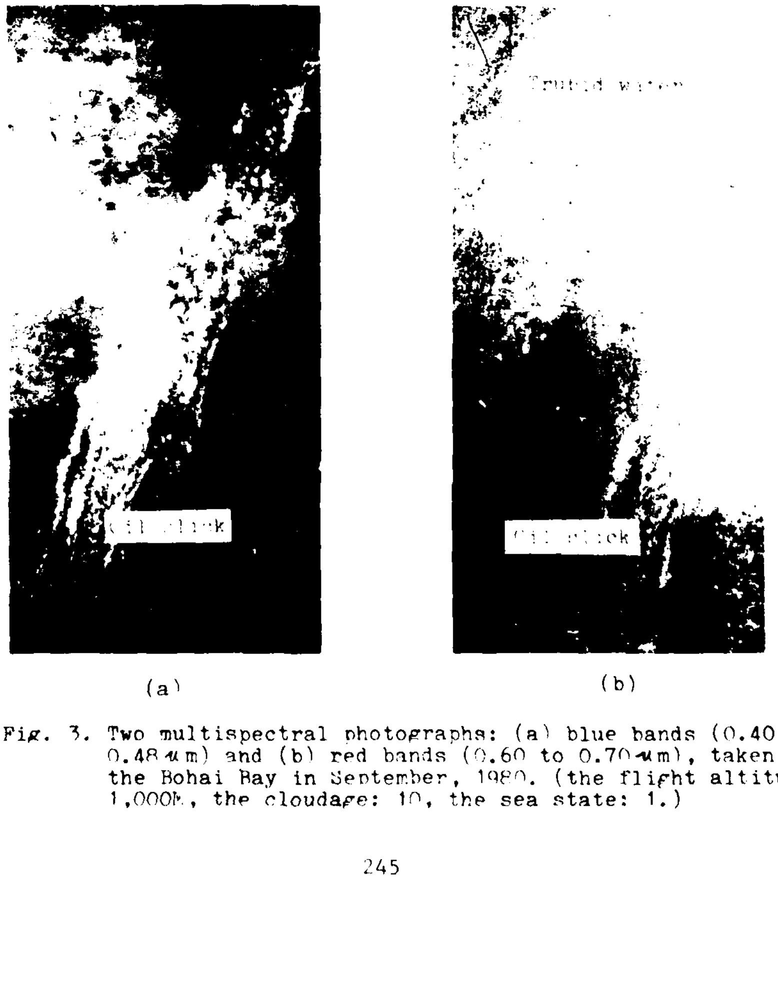

Fig. 3. Two multispectral photographs: (a) blue bands (0.40 to 0.48 μm) and (b) red bands (0.60 to 0.70 μm), taken in the Bohai Bay in September, 1980. (the flight altitute: 1,000k, the cloudage: 10, the sea state: 1.)

Fig. 4. A colored density segmental image made from a multispectral photograph taken at the outlet of a port in Qingdao in September, 1979. (Black and white representation)

(a)

(b)

Fig. 5. (a) A multispectral photograph (red bands) about unlawful oil drainage by a vessel taken in the Bohai Bay in September, 1980. (b) The colored density segmental image of (a). (the flight altitute:1,000M, the cloudage: 8, the sea state: 1) (Black and white representation)

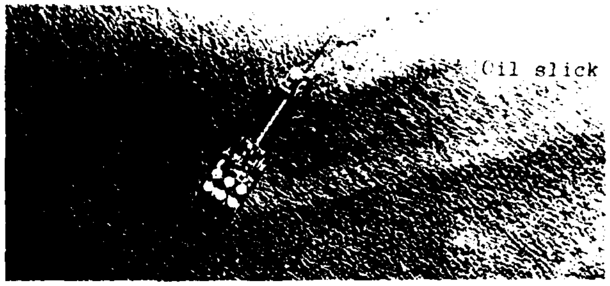

Fig. 6. This ultraviolet (0.32 to 0.38 μm) image of an oil slick was obtained in Bohai Bay in May, 1980. Thin oil film is seen as light against the darker water. (the flight altitute: 1,500M, the cloudage: 0, the sea state: 3.)

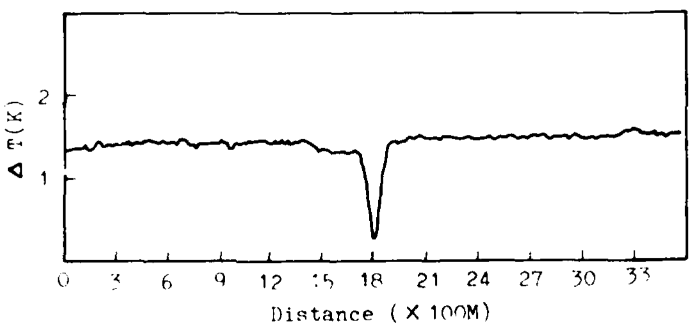

Fig. 7. The infrafed radiometric curve of heavy diesel oil spills taken in Jiaozhou Bay in September, 1979.

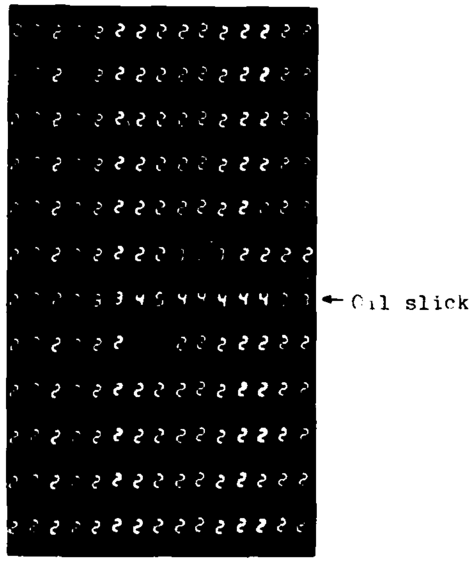

Fig. 8. The microwave radiometric image of crude oil spills acquired at night, where "2" shows sea water, "3" to "5" show oil slick. This image was obtained in Jianzhou Bay in September, 1979. (the flight altitute: 200M, the temperature of water: 23.8°C, the sea state: 1.)

A TECHNIQUE FOR MAPPING ENVIRONMENTAL CHANGE USING DIGITAL LANDSAT DATA

Richard S. Mussakowski

Ontario Centre for Remote Sensing
Ministry of Natural Resources
Toronto, Ontario, Canada

SUMMARY

Digital LANDSAT data is well suited to the monitoring of certain aspects of environmental change because of the comprehensive coverage of individual frames (185 km x 185 km), the repetitive nature of the coverage (on an 18-day cycle), a ground resolution (79 m x 59 m) adequate to relatively broad classification, and the multispectral character of the data, which is digitally recorded and thus readily amendable to analysis using current computer techniques.

In order to develop a LANDSAT-based procedure for mapping environmental change, variations in vegetation density were analyzed and compared on LANDSAT scenes from different years. The area selected for study was the region surrounding the city of Sudbury, an industrial, mining and smelting centre in the province of Ontario, Canada. The terrain of the site is glaciated Precambrian shield covered by a thin layer of drift. The site is located in the Great Lakes-St. Lawrence forest region.

The first problem in comparing successive temporal images of the same location is image-to-image and image-to-map registration. This was successfully accomplished by modeling each image to common ground control points using a polynomial transform, then comparing and resampling to 50 m x 50 m pixels, using the cubic convolution assignment technique. The two dates of imagery selected for analysis and comparison were July 13, 1973 and July 3, 1980. Images obtained as close to the same time of year were selected so as to minimize the effect of seasonal variations.

An unsupervised maximum-likelihood classification was performed for both dates of imagery. Four broad themes were developed:

1. Close vegetation;
2. Scattered vegetation;
3. Barren areas;
4. Water.

A visual comparison of the maps revealed that significant changes had taken place. These changes were better defined by producing a post-classification vegetation change map. Four themes were mapped:

1. Areas of no change;
2. Areas of vegetation increase;
3. Areas of vegetation decrease;
4. Water.

This new classification was developed by ratioing the themes from the two dates. During the unsupervised classifications, bit positions and values were

specified for the themes. (Table 1). When ratioed areas of no change receive the theme bit value of 4 (bit position 3), areas of vegetation increase received the theme bit values of 8 and 16 (bit positions 4 and 5), and areas of vegetation decrease received the theme bit values of 1 and 2 (bit positions 1 and 2)(Table 2). The bit positions and values were expressly selected to create three new change themes. A water theme was later added for reference.

The output consists of three theme maps printed by a computerized colour plotter, with standard legend, title, scale and necessary UTM and latitude and longitude coordinates for reference. Two of the maps are the original unsupervised classification and the third is the post-classification vegetation change map.

The vegetation change map confirmed areas of suspected damage and areas where the closing of a smelter had permitted new vegetation growth. It also revealed unsuspected areas of vegetation change for which ground verification of the cause is required.

This technique should prove applicable to any region of the world, provided at least two successive cloud-free images exist, each acquired at the same time of year so as to minimize the effect of seasonal variations.

	1973		1980	
Theme	Bit Position	Bit Value	Bit Position	Bit Value
Barren	1	1	3	4
Partial	2	2	4	8
Total	3	4	5	16

TABLE I. Theme - Bit Allocation for Ratioing - Sudbury Region

Change Theme	Change Theme Ratio 1980/1973	Bit Value Ratio	Output New Bit Position
Areas of no Change	$\frac{\text{barren}}{\text{barren}}$	$\frac{4}{1} = 4$	3
	$\frac{\text{partial}}{\text{partial}}$	$\frac{8}{2} = 4$	3
	$\frac{\text{total}}{\text{total}}$	$\frac{16}{4} = 4$	3
Areas of vegetation increase	$\frac{\text{partial}}{\text{barren}}$	$\frac{8}{1} = 8$	4
	$\frac{\text{total}}{\text{barren}}$	$\frac{16}{1} = 8$	5
	total	$\frac{16}{2} = 8$	4
Areas of vegetation decrease	$\frac{\text{barren}}{\text{partial}}$	$\frac{4}{2} = 2$	2
	$\frac{\text{barren}}{\text{total}}$	$\frac{4}{4} = 1$	1
	$\frac{\text{partial}}{\text{total}}$	$\frac{8}{4} = 2$	2

TABLE II. Ratioing - Sudbury Region

APPLICATIONS OF IR THERMOMETRY FOR AGRICULTURAL RESOURCE MANAGEMENT

Paul J. Pinter, Jr.

U.S. Department of Agriculture
Water Conservation Laboratory
Phoenix, Arizona

SUMMARY

Infrared thermometry is emerging as a reliable surrogate for many of the methods that were previously used to quantify stress in plants. Its utility arises from the observation that physical or biological stresses which interfere with the movement of water through the plant often result in elevated foliage temperatures. With ample water, for example, evapo-transpiration proceeds at near potential levels, cooling foliage at a rate proportional to the evaporative demand of the environment. As a result, many well-watered agricultural crops have midday radiant canopy temperatures at or below that of the ambient air. As moisture in the root zone becomes depleted, evapotranspiration decreases and canopy temperatures rise relative to non-stressed crops and air temperatures rise relative to non-stressed crops and air temperatures.

Research at the USDA Water Conservation Laboratory in Phoenix, Arizona, has led to the development of a Crop Water Stress Index (CWSI) which is derived from radiant leaf temperatures, air temperatures, and air vapor pressure deficits. In order to calculate the CWSI, observed plant temperatures are scaled relative to minimum and maximum temperatures expected under no-stress (CWSI=0), respectively.

Results from field experiments conducted in alfalfa, cotton and wheat crops have shown that the CWSI is well correlated with concomitant observations of plant physiological status such as leaf water potential, stomata diffusion resistance and net photosynthesis, and to a lesser degree, the extractable fraction of water remaining in the soil. Because an inverse relationship exists between the summation of daily CWSI values and final marketable yield, applications of this technology should result in more efficient management of agricultural resources.

ESTIMATING ACREAGE BY DOUBLE SAMPLING USING LANDSAT DATA

F. Pont
H. Horwitz
R. Kauth

Environmental Research Institute of Michigan
Ann Arbor, Michigan

SUMMARY

Double sampling techniques for estimating the acreages of corn and soybeans by combining ground truth, labor intensive Landsat based estimates and less expensive Landsat based estimates have been investigated and evaluated. The double sampling techniques were evaluated based on estimated costs and correlations within a reasonably realistic operational scenario involving linear cost constraints among two or more types of resources. The costs were estimated from our current experience with the measurement procedures involved and the correlations were estimated from a set of 39 LACIE type sample segments in the U.S. Corn Belt.

For a fixed variance of the estimate double sampling with the two Landsat based measurement procedures can result in a 25% to 50% cost reduction. If ground truth is available then it should be used with the less expensive of the Landsat techniques, in this case. The paper provides a methodology for evaluating which of any competing inexpensive Landsat techniques would be most cost effective when used with ground truth.

This work was sponsored under Contract NAS9-15476 by the U.S. National Aeronautics and Space Administration, NASA Johnson Space Center, Houston, Texas.

USING LANDSAT DIGITAL DATA TO IDENTIFY EROSIONAL ZONES IN THE CUENCA ALTA DEL RIO BOGOTA

Dr. Roland D. Mower

University of North Dakota
Institute for Remote Sensing
Grand Forks, ND 58202

and

Eng. Myriam Ardila T.

Centro Interamericano de Fotointerpretacion (CIAF)
Apartado Aereo 53754
Bogota, Colombia

ABSTRACT

Digital Landsat data for the Embalse de Tomine portion of the Cuenca Alta del Rio Bogota, Colombia were analyzed using a small interactive microcomputer system (IMPAC). Soil erosion within the study region was located and classified according to categories established by CIAF. Results of the digital analysis were then compared with soil erosion maps produced by INDERENA and CIAF. Correlations between the map produced by IMPAC and those produced from extensive field work were good. Based upon this study it appears that small microcomputer systems are useful for the analysis of erosional features in the landscape.

1. INTRODUCTION

Soil erosion has been identified by the Colombian government as one of its principal national problems. Recognition of the need to locate, classify and monitor soil erosion has resulted in strong support for the development of remote sensing techniques. This study focused upon the use of an interactive microcomputer system for the analysis of Landsat digital data acquired in January 1977 (Scene No. E 2716-14184).

2. STUDY REGION

The Embalse (Reservoir) de Tomine region is located in a portion of the Cuenca Alta del Rio Bogota, Departamento de Cundinamarca approximately fifty kilometers northeast of Bogota, Colombia. This region has been severely eroded during the past eighty years and its potential for many forms of

agriculture has been significantly reduced. The study region includes the southern half of Lake Tomine and contiguous portions of the river valley. The small town of Guatavita is located near the eastern shoreline of the lake. This region contains approximately 7,250 hectares (see fig. 1).

The river valley itself is situated between two mountainous ridges, Pena Blanca on the west and Alto de los Mortinos to the east. Slopes within the study region generally range from 25 to 75 percent, and elevations vary from 2,600 to 3,200 meters above sea level. Average monthly temperatures vary from 6 to 12 degrees Celsius, and annual precipitation averages 654 mm. Potential evapotranspiration exceeds precipitation, averaging 781 mm. per year. This corresponds to the "subparamo" and "tierra fria," according to the Holdrige classification of life zones (CIAF, 1981).

Vegetation within the study region is generally sparce, thus reflecting its semiarid conditions. According to Holdrige it is classified as humid mountain forest (bh-m); however, because of severe erosional problems most of the native vegetation has been destroyed. More recently, reforestation has been attempted by governmental agencies such as CAR and INDERENA. Principal species used for reforestation include Eucaliptus globulus, Pinus patula and Pinus radiata. Although reforestation has been successfully applied in some areas, in others it has not stopped the accelerating erosional processes.

Lithologic materials found within the study region were formed during three geological periods: Cretaceous, Tertiary and Quaternary. In the eastern portion of the study region the Guaduas formation acts as transitional formation between Cretaceous and Tertiary. The Guaduas formation, composed primarily of sandstones, is exposed along the roadway that serves Guatavita. Nearby, Guadalupe formation (Tertiary) is composed of fine sandstones and layers of mudstones.

Soils in the study region are generally fragile, and have developed from volcanic ash, and alluvial and lacustrine sediments. The Guasca series, found at higher elevations (above 2,800 meters), is moderately thin and consists of only an A horizon. It has a low pH (3.6 to 5.0), is on slopes greater than 25 percent, and is generally well drained. On the other hand, the Caguas series is found below 2,800 meters; its B horizon is composed of an argilic material which is impervious. As a result, root penetration is severely impeded and little vegetation develops on this easily eroded fine textured material.

3. METHODOLOGY

A set of procedures were developed for this study that linked a large general purpose computer (IBM 4341) and a small interactive microcomputer system (IMPAC). The larger computer was used to preprocess digital data for selected portions of a Landsat scene and to enter data into the microcomputer system. Then the smaller system was used for the analysis of soil erosion within the area. In addition to Landsat MSS digital data, MSS imagery and aerial photos were acquired and visually interpreted using standard optical analysis techniques. Results obtained from visual interpretation were then compared to those obtained by CIAF and INDERENA during their separate studies which were based upon intensive field investigations (INDERENA, 1977).

4. DIGITAL IMAGE ANALYSIS

Landsat MSS digital data for the study area were entered from a CCT to an IBM 4341 computer. After preprocessing the Landsat data were transferred to the IMPAC system and stored in floppy disks. Procedures employed for training and classification with the IMPAC system are quite similar to those

used for other interactive systems (Egbert, 1980). Selection of training pixels was accomplished using band 5 data. Classification involved a "supervised" technique that employed all four MSS bands plus an additional band created by a band rationing. Landsat MSS data proved to be very useful for identifying and mapping regions of soil erosion. Indeed, the Landsat data appeared to contain much more information than needed to produce the level of information contained in the INDERENA and CIAF maps.

5. VISUAL IMAGE INTERPRETACION

Visual interpretation of Landsat imagery and aerial photos was accomplished as part of this study for two principal reasons. Our first objective was to determine the usefulness of Landsat color composits for erosion studies in Colombia. Secondly, we wanted to confirm "ground truth" for the study area. Since the Landsat image was acquired in 1972 and the aerial photos in 1980, we expected to see some changes in the scene. There were significant differences. Erosion appeared to be more extensive in imagery for the later date (see fig. 2). Changes in lake level and erosion along the shorelines were particularly evident.

6. RESULTS

Landsat MSS digital data, when analyzed using the IMPAC system proved to be quite accurate. Two classes of erosion (i.e., severe and moderate) were readily identified and mapped as shown in figure 3. The fact that Landsat data contained sufficient information to identify and locate erosional features in the study region is significant, but another important factor also became evident. It is encouraging to note that a small inexpensive image analysis system is capable of producing useful results.

7. REFERENCES

Centro Interamericano de Fotointerpretacion (CIAF), Metodologia Para la Delimitacion de Areas Homogeneas. Bogota, D.E.: CIAF, 1981.

Instituto Nacional de los Recursos Naturales Renovables y del Ambiente (INDERENA). La Erosion de Tierras en Colombia. Bogota, D.E.: INDERENA, 1977.

Egbert, D. D. IMPAC. Technical Manual. Greenport, NY: Egbert Scientific Software, 1980.

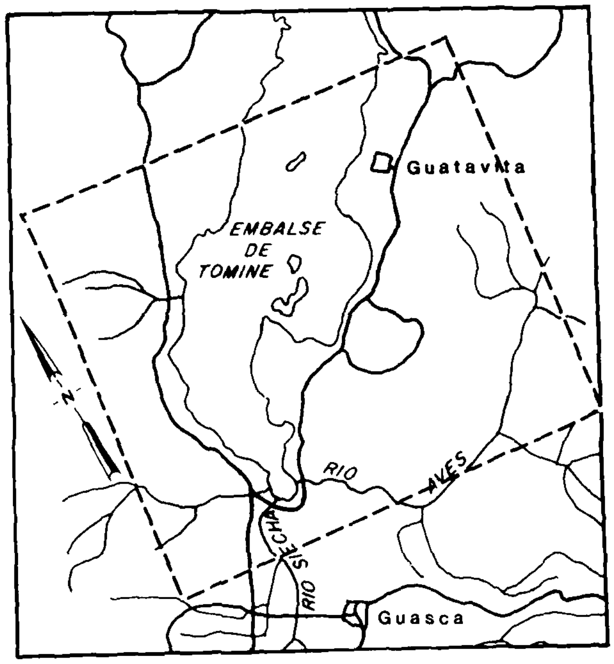

Figure 1: Embalse of Tomine Estudy Region

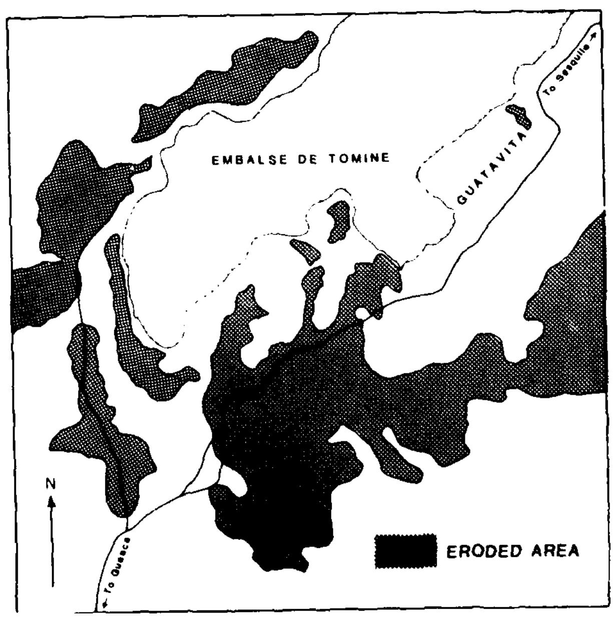

Figure 2: Visual Interpretation of Soil erosion

Figure 3: Computer classified Soil Erosion

MULTISTAGE AND MULTIPHASE SAMPLING WITH NIMBUS AND LANDSAT DATA

J. Colwell
D. Hicks
F. Tanis

Environmental Research Institute of Michigan
Ann Arbor, Michigan

SUMMARY

Landsat data has proved to be a useful tool for inventory of natural resources over large areas. More recently, Nimbus data has been shown to be useful for monitoring general conditions over even larger areas, due to its larger field-of-view.

Landsat data has frequently been found to have greater value for quantitative inventory when it is used in combination with aerial photography and/or field measurements as part of a multistage or multiphase estimation procedure. Utilization of Nimbus data as an additional stage or phase in an estimation procedure could produce added benefits and efficiencies to inventories of very large areas. When Nimbus data is used in this context, some of the apparent deficiences it has (such as very coarse resolution) can be minimized, and some of its potential advantages can be maximized.

One of the advantages of Nimbus data is that it provides a synoptic view of a very large area at a single point in time. This is especially important when an inventory of a rapidly varying resource feature is desired (e.g., rangeland condition, early-season crop area). Nimbus data also has the advantage of the potential for more frequent data acquisition. This facilitates obtaining frequent coverage of rapidly varying phenomena, which is required for analysis of temporal trends. The more frequent coverage also greatly enhances the opportunity to obtain suitable cloud-free coverage. Our experience has shown that there sometimes is not suitable cloud-free Landsat data to enable a complete inventory of very large areas in some developing countries, especially if the data must all be within a narrow time frame.

This paper will illustrate how some of the difficulties of inventory of large, developing countries can be overcome by judicious utilization of Nimbus data in conjunction with Landsat, aerial photo and field data. Both multistage and multiphase estimation procedures will be demonstrated, and their respective advantages and disadvantages will be discussed. Emphasis will be placed on an area in Argentina where Landsat-only estimation procedures are being developed as part of the AgRISTARS program. The result of this activity will be a determination of the most cost-effective inventory procedure possible utilizing various combinations of Nimbus, Landsat, photo, and field data.

AD P002009

AN APPLICATION OF CLUSTER ANALYSIS FOR DETERMINING HOMOGENEOUS SUBREGIONS: THE AGROCLIMATOLOGICAL POINT OF VIEW

Carlos Alberto Cappelletti

Instituto de Pesquisas Espaciais - INPE
Conselho Nacional de Desenvolvimento Científico e Tecnológico - CNPq
Caixa Postal 515, 12200 - São José dos Campos, SP, Brazil

ABSTRACT

A stratification oriented to crop area and yield estimation problems was performed using an algorithm of clustering. The variables used were a set of agroclimatological characteristics measured in each one of the 232 municipalities of the State of Rio Grande do Sul, Brazil. A nonhierarchical cluster analysis was used and the pseudo F-statistics criterion was implemented for determining the "cut point" in the number of strata.

1. INTRODUCTION

In order to predict the crop production of a region it is necessary to estimate two parameters: CA and P, crop area and yield, respectively, and integrate them by the expression

$$TP = CA * P \tag{1}$$

where TP indicates total production.

The estimation of CA and P depends on a data set which can be obtained by different means: statistical sampling system or a census data collecting system in the area of interest. Aerial photograph and/or LANDSAT imagery are important means for CA estimation; for P, a yield prediction model can be implemented, see Baier (1979) and Cappelletti et al. (1981).

Both of the above approaches requires the stratification of the area to be studied for producing an adequate confidence coefficient in the final estimates (Raj, 1968).

This paper reports results obtained in the construction of strat with the application of an algorithm of Cluster Analysis to a set of data consisting of agroclimatological variables, whose values are, in general, averages values of historical series.

The data refers to each one of the 232 municipalities of the State of Rio Grande do Sul, Brazil. The decision to consider as a unity such political division was because the data were published in a municipality level.

The building of homogeneous strata is the first step in a project of crop production estimation. Since the parameters AC and P in Equation (1) depends on different characteristics, two set of strata are required.

2. METHODOLOGY

The technique of clustering has been widely used for grouping similar units. This technique works with a data matrix and a similarity measure.

The data matrix has dimension $N * P$, being N the number of units and P the number of characteristics observed or calculated for each unit.

The similarity measure used in this paper was the Euclidean distance in the observation space.

The objective of the clustering algorithm is to minimize the intracluster sum of squares following the K-means procedure of Mac Queen (1967).

The algorithm works as follows: the i^{th} unit of the j^{th} variable has value $x(i,j)$, $i = 1,\ldots,N$, $j = 1,\ldots,P$, and each of the N unities lies in just one of K cluster. Denoting the mean of the j^{th} variable over the unities by $\bar{x}(\ell,j)$, the distance between the i^{th} unity and the s^{th} cluster is:

$$D(i,s) = \left[\sum_{j=1}^{P} (x(i,j) - \bar{x}(s,j))^2 \right]^{1/2}$$

and the error partition is

$$E\left[P_a(m,k)\right] = \sum_{i=1}^{N} D^2(i,s(i))$$

where $s(i)$ is the cluster containing the i^{th} unity and P_a indicates a partition.

The procedure searchs for a partition with small E by moving unities from one cluster to another and ends when no such movement reduces E (Hartigan, 1975).

Clusters were generated in a nonhierarchical process. The process began with one group and stopped when the number of groups reached the cut point given by the pseudo F-statistics (PFS) criterion function of Vogel and Wong (1979).

The PFS criterion provided the optimal number of groups operating with the weighted ratio of the traces of the matrices B and W, respectively the matrices of sums of squares between and within groups in the multivariate analysis of variance (MANOVA) of the data set.

3. VARIABLES AND DATA SET

The variables used were:

wheat cultivated area (Ha)
wheat yield (kg/Ha)
average farm size (Ha)
agricultural land adequated for wheat (Ha)
average temperature (°C)
potential evapotranspiration (mm)
rainfall in normal years (mm)
rainfall in dry years (mm)
average yearly run-off (%)
useful fraction of rainfall in normal years (mm)
useful fraction of rainfall in dry years (mm)
internal drainage in normal years (mm)
internal drainage in dry years (mm)

moisture deficit in normal years (mm)
moisture deficit in dry years (mm)
necessary minimum rainfall (mm)

The data set was taken from the Anuário Estatístico do Rio Grande do Sul (1968, 1969, 1970 and 1976) and from Ministério da Agricultura (1976).

4. RESULTS AND DISCUSSION

4.1 WHEAT AREA ESTIMATION (AC)

Two variables, relative crop area (RCA) and normalized average farm size (AFS), by municipality, were considered.

The reason for using those variables was that the first one represents the density of cultivated wheat lands and will provide homogeneous strata with respect to the importance of wheat in the agricultural scene. The average farm size was selected to represent problems which might be encountered in LANDSAT data classification with different field sizes.

The clustering algorithm gave four groups as the best partition (Table I).

STRATA No.	MEAN VALUES CRA(%)	AFS(Ha)	STANDARD DEVIATION CRA	AFS	No. OF MUNICIPALITIES
1	8.5	22.7	9.4	9.9	177
2	4.8	85.9	7.6	22.8	34
3	4.2	192.8	6.8	28.2	12
4	1.2	279.1	1.4	24.5	9

Table I. Four strata for CRA and AFS

The columns of the two mean values in Table I show that there exists a negative relationship between the variables CRA and AFS, that is, municipalities with large average farm size dedicate a large percentage of the total land for livestock-raising instead of wheat.

Figure 1 shows the geographical location of the strata.

In order to compare with results showed in Table I, the state was subdivided into four regions with variable CRA alone (Table II).

STRATA No.	MEAN	S.D.	No. OF MUNICIPALITIES
1	35.6	4.1	10
2	21.2	3.4	26
3	10.1	2.6	55
4	1.8	1.9	141

Table II. Four strata for variable CRA

Figure 2 shows the geographical location of these stratas.

4.2 WHEAT YIELD ESTIMATION (P)

The original data set used in this stratification included the last fourteen variables listed in item 3.

The data were those related with the wheat growing season and some of them were average values of historical series.

Those data were treated with a Principal Component Analysis (Cooley and Lohnes, 1971) and after that the scores factor for the first five principal components, which account for 93.5% of the total variance, feeded the clustering algorithm.

The technique of principal components have been described in the book cited. If should be recalled that the method produces uncorrelated linear functions of the original variables without any loss of information. Depending upon the data being used it may be possible to recognize the physical significance of these new variables. When this is possible, this method brings about a reduction in the quantity of basic data that needs to be used.

Table III shows the factor eigenvalues and the cumulated percent of the trace.

FACTOR	EIGENVALUE	CUMULATED PERCENT OF THE TRACE
1	7.69	54.9
2	2.05	69.6
3	1.73	81.9
4	1.01	89.2
5	0.60	93.5
OTHER 9 FACTORS		6.5

Table III. Output of the Principal Components Analysis. First five principal factors

With the factor score coefficients, which are an output of the principal components analysis, the factor scores for each municipality were calculated, and these data feeded the clustering algorithms.

Table IV shows the number of municipalities for each strata.

STRATA No.	No. OF MUNICIPALITIES
1	57
2	72
3	74
4	29

Table IV. Stratas for five principal components with fourteen agro-meteorological variables

Figure 3 shows the geographical position of the strata.

The more relevant characteristics for each strata can be summarized as follows:

Strata I.

This region is called "campanha" and corresponds to an extensive natural grassland zone traditionally used for livestock grazing.

Strata II.

This region is called "depressão Central" and corresponds to a small-scale diversified agriculture.

Strata III.

This region is called "planalto médio". It is the soybean-wheat cropping region in the state. The wheat growing season is the winter and this stratum corresponds to the largest yields of the state.

Strata IV.

In this region wheat is not cultivated because the urban and industrial zone of the great Porto Alegre, the state capital, is in it. Another region in this strata is the atlantic litoral where there are numerous areas of sand dunes. The others two subregions of this strata are in the livestock raising zone.

5. CONCLUSIONS

A stratification oriented to crop area and yield estimation problems was performed.

The algorithm of clustering used produced good results inasmuch as the geographic location of the strata appears to be logical and the strata seem to represent different conditions. Besides that, the within strata sum of squares was minimizes when a set of agro-meteorological variables was simultaneously considered.

The region chosen to apply the procedure has been extensively studied and consequently there exists the possibility of validating the criterium used. In order to improve the final results further work has to be done.

6. REFERENCES

Anuário Estatístico do Rio Grande do Sul, Secretaria de Economia, Departamento Estadual de Estatística, Vol. 1, 2 and 3, 1968, 1969 and 1970; Vol. 5.8 - tomo 1, Agropecuária, 1972-75, publicadc em 1976, Porto Alegre.

Baier, W. Note on the terminology of crop weather models. Agricultural Meteorology, 20: 137-145, 1979.

Cappelletti, C.A.; Reis, J.R.; Lorena, L.A.N.; Dias, N.T.; Cruz Paião, L.B.F. da; Olivo, A.A. de; Costa, S.R.X. Proposta metodológica para a modelagem do crescimento de uma cultura visando estimação de produtividade agrícola. São José dos Campos, INPE, nov. 1981. (INPE-2255-PRE/037)

Cooley, W.W.; Lohnes, P.R. Multivariate data analysis. Wiley, New York, 1971. 364 p.

Hartigan, J.A. Clustering algorithms. Wiley, New York, 1975. 351 p.

Mac Queen, J.B. Some methods for classification and analysis of multivariate observations. Proceedings Symp. Math. Stat. and Prob., 5th, Berkeley 1, 281-297, 1967.

Ministério da Agricultura. Levantamento e avaliação de recursos naturais, sócio-econômicos e institucionais do Rio Grande do Sul. Vols. 1 to 6, INCRA, Brasília, 1976.

Raj, D. Sampling theory. McGraw-Hill, New York, 1968. 302 p.

Vogel, M.A.; Wong, A.K.C. PFS clustering method, IEEE Trans. on Pattern Anal. and Mach. Intel.. Vol. PAMI-1, No. 3, July 1979.

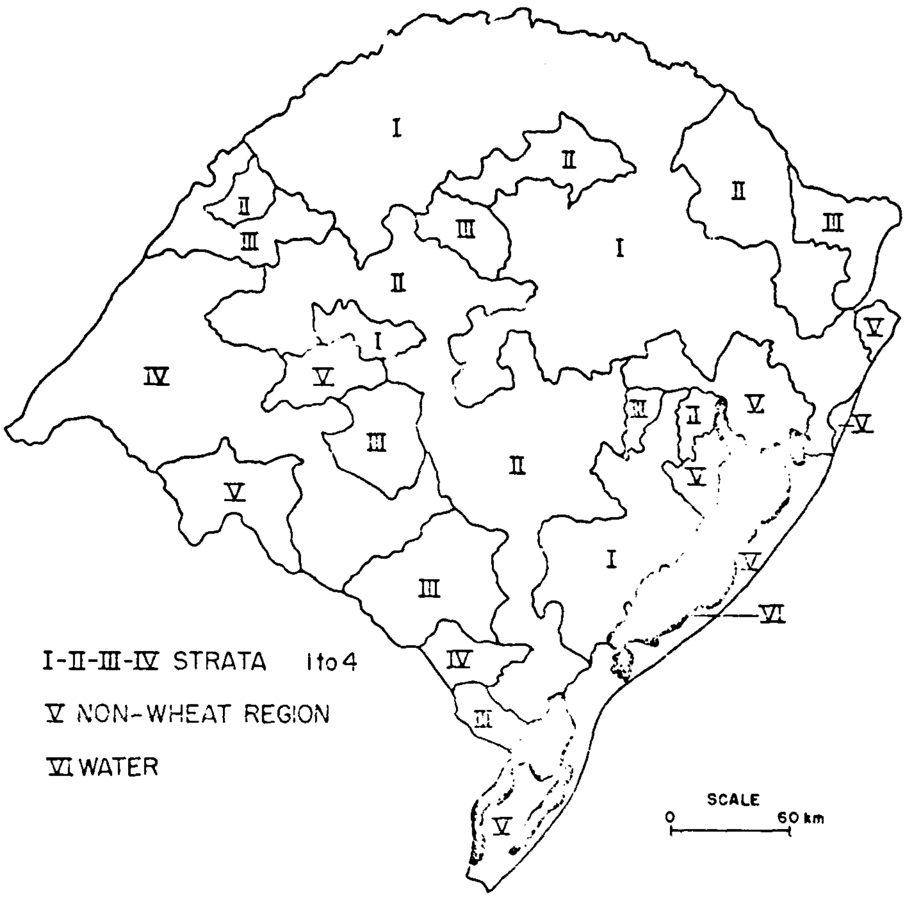

Figure 1. Four strata for CRA and AFS

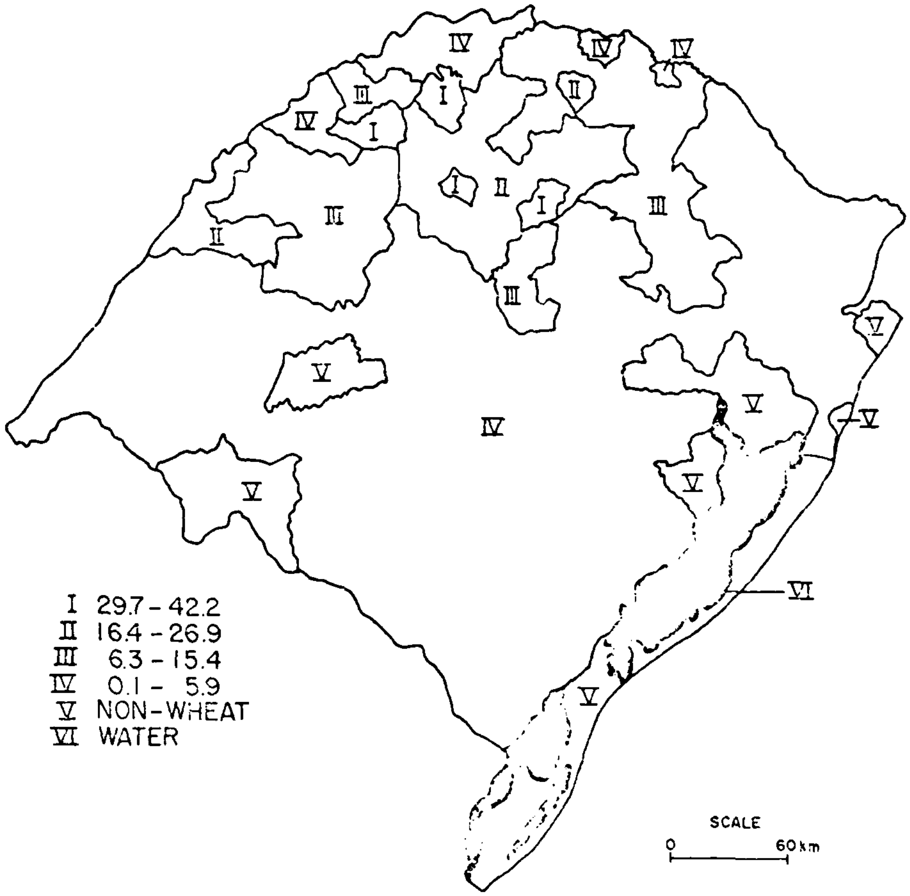

Figure 2. Four strata for CRA (%)

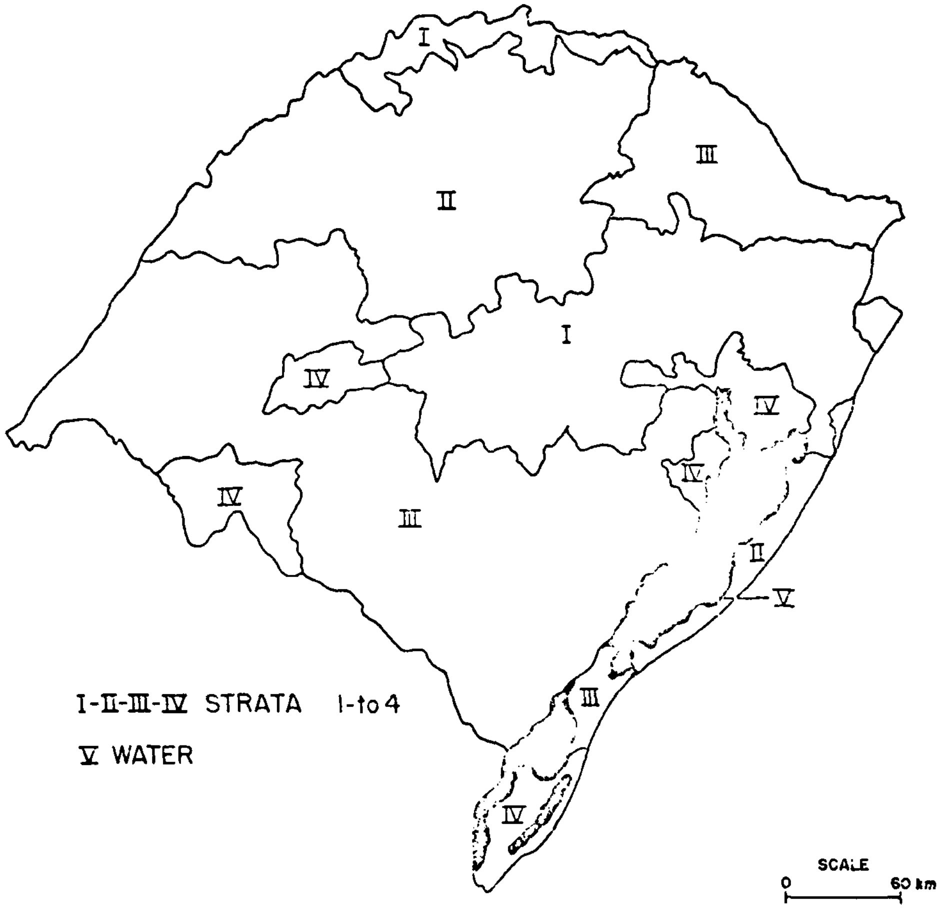

Figure 3. Four strata for five principal components with fourteen agro-meteorological variables

AD P002010

REMOTE SENSING OF WIND EROSION IN CROPLANDS

D.J. Carter
Division of Resource Management
Western Australian Department of Agriculture
Jarrah Road, South Perth 6161 Australia

H.J. Houghton
Western Australian Lands and Surveys Department
Cathedral Avenue, Perth 6001 Australia

ABSTRACT

Wind erosion has caused considerable damage to the wheat growing areas in Western Australia over the last two years. To assess this damage and to create a data base for future events, Landsat data was used.

The Landsat data was found to be accurate for assessing sandblast areas, when there was good backup of aerial and ground information. This was only required for the initial training site identification. The use of Landsat data was found to save both time and money when compared to conventional mapping procedures. It was also sufficiently accurate in a precision processed form to allow for other data sets to be *integrated*.

1. INTRODUCTION

The importance of the cereal industry to the economy of Australia is significant, with net export earnings of $A2.77b. Western Australia contributes some 3.7 m tonnes of wheat which represents 23 per cent of the total wheat export earnings. Wind erosion can limit this production.

The Western Australian crop is grown on soils which have undergone several cycles of weathering. This has produced soils of low fertility and a predominance of sand-sized particles in the soil surface, a fact which renders them prone to wind erosion. This soil condition is exacerbated by the climate, where strong winds coincide with the land being cultivated for seeding. This occurs from May to July, depending on the start of the wet period of the essentially Mediterranean climate.

Sandblast damage to crops is significant in terms of lost production and can affect much of the wheat growing areas. Obviously sandblast events are not fully predictable thus the task of assessment can be difficult. Current procedures include ground inspections complemented by small scale aerial surveys. Aerial photography of the total affected area is not practical in all cases, and an estimate may take some time. In addition the collation and mapping is labour intensive and can make uniform data storage and recall difficult.

Research programmes in Western Australia are currently directed at identifying those conditions under which sandblast occurs, and developing stable farming practices which avoid wind erosion (Gorddard et al., 1982). To most effectively implement such practices requires a knowledge of the extent and history of the problem. These latter factors are associated with climate pattern and soil type. Sandblast events are irregular and sometimes ephemeral so when a problem does occur it is essential that it is rapidly assessed. Regular coverage is also necessary to identify recurrent problem areas and to implement both remedial and preventive measures. The only effective means of monitoring such regional events is by satellite.

The purpose of this paper is to outline the use of broad scale satellite imagery, multispectral and temporal data in identifying wind erosion problems in Western Australia. The justification of the use of Landsat imagery, when compared to conventional aerial surveying and mapping, is also determined.

2. BACKGROUND TO THE STUDY

In the years 1980 and 1981 considerable wind erosion took place on the soils cultivated for cereal production throughout the wheatbelt. A relatively small area (300 000 hectares) out of a total of five million hectares was chosen for the pilot study. The area was located some 100 km from the southern coastline, where damage was consistent and extensive. The damaging north westerly winds moved large quantities of sand in each year and in the process sandblasted the young emerging crops. In many cases the crops were totally destroyed and reseeding was unsuccessful when recurrent strong winds caused further sand drift.

The soils of this general region have been broadly described as ranging from yellow duplex soils (hard, pedal) to sandy apedal mottled yellow duplex soils (Northcote et al., 1975). Deep sands over 1 m in depth are common. The geological map of the area described the soils mainly as sandplain or reworked sandplain of Cainozoic origin (Thom et al., 1981). The sands are yellow to white sand and clay, containing scattered limonite nodules, derived from underlying gravel and laterite. Some soils have developed on the Quaternary deposits of colluvium and alluvium of the above sediments.

The original vegetation of the area was Eucalyptus species in a low scrubland formation grading to a myrtaceous heath (Beard, 1981). This has been removed for the broadacre cropping system which prevails in the district.

Previous surveys of wind erosion have been made in this area. In 1973 a farmer questionnaire estimated that 34 000 hectares had been affected in a survey area of 62 000 hectares. This survey took 15 days to organise and collate results. Several staff were involved in the survey and only part of the total affected area was covered. It was neither possible to validate the results of this survey nor establish a data base for future reference.

First reports of mapping sand blow-outs by ERTS-I imagery indicated a potential for identifying these areas for inventory purposes (Seevers et al., 1975). In 1976 black and white Landsat images (Band 5 only) were used for the first time in Western Australia to estimate wind erosion areas (Birch, 1976). Interpretation difficulties were encountered with the use of this single band imagery. Multi-band MSS data was not used.

3. METHODS

In appearance a wind eroded area has a higher reflectance than normal cultivated soil because the sorting action of the wind removes dark organic matter from the immediate soil surface. The sorting action leaves behind the larger sand size particles on the surface which also increases the reflectance. It was this feature which was thought to be the discriminator on Landsat imagery for wind eroded paddocks, compared to pasture and recently cultivated paddocks.

The data available for the 1980 study included Landsat data in digital form for three dates, aerial photography over portion of the area and ground information. Cloud free Landsat data for the study area was only available for:

117-83	August 15, 1980 (22032-01072) (Image 1)
118-83	November 14, 1980 (22123-01130) (Image 2)
118-83	January 7, 1981 (22177-01124) (Image 3)

In 1981, the only cloud-free Landsat data was 118-83, October 22 (Image 4).

To identify sandblast areas and to assist in the development of appropriate signatures, the aerial photography and a band 4, 5 and 7 colour composite of Image 2 were visually compared. Separate training sites for clay pans and uncleared land were defined for use in classification of the Landsat data.

By using a modified parallelepiped classification procedure (Honey et al., 1974) on a digital interactive analysis system, themes for sandblast areas, clay pans and land not in production (uncleared farm lands, reserves, etc.) were developed. Training sites were first established and then the themes tested over larger areas. The areas unclassified represented an estimate of the land used in agricultural production. A percentage of sandblast damage in the production areas could then be calculated.

Four band radiance statistics were computed for each training site on Image 2, the reference image. The upper and lower boundaries of the signatures were defined by computing two standard deviations either side of the mean reflective values. Similar themes were developed for Image 1, and a theme representing regrowth on sandblast areas was produced for Image 3.

The next phase involved rectification of the Landsat data to permit correlation with existing Australian Map Grid (AMG) cadastral map sheets, and for registration of temporal scenes. Some 20 identifiable ground control points were selected over the study for which both AMG and pixel co-ordinates were computed. A subsequent least square adjustment resulted in a mean error of 67 m.

Data correction using the transformation co-efficients was undertaken on Image 2 using a cubic convolution resampling technique to a 50 m^2 pixel. This resolution was adopted as it corresponds to the 50 micron raster of the Photomation image generating equipment operated by the Department of Lands and Surveys. A corrected and classified sub-scene of Image 2 was produced as a base for future studies.

The identical sub-scene on Image 4 was similarly processed to permit visual assessment and comparison of 1980 and 1981 sandblast areas.

4. RESULTS

The areas classified are quantified in Table I, where data from the 1980 Landsat images are compared. Due to the limitations of the visual display unit, each image was divided into four 512 by 512 pixel sub-scenes. These were registered visually and classification statistics tabulated.

It was found that Image 2 themes were significantly underclassifying due mainly to variations in soil reflection, so buffer classes were used. These were based on visual interpretation of the November aerial photography. Similar anomalies occurred with uncleared areas. The importance of association in identifying sandblast areas has also been reported for high level aerial photography (Fryrear and Wiegand, 1974). A total of nine signatures were necessary to achieve satisfactory correlation with the aerial photography.

Image 1 was processed in a similar manner based on the knowledge gained in interpreting Image 2. Only six themes were required to cover the uncleared and sandblast areas.

In Image 1 some confusion with sandblast and ploughed paddocks occurred, however, it was possible to separate visually, based on shape and association. Claypans in Image 1 were generally moist and could be easily separated spectrally from the higher reflecting sandblast areas. This was not the case in Image 2 because the majority of clay pans had dried. Large areas of salt lakes could not be distinguished from stubble paddocks on any of the images analysed.

Ground inspection including discussions with local farmers confirmed those areas classified as sandblast. No gross discrepancies were evident.

Comparisons of sandblasted areas in Images 1 and 2 showed that the affected areas could increase due to the deposition of sand in adjacent paddocks. Reference to the aerial photography confirmed this conclusion. The frequent north west winds produced stripped paddock areas with an irregular moving sand face to the south east.

Image 3 could not satisfactorily be used to identify sandblast areas because all crop areas had been harvested and only stubble paddocks remained with no growth. The predominant vegetation response proved to be from uncleared native and river vegetation; crop lands reflected brightly in all Landsat bands. The exception proved to be stabilised sandblast areas where regrowth contrasted strongly with surrounding stubble and affected country. An estimate of recovered land could be readily made from Image 3 (Table II).

The classification of sandblast was checked with aerial photography by visual interpolation and grid area estimate. Over a total area of 7 370 hectares the Landsat classification produced 355 hectares of sandblast, the aerial photography 348 hectares. Individual areas coincided.

Sandblast areas in Image 1 are consistently higher than Image 2, possibly indicating mis-classification of freshly seeded paddocks on Image 1.

The 'total production' and 'total non-production' areas vary between Images 1 and 2 due to claypan discrimination problems and spectral similarity between certain fireburn-affected native vegetation and stubble paddocks.

The comparison of sandblast events (Table III) showed that the 1980 problem was more severe than in 1981. The total study area of 1980 (Image 2) could not be used because of missing data in the 1981 image. However in a coinciding subscene the 1981 sandblast damage was only 60 per cent of that of the previous year. By subtraction of Image 4 from Image 2, 1 933 ha of sandblast occurred in different areas from that in the previous year. Therefore with 663 hectares recurring as sandblast, 1 590 hectares of the 1980 problem area had not been stabilised in 1981.

Further, analysis of the precision processed sub-scenes of Image 2 and 4 resulted in a mean relative accuracy approaching one pixel when comparing one image to the other (assessment of some 50 identifiable points), and 70 metre mean absolute error when each image was compared with the AMG. This test confirmed that absolute registration was possible to an accuracy where other data sets, such as soils, contour and cadastral could be integrated. High relative accuracy improved confidence in temporal changes observed.

The cost advantages involved with the use of satellite data in such a study are clearly shown in Table IV. The turn-around time from the date of sandblast damage to processed data is potentially much less for the satellite image but is limited by the availability of cloud-free images and fixed orbit dates.

5. *DISCUSSION*

While Landsat can provide regular coverage of widespread areas, sandblasting is an irregular occurrence associated mostly with winter conditions, consequently cloud can be a problem. This proved to be the case for 1980 where the optimum mid-growing season scene (late September/October) were cloud-affected. In 1981, the October scene (Image 4), sandblast areas were readily discernible, with little confusion.

The obvious visual appearance of sandblasting by its shape and tone could not always be defined spectrally using this classification method. A combination of local knowledge, aerial photography and interactive digital analysis proved most effective. Quantification for the affected area was easily performed on the digital data once themes were developed.

Cultivation and rehabilitation of affected areas and regrowth on soils could change the area of apparent sandblast between multi-date images. The late sown crops affected the estimates.

Signatures developed are unique to each scene and area. Themes could not be easily transported due to atmospheric effects and, more importantly, the difference in soil types as noted by other researchers (Cipra et al., 1980). The importance of generating a reliable data base cannot be overemphasised. Landsat in a precision processed form is a natural reference frame to which later images can be registered and compared. Multi-date images permit a history to be built up, improving spectral classifications.

The data base will identify recurrent erosion areas and point to possible changes in farming practices to maintain and preserve this resource. In a total production area of 303 000 hectares it was estimated that a loss of $750 000 occurred. Preventive measures taken with reference to an accurate historical data base could minimise this loss.

The use of satellite imagery and digital interactive system, has a great cost advantage over conventional aerial photography based systems. This allows for much wider coverage of the study, which would previously have proved impossible because of budgetary and priority constraints.

Landsat derived information on sandblast areas will complement existing research into the economic effects of certain management practices and allow acceptable farming strategies to be implemented.

REFERENCES

Beard, J.S. (1981). Swan 1:1 000 000 vegetation sheet: explanatory notes to sheet 7, "The vegetation of the Swan area". University of W.A. press, 1981, 222 p.

Birch, P.B. (1976). W.A. Department of Agriculture. Personal communication.

Cipra, J.E., Franzmeier, D.P., Bauer, M.E. and Boyd P.K. (1980).

Soil Sci. Soc. Am. J. 44:80-84.

Fryrear, D.W. and Wiegard, C.L. (1974). Trans ASAE 17:892-894.

Gorddard, B.J., Humphry, M. and Carter, D.J. (1982). Jerramungup Soil Erosion Survey, Western Australian Dept. Agric. publication (in press).

Honey, F.R., Prelat, A. and Lyon, R.J.P. (1974). Stansort, Stanford. Remote Sensing Laboratory Pattern Recognition and Classification System. Proc. Ninth Int. Symp. on Remote Sensing of Environment, Ann Arbor, Michigan, April 15-19, 1974, p. 897.

Northcote, K.H., Hubble, G.D., Isbell, R.F., Thompson, C.H. and Bettenay, E. (1975). 'A description of Australian soils', CSIRO, Australia.

Seevers, P.M., Lewis, D.T. and Drew, J.V. (1975). J. Soil Water Cons. 30:181-183.

Thom, R., Hickman, A.H. and Chin, R.J. (1981). Newdegate Sheet SI 50-8, Geological Surveys, Western Australia.

Table I. Statistics of sandblast damage, production area and total area in the study of wind erosion on the south coast of Western Australia in 1980/81

Image date	Sandblast area (ha)	Total non-production area (ha)	Total production area (ha)	% sandblast in production area
1. August 15, 1980	6 636	168 932	302 928	2.2
2. November 14, 1980	5 041	168 494	303 365	1.7

Table II. Area of regrowth on sandblasted areas over the summer period (non-cropping season)

Image date	Area of regrowth (ha)	% of Image 2 sandblast as regrowth
January 7, 1981	194	7.4

Table III. Comparisons of 1980 and 1981 sandblast statistics

Image date	Area of sandblast	% of total land
November 14, 1980* (Image 2)	4 292	1.6
October 22, 1981* (Image 4)	2 596	1.0

* The whole scene of Image 2 was not used, but the two images coincided, with a total of 64 000 ha analysed.

Table IV. Comparison of costs involved for an inventory of sandblast damage between satellite data and conventional aerial surveying techniques based on a 1:250 000 map sheet

	$A
A. Conventional	
a. 1:50 000 B and W aerial photography	13 000
b. Interpretation 15 man days @ $250/day	3 750
c. Transfer to base sheets 2.5 days @ $150/day	375
d. Digitising 2.5 days @ $150/day	375
e. Plotting areas	180
f. Field checking 4 days @ $250/day	1 000
Man days 25	18 680
B. Satellite MSS data (Landsat)	
a. Computer compatible tapes	330
b. Selection of field training sites	1 000
c. Analysis (20 hour) and operator	2 750
d. Photographic output	1 000
e. Verification	1 000
Man days 15	6 080

CROP IDENTIFICATION AND AREA ESTIMATION IN THE SOUTHERN PART OF THE PROVINCE OF BUENOS AIRES - ARGENTINA - USING LANDSAT DATA

Francisco V. REDONDO

Comisión Nacional de
Investigaciones Espaciales
Buenos Aires, Argentina

ABSTRACT

The feasibility of MSS LANDSAT data analysis for crop recognition and area estimation was tested in a pilot area in Argentina, as an attempt to improve the current conventional crop production forecasting method. The main crop in Argentina is wheat and the study area was the Partido of Tres Arroyos. Two contiguous crop years were considered; LANDSAT and ground data were used and two methods (total coverage and sample estimation) were tested.

Results show that oat is an important confusion crop but when considering them together as cereals the identification accuracy level is high.

1. INTRODUCTION

In Argentina, the crop production forecasting system is based on subjective methods. Few enumerators and economic restrictions multiply the problem. Different attempts to improve the system are being done.

The use of satellite data was proposed in order to achieve an objective, timely, reliable and economic area estimation procedure.

The objective of the study was to establish the feasibility of the LANDSAT data digital analysis in identifying wheat and small grains, and its area estimation on a typical wheat production area in Argentina during two contiguous crop years, 1980/81 and 1981/82.

2. STUDY AREA

The wheat production area in Argentina is very large both in N-S and E-W directions. It includes different soil conditions and climatic characteristics. One of the most important subregions is the Southern part of the Province of Buenos Aires. The study was carried out in that area considering the administrative boundaries of the Partido of Tres Arroyos, Map 1. This area has an appropriated infrastructure for crop production, storing and transportation, including the Port of Bahía Blanca.

The main winter crop is wheat, and others like oat, flax, barley are present in a very small proportion. In Summer crops, sunflower is the most important being this one the second crop after wheat in planted area (30% of the wheat area).

The total area of the Partido is 586,000 hectares and from a LANDSAT image stratification, a total agriculture land of 556,000 hectares was obtained. This administrative area represents the minimum area for which official crop statistics are published few months after harvesting (1).

3. GROUND DATA ACQUISITION

The ground data was gathered from sample segments belonging to a sample design developed for this area by the Secretaría de Agricultura y Ganadería de la Nación (S.E.A.G.). Eight random segments were used. Each sample of a 2000 average hectareage includes approximately 27 fields (27 observations). The field size varies from 50 to 100 hectares.

The segments were located on a detailed topographic 1:50,000-scale map made by the Instituto Geográfico Militar (I.G.M.). Aerial photographs of those segments were taken both in black and white and color infrared, in order to have a very clear updated map to be used by enumerators in the field.

The crop calendar for this area is complex. Wheat is planted in a three and a half month period (from May to August) depending on the crop variety cycle length; the harvest period is December and January. Other winter (confusion) crops (e.g.: oat, barley, etc.) have more or less the some growing cycle when they are planted for grain harvesting, but the cycle begins in March-April when they have double purpose (crop and grazing).

The ground data collection work was carried out during the first two weeks of November of 1980 and of 1981, during the post-heading wheat stage, Graphic 1.

4. LANDSAT DATA

The Partido of Tres Arroyos is fully covered by only one LANDSAT frame, code number 241-087. Different LANDSAT CCTs were used during this work with a 0% cloud cover and good transmission quality. Only two free-cloud LANDSAT acquisitions during the wheat growing season in both 1981 and 1982 crop year were available. The LANDSAT data dated October 24, 1980; November 11, 1980; August 8, 1981 and November 6, 1981, were analysed.

The satellite information was received and processed by the Mar Chiquita Receiving Station and Processing Center, both belonging to the Comisión Nacional de Investigaciones Espaciales, C.N.I.E.

5. DIGITAL MULTISPECTRAL ANALYSIS

5.1. 1980/81 Crop Year Analysis

The analysis of ground and LANDSAT data established six main different land uses: wheat, oat, artificial pastures (for grazing), natural ranges, fallow and miscellaneous (dunes, cities, water bodies, roads, etc.). For each one of these classes two files, A and B, were created with the respective LANDSAT data: all the information available in A or B file was used alternatively as a training file to generate a signature file for the maximum likelihood classifier and as a test file for the final result adjustment.

Two LANDSAT acquisition dates were compared within the wheat growing period trying to find the best moment for discrimination between land uses.

In order to carry out classifications and estimations only within the Partido of Tres Arroyos, a masked subimage was developed using maps and visual delineation of the boundaries. Then, a complete coverage automatic classification was carried out.

This analysis was done at the Canadian Centre for Remote Sensing (CCRS)

using the CIAS equipment and at Dipix Ltd., Ottawa, Canada, using the DIPIX analysis system.

5.2. <u>1981/82 Crop Year Analysis</u>

During this analysis some other approaches were tested:

- Both principal land use classes, wheat and oat, were divided into subclasses: 5 for wheat and 3 for oat, trying to define some pure and confussion subclasses for these crops. The artificial pasture class had 3 subclasses, and a new non-crop unit was included: weed fields.

- The signature file was generated in a different way: all the ground segment were used to provide training data but only few fields of each class per segment were chose to create the maximum likelihood classifier signature file.

  The whole set of fields per segment was used like a test file in order to develop the confusion matrix, so ground data was used in a more efficient way.

- The final estimation was done throughout a total automatic pixel classification coverage of the Partido (same 1980/81). At the same time, a sample estimation was attempted by classifying randomly chosen sample segments, (2). Fourteen (14) sample segments of a 10,000 hectare size from a sample design specifically done for this Partido, were classified.

- All the analysis procedures and final calculations were done in the interactive analysis system PI-DARG. This is a software package developed by CNIE's professionals and implemented in a COMTAL VISION ONE interactive system with a CPU PDP 11/34, (3). This package has all the necessary programs for a complete analysis of LANDSAT data for agriculture studies.

6. RESULTS

6.1. <u>1980/1981 Crop Year</u>

6.1.1. <u>Crop Identification</u>

The spectral identification of the different land uses was done with a high accuracy and reliability level bearing in mind land uses as fallow, miscellaneous, some pastures and crop land. Table I.

Some problems appeared when identifying wheat from oat in both October and November dates. A high confusion level existed (20-30%): due to this reason both crops (wheat and oat) were considered as one class, called cereals. This approach achieved good result in identification and classification accuracy. Table II.

This cereal class is acceptable because oat only represents a 10-15% of the wheat cultivated area.

6.1.2. <u>Different dates</u>

The analysis and test carried out on October 24 LANDSAT data resulted with a 98.16% of accuracy when classifying training file (A), and 87.65% when classifying test file (B) (Blind sites). The same procedure used on November 11 LANDSAT data had an accuracy of 97.6% and 79.15%. No differences are detected between the identification and classification accuracy when the training site A is classified but a slight difference (perhaps important to be considered) is shown when the test file B is used. The October 24 data turned to be more adequate for classifying cereals than the November data.

6.1.3. <u>Final figures</u>

The final result was obtained by classifying all the pixels of the sub-image "Partido de Tres Arroyos". A correction was made using the confussion matrix coefficients. The total cereal hectareage was 201,845 and 208,321 through October 24 and November 11 LANDSAT data analysis. The official figures are published 3-4 months after harvest and are corrected with a sample survey and commercialized volume. Wheat plus oat totalized 203,000 hectares. Table III.

6.2. 1981/82 Crop Year

6.2.1. Crop identification

In some cases, the division of wheat and oat in subclasses resulted appropriated for defining pure classes, but in others there was no need for such sub division. Table IV.

The confusion problem appeared once more when identifying wheat from oat on LANDSAT data from November 6, and again the cereal class was created achieving a high accuracy result level. Table V.

6.2.2. Total coverage and sample classification approach

The total coverage classification was developed and the final result of cereal pixels were adjusted with the confusion matrix coefficient. November 6 LANDSAT data gave 247,000 hectares and the official number was 245,000 hectares.

The sample segment analysis and classification was carried out with the same classifier developed for the total coverage approach. The result of the analysis is given in Table VI, where the estimator of the mean ratio is calculated.

A linear regression analysis was carried out with the "Cereal area" LANDSAT data and the ground date for each segment, Graphic 2, in order to have a measurement of the error and an adjustment for the ratio estimator. The obtained equation: $y = 11.4578 + 0{,}84346X$ and the ratio estimator was adjusted and the final estimation was 45.63% of cereals. Graphic 2 and Table III.

Table VI shows an important variance in the variable "percent of cereals". A stratification based on soil capability and crop intensity is recommended in order to reduce the variance and improve the reliability of the estimator.

A hypothes s test was conducted in order to evaluate if the differences between means and variances observed in ground data and calculated through LANDSAT analysis were significant.

Mean Comparison

$$Ho = u_L \text{ LANDSAT data} = u_G \text{ ground data} = \frac{\overline{XL} - \overline{XG} - 0}{\sqrt{\frac{S_L^2(m-1) + S_L^2(m-1)}{2(m-1)}}} = 0.19078$$

and, t value for $P = 0.95$; 12 df = 1.782

Variance Comparison

$$Ho = S_L^2 \text{ LANDSAT data} = S_T^2 \text{ ground data} \qquad F = \frac{S^2_L}{S^2_T} = 1.13170$$

and, $P = 0.95$; 6.6df = 4.28

in both cases the Ho is not rejected at a significat level of 5%.

Although, seven samples are not large enough observations for this kind of statistical analysis, the conclusions are considered valid as orientative start ing point.

7. CONCLUSIONS

- Cereal identification and area estimation can be done using remote sensing information (LANDSAT data in this case) and ground data of some sample areas. The results were consistent with both crop years.

- The accuracy achieved is considered good and satisfactory. In addition, the opportunity of these results is very important: the estimation through LANDSAT data was achieved two months before harvest and these values compared with the official figures from the harvested area published six months later, had no more difference than 3,5%.

- The total coverage approach gave good results but perhaps is not adequate for larger areas. The sample approach showed a good ratio estimator but it has a high variance. Stratification should be done in order to reduce the variance and to increase the reliability of the sample estimator. In addition, to work with samples allows to have more probability of cloud free LANDSAT coverage than in large areas.

- There were some problems when identifying wheat from oat with LANDSAT data. The reason is that both have almost the same growing cycle. Oat as confusion crop is very difficult to eliminate. More research has to be done in multitemporal analysis in order to improve the discrimination. In this study this confusion is not very important because oat area is only 10-15% of wheat area but in some other regions the problem could turn into a real one.

- Considering the available facilities at the Comisión Nacional de Investigaciones Espaciales (CNIE) (LANDSAT Receiving Station, Processing Center and Analysis Center) crop identification and area estimation through LANDSAT data can be analysed in an operational status.

8. REFERENCES

1) E.A.G. Monthly Publication - Secretaría de Agricultura y Ganadería de La Nación.

2) CAPPELLETTI, Carlos A.; Crop Estimation through Remote Sensing Techniques. Report on activities connected with multistage sample design and statistic methodology. FAO-UNDP/ARG/78/016.

3) FERNANDEZ, Severino; CAMPI, Marcelo; A System for Digital Image Processing developed at CNIE. Latin American Satellite Remote Sensing User's Meeting. Brazil, 1981.

4) CRAIG, M; SIGMAN, R.; CARDENAS, M.; Area Estimates by LANDSAT: Kansas 1976 Winter Wheat. SRD, ESCS, USDA, Washington D.C.

5) SCHUBERT, Jane S.; The Canada Land Inventory Program. Environmental Canada. Lands Directorate.

6) RYERSON, R.A.; MOSHER, P.; WALLEN, V.R.; STEWART, N.E.; Three Tests of Agricultural Remote Sensing for Crop Inventory in Eastern Canada. Vth.Canadian Symposium on Remote Sensing, 1978.

7) BROWN, R.; AHERN, F.; et all; Rapeseed: Guidelines for Operational Monitoring. VIth Canadian Symposium on Remote Sensing, 1980.

9. ACKNOWLEDGEMENT

I wish to acknowledge Dr. Carlos Lac Prugent for his statistical advice.

OCT. 80/81	WHEAT	OAT	PASTURE	RANGE	FALLOW
WHEAT	689	205	9	1	0
OAT	218	327	18	0	0
PASTURE	4	8	375	13	0
RANGE	2	3	18	146	3
FALLOW	1	11	0	1	646
MISCEL.	0	0	0	0	0
TOTAL	959	569	440	171	656

Table I. Confusion Matrix

OCT. 80/81	CEREALS	OTHERS	TOTAL
CEREALS	1439	27	1466
OTHERS	17	392	410
NON-CLASS	72	23	

Table II A. Confusion Matrix (on training file A)

OCT. 80/81	CEREALS	OTHERS	TOTAL
CEREALS	345	50	405
OTHERS	17	115	132
NON-CLASS	27	11	

Table II B. Confusion Matrix (on test file B)

	FINAL ESTIMATION (LANDSAT data)	OFFICIAL FIGURES (Conventional)	DIFFERENCE
TOTAL COVERAGE 80/81			
-LANDSAT data OCT.24	201,845	203,000	-0.57%
-LANDSAT data NOV.11	208,321	203,000	+2.62%
TOTAL COVERAGE 81/82			
-LANDSAT data NOV.06	247,000	245,000	+0.81%
SAMPLE ANALYSIS 81/82			
-LANDSAT data NOV. 06			
(45.63%)	253,540	245,000	+3.48%
VARIATION (%)			
80/81 - 81/82	+22	+20	+2%

Table III. Final Estimations (ha.)

NOV. 81/82	W_1	W_2	W_3	W_4	W_5	O_1	O_2	O_3
$Wheat_1$	77	1	4	8	0	0	2	6
$Wheat_2$	0	74	2	0	0	3	9	0
$Wheat_3$	3	8	35	19	0	9	0	24
$Wheat_4$	1	1	32	37	0	1	0	28
$Wheat_5$	0	0	0	0	95	0	4	0
Oat_1	0	1	1	0	0	92	0	0
Oat_2	0	11	0	0	0	0	85	0
Oat_3	0	0	27	0	0	0	0	73

Table IV. Confusion Matrix
Small Grains

NOV. 81/82	C	P_1	P_2	P_3	We_1	R	F
Cereals	97	0.25	2.45	0	0	0	0.13
$Pasture_1$	0	94	0	6	0	0	0
$Pasture_2$	6	0	91	0	0	1	0
$Pasture_3$	0	7	0	93	0	0	0
Weeds	0	0	0	0	95	4	3
Range	0	0	2	0	0	97	0
Fallow	1	0	0	0	6	0.5	91

Table V. Confusion Matrix (Cereals)

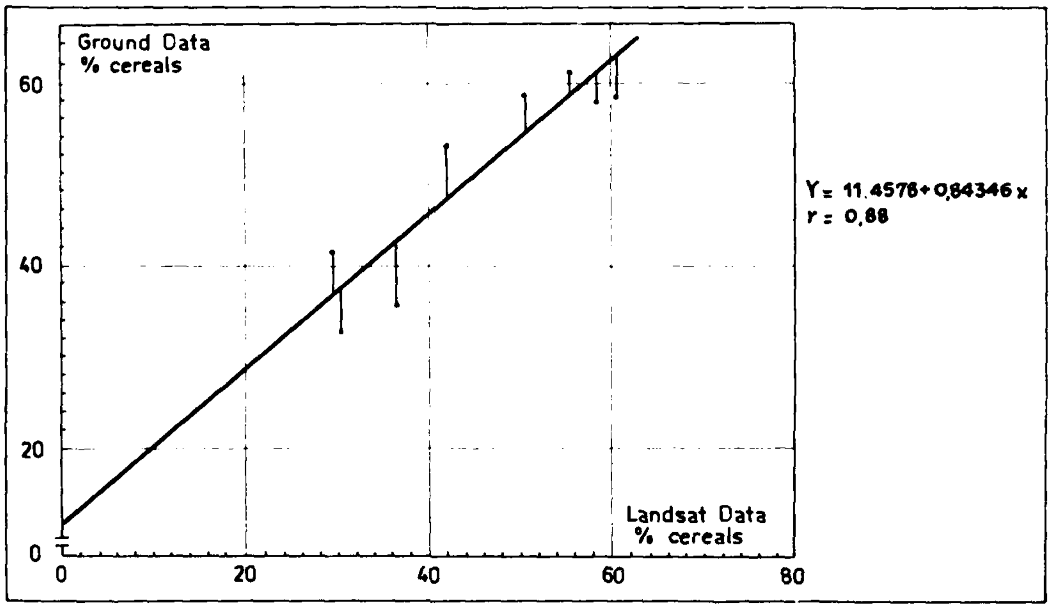

Graphic 2. Linear Regression

Sample Segment	Classif.Result Percent of cereals	Sample Segment	Classif.Result Percent of cereals
1	33.39	9	37.61
2	46.12	10	27.23
3	44.24	11	46.24
4	29.53	12	37.61
5	42.85	13	35.82
6	50.06	14	50.47
7	39.06	X=40.68%	
8	49.42	S= 7.55 (standard deviation of the sample)	

Table VI. Sample segment analysis

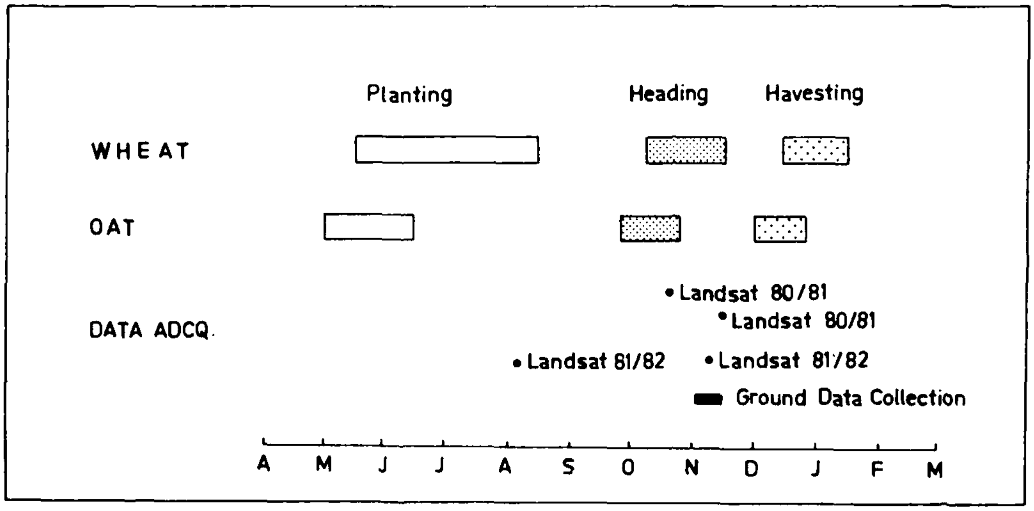

Grafic 1: Crop Calendar

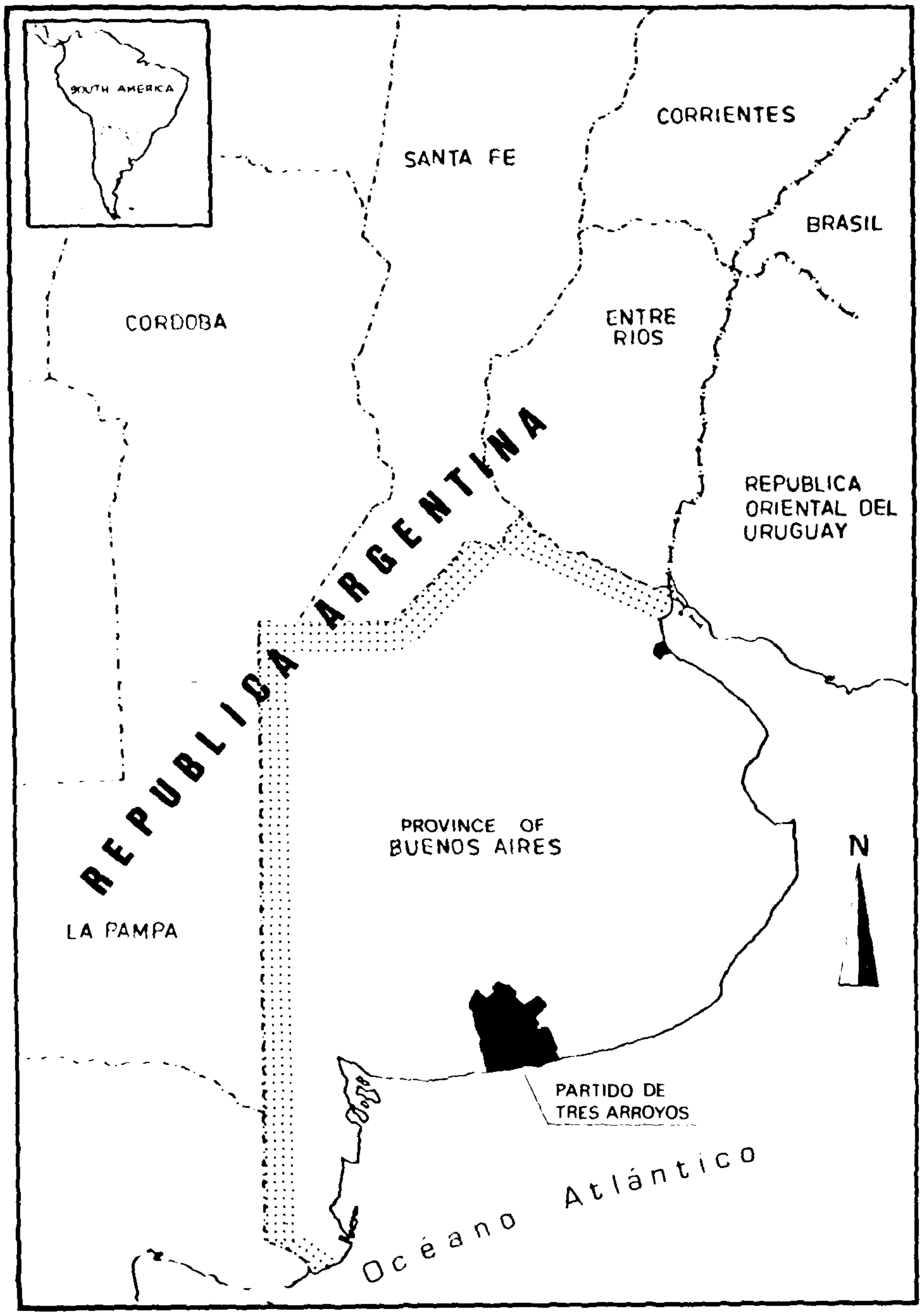

Map 1: Study Area

SOME USES OF REMOTE SENSING FOR URBAN PLANNING

Maria de Lourdes N. de Oliveira
Maria Suelena S. Barros

Instituto de Pesquisas Espaciais
Conselho Nacional de Desenvolvimento Científico e Tecnólogico
Sao José dos Campos, SP, Brazil

SUMMARY

Urban planning consists of a decision making process which requires, as a support, a system for delineating and providing useful information. This paper describes some experiences on urban planning on the Systems Engineering Division of the Institute for Space Research - INPE, using airborne remote sensing techniques to provide information about urban areas.

The main objective is to show the use of remote sensing data in planning networks of social use equipments and as input for implementing mathematical models. The mathematical models considers the following aspects of urban planning: urban quality analysis, allocation of urban population to hospitals, planning of large telephone networks, identification of priority areas for Public Health Care improvements, urban performance analysis, projection and location of the urban population.

Remote sensing techniques are particularly useful in Brazil since urban land in its cities is very not homogeneous. The social, economical and cultural disparity among the human groups, resulting mainly from the existing social organization, shows up also in land aspects. Through urban tissue analysis using air photos at an approximated scale of 1:1000, minor residential areas (homogeneous zones) and their physical aspects are identified, and different resident groups characteristics are indirectly recognized. Remote sensing has been a valuable instrument in Brazil, reducing the necessity of the expensive surveys, either complete or by sampling.

Sao José dos Campos, Sao Paulo, Brazil, with 300,000 inhabitants, has been used as the test area.

AD-A134 719 PAPERS SELECTED FOR PRESENTATION AT THE INTERNATIONAL SYMPOSIUM ON REMOTE..(U) ENVIRONMENTAL RESEARCH INST OF MICHIGAN ANN ARBOR JUN 82 4/6

UNCLASSIFIED F/G 14/5 NL

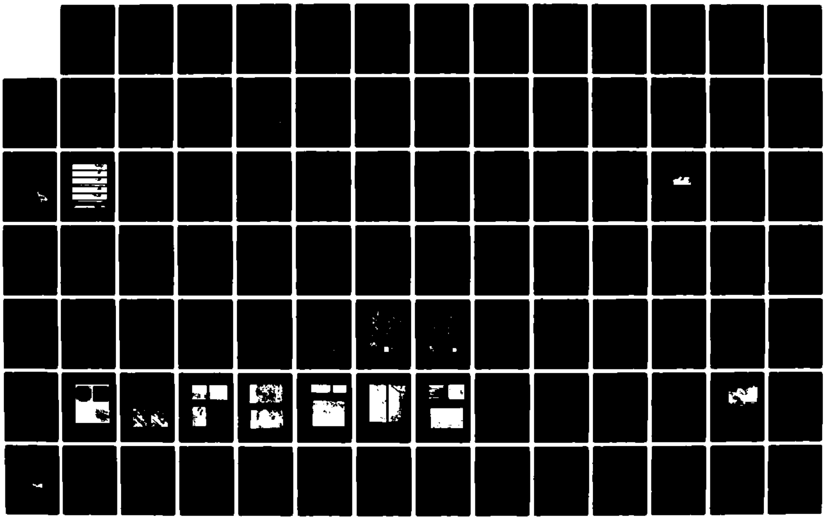

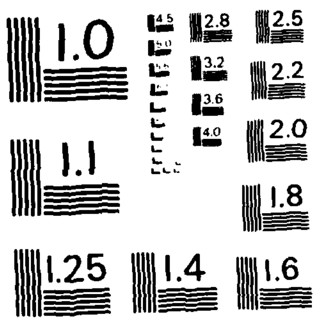

MICROCOPY RESOLUTION TEST CHART

NATIONAL BUREAU OF STANDARDS-1963-A

/

VISUAL AND COMPUTER-ASSISTED TECHNIQUES USED IN LANDSAT MSS DATA FOR GEOLOGICAL RECONNAISSANCE IN AMAZONAS REGION

Chan Chiang Liu

Instituto de Pesquisas Espaciais
Conselho Nacional de Desenvolvimento Científico e Tecnológico
São José dos Campos, SP, Brazil

SUMMARY

The area selected for study is situated in the southern margin of the Amazonas Syneclise, enclosed approximately by 4°00' - 5°50' south latitudes and 55°40' - 57°20' west longitudes and covers approximately 11,200 km². In this tropical terrain with dense virgin jungle coverage, conventional field mapping is almost inaccessible for the most part, and mapping a broad region is also questionable. The temporal and spectral attributes of the Landsat images are barely availble in this region. Therefore, enhancement computer techniques including contrast stretch and digital filtering were applied to the digital MSS Landsat data in order to facilitate the visual analysis and increase the quantity of information to be extracted. These techniques tend to emphasize subtle scene features such as surface texture, topographic elements, etc., that are not perceived in original raw data. The synoptic view provided by Landsat MSS imagery produced different photographic mapping units and structural lineaments. Drainage patterns, landforms, surface textures and their continuities were mapped and a division of mapping units along the Tapajós River, which runs along the southern and southeastern margin of the study area, was performed. The assumption that image signatures and topographic lineaments represent directly or indirectly bedrock conditions led to the designation of: (1) three units of Precambrian rock, (2) three Mesozoic sedimentary rock units and (3) two units of Tertiary sedimentary cover. Topographic lineaments were inferred to be bedrock fractures which may be significant in terms of regional tectonic studies. Field checking along the Trans-Amazon highway, which passes through all of the mapped units, was performed. The study revealed that computer-enhanced techniques can increase the quality of an image and is helpful for visual examination, and that geological mapping of hardly accessible terrain through the analysis and interpretation of Landsat imagery is practicable and may be the best way to establish preliminary geological information in a remote territory.

LANDSAT AND RADAR MAPPING OF INTRUSIVE ROCKS IN SE-BRAZIL

A.R. dos Santos, C.E. dos Anjos, J. C.Moreira, M.P.Barbosa and P.Veneziani
Instituto de Pesquisas Espaciais - INPE
Conselho Nacional de Desenvolvimento Científico e Tecnolóeico - CNPq
C.P. 515 - São José dos Campos - SP - Brazil

ABSTRACT

The objectives of this study were: 1) to study the feasibility to intrusive rock mapping and to establish criteria for regional geological mapping at the scale of 1:500,000 in polycyclic and polymetamorphic areas using Logic Method of photointerpretation of LANDSAT imagery and RADAR from RADAMBRASIL project. 2) to evaluate the spectral behavior of intrusive rocks, using the Interactive Multispectral Image Analysis System (Image -100). The region of Campos (city) in northern Rio de Janeiro State was selected as the study area and digital imagery processing and pattern recognition techniques were applied. Various maps at the 1:250,000 scale were obtained to evaluate the results of automatic data processing.

1. INTRODUCTION

The main objective of this research was to study the viability of identifying intrusive rocks and to establish criteria for regional geological mapping in polycyclic and polymetamorphic areas by meas of visual interpretation of small scale remotely sensed data. It will be also evaluated the spectral behavior of intrusive rocks using the IMAGE-100 System.

The Logical Method of Photointerpretation (Guy, 1966) developped for aerial phothograph was adapted to data acquired from small images such as: MSS/LANDSAT (1:250,000 and 1:500,000) and RADAMBRASIL mosaics (1:250,000). Computer compatible tapes were used for automatic analysis.

2. METHODOLOGY FOR VISUAL INTERPRETATION

To adapt the Logical Method the following aspects had to be taken into account: 1 - the products used in this work (LANDSAT and RADAR data) present scales smaller than usual scales of aerial photography; 2 - These products also present poor spatial resolution and lack of stereoscopic viewing. However, in spite of those limiting factors, the adaptation is possible because MSS and RADAR images are subjected to the same factor which control photrographic texture.

The Logical Method is based upon the following rules:

1) Photographic lecture - it means the recognition and identification of some features on photographic image with corresponding objects;
2) Photographic analysis - it means the analysis of textural photographic elements and shape properties on photographic image so as define homologous areas;
3) Photographic interpretation - it means the indutive and dedutive processing of the data so as to identify their geological meaning.

Texture, structure and shape their main elements for photographic interpretation and they can be related to drainage network properties and relief texture properties.

Textural density, alignments, lineaments, assymetric shape, negative and positive ruptures (for relief), drainage direction and drainge uniformity are the main drainage and relief properties which can be evaluated using LANDSAT and RADAR products.

Shadow effects and tone are also of primary importance for data acquirement since the terrain morphology can be expressed by shadowing effect. This effect also enhaces slope ruptures and relief breakings expressing also the textural density of relief and compensating the lack stereoscopic viewing.

By means of those textural properties, homologous zones can be defined. The limits of these zones can be sharp or difuse and not necessarily coincident with geological contacts. Those textural properties also permit to define the degree of relief and drainage organization and therefore give information about anisotropy of rock material. These properties can indicate the occurrence of faultings and foldings by means of density of alignments and relief and drainage lineaments per unit of area.

The degree of asymmetry (for relief and drainage network) can give information about the dip direction of plane feature and the degree of drainage uniformity so as to deduce the material homogeneity.

The development of this work followed two phases. In the first one, the specific objective was to explore the high density of linear features observed on remotely sensed data and to correlate them to geological structure.

To reach this objective, maps at the scale of 1:250,000 were obtained having the following information:

1) Traces of fault - linear features derived from alignment of drainage or relief texture elements. These features presented dimensions larger than 3.5 km of extension;

2) Traces of fracture - Lines representing zones of fracture concentration. Linear features derived from lineaments of drainage and relief textural elements, presented dimension less than 3,5 km of extension;

3) Traces of foliation - Linear features derived from lineaments cf drainage and relief textural elements;

4) Circular structures - Linear features derived from drainage curvature (classic anelar pattern) radial drainage, and curvature of the relief lineaments.

This phase was complemented in thirty days of field work during which circular structures were checked.

In the second phase of this study the data from field work, bibliography and photointerpretation were combined to establish the relationship geology an intrusive rock occurence.

This phase followed the following steps:

1) Drainage Network Analysis - this analysis gives information about the location and extension of surface material and its control factors; relative permeability, degree of material uniformity; local variations; slope extension; degree of dissection; nature of rock and dip of plane features.

2) Relief Analysis - this analysis gives information about the shape of the geological units present on the surface (landform); the relative degree of resistance to erosion of different materials; degree of influence of structure over the relief. It allows also to infere about the rock nature and plane feature dip. Morphogenetic factors (climate, recent tectonic, etc.), lithological factors (resistance to erosion, permeability, plasticity, anisotropy) and deforming factors (faults and foldings) which control the image texture are directly related to the textural properties of the relief and drainage network.

3) Grey Level Analysis - this analysis allowed to identify great areas whose soil-vegetation-rock-water association could represent regional geological units. The analysis was made primarily using LANDSAT/MSS data.

4) Photointerpretation - photointerpretation models for drainage network and relief were obtained during the analytical phase. These data were interated into 1:250,000 sheet and processed to determine their geological meaning.

The main differences between the results and other published maps were checked during ground observation and new maps were obtained: Photogeological Map with the ground data and bibliography at the scale 1:500,000.

5. DISCUSSION OF VISUAL ANALYSIS RESULTS

The area covered by this study is formed by metamorphic rocks of several ages and complex structures with lithological aspects deeply changed due to various geological events. There are also magmatic bodies with variable ages and composition as well as cenozoic sedimentary cover.

Figure 1 is a simplified map obtained from the maps made by the study of the Intrusive Rocks Project (Santos et al., 1982). The present paper is a summary of that project.

Due to the complex evolution of the area and the poor definition of its lithostratigraphic relationships, the authors decided to adapt Almeida et al., (1977) approach, which divides the precambrian area into structural provinces. These provinces are related to the great tecto--orogenic cycles affecting the area (Jequié - 2,800 my; Trans-Amazonian - 1,800 - 2,200 my; Uruaçuan - 900 - 1,400 my and Brazilian - 450 - 700 my). The area of occurrence of each cycle was tentatively defined for each geological province. Based upon those aspects lithological, dominance units were defined. It is important to emphasize that these units do not present stratigraphic connotation. The precambrian rocks were arranged as follows:

Mantiqueira Province

This unit can be divided into two great regions with particular evolution features.

1) Remobilized Basement - According several authors, this region includes rocks of Transamazonic age or older. These rocks were remobilized in the following tectonic events such as Brasilian Cycle which is the most important of them. The lithology is variable: heterogeneous and homogeneous migmatites (metatexites and diatexites) with different structures; gneiss; granitoid rocks; ectinitic rocks (metasediments); charnockitic rocks; enderbitic rocks; granulitic rocks; marbles, etc.

2) Southeast Folding Region (Almeida et al., 1976). This unit includes rocks of Brazilian age. The main lithologic types are ectinitic rocks (metasediments); heterogenous and homogeneous migmatites with different structural styles and belonging to a single cycle. It presents also gneiss and granitoid.

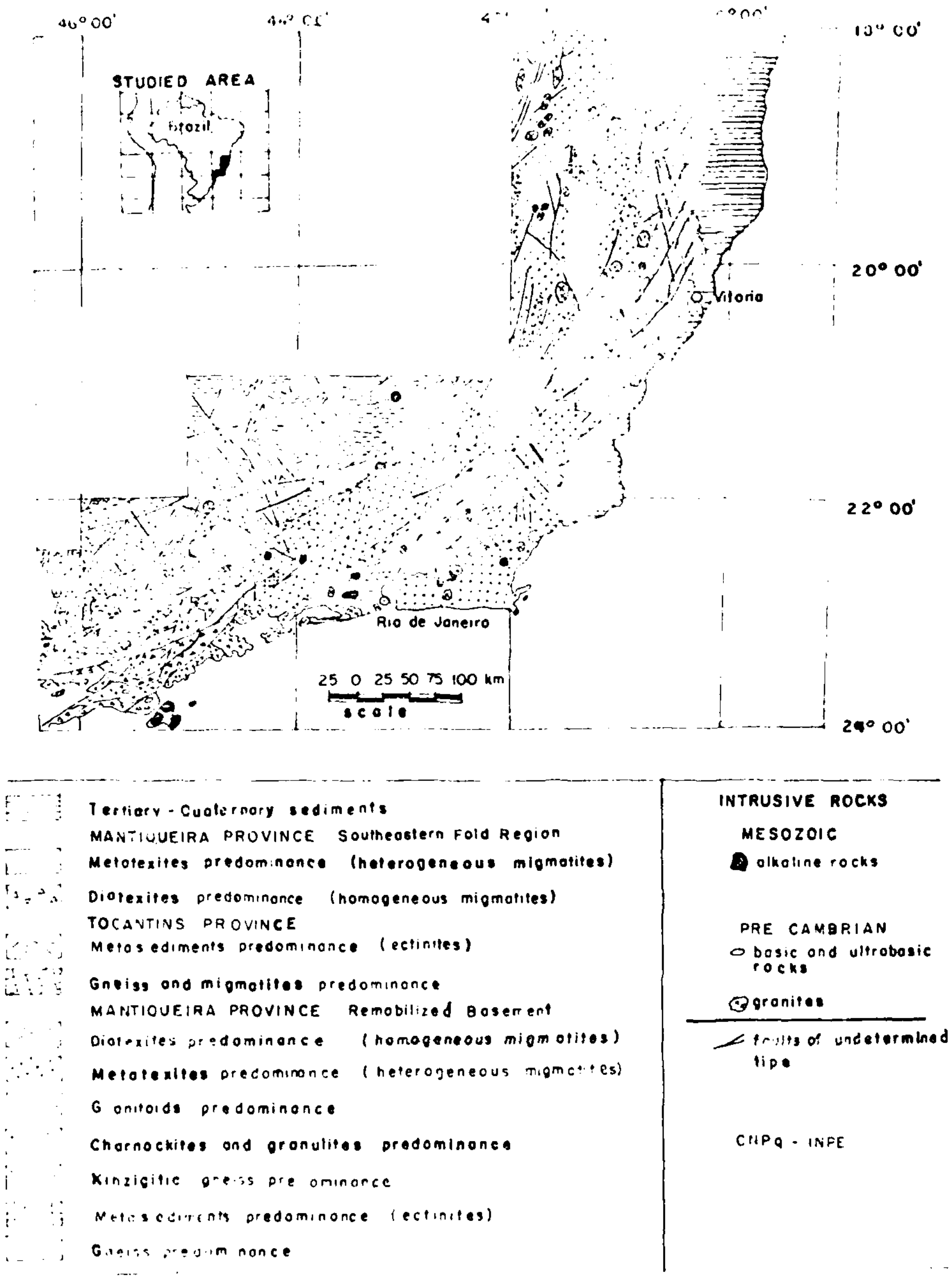

Figure 1. Simplified geologic map.

Tocantins Province

According to Almeida et al. (1973) this unit includes rocks of Uruaçuan and Brazilian cycles. As in the present work it was not possible to distinguish rocks belonging to those cycles, a non-stratigraphic classification was adopted. The main lithologies are: ectinitic rocks (metasediments) marbles; calc-silicate rocks, gneiss and migmatites of different structural styles.

The acid magnetic event with Brazilian age affected intensively all the study area and it is represented by body of different composition and size. In relation to the cycle, this event presents rocks varying from syntectonic to post-tectonic ages (Hasui et al., 1978; Wernick and Penalva, 1978). Part of the ultrabasic and intermediate rocks and all the alkaline bodies are related to tractional tectonic developed during Mesozoic-Cenozoic in the Brazilian Platform. The remaining ultrabasic and intermediate rocks can be related to Pre-cambrian age.

In relation to the geological structure, the southern part of the study area lying west of 42°00W, is characterized by wrench zone faults with ENE - WSW direction. This direction is imposed on different geological units and is associated to cataclastic rocks.

To the eastern side of 42°00' meridian, the great faults are bending to N up to 41°00'W. From Vitoria city towards NNW, there are faulting areas which occur without spatial continuity.

The most important secondary structural directions are the following: NE - SW; EW, N - S.

The foliation is oriented parallel to regional structural direction, presenting only local discodances.

Important and different types of folding structures there are in the area. In the southern part of the area these structures were classified as follows: flexure folds and shear folds (Donath and Parker, 1964 in Hasui, 1973). The largest folds with core area of granitoid bodies were named as "antiformes" by Hasui (1973).

The main areas related to tectonic cycles were identified taking into account the different phases of folding and also by literature reference.

In general way, it can be emphasized the following aspects:

Southeast Folding Region (Mantiqueira Province) - In this area two main folding phases and one secondary and local phase were observed. The second phase is responsible for alignments (EW to ENE - WSW) which can be observed on image.

Three folding phases were observed in the Remobilized Basement (Mantiqueira Province). The two latest phases are related to the two oldest phases of the Southeast Folding Region.

For the Tocantins Province it was observed two foldin phases. The most recent phase is responsible for folds which can be observed on the image. These folds are enhanced mainly when megafoldings are observed in supra-crustal metasediments involving thrusts with NE-SW vergence.

4. METHODOLOGY FOR AUTOMATIC ANALYSIS

As an example of automatic analysis the Campos area, in northern Rio de Janeiro State was selected. The main reason for selecting this area was the presence of the Itaoca granitic massif. Quaternary and Tertiary sediments as well as charnockitic and gneissic rocks of precambrian age are also found in the study area (Figure 2). Topographic enhancement of Itaoca massif makes the visual interpretation easier.

To proceed the spectral discrimination of the granitic massif, the following algorithms were used: single cell signature, grey level slicer, MAXVER System, K-Means algorithm and Spatial Features Acquisition.

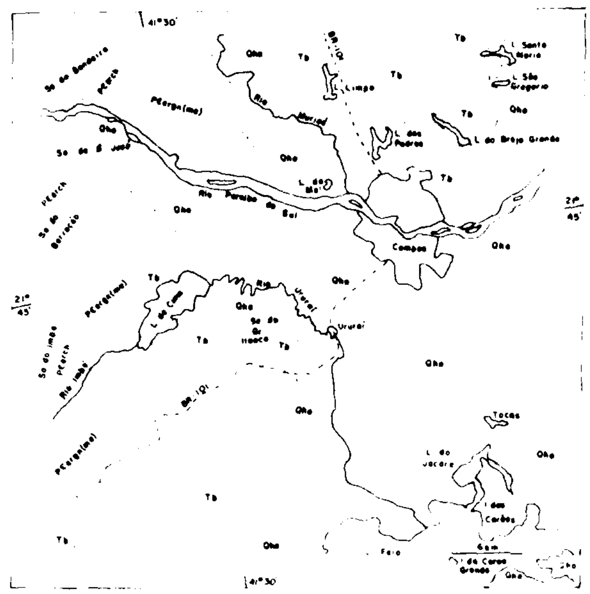

Figure 2. *Distribution of the geologic units-Itaoca Massif.*

Qha - Quarternary sediments; Tb - Tertiary sediments;
PЄergn (me) - gneiss and heterogenous migmatites;
PЄerch - Charnockitic rocks; Gr - granite

Single Cell option was applied to study the spectral behavior of Itaoca Massif in relation to the remaining of the test site. The following classes were analyzed: class g - granite, class Q - quarternary sediments, class T - tertiary sediments, class G - gneiss, class Ch- charnockites; class Ci - Campos town; class V - flooding area; class A - lagoon.

For each class, training area were selected. These training areas were composed by 36 pixels and 180 pixels samples. The total test site was composed by 736 pixels.

Histograms were acquired for each class in order to verify the gaussian assumption.

The Slicer option *is an auxiliary useful program* to divide the total range of grey level within each channel into slices of similar density (GE, 1975). In the present work the normal-slice option was applied and 8 classes of equal interval were obtained. Channel 7 was used because it showed the best enhancement the granitic body.

The MAXVER System was applied for multispectral image classification. It is a supervised system where before starting the classification the number of classes as well as sample areas for each class must be provided by the user (Velasco et al., 1979). To implement MAXVER classification, it was used the same samples as for *the Single Cell option. The sample areas* presented 36 pixel and 180 pixel (5 x 36).

The K-Means algorithm is a non-supervised option for classification multispectral data. It clusters the data based on their natural relationships (Dutra et al., 1982). This algorithm can identify up to 32 classes, but in the present work only 8 classes were selected.

The K-Means option helped to define classes based upon euclidian distance. The classification of each pixel for each test site was based on maximum likelihood criterium (Dutra et al., 1982).

Finally, the Spatial Features Acquisition algorithm was applied as well the MAXVER System and the K-Means System. The image features can be divided into: 1) Natural Features, which are derived from the grey level and texture. 2) Artificial Feature, which are obtained from grey level manipulation. These algorithms allow to generate new channels from the 4 original channels, and to select the best channels to be used for the thematic classification by means of K-Means and MAXVER Systems.

5. AUTHOMATIC ANALYSIS RESULTS

The single-cell option showed that the class g, defined on the granitic body presents the shortest overlap with the other classes.

The results obtained using Slicer option were not good, allowing just to identify the following classes: A, Ci and V.

The MAXVER System allowed a good class discrimination when 36 pixels sample areas were used (Figure 3). Large sample areas determined an increase of the overlap between classes.

The results of K-Means algorithm using 4 and 2 channels were not satisfactory inclusive to the identification of the granitic body (Figure 4).

The use of Spatial Features Extraction and MAXVER (36 pixels) allowed to identify the granitic massif (Figure 5). The use of K-Means System over the modified data doesn't allow meaningful results.

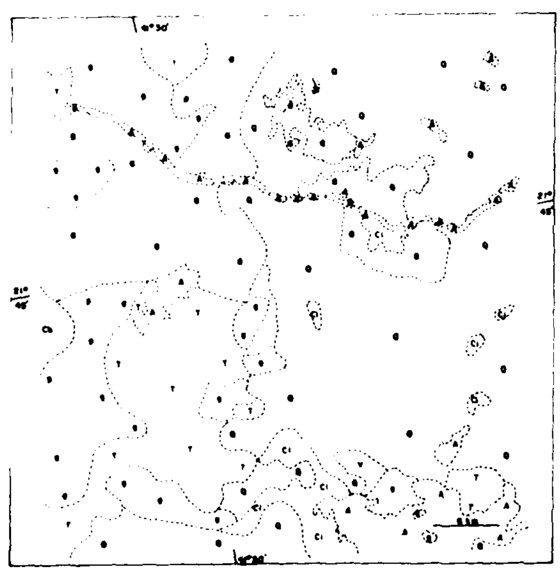

Figure 3. MAXVER Classification (36 pixels) - Itaoca Massif.
(.......) - *Limits of spectral classes.*

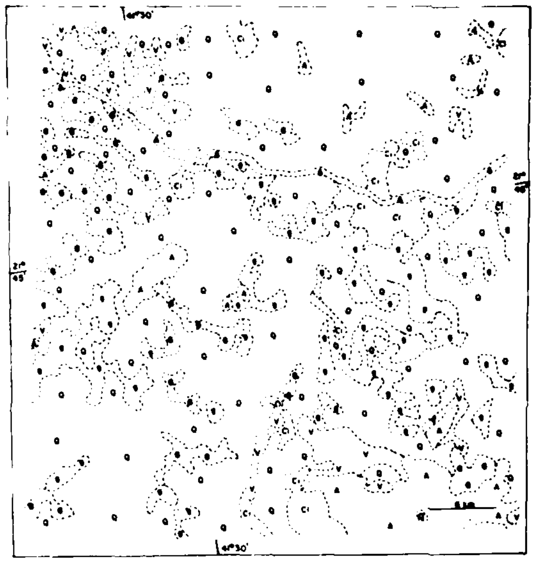

Figure 4. K-Means Classification - Two Channels - Itaoca Massif
(.......) - Limits of spectral classes.

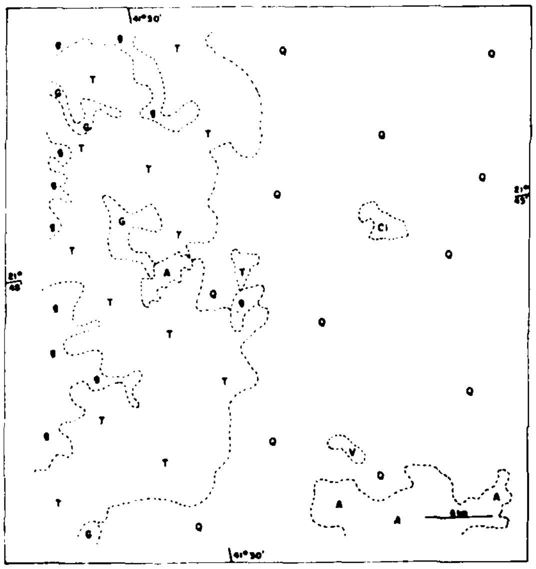

Figure 5. Spatial Features Acquisition. MAXVER Classification Itaoca Massif.
(.......) - Limits of spectral classes.

The combined processing (K-Means and MAXVER) allowed a very good discrimination of the granitic massif.

5. CONCLUSIONS

1. The intrusive bodies could be individualized satisfatorily even though it was considered their dimensions in relation to the spatial resolution of the used products. In spite sometimes the similar nature of the adjacent rocks the bodies could be differentiated by relief contrast.

2. The adaptation of the Logical Method for Photointerpretation allowed the best use of the small scale products used in the present work.

3. The compartmentation into major tectonic units and the division of these units into zones of lithologic dominance was a good classification approach to polycyclic and polymetamorphic area.

4. About the detail found in the final maps of the Study of the Intrusive Rocks Project, it is important to emphasize the following aspects:

   - in the macroscopic point of view, most of, the geological and structural features were identified. It can be emphasized for instance the tectonic conditioning of granite bodies by means of strucutural traces and their relationship to underlying rocks (concordant, partially concordant, discordant).

   - in the mesospic point of view it was possible to identify foliations related to phases of deformation responsible for foldings, but it was not possible to define the foldings themselves over the image. However in some places it was possible to identify the direction of the dip.

5. The use of several remote sensing products of small scalle optimizes the cost/benefit relationship for regional geology.

6. Single-cell option was useful to show the gaussian distribution of the samples, showing in this was the viability to use more accurate techniques for thematic classification.

7. The Itaoca massif could be identified only by supervised classification methods.

8. The results showed that it was not possible to relate a single spectral response to a single geological target.

9. To obtain better separability than it was obtained between two classes it is necessary to find sharp differences of grey level between the target and surroundings.

10. The results of thematic information are only characteristics for the same area. It is not possible to extend target information from one area to another.

6. REFERENCES

ALMEIDA, F.F.M. de; AMARAL, G.; CORDANI, U.G.; KAWASHITA, K. The Precambrian Evolution of the South America Cratonic Margin South of the Amazon River. In: NAIRN. E.M.; STEHLI, F.G. *The Ocean basins and margins.* New York. Plenum, 1973. v. 1, p. 411-446.

ALMEIDA, F.M. de; HASUI, Y.; BRITO NEVES, B.B. de; FUCK, R.A. Provincias Estruturais Brasileiras. In: SIMPÓSIO DE GEOLOGIA DO NORDESTE, 7, Campina Grande, 1977. Atas. p. 363-391.

ALMEIDA, F.F.M de; HASUI, Y.; BRITO NEVES, B.B. de. The Upper Precambrian of South America. *Boletim do Instituto de Geociências da Universidade de São Paulo*, 7:45-80, 1976.

DUTRA, L.V. Extração de Atributos Espaciais em Imagens Multiespectrais. São José dos Campos, INPE, 1982.

DUTRA, L.V.; MOREIRA, J.C.; II, F.A.M. Manual do Usuário dos Sistemas de Tratamento de Imagens Digitais. São José dos Campos, INPE, 1982 (in press)

GENERAL ELETRIC COMPANY (GE). Image-100. *User Manual*. Daytona Beach, F[illegible]ida USA, 1975.

GUY, M. Quelques Principles et Quelques Expériences sur la Methodologie [illegible] la Photo-interpretation. In: SIMPOSIUM INTERNATIONAL DE PHOTOINTERPRETATI[illegible], Paris, 1966. Acte. v. 1, p. 21-41.

HASUI, Y. *Tectônica da Área das Folhas de São Roque e Pilar do Sul*. Tes[illegible] Livre Docência em Geologia. São Paulo, USP, 1975.

HASUI, Y.; CARNEIRO, C.D.R.; BISTRICH, C.A. Os Granitos e Granitoides da [illegible] de Dobramentos Sudeste nos Estados de São Paulo e Paraná. In: CONGRESSO [illegible]ASILEIRO DE GEOLOGIA, 30, Recife, 1978. Anais. v. 6, p. 2594-2608.

SANTOS, A.R.; ANJOS, C.E. dos; BARBOSA, M.P.; VENEZIANI, P. Projeto Estudo de Rochas Intrusivas. São José dos Campos, INPE, 1982. (in press).

VELASCO, F.R.D.; PRADO, L.O.C.; SOUZA, R.C.M. Sistema MAXVER. *Manual do Usuário*. São José dos Campos, INPE, 1979.

WERNICK, E.; PENALVA, F. Contribuição ao Conhecimento das Rochas Granitóides do Sul do Brasil. *Revista Brasileira de Geociências*, 8(2):115-135, 1978.

A NEW GENERATION AIRBORNE SYNTHETIC APERTURE RADAR (SAR) SYSTEM

J.R. Bennett
R.A. Deane
L. Gutteridge
D. Okerson
P. Widmer

MacDonald, Dettwiler & Associates Ltd.
Richmond, B.C., Canada

SUMMARY

Imaging radar is rapidly emerging as an important remote sensing tool in a variety of research and operational applications including oceanography, geology, hydrology, forestry, ice type and movement monitoring, environmental reconnaissance and ocean vessel traffic patrol. The widespread operational use of imaging radar has been limited, however, by the availability of suitable sensor systems. With the exception of the brief operational lifetime of the spaceborne Seasat L-Band Synthetic Aperture Radar (SAR), only airborne systems and data are available for strategic or tactical use. Of these systems, most are real aperture, side looking airborne radars (SLARS), suffering from range dependent azimuth resolution which typically degrades to a few hundred meters at useful ranges. While Synthetic Aperture Radar (SAR) offers the potential for high resolution, wide swath imagery, the few available systems are expensive and require large ground based processors to convert the raw data to imagery. Imagery can hence be obtained only within line-of-sight of the ground stations and is unavailable in the aircraft.

This paper describes a new generation airborne SAR system currently under development. The system, designed specifically for remote sensing applications, produces high resolution, wide swath hard copy imagery in real-time, on-board the aircraft. Processed imagery is downlinked to shipborne or land-based receiving stations in real-time or offline from on-board, high density digital tape. Small, inexpensive ground based receiving and display systems enable imagery interpretation without the need for expensive, ground based processors. The system is compact, light-weight, packages and designed for operation on small aircraft in the 10-12,000 pound gross weight range.

INVENTORY OF RICE PADDIES IN THE LINGAUEN GULF AREA USING LANDSAT MSS DATA

Celso R. Roque
Rolando M. Tomas
Larry Solonga

Natural Resources Management Center
Quezon City, Philippines

SUMMARY

Inventory of rice paddies in the Philippines is usually done by conventional methods which are too costly and time consuming for immediate planning.

Recent studies have shown that Remote Sensing, using Landsat MSS data, is more viable in the inventory of rice paddies than the usual conventional methods, because of it's cost effectiveness, multi-dates coverage, and time effectiveness.

With the development of Remote Sensing Systems, especially the launching of Landsat, the Philippines, through the Natural Resources Management Center (NRMC), is undertaking projects on the inventory of rice paddies, to support the data needs of the Ministry of Agriculture, International Rice Research Institute and other agencies involved in rice research and production.

Inventorying of rice paddies in the Lingayen Gulf Area was conducted as part of the Coastal Resources and Environmental Survey project of the Natural Resources Management Center and the National Science Development Board.

Computer Compatible Tapes (CCTs) which cover the project area were acquired from EROS Data Center. These tapes were processed in a Multispectral Image Analyzer System, called Image 100.

Landsat scenes of the project area with dates that correspond to the planting and harvesting season were generated and pre-processed from CCT's using software techniques such as image enhancement, Radiometric/geometric corrections, grey level inversion to obtain a quality image. These were used in the interpretation and evaluation of rice paddies.

Spectral signatures of rice at planting and harvesting time of the year were extracted to determine their signature difference during those seasons.

The sets of images were compared to determine the extent of rice cultivation and hectares of rice paddies.

PRELIMINARY FIELD TESTS WITH OIL SLICKS USING MICROPROCESSOR CONTROLLED MICROWAVE RADIOMETER SYSTEM

Antti Lääperi

Helsinki University of Technology, Radio Laboratory
Espoo, Finland

ABSTRACT

This paper discusses the two-channel microprocessor controlled microwave radiometer system developed at the Radio Laboratory of the Helsinki University of Technology for oil thickness measurements. The thickness estimations are based on the actual antenna brightness temperatures in real time seen by the two radiometers. For this reason great care has been taken to achieve stable radiometer system. The effects of weather conditions are eliminated by storing the brightness temperature values from a clean water surface into the memory to be used as reference values for thickness measurements. However, the weather and the sea state have great influence on the behaviour of the oil slick and for this reason quite low references, 5 GHz and 16.5 GHz, are selected for the radiometers. This means that the thickness estimations are possible up to 10 mm with an accuracy of 1 mm using the 5 GHz radiometer and up to 3 mm with an accuracy of 0.2 mm using the 16.5 GHz radiometer. Finally some experimental results from field tests are explained.

1. INTRODUCTION

A microwave radiometer system which gives actual antenna brightness temperatures in real time with an accuracy of 1 K over the range 0-320 K at two microwave frequencies has been developed at the Radio Laboratory of the Helsinki University of Technology. The radiometer system is planned for thickness measurements of oil slicks and the whole system operates under microprocessor control. The thickness of the oil slick may vary from 0.1 mm to 10 mm, and it is measured with a resolution of 0.2 mm to 1 mm depending on the thickness of the oil.

Accurate and reliable measurement of the brightness temperature in real time is the basis for estimating the thickness of the oil slick. The limited time available for measurements does not allow for calibration periods, and for this reason a null-balancing Dicke-radiometer is used [1], [2] with the feedback loop and the additional noise source under microprocessor control [3].

2. MICROPROCESSOR CONTROLLED MICROWAVE RADIOMETER SYSTEM

The outputs from the radiometers give the actual antenna brightness temperatures in real time, with an accuracy of 1 K over the range 0-320 K. The radiometers used in the system are Dicke-type radiometers with null-balancing feedback and they operate under microprocessor control, Figure 1. Noise is injected into the antenna branch to balance its noise power with that from a

reference load at a known temperature. Any changes in output power from the diode noise source due to variations in supply voltage or in ambient temperature are accounted for by measuring the voltage and the temperature and accordingly correcting the length of the output pulse from the microprocessor. The physical temperatures of the antenna feedlines and the reference loads are also monitored and used to calculate, in real time, the actual brightness temperatures seen by the antennas. The null-balancing scheme removes all gain variations due to the mixers, amplifiers and detectors. In this way an absolute accuracy of 1 K is achieved in the measurement of the brightness temperature.

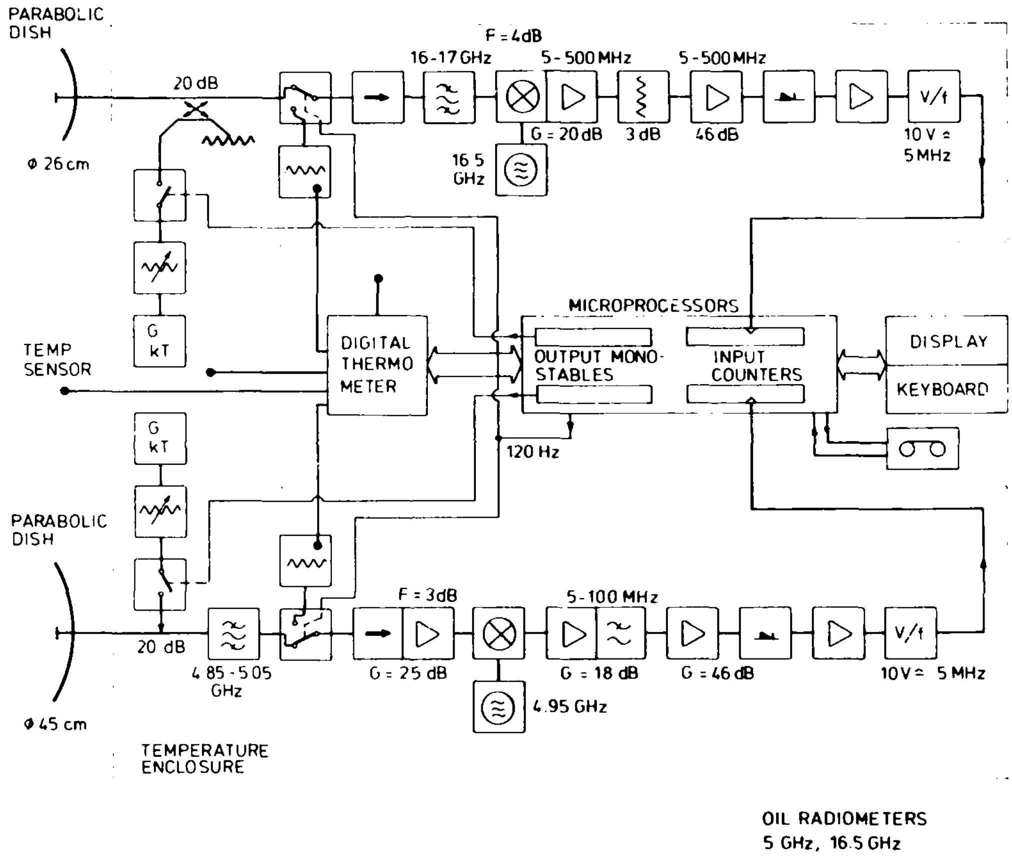

Figure 1. Block diagram of the radiometer system.

The radiometer system is calibrated with two known brightness temperatures. The first is the brightness temperature of the sky, and the second is the brightness temperature in the echo-free chamber. The beam structures of the two antennas have to be measured, and the effects of the side lobes and the back lobe on the antenna brightness temperature have to be calculated before measuring the brightness temperature of the sky. The brightness temperature of the main beam can be taken from the literature [4]. The brightness temperature in the echo-free chamber equals the room temperature.

When the antenna is pointing towards the sky the amplitude of the feedback pulse is adjusted to give the right antenna brightness temperature, T_{A1}, Figure 2. In the echo-free chamber the correct brightness temperature, T_{A2}, Figure 2, is achieved by software means changing the slope of the straight line in Figure 2.

In [2] the calibration is made using one known antenna brightness temperature. However, it can be calculated [3] that the non-ideal characteristics of the Dicke-switch require one more calibration point near the room temperature.

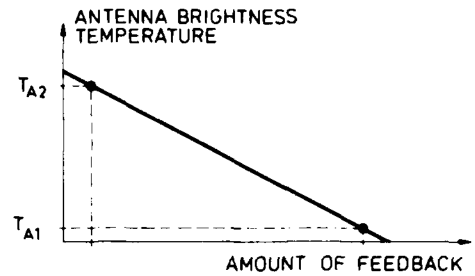

Figure 2. Antenna Brightness temperature as a function of the amount of the feedback value.

3. CHOICE OF FREQUENCIES

The measurement of the thickness of an oil slick with a microwave radiometer is based on the well-known matching effect of oil between air and water [5], [6]. As the thickness of the oil slick increases the brightness temperature also rises. However, it will reach a maximum when the electrical thickness is a quarter wavelength, and then it will fall off towards a minimum at half a wavelength, and so on. The ambiguity which thus arises can be removed by also measuring the brightness temperature at a lower frequency and combining the two measurements.

The calibration curves for both frequencies are stored in the memory of a microprocessor. The curves can be recalculated any time during the measurements due to changes in the physical temperature of the sea water or to different types of oil.

The thickness of an oil slick can be several millimeters. We have recorded thicknesses up to 7 mm. It has been also noted by Hollinger [7] that lower frequencies are much less affected by sea surface roughness and weather conditions. For those reasons the frequencies of 5 GHz and 16.5 GHz were selected.

4. CLEAR WATER REFERENCE

The influence of weather conditions is eliminated by using the clear water surface as a reference for thickness measurements. It is a known fact [8] that hard wind causes increase in the brightness temperature of the sea water due to the formation of white caps. The increase of the brightness temperature is approximately 1 K per white cap coverage percentage [8].

An oil slick removes the white caps and may cause in these cases a decrease of the brightness temperature values compared with the surrounding water areas.

In the radiometer system described above the actual antenna brightness temperatures are measured in real time. This makes it possible to take the clear water reference value from the area where the white cap coverage is small enough, for example behind an island sheltered from the wind. These values for both frequencies are stored in the memory of the microprocessor and they are used as a reference for oil thickness measurements. This kind of a system may give an indication of oil also from clear water in certain conditions, but it should measure correctly the thickness of an oil slick.

5. DATA PROCESSING AND INTERPRETATION

The data processing starts with the average noise powers measured during the times the receiver is connected to the antenna and reference branches, respectively. The processor calculated the noise injection needed for balance, taking into account the various corrections, and it operates a switch to set the required value. The result is one long feedback pulse, the length of which is given by the microprocessor, and the time base of which is given by the crystal oscillator.

The interpretation of the data is based on actual antenna brightness temperatures measured simultaneously at two different microwave frequencies. The upper limit of the interpretation of the thickness of an oil slick is set at 10 mm. This is the thickness, which gives the first maximum value at 5 GHz. Up to thicknesses of 10 mm 3-4 thickness candidates are given by the 16.5 GHz radiometer. Among the possible values obtained at 16.5 GHz, where the thickness resolution is better, the microprocessor selects the value which most closely agrees with the value indicated at 5 GHz.

6. FIELD TESTS

Field tests with an airplane and a helicopter have been carried out above open sea water and ice to test the radiometer system itself. Also one field test with artificial crude oil slick at open sea has been carried out in Norway with very promising preliminary results.

Last May a pool test with light viscosity fuel oil was carried out. It gave an indication of the difficulties which may arise in real situations at open sea. A pool of 2 m x 2 m was used for the experiment. One liter of the oil was poured at a time on the water in the pool causing an increase of 0.25 mm in the film thickness. Figure 3 shows the brightness temperatures recorded during the test, which lasted for several days. During the first day the thicknesses up to 5 mm were measured but the experiment had to be discontinued because the wind began to disturb the measurements too much. The wind caused the oil to move on the water surface and so generated thickness variations. It was difficult to select one brightness temperature value from the 16.5 GHz display to represent the corresponding thickness. This can also be seen from the 16.5 GHz measurements between 2 mm and 5 mm in Figure 3.

The experiment was continued three days later during the night when it was calm. The thicknesses between 5 mm and 10 mm were now measured without difficulties. The lower part in Figure 4 was recorded during that night when the oil thickness was 10 mm. Next morning the test was continued again. Two more liters of oil were poured in the pool. The wind was moderate. The upper part of Figure 4 shows the recorded brightness temperatures. The output variations of the 16.5 GHz radiometer were around 1 K. This means that the thickness variations were approximately 1 mm in the 10 mm oil layer (i.e. ten percent).

To be able to carry out the experiment still further, a plastic shelter was built around the water pool. After that the thicknesses from 10.5 mm to 19 mm were measured. Figure 3 shows that the brightness temperature outputs were now free from interference caused by the wind.

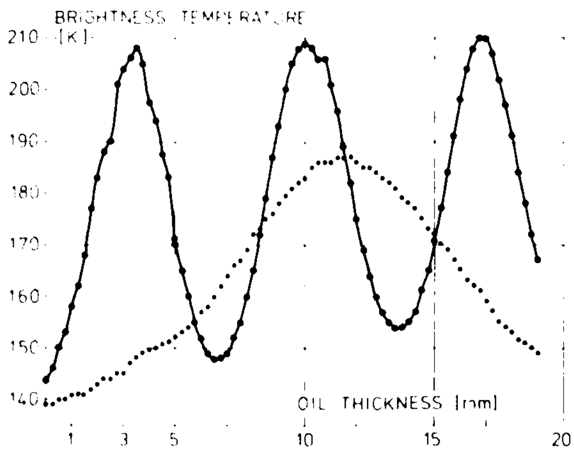

Figure 3. Pool experiment with fuel oil. Brightness temperatures at 5 GHz (dots) and 16.5 GHz (solid line).

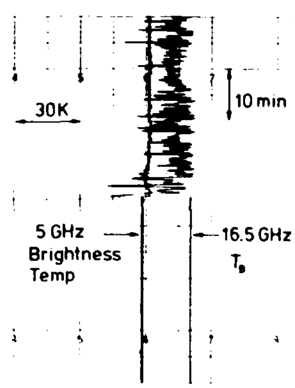

Figure 4. Influence of wind on the brightness temperatures (the thickness of the oil layer is 10 mm).

In normal situations when the radiometer system is installed in an airplane, the foot-prints of the antennas on the sea surface are much larger than in this experiment and the output is an average value of the different thicknesses inside the foot-print. If the thickness variations are of the order of ten percent it is unwise to try to use the 16.5 GHz results beyond the first maximum which occurs at an oil thickness of 3 mm. This means that the accuracy of the thickness measurement is 0.2 to 0.4 mm when the thickness of the oil slick is less than 3 mm. Up to 10 mm the interpretation is based totally on the 5 GHz measurements which gives an accuracy of 1 mm.

7. CONCLUSIONS

The choice of the frequencies, 5 GHz and 16.5 GHz, seems to be quite suitable for oil thickness estimations. The data interpretation algorithm explained in Chapter 5 seems to be too optimistic in real situations. Only if the sea surface is very calm or if the oil is of high viscosity this algoritm can be used. More realistic results can be obtained if the 16.5 GHz radiometer results are used to estimate the oil thicknesses up to 3 mm with an average accuracy of 0.3 mm and the 5 GHz radiometer results for thickness estimations up to 10 mm with an accuracy of 1 mm. The results at 5 GHz are also much less affected by the weather conditions and the sea state than for example those at 16.5 GHz although with poor spatial and thickness resolution. The use of still higher frequencies, for example 35 GHz, in thickness estimations is very difficult because of clouds and thickness variations.

8. REFERENCES

1. Kraus, J.D., "Radio Astronomy", McGraw-Hill, New York 1966.

2. Hardy, W.N. et al, "An S-band radiometer design with high absolute precision", IEEE Trans. on MTT, Vol. MTT-22, No. 4, April 1974.

3. Lääperi, A., "Thickness measurement of an oil slick in real time using microwave radio-meters" (in Finnish), Licentiate Thesis, Helsinki University of Technology, Department of Electrical Engineering, 85 p., 1981.

4. Reeves, R.G., ed., "Manual of Remote Sensing", Vol. I, American Society of Photogrammetry, 1975.

5. Hollinger, J.P. and Mennela, R.A., "Oil spills: measurement of their distribution and volumes by multifrequency microwave radiometry", Science 181, p. 54-55, 1973.

6. Meeks, D.C., Williams, D.P., Wilcox, R.M., Edgerton, A.T., "Microwave radiometer detection of oil slicks", Report No. 1335-2, Aerojet-General Corp., 1971.

7. Hollinger, J.P., "The determination of oil slick thickness by means of multifrequency passive microwave techniques", Naval Research Laboratory, Washington D.C., Report 2953, 1974.

8. Trane, L., "A second generation sea model", Technical University of Denmark, Lyngby, Report 289, 1976.

THE DISTRIBUTION OF CHLOROPHYLL IN THE MALVINAS CURRENT AND THE CONTINENTAL SHELF WATERS OF ARGENTINA AS VIEWED BY THE COASTAL ZONE COLOR SCANNER

Fred J. Tanis

Environmental Research Institute of Michigan
Ann Arbor, Michigan

José A. Alvarez

Universidad Nacional de Mar del Plata
Mar del Plata, Argentina

SUMMARY

The Nimbus-7 Coastal Zone Color Scanner (CZCS) is a scanning radiometer which is capable of viewing the ocean in six coregistered spectral bands. Five of these bands are in the visible and near infrared (443, 520, 550, 670, 750 mm) and the sixth is a thermal band at 11.5 um. From an altitute of 955 km CZCS is able to view a 1600 km wide swath at a resolution of 825 m. At this spatial and spectral resolution CZCS is an ideal instrument to view large sediment transport features and to document the abundance and distribution of phytoplankton at the ocean surface.

CZCS imagery obtained on February 10, 1979 shows clearly the spatial features of the Malvinas Current and complex eddies and gyres along the Argentina coastline from Bahia Grande to the Valdes Peninsula. Using available algorithms and field measurement data these CZCS data were processed to produce a map of the mesoscale distribution of chlorophyll-a. Concentration estimates are correlated with thermal band predictions of surface temperature within the Current and with other ancillary data to confirm spatial features. Interpretations are also made for suspended sediment and other water mass features identifiable in the CZCS imagery. Coastal waters estimated to support high concentrations of phytoplankton can frequently be correlated with available fisheries survey reports. The possible application of CZCS data to fisheries resource management and to location of new fishing grounds is investigated. Potential applications of CZCS imagery to marine studies at the National University of Mar del Plata and other research centers are also discussed.

THE MEASUREMENT OF PARTICLE AND CHLOROPHYLL CONCENTRATION IN WATER USING THE MULTI SCATTERING MODEL*

Yukio Sugahara & Seijiro Hayakawa

Asia Air Survey Co., Ltd.
Tokyo, Japan

ABSTRACT

The authors studied an analytical method to estimate chlorophyll and particle concentration in turbid water using MSS data collected after a heavy rain. The authors introduced the Multi Scattering Model into the analytical method.

It was found that the analytical method employing the Multi Scattering Model was more effective than the method using statistical analysis which uses the relation between sea truth data and remote sensing data for estimating chlorophyll pigment concentrations.

The method employing the Multi Scattering Model requires a number of sea truth data, but this number is less than the number required for the method employing the statistical analysis.

1. INTRODUCTION

In previous studies, a positive correlation has been recognized as existing between chlorophyll pigment concentrations analyzed in the laboratory and MSS (Daedalus's DS-1250) image data processed to enhance the optical properties of chlorophyll.

An MSS data-gathering flight was made on 6 August 1980 over Kitanada Bay. It had rained heavily in the survey and surrounding areas on 5 August with the result that the authors couldn't get a positive correlation between the chlorophyll pigment concentrations and MSS data processed to enhance the optical properties of chlorophyll pigment using the MSS data collected over Kitanada Bay's turbid water. So, the authors decided to introduce the Multi Scattering Model into the analytical method to try to get a better correlation.

The Multi Scattering Model was developed to measure suspended solid concentration. The authors improved on this model in order to estimate the chlorophyll pigment concnetration.

*Presented at the Seventeenth International Symposium on Remote Sensing of Environment, Ann Arbor, Michigan, May 9-13, 1983.

We analyzed two distributions of suspended solid concentrations using the two analytical methods-each with a different MSS band. One distribution was analyzed by the regular method. The other distribution was analyzed by the analytical method using the Multi Scattering Model. (This method emphasizes the effect of light absorption by chlorophyll pigment.). The values of the differences estimated by these two methods were proportional to the chlorophyll pigment concentrations.

From this finding, it was concluded that it would be possible to estimate chlorophyll pigment concentration in turbid waters with different suspended solid concentrations.

2. MULTI SCATTERING MODEL

Chandrasekhar's equation [1] for diffuse reflection from a semi-infinite layer with isotropic scattering is shown in Figure 1.

$$L_\lambda(\mu) = \frac{1}{4\pi}\omega_0 \cdot E \cdot \frac{H(\mu)\cdot H(\mu_0)}{\mu + \mu} \tag{1}$$

L : Radiation

E : Incident Irradiance

ω_0 : Single Scattering Albedo $\left(= \frac{s_\lambda}{s_\lambda + a_\lambda}\right)$

s : Scattering coefficient

a : Absorption coefficient

The Multi Scattering Model was studied by Prewett et al [2] (1973) for measuring particle concentration in lake water. Using Chandrasekhar's equation, the voltage $V_\lambda(\mu')$ measured by the MSS is expressed as:

$$V_\lambda(\mu') = \frac{\omega_0}{4} H(\mu)\cdot H(\mu_0)\cdot N(\mu)\cdot T(2,1,\mu)\cdot T(1,2,\mu_0)\left(\frac{n_1}{n_2}\right)^2 \frac{(V_\lambda)ss}{\mu_0 \cdot \tau_{ss}(\lambda)} + Vb(\mu') \tag{2}$$

$(V_\lambda)ss$: Signal measured by the skylight sensor

$\tau_{ss}(\lambda)$: Throughput of skylight sensor

N : The effect of multiple reflectances at the surface or water

$T(2,1,\mu)$: The transmittance of the water-air interface

$T(1,2,\mu_0)$: The transmittance of the air-water interface

Vb : Background signal

Then, function $G(\omega_0)$ is defined as follows:

$$G(\omega_0) = \left(\frac{\tau_{ss}(\lambda)\mu_0}{(V_\lambda)ss}\right)\left(\frac{n_2}{n_1}\right)^2 \frac{4}{[T(2,1,\mu)][T(1,2,\mu_0')]} \cdot V(\mu') \tag{3}$$

$$\therefore G(\omega_0) = \omega_0 H(\mu) \cdot H(\mu_0) \cdot N(\mu) \tag{4}$$

The quantity $\omega_0 H(\mu)\cdot H(\mu_0)\cdot N(\mu)$ is a monotonic signal-valued function of ω_0. It is defined as a linear correlation between the suspended solid concentrations and both the optical coefficient of absorption and that of scattering. If the following two conditions are satisfied, the relative concentration of suspended solid at any point can be calculated using data from the bands with wavelengths of λ_1 and λ_2.

1. In a body water, the distribution function of a particle's radius is uniform.
2. In two different bands regions, the scattering and absorption cross sections are the same.

The relative concentration $c(r)/c(r_0)$ is given by the formula:

$$\frac{c(r)}{c(r_0)} = \frac{\omega_0(r_0,\lambda_1)\cdot aH_2O}{g(r_0,\lambda_1,\lambda_2) - (r,\lambda_1)\cdot h(r_0,\lambda_1,\lambda_2)} \tag{5}$$

$$g(r_0,\lambda_1,\lambda_2) = \frac{\omega_0(r_0,\lambda_1)\{\omega_0(r_0,\lambda_2)[aH_2O(\lambda_2)-aH_2O(\lambda_1)]\}}{\omega_0(r_0,\lambda_1) - \omega_0(r_0,\lambda_2)}$$

$$h(r_0,\lambda_1,\lambda_2) = \frac{\omega_0(r_0,\lambda_2)\cdot aH_2O(\lambda_2) - \omega_0(r_0,\lambda_1)\cdot aH_2O(\lambda_1)}{\omega_0(r_0,\lambda_1) - \omega_0(r_0,\lambda_2)}$$

c : Suspended solid concentration

r : The location water surface measurement

3. MEASUREMENT

(Survey of suspended solid particles)

In the analysis using the Multi Scattering Model, the measurement of skylight is needed to calculate $G(\omega_0)$. Table 1 shows the spectral response at each band of the skylight sensor.

ω_0 was calculated from scattering and absorption coefficients. These two coefficients were analyzed by the Kubelka-Munk Two Constant Theory using the spectral data of water measured in the survey area by MSS. Figure 2 shows the relation ω_0 and $G(\omega_0)$. The authors applied the single linear regression to ω_0 and $G(\omega_0)$. This regression line passes the point where ω_0 and $G(\omega_0)$ equal zero. Using this regression, the distribution of suspended solid concentration in the survey area was estimated with MSS Band 6 (600-650[nm]) data (This estimation requires that the suspended solid concentration at at least one point in the sea by known. : Photo 1). The wavelength of MSS Band 6 doesn't include the absorption band of chlorophyll pigment. The authors selected Band 6 for λ_1, and Band 7 for λ_2. Symbol ● of Figure 3 shows plotting points from the sea truth data and their estimated values, and the solid line shows the predicted values. The line represented by dashes is a simple regression line.

(Survey of chlorophyll pigment)

The process to estimate chlorophyll pigment concentration is as follows:

1. Conduct a survey for distribution of suspended solid particle concentration. (The authors used results from a previous experiment for suspended solids.)
2. Conduct a survey for distribution of suspended solid particle concentration with MSS Band 4 (500-550[nm]) (photo 2). In this survey, Band 4 was selected for λ_1, and Band 7 (650-690[nm]) was selected for λ_2. In the wavelength of Band 4, photons are absorbed to a relatively high degree by chlorophyll pigment. Symbol ▲ in Figure 3 shows the plotting points from sea truth data and temporary suspended solid concentrations.

3. Perform calculation using the values of difference for suspended solids in processes 1 and 2 for all image pixels.

4. Assuming that no difference in value for suspended solids estimated in processes 1 and 2 mean no existence of chlorophyll pigment, the relation between chlorophyll pigment concentration and value of difference can be calculated using one of the sea truth data (Figure 4). In Figure 4, this relation is indicated as a solid line. The line composed of dashes was obtained by regression analysis. This distribution of chlorophyll concentration was calculated using regression of the solid line.

4. DISCUSSION

Photo 4 shows the pattern of suspended soild concentration estimated by regression analysis using the sea truth data and MSS Band 4's data of point 16. Photo 1 shows the pattern estimated by using one of the analyzed suspended solid data. These patterns almost look like each other. The differences were caused by the influence on changes of skylight sensor's data.

Figure [illegible] shows the plotting points from sea truth data of analyzed chlorophyll pigment concentration and MSS Band 2 (420-450[nm]). The data of MSS Band 2 indicates the best correlation among the data of MSS's bands with chlorophyll pigment concentration. The correlation coefficient was 0.62 and the number of data used were 52, but that correlation was not good enough for a survey of chlorophyll pigment concentration.

Photo 5 shows the distribution of chlorophyll pigment concentration estimated from the data of MSS Band 2.

It can be seen that the pattern of Photo 3 resembles the pattern of suspended solids except where the mouth of the river enters the bay. This phenomenon is a result of the positive relation between the analyzed suspended solids and the analyzed chlorophyll pigment concentrations.

In our analysis, we encountered the following problems using the Multi Scattering Model:

1. The method needs several spectral measurement data.

2. In Figure 4, some points are located away from the solid line. Some of these points were measured by the observation vessel near the land, and others were measured near the tidal front. So, the location of sea truth should be selected carefully.

5. CONCLUSION

In this study the authors confirmed that the analytical method employing the Multi Scattering Model is useful for estimating suspended solid concentrations.

It was also found more useful in estimating the concentration of chlorophyll pigment in turbid water than using the statistical relation between the chlorophyll pigment concentration and MSS image data.

6. ACKNOWLEDGEMENTS

This report represents part of the results obtained through "The Study of Prediction Techniques on Red Tides" which Nansei Regional Fisheries Research Laboratory carried out. This study was funded by The Science and Technology

Agency. The authors wish to express their gratitude to Dr. Akio Murakami, Dr. Masateru Anraku and Dr. Shiro Uno for giving them the opportunity to carry out this research and also for their valuable suggestions. Thanks are also extended to Dr. M. Fuchimoto and Dr. M. Yokota for their valuable suggestions.

7. REFERENCES

[1] S. Chandraskhar, 1960, "Radiative Transfer", Dover Publications, New York.

[2] O.E. Prewett et al, 1973, "Techniques for Measuring Light Absorption, Scattering and Particle Concentration in Water", N62306-71-C-0108.

[3] Y. Sugahara, 1981, "The Relation Between Spectral Radiometric Characteristics of Water Quality", J. Japan Society of Photogrammetry and Remote Sensing, 4, 1981.

[4] D.R. William, 1967, "Kubelka-Munk Formulas Adapted for Better Computation", J. of Paint Tech., 9,511.

[5] Y. Sugahara, S. Hayakawa, S. Uno, 1980, "Remote Sensing of Chlorophyll Found in Bodies of Water", Proceedings of 14th International Symposium of Remote Sensing of Environment.

[6] Y. Sugahara, M. Yokota, S. Hayakawa, Y. Takahashi, 1980, "Survey of Water Quality Using Remote Sensing Techniques", Proceedings of Japan Photogrammetry Soceity, Autumn 1980.

[7] Y. Sugahara, S. Hayakawa, 1978, "Report on Survey Experiment of Water Quality Utilizing Remote Sensing Techniques", J. Association of Photogrammetry & Technology, 5, 1978.

[8] R.C. Ramsey, 1968, "Study of Remote Measurement of Ocean Color", Final Report to NASA, TWA-NASA-1658.

[9] R.W. Austin, 1974, "The Remote Sensing of Spectral Radiance from the Ocean's Surface", Optical Aspects of Oceanography, Academic Press.

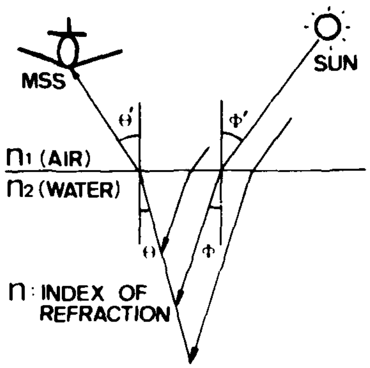

Figure 1. Geometry for infinite depth case.

n_1 : index of refraction of air
n_2 : index of refraction of water

Table 1. Spectral response at each of skylight sensor.

Band	Blue	Green	Red	Infra-red
Center wavelength nm	[illegible]	[illegible]	[illegible]	[illegible]
Half-width nm	[illegible]	[illegible]	[illegible]	[illegible]

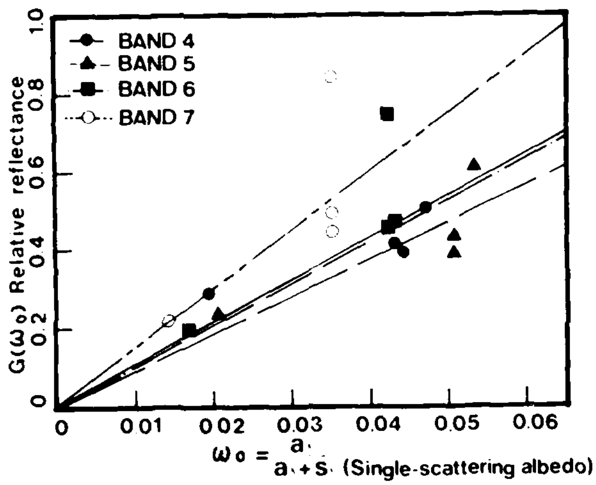

Figure 2. Relation between ω_0 and $G(\omega_0)$.

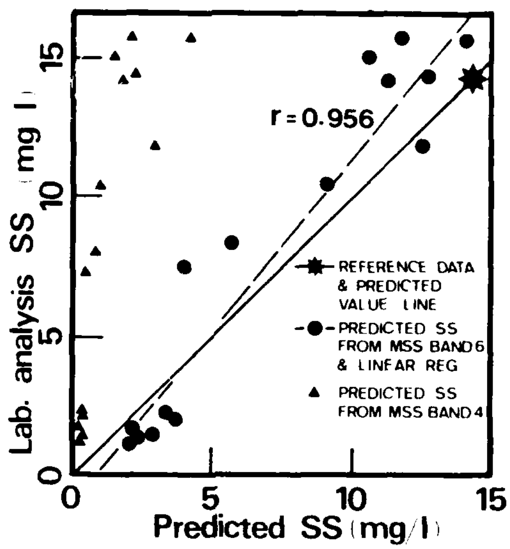

Figure [illegible]. Relation between suspended solid concentration analyzed in laboratory and estimated value.
SS : Suspended solid

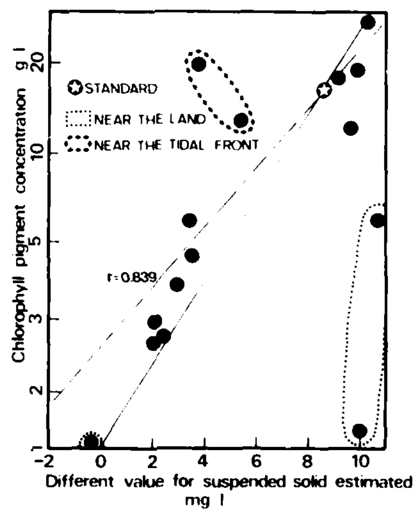

Figure [illegible]. Relation between different value for suspended solid concentration estimated and chlorophyll pigment concentration analyzed in laboratory.

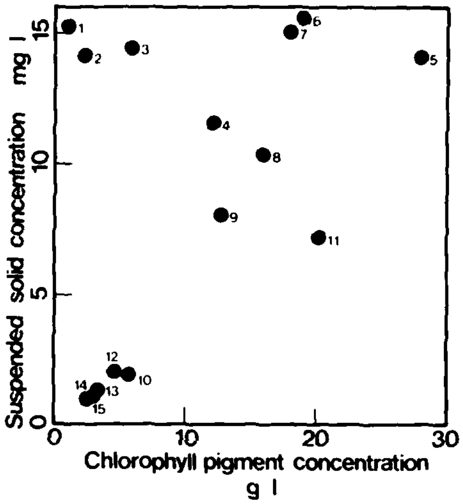
Suspended solid concentration mg l
Chlorophyll pigment concentration g l
0
5
10
15
0
10
20
30
1
2
3
4
5
6
7
8
9
10
11
12
13
14
15

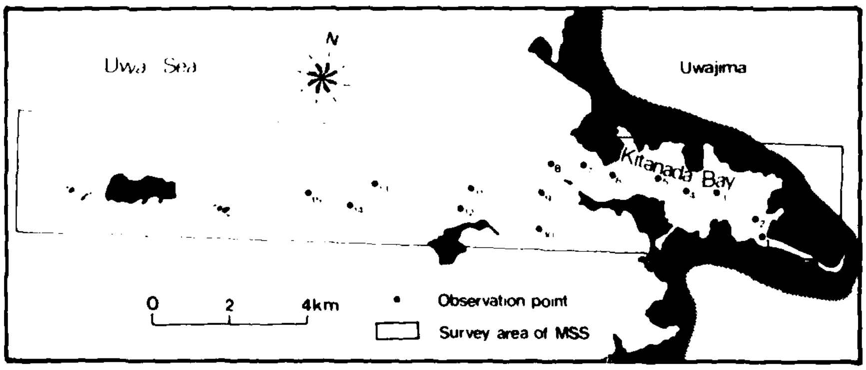
Uwa Sea
N
Uwajima
Kitanada Bay
0
2
4km
Observation point
Survey area of MSS

Fig. [illegible]. Distribution of suspended solids concentration.

Fig. [illegible]. Distribution of temporal suspended solids concentration.

Fig. [illegible]. Distribution of chlorophyll pigment concentration.

CHLOROPHYLL PIGMENT (MICRO-GRAM/L) 0-5 10 15 20 20-

Fig. [illegible]. Distribution of suspended solids concentration.

Fig. [illegible]. Distribution of chlorophyll pigment concentration.

CHLOROPHYLL PIGMENT (MICRO-GRAM L) 0-5 10 10-

SUSPENDED SOLID CONCENTRATION (MG L)
0 2 4 6 8 10 12 14 16 18 18-

CLOUD

SEVERE CONVECTIVE STORM DETECTION BASED ON SATELLITE INFRARED IMAGERY ANALYSIS

R. J. Hung
The University of Alabama in Huntsville
Huntsville, Alabama, U.S.A.

and

R. E. Smith
NASA/Marshall Space Flight Center
Huntsville, Alabama, U.S.A.

ABSTRACT

Several cases of GOES digital infrared data and Doppler Sounder array data during the three-hour time period immediately preceeding the touchdown of the tornado were analyzed. Tornado-associated clouds are compared with non-tornado-associated clouds using satellite infrared data, ray tracing of gravity waves detected by the Doppler Sounder array and rawinsonde data. The satellite observations are at 15-minute intervals. Our study shows that tornado-associated clouds are always accompanied by overshooting turrets penetrating above the tropopause. The growth rate of the overshooting turret above the tropopause for severe storm-associated clouds is much greater than that of non-severe storm-associated clouds.

1. Introduction

Geosynchronous satellite data is a potentially powerful tool for studying enhanced convection and mesoscale systems. Purdom (1976) has noted that intersecting cloud lines observed on GOES imagery can be used in forecasting mesoscale convection and thunderstorms. Sikdar et al. (1970) have used ATS-3 visible data to measure thunderstorm anvil expansion rates. Adler and Fenn (1979) showed examples of cold area expansion rates related to thunderstorm growth using SMS window channel infrared data. Recently, Adler and Fenn (1982) examined cloud top temperature variations from geosynchronous infrared satellite data relative to 11 tornado touchdown times. In 8 of the 11 cases there was a period of rapid cloud top ascent 30-45 min prior to the tornado touchdown. This upward growth appears to be associated with the formulation of a mesocyclone. Adler and Fenn (1982) indicated that, following the ascent of the cloud top, there was a period of no growth or even a height drop preceding, or at the time of the tornado touchdown.

In a study of tropical cyclone intensity, Gentry et al. (1980) suggested that the value of the cloud top equivalent blackbody temperature T_{BB} could serve as an index of current storm intensity, and the growth rate of the cloud

top T_{BB} as a predictor of the future intensity. Hung *et al.* (1980) employed GOES infrared data for studying the May 29, 1977, Oklahoma tornado, to show that both cloud top T_{BB} and the growth rate of the cloud top T_{BB} area can be used to distinguish between thunderstorms which eventually spawned tornadoes and those that did not.

The association between gravity waves and severe convective storms has been studied extensively in the laboratory and in the field during the past decade (Willis and Deardorff, 1974; Adrian, 1975; Curry and Murty, 1974; Gossard and Sweezy, 1974; Stull, 1976; Uccellini, 1975). Gravity waves have been detected in a wide variety of ground-based obersvations as well as in in-situ measurements on satellites (Gossard and Munk, 1954; Bean et al., 1973; Baker and Davies, 1969; Prasad et al. 1975; Smith and Hung, 1975; Georges, 1973; Hung and Smith, 1979; Bertin et al., 1978; Rice and Sharp, 1977; Spencer et al., 1976; Chiu et al., 1979; Browning et al., 1973).

Recently, gravity waves have been associated with tornado activity (Hung et al., 1978a; Hung and Smith, 1978) and hurricanes (Hung and Kuo, 1978). These gravity wave observations were made with a high-frequency CW Doppler array system in which radio receivers located at a central site, NASA/Marshall Space Flight Center, monitored signals transmitted from three independent remote sites on three sets of frequencies and reflected off the ionosphere approximately halfway between the transmitter and receiver sites. Hung et al. (1979a, 1979b), using a ray tracing technique, have shown that the enhanced convection-initiated gravity waves associated with tornadoes were generated by thunderheads embedded in a squall line and/or isolated clouds with intense convection. A comparison of the location of the computed wave sources and the time of wave excitation with published tornado touchdown data showed that the computed wave sources were in the convective clouds with turrets overshooting the tropopause which spawned tornadic storms more than one hour after the waves were excited (Hung et al., 1978a; Hung et al., 1978b).

In laboratory experiments, Townsend (1964), Deardorff, et al. (1969), Willis and Deardorff (1974) and Adrian (1975) observed that gravity waves were excited when convective elements overshot the top of a mixed layer and penetrated a short distance upward into a stable region. Curry and Murty (1974), Gossard and Sweezy (1974) and Stull (1976), among others, have suggested that thunderstorms or fronts could excite gravity waves in the atmosphere. Einaudi and Lalas (1975) indicated that gravity waves can propagate upward through the atmosphere and stimulate cloud growth. Our analytical results also show that gravity waves can be detected at F-region ionospheric height as long as the convection penetrates above the tropopause. This result is in agreement with the study made by Baker and Davies (1969) in which they concluded that gravity waves are detectable at ionospheric height as long as the cloud top is at an altitude of 12 km or higher.

Recently, Hung et al. (1980) investigated the change of cloud top temperature with respect to time for clouds associated with sources of gravity waves compared to clouds which were not associated with gravity waves. The study of GOES infrared data during the time period between when the gravity waves were being excited and the touchdown of the tornado indicated that clouds associated with tornado activity are characterized by both a very low temperature at the cloud top, which is equivalent to a high penetration above the cirrus canopy, and a very high growth rate of the cold region of the cloud top, the signature of enhanced convection in the cloud.

2. Case Study of March 24, 1976 Elton, Louisiana Tornado

2-A. Temperature of Clouds with Intense Convection As Determined from Satellite Infrared Digital Data Analyses

An Image Data Processing System (IDAPS) was developed by NASA/Marshall Space Flight Center to be used for the image processing requirements of the Skylab experiment. IDAPS can be used to process high resolution satellite photographs, both visible and infrared, for studying cloud top height variability, temperature distribution, and the cloud top growth and collapse rates. GOES digital infrared (IR) data for the entire United States during the three-hour time period before the tornado touchdown time on March 24, 1976, were used in this study. The period between satellite observations was 15 minutes and the temperature resolution of the IR data was 1 K in the range of equivalent blackbody temperatures.

In this study, a cumulative histogram is compiled starting from the cold end of the temperature distribution. The number of pixels (picture elements), N_i, with blackbody temperature equal to or less than temperature T_i, is obtained. Physically, the number of pixels, N_i, is proportional to the area of the cold cloud top with temperature $\leq T_i$. This also provides data about the horizontal area of the cloud penetrating above certain altitudes. Only a small portion of the huge cloud extending from Ohio and Illinois down through Arkansas, Mississippi, Louisiana, and Texas had a cloud temperature $\leq$ -68 °C during this time period. GOES IR imagery of the cloud coverage over the entire United States at 2230 GMT is shown in Figure 1.

Figure 2 shows the geographical location of the Louisiana cloud at 2232 GMT. Contour A is the portion of cloud top with temperature $\leq$ -66°C; B, the portion of cloud top with temperature $\leq$ -55°C; and contour C, the area of the entire cloud at Louisiana and its surrounding states in Figure 1. While they were growing, these clouds moved eastward at a speed of approximately 45 km/h, which agrees with the radar observation. A tornado was spawned from the overshooting turret A at 2400 GMT when the overshooting turret had moved to Elton, Louisiana, 30.26 N and 92.42 W.

The areal expansion and growth of the cold element of the cloud top have also been studied. The rawinsonde observation from Lake Charles, Louisiana at 2300 GMT, March 24, 1976, shows that the tropopause height was 11.3 km with a temperature of -58 °C. The comparison between the rawinsonde observation and the IR data shows that the overshooting turrets of the Louisiana cloud started to penetrate above the tropopause about 2131 GMT. Figure 3 shows the changes in the areas of the cloud top at different heights (temperatures) during the time period between the penetration of the tropopause and the tornado touchdown i.e., 2131-2347 GMT. The figure shows the time-dependent increase (or decrease) of the number of pixels for cloud top temperatures $\leq$ -62°C, $\leq$ -66°C, $\leq$ -68°C and $\leq$ -69°C. The cloud area with a temperature $\leq$ -62°C, and a cloud top height just above the tropopause expands very rapidly between 2131 and 2202 GMT and then the expansion slows down during the next 30 minutes. A higher altitude cloud with a temperature $\leq$ -66°C then becomes visible. The top of the cloud continued to rise, reaching a temperature of $\leq$ -68°C at 2247 GMT, and then finally the coldest temperature of $\leq$ -69°C, 11 C° colder than the tropopause, at 2317 GMT. The growth of the cloud top continued until 2332 GMT when the cloud top areas with temperatures of $\leq$ -68°C and $\leq$ -69°C started decreasing, implying that the cloud was collapsing. The cloud collapsed about 30 minutes before the tornado touched down, in good agreement with the results of our earlier investigation of the May 29, 1977 storm (Hung et al. 1980). The overshooting turret can only exist because it is dynamically supported by intensive vertical convection. As the intensive vertical convection conditions disappear, the overshooting turret collapses. This result is also in good agreement with the aircraft observations made by Fujita and his associates (Fujita and Caracena, 1977; Fujita and Byers, 1977).

The following equation was used to calculate the growth and expansion rate of the cloud:

$$\gamma_i = \frac{dN_i}{dt} \qquad \text{(Pixels - sec}^{-1}\text{)}$$

where γ_i denotes the growth rate of the cloud area with a temperature $\leq T_i$; N_i, the number of pixels with temperature $\leq T_i$; and t, the nominal time period between observations. Figure 4 shows the growth rates of the cold cloud areas with temperatures $\leq -62^oC$, $\leq -66^oC$, $\leq -68^oC$, and $\leq -69^oC$ during the time period 2247-2347 GMT. The maximum growth rate of the area with temperature $\leq -62^oC$ occurred during the time period 2302-2317 GMT which was about 43 to 58 minutes before the tornado touchdown. In this case study, the maximum growth rate of the turret above the tropopause occurred approximately one hour before the tornado touchdown.

Similar analyses of both areal expansion rates and growth of cloud top heights during the same time period were accomplished all over the United States. The clouds associated with the severe thunderstorms over Idaho had a temperature only $2C^o$ warmer than the cloud top temperature over Louisiana: however, the growth rate of the Idaho cloud was less than that of the Louisiana cloud.

2-B. Intense Convective Clouds and Gravity Waves

During time periods with severe weather activity, wave-like disturbances are observed in the high frequency CW Doppler records. The records from the CW Doppler sounder array are subjected to a power spectral density analysis to obtain the wave periods of these Doppler fluctuations while the direction of propagation and the phase velocity of the waves are obtained from a cross correlation analysis (Hung and Smith, 1978). Group ray tracing computations using the best available data on the thermodynamic properties of the atmosphere are used in determining the locations of the sources of the waves. A detailed description of the observation system, the data processing techniques, wind data and atmospheric models used in the ray tracing computations is given in Hung and Smith (1978) and Hung et al. (1978a). The probable errors in the determination of the azimuthal angle of the wave arrival and the ray tracing computation have been discussed by Hung et al. (1978a), Hung and Smith (1979), and Hung and Kuo (1978).

Based on our previous analysis of gravity waves associated with tornadic storms, three sources of gravity waves have been determined: (1) Groups of tornadoes (Hung et al., 1978a; Hung and Smith 1979), (2) Isolated tornadoes embedded in a squall line (Hung et al., 1978b; 1979a; 1979b); and (3) Isolated airmass type tornadoes. These gravity waves were excited under a wide variety of meteorological conditions associated with air mass type convective storms to those associated with rapidly moving fronts, pre-frontal squall lines and isolated clouds with intense convection. In each instance, within the combined probable error bands of the detection system and analytical techniques, the wave sources were located in intense convective clouds which eventually developed into tornadic storms (Hung et al., 1979a; 1980).

Doppler records for the 2315-2415 GMT, March 24, 1976, time period which showed wave-like oscillations in the F-2 layer of the ionosphere were analyzed. Figure 5 shows the oscillations in the high frequency, 5.734 MHz, CW transmissions. Four gravity waves were detected and identified. The propagation characteristics of these waves are listed in Table 1. The azimuthal angles of wave arrival were $42\text{-}46^o$ and the horizontal phase speeds were 104-128 m/sec, therefore, it appears as if these waves could be from the same source Ray tracing computations confirmed this.

The results of the computed ray paths and the probable sources of the observed gravity waves are shown in Figure 6. A, B, C and D are the computed tracks of the gravity waves observed during the 2300-2400, 2315-2400, 2315-2415, and 2330-2415 GMT time periods, respectively, of March 24, 1976. The computed sources of these four gravity waves were in clouds in the southwestern corner of Louisiana, about 80 km west of the location of the tornado touchdown. Satellite winds and radar echoes show that these particular clouds were moving eastward at about 45 km/h, which put them over Elton, Louisiana at the time the tornado touched down. A comparison of Figures 6 and 2 shows that the computed locations of the wave sources were within the A contour of Figure 2 where the overshooting turret was penetrating through the tropopause. The wave traveling times from the computed probable source to the receivers were from 112-136 min; therefore, the signals had to be excited about two hours prior to the touchdown of the tornado.

2-C. Airmass Instability from Rawinsonde and Storm Development from Radar Observations

The stability of an air mass can be determined from rawinsonde observations. On the 2300 GMT, March 24, 1976, Lake Charles, Louisiana rawinsonde, the temperature lapse rate was nearly dry adiabatic from 3.7 km (645 mb) to 10.2 km (250 mb). The relative humidity below 3.7 km was 90 - 94%.

The sounding shows that once the warm, moist lower layer of the air mass gained enough energy to break through the inversion at 3.7 km, the updraft motion would continue until the clouds reached the tropopause with the size of the cloud formed, as shown in Figure 2, being dependent upon the amount of moisture available for initiating the updraft motion.

Figures 7 and 8 are the radar summaries of the southern United States at 2235 and 2335 GMT, respectively, March 24, 1976. These radar summaries show that severe thunderstorms were occurring over the states of Illinois, Kentucky, Missouri, Tennessee, Arkansas, Mississippi, Louisiana and southern section of Texas when the overshooting turret of the Louisiana cloud was penetrating the tropopause. The radar echoes over Louisiana were moving eastward at about 25 kts (46 km/h) at the time when the overshooting turret started to penetrate the tropopause, the time when the observed gravity waves were being excited. A comparison of the satellite observations, gravity wave ray tracing calculations, and radar summaries shows that the overshooting turret (contour A in Figure 2) and the computed wave sources (Figure 6) were located in the severe thunderhead shown as a small circle in the southwest section of Louisiana on Figure 7 and the southcentral section of Louisiana on Figure 8. The radar summaries clearly show that the cumulonimbus which spawned the tornado at 2400 GMT had an echo height of 12.2 (40,000 ft) at 2235 GMT (Figure 7), and an echo height of 13.7 km (45,000 ft) at 2335 GMT (Figure 8), after it had moved about 45 km eastward. The cumulonimbus which was responsible for the tornadic storm had the tallest echo height in the entire United States during this 3 hour period.

3. Case Study of May 29, 1977 Ringwood, Oklahoma Tornado

3-A. Satellite Infrared Digital Data Analysis

GOES digital IR data for the entire United States during the 0004-0203 GMT, May 29, 1977 was analyzed in this example. It was found that the isolated cloud in north central Oklahoma was the only cloud with a cloud top temperature $\leq -70.2^{o}C$ during this time period.

The area expansion of the cold elements of the cloud top was studied. Figure 9 shows the changes in the areas of the cloud top at different temperatures during the 0004-0203 GMT time period. Cloud top started to grow to the altitude with equivalent blackbody temperature, $T_{BB} \leq -65.2^{o}C$ at 0004 GMT. At

0033 GMT, cloud top reached to the altitude with temperature $\leq$ -67.2°C; at 0103 GMT, cloud top to the altitude with temperature $\leq$ -70.2°C; at 0133 GMT, cloud top to the higher altitude with temperature $\leq$ -72.2°C; and at 0148 GMT, cloud top finally grew to the highest altitude with lowest temperature at -74.2°C. The area of the cloud top with temperature $\leq$ -72.2°C had its maximum value at 0133 GMT, gradually decreased until 0148 GMT, and then sharply decreased. The tornado finally touched down at 0205 GMT, apparently as the cloud top was rapidly collapsing. This result is in good agreement with the aircraft observations made by Fujita and his associates (Fujita and Caracena, 1977; Fujita and Byers, 1977).

For the purpose of relating the temperature of the penetrating turret to an altitude, the rawinsonde data from Oklahoma City, Olkahoma were analyzed. Based on the rawinsonde data of 2300 GMT, May 28, 1977 and 1100 GMT, May 29, 1977, the temperature of the tropopause was around -64°C and the altitude of the tropopause was around 13 km, while the lowest cloud top temperature observed on the satellite IR imagery was -74.2°C about 14 to 30 minutes before the touchdown of the tornado. It can be seen from Figure 9 that the cloud top started to penetrate above the tropopause approximately two hours before the touchdown of the tornado. The coldest overshooting top temperature was more than 10C° below the temperature of the tropopause. The area of the cloud top penetrated above the tropopause just before the touchdown of the tornado, for this particular case, was 605 pixels.

Figure 10 shows the growth rate of cloud top areas penetrated above the tropopause. The maximum growth rate of the area with temperature $\leq$ -65.2°C (0.5 km or more above the tropopause) with the value of 12.2 x 10^{-2} pixels-sec^{-1} occurred about 45 minutes before the tornado touchdown. In other words, the maximum growth rate of the penetrative overshooting turret above the tropopause (essential for formation of tornadic storms) occurs approximately one hour or less before the tornado touchdown. On the other hand, the growth rate of the high altitude cloud with temperatures $\leq$ -70.2°C, $\leq$ -72.2°C and $\leq$ -74.2°C became negative, implying that the higher altitude cloud began collapsing approximately 15 to 30 minutes before the tornado touchdown.

3-B. Convective Clouds and Gravity Waves

During the period 0200-0245 GMT May 29, 1977, three gravity wave trains, detected by the Doppler sounder array located in Huntsville, Alabama, were analyzed. [See Hung et al., (1980) for a detailed description of the wave analysis for this particular day.] Figure 11 shows the ray tracing results for the three gravity wave trains observed during the 0200-0245 GMT time period. The computed ray path of the waves observed during the 0200-0230 GMT time period is labeled A. B is for the 0200-0245 GMT observation period; and C is for the 0215-0245 GMT observation period. Since the wave traveling times from the computed probable source to the observation point were 138-162 minutes and the actual touchdown time was 0205 GMT, the signals were excited more than one hour prior to the touchdown.

The gravity waves with wave periods of 14.7 - 16 min propagating from north central Oklahoma were the only gravity waves detected by the Doppler array during the 0100-0300 GMT, May 29, 1977 time period. Acoustic waves with wave periods of 3-5 and 6-9 min, which are believed to be excited by enhanced convection associated with severe thunderstorms were also detected. <u>Storm Data</u>, issued by the National Climate Center, and tornado touchdown <u>records</u>, reported by the National Severe Storm Forecasting Center, indicated that while severe thunderstorms were occurring in Kansas, Kentucky, Alabama, Georgia, etc., the tornaod in north central Oklahoma was the only one reported during this entire period.

In this case, the location of the computed probable source of the waves was near the location of the actual tornado touchdown in the north central section of Oklahoma at which the isolated cloud with enhanced convection was observed from satellite IR imagery.

3-C. Airmass Instability from Rawinsonde Observations

Meteorological data shows that there was no front in this area of Oklahoma during the time period of the satellite observations. Gravity wave trains were detected by the Doppler sounder array located in Huntsville, Alabama in these time periods. Results of ray tracing show that a series of gravity waves was excited from the area of cloud at north central Oklahoma. The association between gravity waves and severe convective storms has been shown extensively in the laboratories and in the field during the past decade (Curry and Murty, 1974; Gossard and Sweezy, 1974). The observation of gravity-waves initiated from the cloud located at north central Oklahoma, indicates the existence of strong convection inside the cloud. If any short period waves, with periods of 5 minutes, were excited by other clouds, they were too weak to be detected in the Huntsville area which is 400 km away from the wave source; however, the wave trains with periods of 15 minutes excited by the cloud at north central Oklahoma were detected. This is due to the fact that the damping rate of a wave is inversely proportional to the wave period, and only the waves with longer wave periods can propagate the longer distance without dissipation (Hung et al., 1975).

The stability of an air mass can be determined from rawinsonde observations. On the 2300 GMT, May 28, 1977, Oklahoma City rawinsonde, the temperature lapse rate was dry adiabatic below 2.1 km (790 mb). The relative humidity was around 70 in this lower layer of the atmosphere. There were temperature inversions between 2.1 and 2.5 km, and also between 4.4 and 4.5 km. The air mass was fairly unstable between 6.0 and 7.2 km, because the lapse rate was nearly dry adiabatic. Once this unstable air mass gained enough energy to penetrate the temperature inversions at 2.1 and 4.4 km, the updraft motion continued until the clouds reached the altitude of the tropopause. The precursor oscillations occurred at an altitude of about 4.5 km before the updraft air mass completely overcame the temperature inversion. The size of the cloud formed is partially dependent upon the amount of moisture available to provide the energy source for initiating the updraft motion.

4. Discussions and Conclusions

Special rapid-scan satellite visible and infrared observations have enabled observation of clouds associated with severe convective storms. The satellite data have permitted study of the life cycle of the clouds from the initiation of condensation, through the formation of the clouds, the development of towering cumulus, the penetration of the tropopause, the collapsing of an overshooting turret, and the dissipation of the cloud. During the inception and developing stages of the clouds before they penetrated the tropopause, there are very few apparent differences between the cloud which spawned a tornado and that which ended as a thunderstorm. After the penetration of the tropopause, the differences between the two cloud systems are more readily discernible using satellite observations. The basic characteristics of the cloud associated with the tornado were (1) a large volume of cold cloud above the tropopause (2) a higher growth rate for cloud above the tropopause (3) a cloud top temperature much lower than the tropopause, and (4) a rapid collapsing of the cloud top immediately prior to the touchdown of the funnel cloud. Characteristics of the cloud which terminated in a thunderstorm based on the present study were (1) a small volume of cold cloud above the tropopause, (2) a slow growth rate for cloud above the tropopause (3) a cloud temperature not much lower than the tropopause temperature, and (4) a gradually dissipating cloud above the tropopause.

Since the temperature of the overshooting turret is much lower than that of the surrounding air, the density of the turret is much higher than the surrounding air density, and the overshooting turret can only exist as long as it is dynamically supported by intense vertical convection. The relation between the time rate of change of vertical momentum and energy released by moisture condensation can be shown as

$$\frac{d}{dt} (M_a V_z) = F_z = - \frac{dQ}{dz}$$

where M_a stands for the mass of the moist air; V_z, the vertical velocity of the moist air mass; F_z, the force in the vertical direction; and Q, the total energy released from moisture condensation.

It is clear that, in order to support a tall, large and heavy overshooting turret above the tropopause, a large gradient of thermal energy is necessary. To overcome the temperature inversions, an updraft motion also had to be initiated which was also assisted by a large gradient of thermal energy.

Severe convective storms are a mesoscale phenomena with a short life cycle of a few hours duration; therefore, rapid scans are necessary to insure obtaining effective observations of the future storm development. If the observations are more than 15 minutes apart, the collapsing of cloud top just prior to the formation of the funnel cloud cannot be observed because the collapse of the cloud top normally occurs about 15 to 30 minutes before the touchdown of the tornado based on the case studies on March 24, 1976; April 11, 1976 and May 29, 1977. Neither the current ground or satellite-based observations provide the temporal and spatial data coverage required to establish the detailed life cycles of clouds in mesoscale systems. Imaging systems with rapid scan capabilities, less than 15 minute intervals, and sounders with spatial resolutions of on the order of 25-50 km would be required to insure adequate data coverage for these types of severe weather occurrences.

Areas of localized moisture convergence cannot be determined from the current rawinsonde observation network. It remains to be seen if the proposed satellite sounder systems will provide the data to distinguish such localized areas.

Nevertheless, the present article illustrates the capability of infrared and visible images (from geosynchronous satellite) to describe the life cycles of tornadic clouds. There is evidence of differences between clouds associated with tornadoes and those that are not, after the clouds have penetrated above the tropopause. Earlier detection of severe storms might be possible if localized areas of moisture convergence and instability could be identified.

Acknowledgements

R. J. Hung appreciates the support of present study from the National Aeronautics and Space Administration through contract NAS8-33726.

References

Adler, R. F., and D. D. Fenn, J. Appl. Meteor., 18, 502-517, 1979.

Adler, R. F., and D. D. Fenn, J. Appl. Meteor., 1982 (in press).

Adrian, R. J., J. Fluid Mech., 69, 753-781, 1975.

Baker, D. M., and K. Davies, J. Atmos. Terr. Phys., 31, 1345-1352, 1969.

Bean, B. R., R. E. McGavin, and B. D. Warner, Boundary-Layer Meteor., 4, 201-209, 1973.

Bertin, R., J. Testud, L. Kersley, and P. R, Rees, J. Atmos. Terr. Phys., 40, 1161-1183, 1978.

Browning, K. A., J. R. Starr, and A. J, Whyman, Boundary-Layer Meteor., 4, 91-111, 1973.

Curry, M. J., and R. C. Murty, J. Atmos. Sci., 31, 1402-1408, 1974.

Deardorff, J. W., G. W. Willis and D. K, Lilly, J. Fluid Mech., 35, 7-31, 1969.

Einaudi, F., and D. P. Lalas, J. Atmos. Sci., 32, 536-547, 1975.

Fujita, T. T., and F. Caracena, Bull. Am. Meteor. Soc., 58, 1164-1181, 1977b.

Fujita, T. T., and H. R. Byers, Mon. Wea. Rev., 105, 129-146, 1977.

Gentry, R. C., E. Rogers, J. Steranka, and W. E. Shenk, Mon. Wea. Rev., 108, 445-455, 1980.

Georges, T. M., Rev. Geophys. Space Phys., 11, 571-594, 1973.

Georges, T. M., and G. E. Greens, J. Appl. Meteor, 14, 1303-1316, 1975.

Gossard, E., and W. Munk, J. Meteor., 11, 259-269, 1954.

Gossard, E., and W. B. Sweezy, J. Atmos. Sci., 31, 1540-1548, 1974.

Hung, R. J., and J. P. Kuo, J. Geophys., 45, 67-80, 1978.

Hung, R. J., T. Phan, and R. E. Smith, J. Atmos. Terr. Phys., 40, 831-843, 1978a.

Hung, R. J., T. Phan, and R. E. Smith, AIAA Journal, 16, 763-766, 1978b.

Hung, R. J., T. Phan, and R. E. Smith, J. Appl. Meteor., 18, 460-466, 179a.

Hung, R. J., T. Phan, and R. E. Smith, J. Geophys. Res., 84, 1261-1268, 1979b.

Hung, R. J., and R. E. Smith, J. Appl. Meteor., 17, 3-11, 1978.

Hung, R. J., and R. E. Smith, J. Geomag. Geoelectr., 31, 183-194, 1979.

Hung, R. J., S. T. Wu, and R. E. Smith, J. Geophys. Res. 80, 4325-4335, 1975.

Matsumoto, S., and T. Akiyama, J. Meteor. Soc. Japan, 47, 255-266, 1969.

Prasad, S. S., L. J. Seneck, and K. Davies, J. Atmos. Terr. Phys., 37, 1357-1363, 1975.

Purdom, J. F. W., Mon. Wea. Rev., 104, 1474-1483, 1976.

Rice, C. J., and L. R. Sharp, Geophys. Res. Lett., 4, 315, 1977.

Ruttger, J., J. Atmos. Terr. Phys., 39, 987-998, 1977.

Sikdar, D. N., V. E. Suomi, and C. E. Anderson, Tellus, 22, 521-532, 1970.

Smith, R. E., and R. J. Hung, J. Appl. Meteor., 14, 1611-1615, 1975.

Spencer, N. W., R. F. Theis, L. E. Wharton, and G. R. Carrigan, Geophys. Res. Lett., 3, 313-319, 1976.

Stull, R. B., J. Atmos. Sci., 33, 1279-1286, 1976.

Townsend, A. A., Quart. J. Roy. Meteor. Soc., 90, 248-259, 1964.

Uccellini, L. W., Mon. Wea. Rev., 103, 497-513, 1975.

Willis, G. E., and J. W. Deardorff, J. Atmos. Sci., 31, 1292-1307, 1974.

Figures

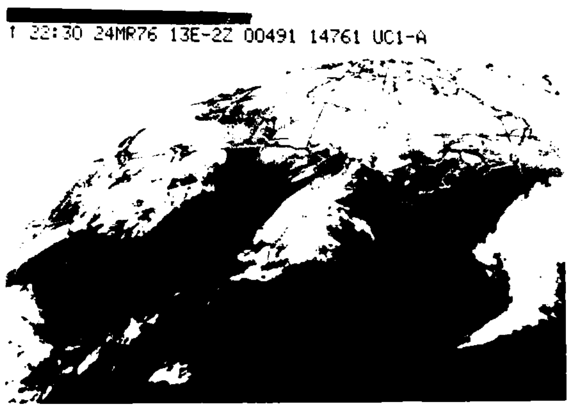

Figure 1. Infrared image from GOES-East at 2230 GMT, March 24, 1976, showing cloud in southwestern Louisiana, responsible for gravity wave generation, and the other non-tornado associated clouds.

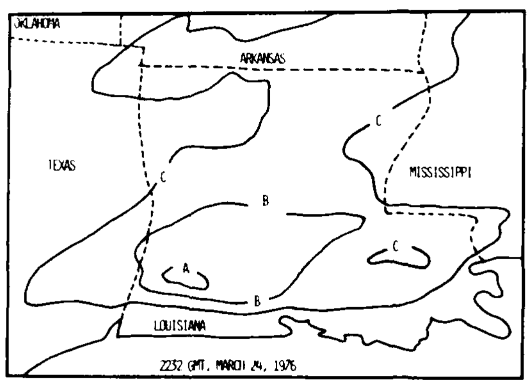

Figure 2. Geographical location of cloud top temperature distribution at 2232 GMT, March 24, 1976. Contour A indicates cloud top with temperature $\leq -60^{\circ}C$; contour B, cloud top with temperature in the range of -55 to $-65^{\circ}C$; C, the area of cloud.

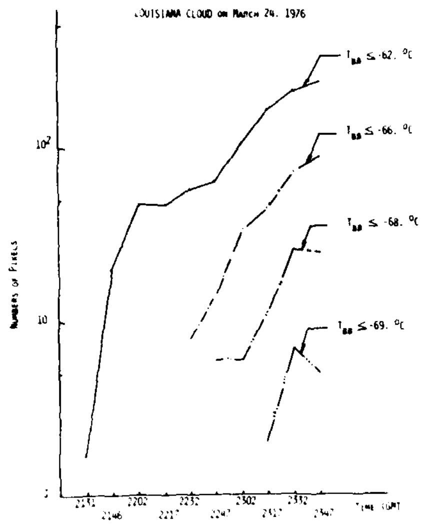

Figure 3. Area expansion and vertical growth of penetrative overshooting cloud top in terms of time change of pixels with temperatures ≤ $-62^{\circ}C$, and ≤ $-66^{\circ}C$, ≤ $-68^{\circ}C$, and ≤ $-69^{\circ}C$ during 2131-2347 GMT, March 24, 1976, for gravity-wave-excited clouds located in southwestern Louisiana.

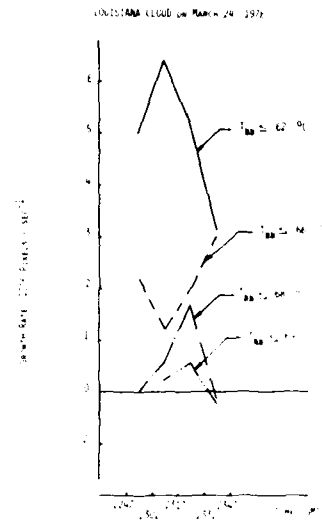

Figure 4. Growth/collapse rate of penetrative overshooting cloud top with temperatures ≤ $-62^{\circ}C$, ≤ $-66^{\circ}C$, ≤ $-68^{\circ}C$, and ≤ $-69^{\circ}C$ during the time period 2247-2347 GMT, March 24, 1976, for cloud at southwestern Louisiana.

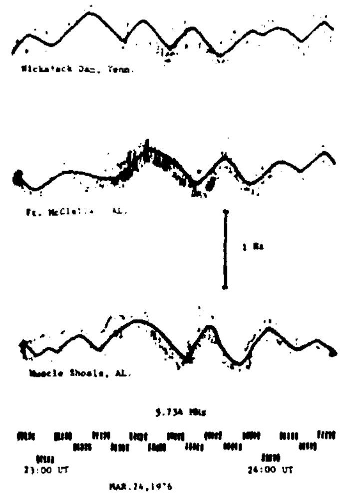

Figure 5. Doppler record on March 24, 1976, during the time period of 2255-2415 GMT, at the operating frequency 5.734 MHz.

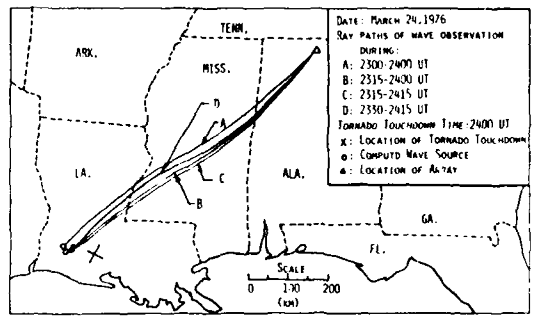

Figure 6. Computed locations of wave sources for waves observed at 2300-2400, 2315-2400, and 2315-2415, and 2300-2415 GMT, March 24, 1976, and the location of tornado touchdown.

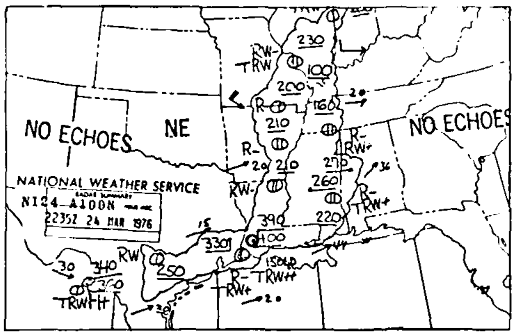

Figure 7. Radar weather summary of the southern United States at 2235 GMT, March 24, 1976. The storm associated with tornado is marked with a small circle.

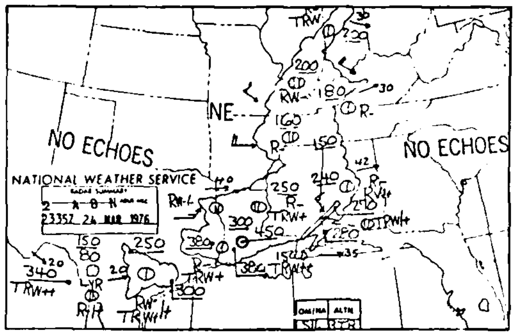

Figure 8. Radar weather summary of the southern United States at 2335 GMT, March 24, 1976. The storm associated with tornado is marked with a small circle.

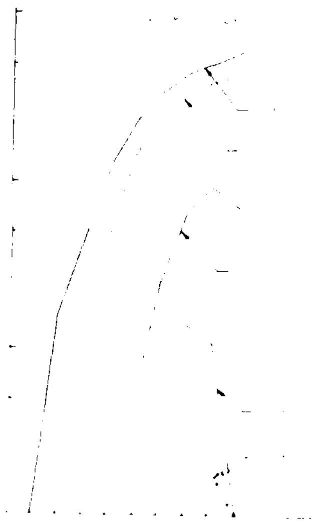

Figure 9. Cold area expansion and vertical growth of the cloud top in terms of time change of number of pixels with temperatures $\leq$ -65.2^{o}C, $\leq$ -67.2^{o}C, $\leq$ -70.2^{o}C, $\leq$ -72.2^{o}C, and $\leq$ -74.2^{o}C during 0004-0203 GMT, May 29, 1977 for an isolated tornado located in north central Oklahoma.

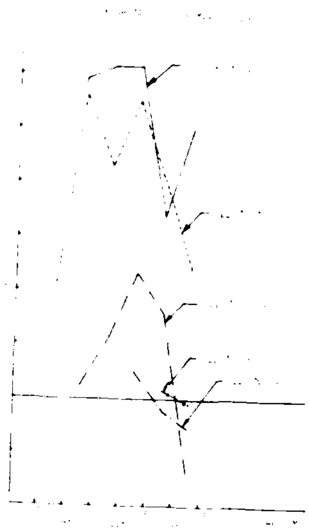

Figure 10. Growth/collapse rate of penetrative overshooting cloud top with temperatures $\leq$ -65.2^{o}C, $\leq$ -67.2^{o}C, $\leq$ -70.2^{o}C, $\leq$ -72.2^{o}C, and $\leq$ -74.2^{o}C during the time period 0004-0203 GMT, May 29, 1977 for cloud at north central Oklahoma.

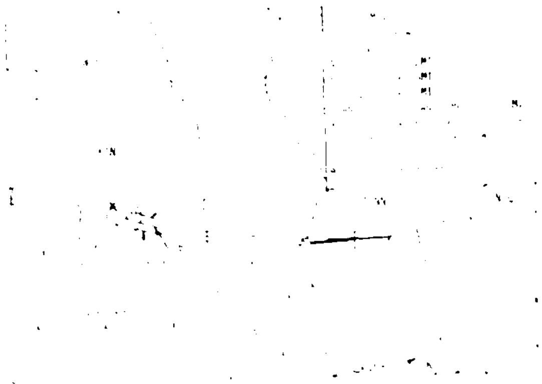

Figure 11. Computed locations of wave sources and the location of the tornado touchdown. Curves A, B and C express the ray paths at 0200-0230, 0200-0245, and 0215-0245 GMT, May 29, 1977. The circle with the broken line is the error circle for ray path B.

Tables

Table 1. Propagation characteristics of the observed gravity waves associated with tornadic storms on March 24, 1976.

[illegible]	[illegible]	[illegible]	[illegible]	[illegible]	[illegible]		Location [illegible]	[illegible]	[illegible]
[illegible]	[illegible]	[illegible]	[illegible]	[illegible]	1	[illegible]	[illegible]	[illegible]	[illegible]
[illegible]	[illegible]	[illegible]	[illegible]	[illegible]	2	[illegible]	[illegible]	[illegible]	[illegible]
[illegible]	[illegible]	[illegible]	[illegible]	111	2	16	[illegible]		
[illegible]	[illegible]	[illegible]	[illegible]	[illegible]	2	16	[illegible]		

DISCRIMINATION BETWEEN RANGELAND PASTURE COMMUNITIES IN THE NORTH-WEST OF AUSTRALIA USING LANDSAT DATA

N.A. Campbell[b], F.R. Honey[a], I.J. Tapley[a],

D.G. Burnside[c] and W.F. Holman[d]

ABSTRACT

The management of the rangelands of Western Australia requires both range inventory and trend estimation. This paper reports the progress of an investigation into the use of Landsat digital data for these purposes. The overall aim of the study is to examine the relationships between Landsat digital data and the vegetative characteristics of some rangeland types from different communities in varying range condition.

The area under investigation is located in the semi-arid north-west region of Western Australia, amidst tussock grassland and tall shrubland communities in a variety of condition classes.

The vegetation characteristics of sites located in five pasture communities in varying range conditions were sampled at regular intervals during 1980 and 1981.

The aspects of the study reported here examine the relationship between measured vegetative characteristics of the pasture communities and the Landsat data, and the discrimination between the pasture communities using Landsat data.

There is one strong canonical correlation between the Landsat bands and the vegetative characteristics, with the canonical vector for the Landsat bands reflecting a contrast between band 5 (B5) and either band 6 (B6) or band 7 (B7), and

[a] CSIRO, Division of Land Resources Management, Wembley 6014, Western Australia

[b] CSIRO, Division of Mathematics and Statistics, Wembley 6014, Western Australia

[c] Department of Agriculture, Kalgoorlie 6430, Western Australia

[d] Department of Lands and Surveys, Perth 6000, Western Australia

that for the vegetative characteristics being dominated by the proportion of green biomass (PG). The relationship between the difference B6-B5 and the vegetative characteristics explains virtually all of the relationship between the two sets of variables.

Canonical variate analysis is used to discriminate between the pasture communities. Bands 5 and 7 give the best discrimination.

Excellent allocation of individual pixels is achieved. Atypical pixels are identified and discussed.

OBJECTIVES OF PROJECT

This paper reports the progress of an investigation into the use of Landsat digital data for the management of the rangelands of Western Australia. The area under investigation is located in the semi-arid northwest region of Western Australia, amidst tussock grassland and tall shrubland communities in a variety of condition classes.

The overall aims of the project are:

(1) to develop relationships between Landsat bands and parameters characterizing the vegetation, hereafter referred to as vegetative characteristics, for a range of communities in varying condition; and

(2) to develop relationships over time between Landsat bands and vegetative characteristics which will discriminate between, and determine the condition of, the communities and provide a means of determining trend.

This paper describes analyses of data related to these objectives, using multiple regression, canonical correlation analysis, canonical variate analysis and allocation procedures.

DATA ANALYSIS

Canonical correlation analysis is applied to the analysis of the relationships between the Landsat bands and the vegetative characteristics. The technique is reviewed by Gittins (1979). Linear combinations of the two sets of variables - the Landsat bands and the vegetative characteristics - are derived such that the correlation between these linear combinations is a maximum. Multiple regression may be considered as a subset of canonical correlation in which only one variable is considered in one of the sets. There are high correlations between the Landsat bands and between some of the vegetative characteristics, and this may lead to unstable estimates of the coefficients defining the linear relationships (see, e.g., Phillips, et al., 1973; Marquardt and Snee, 1975).

Ridge-type procedures, which tend to offset ' effect of the high correlations, are incorporated into the analysis. Tne analysis implemented here restricts the solution to a subspace spanned by the first few principal components of the Landsat bands and to that spanned by the first few principal components of the vegetative characteristics.

Canonical variate analysis is used to provide a description or ordi-

nation of the differences between the sites. Linear combinations of the Landsat bands are chosen to maximize the ratio of the between-groups sum of squares to the within-groups sum of squares; successive linear combinations are chosen to be uncorrelated within sites (see, e.g., Campbell & Atchley, 1981). The ratios of sums of squares are referred to as the canonical roots.

Pixels from the different sites are allocated using leave-one-out calculations. Posterior probabilities are estimated using multivariate Student densities (see, e.g., Anderson, 1958, Section 6.3; Aitchison, et al., 1977). In view of the relatively small number of pixels at a site (minimum 12, maximum 28), equal covariance matrices are assumed in the calculation of the multivariate Student densities. An index of typicality is also calculated for each pixel (see Aitchison et al., 1977, for a formal definition). This index reduces to the probability associated with the individual squared Mahalanobis distance for the pixel. For leave-one-out calculations or for pixels from additional testing sites, the probability is calculated by referring the squared Mahalanobis distance to the F distribution.

STUDY AREA

The study area, covering approximately 30 km E-W and 20 km N-S, is on Minderoo Station, which straddles the Ashburton River along 80 km of its course near Onslow, Western Australia. The land systems of the area have been described by Payne, Mitchell and Holman (1983). Much of the area consists of depositional surfaces comprised mainly of Quaternary alluvium with some areas of Quaternary aeolian sand.

The region has an average annual rainfall of 250 mm, with winter and summer rainfall, winter dominating. There may be heavy falls during the period January to March as a result of cyclone activity or tropical depressions. Daily maximum temperatures range from 25 degrees in winter to 45 degrees in summer.

VEGETATION TYPES

The data have been collected over seventeen sites chosen to represent the major pasture groups occurring in the area at varying condition levels. These vegetation types are:

1. *Cenchrus* spp. (Tussock grassland)
2. *Astrebla elymoides* (Tussock grassland)
3. *Eragrostis* spp (Tussock grassland)
4. *Eriachne* spp. (Tussock grassland)
5. *Acacia victoriae* (Shrubland with sparse under-storey)

Each of the sites was chosen within a large (> 20 ha) uniform area and aligned with major axes either in a 10-190 degrees or 100-280 degrees orientation to coincide with the ground sampling grid of the satellite. This was done in order to avoid sampling transition from the Landsat computer compatible tapes. Site dimensions average 400 x 400 metres.

GROUND DATA

The seventeen sites were sampled on 5 occasions during the 1980-81 season. Sampling times were chosen to coincide as closely as possible with Landsat times. At each sampling date, the following vegetative characteristics were estimated:

1. Fresh biomass (kg/ha) (FW)
2. Dry biomass (kg/ha) (DW)
3. Proportion of green biomass (percentage) (PG)
4. Projected foliage cover (including litter), for grasses and annual

species (percentage) (PFCT)

5. Botanical composition (units)
6. Projected shrub and tree cover (percentage) (PFCS)
7. Percentage moisture of perennial grasses (PM)

The projected shrub and tree cover was estimated using the Bitterlich technique (Cooper, 1957). Thirty random observations were made at each site. The remaining ground data were obtained by sampling with a 0.5 x 1 metre quadrat. Sixty quadrats were dropped along six random transects to sample the entire site. A double sampling method based on that developed by Wilm et al. (1944) was used by three observers to obtain estimates of fresh biomass. Sufficient samples were cut and dried to allow the determination of dry biomass. The proportion of green biomass and projected foliage cover were estimated for each quadrat.

A modification of the dry weight rank method of t'Mannetje and Haydock (1963) was used to estimate the proportion of perennial grasses, annual species and litter on each site. Percentage moisture was calculated as 100(FW-DW)/FW and is denoted here as PM.

LANDSAT DATA

Five LANDSAT scenes covering the area were analysed. The scene identifications and dates are:

E 22037-01324	20 August 1980
E 22056-01384	8 September 1980
E 22092-01385	14 October 1980
E 22164-01381	24 December 1980
E 22272-01370	12 April 1981

The 4-band data for the experimental sites were extracted for each of the scenes. The data were corrected for atmospheric backscatter by dark-target (averaged deep ocean areas) subtraction, and converted to "normal sun" values by dividing by the sine of the sun elevation.

RELATIONSHIPS BETWEEN LANDSAT BANDS AND VEGETATIVE CHARACTERISTICS OVER ALL DATES

The means of each of the bands are used to characterize the Landsat bands for each site.

There are strong correlations among the Landsat bands, particularly between band 4 and the remaining bands, and among the vegetative characteristics, particularly between FW and DW, PG and PFCT.

A canonical correlation analysis of the interrelationships between the Landsat bands and the vegetative characteristics shows one strong canonical correlation ($r^2_{c1} = 0.95$; $r^2_{c2} = 0.22$), with the first canonical vector for the Landsat bands reflecting a contrast between B5 and either B6 or B7, and that for the vegetative characteristics being dominated by PG (see Honey et al., 1980, Table 2). The difference B6-B5 explains virtually all of the relationship with the vegetative characteristics ($R^2 = 0.93$). Further examination shows that the relationship between B6-B5 and PG ($r^2 = 0.78$) explains much of this variation. Other bands contribute to the relationships between each vegetative characteristic separately and the Landsat bands.

An examination of the interrelationships for the different communities shows similar degrees of relationship between the Landsat bands and the vegetative characteristics for *Acacia* shrub when compared with the overall data set, while those for *Eragrostis* spp. are a little lower. The relationship between the difference B6-B5 and the vegetative characteristics is again

similar to that for the relationship between the two sets of variables.

The vegetative characteristics have higher values for PG and FW for the samples taken on 20-08-80 than at the other dates. To evaluate the effect of the different times of sampling, and the predictive ability of the relationships, the data are examined with each date excluded in turn. Comparison of the relationships from these analyses with those of the relationships over all times shows that leaving out the data collected on 20-08-80 gives consistently lower r^2_{c1} and R^2 values. Once again, the relationship between B6-B5 and the vegetative characteristics explains virtually all of the relationship between the two sets of variables for the various analyses. Only for PFCT is there a noticeable decrease in the magnitude of the relationship when the four bands are replaced by B6-B5.

DISCRIMINATION BETWEEN THE SITES

There is marked separation between the 17 sites, with virtually all sites being separated along one or more of the first five canonical variates.

Table I summarizes the first five canonical roots when all bands are analyzed for all dates, and when various subsets of the bands and dates are analyzed. An analysis based on B5 and B7 gives virtually the same description of site differences as that based on all bands, while the separation based on B5 and B6 is less marked.

Table I. Summary of First Five Canonical Roots (f_1-f_5) for Minderoo data

	f_1	f_2	f_3	f_4	f_5
B4,...,B7 all dates	18.80	8.75	4.06	2.90	1.66
B5,B7 all dates	17.08	8.01	3.27	2.49	0.73
B5,B6 all dates	16.38	5.73	2.28	1.28	0.86
B7-B5 all dates	12.36	4.47	1.95	0.81	0.36
B6-B5 all dates	6.59	2.78	0.81	0.59	0.19
B5,B7 with B7 on 14-10-81 excl	15.56	6.35	3.27	2.10	0.60

Figure 1 shows the relationships between the sites based on all bands for all dates (Figure 1(a)) and on B5 and B7 for all dates (Figure 1(b)), while Figures 2(a) and 2(b) show a plot of B5 and B7 respectively for a selection of sites. B5 on 20-08-81 and B7 on 14-10-81 make little contribution to the site separation.

The first canonical variate separates and ranks sites on the basis of total projected foliage cover, especially in the period August-October, 1980 (Table II). For example, sites 57, 72 and 65 are relatively well covered, while site 98 is poorly covered.

Table II. Variation in Projected Foliage Cover for a Selection of Sites

Site	Aug 80	Oct 80	Dec 80	Apr 81
57	59	50	42	32
72	40	37	36	27
65	31	39	26	27
71	21	21	17	7
97	27	24	29	25
201	13	13	15	16
98	17	12	15	5

The first canonical variate is dominated by B5 for the first three dates. For example, site 33 has high values (means of 110.3, 108.3 and 130.5

with a standard deviation of approximately 6.5) while sites 57 and 58 have low values (means of 35.9, 40.8 and 91.1 and 43.2, 48.1 and 105.3).

The second canonical variate to some extent separates and ranks sites with similar ground cover on the basis of percentage of biomass which is green, again especially in the period August-October, 1980 (Table III).

Table III. Variation in Percent Greenness for a Selection of Sites

Site	Aug 80	Oct 80	Dec 80
58	93	28	5
200	81	65	3
72	61	61	14
50	92	26	2
4	74	55	7
71	82	67	3

The second canonical variate is dominated by differences in B7 on 20-08-80, B5 on 8-9-80, and the contrast between B7 and B5 on 24-12-80.

The third canonical variate is dominated by differences in B5 and B7 at 12 April. For example, site 19 has means of 87.8 and 95.3 (with standard deviations of 7.3 and 4.9) while site 50 has means of 82.6 and 100.9.

There is no ready interpretation of the remaining canonical variates in terms of the associated vegetative characteristics.

There is no obvious grouping of sites into communities in Figure 1. This is to be expected due to the wide range of condition types, from good to poor, within each community. There is some tendency for sites which are predominantly _Acacia_ shrubland with grassland understory (sites 1, 19, 57, 58) to group together; they have low scores on the first canonical variate and high scores on the second canonical variate. There is also some tendency for tussock grasslands (sites 65, 72, 78, 200) to group together; they have low scores on the first two canonical variates. In what follows, the sites are considered as seventeen potentially distinct classes.

The results of the allocation of individual pixels to the seventeen classes based on B5 and B7 for all dates and using leave-one-out calculations with equal covariance matrices are summarized in Table IV.

Misallocated pixels are usually identified as belonging to the site nearest to the relevant reference site in Figure 1. Site 4 is an exception.

Site 4 consists of four lines by four pixels (Figure 3(a)), with pixels in positions (3,1) and (4,1) being wrongly identified. While Site 4 is generally covered by tussock grassland, some _Acacia victoriae_ shrubs are found in the S-W corner. Pixel (3,1) is identified as belonging to site 201 and has a typicality index of 0.16, while pixel (4,1) is identified as belonging to site 1 but is also atypical for that site (index of 0.02).

For site 72, one pixel is strongly allocated to site 65. A further three pixels are allocated to other sites using a forced allocation (Figure 3(b)), though all three should be indicated as doubtful. They are, in fact, typical for both their reference site and the site for which they have the highest probability of group membership.

Site 201 is located on a broad sand-dune, with the western side of the site bordered by scald patches. These pixels have been identified as atypical, with two being allocated to other groups (Figure 3(c)). Due to small fluctuations in the path of the satellite, these pixels are best considered as

mixed pixels.

Table IV. Results of Forced Allocation of Individual Pixels using Leave-One-Out Calculations for the Seventeen Sites

Group No in Figure 1	Site No	No of Pixels	Number Correctly Allocated (with Relative Frequency)	Pixel(s) Incorrectly Allocated with Identity of Site(s)
1	57	20	20 (100)	
2	1	16	14 (87)	2 to site 19
3	19	16	12 (75)	1 to site 1; 3 to site 50
4	58	16	16 (100)	
5	98	25	24 (96)	1 to site 202
6	33	20	20 (100)	
7	72	28	24 (85)	2 to site 65; 1 to site 71; 1 to site 200
8	4	16	14 (87)	1 to site 201; 1 to site 1
9	201	16	13 (81)	1 to site 71; 2 to site 202
10	65	16	14 (87)	2 to site 78
11	78	28	25 (89)	2 to site 72; 1 to site 65
12	50	16	15 (93)	1 to site 19
13	70	12	9 (75)	2 to site 78; 1 to site 71
14	71	18	16 (88)	1 to site 70; 1 to site 78
15	97	18	18 (100)	
16	202	15	11 (73)	4 to site 201
17	200	18	18 (100)	

DISCUSSION

There is clear and marked separation between most of the sites. Very little overlap of individual pixels is evident.

The detailed examination of pixels which are wrongly identified or which are atypical highlights the need for careful selection and definition of the reference sites. At least one additional class is necessary, to define scald patches.

Future work will concentrate on the analyses of further sites in the area, with data for additional dates being extracted if possible. The data for the reference groups will be based only on those pixels for a site which are considered to belong to the site and which are typical for the site.

ACKNOWLEDGEMENTS

The authors are grateful to Peter Hennig, W.A. Department of Agriculture, Carnarvon, for his assistance with the field sampling.

REFERENCES

Aitchison, J., Habbema, J.D.F. and Kay, J.W. (1977). A critical comparison of two methods of statistical discrimination. Appl. Statist., 26, 15-25.

Anderson, T.W. (1958). An Introduction to Multivariate Statistical Analysis. Wiley.

Campbell, N.A. & Atchley, W.R. (1981). The geometry of canonical variate analysis. Syst. Zool., 31, 268-280.

Cooper, F. (1957). The variable plot method for estimating shrub density. J. Range Management, 10, 111-115.

Gittins, R. (1979). Ecological applications of canonical analysis. In Multivariate Methods in Ecological Work (L. Orloci, C.R. Rao and W.M. Stiteler, eds). pp. 309-535.

Honey, F.R., Campbell, N.A., Tapley, I.J., Burnside, D.G., and Holman, W.F. (1981). Range inventory and monitoring used Landsat data in the semi-arid perennial grasslands of North-Western Australia. Proc. Landsat 81, 2.13.1-2.13.14.

Marquardt, D.W., and Snee, R.D. (1975). Ridge regression in practice. The Amer. Statist., 29, 3-20.

Payne, A.L., Mitchell, A.A. & Holman, W.F. (1983). A report on the condition of the Ashburton catchment. W.A. Dept. of Agriculture Report.

Phillips, B.F., Campbell, N.A., and Wilson, B.R. (1973). A multivariate study of geographic variation in the whelk Dicathais. J. Exp. Mar. Biol. Ecol., 11, 27-69.

t'Mannetje, L., and Haydock, K.P. (1963). The dry weight rank method for the botanical analysis of pasture. J. Brit. Grassl. Soc., 18, 268-275.

Wilm, H.G., Costello, D.F., and Klipple, G.E. (1944). Estimating forage yield by the double sampling method. J. Americ. Soc. Agron., 36, 194-203.

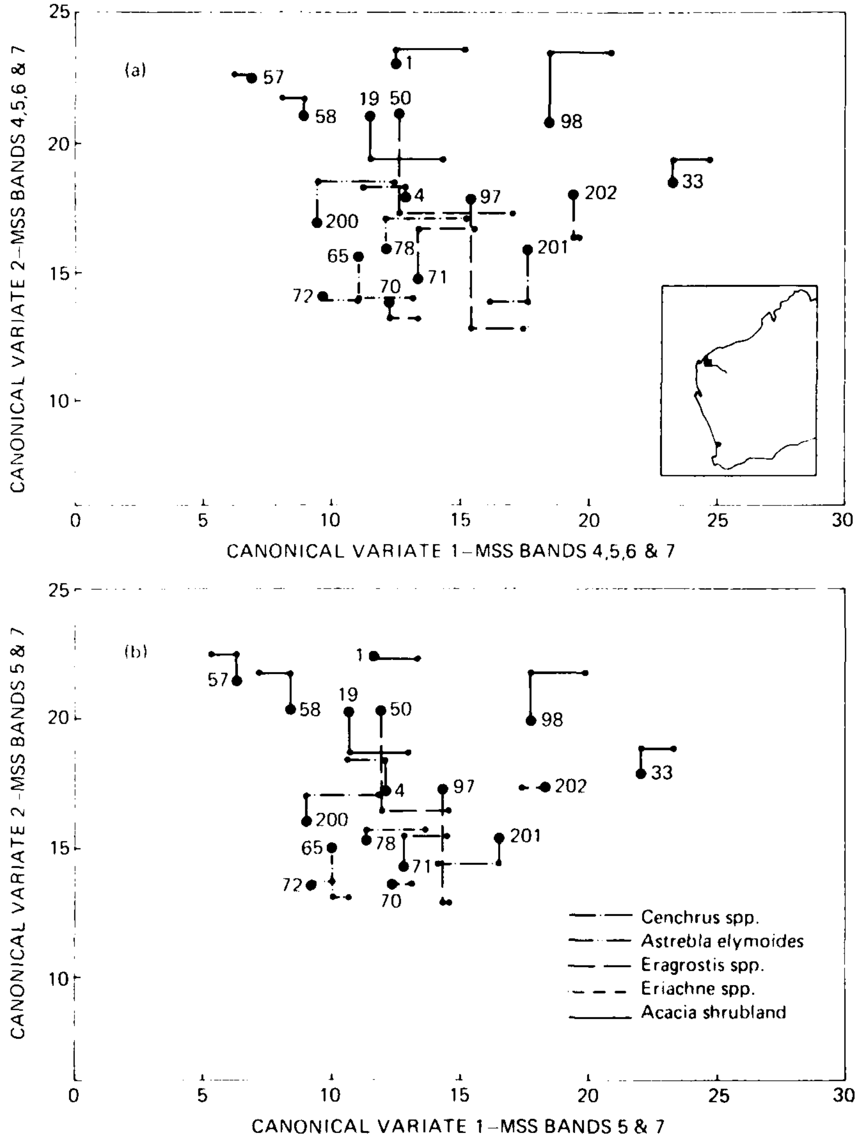

Figure 1 Means for 17 sites for first two canonical variates based on (a) all bands for all dates and (b) bands 5 and 7 for all dates. The canonical vectors are scaled to unit standard deviation within sites. The third and fourth canonical variates are indicated by vertical and horizontal lines.

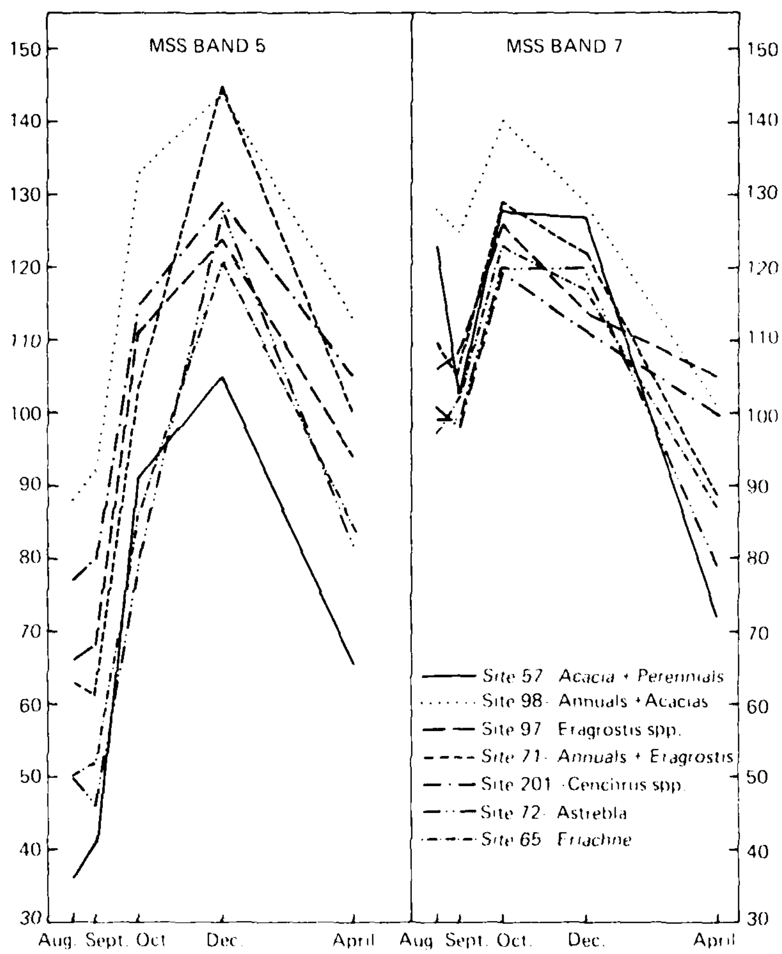

Figure 2 Plots of (a) band 5 and (b) band 7 against time for a selection of the sites from Figure 1.

3(a) Site 4 – Cenchrus spp.

3(b) Site 72 – Astrebla elymoides – excellent condition.

3(c) Site 201 – Cenchrus spp – good condition.

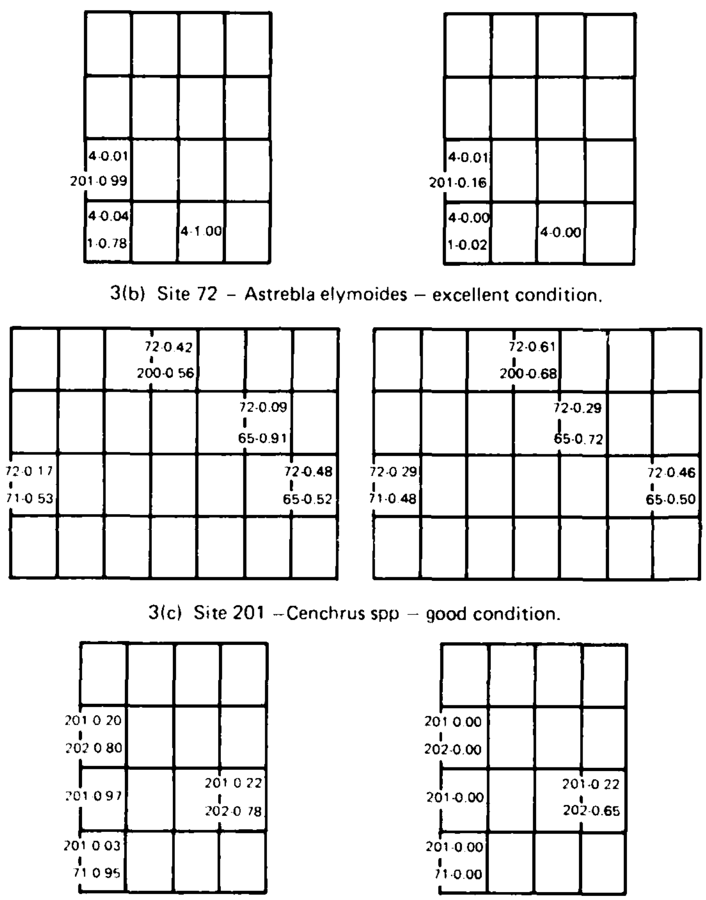

Figure 3 Representation of (i) group membership probabilities and (ii) typicality indices for a selection of sites where pixels are wrongly allocated and/or are found to be atypical. When group membership probabilities are given for two sites, the first refers to the reference site while the second refers to the site to which the pixel would be allocated if the usual forced allocation procedure was to be adopted. The corresponding typicality indices are given in (ii). Note that some pixels are atypical for both the reference and alternative sites. When only one group membership probability is given, this indicates that the pixel is atypical for the site, though the pixel would be allocated to the reference site if the usual forced allocation procedure was to be adopted.

REMOTE SENSING ANALYSIS OF FLOODING AND SALINITY PROBLEMS IN THE NW AREA OF BUENOS AIRES PROVINCE, ARGENTINA

Oscar Domínguez and Stella Carballo

Instituto Nacional de Tecnología Agropecuaria
Buenos Aires, Argentina

ABSTRACT

Many countries suffer great inundations that generally and periodically overwhelm regions of great productivity.

Governments are trying to study these inundations to become familiar with the origen, surface, velocity, depth, and the time of permanence of the waters. They are also trying to estimate damage, in order to program short and long term measures, to prevent or at least mitigate damage.

It was lamentable that countries of great extension and little development, due to technical and/or economic motives, could not concrete these studies.

Recently, since the last decade, satellite images have made possible this type of research.

In this paper it is shown, how, with minimum cost, time and personnel, it was possible to comprehend, map and measure five inundations, that caused great damage to a region of approximately 65.000 km^2 of the Argentine Republic.

Color composite diapositives (scale 1:1.000.000) and paper enlargements (scale 1:200.000) of bands 5 and 7 were used.

The interpretation was realized by two professionals, in four months of effective work, using a manual technique.

Ten maps covering an area of 70.000 km^2 were elaborated showing the different percentages of land-flood water. Two maps showing areas with different risk of flooding and maps showing outcropping salinity were made too.

1. INTRODUCTION

Due to the tragic effects that periodically and since remote times great inundations have had over lives and properties, man has had to preoccupy himself to learn the reach of this natural phenomenon, over determined sectors of the earth's surface.

The first written mention known to us of great floods and the technique utilized to detect the situation in a given moment, is mentioned in the Bible when the patriarchal NOAH, sends, form his arc, first a crow then later two doves, to inform him of the descent of the water and the presence of land not covered by water.

For as strange as it might seem, NOAH, utilized the most advanced technique: to receive information from the air of the situation below, just as today we use airplanes or satellites.

For its evaluation, traditionally, land control was the technique utilized. Unfortunately, this method becomes unpractical when the inundation blocks the roads and, also, the so obtained information generally results fragmented, subjective and inaccurate.

With the aerial photography development later the first World War, man had the possibility to study the inundations from an aerial perspective.

But the cost of this technique for developing countries, is such that, up to the present, it has only been utilized for evaluating natural resources.

Because of this, before phenomena of such magnitud and dynamics, such as are the inundations of regional extension, in which the information must be registered in sequencial form, the only practicable technique, until only a few years ago, continued to be terrestrial control, only sometimes complemented with aerial recognition.

Fortunately, in the world, since 10 years ago, there exists great possibility to investigate and evaluate inundations and salinization processes, by means of the information registered by remote sensors, transported by satellites.

The study of an inundation, be it local or regional, infers research about: 1) causes: Natural (by rain, by rising of rivers, lakes or seas). Anthropic (indikement incited by railroads, roads and canals, etc.) 2) evolution: (limit reached by the water in different dates, depth in different places; time of superficial and vertical drainage, direction, velocity of the currents, etc.). 3) consequences: loss of lives, damage to properties and installations (fences, etc), crop damage, soil deterioration by salinization, erosion or deposits of harmful sediments; contamination; destruction of natural vegetation and constructions (bridges, roads, etc.).

It must be remembered that when an inundation is surveyed by means of satellite images, what is obtained is the real representation of the flooding at the same date the image was taken. Nobody could cuestion that at that day and time, the water were not found where they were delimited. This technique resolves all types of doubt and prevents any fantasy that migth be weaved over the distribution, source or movement of the water, etc.

For a developing country, like the Argentine Republic, where big sectors of productive lands (approximately 1 million sq km) are cyclically devastated by droughts and inundations, it is of essential necessity to distinguish objectively and with great precision, the range and consecuence of these phenomena. The fact that from these lands dedicated essentially to agriculture crops and livestock, it is obtained the 80% of our country's commercial ingrees, makes it even more indispensable.

The introduction of this technique in the Argentine Republic, takes place in 1972 in the Instituto Nacional de Tecnología Agropecuaria (I.N.T.A.) but its concrete aplication in inundation and/or salinization studies, just takes place for first time in

the country, in 1978, when this work was started.

2. OBJECT

In 1978, the agricultural producers of the area enclosed by this study, solicited economical assistance to Buenos Aires Province Gobernment, considering that the inundations of previous years had produced salinization in the soil, and had prevented them from obtaining any benefits of their land and, on the contrary, suffered considerable losses.

The Government considered it necessary to accomplih an study to evaluate the real situation of the land. For such goal, it were used satellite images, to delimit the inundations and salinization of the lands and draw out conclusions regarding both phenomena.

3. ANTECEDENTS

Abundant Cartographic representations on microscopic scale, appear inmediately in the newspaper when an inundation is produced. These cartographic apart from their heavy errors, attemps to magnify the surface covered by water and the time of permanence of these waters. Also, they exagerate damage caused to the agricultural production, on account that the same who are damned by the incident, are the informants of the same, unable to give an objective view of the phenomenon because of the situation that directly affects them.

In 1973, in the maximum moment of the inundation affecting the zone of the present work, the Instituto Nacional de Tecnología Agropecuaria employed a lot of technicians to accomplish the map of the inundation, delimiting areas of different degrees of overflowing and, also, representing through arrows, the various movements of the waters.

Upon confronting this work with the satellite images, it was inmediatelly deduced that there was no relation between one information and the other. The work prepared using only land control technique, shows heavy errors in the limits of the waters and a whole error with respect to the movement and circulation of the superficial waters.

In 1978, before the present work were started, a map showing different soil salinity degrees was done by INTA technicians using the soil map, surveyed in previous years at 1:50.000 scale, complemented with land control.

Upon confronting this work with the flooding frequency map, elaborated from satellite images, it was met great correspondence between the limits of both maps.

4. LOCATION

The affected area is of approximately 65.000 km^2 and is limited on the N-NE with the Salado River, on the SE with the Arroyo Vallimanca depression, and has as limit W, the meridian that separates the Provinces of Buenos Aires and La Pampa (see Figure Nº 1).

The studied area, including almost 80 % of the whole affected area is included in two satellite images, numbered according to LANDSAT Worldwide Reference System as 243-084 and 243-085 (See Fig. 1).

5. PHYSIOGRAPHY

It deals with a great plain that on the west coincides with the datum level, of 110 m and at 280 km, with the datum level of 50 m. This makes the gradient become very scarce, which oscillates between 0,10 ‰ and 0,30 ‰.

This great plain, except in some sectors, is covered by a variably thick mantle of sand with dune formation of various ages, that in one sector of approximately 2 mil-

lion hectares, presents a marked disposition in parallel arcs, with SO-NE orientation, which contribute to obstruct natural drainage.

This large parallel arcs of more than 100 km in longitude, with widths varying between 500m to 4km and smooth slopes, constitute real palo-sandbanks. In the past, they were the advance toward the east of dune formation. Nowadays we can find a similar relief in the proximities of the Andes.

The great parallel arcs of this zone do not surpass, to the E, the depression of Vallimanca. Starting from this depression and outside the area of this study, the sand accumulations appear in other different patterns.

These patterns were discovered by the authors when they studied the satellite images taken when flooding occurred. It is say, that the water actted as a photographic developer of the existent morphology.

Previously, no naturalist had mentioned them and even less the settlers of the area. The motive of this unknowledge is that the great expansion of the dune formations and the distance between them, added to the exiguous slopes, had prevented the visualization of the relief from a terrestrial point of view.

Outside of these sandbanks, in arcs, exist plains covered with various thicknesses of sand (from 0,20cm to 2 or 3m) and, also, a large South sector where the sand accumulation takes the form of barchans. In this last sector superficial water accumulation do no exist, even in moments of great rainfalls.

All these sands are deposited directly over loess of variable composition that countain limestone in nodule form or in lenses of different magnitudes. All this contributes so that the permeability of the subsoil is not the same in all the area.

In the low zones, in general, predominates fine material accumulations, came from higher levels that have originated soils with horizons of slow permeability.

6. USE OF THE LAND

The main activities are agriculture crops and livestock, where the predominance of one activity over the other varies by sectors, depending on factors like: natural aptitude of the soils, size of properties, etc.

7. HIDROGRAPHY

In the south half of the studied area (present in satellite image 243-085) does not exist superficial natural drainage. It was only observed very few permanent lagoons and numerous depressions that act as temporary lagoons in moments of continuous precipitations. The north half of the area (present in satellite image 243-084) has a net-work of blinded drainage unknown in time of draught, but clearly manifestated in satellite images after a long period of precipitations upon appearing a lot of lagoons connecting together that conforms the outline of an old drainage net-work toward the Salado River.

8. CLIMATE AND PLUVIOMETRY

8.1 GENERALITIES

The anual average temperature oscillates around 16ºC, increasing, from south to North. The average temperature of the warmest month, January, is superior to 23ºC and the average temperature of the coldest month, July, oscillates between 8 and 9ºC and reaches the lowest values to the west of the region.

The absolute maximum temperature, in some cases, reachs 44ºC and the absolute minimum (observed between 1940 to 1960) reaches 6 and 7ºC below zero, to the east, and 10 and 11ºC below zero, to the west.

The predominant winds are from the N and NE. Spring, being the windiest season.

The anual average rainfall of the area is of 800mm, decreasing from east to west, starting from values of 900mm in eastern localities to reach values near to 70mm to the west.

8.2 WATER BALANCE AND PLUVIOMETRIC RATE

The region presents a water balance equilibrated to negative, existing major possibility of excess to the east and of deficiencies to the west. The fact that in the region, the average temperature values are maintained practically always above 0ºC makes the process of evaporation continuous. To this we must add the desiccating effect of the winds.

Rainfalls are produced during all the months of the year, but with a marked estival concentration (from October to March 65% of the precipitations are produced). The months of less precipitation are July and August. March, being the one of mayor precipitation, surpassing in all the localities analized, 100mm.

On the basis of 30 years statistics corredponding to 1921-50 we obtain the following average and extreme values of precipitation for six localities of the region:

Table I

Locality	Average value	Maximum value	Minimum value
Bragado	943 mm	1.333	632
Junín	879 mm	1.228	590
Nueve de Julio	854 mm	1.151	632
Pehuajó	840 mm	1.206	511
Carlos Tejedor	796 mm	1.226	483
Trenque Lauquen	689 mm	1.178	447

8.3 EXTREME RAINFALLS YEAR 1972-73

The rainfalls occurred during August 1972 to July 1973 caused a flooding that had catastrophic chracteristics for a great part of this region.

If the mentioned period is considered a calendar year, we can determine, for the previous localities, the following precipitacion values and their respective differences with relation to the average value.

Table II

Locality	Rainfalls from August 72-July 73	Difference with relation to the average	
		in mm	in %
Bragado	1210	267	28
Junín	1207	328	27
Nueve de Julio	1400	546	64
Pehuajó	1486	646	77
Carlos Tejedor	1311	515	65
Trenque Lauquen	1356	667	97

9. TECHNIQUE EMPLOYED AND MATERIAL USED

It was used manual interpretation of satellite images helped by an illuminated table and magnifying glasses.

Image enhacement techniques and automatic processing were not used.

The using of a more advanced technique, did not depend on authors decision.

In the selection of the material two fundamental aspects were taken into consideration: 1º cloud scarcity; 2º the different states of flooding and salinization present in the images.

Enlargements to scale of 1:200.000 from infrarred (MSS7) and color composited images to scale of 1:1.000.000 were used to delimit the water. Enlargements to scale of 1:200.000 from red (MSS5) were used for salinity studies.

From each of both images studied (243-084 and 243-085) five sequences (different dates) were selected for interpretation.

The sequences of the images are as follow:

Table III

Image	Dates				
	1	2	3	4	5
243-084	11-10-72	2-26-73	12-28-75	3-27-76	9-23-76
243-085	10- 5-72	2-26-73	1-15-76	3-27-76	9-23-76

10. TIME AND PERSONNEL

All the work was realized by two persons (authors) in four months of effective work.

11. METHODOLOGY

By the experience adquired over the satellite images, we knew that they always offer totally new and unexpected information. Because of this, the interpretation of the images was accomplished without taking into consideration any previous knowledge of the region.

It was not possible to obtain information from ground truth because it was an historical work, but when work was concluded and it was presented to technicians and producers of the zone they themselves agreed with the limits of salt and water traced on their properties.

For each date and image (see Table 3) it was possible to identify six different patterns according the existent proportion between the land and the flood water.

Saturated soils were not differentiated, because in manual interpretation it could be confused with other elements.

Over band 5 enlargement outcropping salts were delimited. The different soil salinity degrees were not subdivided because the laking of land control.

12. RESULTS

For each date and image, a map of distribution of water and salts was accomplished.

Two flooding frecuency maps were done on the basis of water distribution maps. These maps, covering an area of 70.000 Km2 (included in images 243-084 and 243-085) show sectors affected by floodings in different grades and frecuencies (See Table 4).

The map appearing as figure 2 is a portion of one of those flooding frecuency maps where the eight original categories were reduce to four because black and white print problems. The flooding values appearing at the foot of the figure belongs to the whole area included in 243-085 image.

Table IV

Flooding frecuency during 1972-1976

Categories		Flooding Frequency	Surface values sc Km	
			image 243-084	image 243-085
1	100% of water	5 times	463	255
2	"	4 times	318	385
3	"	3 times	550	285
4	"	2 times	308	355
5	"	1 times	1150	810
6	30-70% of water	one or more times	2466	2580
7	5-30% of water	one or more times	1445	2090
8	Non affected		28300	78240

The map appearing as figure 3 is a portion of the outcropping salts map belonging to 243-085 image dated on 9-23-76.

13. CONCLUSIONS

1) This work permitted to amplify and in some cases, totally revert concepts considered irremovable about floods and salinization origin, affected surface for both phenomena, water movement, damage evaluation, etc.

2) About flooding origin it was determined the floodings depended exclusively on rains fallen directly on the place. The idea of water coming from other zones was desvirtuated by satellite images.

3) About water drainage it could be established three different sectors. One located in the south part of 243-085 image that appears perfectly drained.

   Other in north sector of the same image presents the water endammed between sandy dunes and without any possibility of movement. (Water must dessapear by evaporation and infiltration).

The third one, included in 243-084 image presents a blinded drainage network that formerly drained in the Salado River. During great rainfalls this basin is activated by natural and artificial channels, but still the drainage is insufficient. So it must be increased.

4) About flooding surface it was determined what was the maximum of land surface affectation, aproximately 12.400 Km2, almost 20% of whole studied surface (70.000 Km2.)

   This measure resulted substancially lower than the forward approachments given by other studies and from agrarian producers estimations.

5) About soil salinization processes it was determinated that they do not depend on the salt contribution from the circundant sectors as the agrarian producers hold.

   The salts are present in the water-table and after a long period of precipitations follows by a windy and dry season are fully manifestated on the landsurface.

6) After this study it becomes easier to establish the strategy to mitigate damages in similar cases. Routes could be stablished for the evacuation of inhabitans and livestock.

REFERENCES

Datos pluviométricos 1921-1950. Servicio Meteorológico Nacional, Buenos Aires, 1963.

Estadísticas climatológicas 1951-1960. Servicio Meteorológico Nacional, Buenos Aires, 1963.

"La inundación del Oeste Bonaerense vista por el INTA en un primer relevamiento", Buenos Aires, 1973.

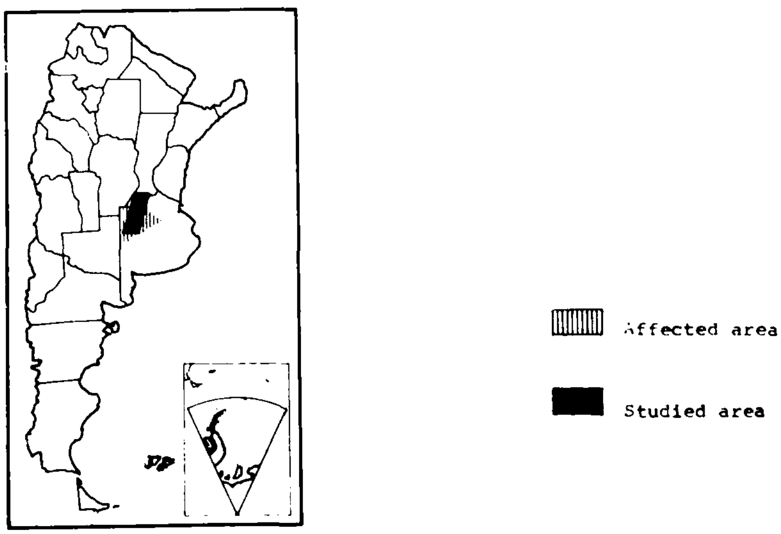

Fig. 1 : Geographical Location

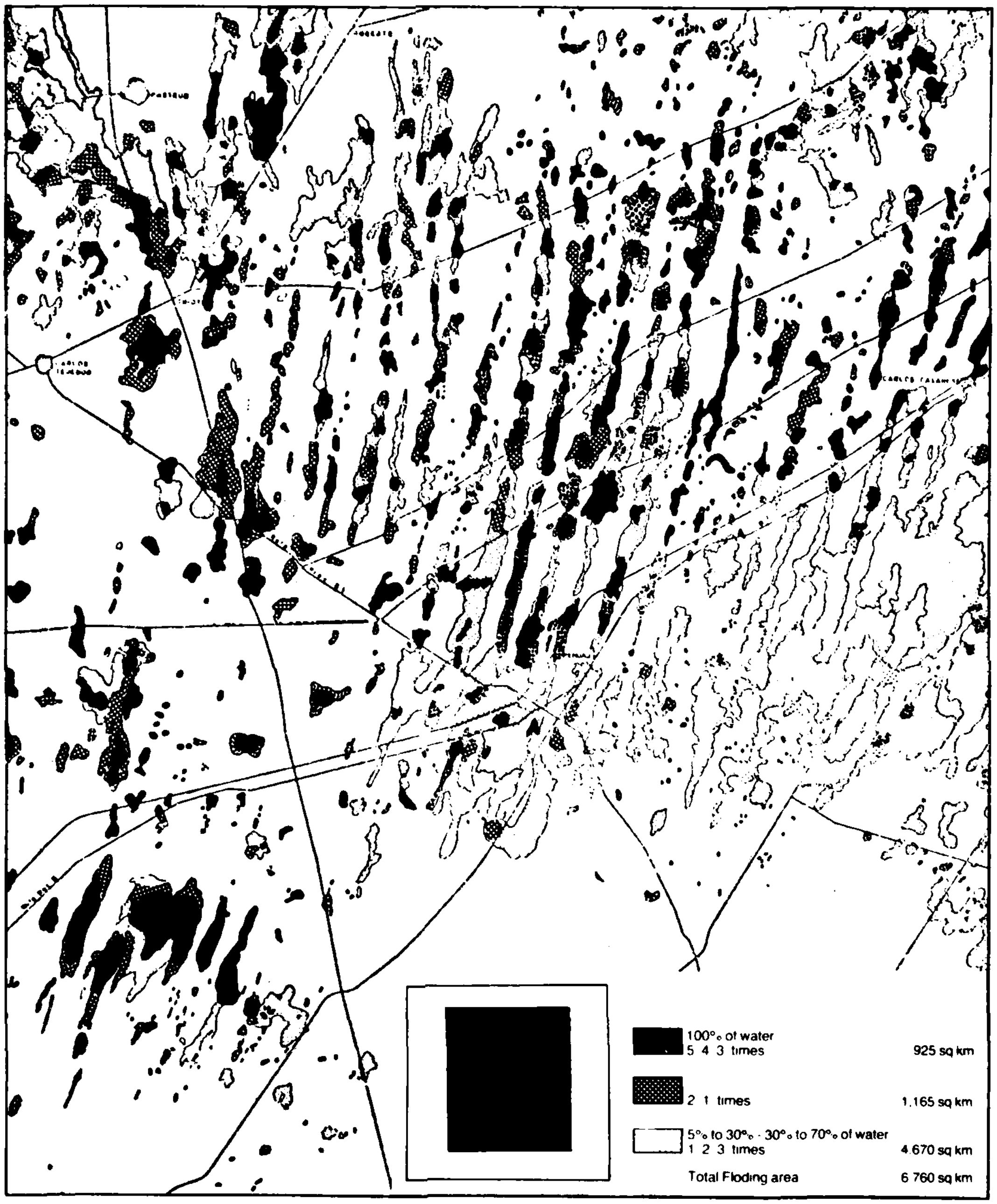

Figure ?: Frequency of flooding between the years 1972 and 1976. The map shows a portion of ?4?-085 image. (Scale 1:500.000).

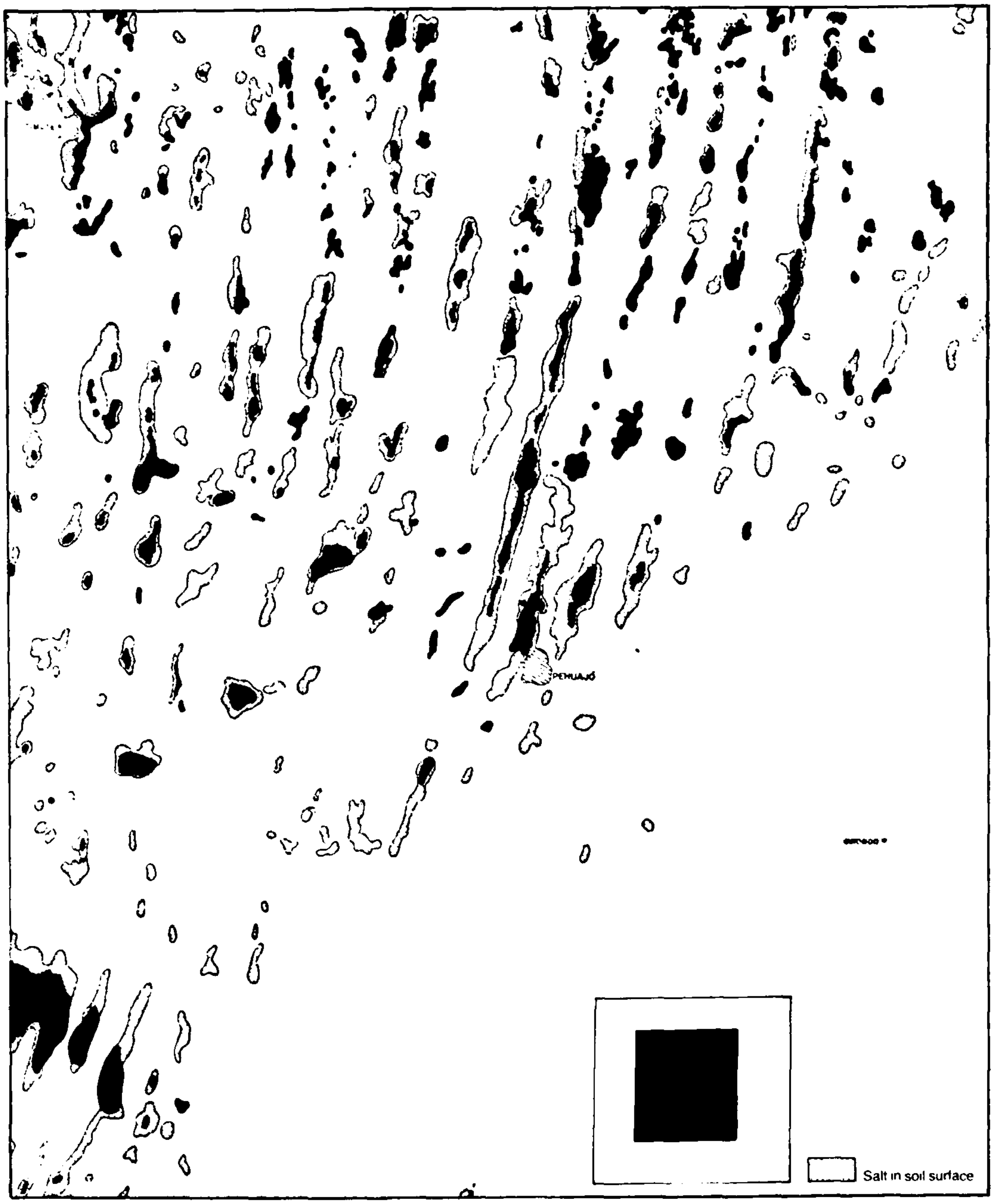

Figure 3: Outcropping salts. The map shows a portion of 243-085 image dated on 9-??-76. (Scale 1:400.000).

STUDIES ON SOME URBAN PROBLEMS BY USING AIRBORNE REMOTE SENSORS IN SANTIAGO, CHILE

Mauricio Araya F.(1), Jaime Gibson (2), Rodrigo Fernández (3) and Nelly Nussbaum (3)

(1) Research Engineer, Departamento de Geología y Geofísica
(2) Research Engineer, Departamento de Ingeniería Civil
(3) Research Assistant, Dptos. Ing. Civil y Geología y Geofísica

Facultad de Ciencias Físicas y Matemáticas, Universidad de Chile.
Beauchef 850, Casilla 2777. Santiago, Chile.

ABSTRACT

A cooperation agreement between Aerophotogrammetric Service of Chilean Air Force (SAF) and the Faculty of Physical and Mathematical Sciences, University of Chile, has allowed to perform several interesting pilot experiences to study some problems regarding environmental pollution, urban road traffic and other aspects related to civil engineering designs. The use of multiband camera and thermal infrared scanner has been very useful to foresee operational methodologies to study these problems in the next future. The use of conventional black/white aerial photographs to study urban traffic has allowed to obtain successful preliminary results. The main aspects of these experiences, its results and derived future activities are summarized in this paper.

1. INTRODUCTION

Several preliminar projects related to some urban problems have been successfully developed thanks to a joint cooperation program between Servicio Aerofotogramétrico de la Fuerza Aérea de Chile (Aerophotogrammetric Service of Chilean Air Force, SAF) and the Facultad de Ciencias Físicas y Matemáticas, Universidad de Chile (Faculty of Physical and Mathematical Sciences, University of Chile) through its Remote Sensing Section, Departamento de Geología y Geofísica and the Transport Section, Departamento de Ingeniería Civil. These experiences were addressed to determine the usefulness of several airborne remote sensors and the best methodology that could be used in the next future for operational programs to study several urban problems such as environmental pollution (air and water), thermal isolation in buildings, urban traffic congestion, and others. Although one urban area was selected as test site, the potential applications of this technology to other zones of the country could also be foreseen through these pilot experiences. The use of non conventional remote sensors (multiband camera and thermal infrared scanner) is described in Section 2, including preliminary results and future operational programs. Section 3 contains the main aspects of an experience developed to quantify urban traffic problems by using conventional black/white aerial photographs.

2. STUDY OF ENVIRONMENTAL POLLUTION AND OTHER CIVIL ENGINEERING PROBLEMS.

2.1 BASIC ANTECEDENTS ON THE REMOTE SENSING DATA USED.

The use of passive photooptic (multiband camera, conventional aerophotogrammetric cameras) and passive electrooptic airborne remote sensors has interesting potential applications in the study of urban environmental pollution and other problems related to civil engineering buildings designs. Meanwhile multiband camera obtains information on the reflection properties of different matterials along different spectral bands, thermal infrared scanner is specially designed to register data on the energy emission properties of different matterials on earth surface.

The use of both type of information allows to obtain interesting conclussions that could support the future use of this technology in several operational programs.

The multiband camera was used to obtain a real view of the city (without spatial deformation) and by using analogic techniques (Diazo films) it was possible to enhance certain features (vegetation, water conditions, open spaces) by making special color composites (derived from the original B/W products) over selected areas. The four spectral bands used were: AMB-1 or blue (0.4 - 0.5 um), AMB-2 or green (0.5-0.6 um), AMB-3 or red (0.6-0.7 um) and AMB-4 or near infrared (0.7 - 0.9 um). These spectral bands have similar wavelenghts ranges than Landsat MSS-4,5,6 (Fig. 1). Specially interesting was the spectral band AMB-4 or near infrared because of its capability to penetrate light fog (Photo 1) which is an usual phenomena that occurs in Santiago during winter time. Because this passive photooptic remote sensor is specially designed to obtain information on electromagnetic energy reflection properties of the matterials through different wavelenghts or spectral bands (the Sun is the normal source of energy), these photographs were obtained during the day, at the conventional aerophotogrammetric hours (optical light conditions).

The thermal infrared linescanner operated in the spectral band 8-14 um, with thermal resolution of 0,25° C and spatial resolution (IFOV) 1,5 milirad. These characteristics allowed to obtain very good analogic products (no digital recording capability) and special enlargements and enhancements (density slicing techniques) were made for specially interesting areas by using the original B/W products. This passive electrooptic remote sensor is specially designed to obtain information on the internal energy of the different matterials on earth surface by registering the emitted energy in the electromagnetic wavelenght range 8-14 um (Fig. 2). For this reason,if no Sun interference is desired (to register the internal energy conditions of the matterials), these images must be obtained during the night or very early in the morning. Otherwise Sun interference will be important and the sensor will register both the reflected energy (coming from the Sun) and the emitted energy (coming from the matterial) in the wavelenght range 8-14 um. Photo 2 shows an example of this phenomena; thermal contrast during the day is not good due to the Sun influence.

It is possible to combine the information coming from thermal images taken at different hours (day and night) and so to perform studies on thermal inertia for different matterials on earth surface. It is important to notice the special characteristics of the 8-14 um spectral band and so to obtain the maximum benefit from this sensor. As shown in Fig. 2, if emitted energy is registered the maximum sensibility or thermal discrimination capability of this sensor occurs for matterials having external temperatures ranging 0°-35° C. In this way, the use of thermal scanners having more than one spectral band (for instance, 3-5 um and 8-14 um) would allow to develop more detailed and accurate studies. The use of thermal scanners having digital recording capability would allow to improve more yet these studies. In this pilot experiences, thermal images were obtained during winter time (July) about 6 A.M.

Finally, the use of conventional aerophotogrammetric cameras equipped with panchromatic B/W film, scale 1: 2000 approx (about 3000 ft altitude) , was successfully tested in pilot experiences to quantify some urban traffic flow problems in downtown Santiago. A Twin Otter airplane (S.A.F.) was used to obtain these photographies (and also multiband photographies and thermal images).

2.2 AIR POLLUTION : IDENTIFICATION OF POTENTIAL SOURCES OF SMOG

The identification of "hot spots" that could represent potential sources of smog can be easily accomplished by using thermal images. Because of the "stretching effect" on these images, it was quite advisable to compare these images with undeformed registers (such as conventional B/W photographies or multiband photographies). In this sense, the use of multiband photographs was very useful and ,besides, it was possible to make color composites to enhance certain features over selected areas in pilot areas in Santiago. The near infrared band was also very useful to penetrate light fog and to obtain better contrast in vegetated areas and between cars and streets.

This pilot experience showed the different charcteristics of hot spots distribution in residential and industrial zones in the city. Residential areas are characterized by a rather high density level of small hot sources, usually represented by chims of houses and residential buildings, as it was proved in terrain activities(Photo 3a,3b).Industrial areas are mainly charcterized

by a rather low density level of big hot sources, represented by factories or industries (Photo 3e). In this pilot study the sources were classified (and field verified) in different orders of magnitude: level 1 or vehicles and other machines, level 2 or houses, level 3 or residential buildings, level 4 or small industries or big residential buildings, level 5 or big industries.

This preliminar study proved that it is feasible to make a map of potential pollution sources of smog (through the identification of hot spots) and to have a real and updated view of the different contributing areas of the city to the global problem. It is also possible to evaluate the relative quality and spatial contribution of these sources. As a general concept, the sources located in the North West zone of Santiago have the minor contribution to the global smoke problem due to the special topography and wind conditions of the city. Wind usually flows from South-West and accumulates smoke in the North-East mountains surrounding Santiago, as it can be clearly seen in the Landsat image shown in Photo 4. This satellite image allows to evaluate the general situation of Santiago and the natural ways to accumulate and to evacuate smoke in the city; under these conditions, a better location for industries and other pollutant agents could be planned.

2.3 WATER POLLUTION

Thermal images showed its great capability to identify problems related with water pollution. A thermal tracking along Mapocho River since Los Leones Ave. to Independencia Ave. (about 6 km) allowed to identify all the water discharges joining to Mapocho River. Photo 5 shows some clear examples (and also Photo 2a). The situation in San Carlos channel is very explanatory about the industrial use of water and its former pollutant discharge to water streams. These images allow to accomplish qualitative evaluations on these problems. However, if quantitative relations are needed, ground truth data should be obtained to be correlated with thermal images (water temperature, analysis of suspended particles, etc.).

The use of thermal images to find sources of water pollution in coastal zones would allow to obtain important positive results. Chilean central coastal zone has a rather high population density (specially during summer period) and several industries also discharge pollutant materials in river streams and ocean. The exact location of human made water discharge sources could be very well accomplished by using thermal images (sometimes this location does not appear in old maps). The use of multispectral and multitemporal satellite images (such as Landsat images showed in the example of Photo 6) would allow to perform studies on oceanic currents and its variations along the year, by studying the suspended matterials on oceanic water. Landsat MSS-4 (0.5-0.6 um or green) is very sensible to suspended materials on water due to the high reflectance registered in this spectral band. Landsat MSS-5 (0.6-0.7 um or red) is less sensible than MSS-4 and only the main concentration level areas can be identified. These Landsat images can be obtained every 18 days, with a spatial resolution of 80 meters (40 meters in the panchromatic RBV cameras, Landsat-3). Landsat-D (1982) will allow to obtain multispectral information (including thermal images, 200 m spatial resolution) with 30 m spatial resolution. The French SPOT satellite will register multispectral data with 20 m spatial resolution (10 meters in the panchromatic B/W image), and images could be obtained about 7 days if necessary. Nimbus CZCS sensor (Coastal Zones Color Scanner,CZCS) allow to obtain daily multispectral data (including thermal images) with a lower spatial resolution (about 800 m). The combined use of aerial and satellite information is very useful to better design the location of future pollutant discharge sources (and also to evaluate the actual influence of theses sources in the global water pollution problem).

Besides water pollution, important studies on coastal ground water location could be developed by using aerial thermal images. If any ground water discharge (coming from the continent) joins to the oceanic water, this fresh water will go up (because its minor salinity) and thermal images will register the thermal differences in surficial oceanic water (thermal discrimination 0,5°C). Usually these discharges appears such as water plumes of different temperatures. In this sense, the great capability of these images for temperature discrimination would allow to study local coastal phenomenas of "upwellings" (surgencias), that are related with favorable conditions for fishery. The adequate combined use of satellite and aerial multispectral and multitemporal images would be again very useful to develop these studies. Aerial images should be of course used for detailed studies of previously identified interesting areas(which could be determined through satellite images).

2.4 BUILDING THERMAL ISOLATION AND OTHER CIVIL ENGINEERING PROBLEMS

Heat loss problems in houses and residential buildings were clearly identified (Photo 7a). The different building matterials and its thermal properties could also be identified, as showed in Photo 7b. Opened spaces and its influence in thermal variations can also be studied. These factors are very important to be considered for energy saving purposes. A better building isolation design could allow to save important amounts of energy (usually represented by petroleum) to obtain warmer conditions inside the residences. Photo 7c shows an example on how thermal inertia can be determined through these thermal images: a terminal for rural buses in Santiago shows the relative colding of the buses, depending on its recent use.

A global project to obtain thermal distribution of the different zones of the city could be intended in the next future. For instance, it is known that downtown area (central zone of Santiago) acts as a thermal focus that produces the elevation of hot air and this effect is specially important during the night (when all the matterials are becoming colder). Due to the mountains that surround the city in the East zone, that hot air contacts the residential area (at higher level due to the mountains topography). In this way, the intermediate zone should be the colder area during the night and the early morning. This phenomena has been studied (*) through conventional data measurements in the city (temperatures measured at different hours, in representative streets along N-S and E-W of the city). If thermal mosaics (obtained at different hours along day and night) were available , these studies could be very well accomplished. The identification of the different thermal zones of the city (thermal inertia, specially during the night) would allow to select the best building matterials and designs to be used in these different areas in Santiago (or other cities), through the knowledge of the different thermal gradients, day-night, for every zone.

The study of different materials (sand, clay, rocks) or soil conditions, water loss in dams, irrigation conditions and other problems related to civil engineering activities could be also improved by using remote sensing techniques. The use of both satellite and aerial information is very important to accomplish these studies. Many of these experiences have been successfully performed in other countries. However, it was very useful to prove that such technology could be also employed in Chile, by using the Chilean infrastructure. Due to the positive results obtained in these and other preliminar experiences (see References 1,2,3) , many potential applications for future operational programs have been foreseen. The acquisition of improved remote sensors (multispectral scanners with digital recording capability) and interpretation equipment is being considered by now. As a first and important step, the Aerophotogrammetric Service (SAF) has already installed a complete B/W and color photographic laboratory and an equipment for digital interpretation of satellite and aerial images is almost ready to be used. The future availability of Landsat-D and SPOT images will allow to improve methodologies to be applied in future operational programs, such as the existing programs to study geothermal resources in Chile by using remote sensing techniques (Refs. 1,3) and antarctic environmental conditions and natural resources (Ref.2), where positive results have been obtained by now. The improved infrastructure,for data acquisition/interpretation, besides the improved satellite data and the experience accumulated by national researchists, will allow to obtain important results for different programs in the next future.

3. ISO-DENSITY CURVES IN URBAN TRAFFIC FLOW.

Aerial photographs give an instantaneous picture of the traffic situation on a road section. A sequence of them along an arterial route can illustrate not only stationary conditions but dynamic ones because sections are photographed at different moments in time. A technique, already used at least in freeways (Ref. 4), to represent this dynamic information is to draw iso-density curves in a time-space diagram.

Density is a property of traffic flow defined as the number of vehicles per unit distance present in a road section at a given moment. For the sake of spatial homogeneity when geometric design is not standard, it can be expressed on a per lane basis. Then, density can be calculated as:

(*) Eng. Pablo Ulriksen, Dpto. Geología y Geofísica, Facultad de Ciencias Físicas y Matemáticas, Universidad de Chile.

$$k(x,t) = \frac{N(x,t)}{L(x)D(x)} \qquad [1]$$

where:

- $k(x,t)$ = density in section x at time t (veh/km/lane)
- $N(x,t)$ = number of vehicles in section x at time t (veh)
- $L(x)$ = number of lanes in section x
- $D(x)$ = lenght of section x (km)

Each photograph contains one or more sections where $N(x,t)$ can be computed. Each value $k(x,t)$ is a point (*) in a space-time diagram with a density value associated. In this way, a map of such points can be obtained and then iso-density level curves drawn.

To investigate the usefulness of this approach in urban transport, a circuit embracing four main roadways of Santiago (Fig. 3) was selected to be flown over between 7:30 and 9:55 A.M. A Twin Otter airplane (SAF), equipped with a conventional aerophotogrammetric camera (B/W film) and flying at 3000 ft altitude was used. The cycle time was between 10 and 15 minutes, so an average of 10 observations for each section of the circuit was obtained. The original scale of the photographs was about 1: 7000.

In a first stage, only Ave. L. B. O'Higgins has been studied, eastbound and westbound traffic separately. This is the main street of the city and has similar design characteristics in each traffic direction. Eight photo sets, ranging 7:30 and 9:55 A.M., have been considered. In each way, sections were defined block by block where signalised intersections exist. If distance between signals exceeded one block, two sections were defined: one, the block immediately upstream the signal, being the other the remaining road portion. This criterion arose from the fact that such junctions tend to be bottlenecks. Three vehicle types were significant: light vehicles, buses and minibuses. There are bus carriageways, with two lanes, in a considerable extension of the Avenue. Taking into account that out of this zone transit vehicles tend to use exclusively one or two lanes, light vehicles were separately analysed assigning them a number of lanes accordingly with the space they form.

Density is a measure defined for a road section. This would lead to stepwise functions in a space-time plane. On the other hand, density varies along the section as the existence of signals make the pattern of variation dependent on the stage of the cycle in which the photo was taken. Then, continuity can be reasonably introduced but it is not clear how to do it. Considering that usually junctions are the critical points in terms of capacity, it was decided to assign the density value of a section to its downstream end.

Density levels meaningful to be drawn were selected relying upon traffic flow theory. It states that the congested situation arises when density approximates one half of the jam value. Deriving it from the mean vehicle length (5m for light vehicles in Santiago) the congestion limit is 100 veh/km/lane. Curves for 150 and 200 veh/km/lane are also used to qualify congestion conditions. Finally, a free flow limit was somewhat arbitrary chosen at 65 veh/km/lane. Equivalent values for buses can be easily obtained considering its own length (about 8-9 m). Curves for each level result from linear interpolation between corresponding points. Two examples are presented in Figs. 4 and 5. Distances are measured in the direction of flows. Road sections are identified by the name of the opposing street in each junction used as a boundary, in the abscissa axis.

As can be seen, iso-density curves allow a rapid and detailed view of the traffic situation along the road, in space and time. For this reason, they seem to be very useful as a congestion diagnostics tool helping in at least two major tasks: bottlenecks identification and congestion characteristics quantification. They provide valuable information for selection of sites where capacity increments would render higher benefits.

Generally, iso-density curves are closed. Otherwise, density should be constant-or even comprised between a pair of selected levels- along time and/or space. Nevertheless, it can sometimes happen that a curve is open in one axis because the associated congestion level remains farther than the end of the observed period or road segment (see left-hand side of Fig. 5).

(*) Strictly speaking, a straight line segment. See discussion below.

So, the time-space plane can be divided into different classes:
- uncongested: outside the 65 veh/km/lane curve
- moderately congested: between 65 and 100 veh/km/lane curves
- heavily congested : between the 100 and 150 veh/km/lane curves
- extremely congested: inside the 150 veh/km/lane curve

A gross index of the magnitude of congestion situation in a given section (or set of sections) is the proportion of the whole corresponding time-space area that belongs to the uncongested class. Looking at Figures 4 and 5 the impact of the city centre's trip attractions at A.M. peak period can be seen. The centre is located between Santa Rosa and R. Pretot-Dieciocho streets. It is also apparent that congestion levels are higher in the E-W direction reflecting the fact that car ownership is heavily concentrated in the eastern neighbourhoods of the city. Of course, congestion severity can be judged according to the distribution of congested portion among the abovementioned classes. In our example, heavy congestion is confined, with a few exceptions, to a relatively short period and does not spread out dramatically in space.

Iso-density curves allow too a more precise characterisation of a congested zone. The horizontal distance between the farthest two vertical tangents to a curve measures the maximum extension (in space) of a continuous road segment in which a given congestion level is overpassed. Similarly, the vertical distance between the farthest two horizontal tangents, represents the maximum duration of this situation in that segment. The greater these distances, the larger the importance of congestion in it. For instance, in Fig. 4 the section between Namur and Miraflores is much more problematic than the one between Esperanza and Maipú streets.

Bottlenecks are points of a road where flow-capacity ratio has a local or global maximum. So, congestion levels are first reached at them and then, through queuing back, are propagated upstream. This happens because the queue reduces the capacity of precedent links. Accordingly, density rises in those links. This is reflected by iso-density curves: points, in space, where the slope changes from a negative value to a positive one (like in Exposicion, point A in Fig. 5) represent bottlenecks. It is equivalent to find the point, in space, where the curve has a minimum in time.

The rationale is the following. From eqn. [1],

$$\frac{\partial K(x,t)}{\partial t} = \frac{1}{L(x)D(x)} \frac{\partial N(x,t)}{\partial t} \qquad [2]\ ☆$$

It can be shown that

$$\frac{\partial N(x,t)}{\partial t} = \lambda(x,t) - \mu(x,t) \qquad [3]$$

being $\lambda(x,t)$ and $\mu(x,t)$ the arrival and discharge flow rates at section x and instant t. When the queue in section x is long enough, it reduces $\mu(x-1,t)$ rate at the preceding section. But this takes place with a time displacement because queue building up is not instantaneous. As a result $K(x-1,t+\Delta t) > K(x-1,t)$ even at a constant arrival rate to section (x-1).

On the other hand, a bottleneck plays a regulatory role downstream because its exit rate (capacity, if saturated) is the arrival rate for the next road section. Then, unless other flows enter this section or the number of lanes is reduced, its density will tend to be stable in time as long as saturation upstream remains. This explains discontinuity in congestion levels and the quasi-verticality of the slope of the curve after a bottleneck. The linear interpolation proceed re sortens this effect.

Two additional properties of the curves can now be discussed. One is the propagation speed of congestion arising from a given bottleneck. A mean value of it is given by $\Delta s/\Delta t$, where Δs is the distance in abscise axis between the bottleneck and the farthest vertical tangency point upstream (at the same curve). Δt is the analogous distance in ordinate axis. The greater the

---

(☆) It should be noted that the derivative value is inversely related to L(x)D(x), which indicates the storage capacity of a road section.

propagation speed, the more dangerous the bottleneck. Just compare situation at Exposición in Fig. 5 and at Santa Rosa in Fig. 4. The other property is the congestion variation rate in time. From eqns. [2] and [3] , this variation at a given section only can derive from timely changes in λ and/or μ . Besides, it can be positive (vehicles accumulation) or negative (the opposite case). Vertical distance, at a point, between two consecutive level curves is a measure of this rate. The lesser the value, the greater the unstability in the traffic conditions originated by the bottleneck. In some cases, specially when positive and negative values are small, it is likely that we are facing an unusual situation, produced by a random perturbation (i.e. an accident). Both properties are used to assess how sensitive to minor changes in capacity is the bottleneck.

However, this diagnostic does not provide direct information on congestion causes. Then, immediate decisions on development of projects are not advisable; maybe infrastructural works will be necessary, maybe operational improvements will suffice. But one can turn to photographs and observe in detail identified critical points or sections in order to get a more precise approach to this issue.

In summary, aerial photographs are a powerful technique whose potential value is still to be fully explored. Some further research directions have been identified. Prior to apply the method in engineering contexts the following issues should be settled:

- dependence of density measures in adjacent sections separated by a signal on the stage of cycle in which the photo was taken ;

- validity of criteria used for meaningful congestion levels definition and for interpolation to construct the curves.

In addition, information provided by aerial photographs could be better used if research is conducted regarding:

- other properties of the curves, linked with enclosed area;

- other data obtainable from photographs, as lane use, patterns speeds, vehicle equivalence factors and average delays;

- photo processing mechanisation, to improve efficiency.

Some of these topics are being currently dealt with by the authors and positive results are hoped in the next future.

4. REFERENCES

1. Araya M. and Piracés R., Use of Remote Sensing techniques to study geothermal resources in arid and semi-arid zones in Chile, First ERIM Thematic Conference on Remote Sensing of Arid and Semi-Arid Lands,(Paper A-19),El Cairo, Egypt, January 1982.

2. Araya M., Use of remote sensing techniques to study environmental conditions and natural resources in Antarctic Peninsula, International Geosciences and Remote Sensing Society Symposium (IGARSS-82), Munich, Federal Republic of Germany, June 1982 (Paper TA-8.3).

3. Araya M., Main aspects of some remote sensing projects developed at the Facultad de Ciencias Físicas y Matemáticas, Universidad de Chile, Second Brasilian Symposium on Remote Sensing (INPE), Brasilia, Brasil, May 1982 .

4. Wagner F. A. and May A. D. , Use of aerial photographs in freeway traffic operations studies, U. S. Highway Research Board, Highway Research Record N 19,pages 24 - 34 (1963).

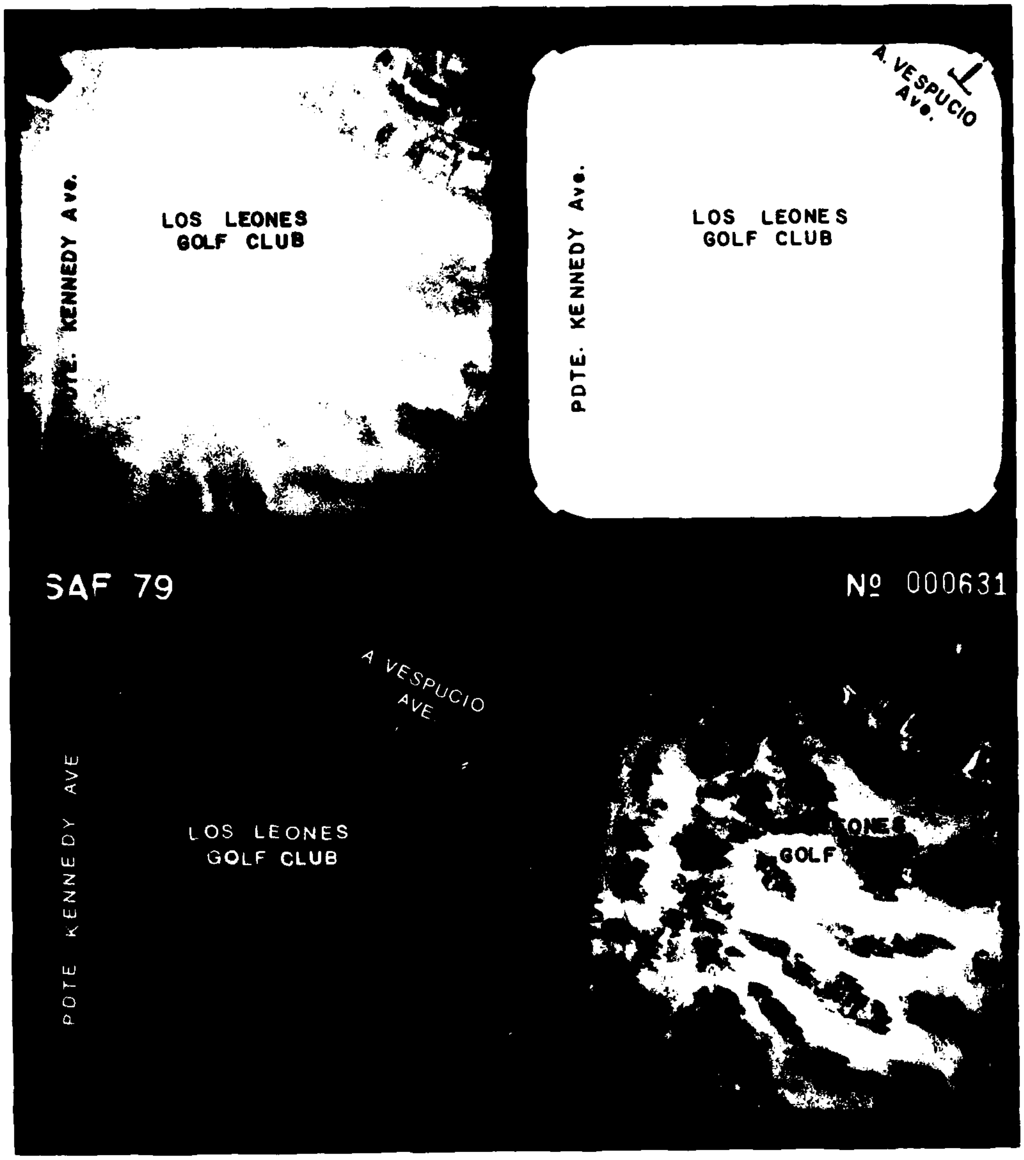

FIGURE 1. [illegible] BAND PHOTOGRAPHY OVER A [illegible] AREA IN SANTIAGO, [illegible] 10 A.M., WINTER [illegible].

The spectral bands used were: AMP-1 or [illegible] (0.4-0.5 [illegible]), AMP-2 or green (0.5-0.6 [illegible]), AMP-3 or red (0.6-0.7 [illegible]) and AMP-4 or near infrared (0.7-0.9 µm), approx. The capacity of near infrared band to penetrate light fog (a very [illegible] phenomenon during winter time) is clearly showed in this photography.

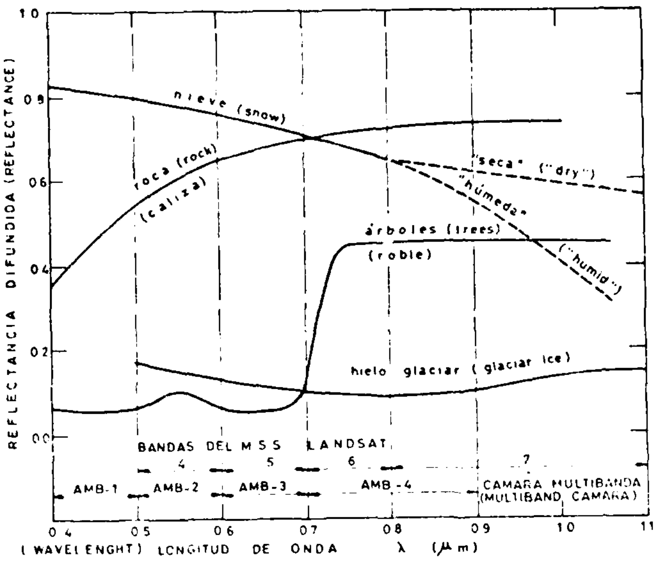

FIGURE 1. TYPICAL SPECTRAL CHARACTERISTICS, REFLEXION VS. WAVELENGTH, FOR DIFFERENT MATERIALS.

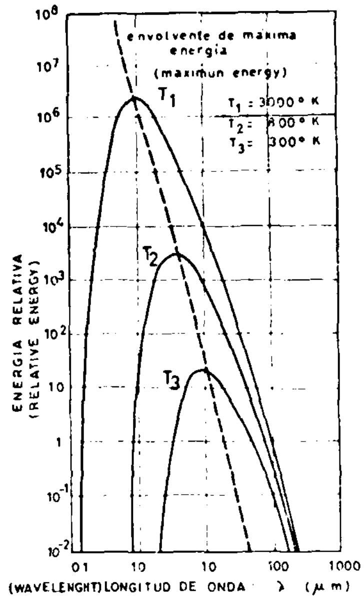

FIGURE 2. ENERGY EMMISSION OF BLACKBODY, DEPENDING ON WAVELENGTH AND SURFICIAL TEMPERATURE.

PHOTO 2a. THERMAL IMAGE OVER SANTIAGO (ABOUT 6 A.M., WINTER TIME). It is very clear the water discharge (W) and the building heat loss(E).

PHOTO 2b. THERMAL IMAGE OVER SANTIAGO (ABOUT 1 P.M.,WINTER TIME).Better contrast is obtained in green areas but water appears uniform.

PHOTO 3a. POTENTIAL SOURCES OF SMOG IN A RESIDENTIAL AREA IN SANTIAGO.

Building chims and fire places(1,2,3,4) are clearly identified. Unused new buildings with metalic roof (N) are also seen.

PHOTO 3b. POTENTIAL SOURCES OF SMOG IN A RESIDENTIAL AREA IN SANTIAGO.

Similarly than Photo 3a, fire places and chims are clearly identified (1, 2, 3, 4). The different building materials are also seen in these thermal images obtained about 7 A.M., during winter time.

PHOTO 3c. POTENTIAL SOURCES OF SMOG IN AN INDUSTRIAL AREA INSANTIAGO.

This thermal image (obtained about 7 A.M., winter time) clearly shows the pattern of big industries activity.

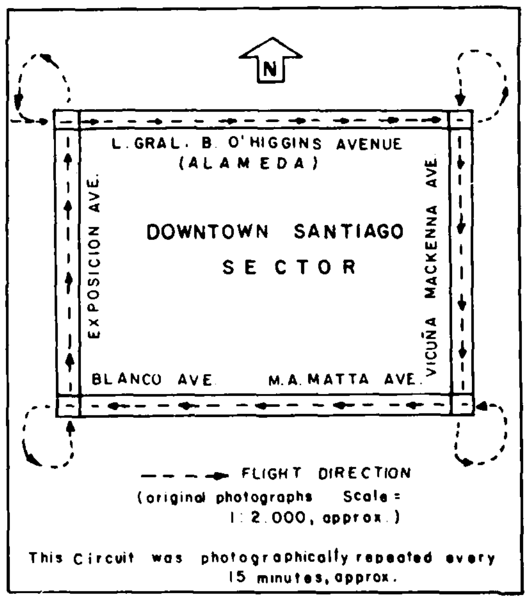

FIGURE 3. CIRCUIT PHOTOGRAPHED OVER A PILOT AREA IN SANTIAGO, TO OBTAIN ISO-DENSITY CURVES FOR URBAN TRAFFIC. These photographies allowed to draw the space-time diagrams (Figs. 4,5) of vehicles concentration variations in this area.

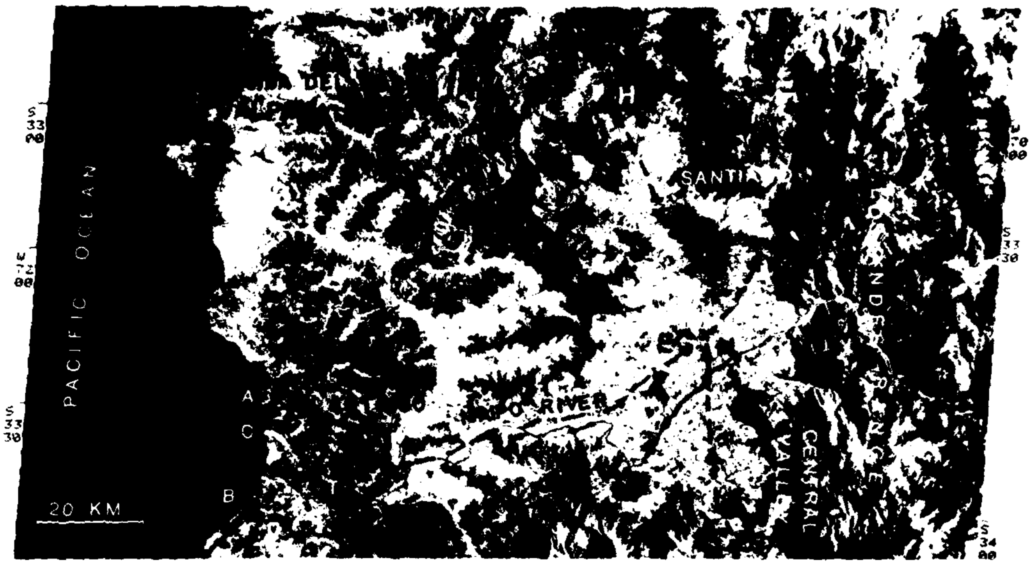

PHOTO 4a. SECTOR OF LANDSAT IMAGE OVER SANTIAGO, SAN ANTONIO AND VALPARAISO ZONE(MSS-7 or near infrared, 0.8-1.1 μm; December 11,1976, INPE,Brasil). The natural ways for wind arrivals to Santiago are clearly observed in W-E and S-N ways; 1 and 2 hills could be disturbance elements for helping the accumulation of smoke in East area of Santiago, being H the natural exit way.

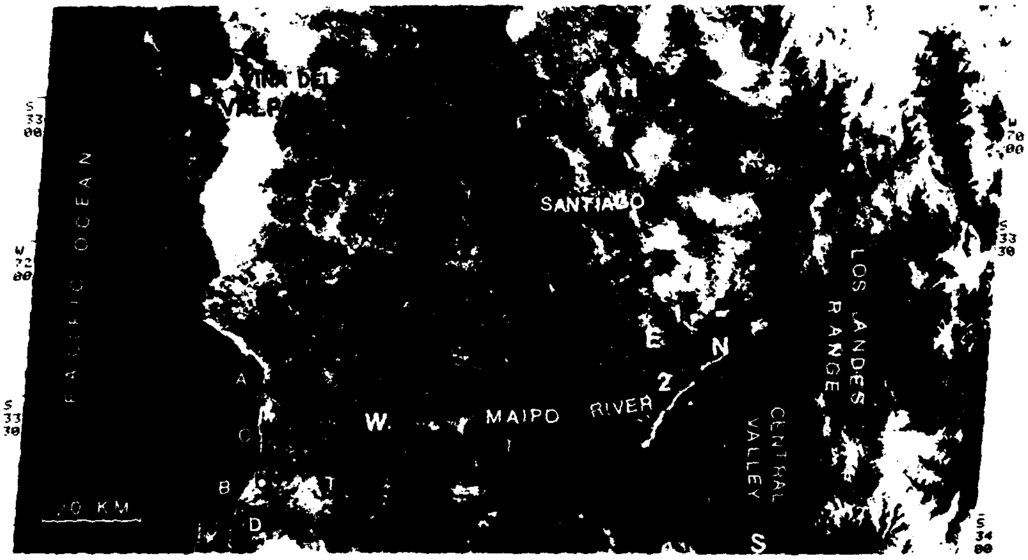

PHOTO 4b. THE SAME IMAGE IN MSS-4 or green (0.5-0.6 μm) spectral band. Sediment flux is clearly observed in San Antonio area; A-C probably produced by Maipo River. Wetlands (D) and B plume could probably be produced by ground water of Maipo River, considering T-T alignment.

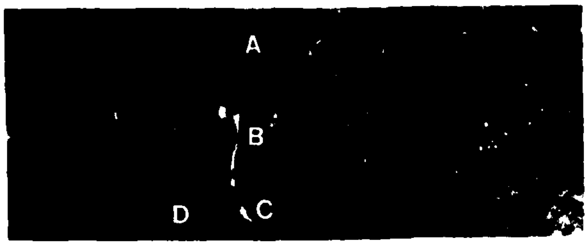

PHOTO 5a. WATER POLLUTION IN MAPOCHO RIVER, SANTIAGO, AS SHOWED IN THERMAL IMAGES (6 A.M.).

San Carlos Channel normal temperature(A) is heated (B) after passing an industry. Mapocho River normal temperature (D) is increased(C) after joining with the channel water.

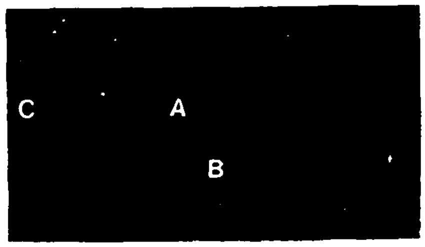

PHOTO 5b. DISCHARGE OF POLLUTED WATER TO MAPOCHO RIVER ,SANTIAGO(6 A.M.).

Mapocho River temperature (C, heated after passing San Carlos Channel) is again changed by new water discharge (A and B).

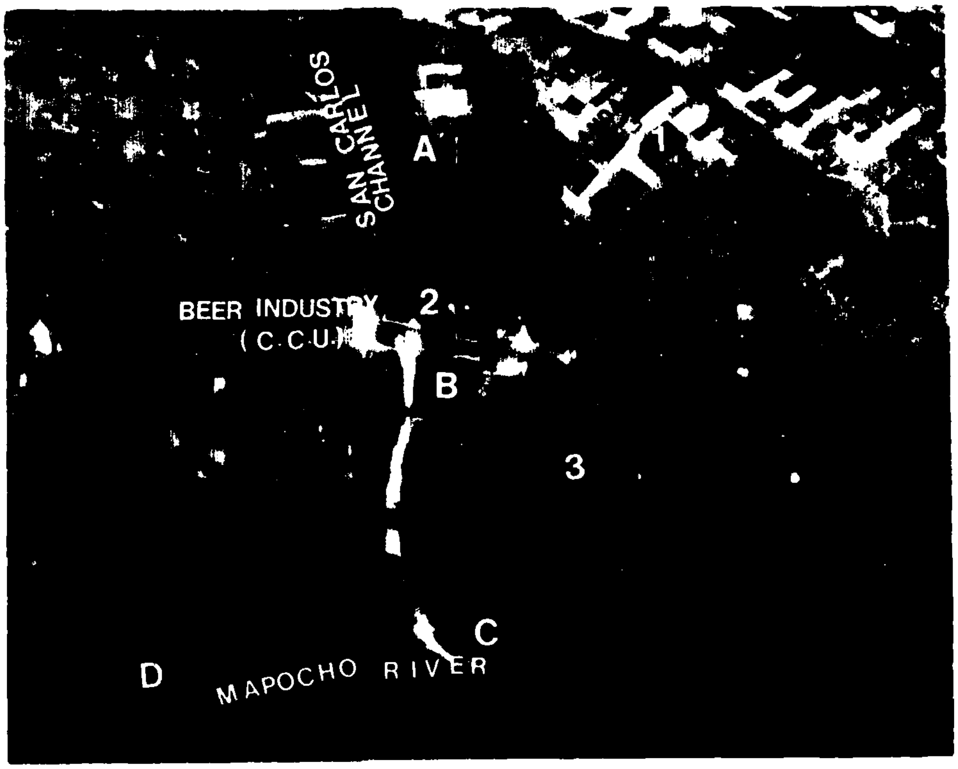

PHOTO 5c. DETAILED STUDY OF WATER POLLUTION IN PILOT AREAS IN SANTIAGO, BY USING THERMAL IMAGES OBTAINED ABOUT 6 A.M., WINTER TIME.

This enlargement of Photo 5a shows the detail of the industry effect on San Carlos channel water. It is also possible to observe the industrial water waste(2), a free terrain (3) and heat loss in an Hospital building complex(1).

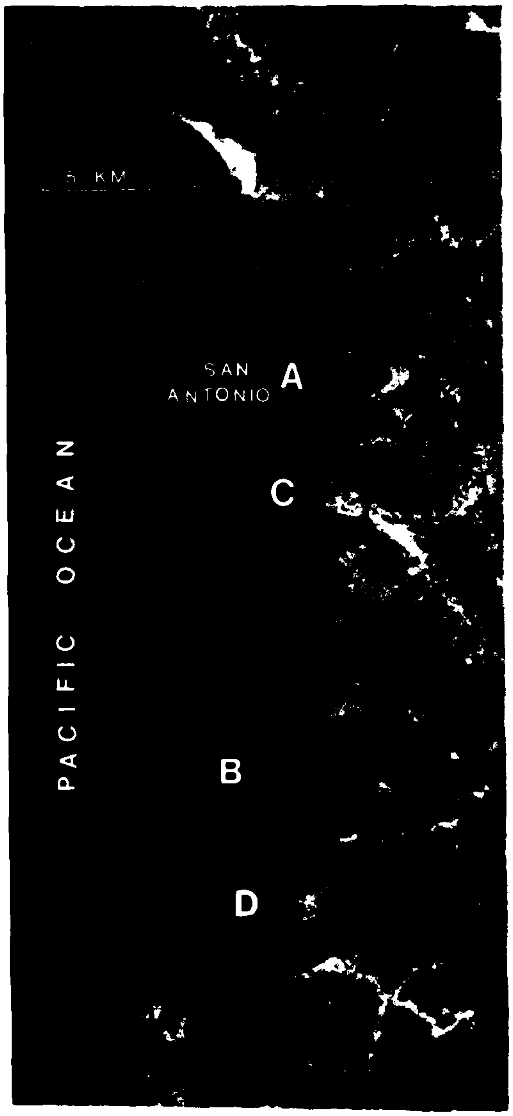

PHOTO 6a. ENLARGEMENT OF SAN ANTONIO AREA SHOWED IN PHOTO 4a, LANDSAT MSS-7 .

This spectral band is not sensible to suspended materials on water and so it is clearly seen San Antonio harbor (A), Maipo River and Pacific ocean junction (C), the area of special plume (E) and the water bodies in the wetland (D). These images show the interesting area that could be studied with more detail using airborne remote sensors and satellite data.

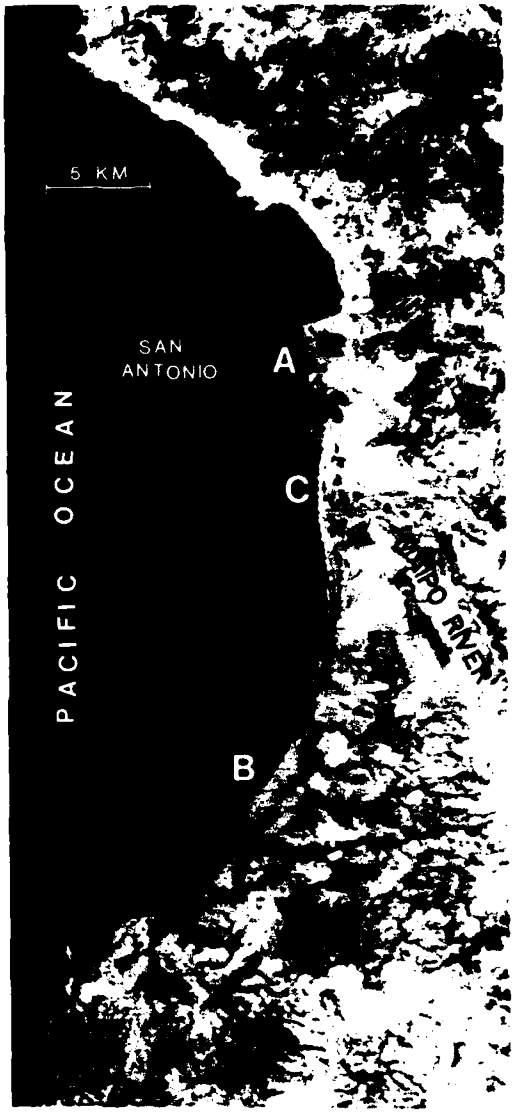

PHOTO 6b. ENLARGEMENT OF SAN ANTONIO AREA SHOWED IN PHOTO 4b, LANDSAT MSS-5.

This spectral band (0.6-0.7 μm or red) is less sensible than Landsat MSS-4 to suspended materials on water. Only the main sources appears and the A and B phenomenas showed in Photo 4b still remain. The special pattern of oceanic current near San Antonio area is observed here. A multitemporal analysis would be very useful for these purposes.

PHOTO 7a. HEAT LOSS IN RESIDENTIAL BUILDINGS IN A PILOT AREA IN SANTIAGO.

These are identical buildings (near Las Rejas Ave) show a typical phenomena: heat loss in window areas. The subway ventilations are also seen(A). This thermal image was obtained about 7 A.M., during winter time.

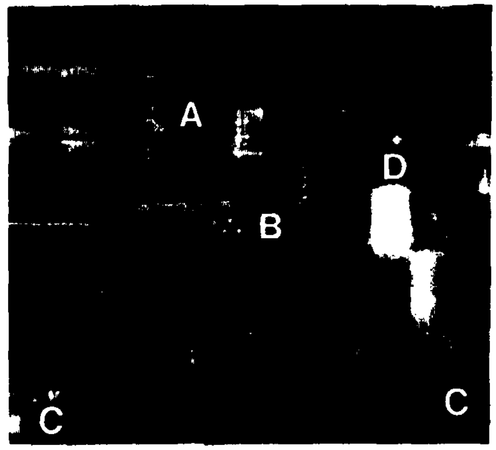

PHOTO 7c. THERMAL IMAGE OVER A BUS TERMINAL IN DOWNTOWN SANTIAGO.

Temporal use of buses is clearly seen in A area: recent used buses are showed in white and viceversa. Parking place(B), subway ventilation (C) and one industry(D) are also seen in this thermal image (about 7 A.M.).

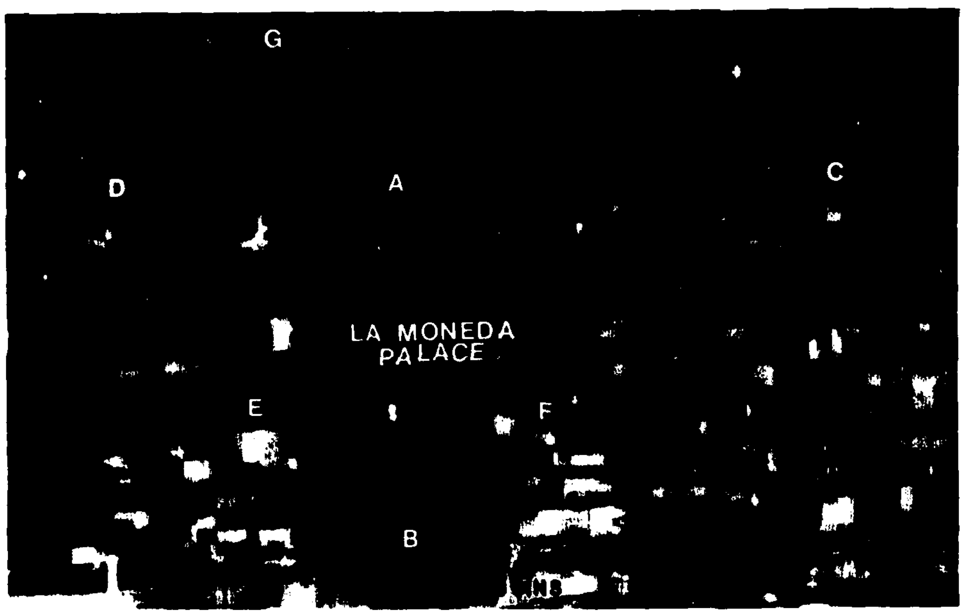

PHOTO 7b. THERMAL IMAGE OVER CENTRAL SECTOR IN SANTIAGO, SHOWING DIFFERENT MATERIALS. Open spaces influence is observed in the colder areas (A,B) in contrast with D and C zones. Different building mattetials(F,E) and unused field (G) are also identified.

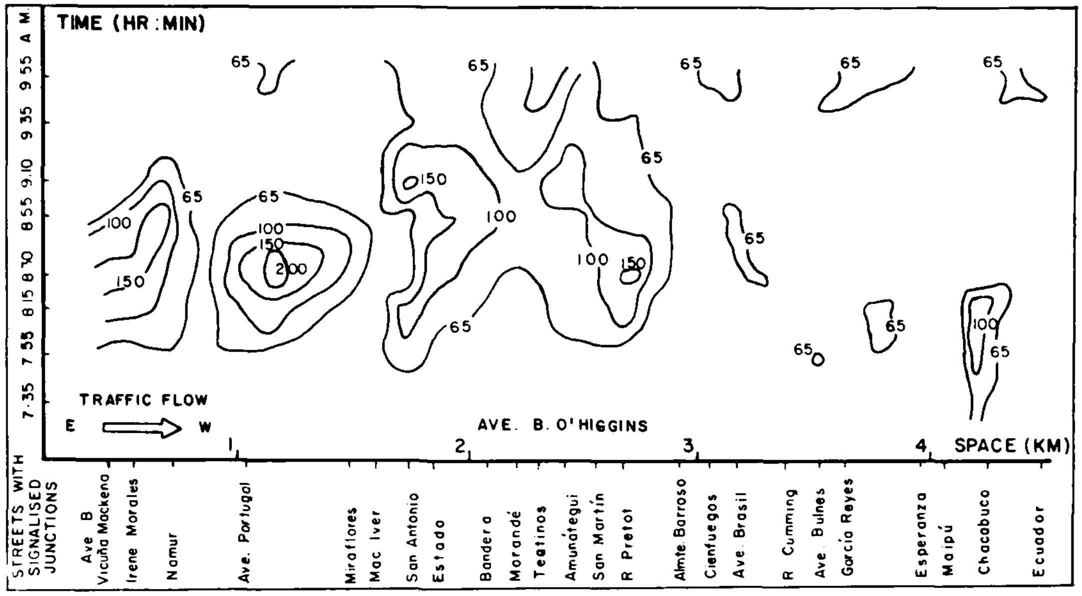

FIGURE 4. ISO-DENSITY CURVES (VEH/KM-LANE) FOR LIGHT VEHICLES IN BERNARDO O'HIGGINS AVENUE, WESTBOUND DIRECTION.

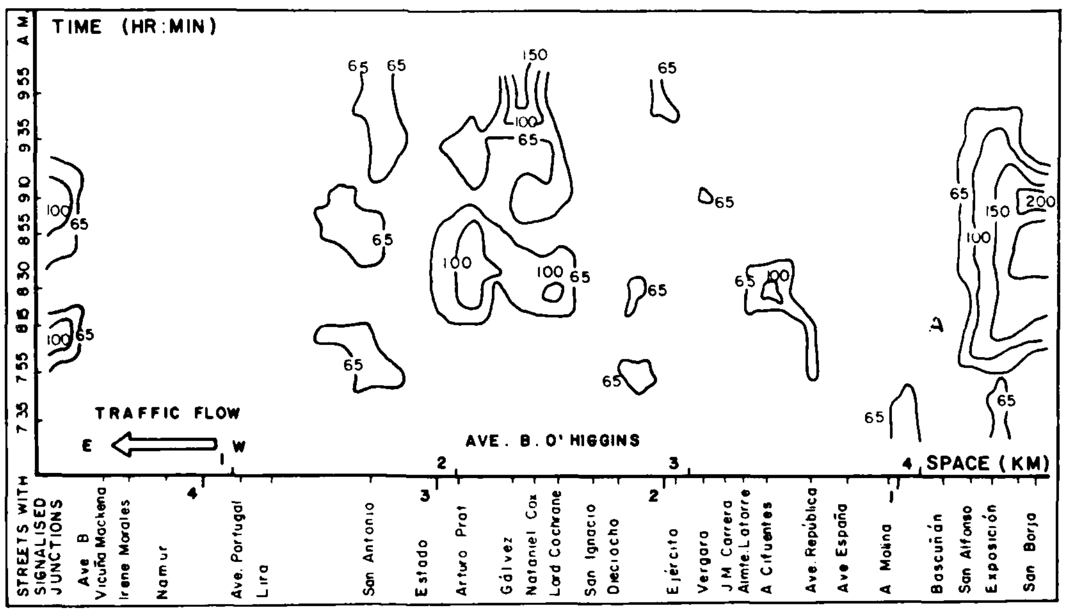

FIGURE 5. ISO-DENSITY CURVES (VEH/KM-LANE) FOR LIGHT VEHICLES IN BERNARDO O'HIGGINS AVENUE, EASTBOUND DIRECTION.

THE USE OF A GEOGRAPHIC INFORMATION SYSTEM TO COMBINE LAND USE INFORMATION DERIVED FROM LANDSAT WITH SOILS DATA TO STRATIFY AN AREA IN ARGENTINA FOR CROP FORESCASTING*

Mary DeVries, Frederick Westin, Francisco Redondo, Claudia Gargantini, Natalia Marlenko, Guido Vassallo, Michael Wehde**

ABSTRACT

Area frame sampling is currently used extensively for providing agricultural crop production data. One of the requirements for the implementation of a successful area frame is the initial stratification of the country or region into relatively homogeneous areas. Soils and land use information play an important role in identifying these homogeneous areas. A technique which utilizes the Area REsource Analysis System (AREAS) geographic information system for processing the soils and land use information in order to obtain output products which are useful for homogeneous area delineations is demonstrated. The area chosen for the study includes portions of the Argentine provinces of LaPampa and Buenos Aires. Political boundary (partido) information was also processed by AREAS in order to provide areal tabulations on a partido basis.

1. INTRODUCTION

The ability of a government to make sound decisions concerning a country's agricultural economy is dependent to a large degree on the availability of accurate and up-to-date agricultural crop production data. Area frame sampling (Wigton et al., 1978) is a technique which is currently used extensively for providing such data. One of the requirements for the implementation of a successful area frame is the initial stratification of the country or region into relatively homogeneous areas. A technique which utilizes land use information derived from Landsat MSS imagery, soils data and the Area REsource Analysis System (AREAS) (Wehde et al., 1980) geographic information system to aid in the delineation of these homogeneous areas is demonstrated for portions of the Argentine provinces of Buenos Aires and LaPampa. This study was conducted during the period of January through April, 1981, while the four authors from the Comisión Nacional de Investigaciones Espaciales participated in the Visiting International Scientist Program at the Remote Sensing Institute under the sponsorship of the United Nations Food and Agriculture Organization.

2. DESCRIPTION OF THE STUDY AREA

The location chosen for this study was 38° S to 39° S latitude and 60° W to 64 W longitude. Figure 1 is a false color composite Landsat mosaic reproduced in black and white of a large portion of the project area. This area lies in the southwestern part of Buenos Aires Province and the southeastern part of LaPampa Province, approximately 550 km southwest of the city of Buenos Aires. One of the reasons this location was selected is because it contains differences in soil types and crops. The eastern portion is one of

---

* SDSU-RSI-J-82-03

** Ms. DeVries, Dr. Westin and Mr. Wehde are associated with the Remote Sensing Institute (RSI), South Dakota State University, Brookings, SD, USA. Mr. Redondo, Ms. Gargantini, Ms. Marlenko and Mr. Vassallo are associated with the Comisión Nacional de Investigaciones Espaciales (CNIE), Buenos Aires, Argentina.

the most productive agricultural areas in Argentina in which the main crop is wheat. It is humid with precipitation as high as 900 mm/year. The soils mostly are Argiudolls and Hapludolls (Prairie soils) developed from loess. The western portion of the project area is less moist and the predominant soils are Haplustolls and Argiustolls (Chernozems and Chestnuts). There are more summer crops, such as sunflowers and sorghum, and the farms are diversified with livestock as well as crops.

3. MATERIALS AND METHODOLOGY

The AREAS input data used in this study were (1) political boundaries (partidos) obtained from an Operational Navigation Chart (ONC), (2) soils maps and legend material obtained from the World Soils Maps of the Soil Geography Unit of the U.S. Soil Conservation Service, and (3) land use (crop use intensity--CUI) data produced by the interpretation of Landsat false color composite imagery (Westin et al., 1981). All of the input data maps were at a scale of 1:1,000,000 and are presented in Figures 2, 3, and 4 as drafted versions at a reduced scale.

Each of the three input maps was digitized using a transparent mylar grid and a manual encoding technique. The grid was generated using the South Dakota State University (SDSU) Calcomp drum plotter, the SDSU IBM 370/148 computer and the AREAS GRID program. (See Table I for a listing of the AREAS programs.) Each grid cell represented an area of 4 km^2 when overlaid on the 1:1,000,000 scale maps. The manual digitization process involved recording the column numbers where category changes occurred on a row-by-row basis.

The encoded data were processed using the CARDSIN program which checks for coding errors and creates a map data set on a disk file. This data set was then used by the PLOTTER program to produce a computer-plotter map which was compared to the original map for error checking. Errors detected by the CARDSIN program or on the plotted map were corrected and the data were again processed using CARDSIN and PLOTTER. This error-detection loop was executed until the data were error-free. Figure 5 is the plotted version of the soils map (compare with Figure 3).

It was necessary to check for registration among the three basic input data sets because of accuracy problems which result from mis-registration during subsequent compositing of the data sets. The registered, error-free data sets were then processed using the TABULATE program to determine the areal extent of each category within the individual data sets.

4. RESULTS AND DISCUSSION

One of the analysis functions within AREAS is the INTERPRT program. This allows the user to group map units and create thematic maps. The utility of this program was demonstrated using the soils data set. Table II is an interpretation of each of the soil map units for several internal and external characteristics and the comprehensive soil taxonomy classification for each unit. Table III is an interpretation of each of the units for land use capability and suitability for various crops. The interpretation information was used in conjunction with the INTERPRT program and the soils data set to create several thematic maps such as the suitability for oats map in Figure 6. This film printer map was produced using the IMAGEOUT program in AREAS to create a magnetic tape file which was then used to generate the map.

Another AREAS analysis function is the COMPOSIT program. This program overlays two to four input data sets and results in a data set which is a composite of the input maps. Because an unwieldy number of combinations can result, it is often desirable to refine the output data set by subsequent INTERPRT processing or to present the combinations in tabular form as in Table IV. This table shows the results of compositing the political boundary

and crop use intensity data sets and provides useful information concerning the crop use intensity within each partido. Figure 7 is a line printer map (PRINTMAP option) and tabulation of the composited crop use intensity and soils data sets.

The map shown in Figure 7a can be used to locate homogeneous areas for area frame sampling. The soils data presented in Tables II and III indicate that the soils CH U/L and CT U/L are potentially the most productive. The areal tabulation data in Figure 7b show that together these two soils make up 78.9 of the CUI class 1 category (greater than 70% cultivated). The CH U/L soil unit within CUI class 1 is designated by an N on the map (Figure 7a) while the CT U/L soil unit within CUI class 1 is designated by a hyphen. By compositing the partido data set with the composited data set shown in Figure 7, homogeneous sampling areas can be located within the political units for planning purposes.

The data in Table III can be used to provide an agronomic check for the crop production figures that ultimately are to be derived from the area frame sampling. It is noted that the soil CH U/L has a good rating for all land uses listed. The soil CT U/L has either fair or good suitability ratings. The principal difference between these soil units is that the CT U/L soil unit is the product of a drier environment so that yields will be lower than for the CH U/L soil unit.

5. CONCLUSION

Soil maps, used alone, tell something about the potential of an area but do not indicate land use. Maps generated using Landsat imagery show land use but not soil potential. When these two data sources are combined in an information system, the resulting delineations are homogeneous with respect to potential and crop use intensity and would appear to be useful for area frame sampling.

6. REFERENCES

Wehde, Michael E. 1978. The operation of AREAS: Area REsource Analysis System. Remote Sensing Institute, South Dakota State University, SDSU-RSI-78-10.

Wehde, Michael E., K.J. Dalsted and B.K. Worcester. 1980. Resource applications of computerized data processing: The AREAS example. J. Soil and Water Cons., Vol. 35, No. 1.

Westin, F.C. and T.M. Brandner. 1981. Combining land use data acquired from Landsat with soil map data. Digest Vol. II, 1981 Int. Geoscience and Remote Sensing Symp., June 8-10, 1981, Wash. D.C., IEEE Cat. No. 81CH1656-8, pp. 1413-1424.

Wigton, W.H. and P. Bormann. 1978. A guide to area sampling frame construction utilizing satellite imagery. Submitted to United Nations Outer Space Affairs Division.

Figure 1. Black and white reproduction of the false color composite mosaic of Landsat scenes 2322-13104 and 2321-13045 acquired on December 10, 1975, and December 9, 1975, respectively, covering a large portion of the study area.

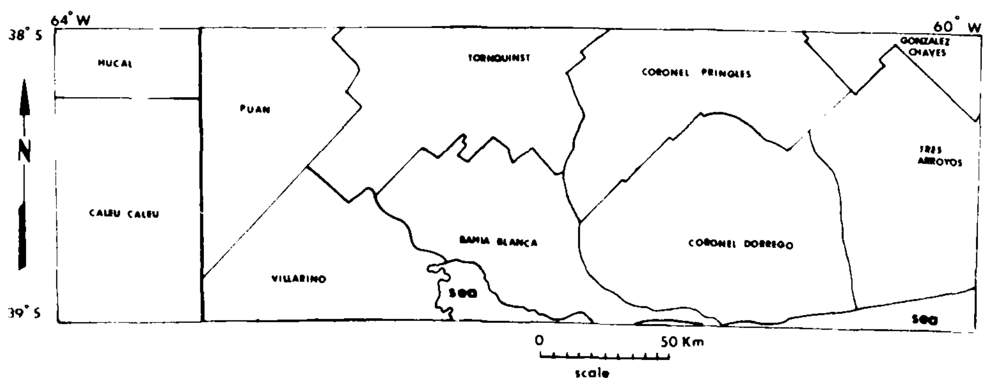

Figure 2. Drafted version of the AREAS input map showing political boundaries (partidos).

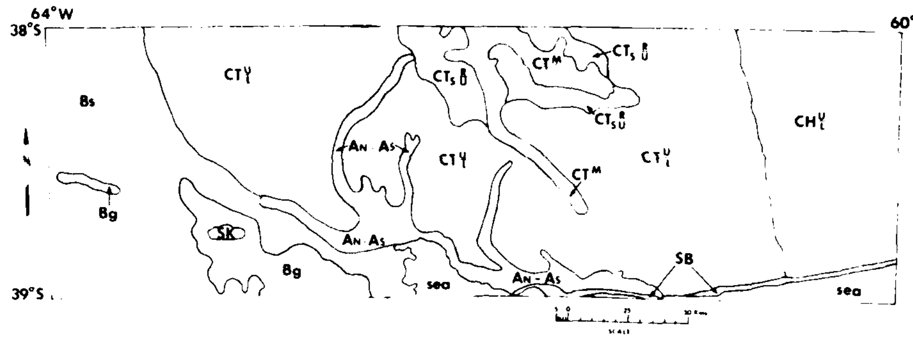

LEGEND

Soil Map Unit	Description	Soil Map Unit	Description
A_N-A_S	Calcareous and saline alluvial soils	CTs R/U	Sandy chestnut soils from unconsolidated materials on rolling terrain
Bg	Brown soils on gravel plains		
Bs	Sandy brown soils on level to rolling plains	CT U/L	Chestnut soils from loessial parent materials on undulating to rolling topography
CH U/L	Chernozem soils on nearly level to gently sloping loessial plains	SB	Sandy beaches
CT M/	Lithosolic chestnut soils on mountains	SK	Sononchak and associated soils

Figure 3. Drafted version of the soils maps used as input data for AREAS and legend for the map.

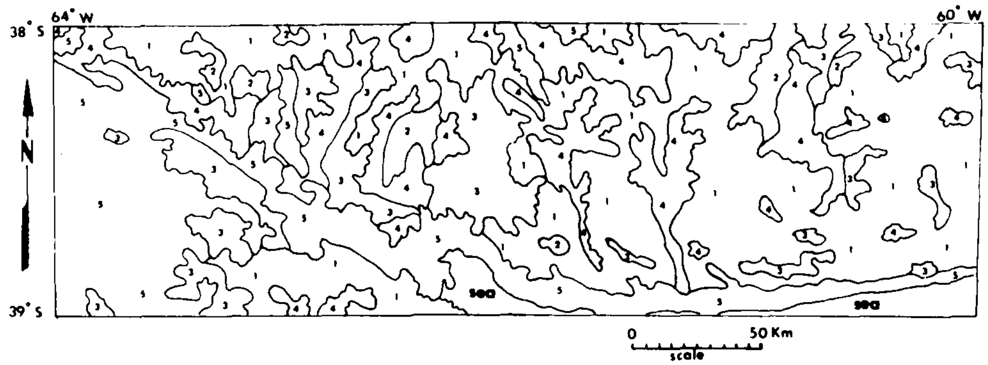

LEGEND

1. >70% cultivated
2. 50-70% cultivated
3. 30-50% cultivated
4. 5-30% cultivated
5. < 5% cultivated

Figure 4. Drafted version of the crop use intensity map used as input data for AREAS and the legend for the map.

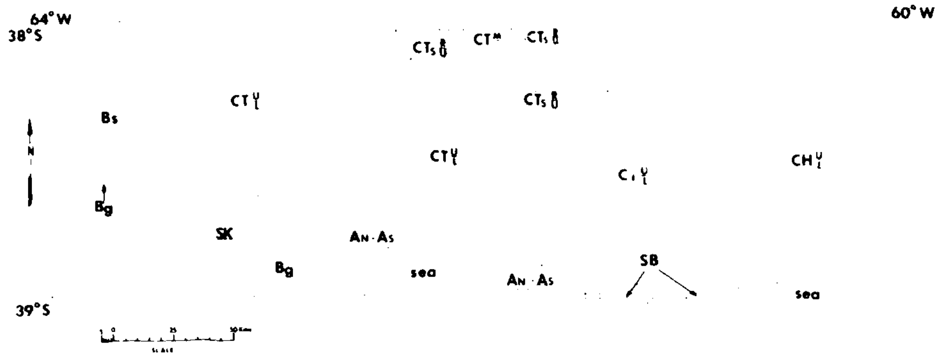

Figure 5. Digitized, plotted version of the soils input map with annotation added manually. See Figure 3 for legend.

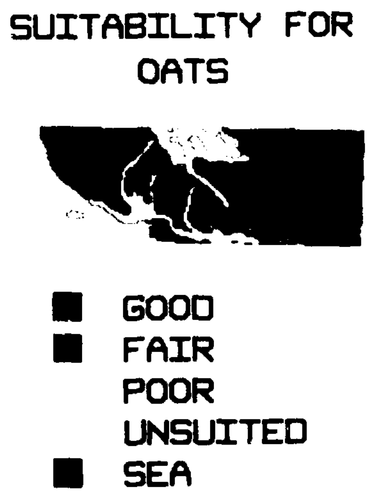

Figure 6. Suitability for oats thematic data set created using the INTERPRT program for soils data interpretation and the IMAGEOUT program for generation of the film printer map.

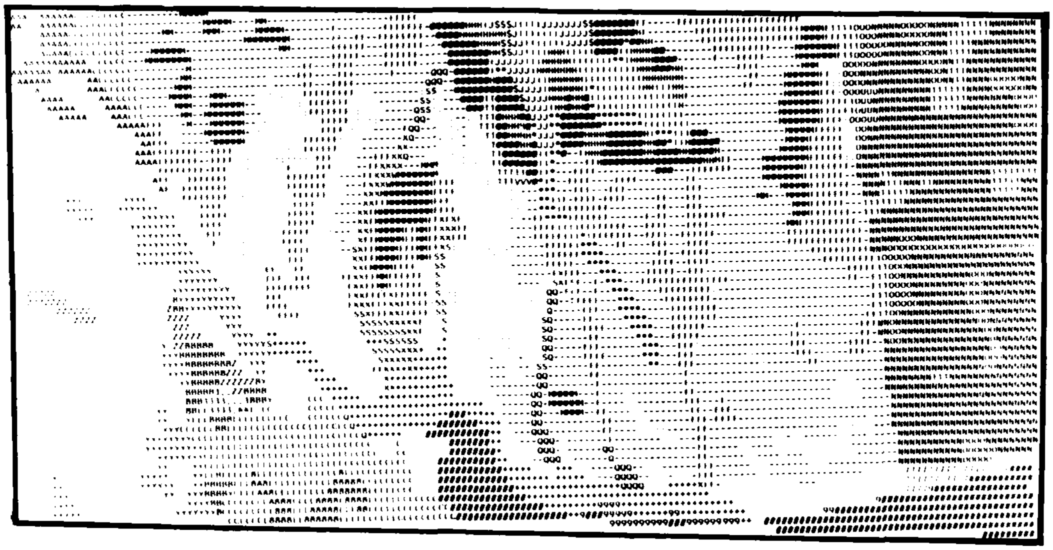

(a)

(b)

Code	CUI	Soil	Percent Area	Area (Hectares)	Code	CUI	Soil	Percent Area	Area (Hectares)
Q	1	An-As	0.68	26,000	3	3	SK	0.10	4,000
L	1	Bg	2.27	86,800	X	4	An-As	0.86	32,800
C	1	Bs	2.24	85,600	8	4	Bg	0.50	19,200
N	1	CH U/L	11.08	424,000	A	4	Bs	1.19	45,600
*	1	CT M/	1.02	39,200	1	4	CH U/L	1.19	45,600
@	1	CTs R/U	2.26	86,400	I	4	CT M/	1.56	59,000
-	1	CT U/L	20.68	791,000	H	4	CTs R/U	1.25	48,000
K	1	SK	0.02	800	F	4	CT U/L	10.44	399,600
W	2	An-As	0.02	800	+	5	An-As	3.01	115,200
U	2	CH U/L	0.09	3,600	2	5	Bg	0.51	19,600
M	2	CT U/L	3.32	127,200	.	5	Bs	12.58	481,000
S	3	An-As	0.59	22,400	7	5	CH U/L	0.42	16,000
B	3	Bg	0.75	28,800	J	5	CT M/	0.62	23,600
Y	3	Bs	2.56	98,000	$	5	CTs R/U	0.15	5,600
O	3	CH U/L	1.94	74,400	=	5	CT U/L	4.55	174,000
V	3	CT M/	0.03	1,200	9	5	SB	0.37	14,000
T	3	CTs R/U	0.26	10,000	,	5	SK	0.06	2,400
:	3	CT U/L	7.39	282,800	#	5	Sea	3.43	131,200
							Totals	100.00	3,826,400

Figure 7. Results obtained from compositing the crop use intensity (CUI) and soils data sets. (a) Line printer map created using the PRINTMAP option. (b) Legend for map and areal tabulation.

Table I. Listing and brief description of the AREAS programs.

ADJACENT	-	Report which codes adjoin (spatially)
AGREGATE	-	Reorient boundaries to simulate larger cell size
BOUNDARY	-	Analyze inter-boundary distances
CARDSIN	-	Create a map data set from coded card deck
COMPOSIT	-	Overlay two to four maps into one data set
DELETE	-	Remove a data set from the disk directory
DISTAP	-	Copy AREAS data set disk-to-tape
EXPAND	-	Increase matrix dimensions to simulate a smaller cell size
FILLER	-	Generate a dummy data set for filler in merge operations
GRID	-	Generate cellular grids of rectangular shapes
IMAGEIN	-	Convert digital image to AREAS data base
IMAGEOUT	-	Convert AREAS data to various forms of digital images for film recording
IMAGSTAT	-	Calculate the mean and variance of subsets of a digital image corresponding to an AREAS data set
INTERPRT	-	Tabulate areal extents or alter data codes to take on a new meaning
LISTING	-	List a data set on the line printer
MERGER	-	Join up to 5 data sets per pass at edges or ends
PLOTTER	-	Plot AREAS data set on Calcomp drum plotter
PRINTMAP	-	Create a map on the line printer
SHRINK	-	Reduce matrix dimensions to reflect cell output of AGREGATE program
SUBSET	-	Select a subset of data codes for analysis characteristics
SUMMARY	-	Generate a one page report of data set characteristics
TABULATE	-	Generate area tables (inventory)
TAPDIS	-	Copy AREAS data set tape-to-disk
WINDOW	-	Build a smaller rectangular output data set from an input data set

Table II. Characteristics and qualities of the soil map units and the comprehensive soil taxonomy classification for each unit.

Soil Map Unit	Precipitation (mm)	Texture	Depth	Internal Soil Drainage	Salinity mmhos/cm	Slope	Water Holding Capacity	Regime Temp.	Regime Moist.	Soil Rating: Texture	Soil Rating: Depth	Soil Rating: Drainage	Soil Rating: Salinity	Soil Rating: Slope	Wheat Yield Rating	Comprehensive Classification
A_N-A_S	530	Vf	d	p	sl-m	nl	h	T	UST	2	1	3	2-3	1	3	EAFa Typic Fluvaquent, fine, mixed (calcareous), thermic, DOSa and Typic Salorthid, fine, mixed, thermic
B_g	520	Vc	sh	se	0	gr	l	T	UST	2	3	3	1	2	3	MUHc Aridic Haplustoll, fine-loamy, mixed, thermic
B_s	515	Sl	d	se	0	gr-r	m	T	UST	2	1	3	1	2-3	3	EPHa Typic Torripsamment, mixed, thermic
$CH\frac{U}{L}$	630	Sil	d	w	0	nl	h	T	UST	1	1	1	1	1	1	MDAa Typic Argiudoll, fine-silty, mixed, thermic
$CT\frac{M}{}$	630	Vc	vsh	e	0	m	l	T	UST	2	4	4	1	4	4	MUHi Lithic Haplustoll, loamy-skeletal, siliceous, thermic
CT_{SU}^{R}	650	Sl	d	w	0	r	h	T	UST	2	1	1	1	3	3	MUHa Typic Haplustoll, coarse-loamy, mixed, thermic
$CT\frac{U}{L}$	570-670	Sil	d	w	0	gr	h	T	UST	1	1	1	1	2	2	MUAa Typic Argiustoll, fine-silty, mixed, thermic
SB	570-670	Fs	d	e	0	nl	l	T	UST	4	1	4	1	2	4	EPQa Typic Quartzipsamment, thermic, uncoated
SK	500	Sic	d	p	se	gr	h	T	UST	2	1	3	4	2	4	DOSa Typic Salorthid, fine-loamy, mixed, thermic

Texture

Fs = fine sand
Sl = sandy loam
Sil = silt loam
Sic = silty clay
Vc = variable, mostly coarse
Vf = variable, mostly fine

Depth

d = deep >36 inches
sh = shallow 10-20 inches
vsh = very shallow <10 inches

Internal Soil Drainage

p = poorly drained
w = well drained
se = somewhat excessively drained
e = excessively drained

Salinity - (mmhos/cm)

0 = none <2
sl = slight 2-4
se = severe 8-16

Slope

nl = level gently sloping 0-5%
gr = gently rolling 5-10%
r = rolling 10-15%
m = mountainous

Soil Rating (based on potential for growing wheat)

1 = excellent
2 = good to fair
3 = poor
4 = unsuitable

Water Holding Capacity

h = high >6.4" in root zone
m = medium 4.8-6.4" in root zone
l = low 3.2-4.8" in root zone

Temperature

T = Thermic 15-22°C

Moisture

UST = Ustic, moist part of year, dry for periods amounting to more than 3 months per year

Table III. Interpretation of the soil map units for land use capability and suitability for various crops.

Soil Map Unit	Composition		Land use Capabilities (Class and Subclass)	Suitability: Corn	Wheat	Sunflower	Oats	Grazing	Wood Crops	Feature Limiting Use
A_N-A_S	A_N	70	I	1	1	1	1	1	1	---
	A_S	30	VIs	4	4	4	4	2	2	Salinity
Bg		100	IVs	4	3	3	3	1	1	Excessively drained, aridity
Bs		100	IIIs	2	2	3	3	1	1	Excessively drained, wind erosion
$CH\frac{U}{L}$		100	I	1	1	1	1	1	1	---
$CT\frac{M}{-}$		100	VIIe	4	4	4	4	3	2-3	Very shallow, wind erosion
$CT_S\frac{R}{U}$		100	IVe	3	3	3	3	2	1	Slope-hilly, erosion
$CT\frac{U}{L}$		100	IIIe	2	2	2	2	1	1	Erosion
SB		100	VIIs	4	4	4	4	4	2	Coarse texture, excessively drained
SK		100	VIs	4	4	4	4	2	2	Salinity

Land Use Capability Classes determine the degree of land use capability: I-IV are capability for croplands, V-VII are capability for grasslands.

Suitability
1 = Good
2 = Fair
3 = Poor
4 = Unsuited

Land Use Capability Subclasses determine the limitation of the soil: e - erosion, s = limitations in the root area for salinity, excessive drainage.

Table IV. TABULATE resul.s for the composited political boundary and crop use intensity data sets.

Code Number	Code* Label	Percent Area	Area (Hectares)	Code Number	Code* Label	Percent Area	Area (Hectares)
1	4H	0.92	39,600	23	3T	2.15	92,800
2	5H	0.88	38,000	24	5C	8.98	388,000
3	1H	1.38	54,600	25	4C	0.22	9,600
4	1PU	1.91	82,400	26	2T	0.66	28,400
5	2PU	0.79	34,000	27	1D	8.85	382,400
6	1T	3.54	152,800	28	2D	0.07	3,200
7	4T	2.95	127,600	29	3C	1.05	45,200
8	2H	0.07	3,200	30	3B	2.44	105,600
9	5T	0.68	29,200	31	4B	0.94	40,400
10	1PR	4.33	187,200	32	4D	2.21	95,600
11	4PR	3.53	152,400	33	2B	0.25	10,800
12	2PR	1.05	45,200	34	1B	2.09	90,400
13	4G	0.18	7,600	35	4V	0.84	36,400
14	3G	0.50	21,600	36	5V	2.84	122,800
15	1G	1.45	62,800	37	3V	1.07	46,400
16	4PU	1.42	61,200	38	5B	2.17	93,600
17	13A	7.80	336,800	39	3D	0.63	27,200
18	3PU	2.32	100,400	40	1V	3.19	137,600
19	3PR	0.39	16,800	41	5D	1.34	58,000
20	33A	0.81	34,800	42	53A	0.38	16,400
21	43A	0.61	26,400	43	SEA	2.96	128,000
22	5PU	1.57	67,600				

* First digit of code label corresponds to crop use intensity (see Figure 4). Coding following digit indicates partido:

H = Hucal
PU = Puan
T = Tornquinst
PR = Coronel Pringles
G = Gonzalez Chaves
3A = Tres Arroyos
C = Caleu Caleu
D = Coronel Dorrego
B = Bahia Blanca
V = Villarino

BIOPHYSICAL MAPPING OF THE REPUBLIC OF HAITI THROUGH THE USE OF ENHANCED LANDSAT IMAGERY

Bernard Kientz

Societe Francaise d'Etudes et de Recherches Economiques et statistiques
Paris, France

L.A. Rivard

Montreal, Quebec, Canada

William A. Tyler

Environmental Research Institute of Michigan
Ann Arbor, Michigan, USA

ABSTRACT

Landsat data in imagery form at 1:250,000 scale were utilized to produce mapping of biophysical features of the Republic of Haïti. The results of this study will serve as a baseline inventory of resources for the Direction de l'Aménagement du Territoire et de la Protection de l'Environnement. As a comprehensive reconnaissance inventory, the map products should permit an initial selection of agricultural management areas or priority zones of erosion control.

The Haitian environment is highly sensitive to erosion primarily because of:

1. Rugged relief
2. High rural population density,
3. Climatic conditions.

PREPROCESSING OF LANDSAT DATA

The territory of the Republic of Haïti is included on portions of four Landsat frames. Four geometrically corrected enhanced false color images were produced at a scale of 1:250,000.

1. Most recent cloud-free imagery was obtained from the EROS data center. Most of the country is included within two frames imaged in January, 1979.
2. Each scene was geometrically corrected utilizing the best available topographic maps and nautical charts.
3. Landsat data were resampled into 50 meter cells in UTM map projection.
4. Four geometrically corrected, radiometrically balanced digital mosaic images were produced at 1:250,000 scale.

*Presented at the Seventeenth International Symposium on Remote Sensing of Environment, Ann Arbor, Michigan, May 9-13, 1983.

INFORMATION EXTRACTION

Three map products were generated at 1:250,000 scale by visual interpretation of enhanced false color images, supported by 285 ground-truth stereophoto pairs at 1:40,000 scale taken in 1978.

1. A geomorphology map (22 categories),
2. A biomass map (17 categories),
3. An erosion susceptibility map delineating 4 classes of erosion risk.

In addition, the geomorphology classification was produced in report form to define the attributes of the categories.

INTRODUCTION

The biophysical thematic mapping activities described in this paper were carried out in 1981 at the request of DATPE (Direction de l'Aménagement du Territoire et de la Protection de l'Environnment de la secrétairerie d'etat de Plan) of the Republic of Haïti and was financed by the Fonds d'Aide et de Cooperation francais. Specifically the request was to obtain rapidly an up-to-date country-wide inventory (28,000 km) of biophysical resources, the purpose of such inventory being to serve as basic information for the development of the national 5-year management plan for the period 1981-1986. Priority needs included (1) a means of initially locating districts most favorable for agricultural development; (2) areas requiring soil erosion control. The Haitian environment is particularly sensitive to such erosion due to a) its climatic regime, b) its generally very rugged relief and c) high population pressure on the land.

Budget and time constraints led to the use of Landsat MSS data as the most practical means of producing reconnaissance scale maps (1:250,000). The following products were delivered to the client:

- An enhanced imagery mosaic described elsewhere in this paper.
- A map of geomorphological terrain type.
- A land cover/land use map.
- A map of susceptibility to soil erosion.

DATA PROCESSING

The Republic of Haïti is included on portions of four Landsat frames. Cloud-free images were obtained during successive day passes in January 1979 for most of the country. Cloudy areas were supplemented by using data obtained during February 1976 for a small portion of the country. It should be stressed that a considerable degree of freedom is allowed in finding cloud-free areas due to the overlap and sidelap of Landsat images. Areas that are cloudy on one acquisition date may be clear on the previous satellite pass (one day earlier) or the next satellite pass (next day). If this area corresponds to an overlap area where cloud-free data are available, cloudy data may be "written over" with clear.

All digital processing was done at the Environmental Research Institute of Michigan's Earth Resources Data Center (ERDC). The initial steps involved in producing the images used in this study were running a scene search and ordering recent cloud-free data. After digital CCT's were received from the EROS Data Center, preliminary processing steps were performed on the data. These involved destriping, geometrically correcting and resampling the Landsat data.

Geometric corrections are required to convert the data from the uncorrected Landsat grid system to a more useful mathemetically defined map projection. The characteristics of the Landsat data that necessitate geometric correction include parameters related to the orbit of the satellite, the design of the multispectral scanner, and the requirement for use of projections to map a curved earth surface onto a flat piece of film. Satellite and orbital parameters requiring correction include: (1) tilt of the Landsat orbit with respect to the axis of the earth, (2) rotation of the earth under the satellite, (3) non-spherical shape of the earth, (4) satellite altitude, roll, pitch, and yaw and the changes on these attitude parameters.

The most accurate method of correction, and the one applied in this study, uses the ERIM nonlinear rigid model to map Landsat data into the desired map projection, correcting spacecraft and sensor distortions and perturbations in the process. The model uses a combination of defined Landsat parameters and the information contained in the Landsat SIAT file (an ancillary file contained on the EROS CCT) which includes spacecraft latitude and longitude and altitude, pitch, roll, and yaw as reported at several points through the scene. Parameters which are rigidly defined by the model include:

- Sweep-to-sweep skew due to earth rotation,
- Sampling delays and errors due to repeated pixels,
- Variations in scan mirror velocity with scan angle (empirically derived for Landsat 1, 2, and 3),
- Perspective or panoramic distortion,
- Oblateness of the earth,
- Elevation of map control points.

To apply the model, a regression analysis is performed between a set of map control points and image control points to refine the reported spacecraft roll, pitch, and yaw and to calculate roll and pitch rates and accelerations. Image control points are identified within the scene in row and column coordinates as it is displayed on a color monitor, and the corresponding points are marked on large-scale topographic maps. Control points should be single pixel permanent features that are visible in both the image and on the map. Examples include road intersections, bridges over streams, and other high contrast features. Map control points are digitized on a digitizing table to define their latitude, longitude, and elevation information is entered (if available). The refined attitude parameters are subsequently combined with the rigidly defined model parameters to generate a pair of geometric transformations that are used to convert the raw data into the desired map projection.

In principle, only three control point pairs are needed if no attitude maneuvers have been performed by the satellite during the collection of the data being corrected. In practice, however, a larger number of control point pairs are used to (1) reduce the effects of and permit detection of a bad point, (2) permit averaging to achieve subpixel accuracy in image control point location, and (3) to correct for pitch and roll rates and accelerations. The accuracy of the correction is limited by the resolution of Landsat data, map accuracies (usually a function of scale), and the precision with which image and map control points are located.

Mapping the data from the Landsat coordinate system to the desired map projection requires resampling of the data. Since new pixels will generally be required from locations between original pixels and transformed pixels, some form of interpolation is needed to estimate the new value. Common resampling techniques include nearest neighbor, bili ear, cubic convolution, and restoration. The first three are interpolations, while the fourth (restoration) is not. Restoration is a deconvolution technique. Because this project required the highest quality images, the restoration resampling technique was used. This technique recognizes that the terrain informatin has been convoluted by the scanner point spread function which includes the optical blur circle, the

moving detector area, the presampling electronic filter, and the digitizing or sampling process. The intent of restoration is to deconvolve the data by using a priori knowledge of the characteristics of the MSS to develop a set of processing coefficients which, when multiplied by an array of Landsat data values, will yield the best estimate of the desired resample point. Further, through the use of a priori knowledge, the inverse of the scanner convolution can be applied to synthesize the new sample point with a desired scanner point spread function to replace the original point spread function. Using a 4 x 8 array of Landsat pixels and the appropriate processing coefficients, data with better spatial and radiometric quality than the tape recorded Landsat data can be synthesized during the resampling process. For this project a 50 meter by 50 meter resampling interval was used. The data were resampled into a UTM map projection.

Resampled subscenes were then digitally mosaicked into four geographic areas labeled northwest, northeast, southwest, and southeast. The resampled images were filmed at 1:1,000,000 scale (using a 50 μ film aperture) and final scale enlargements (4X) were produced at 1:250,000.

INTERPRETATION ACTIVITIES

Methodology

The work followed a normal multi-stage approach for a reconnaissance level base line survey proceeding from a study of collateral information (see site-specific items in Selected References) to a correlation with the imagery spectral patterns to establish classification categories and their subsequent mapping.

Landsat imagery-based visual interpretation methodology can be viewed as situated between the standard type based on airphotos on the one hand and digital classification of the spectral data on the other.

Ground Data

Since field investigations were precluded by available funds, Landsat image classification accuracy was maintained by comparison with interpretation of black and white stereo airphoto pairs, scale 1:44,000 flown a year before the multispectral data. These were available for 285 sample localities scattered throughout the country.

Time

The time required to complete the delineation of the geomorphology and biomass classifications for 28,000 km^2 was approximately two man-months per classification.

THEMATIC CLASSIFICATIONS

Mapping Unit Signatures

As in the interpretation of conventional airphotos, biophysical mapping units are delineated on Landsat MSS imagery by combining a number of diagnostic elements of which the integrated radiance unit of the pixel is but one.

The detection and recognition of classification categories in Haïti was based on the following image elements:

Element	Geomorphology	Biomass
Direct Spectral	- slope aspect shadows and illumination - biomass association	colour (infra-red)
Locational	physiographic site	geomorphic association
Patterns	stream drainage	- stand density - relative height
Shape	unit polygon outline	crop polygons

GEOMORPHOLOGY

The 1968-70 OAS survey produced a geologic map and a soil/land capability map of Haïti. For the needs of the 1981-86 five-year plan we were asked to produce a geomorphologic map of the national territory.

The physical framework of the country is dominated by northwest-southeast and east-west tectonic trends and is characterized by anticlinal mountain ranges and alluvium-filled synclinal or down-faulted valleys arranged in continuous sequence from the north to the south coasts of the island. The highest point in the country is 2660 m while the average elevation of the ranges is about 1200 m.

The geomorphology classification is based on geological genetic principles and the categories are essentially lithomorphic. In land systems terminology our interpretation of the airphotos delineated "land units/facets", initial analysis of the Landsat mosaic delineated "land systems" and the latter were refined as much as possible into units/facets by comparison with the photos.

The developed classification of geomorphologic units is as follows:

GEOMORPHOLOGY MAP

Group 1 - Coastal deposits and fossil forms

11 - plains and deltas
12 - mangrove wetlands
13 - fringing and barrier coral reefs
14 - raised reef cliff terraces and plateaux (maximum elevation 690 meters)

Group 2 - Detrital fluvial deposits

21 - valleys > 500 m wide, including floodplains and terraces
22 - alluvial fans
23 - level plains
24 - inland wetlands
25 - dissected plains

Group 3 - Residual high mountainous massifs

31 - dissected volcanic
32 - dissected granitic
33 - karstic limestone
34 - mixed/interbedded sedimentary rocks
35 - altered sedimentary rocks

Group 4 - Hills and low mountains

41 - karstic
42 - mixed/interbedded sedimentary rocks
43 - volcanic rocks strongly dissected
44 - altered sedimentary rocks
45 - dissected granitic rocks

Group 5 - Plateaux

51 - relatively flat-lying limestone
52 - relatively flat-lying interbedded sed. rocks
53 - granitic rocks

Expanded Legend

The geomorphology classification was also produced in report form to define the attributes of the categories under a number of headings:

- Representative Location: - this was illustrated by reproductions of a sample airphoto and the corresponding area from the Landsat mosaic.
- Material: - relative induration, lithology
- Topographic characteristics: - relief range, regional pattern and local morphology
- Morphogenesis: - relative permeability, relative resistance to water degradation and susceptibility to chemical weathering.

BIOMASS

In the Caribbean region easterly trade winds blow off the sea constantly throughout the year. This dominant climatic factor acting on the structural arrangement and relief of Haïti described in the geomorphology theme produces great differences in rainfall on the northeast and southwest sides of the mountains, the rains being heaviest on the windward side with moisture deficiencies in the lee valleys. This generalization does not apply to the southern mountains where both north and south slopes are wet.

These orographic and climatic factors strongly determine the type and distribution of both vegetation and land use in the country. The basic patterns are strikingly apparent on the Landsat mosaic particularly since it was produced from data acquired during the local dry season.

As indicated in the discussion of mapping unit signatures, the biomass categories were established on the basis of spectral and physiognomic features which were then subdivided according to the geomorphic factors of topography, slope aspect and geomorphic type.

The classification is as follows:

A. Land Use

Intensive agriculture in plains and valleys

Irrigated:
11 - Sugar cane
21 - Multiple Cropping

Non-Irrigated:
12 - Sisal
22 - Multiple Cropping

Land Use on hill lands and mountains

23 - subsistence agriculture and extensive pastures
24 - coffee
25 - cocoa

B. Natural Vegetative Cover

Savannahs

31 - Wooded
32 - Herbaceous
33 - Regeneration forest/bush fallow

Forests

41 - Dense forest (mature)
42 - Degraded forests

Xerophytic Associations

51 - Barren land

Hydrophytic Associations

61 - inland wetlands
62 - mangrove swamps

C. Non-vegetative Land

71 - inert lithosols
81 - inert urban

Comments

The biomass classi˙ ˉ .tion may be compared to two earlier surveys:

1. The paper by Lafortune Seme and Laurin on the Cul-de-Sac Plain lists a number of limitations in the digital processing of their data (P. 1474):
- 7% of the land remained unclassified
- sparsely vegetated land (71) was confused with light forest (42)
- Xerophytes (51) could not be separated from savannahs (31/32)
- multiple cropping without irrigation (22) could not be separated as a category because of its inherent heterogeneity and the small size of individual fields.

Neither their visual interpretation nor ours encountered difficulties in discriminating these categories. Their visual interpretation yielded 20 categories compared to 17 for their digital classification.

2. Although it was not intended by the client that we maintain compatibility with earlier classification schemes, it is worth noting the ways in which our map of land cover and land use differs from the only other comparable nation-wide survey to come to our attention, the OAS 1968 ecologic and cash crop maps:
- scale: 1:250,000 vs 1:500,000 for OAS
- survey date: 1979 vs 1968 for OAS
- content: the OAS ecology map classification logically depicts nine categories of theoretical or "climax" forest vegetation while our 10 land cover and land categories show the occurrence of actual natural vegetation.

The OAS cash crops map shows the distribution of six specific crops in nine plains areas of intensive agriculture, while our land use information shows the distribution of four cash crops and subsistence agriculture in seven categories throughout the country.

Susceptibility to Erosion

The static nature of the information presented in the geomorphology and biomass maps is complemented by the map of susceptibility to erosion which can be considered a type of morphodynamic map. It was produced as a derivative cartographic task in the manner described below.

Bearing in mind the major environmental variables that control soil erosion - climate, geologic material, vegetation cover and topography, it was judged that a map depicting relative risk in a manner adequate to the working scale (1:250,000) could be produced by relating these variables to the categories of the two other thematic maps. This decision was based on the following assumptions:

1. That the effect of climate is well expressed in the natural vegetative cover.
2. That the geomorphic categories integrate relative resistance of geologic materials and topography to fluvial erosion and weathering.

The biomass categories were rated according to their relative deterrence of erosion as follows:

Classes	Biomass Categories
1. High Deterrence	11, 12, 21, 22, 23, 34, 25, 41, 61, 62
2. Moderate Deterrence	31, 32, 33, 42
3. Weak Deterrence	51, 71

The geomorphic categories were noted in ascending order of susceptibility:

Classes	Geomorphic Categories
0 Stability	12, 13, 14, 24
1 Low Susceptibility	11, 21
2 Moderate Susceptibility	22, 23, 33, 34, 35, 41, 44, 51, 52, 53
3 High Susceptibility	25, 31, 32, 42, 43, 45

Tracings of the two sets of regrouped categories were then superimposed and the susceptibility map was drawn according to a final classification which was arrived at by combinin. the separate ratings as follows:

Susceptibility to Erosion
(G = geomorphic ratings; B = biomass ratings)

- Class stability: G0 category
- Class low Susceptibility: G1 and B1 categories
- Class high Susceptibility: G2 and B3, plus G3 and B2, B3
- Class moderate susceptibility: all remaining areas not included in the above.

CONCLUSION

This biophysical mapping experience leads us to comment briefly on alternative remote sensing approaches to these types of terrain analysis:

- The use of satellite data as opposed to airphotos for regional surveys.
- The use of a visual as opposed to digital classification method.

Dent and Young state (p. 107) "Reconnaissance land surveys based on satellite imagery may not be as good as those based on airphoto interpretation but they are not demonstrably very much worse. Comparisons between unit boundaries initially based on satellite imagery with those subsequently derived

AD-A134 719 PAPERS SELECTED FOR PRESENTATION AT THE INTERNATIONAL SYMPOSIUM ON REMOTE..(U) ENVIRONMENTAL RESEARCH INST OF MICHIGAN ANN ARBOR JUN 82

96

UNCLASSIFIED F/G 14/5 NL

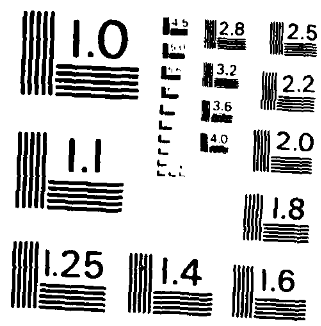

MICROCOPY RESOLUTION TEST CHART
NATIONAL BUREAU OF STANDARDS-1963-A

/

from airphoto interpretation show an acceptable measure of agreement. The value of the results of satellite-based survey is lower, but not by a large margin, but the cost of completing such a survey is lower by a factor of ten or more. Hence, the results obtained per unit cost are certainly greater. In addition, they are attained much more quickly."

Two main factors operated against the application of a digital classification method in these surveys. First, our analysis work was limited to using single date data. Further, these data were acquired in the month of January. Along with a limited budget, this constraint was dictated by one of the client's product requirements - the creation of a digitally-matched mosaic of the whole country.

The search for single-date cloud-free imagery for this purpose means that, for low-latitude environments, the useable data will usually be found to coincide with the local dry season. In the case of Haiti this is during the winter. The 34 degree sun angle and 134 degree azimuth, combined with the frequency and orientation of strong topographic relief, did not provide ideal data for digital analysis.

Secondly, the inability to collect a substantial quantity of ground information is usually considered to be an important factor limiting digital classification of an area in a tropical environment. Our budget and time constraints precluded a field study.

Finally, we believe the map products described here, generated by the visual interpretation method, constitute an added illustration of the fact that, in the present state-of-the-art human interpretation remains an efficient method of extracting information from enhanced remotely sensed data in imagery form. To paraphrase Townshend - other analysis methods may be potentially better, but are they sufficiently better in terms of cost and available expertise or timeliness?

SELECTED REFERENCES

GEOMORPHOLOGY

Haiti

Maps

- topographic - A.C.I.C., 1969 1:250,000, sheets NE 18-4, NE 18-7, NE 18-8 (50 meter contours)
- geologic - O.A.S. 1970, 1:250,000 (stratigraphy, lithology and structure)
- pedologic - O.A.S. 1970, 1:250,000 (ITC "soil units")

Reports

- Mission d'Assistance Integree du Secretariat General de L'O.E.A., 1968-1970 chap. 2, geology & physiography, chap. 4, soils
- Geology, Morphotectonic Analysis & Soils Mapping of Central Haiti Based on Landsat Image & Aerial Photographs, N. Munoz et al pp. 1529-1535, Proceedings 14th International Symposium on Remote Sensing, Costa Rica, 1980

General

- Integrated Terrain Mapping with Digital Landsat Images in Queensland, Australia, C. Robinove, U.S.G.S. Professional Paper 1102, 1979
- ERTS 1 Imagery in Biophysical Studies, P. Gimbarzevsky, pp. 391-403, Proceedings, 2nd Canadian Symposium on Remote Sensing, 1974
- The Application of Landsat Imagery to Soil Degradation Mapping at 1:1,000,000, C. Mitchell & J. Howard, FAO Report AGLT4/78, 1978
- Terrain Analysis and Remote Sensing, J. Townshend ed. Allen and Unwin, 1981. chaps. 3, 5, 6, and 7
- Terrain Classification, C. Ollier, chap. 8 in Applied Geomorphology, J. Hails ed., Elsevier, 1977

- Géomorphologie Applicable, J. Tricart, Masson, 1978, chap. 2
- Geomorphology in Environmental Management, R. Cooke and J. Doornkamp, Oxford, 1974, chaps. 13 and 14
- Terrain Evaluation, C. Mitchell, Longman, 1973, chaps, 5 and 8
- Soil Survey and Land Evaluation, D. Dent and A. Young, Allen and Unwin, 1981, chaps. 7 and 8
- Review of Concepts of Land Classification, J. Mabbut, pp. 11-28 in Land Evaluation, G. Stewart ed. MacMillan, 1968

BIOMASS

Haiti

Maps
- ecologic zones - O.A.S. 1970, 1:500,000
- cash crops - O.A.S. 1970, 1:500,000

Reports
- Mission d'Assistance Intégrée du Secrétatiat Général de L'OEA, 1968-70 chap. 5 ecology, chap. 7 land use
- Department du Nord, Haïti, a Study of Land Use and Settlement, H. Wood, University of Toronto, 1963
- Landsat Applications to Land Use Mapping of the Cul de Sac Plain of Haiti, R. Lafortune, F. Seme, R. Laurin, 1978, pp. 1465-1475, Proceedings 13th International Symposium on Remote Sensing, Ann Arbor, Michigan, 1979

General
- Application of Landsat Data to Tropical Forest Surveys, R. Baltaxe, FAO Report FOR: TF/INT/333 (SWE), 1980

Analogs
- Mapping Tropical Vegetation Zones in the State of Veracruz, Mexico, M. Soto et al. pp. 1871-1882, Proceedings, 12th International Symposium on Remote Sensing, Manila, 1978
- Remote Sensing of the Los Andes Region, Venezuela, J. McKeon, ERIM Report 305200-7-F, 1979
- Interpretation of Forest Vegetation of the Doon Valley, India, E. Van Es, pp. 650-656 I.T.C. Journal 74-5

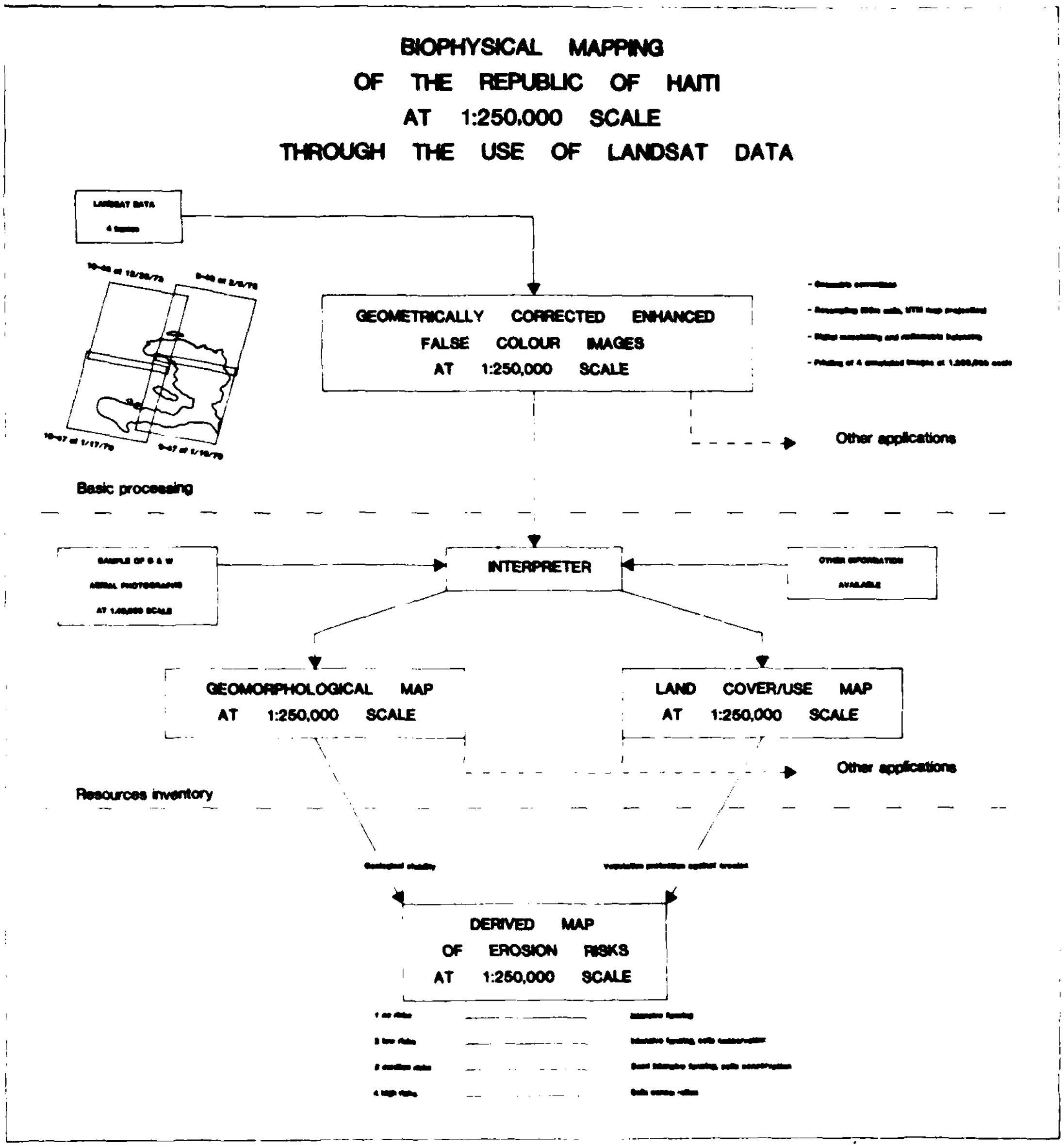
BIOPHYSICAL MAPPING
OF THE REPUBLIC OF HAITI
AT 1:250,000 SCALE
THROUGH THE USE OF LANDSAT DATA
GEOMETRICALLY CORRECTED ENHANCED
FALSE COLOUR IMAGES
AT 1:250,000 SCALE
Other applications
Basic processing
INTERPRETER
GEOMORPHOLOGICAL MAP
AT 1:250,000 SCALE
LAND COVER/USE MAP
AT 1:250,000 SCALE
Other applications
Resources inventory
DERIVED MAP
OF EROSION RISKS
AT 1:250,000 SCALE

FIGURE 1.

REPUBLIQUE DE HAITI

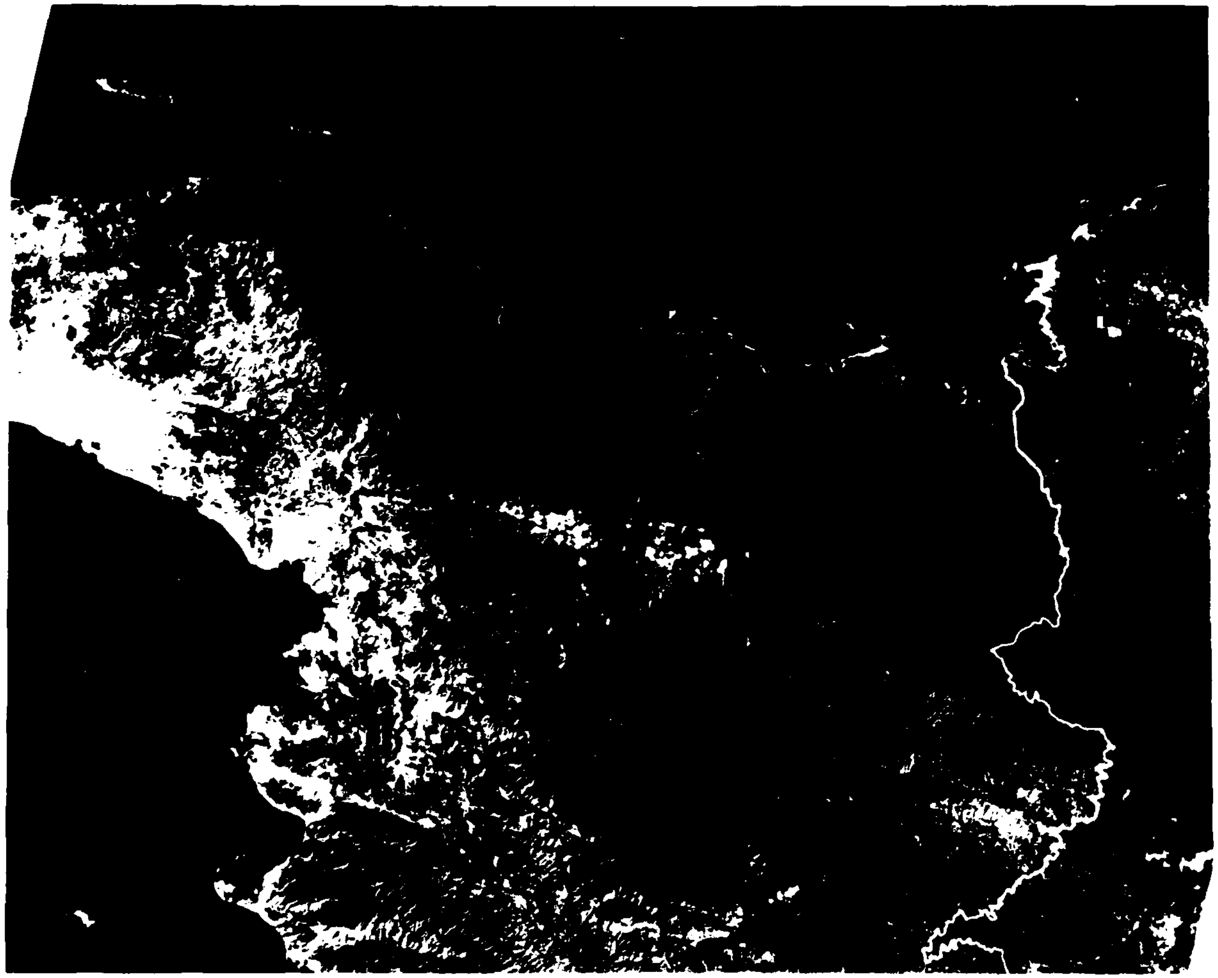

Echelle : 1 250 000 ème

FIGURE 2.

REPUBLIQUE FRANCAISE
MINISTERE DE LA
COOPERATION

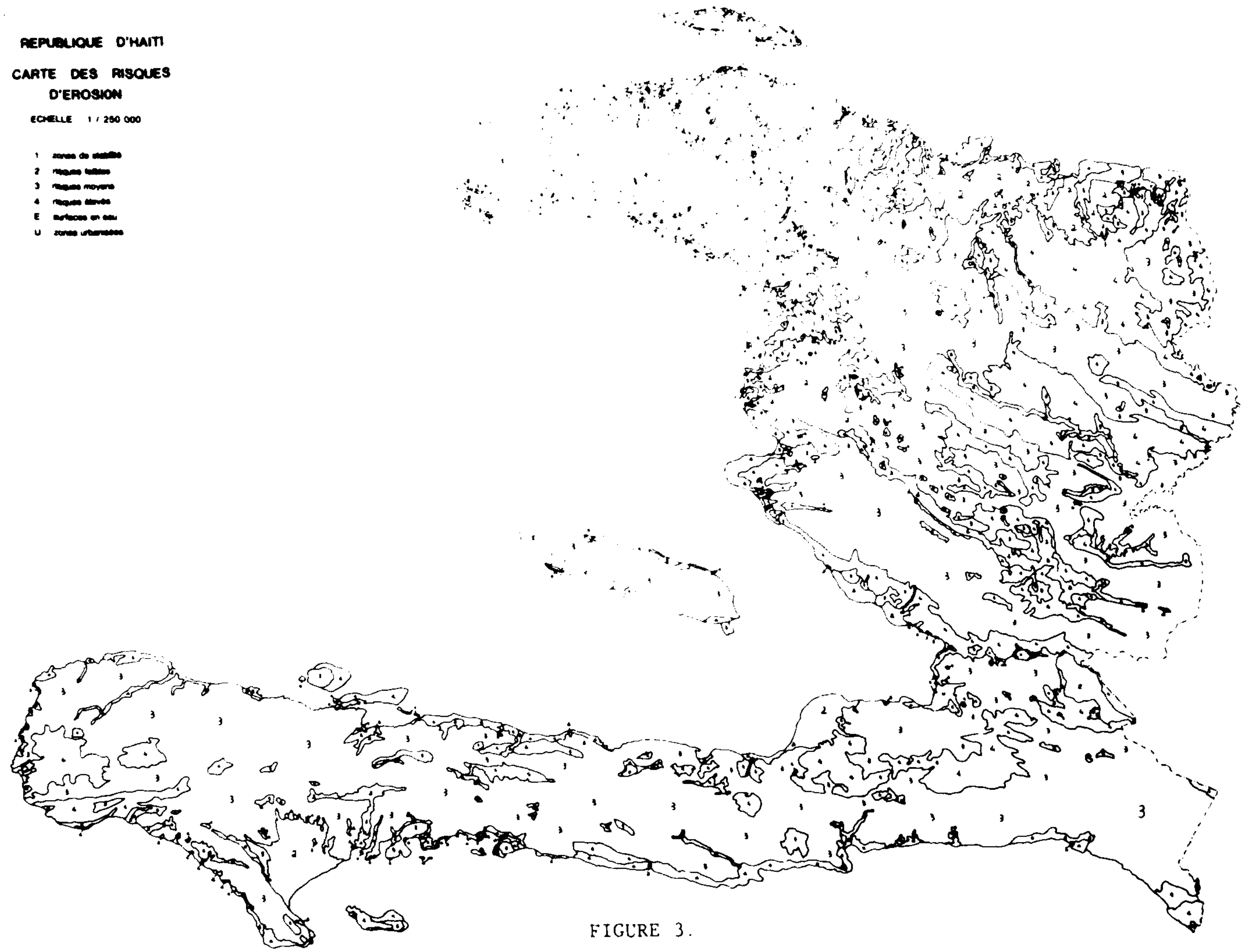

REPUBLIQUE D'HAITI
CARTE DES RISQUES D'EROSION
ECHELLE 1 / 250 000

FIGURE 3.

THE USE OF LANDSAT IMAGERY FOR LINEAMENT ANALYSIS IN ARGENTINA

Carlos Esteban Castro
Héctor Horacio Puigdomenech
Leonor Ines Salinas
Maria Angélica Matar de Sarquís
Gustavo Héctor Tabbia

Instituto de Investigaciones Mineras
Universidad Nacional de San Juan
San Juan, Argentina

SUMMARY

The regions under study belong to: a) north-western Patagonia Provinces, in the south of Argentine Republic, between parallels 38°00'S and 42°00' S, and meridians 68°00' W and 71°00' W; and, b) the Pie de Palo Range in the central part of San Juan Province.

The basic objective was to determine the pattern and regional trends of the dominant sets of lineaments, and to prepare an iso-lineament map of the area in order to obtain structural data to identify what systems of forces gave rise to those anomalies; and in b) a structural analysis was done by means of the lineament interpretation on Landsat imagery 1:500,000, in order to develop a mineral deposit prospecting project.

The work was run on a mosaic of Landsat imagery at scale 1:1,000,000 in band 7, and F.C.C., with the aid at times of F.C.C. in 1:250,000. The first step was to prepare a schematic geologic map of the region, and a map of meso, macro and megatraces (lineaments). A correlation was done over areas covered by conventional geologic surveys, and then each data was extrapolated to not-well-known areas supported by satellite imagery interpretation.

Every set of lineament data (strike and long) was processed by means of a digital table and ordinator, obtaining circular histograms and iso-density curves. For regional patterns, a detailed field survey was also accomplished.

The north-western Patagonia (Argentina) is characterized by several morphostructural features: Comarca Norpatagónica, Cordillera Neuquina, Cordillera Patagónica, Cuenca de Ñirihuau-Norquinco-Cushamen. So, from a geological point of view, the whole area is quite difficult to schematic simplications.

Inferences are done to identify correlations between geologic provinces with orientation and frequency of lineament patterns.

In the Pie de Palo Range, two regional trends have been defined in the system of lineaments: N 30°-40° W and N 60°-70° E, and the next step was the design of isodensity curves and intersections, whose maximum figures focus was at the NE sierra's quadrant.

OPTIMUM ASSESSMENT OF SUBSURFACE WATER PARAMETERS USING RADIANCE MEASUREMENTS FROM SPACE*

S. Ueno and Y. Kawata

Kanazawa Institute of Technology,
P.O.Kanazawa-South,Nonoichimachi,
Ishikawa 921,Japan

ABSTRACT

In recent years, with the advent of LANDSAT, Skylab.,and advanced Earth monitoring spacecrafts, there have been many examples of terrestrial imagery obtained from space over ocean and coastal regions. Whereas some show clearly ocean bottom surface, however,some show turbid plumes of sediment-bearing water in the littoral zone, or effluent extending seaward from river mouths. Then, it has become increasingly important to evaluate the extent of the atmospheric degradation of the signal, because of the presence of the terrestrial atmosphere between target and backgrounds. In remote sensing of oceans the extent of the atmospheric effects on the MSS data is estimated for clear sky and under stable condition.

An aim of the present paper is to show how to compute the ordinary and inverse initial-value solutions of the transfer equation of radiation for the atmosphere-ocean system, in order to remove the atmospheric blurring effects on the oceanic imagery. An introduction of the effective surface albedo of the calm sea into the solution of the transfer equation for the composite system enables one to evaluate the ratio of the upward radiance just below water to the downward radiance just above water, which is related to the optical parameters in the composite system. As a result, contour map of the digital counts near Kanazawa harbor in Hokuriku region of Japan is produced from LANDSAT MSS data in band 5, and the associate map of the albedo of the sea surface is also presented. These maps are useful not only in monitoring the flow patterns, but also in providing the relative detailed features of turbidity of the coastal water from LANDSAT, allowing for the logarithmic relation between the diffuse reflectance and the suspended sediment concentration.

I. INTRODUCTION

The multiple scattering problems in atmospheres bounded by specular reflector have been reduced to the determination of the scattering and transmission functions (cf.Sobolev 1963;Casti , Kalaba and Ueno 1969; Ueno and Mukai 1973;Matsumoto and Ueno 1976). Another problem of the specular reflection is the evaluation of the radiation field within the sea in quiet condition. In a rigorous manner the spectral radiance emanating from the air-water system with allowance

*Presented at the Seventeenth International Symposium on Remote Sensing of Environment, Ann Arbor, Michigan, May 9-13, 1983.

for both reflection and refraction at the system interface has been dealt with by several authors(cf. Ambarzumian 1964;Sobolev 1963, 1975; Gutshabash 1963;Raschke 1972;Tanaka and Nakajima 1977; Mukai and Ueno 1978). Furthermore, *in recent years the approximate solution approach* to the above problems has been developed by several authors(cf.Duntley 1963; Plass and Kattawar 1969;Jain and Miller 1976;Gordon and Clark 1981).

In recent years an inverse problem of determining the optical parameters of air-water system from the remotely sensed reflected radiance of water has deserved much attention in the field of environmental monitoring(cf. Jerlov 1968; Jerlov and Steeman 1974). Particularly, optimization approach to the inference of the optical properties of subsurface waters from the measurements of space-borne Multi-spectral Scanners data over the sea has been theoretically and observationally dealt with (cf. Gower 1981; Vernberg and Diemer 1982). In satellite observations of oceanic turbidities, the background radiance of light scattered by the atmosphere and the water surface is predominant compared with that due to the water color and suspendid solids. Thus, in monitoring the low concentration of turbidities by the space-borne sensors, it is first required to remove the atmospheric scattering and sea-surface reflection effects on the imagery(cf.Jain and Miller 1976;Dechamps et al. 1977; Holyer 1978; Munday and Alföldi 1979;Gordon and Clark 1981; Aranuvachapun and Leblond 1981; Okami et al.,1981). In a series of our papers(cf.Ueno,Haba et al. 1978;Haba,kawata et al. 1979;Kawata, Kusaka et al. 1981;Ueno,Kawata et al. 1980; Ueno 1980; Ueno 1981a) , an invariant imbedding and quasilinearization (cf.Bellman and Kalaba 1965; Kagiwada, Kalaba and Ueno 1975; Kagiwada 1974;Ueno 1981a) have been applied to the inversion of the total reflected radiance at top of the atmosphere-ground system. On extending the quasilinearization approach , inference of optical parameters of air-water system from the total reflected radiance by the space-borne sensors have been dealt with (cf.Ueno 1981b; Ueno 1981c).

An aim of the present paper is to show how extension of the quasilinearization algorithm to the least-squares estimation of the sea surface albedo from the LANDSAT MSS data will be performed, allowing for the albedo mapping of the sea surface which is related to the turbidity patterns in coastal waters. In text, the second section deals with the initial-value solution of the transfer equation for the air-water system, allowing for the interaction of radiation through the system interface. On keeping in mind the *interaction of radiation at the system* surface, the simultaneous determination of the radiation field in air and in water is reduced approximately to the esimation of the radiation field in the atmosphere bounded by the effective surface albedo of the specular reflector. In the third section, it is snown how to use the quasilearization for the least-squares estimation of the effective water surface albedo from the noisy measurements of the spectral radiance emergent from the air-water system. The numerical experiments for the successive approximation of the effective water surface albedo in the simulation model showed rapid convergence towards to the true value. As a result,the contour map of digital counts produced from LANDSAT data in band 5 near Kanazawa harbor is illustrated and furthermore, based on the atmosphere-ocean model appropriate to this case, the associate map of the sea-surface albedo is presented. The above associated map may be similar in form to the turbidity patterns , provided that the logarithmic relation between diffuse reflectance and the sediment concentration holds approximately(cf.Maul and Gordon 1975;Munday and Alföldi 1979;Aranuvachapun and Leblond 1981). Hence such associated maps may be not only useful for the preparation of the turbidity patterns, but also they are related to many oceanographic parameters such as the attenuation and scattering coefficients, ocean color and others.

II. TRANSFER PROBLEM OF RADIATION

1. ATMOSPHERE-OCEAN SYSTEM WITH INTERACTING SEA-SURFACE

i. Basic Equations

Suppose that the top of a plane-parallel, anisotropically scattering, inhomogeneous atmosphere-ocean system of the overall optical thickness L is illuminated in a direction Ω by parallel rays of net flux πF per unit area normal to the direction of propagation. Let the upwelling intensity of radiation in the direction Ω at any level t $(0 \leq t \leq L)$ be denoted by $I(t, \Omega)$;similarly let the downwelling intensity of radiation at level t be denoted by $I(t, -\Omega)$. In the above the direction Ω (or Ω_0) stands for (v, ϕ) (or u, ϕ_0), where v (or u) is the cosine of inclination to the normal and ϕ (or ϕ_0) is the azimuth referred to the suitably chosen horizontal axis. Furthermore,let the albedo for single scattering be denoted by λ $(0 \leq \lambda \leq 1)$, which depends on the optical height. The atmosphere-ocean system consists of the atmospheric layer and the oceanic lay-

er , whose anisotropic scattering property is described by the normalized phase function P. The interacting interface is assumed to reflect specularly the radiation.

The equation of transfer appropriate to to this case takes the form

[illegible] (2.1)

where $d\Omega' = dv'd\phi'$, together with the boundary conditions

$$I(L,-\ [illegible]) = [illegible], \qquad (2.2)$$

$$I(0,+\ [illegible]) = 0. \qquad (2.3)$$

[illegible].(2.3) refers to the boundary condition at the non-reentrant surface t=0. Furthermore, we should take into account the redistribution in direction of radiation at the interface t=y, whose y is the optical thickness of the oceanic layer.

In the case of specular reflection from the water surface, the angle of incidence is equal to that of reflection from the surface, and moreover the incident ray, the normal, and the reflected ray are together in the same plane. Generally speaking, a fraction r(u) of the radiation incident on the interacting surface will be reflected, whereas the remainder (1-r(u)) goes through the water. In other words, both reflection and refraction take place at the interacting surface, where the redistribution of radiation in various directions occurs.

Let the upwelling and downwelling intensities of radiation just above the surface be denoted by I(y,+[illegible],A) and I(y,-[illegible],A), respectively. Similarly, let the upwelling and downwelling intensities of radiation just below the [illegible] I(y,+[illegible],W) and I(y,-[illegible],W), respectively. In the above A(or W) represents the abbreviation of Air(or Water), and each component layer is assumed to be free from the reflecting boundary. Furthermore, let the scattering and transmission functions of the air (or water) be denoted by S(x(or y);[illegible],Ω_0) and T(x(or y);[illegible], [illegible]),respectively, where x represents the optical thickness of the atmosphere. In Appendix system of the Riccati type of the integro-differential equations governing the scattering and transmission functions in the air and the water is presented.

Based on the invariance principles (cf.Chandrasekhar 1960)we get the redistribution laws of radiation in various directions at the interaction surface as follows:

[illegible] (2.4)

[illegible] (2.5)

[illegible] (2.6)

$$I(y,+\bar{\ }\ ;w) = [illegible]\ I(y,-\Omega';w)d\Omega' + \frac{1}{4v} e^{-x/u}(1-r(u))n^2 s(y;\bar{\Omega}, \bar{\Omega}_0), \qquad (2.7)$$

where

$$\bar{\ } = ([1-n^2(1-w'^2)]^{1/2}, [illegible]), \qquad (2.8)$$

$$\bar{\ } = ([n^2 - (1-v^2)]^{1/2}/n, [illegible]), \qquad (2.9)$$

$$[illegible]\,\{[n^2-(1-u^2)]^{1/2}\,[illegible]\,n,\,[illegible]\}. \qquad (2.10)$$

In Eqs.(2.4) through (2.7) r(v) is given by Fresnel's formula

$$r(v) = \frac{1}{2}\left[\frac{\sin^2(\ [illegible]\ )}{\sin^2(\ [illegible]\ )} + \frac{\tan^2(\ [illegible]\ )}{\tan^2(\ [illegible]\ )}\right], \qquad (2.11)$$

where $v=\cos\theta$, $u=\cos\theta_0$, and furthermore,

$$[illegible] \qquad (2.12)$$

In Eq.(2.12) n is the index of refraction of the second medium to the first one.

In the case of LANDSAT MSS data the effect of sun glint and wind wave on the oceanic imagery should be taken into account (cf.Cox and Munk 1954; Plass,Kattawar, and Guinn 1977).

ii. Total Reflected Radiance at Top

On keeping in mind Eqs.(2.4) through (2.7), the required total spectral radiance emerging from the top is expressed in terms of S-,T*- and I-functions as follows:

$$[illegible]$$

$$[illegible] \qquad (2.13)$$

where I(y,+[illegible],A) is given by Eq.(2.5), and T*-function is the transmission function of the atmospheric layer , when upward parallel rays are incident at t=y.

3. ATMOSPHERE-OCEAN SYSTEM WITH EFFECTIVE SPECULAR REFLECTOR

i. Basic Equations

Exact solution of the total spectral radiance I(L,+[illegible]) with allowance for the redistribution in direction of energy in the air-water system is not so readily computed(cf. Mukai and Ueno 1978). Then, in order to make tractable the inverse problem, we shall take into account approximately the contribution of the upwelling intensity of radiation just below the surface to the upwelling intensity of radiation just above the surface. In other words, in place of the surface albedo r(v), we deal with the effective surface albedo R(v), allowing for the interaction of radiation at the interface. The quantity R corresponds to the effective specular reflector albedo. The equation of transfer appropriate to this case takes the form in Eq.(2.1), where the overall optical thickness L is replaced by the atmospheric optical thickness x. Furthermore it should be solved subject to the boundary conditions

$$[illegible] \qquad (2.14)$$

$$[illegible] \qquad (2.15)$$

where stands for (v,[illegible]). In this case , allowing for Eqs.(2.5) and (2.7), the effective surface albedo R(v) takes the form

$$R(v) \simeq [r(v) + \frac{(1-r(\bar{v}))\,[illegible]}{[illegible]}\,\frac{I(y,+[illegible];A)}{I(y,-[illegible];A)}], \qquad (2.16)$$

where R-function includes the contribution due to the upward radiance just below the surface. Eq.(2.16) is similar in form to that given by Jerlov(1968).

ii. Effective Scattering Function

The total spectral radiance at top in the diffuse radiation field is expressed in terms of the effective scattering function $S(x,R;\Omega,\Omega_0)$

[illegible]

where the interaction effect of radiation at the calm sea surface is included approximately in the effective surface albedo $R(v)$. Now, the phase function $P(t;\Omega,\Omega_0)$ is expressed in Legendre polynomials

[illegible]

where $P_k^m(t)$ is the associated Legendre function of degree k and order m, and

[illegible]

Then, the effective scattering function is expressed in terms of the Fourier [illegible]

[illegible]

In a manner similar to our preceding paper (cf. Bellman and Ueno 1972), it is shown that the Fourier component of the scattering function $S^{(m)}(x,R;\Omega,\Omega_0)$ fulfills

[illegible]

where

[illegible]

for m=0,1,2,...,M. The initial condition of Eq.(2.22) is given by

[illegible]

Furthermore, the $S^{(m)}$-function has the angular symmetric property, i.e. the reciprocity principle

[illegible]

III. INVERSE TRANSFER PROBLEM OF THE EFFECTIVE SURFACE ALBEDO

1. LEAST-SQUARES ESTIMATION

In a series of papers (cf. Bellman et al. 1965), the least-squares estimation of optical properties such as the optical thickness, phase function, albedo for single scattering and others has been performed with the aid of the quasilinearization and invariant imbedding, assuming an atmosphere bounded by a completely absorbing background. In what dollows, we shall consider the estimation of the effective surface albedo.

The inverse problem which we wish to solve is to estimate the effective surface albedo of the air-water surface discussed in the preceding section, in the least-squares sense, using the noisy total spectral radiance measurements. Mathematically speaking, we wish to minimize the following expression.

[illegible] (3.1)

over all choices of the unknown parameter R, provided that the phase function, the optical thickness and others are together provided. In Eq.(3.1) b_{ijk} represents the radiance of the diffusely reflected light, i.e., $b_{ijk} = I_{ijk}(x,R)$, for incident directions [illegible] N. The subscript k denotes the k-th component of the azimuth of the view angle. In Eq.(3.1) $I_{ijk}(x,R)$ is given by

[illegible]

On making use of quasilinearization, the problem will be successively solved. Putting the function $S_{ij}^{(m)}$ as S_{mij} and similarly, writing [illegible] as [illegible], $P_k^m(v_i)$ as P_{mki} we get a system of linear differential equations for the $(n+1)^{st}$ approximation of S_{mij} and R. A Cauchy system of the S-component takes the form

[illegible]

[illegible]

where

[illegible]

and S^0 is a known set of first approximation to the solution. In Eq.(3.5) [illegible]$_{mki}$ is given by

[illegible] $+ P_{mki}$ [illegible] e^{-2x/v_i} [illegible]

In Eq.(3.6) $\{v_i\}$ is the set of N roots of the shifted Legendre polynomial of degree N, $P_N^*(v) = P_N(1-2v)$. Furthermore, w_i is the Christoffel weight corresponding to the value of v_i. The initial condition of S_{mij}^n is such that it vanishes as x tends to zero. In Eq.(3.3) the Fourier component S_{mij}^n satisfies the principle of reciprocity with respect to the angular argument.

[illegible]

There are basically (MN^2+1) differential equations, which reduce to [illegible] differential equations with the aid of the reciprocity relation Eq.(3.7), whereas the full set of values S_{mij}^n representing MN^N matrix is always available. The solution is subject to the initial condition (2.24) and the boundary condition (3.1) with Eq.(3.2).

Since S_{mij}^{n+1} is a solution of a system of linear differential equations, we express it in terms of a linear combination of a particular solution q_{mij} and a homogeneous solution h_{mij}

[illegible]

The particular solution is defined by the equation

[illegible]

[illegible] (3.10)

while the homogeneous solution is defined by the differential equations

[illegible] (3.11)

where δ is the Kronecker delta function, which vanishes except for the last component of unity. From the definition of the initial condition in Eqs. (3.10) and (3.12), the coefficient R in Eq. (3.8) is identified with the initial conditions of the system at x. Given an initial approximation for the solution S, both the particular solution q and the homogeneous solution h can be computed from Eqs.(3.9) and (3.11).

By a simple differentiation of Eq.(3.1) with respect to R, we get the valus of R minimizing the performance function

$$\ldots \sum_{m=0}^{M} b_{mij} \cos m\phi_k)^2]^{-1}, \quad (3.13)$$

where ϕ_0 is put to be zero. Eq.(3.13) is the required expression, permitting the least-squares estimation of the effective surface albedo from the noisy spectral radiance measurements.

i. Numerical Simulation

In our preceding papers (cf.Kagiwada 1974;Kagiwada et al. 1975), the inverse problems of inhomogeneous and anisotropically scattering atmospheres bounded by diffuse reflectors have been solved numerically. Initial estimates of the optical parameters such as the optical thickness, phase function, and others have been sequentially refined.

For the sake of simplicity of presentation, the inverse problem of homogeneous, isotropically scattering atmosphere bounded by quiet water surface is computed for the case in which true values of the parameters are λ =1, x=0.3, [illegible] division points are made , allowing for the numerical solution of Eq.(2.22) under consideration. On Making use of the reciprocity relations, the result of numerical experiments with initial guesses R=0, 0.1, and 0.2, respectively, is listed (cf.Ueno 1981b). The values of R obtained in the first, second, third and fourth experiments are tabulated. The initial guess of R in Run 1 is too low, in Run 2 and 3 too high. Yet the correct value of R is almost accurately found in 3 to 4 iterations. The time required for each run is less than a few minutes on IBM 3031 digital computer, using Runge-Kutta forth order integration scheme with a grid size of Δx=0.01.

In the case of LANDSAT II MSS data, making use of the Takayama scene in the north side of Japan on May 23,1979, the test site of ten by ten pixels is fixed in the coastal area of Japan sea in the neighbourhood of Kanaza. At the local transite time $9^h 45^m$ the used parameters are θ=31°25' and ϕ=0°. On making use of the optical parameters as x=0.35, λ =1, in atmospheric model similar to Elterman's model, the mean effective surface albedo R=0.02 in band [illegible] the minimization of the performance function for the inversion of spectral radiance.

ii. Models of Atmosphere-Ocean System

In the present paper the atmosphere-ocean system is composed of the atmospheric and oceanic layers, whose optical parameters are assumed to be vertically inhomogeneous, in addition to the calm interacting surface of the sea.

Atmospheric Model

In addition to the absorption by molecules and aerosols, the scattering by molecules and aerosols are taken into account. The index of refraction of aerosols is denoted by 1.330, and its size distribution is assumed to be that of aerosols in coastal zone,i.e. the haze M model (cf. Deirmendjian 1969). The number density function is given by

$$n(r) = 5.3333\times10^4 r \exp[-8.9443r^{1/2}], \quad (3.14)$$

where r is the radius of a spherical particle. Once when the effective wave-length, the index of refraction, and the size distribution of aerosols have been given, the phase function and the albedo for single scattering are computed with the aid of Mie"s theory of aerosols. So far as the vertical distribution of the optical parameters is concerned, based on the Elterman model (cf.1968), we tried to make minor change of the optical thickness of the aerosols in lower layer than the altitude of three kilometers (cf.Haba et al.1978;Ueno et al. 1980; Kawata et al. 1981). The effective wave-length is assumed to be the mean value of each band 4,5,6, and 7 , and the albedo for single scattering is given by the ratio of the scattering coefficient

to the extinction coefficient. The phase function in transfer equation takes the form

$$P(t;\Omega;\Omega_0) = f_g P_g(t;\Omega,\Omega_0) + (1-f_g) P_g(t;\Omega,\Omega_0), \tag{3.15}$$

where P_g and P_a represent the phase function of molecular gas and aerosols, respectively, and f_g is the ration of the optical height by the molecules to that by the total components. The molecular phase function is given by Rayleigh phase function (cf. Chandrasekhar 1960). The optical parameters such as the wave-length (nm), altitude h(km), optical height t, albedo for single scattering , and the turbidity factor f_g in band 5 are listed in Table 1.

Oceanic Model

In the oceanic model, in a manner similar to the atmospheric case, the absorption and scattering by water molecules and hydrosols are taken into account (cf. Jerlov and Nielsen 1974; Tanaka and Nakajima 1977). The scattering phase function for ocean water is the sum of the molecular Rayleigh function and the scattering function by hydrosols,i.e., aquatic suspended solids. Because of the very sharp forward peak, the shape of the phase function for the medium may depend not only on the location but also on the time of measurements. Then, up to now many realistic oceanic models based on the measurements at different depths at different locations alistic oceanic models based on the measurements at different depths in different locations have been presented (cf. Jerlov and Nielsen 1974). Assuming an extension of the phase function in clear oceanic model to turbid model (cf. Gordon and Clark 1981), we computed the radiance in the oceanic medium in band 5.

iii. Effective Surface Albedo Mapping

On making use of Eq.(3.13), based on the simulation model of the atmosphere-Ocean system, we computed successively the effective albedo of the sea surface, which permitts us to estimate the ratio of the upward radiance just below the surface to the downward radiance just above the surface(cf.Eq.(2.16)). The above ratio depends on the concentration and type of hydrosols. On the other hand, it is observationally known that there may reasonably be the non-linear (or logarithmic) relation between the diffuse reflectance and the concentration of aquatic suspended sediment(cf. Maul and Gordon 1975;Munday and Alfoldi 1979;Aranuvachapun and Leblond 1981). On keeping in mind that the diffuse reflectance corresponds to the difference between the effective surface albedo and reflectance in air , the contour map of the sea surface albedo represents approximately the turbidity map. Then, in Figure 1 the contour map of digital counts (uncalibrated) in band 5 on May 23, 1979, (ID:21582-00450) near Kanazawa harbor is shown in low gain. Furthmore, based on the atmospheric and oceanic models appropriate to this case, after deblurring, the associated map of the sea surface albedo is illustrated in Figure 2. Based on the logarithmic model of the diffuse reflectance, the above associated map may be similar in form to the turbidity map. The reference area chosen in image is around 104X40 pixels in the plume, breakwater, and land. Whereas the comparison of Figures 1 and 2 presents the similar patterns of distribution, the map of the surface albedo may show more detailed features of the turbidity information, because of the degradation effect.

IV. SUMMARY

In the present paper, making use of an invariant imbedding and quasilinearization, we showed how to find an initial-value solution of the inverse transfer problem of radiation in atmosphere-ocean system with the interacting sea surface, and then performed the numerical simulation of the LANDSAT II MSS data. In other words , the removal of the degration of signals is analytically and numerically processed such that the surface albedo is estimated, in the least-squares sense, to provide an information of turbidity in the coastal subsurface waters. Whereas in Figure 1 the contour map of the digital counts in band 5 on May 23, 1979, near Kanazawa harbor is presented, however, the refinement of the mapping will be tried again in high gain. Furthermore, the associated map of the effective surface albedo will subsequently be presented, allowing for the sea-truth data concerning the diffuse reflectance and the concentration of suspended sediments. Finally, it is of interest to mention that our effective surface albedo will be more details discussed in connection with the non-linear model of diffuse reflectance.

APPENDIX

In a preceding paper (cf. Ueno [illegible]) a system of nonlinear integrodifferential equations governing the scattering and transmission functions in an inhomogeneous, isotropically scattering atmosphere bounded by a completely absorbing medium has been provided, allowing for the polarity of the diffuse radiation field. On extending the algorithm to the inhomogeneous and anisotropically scattering atmosphere, a system of Riccati-type of integrodifferential equations governing the scattering and transmission functions in atmospheric and oceanic layers takes the form

$$[illegible] \; T(x;\Omega,\Omega')P(x;-\Omega',\Omega'')X \; [illegible] \qquad (A.1)$$

$$[illegible] \qquad (A.2)$$

$$[illegible] \; P(y;\Omega,\Omega'')S(y;\Omega'',\Omega_0)\frac{d\Omega''}{v''} \; [illegible] \qquad (A.3)$$

together with the initial conditions

$$[illegible] \qquad (A.4)$$

$$[illegible] \qquad (A.5)$$

$$[illegible] \qquad (A.6)$$

In [illegible] the subscript x represents the differentiation with respect to x. The integrodifferential equation governing [illegible] is expressed by Eq.(A.[illegible]), whose argument [illegible] is replaced by x. Furthermore, the reciprocity principles for the scattering and transmission functions take the form

$$[illegible] \qquad (A.7)$$

$$[illegible] \qquad (A.8)$$

$$[illegible] \qquad (A.9)$$

REFERENCES

Ambarzumian, V.A.. 1944. On the problem of multiple scattering of light in a plane parallel medium with internal reflection at the bounding surface. Turdy Astron. Obs. Leningrad, Gos. Univ., Vol. 20.

Aranuvachapun, S., and P.H. Leblond. 1981. Turbidity of coastal water determinded from Landsat. Remote Sens. Environ. Vol. 10, pp.113-132.

Bellman, R.,and R. Kalaba. 1965. Quasilinearization and Non Linear Boundary Value Problems. American Elsevier Publ. Co.,Ltd.

Bellman, R., and S. Ueno. 1972. Invariant imbedding and Chandrasekhar's planetary problem of radiative transfer. Astrophys. Space Sci., Vol. 16, pp.241-248.

Casti, J.L., R. Kalaba, and S. Ueno. 1969. Reflection and transmission functions for finite isotropically scattering atmospheres with specular reflectors. J. Quant. Spectrosc. Radiat. transfer. Vol. 9, pp.537-552.

Chandrasekhar, S.. 1950. Radiative Transfer, Oxford University Press.

Cox, C., and W. Munk. 1954. Measurement of the roughness photographes of the sun's glitter. J. Opt. Soc. Am., Vol.44, pp.838-850.

Dechamps, P.Y., P. Lecomte, and M. Viollier. 1977. Remote sensing of ocean color and detection of chlorophyll content, in Proc. 11th Int. Symp. on Remote Sensing of Environment. April. 25-29, 1977, ERIM, Michigan, pp.1021-1033.

Deirmendijian, D. 1969. Electromagnetic Scattering on Spherical Polydispersions., American Elsevier, New York.

Duntley, S.Q.. 1963. Light in the Sea. J. Optical. Soc. Am. Vol.53, pp.214-233.

Elterman, L.. 1968. UV, visible and IR attenuation for altitude to 50 km, Rept. AFCRL-68-0153, Bedford, Mass..

Gordon, H.R., and D.K. Clark. 1981. Clear water radiances for atmospheric correction of coastal zone color scanner imagery. Appl. Opt. Vol. 20, pp.4175-4180.

Gower, J.F.R.. 1981. Oceanography from Space. Plenum Press, New York.

Gutshabash, S.D.. 1963. The diffusion of radiation in two medium with effects at the interface taken into account. Izv. Geophys. Ser., pp.1117-1124.

Haba, Y., Y. Kawata, T. Kusaka, and S. Ueno. 1979. The system of correcting remotely sensed Earth imagery for atmospheric effects. In Proc. 13th Int. Symp. on Remote Sensing of Environment, April 23-27, Ann Arbor, Michigan, pp.1583-1694.

Holyer, R.J.. 1978. Toward universal multispectral suspended sediment algorithms. Remote Sens. Environ. Vol. 7, pp.323-338.

Jain, S.C., and J.R. Miller. 1976. Subsurface water parameters: optimization approach to their determination from remotely sensed water color data. Appl. Opt., Vol. 15, pp.886-890.

Jerlov, N.G.. 1968. Optical Oceanography. Elsevier Publ. Co.,Ltd. Amsterdam, London and New York.

Jerlov, N.G., and E. Steemann Nielsen(Eds.). 1974. Optical Aspects of Oceanography. Academic Press, London and New York.

Kagiwada, H.. 1974. System Identification: Methods and Applications. Addison-Wesley Publ. Co., Inc., Reading, Mass..

Kagiwada, H., R. Kagiwada, and S. Ueno. 1975. Multiple Scattering Processes: Inverse and Direct. Addison-Wesley Publ. Co. Inc., Reading, Mass..

Kawata, Y., T. Kusaka, Y. Haba, and S. Ueno. 1981. A new approach to automatic identification of ground objects via the reflectance look-up tables, in Proc. 7th Int. Symp. on Machine Processing of Remotely Sensed Data, Purdue University, June 23-26, 1981, pp.331-335.

Matsumoto, M., and S. Ueno. 1976. Diffuse reflection and transmisson of radiation by finite atmospheres with specular reflectors. Astrophys. Space Sci., Vol. 43, pp.475-490.

Maul, G.A., and H.R. Gordon. 1975. On the use of the earth resources technology satellite(LANDSAT-I) in optical oceanography. Remote Sens. Environ, Vol. 4, pp.95-128.

Mukai, S., and S. Ueno. 1978. Apparent contrast of an atmosphere-ocean system with an oil polluted sea surface. App. Math. Modelling, Vol.2, pp.254-260.

Munday, J.C., and T.T. Alföldi. 1979. LANDSAT test of diffuse reflectance models for aquatic suspended solids measurement. Remote Sens. Environ. Vol. 8,pp.169-183.

Okami, N., M. Kishino, S. Sugihara, and S. Unoki. 1981. Measurements of spectral irradiance in Tokyo Bay. Techn. Rep. Phys. Oceanogr. Lab., The Inst. Phys. and Chem. Res. Tokyo, No.5, pp.1-75.

Plass, G.N., and G.W. Kattawar. 1969. Radiative transfer in an atmosphere-ocean system, Appl. Opt., Vol. 8, pp.455-466.

Plass, G.N.,G.W. Kattawar, and J.A. Guinn. 1977. Isophotes of sunlight glitter on a wind-ruffled sea, Appl. Opt.,Vol. 16, pp.643-653.

Raschke, E.. 1972. Multiple scattering calculation of the transfer of solar radiation in an atmosphere-ocean system. Beitr. Phys. Atmos., Vol. 45, pp.1-19.

Sobolev, V.V.. 1963. A Treatise on Radiative Transfer, Van Nostrand, Princeton, N. J..

Sobolev, V.V.. 1975. Light Scattering in Planetary Atmospheres. Pergamon Press, Oxford and New York.

Tanaka, M., and T. Nakajima. 1977. Effects of oceanic turbidity and index of refraction of hydrosols on the flux of solar radiation in the atmosphere-ocean system., J. Quant. Spectrosc. Radiat. Transfer, Vol. 18, pp.93-111.

Ueno, S.. 1960. The probabilistic method for problems of radiative transfer. X. Diffuse reflection and transmission in a finite inhomogeneous atmosphere. Astrophys. J., Vol. 132, pp.729-745.

Ueno, S.. 1980. Inversion of solar transmitted radiance profiles of the atmospheric optical thickness., Appl. Math. Comp., Vol. 17, pp.177-186.

Ueno, S.. 1981a. Parameter identification of multiple scattering systems via the quasilinearrization, in Proc. IFAC 8th Triennial World Congress, Aug.24-28,1981, Pergamon Press, VI pp.89-94.

Ueno, S.. 1981b. Retrieval of coastal water information from LANDSAT MSS data, in Proc. 7th Int. Symp. on Machine Processing of Remotely Sensed Data, Purdue University, June 23-26,1981, pp.703-709.

Ueno, S.. 1981c. Estimation of diffuse reflectance of surface water from remotely sensed MSS data, in Extended Abstracts of IAMAP, 3rd Scientific Assembly, Hamburg, Aug. 17-28, 1981, pp.64-68.

Ueno, S.. 1982. Remote sensing-research experience and problems., in Processes in Marine Remote Sensing(ed. by F.J. Vernberg, and F.P. Diemer). University of South Carolina Press, 1982, pp.451-510.

Ueno, S., Y. Haba, Y. Kawata, T. Kusaka, and Y. Terashita. 1978. The atmospheric blurring effect on remotely sensed Earth imagery: Inversion Methods and Application(Edit. by Fymat and Zuev), Elsevier Publ. Co. Inc., Amsterdam, pp.305-310.

Ueno, S., Y. Kawata, T. Kusaka, and Y. Haba. 1980. Ground albedo mapping from remotely sensed Earth's imagery data, in Proc. of 1980 IFAC Symp. on Water and Related Land Resource System, Pergamon Press, pp.165-172.

Ueno, S., and S. Mukai. 1973. Reduction of Chandrasekhar's planetary problem in the case of a specularly reflecting surface to the standard problem, J. Quant. Spectrosc. Radiat. Transfer, Vol. 13, pp.1261-1271.

Vernberg, F.J., and F.P. Diemer(Eds.). 1982. Processes in Marine Remote Sensing., University of South Carolina Press., Columbia, S. C.

Table 1. Optical parameters of Elterman's model atmosphere

Wavelength (nm)	Layers* (km)	Extinction optical thickness	Albedo for single scattering	f_g
	1.(0 - 1)	0.108	0.9998	0.0556
0.65	2.(1 - 3)	0.074	0.9991	0.1216
	3.(3 -50)	0.113	0.9909	0.3097

* Layer 1.,2., and 3. is lower, middle, and upper layer , respectively.

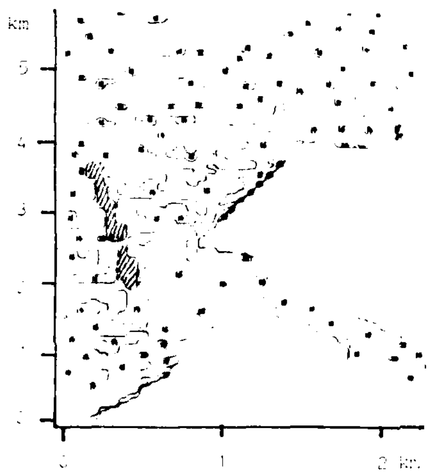

Figure 1. Map of LANDSAT II MSS data on May 23, 1979, in Band 5.

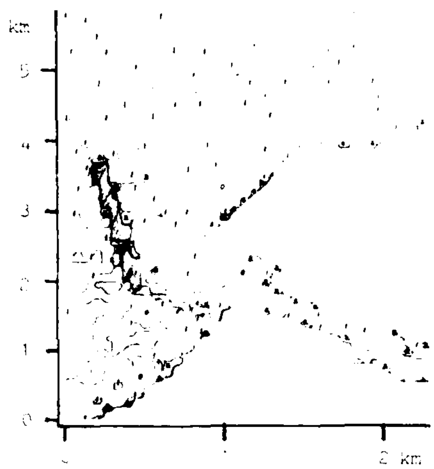

Figure 2. The associated map of the surface albedo in Band 5. The shaded area represents the breakwater appeared distinctly after the deblurring. The symbol 0,1,2, and 3 in the map denotes the effective surface albedo, 0.02,0.04,0.06, and 0.08, respectively.

LIMNOLOGICAL STUDY OF THE COASTAL LAGOON "COYUCA DE BENITEZ, GRO." DURING AN ANNUAL CYCLE (SUMMER 1981 - SPRING 1982).*

P. Ruiz Azuara, A. Ma. Pérez Zea and Ma. del P. Segarra Alberú

Laboratorio Interdisciplinario, Facultad de Ciencias, U.N.A.M.
04510, México, D.F., MEXICO

ABSTRACT

A limnological study of the Coastal Lagoon "Coyuca de Benítez, Guerrero" was initiated in August 1981. Seasonal variations of water net primary productivity during an annual cycle (Summer 1981 Spring 1982) were our principal interest. The main goal was to explore the real capabilities of the remote sensing techniques that are available in our country for this kind of studies. The program was composed of three principal parts: water truth sampling, later laboratory process (water samples and recorded films "in situ") and aerial images of the lagoon. Physical, chemical and biological parameters were seasonally measured for ten sample points previously selected. The main parameters were: air and water temperatures, pH, depth, Secchi disk transparency, superficial water velocity, water dissolved oxygen, water conductivity, hardness, total suspended solids, salinity, chlorophyll a and water net primary productivity. Zooplankton and fitoplankton samples are being studied. Normal and infrared color photographies were taken "in situ". Aerial B/W infrared photographies and multispectral images of the lagoon corresponding to summer and winter were also available. Correlations among measured parameters are shown. The results obtained from the images are also discussed. The annual limnological study indicated that the lagoon showed an oscillating dynamics with a destrophic tendency.

1. INTRODUCTION

The coastal lagoon "Coyuca de Benítez, Guerrero" is located at Long. 100 and Lat. N. 17 . It has an approximately area of 28.5 km (1). This zone corresponds to high primary productivity oceanic areas (2). However, the primary productivity in the lagoon had not been studied in a sistematic way (1,3,4,5,6) (Figure 1).

Seasonal variations of the water net primary productivity in the Coastal Lagoon "Coyuca de Benítez, Gro." during an annual cycle were obtained from summer 1981 to spring 1982.

*Presented at the Seventeenth International Symposium on Remote Sensing of Environment, Ann Arbor, Michigan, May 9-13, 1983.

2. METHODOLOGY

The general program included:

a) Ground-truth or water truth program (in situ sampling).
b) Laboratory analysis (chemical, spectrophotometric, etc.).
c) Normal and infrared color photography.
d) Images analysis (by photointerpretation and densitometry).
e) Aerial B/W infrared photography.
f) Multispectral analysis of aerial images in the visible and near infrared wavelenghts.

Ten sample points were previously chosen (Figure 2). For each sample point, normal and infrared color photographies were taken "in situ". Samples at three levels: superficial, 0.5 m and 1 m depth were taken for each season in the mentioned sample points. Aerial B/W infrared photographies and aerial multispectral images in the visible and near infrared wavelenghts (Scanner DS-1280) were taken by DETENAL for summer and winter seasons.

Water-truth program and later laboratory analysis let us estimate physical, chemical and biological parameters as: air and water temperatures, pH, conductivity, hardness, superficial water velocity, Secchi disk transparency, depth, dissolved oxygen, concentration of chlorophyll a, concentration of total suspended solids, salinity and water net primary productivity. Zooplankton and fitoplankton samples are being studied.

The main laboratory techniques that had been used are: chemical analysis, spectrophotometry U.V. and Visible, densitometry and optical microscopy.

Correlations between the water truth data and the available remote sensor data are discussed.

3. RESULTS

The dynamics of the Coastal Lagoon "Coyuca de Benítez, Guerrero" corresponding to the annual cycle (Sammer 1981 - Spring 1982) was studied from August 1981 to May 1982.

Seasonal mean values corresponding to water temperature (T), pH, Secchi disk transparency (S.D.T.), chlorophyll a (Cl. a) and water primary productivity (N.P.P.) are shown in Table 1.

Table 1. Seasonal Mean Values.

	$[T]_{d,s.p.}$	$[pH]_{d,s.p.}$	$[S.D.T]_{s.p.}$	$[Cl.\ a]_{d,s.p.}$	$[N.P.P]_{d,s.p.}$
SUMMER	31.83	7.99	28.75	3.79	0.68
AUTUMN	29.33	7.2	38.75	3.02	2.49
WINTER	30.1	7.33	36.3	4.05	1.45
SPRING	31.39	7.8	41.0	5.04	1.77

Units: T(C), S.D.T. (cm), Cl. a (mg/l) and N.P.P. (mg/l).
Key: [ ], mean; d, depth (superficial, .5 m, 1 m); s.p., sample points (1-10).

Chlorophyll a values were obtained using membrane filters (7) and later spectrophotometric determination (8, 9). Water net primary productivity was calculated using Gaarder and Gran's method (9) and Winkler's technique (10, 11).

Seasonal mean values for Secchi disk transparency showed small variations: 29 to 41 cm. This values are presented versus concentration of suspended solids and salinity in figures 3 and 4.

The limnological results for the full cycle exhibited an oscillating dynamics, with a dystrophic tendency, for the Coastal Lagoon "Coyuca de Benítez, Gro." due to the contribution of sweet-water from the main tributaries: the Coyuca river and the De Las Cruces rivulet (Figure 2), and the sea water contribution when the sand bar is opened (Figure 5). An inverse relationship between chlorophyll a and Secchi disk transparency was suggested (as Brezonik (12) reported) (Figure 6). Summer, autumn and winter mean chlorophyll a data showed an inverse correlation with concentration of suspended solids (Figure 8) and salinity (Figure 9). Water net primary productivity showed a similar behaviour that chlorophyll a with c.s.s. and salinity (Figures 10 and 11). However, as the lagoon is very homogeneous this correlation can just be suggested. In general terms, we observed that the water net primary productivity showed a similar behaviour to chlorophyll a with the estimated variables (Figures 7, 10 and 11).

The remote sensing data for summer (Figures 2 and 12) were useful to show superficial currents. The corresponding data for winter (Figure 1) reported an homogeneous water body. The same result was found by photointerpretation of the photographies "in situ".

The chlorophyll a has an absorption peak at .665 microns. The channel 2 of the Scanner DS 1284 includes this region. Then, we decided to explore the possible use of the multispectral images containing these channel data. The atmospheric absorption has to be considered.

The available summer multispectral images (Figures 13 and 14), containing data from channels 2 and 3, covered only two of our sample points: 4 and 9. For these, we observed less reflectance in channel 2 where the concentration of chlorophyll a was larger (Table II).

These preliminary results with the multispectral images suggested the general capabilities of the remote sensing techniques for this kind of studies (as Klemas et al. (13) discussed) but we need complete images of the lagoon before to stablish any correlation. We are looking for that data now.

This limnological studies may be applied, within an ecological context, to the rational use of the natural resource considered. To avoid the dystrophication of the water body we recomend the introduction of different fish species at specific periods.

4. ACKNOWLEDGMENTS

We would like to thank the following for their cooperation: Departamento de Pesca de Coyuca de Benitez by the facilities during the sampling; E. Schroeder and A. Lozano from the Laboratorio de Quimica del Institute de Geologia de la UNAM for the chemical analysis of summer, autumn and winter samples, Direccion General de Geografia del Territorio Nacional de la Secretaria de Programacion y Presupuesto (DETENAL) for the aerial images, Division de Estudios Superiores de la Facultad de Ciencias Quimicas de la UNAM by let us use the UV Visible Spectrophotometer and to our colleagues R. Llanos (Chlorophyll a and sampling), Ma. del R. Aguilar and Dr. L. Segura (summer zooplankton composition), G. Carvallo, E. Uribe, O. Perez and R. Aguirre (sampling) and G. Vidargas (computer graphics).

5. REFERENCES

1. Stuardo J., Martínez A., Yañez L.A., Prospección de recursos biológicos y pesqueros del sistema lagunar de Guerrero y en parte del litoral rocoso de Michoacán. An. Centro de Ciencias del Mar y Limnología, UNAM, 1974.

2. Margalef R. and Estrada M., Las áreas oceánicas más productivas, investigación y Ciencia, 49, 8-20, Octubre, 1980.

3. Ramírez R., Estudio ecológico preliminar de las lagunas costeras cercanas a Acapulco, Guerrero, Rev. Soc. Mex. Hist. Nat. 13, 199-218, 1952.

4. Cárdenas M., Pesquerías de las lagunas litorales de México, Mem. Symp. Intern. Lagunas Costeras (A. Ayala, ed.) UNAM-UNESCO, 1969.

5. Stuardo J. y Villarroel M., Aspectos ecológicos y distribución de moluscos en las lagunas costeras de Guerrero, México. An. Centro de Ciencias del Mar y Limnología, 3(1), 65-92, UNAM, 1976.

6. Several Authors, Ciencia y Desarrollo, Marzo-Abril, núm 3 año VIII, CONACYT, 1982.

7. Clark J.W. and William L.S., Method of concentrating Phytoplankton samples using membrane filters. Limnology and Oceanography, 8, 127-129, 1963.

8. Strickland J.D.M. and Parsons T.R., Practical handbook of seawater analysis Fish. Res. Board of Canada, 1977.

9. Lieth H. and Whittaker R.H., Primary Productivity of the Biosphere, Ed. Springer Verlag, New York, 1975.

10. APHA, AWWA, WPCF, Standart Methods for the examination of water and waste water, Fourteenth Ed., 1976.

11. Wetzel R.G. and Likens G.E., Limnological Analysis, Saunders, 1979.

12. Brezonik P.L., Effect of organic color and turbidity on Secchi disk transparency. J. Fish. Res. Board Can. 35, 1410-1416, 1978.

13. Klemas V., Bartlett D.S., Philpot W.D., Remote Sensing of marine fisheries resources in: *Advanced Concepts in Ocean Measurements for Marine Biology* (F.P. Diemer, F.S. Vernberg and D.Z. Mirkes, eds.) Univ. of South Carolina Press, Columbia, 1980.

6. FIGURES

Figure 1. Coastal Lagoon "Coyuca de Benitez, Guerrero".

Aerial B/W infrared photography corresponding to winter. The water body appears homogeneous (3 months after that the sand bar was closed). The same result was obtained by photointerpretation and densitometric analysis of the photographies "in situ". These results are consistent with all the other data, including the multispectral images.

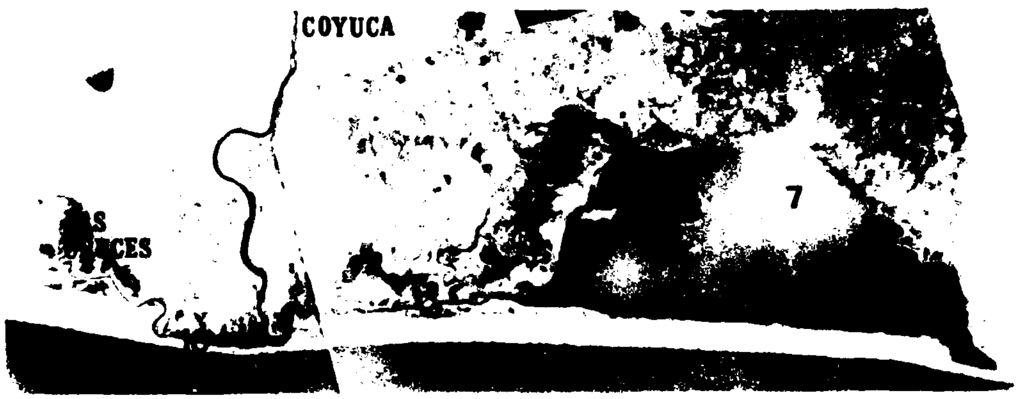

Figure 2. Sample Points.

Aerial B/W infrared photography corresponding to summer. The approximate depth of points 3, 7, 8 and 9 is 9 m; the mean depth of the other six points is 2.26 m. Points 5 and 10 are not lagoon points. They are in the Coyuca River with point 5 corresponding to the sand bar (opened in summer). Point 4 is in the mouth of river. Point 1 is in front of an inhabited place and point 8 is between two currents, one coming from the sea and the other from a small tributary.

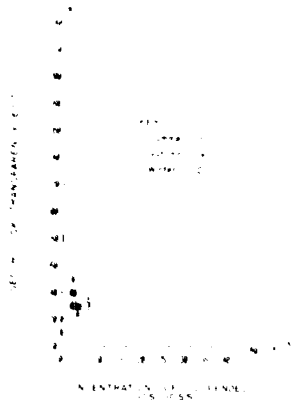

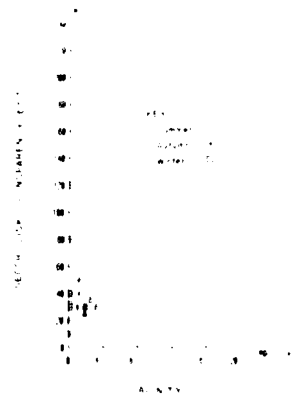

Figure 2. Secchi Disk Transparency vs. concentration of suspended solids (...).

Figure 3. Secchi Disk Transparency vs. salinity (i.e. chlorine concentration).

As the lagoon is very homogeneous most of the points are in a small area being this a great difficulty to suggest any relationship. Autumn and winter data are from superficial and 1 m. depth samples, summer are only superficial.

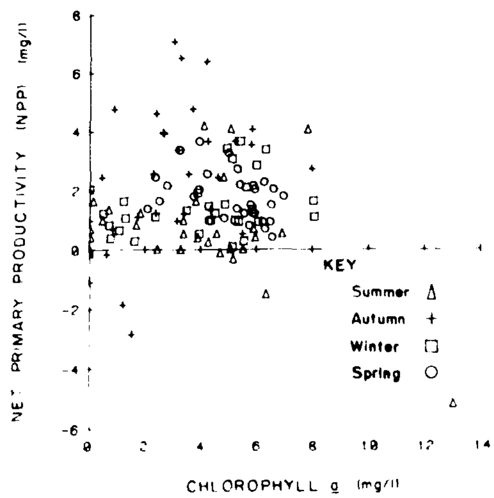

Figure 4. Net Primary Productivity vs. Chlorophyll a.

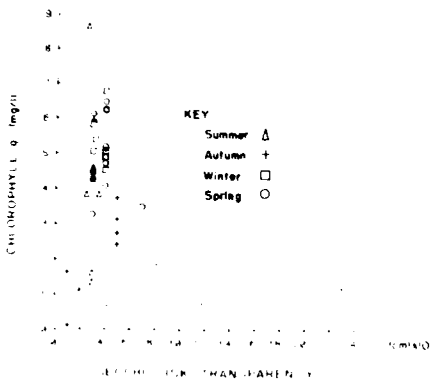

Figure 6. Chlorophyll a vs. Secchi Disk Transparency.

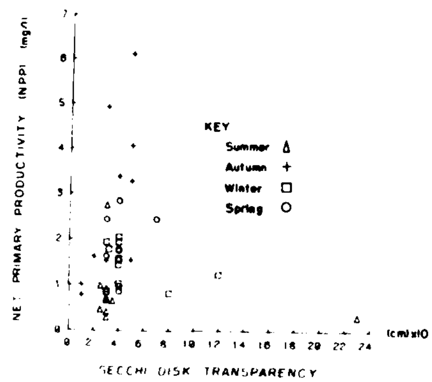

Figure 7. Net Primary Productivity vs. Secchi Disk Transparency.

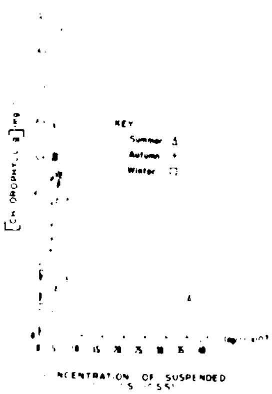

Figure 8. Mean Chlorophyll a vs. Concentration of Suspended Solids (CSS).

Figure 9. Mean Chlorophyll a vs. Salinity.

*The mean values were calculated for 3 depths (superficial, 0.5 m and 1 m).

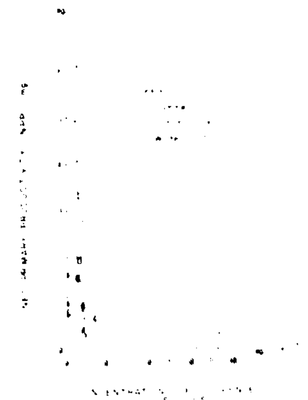

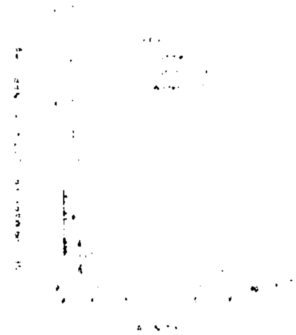

[illegible] Net [illegible]

[illegible] Net Primary Productivity [illegible] Salinity.

[illegible] depth values [illegible] calculated [illegible] have the [illegible] behavior [illegible]

Figure 12. Currents detected by Aerial [illegible] Infrared Photography

This picture shows the capacity of this type of photography for detecting superficial currents. The current marked with number 1 is similar to class "b" (Figure 15) detected by the scanner. These currents were verified in the water truth program.


a
b
9
c
4"

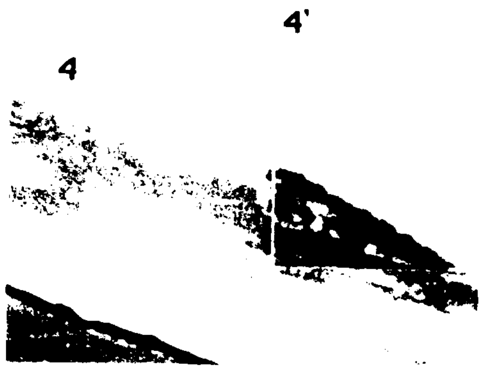

Figure 11. Sample points 4 and 9.

The only available remote sensor data correspond to points 4 and 9 for summer. Then, for these points the next table summarized both water truth and remote data. The reflectances for class 1* are ρ_2 73.75 and ρ_3 30.10.

Table 11. Data for sample points 4 and 9.

SAMPLE POINT	S (‰)	pH	N.P.P. (mg/l)	Cl. a (mg/l)	S.S.S. (mg/l)	S.D.T. (cm)	DEPTH (cm)	ρ_2	ρ_3
4 s	31.8	6.2	0.82	1.67	6371	30	150	73.83	28.97
m	31	6.8	1.31	0.68					
d	30.5	7.8	0.00	2.11					
9 s	35	8.7	0.00	3.20	8750	30	1250	[illegible].91	29.12
m	[illegible]	[illegible]	0.69	3.87					
d	35	8.8	0.33	1.[illegible]					

KEY: ρ_2, ρ_3 Reflectances in bands 2 and 3 respectively; s superficial, m=0.5 m. and d 1 m. sampling respectively.

AD P002023

CULTURAL AND ENVIRONMENTAL EFFECTS ON CROP SPECTRAL DEVELOPMENT PATTERNS AS VIEWED BY LANDSAT*+

E. P. Crist

Environmental Research Institute of Michigan
Ann Arbor, Michigan 48107

ABSTRACT

The typical patterns of spectral development (profiles) for corn and soybeans are presented, based on field-collected reflectance data transformed to correspond to Landsat-MSS Tasseled Cap coordinates. Reasonable variations in field conditions and cultural practices are shown to significantly influence profile features. The separability of the two crops is determined to be primarily related to the maximum value of the reflectance equivalent of Greenness, and to the plateau effect seen in corn Greenness profiles. The impact of changes in conditions on separability is described. In addition, association is made between profile features and stages of development for corn and soybeans. Corn is shown to peak at a stage well before tasseling or maximum LAI, while the characteristics of the soybean profile are shown to be unrelated to any particular stage of development.

1. INTRODUCTION

Central to the successful use of remotely sensed data for agricultural inventories is the ability of human analysts or computer algorithms to detect differences in the spectral characteristics of various cover classes. Experience with Landsat data in the Large Area Crop Inventory Experiment (LACIE) and other studies has demonstrated that the use of multitemporal, spatially-registered data greatly enhances the ability to distinguish between various crop spectral patterns [1]. In recent years interest has been renewed in utilizing characterizations of the continuous patterns of crop spectral development over time, termed "profiles", in automatic crop identification techniques [2,3,4]. These and other automated approaches offer substantial gains in efficiency over manual techniques, and would therefore be of great value if their accuracies were similar to or better than those associated with human analysts.

One substantial cause of error in both automatic and manual crop labeling techniques is the deviation of a crop from its expected spectral pattern due to cultural or environmental influences (e.g., fertilization, moisture stress, changes in planting practices, etc.). This spectral deviation is the result

*This work was sponsored under Contracts NAS9-15476 and NAS9-16538 by the U.S. National Aeronautics and Space Administration, NASA Johnson Space Center, Houston, Texas 77058.

+Presented at the Seventeenth International Symposium on Remote Sensing of Environment, Ann Arbor, Michigan, May 9-13, 1983

both of physiological changes in the plants themselves, resulting in changes in the spectral properties of the plant parts, and of changes in the canopy geometry, including the orientation of plant parts, number and size of leaves or other plant parts, and amount of soil visible through the canopy. Particularly for computer algorithms, which lack the flexibility and adaptive capabilities of the human mind, it is essential that major external influences on crop spectral patterns be known in advance and taken into account, if the algorithms are to perform adequately over broad regions or many growing seasons.

This paper presents the results of research aimed at characterizing and understanding the spectral development patterns of corn and soybeans, using field-collected reflectance data. Average profiles are described, as are the changes in those profiles brought about by changes in some major cultural and environmental factors. In addition, the association of profile features with stages of development of the two crops is discussed. Finally, the separability of corn and soybeans, both in a general sense and in the context of particular field conditions, is considered.

2. DESCRIPTION OF DATA

Evaluation of crop spectral characteristics can best be accomplished with data collected at frequent intervals over plots whose conditions are controlled or known. Such data have been collected for several years by and at Purdue/LARS as part of a field research program carried out for NASA. For the analyses reported in this paper, data were selected from experiments carried out in the 1978 through 1980 growing seasons, which included as experimental treatments nitrogen fertilization, planting date, and plant population for corn, and variety, planting date, and row spacing for soybeans [5,6,7]. Reflectance measurements were made on clear days, resulting in gaps between successive observations of several days to weeks. All reflectance data were collected as or converted to Landsat-MSS inband reflectance values, and multiple observations of a single plot on a single day were represented by their mean.

A reflectance equivalent of the Tasseled Cap transformation [8] was used to provide spectral variables that were physically-interpretable. This transformation, in its Landsat-MSS form, captures 95% or more of the total data variability over agricultural areas in two variables. A rotation of the first two principle components in the reflectance data set was used to derive reflectance equivalents of the two variables [9], termed Green Reflectance and Bright Reflectance. These two variables contained 99% of the total variability in this data set. Green Reflectance serves as a green vegetation indicator, while Bright Reflectance is related to soil brightness or plot albedo.

The total data set consisted of observations from 118 corn plots and 171 soybean plots. However, some plots were not suitable for all analyses, so the actual number used in any particular evaluation varied.

3. PROFILE ANALYSIS TECHNIQUE

Although the field reflectance data set provided more frequent observations and more detailed agronomic information than would be available using Landsat data, the problems of temporal gaps in spectral measurements and inexplicable data variations were still apparent. As a result, it was necessary to devise a technique by which profile values could be interpolated between actual measurements, and some smoothing of the measured values could be achieved. One approach to accomplishing these objectives is use of a mathematical model to describe the spectral development patterns [2]. Such models have been developed for and successfully applied to spring small grains [10,11]. However, the plateau feature commonly observed in corn Greenness and Green Reflectance data (Figure 1) cannot be adequately described by previously developed profile models [9], so some other approach - either a new model or a more general technique - was required.

Two techniques were selected for profile characterization. For analysis of soybeans, which exhibit a less complex profile shape in Green Reflectance, and for some analyses of corn, a cubic smoothing spline [12] was used. This method provided the desired degree of smoothing, and captured the plateau feature given that sufficient data points were present in that portion of the profile. However, when significant data gaps existed in critical periods, the cubic smoothing spline result for corn was less acceptable. Accordingly, a profile model form, developed at ERIM specifically for this purpose [9], was used on the corn data when the plateau feature was of prime interest.

For Bright Reflectance data, early season variations caused by soil moisture differences and other unknown factors rendered automatic curve-fitting impractical. Therefore, Bright reflectance profiles were derived for each plot manually, based on the available data points and soil moisture information. Since planting dates were known, a "days since planting" time axis was used in describing and comparing both Green Reflectance and Bright Reflectance profiles.

In order to facilitate comparison of profiles, a set of features was defined which described their major characteristics. These features (illustrated in Figure 2) included the peak profile value (PMAX), the time at which the peak occurred (PT), the times of occurrence of one-half the peak value (HP1 and HP2), and the time intervals between HP1 and PT (SPAN1), PT and HP2 (SPAN2), and HP1 and HP2 (SPAN3). In Green Reflectance, these features are related to the maximum amount of green vegetation (PMAX), the rate of vegetative development (PT,HP1,SPAN1), the rate of senescence (SPAN2), and the overall development rate (HP2 and SPAN3). For corn, two additional features were used to describe the duration and slope of the plateau.

Features of Green Reflectance profiles were derived explicitly, and analyzed quantitatively by analyses of variance. For Bright Reflectance, the features were derived implicitly by visual analysis of the profiles, and compared qualitatively.

4. NORMAL PROFILES

Figures 3 through 6 illustrate the average profiles of corn and soybeans, using the corn profile model results for 57 corn plots and the cubic smoothing spline results for 167 soybean plots. The dashed lines around the Green Reflectance profiles represent one standard deviation about the mean. The asymmetry of the soybean variability about the mean, most noticeable in the declining phase of the profile, is largely the result of differences in timing of leaf senescence between maturity classes.

The Bright Reflectance profiles, illustrated with a dark and light soil background, are delimited by dashed lines representing the range of mean profiles (by treatment) used to derive the overall average profiles. It should be noted that for corn, the very bright soil completely obscures the peak in the Bright Reflectance profile seen with darker soils. For both corn and soybeans, soil effects were undetectable in the latter portions of the profiles.

Figures 7 and 8 present the spectral trajectories of the two crops in Green Reflectance and Bright Reflectance, using the dark soil Bright Reflectance profiles. The plateau in corn Green Reflectance, when combined with the Bright Reflectance profile, is expressed as a movement away from and then back to the "Green Arm" of the Tasseled Cap.

5. CULTURAL AND ENVIRONMENTAL EFFECTS ON PROFILE FEATURES

This section summarizes the results of both a literature review of the effects of environmental factors on corn and soybean characteristics and the profile features analyses. Reference [9] contains a more detailed description

of many of the results. For Green Reflectance profiles, results reported are those found to be significant to the 0.9 level of confidence.

5.1 CORN EFFECTS

Nitrogen Fertilization. The availability of nitrogen, which is required for synthesis of chlorophyll, influences the vegetative development of corn. Abundant nitrogen results in more and larger leaves, longer vegetative stages, and increased longevity of green leaf area. These effects were expressed in a later and higher peak Green Reflectance value and a longer and flatter plateau. While the quality of Bright Reflectance data for these experiments was low, some indication of a higher peak Bright Reflectance value was observed.

Planting Date. Later planted corn experiences higher temperatures at any given stage of development than does earlier-planted corn. As a result, the rates of plant emergence and development are increased, as are the rates of leaf emergence and leaf area development. Very early planting exposes the plants to lower temperatures, and would thus be expected to delay emergence and retard early growth.

Both late and very early planting reduced the peak Green Reflectance profile value, probably an indication of the less conducive growing conditions encountered. Both also reduced the overall development time (HP2). Late planting, in addition, hastened the rate of green-up, the time of peak, and the rate of green decline. Late planting similarly hastened the time of occurrence and reduced the value of the Bright Reflectance profile peak.

Plant Population. Increases in corn plant population density cause reduced rates of leaf area production, faster early height increase, greater maximum leaf area index, and faster decline in LAI after peak. These effects were expressed in an earlier and higher peak Green Reflectance value, a faster rate of green-up, and a steeper plateau slope. In Bright Reflectance, a higher peak value was observed, and the elimination of soil effects occurred earlier, indicating earlier canopy closure.

5.2 SOYBEAN EFFECTS

Variety. Soybean varieties exhibit differences in days to maturity (maturity class), plant height, leaf size, number, and orientation, rate of accumulation and maximum leaf area, ability to achieve full closure, response to row spacing or planting delays, etc. Not surprisingly, all the profile features were significantly affected by varietal differences at some row spacing.

Planting Date. Both early and late planting tend to cause reductions in the final height of soybean plants, and to reduce the rate of canopy closure. The higher temperatures associated with later planting hasten emergence and early growth, and reduce the duration of the vegetative phase.

The peak Green Reflectance value was reduced with both early and late planting, and was substantially earlier for late planting. In addition, late-planted soybeans had a faster rate of green-up and a shorter overall development time. Similarly, late-planted soybeans exhibited an earlier peak Bright Reflectance value and a more rapid increase in Bright Reflectance, as well as a reduced overall profile span.

Row Spacing. Soybean varieties differ in their response to row spacing. In general, however, wider rows tend to cause a reduction in the rate of leaf area accumulation and a delay in achievement of full canopy closure. These effects were expressed in lower and later peak Green Reflectance values and a slower rate of green-up. Also observed was a more rapid green decline after peak, probably an indication of the lower leaf area density, which allowed brown lower leaves or soil to show through the canopy sooner after the peak.

6. ASSOCIATION OF SPECTRAL AND DEVELOPMENTAL EVENTS

Another aspect of understanding crop profiles is knowing the stages of development associated with some of the key profile features. Such knowledge allows development of crop identification techniques which utilize the most fundamental and therefore most stable differences between crops, and could aid the assessment of crop condition or prediction of yield by providing a means of pinpointing certain key developmental events from spectral data.

In order to carry out this analysis, development stage data collected for the experimental plots were smoothed and interpolated by polynomial regression. The time of occurrence of each stage, or the stage at any particular time, could then be easily determined. Figure 9 illustrates the result of combining the development stage data with the Green Reflectance data for a typical corn plot.

6.1 CORN RESULTS

Stages of development defined by Hanway [13] were used for corn. Peak Green Reflectance was found to occur at Stages 2.5 to 3.0, which correspond to 10 to 12 leaves fully emerged. These stages occur about two weeks prior to tassel emergence, and three weeks before the stage normally associated with peak LAI (Stage 5 - silking). Although this result seems to contradict the normally expected correlation between vegetation indices and LAI or percent cover, a plausible, if hypothetical, explanation can be given.

At Stage 2.5 to 3.0, all or nearly all of the green leaf area is developed, but much of it is still furled into a pseudostem. Because the stem itself is only about half as tall as the total corn plant at this point, there is a dense and fairly shallow layer of pure green leaf matter at the top of the canopy, which contains all the green leaf matter that the plant will have. Development after this point, including continued stem elongation, changes in leaf angular orientation, and emergence of tassels, serves to reduce Green Reflectance by increasing shadowing or changing the mix and distribution of plant parts in the canopy.

The plateau in corn Green Reflectance ended around Stage 8, the early dent stage. This stage falls about one month after initiation of rapid dry matter accumulation in the kernels, which would correspond to an accelerated rate of senescence in the vegetative parts. Since one would expect a time lag between senescence, which proceeds from the bottom of the plant to the top, and any noticeable effect on the Green Reflectance of the canopy, the observed delay is not surprising.

6.2 SOYBEAN RESULTS

The stages of soybean development defined by Fehr and Caviness [14] were used. Since many varieties of soybeans are indeterminate, the Fehr/Caviness system provides separate vegetative and reproductive stage progressions.

Peak Green Reflectance occurred between vegetative stages 12 and 21 (12 to 21 nodes with fully emerged leaves), or reproductive stages 3.5 to 6 (beginning pod to full seed). The extremes of these stage ranges normally occur about 30 days apart, suggesting that there is little if any correlation between peak Green Reflectance and any particular soybean stage of development.

In some of the plots, peak Green Reflectance did coincide with the maximum vegetative stage reached, but in many others, the Green Reflectance peak occurred at a vegetative stage well before the maximum. In most of these cases, however, lodging was reported at the time of maximum vegetative development, and at all observation times after the peak. While the severity of lodging was not recorded, one can speculate that it was enough to reduce the Green

Reflectance of the canopy by exposing more stems and changing the overall geometry.

It would appear, then, that maximum Green Reflectance in soybeans occurs at the end of vegetative development except when lodging occurs. When lodging was a factor in these data, the end of vegetative development sometimes occurred at a point well down the declining side of the Green Reflectance profile. Thus it must be concluded that Green Reflectance profile features can give little or no reliable information as to the stages of soybean vegetative or reproductive development.

7. SEPARABILITY OF CORN AND SOYBEANS

Based on the profile-derived features for the entire set of experimental plots, an analysis of the separability of corn and soybeans profiles was carried out. Both the corn model and cubic smoothing spline were used to characterize corn Green Reflectance profiles, the model because it more accurately describes the actual spectral development pattern, and the spline because it more closely resembles the kind of approach that might be used in an operational setting where the crop type of a sample was not known. Each feature was histogrammed, and the histograms were compared to determine separability. Evaluation of Bright Reflectance profile separability was carried out qualitatively.

7.1 OVERALL RESULT

Using the corn model, the peak Green Reflectance profile value (PMAX), the time of occurrence of that peak (PT), the rate of vegetative development after emergence (SPAN1), and the rate of Green Reflectance decline after the peak (SPAN2) all provided substantial separability. Corn tended to reach a lower peak value earlier, had a more rapid relative green-up rate, and declined in Green Reflectance much more slowly than soybeans. The separability related to green decline was the result of the corn Green Reflectance plateau.

When the cubic smoothing spline was used for both crops, substantial separability was still found in the height of the Green Reflectance profile peak (PMAX), with reasonably good separation also in the rate of Green Reflectance decline (SPAN2). Most notably, in this data set 100% separability was achieved using the peak Green Reflectance profile value and the rate of Green Reflectance profile decline (Figure 10). While the peak value, or something similar to it, is a feature used in several current corn/soybean discrimination techniques [15], the plateau feature is little used at this time. However, apparent rates of green-up and decline, as derived by simpler profile models, are used in current techniques [16], and the separability found in these features is probably an indirect result of the corn plateau.

Early season features such as the rate of early vegetative development (HP1) provided little or no separability, particularly with the spline technique. In addition, comparison of the slopes of the ascending portions of the average corn and soybean profiles revealed little or no difference between the two crops in this respect. Planting date differences, ignored in this analysis, may provide a greater potential for separation, depending on local crop calendars, but there is little indication of purely spectral separability in the early season.

In Bright Reflectance the only obvious source of separability was, again, the height of the profile peak. As can be seen by comparing Figures 7 and 8, this is an expression of the same phenomenon expressed in the Green Reflectance profile peak height - Soybeans move farther up the "Green Arm" of the Tasseled Cap than does corn. This feature too has been used in crop identification techniques [17].

7.2 EFFECTS OF CHANGES IN FIELD CONDITIONS

Comparison of the results in Sections 5 and 7.1 reveal that many of the environmental and cultural factors considered affect precisely those features most important in corn and soybean discrimination. Both nitrogen fertilization and increased planting density tend to raise the peak Green Reflectance value of corn, while early or late planting and wider row spacing tend to lower the peak soybean Green Reflectance value. Similarly, nitrogen deficiency and late planting tend to shorten or soften the plateau effect in corn. Under particular sets of conditions, then, one should expect a degradation in the separability of corn and soybeans.

8. CONCLUSIONS

Comparison of the curves fit to each plot in the set of corn and soybeans transformed field reflectance data indicates that there are indeed characteristic profile shapes for these two crops, shapes which show some variation but which nonetheless retain characteristic attributes. At least some of the variation is caused by changes in field conditions and cultural practices, and it has been shown that variations in these factors within a range that could be reasonably expected in an operational setting cause significant changes in profile features. Furthermore, while corn and soybeans are distinguishable based on their profile features, the effects of changes in conditions or practices are such that separability could, under particular sets of circumstances, be substantially degraded.

The evaluation of development stage association with profile features shows a clear relationship between corn Green Reflectance features and stages of development, and further shows that the peak in corn Green Reflectance occurs earlier than would have been expected, before either maximum LAI or maximum canopy closure. Conversely, soybean Green Reflectance features cannot be associated with any particular stage of development. In the absence of lodging, a strong correlation can be seen between peak soybean Green Reflectance and maximum vegetative development.

The profiles described in this report, and the changes in those profiles attributable to field conditions and cultural practices, provide a foundation for development of an automatic crop identification technique using Landsat data. These analyses indicate that the inference of field conditions from profile characteristics alone is not likely to be successful, since the same type of change in profile characteristics can be caused by a number of different factors. However, if, using meteorological or other available information, such inference could be made for a particular region of interest, expectations regarding corn and soybean profile shapes could be modified based on the presented results, an approach which could yield a substantial increase in labeling accuracy. A technique adaptable in such a manner, and therefore applicable over wide regions and many years, would be of considerable value.

REFERENCES

1. Hay, C.M. 1979. Manual interpretation of Landsat data. Proceedings of the Technical Sessions, Vol. I, The LACIE Symposium. NASA Johnson Space Center, Houston, Texas.

2. Crist, E.P. and W.A. Malila. 1980. A temporal-spectral analysis technique for vegetation applications of Landsat. Proceedings of Fourteenth International Symposium on Remote Sensing of Environment. San Jose, Costa Rica.

3. Crist, E.P. and W.A. Malila. 1981. A technique for automatic labeling of Landsat agricultural scene elements by analysis of temporal-spectral patterns. Proceedings of Fifteenth International Symposium on Remote Sensing of Environment, Ann Arbor, Michigan.

4. Badhwar, G.D. 1979. A semi-automatic technique for multitemporal classification of a given crop. AgRISTARS Report SR-J0-00481, NASA Johnson Space Center, Houston, Texas.

5. Bauer, M.E., M.H. Hixson, L.L. Biehl, C.S.T. Daughtry, B.F. Robinson, and E.R. Stoner. 1978. Agricultural scene understanding. LARS Report 112578. Laboratory for Applications of Remote Sensing, Purdue University, West Lafayette, Indiana.

6. Bauer, M.E., L.L. Biehl, C.S.T. Daughtry, B.F. Robinson, and E.R. Stoner. 1979. Agricultural scene understanding and supporting field research. NASA Report SR-P9-00410. Laboratory for Applications of Remote Sensing, Purdue University, West Lafayette, Indiana.

7. Bauer, M.E., L.L. Biehl, and B.F. Robinson. 1980. Field research on the spectral properties of crops and soils. NASA Report SR-P0-04022. Laboratory for Applications of Remote Sensing, Purdue University, West Lafayette, Indiana.

8. Kauth, R.J. and G.S. Thomas. 1976. The Tasseled-Cap -- a graphic description of the spectral-temporal development of agricultural crops as seen by Landsat. Proceedings of the Symposium on Machine Processing of Remotely Sensed Data. Purdue University, West Lafayette, Indiana.

9. Crist, E.P. 1982. Cultural and environmental effects on the spectral development patterns of corn and soybeans - field data analysis. NASA Report SR-E2-04224. Environmental Research Institute of Michigan, Ann Arbor, Mich.

10. Badhwar, G.D. 1980. Crop emergence date determination from spectral data. Photogrammetric Engineering and Remote Sensing. 46:369-377.

11. Cicone, R.C., E. Crist, R. Kauth, P. Lambeck, W. Malila, and W. Richardson. 1979. Development of Procedure M for multicrop inventory, with tests of a spring wheat configuration. Final Report 132400-16-F, Environmental Research Institute of Michigan, Ann Arbor, Michigan.

12. DeBour, C. 1978. A practical guide to splines. Springer-Verlag, New York.

13. Hanway, J.J. 1963. Growth stages of corn (*Zea Mays, L.*). Agronomy Journal 55:487-492.

14. Fehr, W.R. and C.E. Caviness. 1977. Stages of soybean development. Special Report 80. Iowa State University, Cooperative Extension Service, Ames, Iowa.

15. Metzler, M., R. Cate, and J. Odenweller. 1982. Automatic crop inventory in Argentina with multitemporal Landsat data. Proceedings of Sixteenth International Symposium on Remote Sensing of Environment, Buenos Aires, Argentina.

16. Badhwar, G.D., J.G. Carnes, and W.W. Austin. 1982. Use of Landsat-derived temporal profiles for corn-soybean feature extraction and classification. Remote Sensing of Environment 12:57-79.

17. Roller, N., K. Johnson, J. Odenweller, and C. Hay. 1981. Analyst handbook for the augmented U.S. baseline corn and soybean segment classification procedure (C/S-1A). NASA Report FC-E1-00723. Environmental Research Institute of Michigan, Ann Arbor, Michigan and University of California at Berkeley, Berkeley, California.

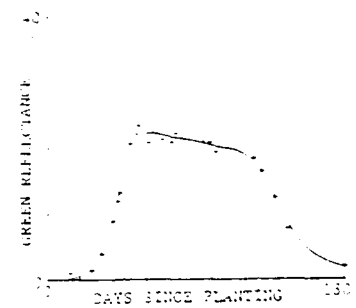

Figure 1. Plateau in Corn Green Reflectance Profile

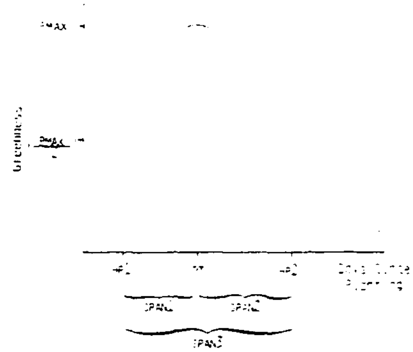

Figure 2. Green Reflectance Profile Features

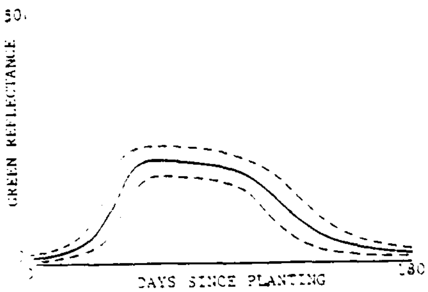

Figure 3. Average Corn Green Reflectance Profile

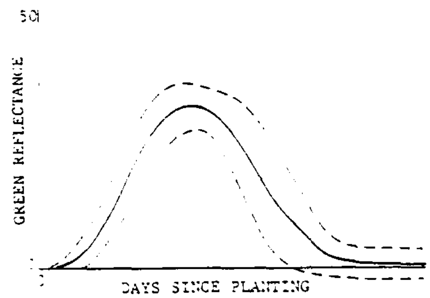

Figure 4. Average Soybean Green Reflectance Profile

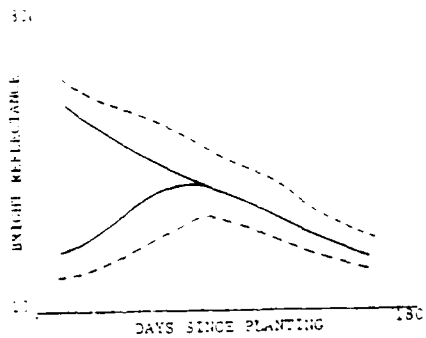

Figure 5. Average Corn Bright Reflectance Profile (Light and Dark Soil)

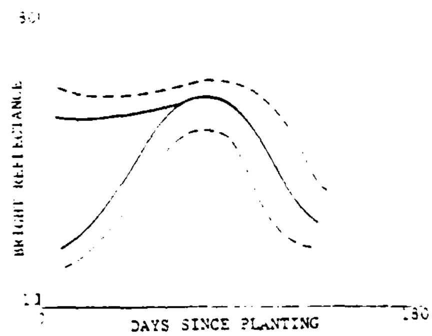

Figure 6. Average Soybean Bright Reflectance Profile (Light and Dark Soil)

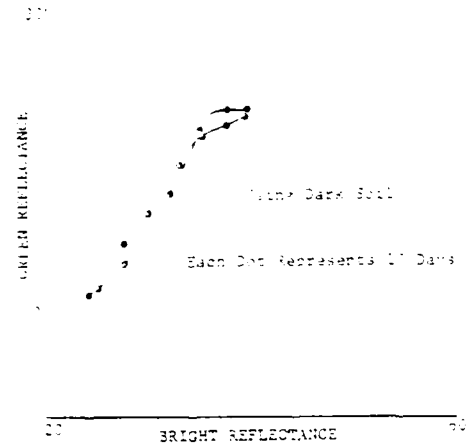

Figure 7. Average Corn Green Reflectance/Bright Reflectance Trajectory

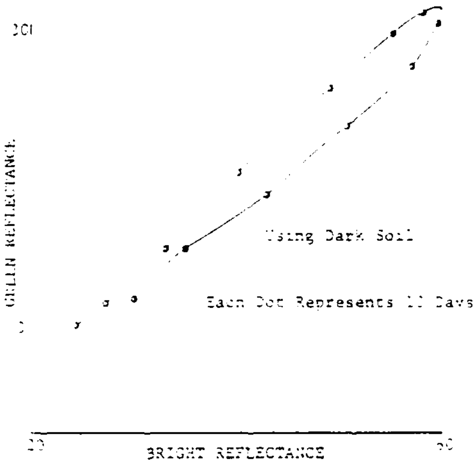

Figure 8. Average Soybean Green Reflectance/Bright Reflectance Trajectory

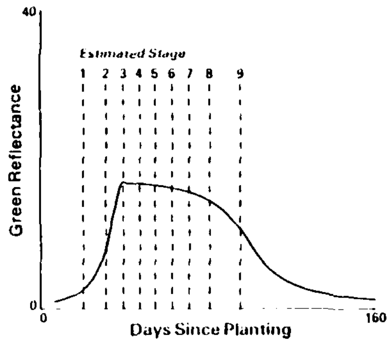

Figure 9. Sam[illegible] Result — Profile/St[illegible]ociation

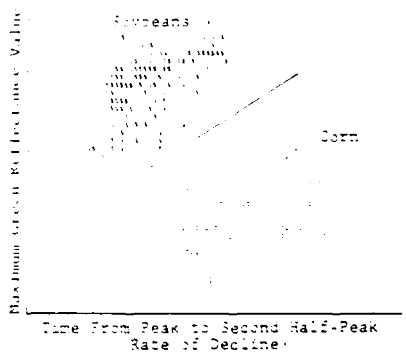

Figure 10. Separability of Corn and Soybeans Based on Spline-Derived Profile Features

ASSESSMENT OF DISEASE-INDUCED YIELD REDUCTION IN COTTON USING SIMULATED SATELLITE IMAGERY*

M. C. Parton

Office of Arid Lands Studies
University of Arizona
Tucson, Arizona

E. N. Mulrean

Department of Plant Pathology
University of Arizona
Tucson, Arizona

O. A. Chadwick

Office of Arid Lands Studies
University of Arizona
Tucson, Arizona

ABSTRACT

Phymatotrichum (Cotton) root rot is a plant disease endemic to the southwestern United States and northern Mexico. This disease, caused by the fungus Phymatotrichum omnivorum, can infect more than 2000 species of cultivated crops and native trees and shrubs. While the extent of infestation can be detected with aerial photography, the cost of periodic coverage makes this data source uneconomical. Landsat multispectral scanner coverage, while frequent, is unsatisfactory because of poor spatial resolution. Thematic Mapper Simulator (TMS) data, flown over a study area near Tucson, Arizona, are demonstrated to possess sufficient spatial and spectral resolution for the detection, tabulation, and mapping of Phymatotrichum root rot. The scheduled July 1982 launch of Landsat D will make Thematic Mapper data available for subsequent mapping and monitoring of root rot throughout the North American area of infestation.

1. INTRODUCTION

1.1 PHYMATOTRICHUM ROOT ROT

Phymatotrichum root rot (Texas root rot) is a plant disease that has a host range of more than 2,000 species of dicotyledonous plants. The causal fungus, Phymatotrichum omnivorum, is endemic on many native trees and shrubs at lower elevations in the southwestern United States and northern Mexico (Figure 1). Cotton, alfalfa, almonds, pecans, apricots, pistachio, apples and other economically important irrigated crops are also susceptible to root rot.

*Presented at the Seventeenth International Symposium on Remote Sensing of Environment, Ann Arbor, Michigan, May 9-13, 1983.

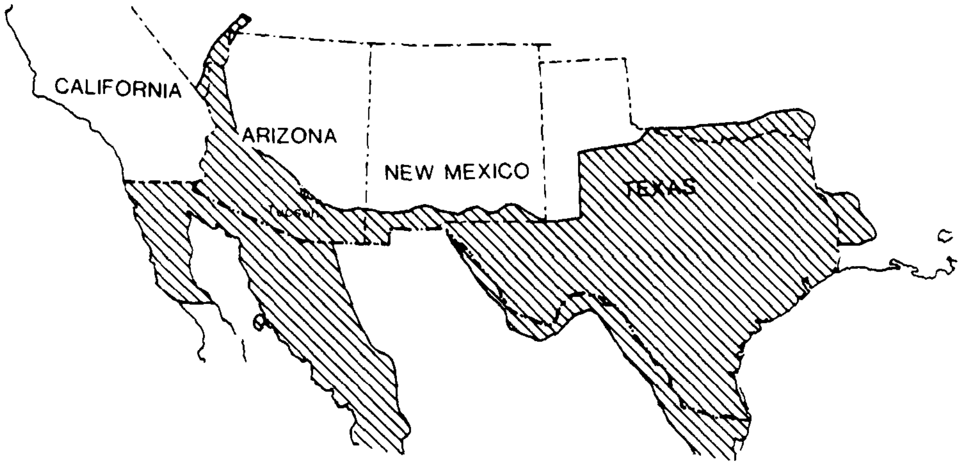

Figure 1. Distribution of Phymatotrichum in North America

The fungus survives in the soil and initially infects the tap root of susceptible plants before ramifying through the entire root system. The first symptom observed is a wilting of the leaves and petioles followed by leaf bronzing and plant death (Figure 2). The fungus is not readily spread in the field, so the affected areas within a given field remain largely unchanged from year to year. Yield reduction results from two factors: 1) early termination of the boll maturation, and 2) lowering of the grade of the fiber due to the introduction of excessive amounts of dead plant material into the lint during the harvesting process.

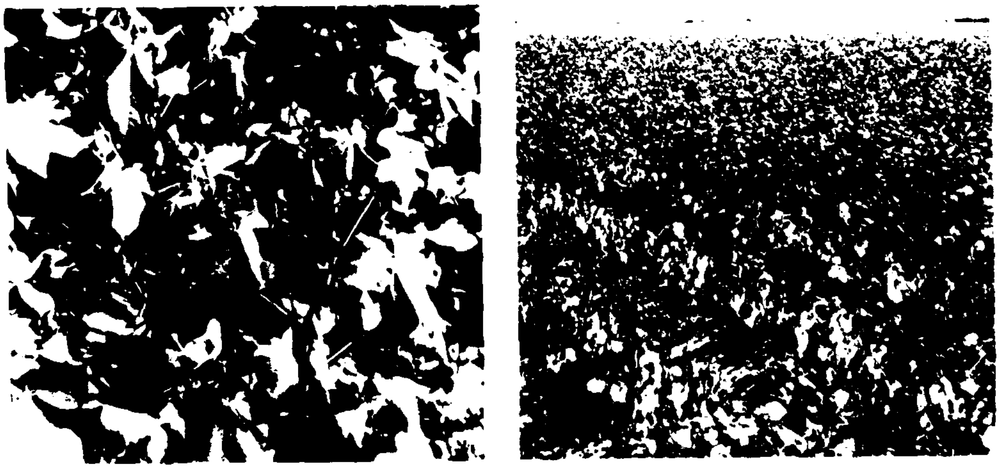

Figure 2. A) Early wilt on cotton plants; B) Phymatotrichum infestation in cotton field

An accurate assessment of crop losses attributable to Phymatotrichum root rot is essential for cost-benefit analysis of disease control strategies. Conservative estimates of losses due to this disease for all crops in Arizona are $5 million annually, while in Texas, the annual loss is estimated to be $100 million with about 60 percent loss in cotton alone.

1.2 DETECTION WITH AERIAL PHOTOGRAPHY

Accurate estimates on crop loss and areal extent of disease damage are difficult to appraise from ground survey. While studies of root rot from aerial photography in Texas and Arizona indicate that large- to medium-scale imagery (1:3,000 to 1:20,000) is satisfactory for monitoring the extent of the disease in cotton fields, the size of the combined southwestern United States/northwestern Mexico infestation region makes regular acquisition of photographic coverage economically prohibitive.

1.3 LANDSAT IMAGERY

The use of Landsat multispectral scanner (MSS) imagery has been investigated as an alternative to conventional aerial photography. While the 18-day repetitive coverage potential provides the necessary monitoring capability, the relatively coarse spatial resolution of this imagery (80m) renders it impractical for the detection of small infestation spots characteristic of root rot (Figure 3).

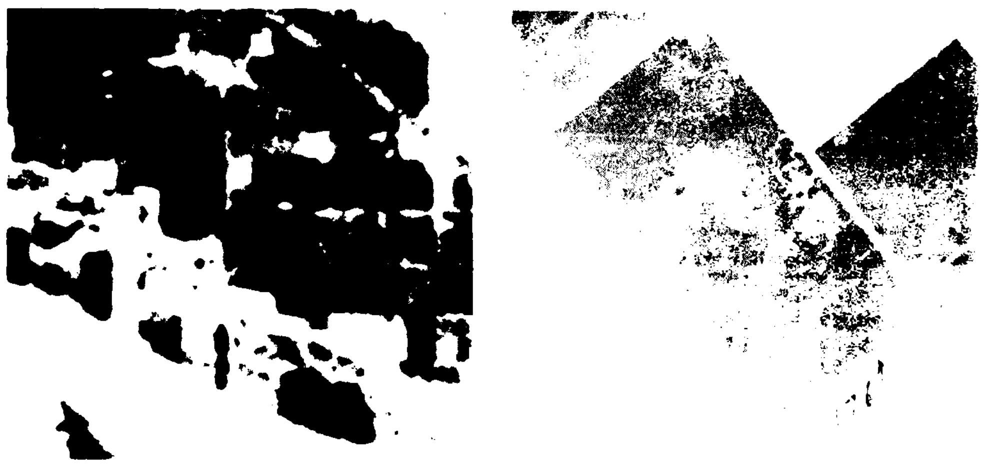

Figure 3. Comparison of A) Landsat and B) Low-Altitude Photography of Marana Study Area

1.4 THEMATIC MAPPER SIMULATOR

In September 1981, the National Aeronautics and Space Administration (NASA) conducted a simulation of an improved-resolution multispectral scanner, named "Thematic Mapper," over an agricultural area that has been the focus of the University of Arizona's five-year research project on Phymatotrichum. This instrument, scheduled for orbital launch as a part of the Landsat-4 payload in July 1982, has a ground resolution of approximately 30 meters and a multispectral range of .38 - 1.10 μm across 10 bands (Table I). This study assesses

the use of Thematic Mapper Simulator (TMS) multispectral data for the detection, tabulation of areal extent, and mapping of Phymatotrichum root rot.

Table I. Thematic Mapper Simulator Spectral Bands

TMS Channel*	Wavelength Range	Landsat MSS Band
1	.38 - .42μm	-
2	.42 - .45μm	-
3	.45 - .50μm	-
4	.50 - .55μm	4
5	.55 - .60μm	4
6	.60 - .65μm	5
7	.65 - .69μm	5
8	.70 - .79μm	6
9	.80 - .89μm	7
10	.90 - 1.10μm	7

*The Thematic Mapper scheduled for launch will have only seven channels. The overall TMS mission includes an evaluation of the utility of 10 visible/near infrared channels and two thermal channels in the ultimate selection of a Landsat-4 thematic mapper configuration.

2. PROCEDURE

2.1 FIELD DATA

A conventional ground-based survey of the Marana study area was conducted in fall 1981 by the University of Arizona, Plant Pathology Department. Large-scale aerial photographs were used for infested-area tabulations, while field sampling was used for yield estimates in Pima (Gossypium barbadense) and Upland (G. hirsutum) cotton. The calculation of infestation area and total field area used 1:3,000 scale color infrared photography flown over the area in September 1981. Tabular results for 28 fields in the study area are provided in Table II.

Table II. Field Survey Tabulations for Marana Area

Field Number	Total Area	Area Healthy (Ha)	Area Rot (Ha)	Field Number	Total Area	Area Healthy (Ha)	Area Rot (Ha)
99	30.57	11.25	19.32	172	24.13	22.75	1.38
106	29.80	13.48	16.32	174	14.17	9.21	4.96
122	44.53	33.35	11.18	179	24.90	17.80	7.10
123	39.84	26.53	13.31	180	21.86	18.36	3.50
129	30.24	11.97	18.27	181	13.36	8.35	5.01
130	31.09	21.61	9.48	182	24.01	19.62	4.39
133	58.70	44.55	14.15	184	25.51	18.93	6.58
142	43.31	33.81	8.50	185	30.36	17.24	13.12
146	44.13	35.35	8.78	188	33.40	28.12	5.28
147	16.88	8.67	8.21	189	29.15	24.83	4.32
148	41.70	36.11	5.59	190	15.38	10.93	4.45
150	18.79	14.66	4.13	191	13.36	10.69	2.67
153	29.92	26.96	2.96	192	14.98	10.44	4.54
171	31.38	23.51	7.87	193	22.79	18.69	4.10

Source: Upland/Pima Fields, Marana, 1981. University of Arizona, Plant Pathology Department

2.2 THEMATIC MAPPER SIMULATOR DATA PROCESSING

A computer-compatible tape of TMS digital data was supplied to the University of Arizona by NASA-Ames Research Center, the testing facility for the Thematic Mapper. A working image of 512 lines-by-512 pixels was extracted to include 28 fields sampled in the Marana area (Figure 4). The image display and classification was performed on an I^2S Model 70 image processor at the Digital Image Analysis Laboratory, University of Arizona.

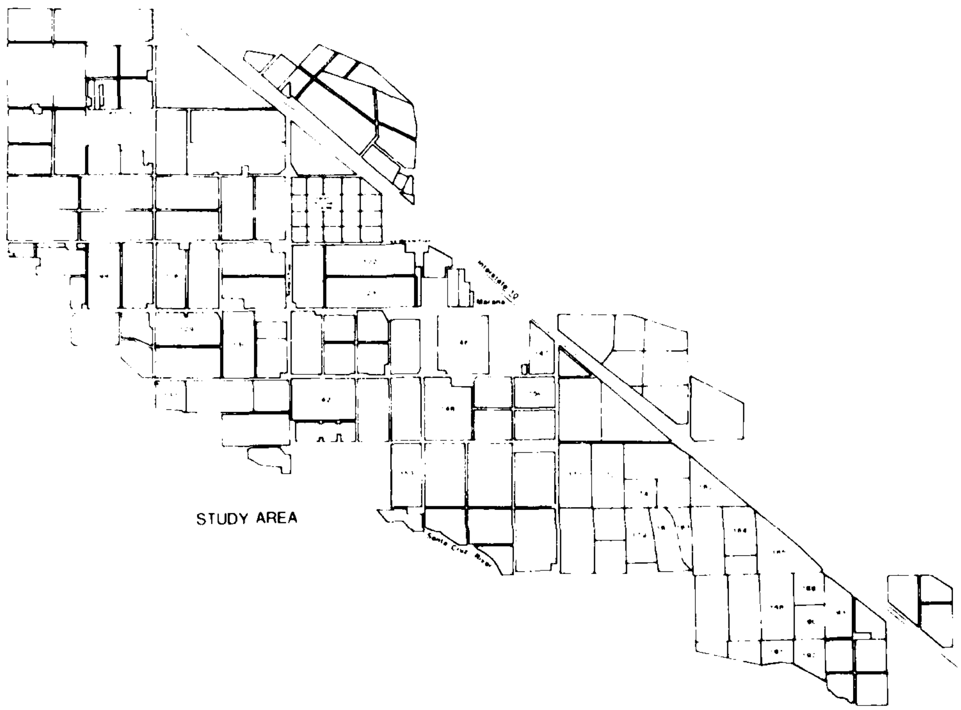

Figure 4. Marana study area

2.3 SEPARABILITY ANALYSIS

Selection of optimal spectral channels from the 10 provided was based on separability analysis of four classes of information needed for root rot mapping and yield estimation:

1. Healthy fields, showing predominantly vigorous individuals with little or no observable canopy reduction;
2. Phymatotrichum infestation, indicated by reduced vigor in a characteristic pattern within a field;
3. Low-vigor strips within fields, typically in a linear pattern, indicating low-yield conditions resulting from factors other than Phymatotrichum; and,
4. Field edges, including paths, irrigation canals, and roads.

Mean pixel values sampled within training sets for each of the four classes were plotted by channel (Figure 5) and evaluated to determine which of the 10 channels were most useful in separating the features desired. A combination of channels 3, 5, and 9 provide the best apparent discrimination between the field features listed above.

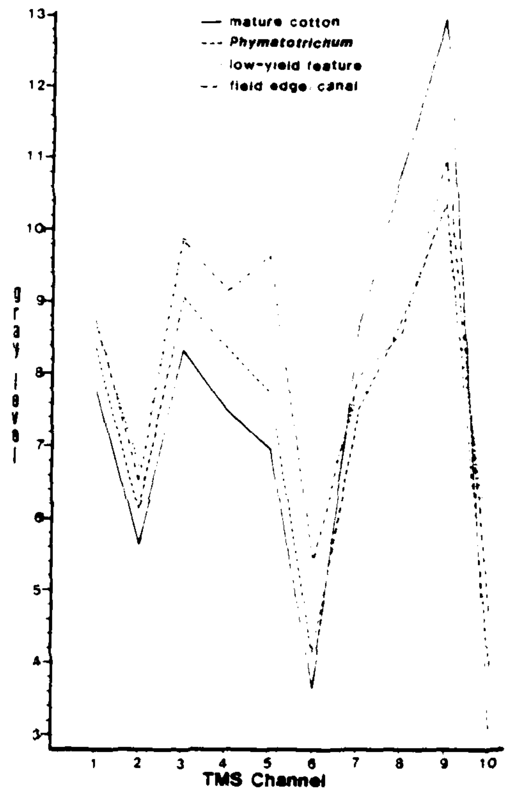

Figure 5. TMS channel separability analysis

2.4 FIELD POLYGON GENERATION

To allow for the tabulation of root rot classes for the sample fields selected, a polygon mask was generated to overlay onto a multichannel image composite. This mask was created using a set of coordinates corresponding to corner points of the 28 fields, which was subsequently converted to a raster-based polygon file. This was merged with each of the three TMS channels selected for classification, which, in turn, were composited. The resulting "mask" isolated the sample fields from the remaining image, simplifying the task of tabulating pixel sums by class for area calculation.

2.5 CLASSIFICATION

While a number of classification algorithms are available with the I^2S System 500 interactive software, a simple supervised minimum-distance routine (MINDIST, I^2S, 1981) was found to be satisfactory in classifying areas of Phymatotrichum root rot, healthy field vegetation, and low-vigor growth within the sample fields. Training sites were selected interactively using both low-altitude color infrared aerial photography and a trained observer familiar with the study area and its field characteristics. Several iterations of the routine were performed with increasing values of thresholding to approximate the infestation patterns observable on aerial photography used for the ground survey. The tabular results of this classification are listed in Table III.

Table III. Thematic Mapper Simulator Tabular Summary

Field Number	Infested Area (Ha)	Uninfested Area (Ha)	Low-Yield Area (Ha)	Total Area (Ha)
99	13.58	11.78	5.21	30.57
106	8.82	9.74	11.23	29.80
122	5.82	29.29	9.42	44.53
123	9.33	21.97	8.54	39.84
129	9.51	9.19	11.54	30.24
130	2.54	25.82	2.74	31.09
133	2.22	52.02	4.46	58.70
142	4.39	32.95	4.97	42.31
146	9.09	19.31	15.73	44.13
147	0.88	13.33	2.67	16.88
148	1.31	37.73	2.66	41.70
150	.46	16.65	1.69	18.79
153	.83	27.01	2.09	29.92
171	6.45	18.66	6.27	31.38
172	3.01	14.00	7.13	24.13
174	5.72	6.42	2.03	14.17
179	3.48	20.02	1.39	24.90
180	3.70	14.85	3.31	21.86
181	1.45	5.93	5.97	13.36
182	2.25	20.01	1.75	24.01
184	6.02	10.36	9.12	25.51
185	10.16	11.70	8.50	30.36
188	4.05	27.30	2.05	33.40
189	10.63	14.31	4.22	29.15
190	4.14	10.43	0.81	15.38
191	1.23	9.87	2.26	13.36
192	3.35	8.49	3.14	14.98
193	3.04	17.46	2.29	22.79

3. RESULTS

A direct comparison of results from field and TMS tabulations is not possible since the latter includes a low-yield class that may be included either in infestation or healthy area categories derived from the field/aerial photo method. With this deficiency in mind, a review of the percentage difference results between the methods (Table IV) reveals that the two techniques are significantly close in many cases. Further examination shows that nearly all of the substantial percentage-difference cases have large values for the low-yield category, accounting for the deviation between aerial photo and TMS calculations.

A simple classification map is illustrated in Figure 6 which depicts Phymatotrichum infestation, healthy field cotton, and low-yield areas within the study fields. This map was produced from the classification file from which the tabular results by class and field were obtained.

Table IV. Comparison of Aerial and TMS Area Data (area in hectares)

Field Number	Total Area	Healthy Area Aerial	Healthy Area TMS	Healthy Percent Differ.	Rot Area Aerial	Rot Area TMS	Rot Percent Differ.	Low-Yield Area TMS Only
99	30.57	11.25	11.78	-1.37	19.32	13.58	18.78	5.21
106	29.80	13.48	9.74	12.55	16.32	8.82	25.17	11.23
122	44.53	33.35	29.29	9.12	11.18	5.82	12.04	9.48
123	39.84	26.53	21.97	11.45	13.31	9.33	9.99	8.54
129	30.24	11.97	9.19	9.19	18.27	9.51	28.97	11.54
130	31.09	21.61	25.82	-13.54	9.48	2.54	22.32	2.74
133	58.70	44.55	52.02	-12.73	14.15	2.22	20.32	4.46
142	42.31	33.81	32.95	2.03	8.50	4.39	9.71	4.97
146	44.13	35.35	19.31	36.35	8.78	9.09	-0.70	15.73
147	16.88	8.67	13.33	-27.61	8.21	0.88	43.42	2.67
148	41.70	36.11	37.73	-3.88	5.59	1.31	10.26	2.66
150	18.79	14.66	16.65	-10.59	4.13	0.46	19.53	1.69
153	29.92	26.96	27.01	-0.17	2.96	0.83	7.12	2.09
171	31.38	23.51	18.66	15.46	7.87	6.45	4.53	6.27
172	24.13	22.75	14.00	36.26	1.38	3.01	-6.76	7.13
174	14.17	9.21	6.42	19.69	4.96	5.72	-5.36	2.03
179	24.90	17.80	20.02	-8.92	7.10	3.48	14.54	1.39
180	21.86	18.36	14.85	16.06	3.50	3.70	-0.91	3.31
181	13.36	8.35	5.93	18.11	5.01	1.45	26.65	5.97
182	24.01	19.62	20.01	-1.62	4.39	2.25	8.91	1.75
184	25.51	18.93	10.36	33.59	6.58	6.02	2.20	9.12
185	30.36	17.24	11.70	18.25	13.12	10.16	9.75	8.50
188	33.40	28.12	27.30	2.46	5.28	4.05	3.68	2.05
189	29.15	24.83	14.31	36.09	4.32	10.63	-21.65	4.22
190	15.38	10.93	10.43	3.25	4.45	4.14	2.02	0.81
191	13.36	10.69	9.87	6.14	2.67	1.23	10.78	2.26
192	14.98	10.44	8.49	13.02	4.54	3.35	7.94	3.14
193	22.79	18.69	17.46	5.40	4.10	3.04	4.65	2.29

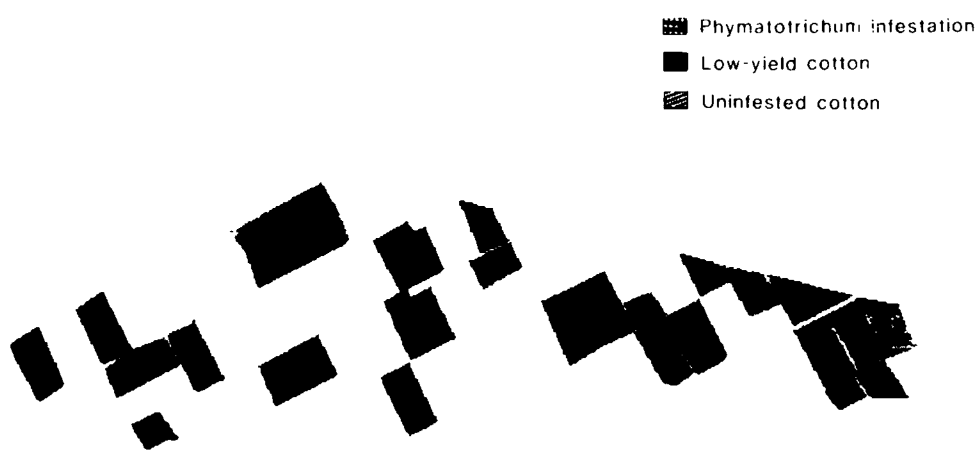

Figure 6. Classification Map of Marana Study Area

4. CONCLUSIONS

The results of the aerial photo and TMS comparison suggest that satellite-borne multispectral scanning image data can effectively provide data on Phymatotrichum infestation which is comparable to that produced from manual interpretation of aerial photography. The immediate benefits that can be recognized by TMS data utilization include 1) frequent (16-day) coverage potential for infestation monitoring, 2) consistency in classification, and 3) direct data tabulation and analysis.

Further investigation is suggested for the following areas:

1) Calibration of reflectance with actual sample yields to derive direct yield estimates on a field-by-field basis;
2) Seasonal and multitemporal changes in the extent and degree of infestation effects; and
3) Comparison of TMS classification results with actual harvest analysis to evaluate the effectiveness of machine-derived yield estimates over field sample estimates.

5. REFERENCES

Bloss, H.E. 1973. Application of Aerial Infrared Photography to Ecology of Phymatotrichum Root Rot. Progressive Agriculture in Arizona, 25:3, p 10

Hine, R.B., J.F. Armstrong, and B.B. Taylor. 1980. Texas Root Rot of Cotton. Cooperative Extension Service Pamphlet No. Q-410, University of Arizona, Tucson. 2 pp.

I^{2}S (International Imaging Systems, Inc.). 1981. System 500 Image Processing System Users Manual. Version 2.2 (February, 1981). 152 pp.

NASA (National Aeronautics and Space Administration). 1981. Flight Summary Report - No. 81-180 (25 September 1981). NASA Airborne Missions and Applications Division, Ames Research Center, FSR-1550. 6 pp.

Streets, R.B., and H.E. Bloss. 1973. Phymatotrichum Root Rot. Monograph No. 8, The American Phytopathological Society. 38 pp.

Toler, R.W., B.D. Smith, and J.C. Harlan. 1981. Use of Color Infrared Photography to Evaluate Crop Disease. Plant Disease, 65:1, pp. 24-31.

U.S. Geological Survey, EROS Data Center. 1982. Band Numbering to Change with Landsat D. Landsat Data Users Notes, No. 22 (March), p. 5.

APPLICATION OF NOAA-AVHRR DATA TO REGIONAL GEOLOGIC MAPPING AND ROCK AND SOIL DISCRIMINATION

F.R. Honey

CSIRO
Wembley, Western Australia

SUMMARY

Data and imagery from the polar orbiting weather satellites have received little attention to determine their potential for mapping geology, soils, and soil moisture. This is due in part to their poor spatial resolution when compared to Landsat, and to the broad spectral bands used on early system designed primarily for cloud studies.

The NOAA-6 and NOAA-7 Advanced Very High Resolution Radiometers, with four and five spectral bands respectively, with resolutions of 1.1 km, and with two overpasses per satellite over any area of the earth each day, provide data which is being evaluated in Australia, for geologic mapping and soil moisture studies, as well as atmospheric and oceanographic application.

Linear features greater than 100 km in length have been mapped, using the visible, reflective infrared and thermal images. Some lineaments mapped in the Canning Basin using the thermal data are not apparent in the visible and reflected infrared images. Night time imagery has highlighted several thermal anomalies in the granite plutons in the Pilbara region, which correlated with geochemical anomalies mapped independently.

Ratios of the two long wavelength bands on NOAA-7 are providing some discrimination of rock and soil types, based on their silicate content.

Results in the form of images and maps will be presented to illustrate the capabilities of the AVHRR data for mapping.

OPTIMAL LANDSAT TRANSFORMS FOR FOREST APPLICATIONS[1]

Thomas L. Logan

Jet Propulsion Laboratory, California Institute of Technology
4800 Oak Grove Drive, Pasadena, California 91109

Alan H. Strahler[2]

Department of Geography, University of California
Santa Barbara, California 93106

ABSTRACT

In agricultural applications of remote sensing, linear transforms of Landsat data, such as those of Kauth and Thomas, are known to be highly effective both for data compression and enhancement of crop identification accuracies. Typically, such transforms are based on the time-trajectory of crop pixels through measurement space as the crop increasingly obscures the soil, matures, scenesces, and is harvested. In natural vegetation applications, temporal variations are less important-- life-form differences among vegetation types lead to distinctive signatures for natural vegetation types that are more or less distinctive, independent of season. However, the signatures of natural vegetation types are greatly influenced by their topographic position on the landscape, due to factors of differential illumination and complex bidirectional reflectance distribution functions. Thus, the question arises whether there are one or more transforms of Landsat data, beyond those already explored, that can accentuate the separability of natural vegetation classes in areas of diverse topographic relief. To answer this question, we investigated eleven transforms of four Landsat MSS channels as shown below.

1. MSS5/MSS6

2. MSS5/MSS4

3. $\left(\frac{MSS4 + MSS5}{2}\right) / \left(\frac{MSS6 + MSS7}{2}\right)$ (RAVE)

4. $\frac{(MSS4 + MSS5 / (MSS6 + MSS7)}{(MSS6 + MSS7 - (MSS4 + MSS5)}$ (RASD)

5. $\sqrt{\frac{MSS6 - MSS5}{MSS6 + MSS5} + .05}$ (TV16)

6. $\sqrt{(SOIL5 - MSS5)^2 + (SOIL6 - MSS6)^2}$ (PV16)

Where SOIL5 = -0.498 + 0.543*MSS5 + 0.498*MSS6

---

[1]This paper represents one phase of research carried out under NASA Contract NAS7-100 with the support of California Institute of Technology President's Fund Award PF-168.

[2]Now with Department of Geography, Hunter College, City of New York University.

SOIL6 = 2.734 + 0.498*MSS5 + 0.498*MSS6

7. .2120*MSS4 + .2962*MSS5 + .6051*MSS6 + .7079*MSS7 (E1)

8. .4648*MSS4 + .7847*MSS5 - .0752*MSS6 - .4031*MSS7 (E2)

9. MSS5/E2

10. $\frac{\text{MSS5/E2}}{\text{E2}}$

11. RAVE/E2

These transforms were evaluated for their ability to distinguish among thirteen classes of natural vegetation in a small area of the Klamath Mountains in northern California, USA. The thirteen classes included seven types based on life form: open canopy conifer forest, closed canopy conifer forest, hardwood forest, sparse forest, meadow, grass and small trees. The open and closed conifer types were further subdivided by dominant species: red fir, white fir, Douglas-fir, and ponderosa pine. Landsat data were from a July 1973 image received from Landsat 1. Identification of classes and training areas was carried out in the field during the summer of 1977.

Two contrasting methods were employed to rate the information content of the eleven transforms and four raw Landsat channels: divergence analysis and classification accuracy. Although the divergence analysis appeared to be quite sensitive to minor variations in computation induced by quantization of the raw Landsat data, divergence values were highest for the three transforms (9, 10, and 11) in which the second eigenvector, E2, appeared in the denominator. This result suggests that the second eigenvector performs a useful scaling function. For the Landsat image analyzed, the second eigenvector emphasizes the difference between MSS7 and the weighted sum of MSS4 and MSS5. Since this linear function is orthogonal to the first eigenvector, which weights all MSS bands positively and accounts for the overall "brightness" of the image, it reduces the effects of shadowing and differential illumination on vegetation signatures, producing the observed enhanced values for divergence.

In accuracy analysis, transform 11, the ratio of MSS4 and 5 and MSS6 and 7 averages (RAVE) divided by the second eigenvector (E2), archieved highest accuracies, followed by raw MSS4 and MSS5 bands. Band ratios such as RAVE are known to reduce the effects of differential illumination, but do so in a fashion clearly different from linear compounds such as E2. Since only one multichannel transform performed better than the two raw Landsat channels, the results suggest that transforms should be chosen with care for a particular application to natural vegetation.

1.0 BACKGROUND

Resource managers of state, federal, and private agencies constantly face the need to assess and inventory large areas of natural land cover in a timely and cost-effective manner. Thus far, Landsat classifications have been helpful in providing the data needed for such inventories. However, classification accuracies degrade when classification must distinguish between land cover classes which are similar in vegetation form and pattern, but differ in species composition. Spectral information alone is often insufficient to accurately distinguish stands of different coniferous tree species, or to differentiate various types of chapparal. This failure can make resource management difficult when the stands or vegetation types require widely different management practices.

Early research in the Doggett Creek vicinity of the Klamath National Forest (Strahler, et al., 1978) demonstrated that the incorporation of U.S. Geological Survey-Defense Mapping Agency elevation and derived compass-aspect information with multidate Landsat spectral data in conventional supervised classification of western North American forest species could produce average accuracies as high as 85 percent. The use of elevation data with spectral data in unsupervised classification, however, resulted in the swamping of spectral information by the topographic data.

Subsequent research (Strahler, 1981) showed that a standard deviation texture channel (derived from MSS5) combined with Landsat spectral data in an unsupervised procedure could produce classes that differentiated timber stands of uniform height and density reasonably well. When combined with an image predicting regional forest type (which denotes species composition) using elevation and aspect data, accurate timber stratum maps resulted that could be used to allocate timber volume samples as well as provide other forms of useful timber management information.

The combination of spectral tone, spatial texture and independent terrain information, therefore, appears to provide sufficient information for automatic characterization of natural vegetation resources. Tone is most important for recognizing the existence and presence of a feature. Texture combines with tone to measure local tonal variation. The topographic terrain information provides a powerful independent parameter well known for improving forest classification accuracies.

The work of several researchers in agriculture (Kauth and Thomas, 1976), geology (Soha and Schwartz, 1978), and forestry (Deering, et al., 1975), have suggested that certain transforms of Landsat data can enhance inherent information or at least permit a reduction in the number of data channels without substantial data loss (data compression). Use of such transforms offers a potential for improved classification accuracy with reduced computer costs. A single enhanced channel could prove particularly useful as a base for the standard deviation texture convolution. The purpose of this research is to investigate several of the better known Landsat transformations and assess their utility for accentuating the separability of general coniferous forest and related vegetation classes.

The computer processing for this research was carried out at JPL and UCSB using the Video Image Communication and Retrieval (VICAR) image processing system. Under continual development at JPL for the past ten years, the VICAR system was originally designed for enhancement of satellite pictures from the nation's unmanned space exploration programs such as Mariner, Viking and Voyager. VICAR manipulates digital images expressed as eight-bit bytes, ranging in value from zero to 255. As part of the log-in procedure under which Landsat images in CCT format are converted to VICAR format, six and seven-bit sensor values are stretched to eight bits.

1.1 STUDY AREA

The study area used in this research is located in the Doggett Creek vicinity of the Klamath National Forest (Figure 1). The area comprises about 220 sq. km. of private and publicly-owned forest land in Northern California near the town of Klamath River. Located within the Siskiyou Mountains, elevations in the area range from 500m at the Klamath River, which crosses the southern portion, to 2065m near Dry Lake lookout on an unnamed summit. The extensive topographic relief of the Doggett Creek area can be seen via a synthetic stereogram of the July 4, 1973 Landsat MSS5 (1346-18221) in Figure 3.

A wide variety of distinctive vegetation types are present in the area. Life-form classes include alpine meadow, fir park, pasture, cropland, and burned, reforested areas. Forest vegetation includes, from high elevation to low elevation, such types as noble fir, mixed fir (noble, red and white), douglas fir, ponderosa pine-incense cedar, pine-oak, and oak-chaparral. Thus, the topographic and vegetational characteristics of the area are well differentiated.

2.0 LANDSAT TRANSFORMS

A textural transform of the type used by Strahler, et al. (1979) can provide transformed information only at a level relative to the amount present in the original data. A channel

endowed with more pertainent information than another will provide more textural information after transformation. Landsat data, however, contain a range of vegetation reflectance information apportioned over four separate bands covering the 0.5 to 1.1 micron wavelenghts. While MSS4 band provides most coniferous vegetation information, there is still important data to be found within the MSS5 and infrared channels. Producing textural transforms of all four bands would provide too much non-vegetation information as well as over emphasize the redundant nature of Landsat data due to high channel intercorrelations. The redundant property of Landsat data, however, makes it a candidate for data compression. A single channel of compressed Landsat data could provide a powerful foundation for a textural transform.

Many techniques such as ratioing, principal components and discriminant analysis, have been used for the purpose of removing redundancy while retaining desired information. The success rate tends to vary with the purpose and procedure that are utilized. Considerable success has been reported in the literature when the emphasis has been on enhancing one particular feature such as gypsy moth defoliation (Williams, et al., 1979) or the urban/rural boundary (Friedman, 1980). Often, enhancement of one feature coincidentally enhances another. In this research, several of the more common compression techniques are investigated to determine if any have the potential for condensing Landsat data into a single channel which enhances the range of coniferous species-type classes. Fifteen channels of data are investigated.

Two families of data compression procedures have tended to be most popular largely because of the ease with which they can be formed: ratioing and principal components analysis (PCA). The most common ratio for vegetation purposes is:

$$(1) \qquad \frac{MSS\ 5}{MSS\ 6}$$

(or visa versa or MSS7 in lieu of MSS6) as suggested by Kriegler, et al. (1969), Billingsley (1973), Vincent (1973) and Maxwell (1976). The ratio:

$$(2) \qquad \frac{MSS\ 5}{MSS\ 4}$$

has also been used to emphasize just the key vegetation channels within Landsat data. A slight variation of this theme which retains the use of all four bands is the ratio of averages (RAVE):

$$(3) \qquad \frac{\frac{MSS4\ +\ MSS5}{2}}{\frac{MSS6\ +\ MSS7}{2}}$$

and the ratio of sums divided by the differences (RASD):

$$(4) \qquad \frac{(MSS4\ +\ MSS5)\ /\ (MSS6\ +\ MSS7)}{(MSS6\ +\ MSS7\ \ -\ (MSS4\ +\ MSS5)}$$

Richardson and Weigand (1977) evaluated several vegetation models and found TV16 (Transform Vegetation Index with MSS6) as suggested by Rouse, et al. (1973) and Deering, et al. (1975) to be the most useful for estimating relative greenness:

$$(5) \qquad \sqrt{\frac{MSS6\ -\ MSS5}{MSS6\ +\ MSS5} + 0.5}$$

They also developed the PV16 (Perpendicular Vegetation Index) to distinguish the spectral response of green vegetation from the response contributed by background soils:

$$(6) \qquad \sqrt{(SOIL5\ -\ MSS5)^2 + (SOIL6\ -\ MSS6)^2}$$

where: SOIL5 = -0.498 + 0.543 * MSS5 + 0.498 * MSS6

SOIL6 = 2.734 + 0.498 * MSS5 + 0.498 * MSS6

Ratioing techniques are popular because they can often be easily performed digitally as well as photographically, and they also tend to reduce the effects of shadowing and atmospheric degradation.

Principal Components Analysis (PCA) techniques have also been found to be useful for data compression (Ready and Wintz, 1973, Fontanel, et al., 1975, and Jenson and Waltz, 1978). Principal components seeks to determine the best orthogonal linear combinations of data which can account for more variance in the data as a whole than any other linear combinations. The principal components were derived from the covariance matrix (Karhunen-Loeve transform). Each component was automatically scaled after transformation so that its histogram assumed a distribution centered at a DN of 128, and the spread encompassed the full 256 DN range. With Landsat data, the first principal component:

(7) .2120*MSS4.+.2962*MSS5+.6051*MSS6.+.7079*MSS7 (E1)

weights all four channels positively according to the magnitude of their standard deviations. It thus generally reflects overall brightness, and is likely to be strongly influenced by differential illumination. The second principal component:

(8) .4648*MSS4+.7847*MSS5-.0753*MSS6-.4032*MSS7 (E2)

emphasizes the difference between visible and infrared bands; and contains the feature-specific information derived from the four Landsat channels that is the most useful PCA contribution to feature data compression. Haralick, et al. (1972) found that of the several transforms he tested, the principal components procedure best approximated the original picture.

A variation of the above ratioing and PCA techniques combines the two to produce the following channels:

(9) MSS5 / E2

(10) (MSS5 / MSS6) / E2

(11) RAVE / E2

Conceivably a synergism could occur as a result of transforming the four Landsat channels by the two very different mechanisms, and ratioing the two products (as in the case of RAVE/E2).

The last four channels of data to be tested consist of the Landsat bands, included so as to provide a scientific control to the experiment as well as provide a relative measure with which to rate and evaluate the merits of the other channels. Most remote sensing scientists are familiar with the relative information content of these channels, and can therefore use them to place the ratio and PCA channels in perspective.

3.0 TRANSFORM EVALUATION

Two contrasting methods were employed to rate the information content of the fifteen selected channels. The first is a divergence analysis test and the second is back-classification of the training sites. Both methods use training site data as the basis for their calculations.

3.1 DIVERGENCE ANALYSIS

Divergence analysis uses a covariance-weighted distance measure of class means to determine the total separability of class categories within a given channel. The total divergence value that is calculated can then be used to rate the individual channels, with the underlying assumption being that, for the purposes of this research, greater separation is an indication of more "information." Divergence analysis has been employed by Shlien, et al. (1973) and Goodenough and Narendra (1976), and is a common-place practive among users of LARSYS.

Results of the divergence analysis are reported in Table 1, but are not considered reliable. The technique requires that the spectral data within the training sites have a Gaussian distribution. This is a common requirement among multivariate techniques including maximum likelihood classification that is often relaxed because it is virtually impossible to obtain. However, there are limits to which the Gaussian rule can be relaxed. The fundamental problem in this case lies with the nature of natural vegetation. Unlike agricultural training sites which tend to be homogeneous, well defined, and easily delineated, natural vegetation nearly always has a high variation due to spacing of the vegetation (which lets in ground signature), modulating height, health, and other factors. Every effort was made in the selection of training sites to make them as homogeneous and demonstrative of the class to which they represent. However, many of the variations typical of natural vegetation do not appear in a single Landsat channel. Thus, training sites delineated based on MSS5 that look homogeneous in MSS5 may be rather heterogeneous when viewed in MSS7 or MSS4. This problem is particularly compounded in the ratio process when the second eigenvector image is involved. When a set of overlaying pixels from the four Landsat bands are very contrasting, the principal components process can produce an unusual grey value (DN). When such an odd DN is divided into its band 5 counterpart (as in the case of 5/E2), a very large or small output DN value may result that is uncharacteristic of the surrounding norm (Figure 2). If this high variance pixel falls in a training site, it will artificially raise or lower the mean of the training class. The divergence analysis technique, which relies on the class means for determining separability, will then be inflated producing unreliable results. Thus, divergence analysis is likely to be misleading in the analysis of classes of natural vegetation.

3.2 CLASSIFICATION TEST

Back-classification of training sites is a technique that allows easy and rapid comparison of relative accuracies; however, its use for measuring absolute accuracies is suspect. The technique employs the same training sites areas utilized in the classification process to determine the number of correctly classified pixels. Thus, the same set of data used to train a classifier is also used to evaluate it. While this method has obvious short-comings for evaluating the exact accuracy of a classification, it is an acceptable technique when relative accuracies are to be compared.

The results of separately back-classifying the fifteen channels are shown in Table I. As would be expected for single channel classifications, the numerical accuracies are low. No "tuning" of the classifications was performed to enhance accuracies.

3.3 RAVE/E2 ANALYSIS

Of the fifteen channels investigated, the RAVE/E2 (Figure 4) contained the most vegetation information, with an average classification accuracy of 13.2% compared to 11.7% for the closest rival. This channel represents an enhancement in information relative to all other tested ratio transform channels, which lost information over the raw Landsat classification. This is apparent from the number two position of MSS4, which theoretically should be the best single Landsat band for vegetation because of the strong reflectance peak of coniferous forests at 0.55 microns. Channels scoring lower than MSS4 would indicate a loss of information content, and channels scoring higher would represent a gain in information.

Other evidence suggesting utility for the RAVE/E2 channel can be found by looking at the percentages of unclassified pixels. In addition to having the highest classification accuracy, the RAVE/E2 channel also had the lowest percentage of unclassified pixels: 37.9%. This compares to 41.7% for MSS4 and 58.9% for MSS5. Thus, not only did the RAVE/E2 channel classify more pixels than the other channels, but it also classified a higher percentage of them correctly.

The mechanism which gives the RAVE/E2 channel an advantage over the others is likely related to an overall reduction in the effects of shadowing. Comparison of the transformed image (Figure 4) with the original Landsat band 5 (Figure 3) suggest that several of the steeper slopes that appear darker in the original imagery are being equalized in grey tone with related timber types on flater slopes in the transformed image. Indications of this effect appear in the left-middle bottom and upper middle-right edge of the imagery, where opposing slopes of similar types but differing DN due to shadowing in the original imagery receive similar DN in

the transformed data. Classification accuracy would certainly be expected to improve if similar timber types on differing slopes were to receive similar DN ranges.

An overall reduction in the effects of shadowing could be expected from the RAVE/E2 channel. When shadowing affects all four Landsat bands equally, ratioing is known to remove most of the negative effects. At the same time, the second eigenvector from PCA displays most of the information left after overall brightness, as influenced by relative illumination, is accounted for in the first eigenvector image. Note that topographic shadowing is very evident in the first eigenvecotor image (Figure 5) when compared to the second eigenvector (Figure 6). It would, therefore, seem very plausible that the ratio of two transforms that are each known to compensate for differential illumination in a unique way could result in a synergistic output of superior quality to either taken separately. Further research is necessary to fully investigate and confirm this hypothesis.

The quality of the RAVE/E2 channel is heavily influenced by the PCA factor loadings. Variations in these values due to the presence or absence of clouds or snow, for example, could negatively or positively effect the discrimination capability of the RAVE/E2 channel. Table II shows the varying results that such effects can have. A minor change in the infrared loadings (.4648, .7847, -.0752, -.4031) improved classification performance to 14.0%, and had an effect in helping to discriminate open canopy Ponderosa Pine (POP_o). The number of unclassified pixels dropped to 33.2%*. Other changes had significantly negative effects. Rounding the factor loadings to (.5000, .8000, 0,-.4000) produced the worse average coniferous classification accuracy of 4.6%.

Indiscriminant scaling during creation of RAVE/E2 can also have deleterious effects. Throughout all ratio channel processing, the attempt was made to produce an output standard deviation that was close to or within the Landsat range, since previous research had indicated that channels with extremely small local standard deviations, such as those typical of digital elevation, could easily swamp spectral data in an unsupervised classification operation. Thus, the RAVE portion of the RAVE/E2 transform was multiplied by 110, and after division by E2 (which was initially scaled), the quotient was multiplied by 60 (denoted as 110;60). This produced a standard deviation reasonably close to the range of Landsat standard deviations.

The (110;60) scaling combination produced the best results for the RAVE/E2 channel. A neutral scaling of (100;100) produced poor results substantiating the need for a scaling of some design. Minor adjustments (Table II) to (100;60) and (100;50) produced some rather significant changes in individual category accuracies suggesting that like PCA, ratio scaling is a critical component of the channel transformation process.

That ratio transforms can provide a valuable tool for selective enhancement of specific features is very evident in this research. While the RAVE/E2 channel would appear to offer the best all around general enhancement of coniferous forest vegetation, the (5/6)/E2 channel might be better for examination of open canopy douglas fir, or the green band for high and low density white fir. The best channels for specific conifer and general vegetation types are highlighted in Tables I and II.

4. CONCLUSIONS

Coniferous Landsat data can be compressed into a single channel containing more information than any of the original individual inputs using the following transform (RAVE/E2):

$$\left(\left(\left(\left(\frac{MSS4 + MSS5}{2}\right) / \left(\frac{MSS6 + MSS7}{2}\right)\right) *110\right) / \text{ Second Eigenvector}\right) *60$$

where the second eigenvector has linear factor loadings of (.4648, .7847, -.0752 -.4031) and was scaled to spread the distribution over 256 DN levels with the center at 128. This information gain appears to be unique among similar transforms discussed in the literature, which all

* Part of the seemingly large percentage change occurring here may be due to the statistically small number of pixels in some of the training classes.

suffer an informational loss during the compression process. However, RAVE/E2 is a technologically complex channel to generate, and considering the radiometric variation common between Landsat scenes, it is unlikely that the PCA loadings disclosed here would be of wide applicability. It is probable that Landsat MSS4 which ranked second best in coniferous information content is the best all-around dependable single channel of data. The extra effort to utilize transformed Landsat channels will probably provide only a subtle, if any, improvement in average classification accuracy. For enhancement of specific classes, the use of certain transforms may be quite beneficial (Table I). But for the general classification of coniferious forest Landsat data, the raw channels will probably provide a result comparable to the best of any classification based on transformations of the raw channels tested herein.

5.0 REFERENCES

1. Billingsley, F.C, 1973. "Some Digital Techniques for Enhancing ERTS Imagery," Management and Utilization of Remote Sensing Data. Symposium of the American Society of Photogrammetry, Sioux Falls, South Dakota.

2. Deering, D.W., J. Rouse, Jr., R. Haas and J. Schell, 1975. "Measuring 'Forage Production' of Grazing Units from Landsat MSS Data," in: Proceedings 10th International Symposium on Remote Sensing of Environment, Environmental Research Institute of Michigan, Ann Arbor, pp. 1169-1178.

3. Fontanel, A., C. Blanchet and C. Lallemand, 1975. "Enhancement of Landsat Imagery by Combination of Multispectral Classification and Principal Component Analysis," in Proceedings NASA Earth Resources Symposium, Vol. 1-B, NASA TMX-58168, pp. 991-1012.

4. Friedman, Steven Z., 1980. Mapping Urbanized Area Expansion Through Digital Image Processing of Landsat and Coventional Data, JPL Publication 79-113, NASA Jet Propulsion Laboratory, Pasadena, California.

5. Goodenough, David and P.M. Narendra, 1976. "Feature Subset Selection in Remote Sensing," Presented at the Milwaukee Symposium on Automatic Computation and Control.

6. Haralick, R.M., J.D. Young, D.K. Goel, and K.S. Shanmugam, 1972. "A Comparative Study of Data Compression Techniques for Digital Image Transmission," in Fourth Annual Earth Resources Program Review, Vol. II, Chapter 38, NASA-TM-X-68397, p. 27-33.

7. Jenson, S.K., and F.A. Waltz, 1978. "Canonical Analysis and Principal Components Analysis in Remote Sensing," Prepared under U.S. Geological Survey Contract No. 14-08-0001-16439, by Technicolor Graphic Services, Inc., Sioux Falls, South Dakota.

8. Kauth, R.J., and G.S. Thomas, 1976. "The Tasselled Cap -- A Graphic Description of the Spectral-Temporal Development of Agricultural Crops as seen by Landsat," in: Proceedings of the Symposium on Machine Processing of Remotely Sensed Data, Purdue University, West Lafeyette, Indiana, (June-July).

9. Kriegler, F.J., W.A. Malila, R.F. Nalepka and W. Richardson, 1969. "Preprocessing Transformations and their Effects on Multispectral Recognition," in Proceedings of the Sixth International Symposium on Remote Sensing of Environment, Environmental Research Institute of Michigan, Ann Arbor, pp. 97-122.

10. Maxwell, E.L., 1976. "Multivariate System Analysis of Multispectral Imagery," Photogrammetric Engineering and Remote Sensing, Vol. 42, No. 9, September, pp. 1173-1186.

11. Ready, P.J., and P.A. Wintz, 1972. "Information Extraction, SNR Improvement, and Data Compression in Multispectral Imagery," IEEE Transactions on Communications, Vol. COM-21, No. 10, October, pp. 1123-1130.

12. Richardson, A.J., and C.L. Wiegand, 1977. "Distinguishing Vegetation from Soil Background Information, "Photogrammetric Engineering and Remote Sensing, Vol. 43, No. 12, December, pp. 1541-1552.

13. Rouse, J.W., R.H. Haas, J.A. Schell and D.W. Deering, 1973. "Monitoring Vegetation Systems in the Great Plains with ERTS," in *Third Earth Resources Technology Satellite-1 Symposium*, Vol. 1, NASA Goddard Space Flight Center, Maryland, pp. 309-317.

14. Shlien, Seymour, and David Goodenough, 1973. "Automatic Interpretation of ERTS-A Imagery Using the Maximum Likelihood Decision Rule," *Canada Centre for Remote Sensing Research, Report 73.2*.

15. Soha, J.M., and A. Schwartz, 1978. "Multispectral Histogram Normalization Constrast," in: *Proceedings of the Fifth Canadian Symposium on Remote Sensing, Victoria, British Columbia.* (August).

16. Strahler, A.H., 1981. "Stratification of Natural Vegetation for Forest and Range land Inventory Using Landsat Digital Imagery and Collateral Data; *International Journal of Remote Sensing*, Vol. 2, pp. 1515-41.

17. Strahler, A.H., T.L. Logan and N.A. Bryant, "Improving Forest Cover Classification Accuracy from Landsat by Incorporating Topographic Information," in *Proceedings Twelfth International Symposium on Remote Sensing of Environment*, Environmental Research Institute of Michigan, Ann Arbor, Michigan, pp. 927-942.

18. Strahler, A.H., T.L. Logan and C.E. Woodcock, 1979. "Forest Classification and Inventory System Using Landsat, Digital Terrain, and Ground Sample Data," in *Proceedings Thirteenth International Symposium on Remote Sensing of the Environment*, Environmental Research Institute of Michigan, Ann Arbor, pp. 1541-1557.

19. Vincent, R.K., 1973. "Ratio Maps of Iron Ore Deposits Atlantic City District, Wyoming," in *Symposium on Significant Results Obtained from the Earth Resources Technology Satellite-1*, Vol. 1, SP-327, NASA Goddard Space Flight Center, Greenbelt, Maryland, pp. 379-386.

20. Williams, D.L., M.L. Stauffer, and K.C. Leung, 1979. "A Forester's Look at the Application of Image Manipulation Techniques to Multitemporal Landsat Data," in *Fifth Machine Processing of Remotely Sensed Data Symposium*, LARS, Purdue University, West Lafayette, Indiana, pp. 368-376.

TABLE I - CLASSIFICATION AND DIVERGENCE RESULTS

Overall and individual classification accuracies for each of the fifteen tested data channels are provided below. Outlined boxes highlight the best channel for a given class category. Total divergence scores are not considered reliable.

	CHANNEL	Hd	DF_O	POP_O	WF_O	RF_O	RF_C	WF_C	DF_C	POP_C	MEAD	SPARSE	SMALL TREES	GRASS	SCALING	AVERAGE CONIFEROUS ACCURACY	AVERAGE OVERALL ACCURACY	TOTAL DIVERGENCE
1	$\frac{RAVE}{E2}$	$\boxed{19.0}$	$\boxed{18.1}$	0	11.1	$\boxed{29.7}$	$\boxed{19.2}$	12.8	5.2	9.4	$\boxed{16.6}$	$\boxed{37.4}$	0.5	0	110;60	13.2	13.8	1153
2	GN	15.6	11.1	0	$\boxed{17.0}$	2.1	$\boxed{19.2}$	$\boxed{21.0}$	12.7	$\boxed{10.3}$	7.6	13.7	0	$\boxed{19.3}$	-	11.7	11.5	690
3	RD	10.6	10.0	8.0	10.0	4.2	13.2	10.6	11.9	6.6	4.8	5.9	6.0	7.1	-	9.3	8.4	836
4	E/E2	15.3	7.4	0	16.4	17.0	15.6	3.0	0	1.8	0	3.6	1.1	11.5	100	7.65	7.1	952
5	5/6	6.9	5.9	4.5	5.8	12.7	10.8	6.7	11.5	0	9.0	9.2	8.8	6.2	90	7.2	7.5	760
6	RAVE	10.6	5.9	3.8	4.7	10.6	10.8	12.1	2.7	2.8	8.3	1.5	6.0	5.6	110	6.7	6.6	724
7	TVI6	8.3	5.1	6.2	8.2	8.5	9.6	6.7	8.3	0	5.5	1.7	9.9	3.4	200	6.6	6.3	755
8	IR2	9.2	5.1	4.5	6.4	14.8	9.6	0	6.7	4.7	0	5.8	1.1	2.1	-	6.5	5.4	645
9	$\frac{5/6}{E2}$	18.2	2.9	$\boxed{13.6}$	0	10.6	14.4	3.0	2.0	2.8	11.1	14.1	1.1	19.0	90;100	6.2	8.7	1025
10	5/4	10.1	7.4	0	11.1	0	0	8.2	$\boxed{14.3}$	2.6	7.6	11.8	0	3.4	100	5.5	5.9	711
11	RATSD	15.3	10.0	6.2	0	8.5	7.2	0	7.5	0	5.5	5.3	$\boxed{32.5}$	4.6	20	4.9	7.9	800
12	E2	5.7	4.8	3.1	5.8	6.3	0	8.8	4.3	2.8	4.8	5.3	3.3	5.0	-	4.5	4.6	794
13	PVI6	7.8	5.5	4.8	7.6	4.2	6.0	0	3.5	0.9	0	5.1	5.5	5.3	1.9	4.1	4.3	625
14	IR1	7.8	6.6	0	4.7	6.3	2.4	8.5	4.3	0	3.4	5.3	3.8	6.8	-	4.1	4.6	610
15	E1	1.7	3.3	1.3	2.9	2.1	1.2	0.9	0.7	0	2.0	6.1	2.2	3.4	-	1.6	2.1	662
Number of Training class Pixels		383	268	286	169	47	83	327	250	105	144	633	179	320				

TABLE II - PCA AND SCALING EFFECTS

Overall and individual classification accuracies for each of the fifteen tested data channels are provided below. PCA Test assumes (110;60) Scaling. Scaling test uses PCA factor loading of (.4648, .7847, -0.752 -.4032). Outlined boxes highlight the best channel for a given class category.

PCA TEST

HD	DF_O	POP_O	WF_O	RF_O	RF_C	WF_C	DF_C	POP_C	MEAD	SPARSE	TREES	GRASS	PERCENTAGE UNCLASSIFIED	AVERAGE CONIFEROUS ACCURACY	AVERAGE OVERALL ACCURACY	PCA FACTOR LOADINGS
19.0	18.8	$\boxed{9.4}$	12.3	29.7	18.0	10.6	4.0	$\boxed{9.4}$	15.9	37.6	0	0	33.2	14.0	14.2	.4648, .7847, -.0752, -.4031
19.9	16.6	0	8.8	0	18.0	10.0	$\boxed{5.2}$	$\boxed{9.4}$	15.9	36.8	0	0	47.5	8.5	10.8	.4648, .7847, -.0742, -.4021
18.4	19.6	0	9.4	0	16.8	13.4	3.2	5.6	17.3	36.8	0	0	45.9	8.5	10.8	.4648, .7847, -.0762, -.4041
19.3	18.8	0	10.5	0	18.0	12.1	3.2	5.6	16.6	36.8	0.5	0	45.5	8.5	10.9	.4638, .7837, -.0752, -.4031
21.0	15.9	0	9.4	0	18.0	12.5	4.7	5.6	15.9	23.9	0	0	51.5	8.3	9.8	.4658, .7857, -.0752, -.4031
15.0	12.2	0	9.4	0	0	7.9	4.7	2.8	16.6	29.2	0.5	15.0	56.9	4.6	8.7	.5000, .8000, 0, -.4000
14.1	16.6	0	0	0	10.8	10.9	2.7	3.7	15.2	29.7	0	$\boxed{27.8}$	52.1	5.6	10.1	10000, 20000, 0, -10000

SCALING TEST

HD	DF_O	POP_O	WF_O	RF_O	RF_C	WF_C	DF_C	POP_C	MEAD	SPARSE	TREES	GRASS	PERCENTAGE UNCLASSIFIED	AVERAGE CONIFEROUS ACCURACY	AVERAGE OVERALL ACCURACY	SCALING
4.0	5.5	0	7.0	10.6	8.4	3.3	1.2	0.9	4.8	21.7	$\boxed{1.1}$	13.7	71.1	4.6	6.3	200;100
10.6	10.0	0	8.2	0	12.0	7.0	1.2	2.8	9.0	24.7	0	10.6	62.3	5.2	7.4	200;60
11.[illegible]	10.3	0	5.8	0	10.8	9.4	2.3	5.6	10.4	24.8	0	13.4	59.8	5.5	8.0	100;100
15.8	18.8	0	0	$\boxed{34.0}$	$\boxed{24.0}$	13.1	4.7	8.4	21.5	22.6	0	17.1	38.0	12.9	13.8	100;60
$\boxed{22.2}$	$\boxed{23.7}$	0	$\boxed{15.8}$	0	$\boxed{24.0}$	$\boxed{17.6}$	4.3	7.5	$\boxed{22.2}$	$\boxed{38.7}$	0	0	29.9	11.6	13.5	100;50

Figure I - LOCATION MAP. The Doggett Creek study area is located in the Condrey Mountain 15 minute quadrangle near the town of Klamath River in Klamath National Forest, California.

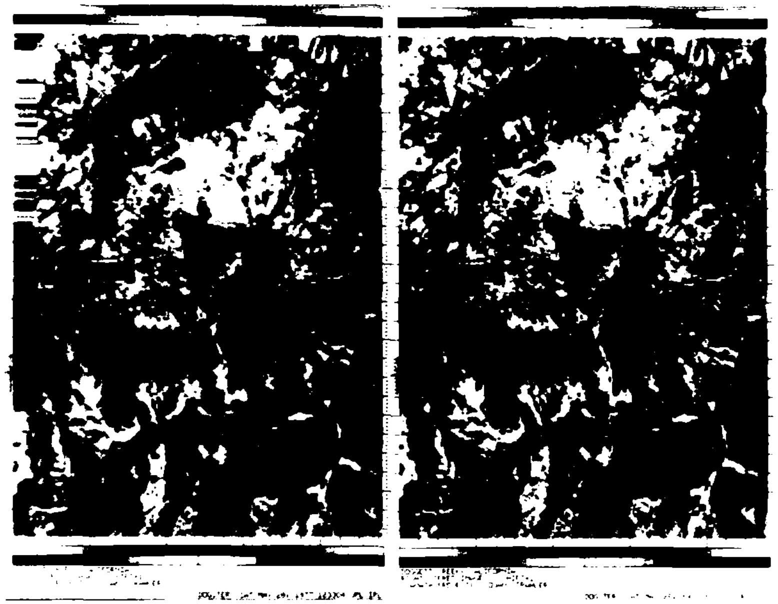

Figure 3 - MSS5. Landsat synthetic stereogram of the Doggett Creek study area showing the interplay of extensive topographic relief and the ecological relationships of forest vegetation reflectance values (DN). Parallax was artificially introduced by proportionally shifting pixels to the right based on their elevation.

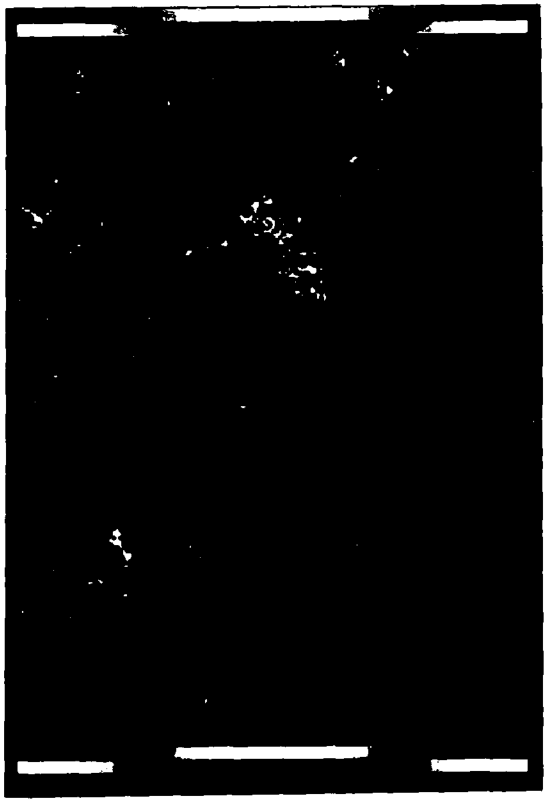

Figure 2 - SATURATED PIXELS. MSS5/E2 unenhanced transform channel showing the saturated white and black pixels that occasionally occur when Landsat or ratioed Landsat data is divided by the second principal component. Saturated pixels represent areas of unusual contrast between Landsat bands. Any saturated pixel falling into a training site used for divergence analysis would significantly alter statistical means rendering the technique unreliable.

Figure 4 - RAVE/E2. This transform represents the ratio of the four Landsat band averages divided by the second principal component of the four bands. It was the only transform to gain in information content relative to Landsat MSS4. Comparison with Figure 3 of the upper middle-right edge shows how the grey tones of similar timber types on opposite slopes are equalized in the RAVE/E2 channel.

Figure 5 - EIGEN 1. The principal component (Eigenvector 1) of Landsat PCA highlights the reflectance differences between spectral channels due to wavelength, and therefore contains only marginal vegetation information. Comparison of this channel with the topographic stereogram of MSS5 (Figure 3) shows the strong correlation with relief typical of most eigenvector 1 images.

Figure 6 - EIGEN 2. Comparison with the first eigenvector (Figure 5) shows how the second eigenvector from Landsat PCA displays the subtle variations within image features, with most interband wavelength contrasts removed. The combination of PCA data compression with conventional rotioing of Landsat bands produces a potentially useful synergism.

LANDSAT AND COLLATERAL DATA AS AN AID IN DETERMINING FUEL-BED PROPERTIES FOR WILDFIRE SIMULATION PURPOSES

Michael J. Cosentino

University of California
Santa Barbara, California

SUMMARY

When broad expanses of fire-prone vegetation are in close proximity to, and intermingled with, urban areas, uncontrolled wildfires constitute an immediate danger to lives, homes, property, and natural resources. Other dangers persist into the rainy season when burned slopes, lacking in protective vegetative cover, are susceptible to rapid runoff, soil erosion, and landslides. Wildfires can have catastrophic consequences and require proper planning and swift suppression to keep damages to a minimum. This necessitates that land managers be able to predict fire behavior in order to effectively deploy firefighting resources.

The behavior of fire in natural vegetation is influenced by the structure, composition, and size distribution of the vegetative biomas. In order to predict fire behavior (fire spread rate and heat release) using existing mathematical models, the vegetation must be categorically described in terms of several physical parameters including the distribution of the living and dead biomass by size-class.

The Geography Remote Sensing Unit at the University of California, Santa Barbara and the United States Forest Service are conducting cooperative research to map the physical characteristics of the vegetative fuels for a 6.5 million hectare (16 million acre) area in Southern California using remotely sensed and collateral data. The final classification will comprise a fuels database for fire simulation by the U.S. Forest Service's FIRESCOPE Program (Firefighting Resources of Southern California Organized for Potential Emergencies). FIRESCOPE was organized to coordinate multi-agency fire suppression efforts in Southern California, and fire simulation and modeling are integral components of a program which includes digital terrain modeling and automated weather monitoring.

Initial testing is being conducted on a 7.5 minute quadrangle in the Santa Ynez Mountains northwest of Santa Barbara, California. This test site is a small portion of the FIRESCOPE Program area and is characterized by diverse topography, a Mediterranean climate, with mild wet winters and warm dry summers. There is a wide array of cover types in the test area, and these typify most of the diversity in Southern California fire-prone areas.

Unsupervised training procedures are being used to produce a physiognomic classification of vegetative fuel types (communities or species associations) and densities (percent crown closure). The assumption is that fuel densities will indicate areas of homogeneous biomass which are further partitioned by fuel types to indicate size-class differences. These physiognomic classes can then be further stratified using fire history data (time since last burn) as an indication of the age of the vegetation to estimate height and percent dead. Six input data channels, represented by four raw Landsat reflectance channels, one synthesized Landsat "texture" channel, and one terrain-derived solar illumination channel, are being utilized with highly detailed clustering procedures.

These procedures result in numerous spectral classes which are constrained to represent very small portions of measurement space such that several spectral classes may comprise a single physiognomic class. These physiognomic classes, which are actually fuel type and density strata, can be further partitioned by overlaying digitized fire history data. Ground plots may then be allocated, using a stratified sampling approach, for detailed measurements of fuel parameters.

For this project, the normal procedure for deriving a standard deviation "texture" image was modified to operate on a ratio image of Landsat bands 7 over 5, rather than the typical band 5 alone. The rationale being that since these ratio values correlate well with vegetative biomass, standard deviation values derived from a three-by-three moving window will indicate whether a pixel lies within an area of change or stability in biomass characteristics.

Another unique component of this project is the use of a solar illuminated terrain channel, derived from a high resolution (30 meter) digital terrain image, which is processed to represent the expected solar illumination at the time of the Landsat overpass. By incorporating the solar illuminated terrain data as a pseudospectral channel, the resulting classes are constrained to include pixels which are not only similar spectrally, but also have the same illumination characteristics. This approach should help overcome the "shadowing" problems inherent in the classification of Landsat data in areas of high topographic relief.

SMALL GRAINS AREA ESTIMATION FOR TRENQUE LAUQUEN PARTIDO USING DIGITAL IMAGE PROCESSING TECHNIQUES

Claudia GARGANTINI

Comisión Nacional de
Investigaciones Espaciales
Buenos Aires, Argentina

ABSTRACT

An efficient methodology for production forecast is very important in an agricultural country like Argentina. This paper describes a first attempt to develop a methodology based on digital LANDSAT analysis for small grains area estimation in a pilot area of the Pampa Húmeda, which is the main crop area of the country.

1. INTRODUCTION

Agricultural production is one of the main activities in Argentina, for this reason it is very important to develop a fast and efficient methodology to estimate crop production accurately to improve the conventional techniques.

This work is being carried out within the United Nations Development Programme for crop production estimation in the Pampa Húmeda area.

This paper presented is focussed in one of the three pilot areas selected for the first step of the project programme: the Trenque Lauquen Partido. This area is located west of Buenos Aires Province and covers about 550,000 hectares. The main crops in the area are wheat, corn, sorghum and sunflower and it is a region where agricultural activity and cattle have the same importance.(Fig. N°1)

2. GOALS

The main goal of this work is the wheat area estimation for Trenque Lauquen Partido using digital image processing techniques to be compared the results with the annual estimation results provided by the Agricultural Ministry.

The importance of this paper is the possibility of proving a methodology for our country in three pilot areas and improving it to be applied lately in the crop area estimation for the whole Pampa Húmeda.

3. MATERIALS AND METHODS

It has been used for this study one CCT corresponding to the coordinates 243-085, dated October 9th., 1981, the only one available within the wheat growing season. The phenological stage for that special date is heading. This CCT covers the 91% of Trenque Lauquen Partido.

A trip of four days to the field, to the area of interest has been realiz-

ed in October 22nd.

Each one of the segments located in the partido by a random sampling design prepared by the MAG for their annual periodic production estimates, has been visited. These segments cover approximately 10% of the total area of the Partido, and they have been determined by the MAG without any previous stratification based on LANDSAT data.

Each one of the farms belonging to the segments has been visited and maps with the location of fields, in most of cases provided by the farmers have been filled with the ground truth data (crop, planting date, and phenological stage).

For the location in the field it has been used a map of the partido with the boundaries of each farm with the owner's names, provided by the MAG with the segments drawn in it.

It has been used too a LANDSAT image of 1:250,000 that because of the big size of the fields of this area (average 100 has.) it was more useful than the topographic maps 1:100,000 used in other areas of Buenos Aires Province with an intensive agricultural use and with small sizes of fields. In some cases it has been used two photographs of some of the segments taken from the monitor, being as good or better material than aerial photographs.

Once finished this first step, the digital image processing with the PI System, developed in CNIE has been done.

A subimage with the area of interest has been created delineating the boundaries of the Partido in the original image.

Once being this done the segments were located and the unsupervised classifier algorythm was applied in one of the segments. Two different classes of wheat were separated by the clustering with very different values in bands 6 and 7, the rye was confussed with wheat: pastures and two classes of bare soil (one seeded and the other ploughed) were separated.

The training sites to be used in the analysis were selected applying the clustering results. The spectral separability of the training sites was evaluated using hystogram analysis, spectral coincidence maps for the different classes, confusion matrix and covariance matrix. Figure N°2, Table N°1. show the statistics of the different polygons (fields) and the similarity between wheat and rye.

After the statistics were analysed and the training sites were chosen for the classification performance, an accuracy evaluation was done by classifying the rest of the segments. (Fig. N° 3)

The classification of the segments for the accuracy evaluation was done in 7 of the 12 segments, because almost the total area of 3 of them were located within the 9% of the Partido not covered by the image, other segment was impossible to be visited and the other showed a confussed spectral behavior.

Once being this done the whole Partido area was classified, and the results were evaluated and matched against the ones obtaining at the Ministry of Agriculture by the conventional method by the use of non remote sensing techniques.

4. RESULTS

The confusion matrix of the polygons used in the classification (Table N° 2) shows the two classes of wheat, and the spectral separability of pastures, bare soil (seeded) and fallow. The rye is completely confussed with wheat, for

that reason in the classification they were used as a unique class.

The classification of the seven segments showed an excellent behavior in the segment to which the training sites used belonged, and in the segments close to the first one; although the results were good too in the segments more separated in distance from the first one, they were not as good as in the others.

After the accuracy evaluation was done the whole partido was classified with for polygons, the two classes of wheat and rye as one class and pasture as a second class.

The first result was 126,797 pixels of wheat + rye, 62,000 hectares, this value belongs to the 91% of the total area of the Partido covered by the image.

As three of the segments belong to the rest of the area, 3.7% of the 9% were covered by ground truth and there were in it 1600 ha. of wheat and 650 ha. of rye, and without any statistics criteria, but by a simple extrapolation the result for this 9% of the area was 3600 hectares of wheat and 1600 hectares of rye.

The final result for the whole Partido of Trenque Lauquen was 67,200 hectares of wheat and rye.

To evaluate the accuracy of the classification, a regression analysis was realized and the result was a regression coefficient = 0.89, which is reasonable value of acceptability. Figure N°4.

5. CONCLUSIONS AND RECOMMENDATIONS

- The annual periodic acreage estimation done by the Ministry of Agriculture for Trenque Lauquen Partido was 60,000 hectares for wheat and 9,000 hectares for rye.

The comparison between the total value of 69,000 ha. with the conventional method and the 67,200 ha. estimated with the digital analysis shows the similarity of both values.

Although the best way to compare the results of the classification analysis would be to have a complete census of the Partido, the only data available to be compared was this one provided by the Agricultural Ministry.

- The spectral separability of wheat and rye is almost impossible if it is considered that the planting and harvesting dates of both crops are very similar. It would be possible to separate with a multitemporal analysis the portion of double purpose rye which is planted in March for pasture first and is harvested then for grain. But anyway it is not a solution for wheat estimation, it doesn't discard the rye at all, because the one planted in July for grain would be confussed with wheat. For that reason, in the present paper they have been estimated together.

It has been reviewed the historical data to see if the relation between the areas planted with the two crops had been constant in the last ten years to allow knowing for future estimation which percent of the total value belongs to each crop. But the behavior of wheat and rye was different from one year to the other.

- The fact that the bigger the distance between the original segment and the other ones was, the less efficient the classification performance resulted, shows clearly that a previous stratification based on LANDSAT is necessary for a new sampling design. A roughly visual analysis of the Partido in the LANDSAT image shows two different areas, one in which the percent of agriculture is lower than in the other associated to a more defficient drainage pattern.

It is very important that future estimations will be done based on a new samping design based on stratum, and not based on administrative limits.

6. ACKNOWLEDGEMENTS

My gratitude is for the Dipl. Eng. Severino Fernández and Dipl. Eng Marcelo Campi for the PI system by them developed which gave me the possibility of realizing this work.

A special word of thanks goes to Dipl. Eng. Severino Fernández for his help and assistance in the use of the different programmes of the PI System.

7. LIST OF REFERENCES

- Schubert J.S. and Chagarlamudi, P. "Development and Evaluation of Methods for Estimating Rapeseed Acreage.
- Schubert, J.S. "The Canada Land Inventory".
- Craig, M.T.; Sigman, R.S.; Cárdenas, M. "Area Estimates by Landsat: Kansas 1976 Winter Wheat".

Polygon Statistics
15. Wheat-LAN 1

Mean values

Channel:	1	2	3	4
	22	25	52	66

Covariance matrix

Channel:	1	2	3	4
1	1	0	0	0
2	0	2	-1	-1
3	0	-1	4	4
4	0	-1	4	9

Polygon Statistics
3. Wheat-LAN 1

Mean values

Channel:	1	2	3	4
	22	24	61	83

Covariance matrix

Channel:	1	2	3	4
1	1	0	0	0
2	0	2	0	-1
3	0	0	6	5
4	0	-1	5	12

Polygon Statistics
1. Rye-LAN 1

Mean values

Channel:	1	2	3	4
	24	28	54	68

Covariance matrix

Channel:	1	2	3	4
1	1	1	0	-1
2	1	4	0	-1
3	0	0	3	1
4	-1	-1	1	7

Polygon Statistics
10. Pasture-LAN 1

Mean values

Channel:	1	2	3	4
	25	30	79	111

Covariance matrix

Channel:	1	2	3	4
1	2	0	1	1
2	0	2	1	2
3	1	1	9	8
4	1	2	8	13

Polygon Statistics
1. Fallow-LAN 1

Mean values

Channel:	1	2	3	4
	29	44	49	57

Covariance matrix

Channel:	1	2	3	4
1	3	3	3	2
2	3	10	6	5
3	3	6	10	7
4	2	5	7	12

Polygon Statistics
1. Seeded-LAN 1

Mean values

Channel:	1	2	3	4
	21	27	29	32

Covariance matrix

Channel:	1	2	3	4
1	1	0	0	0
2	0	1	0	1
3	0	0	3	2
4	0	1	2	5

Table N° 1

	3. Wheat LAN 1	15. Wheat LAN 1	1. Rye LAN 1	10. Pasture LAN 1	1.Seeded LAN 1	1.Fallow LAN 1
3. Wheat-LAN 1	92	1	7	0	0	0
15. Wheat-LAN 1	1	83	15	0	0	0
1. Rye-LAN 1	2	26	72	0	0	0
10. Pasture-LAN 1	0	0	1	99	0	0
1. Seeded-LAN 1	0	0	0	0	100	0
1. Fallow-LAN 1	0	0	0	0	0	100

Table N°2. Confusion Matrix

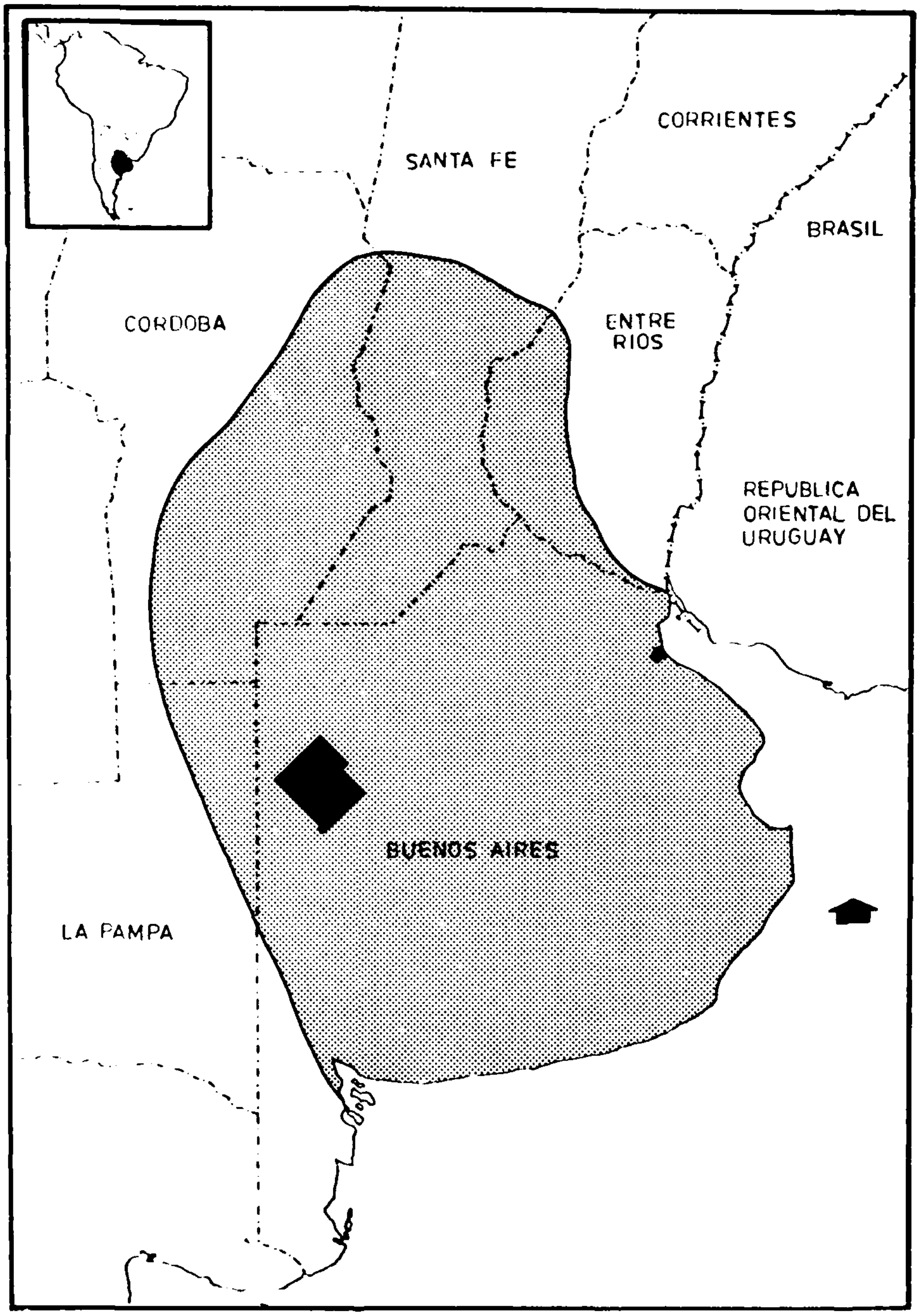
CORRIENTES
SANTA FE
BRASIL
CORDOBA
ENTRE RIOS
REPUBLICA ORIENTAL DEL URUGUAY
BUENOS AIRES
LA PAMPA

Fig. N° 1

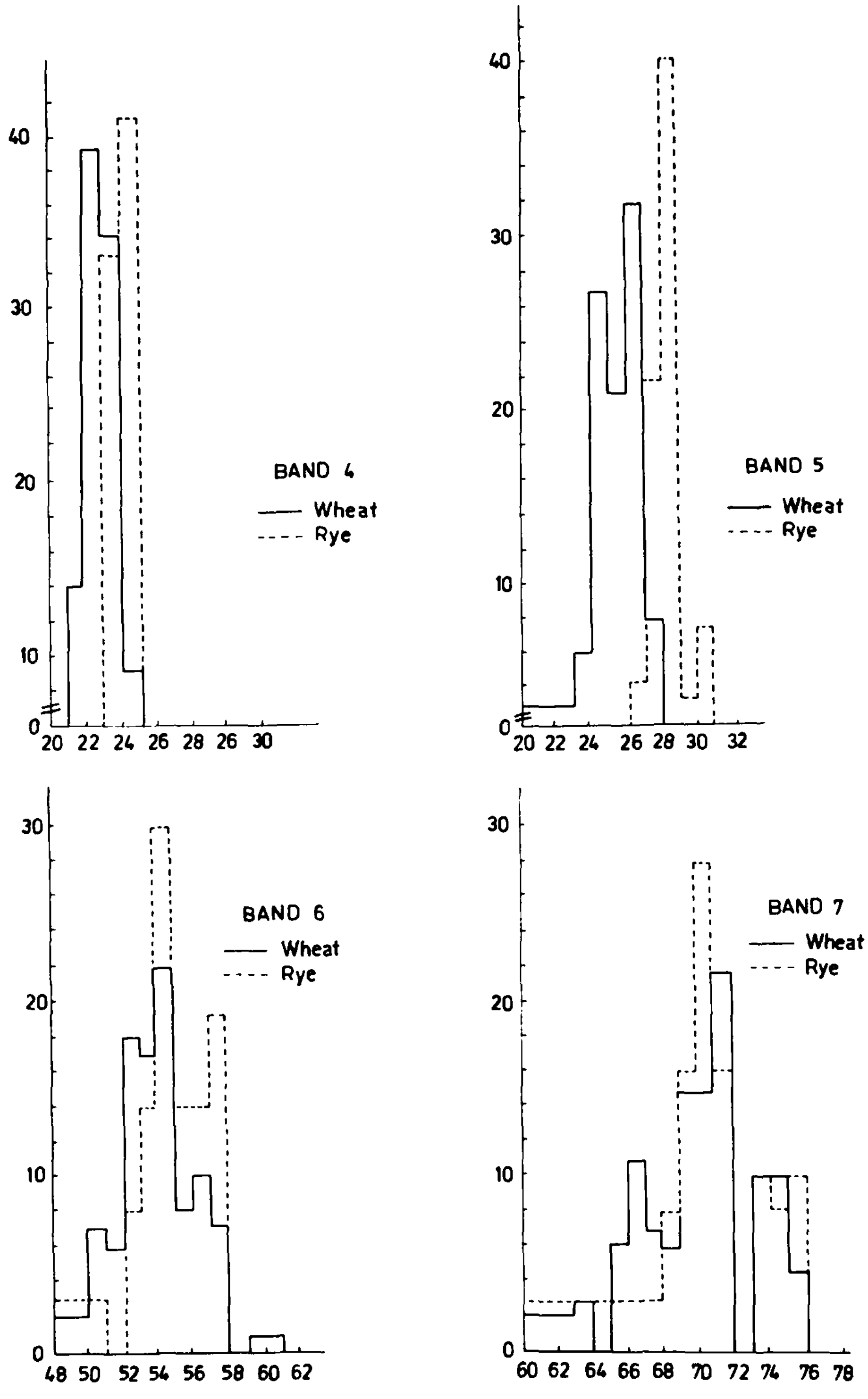
BAND 4
Wheat
Rye
40
30
20
10
0
20 22 24 26 28 26 30
BAND 5
Wheat
Rye
40
30
20
10
0
20 22 24 26 28 30 32
BAND 6
Wheat
Rye
30
20
10
0
48 50 52 54 56 58 60 62
BAND 7
Wheat
Rye
30
20
10
0
60 62 64 66 68 70 72 74 76 78

Fig. N° 2

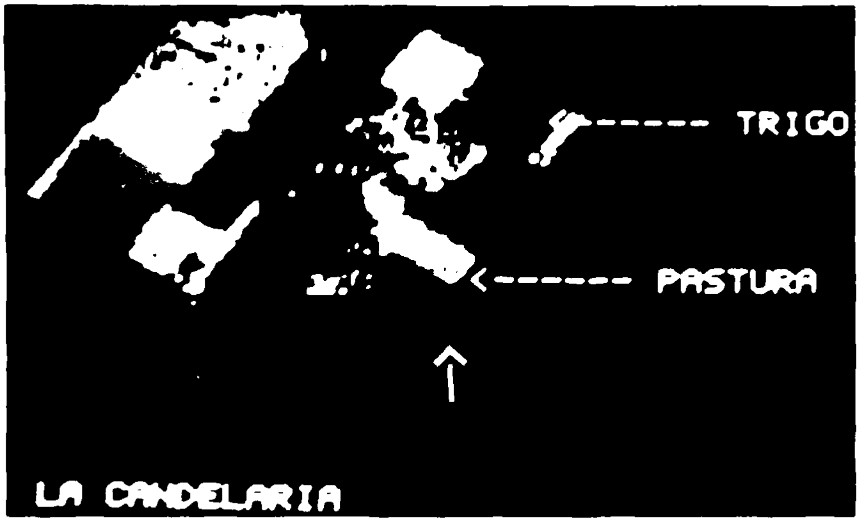

Estancia "LA CANDELARIA"

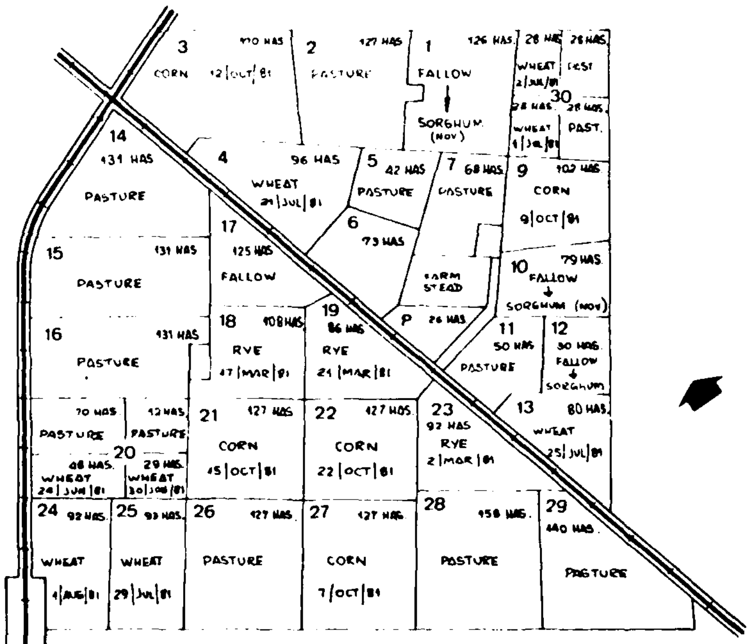

Fig. N° 3

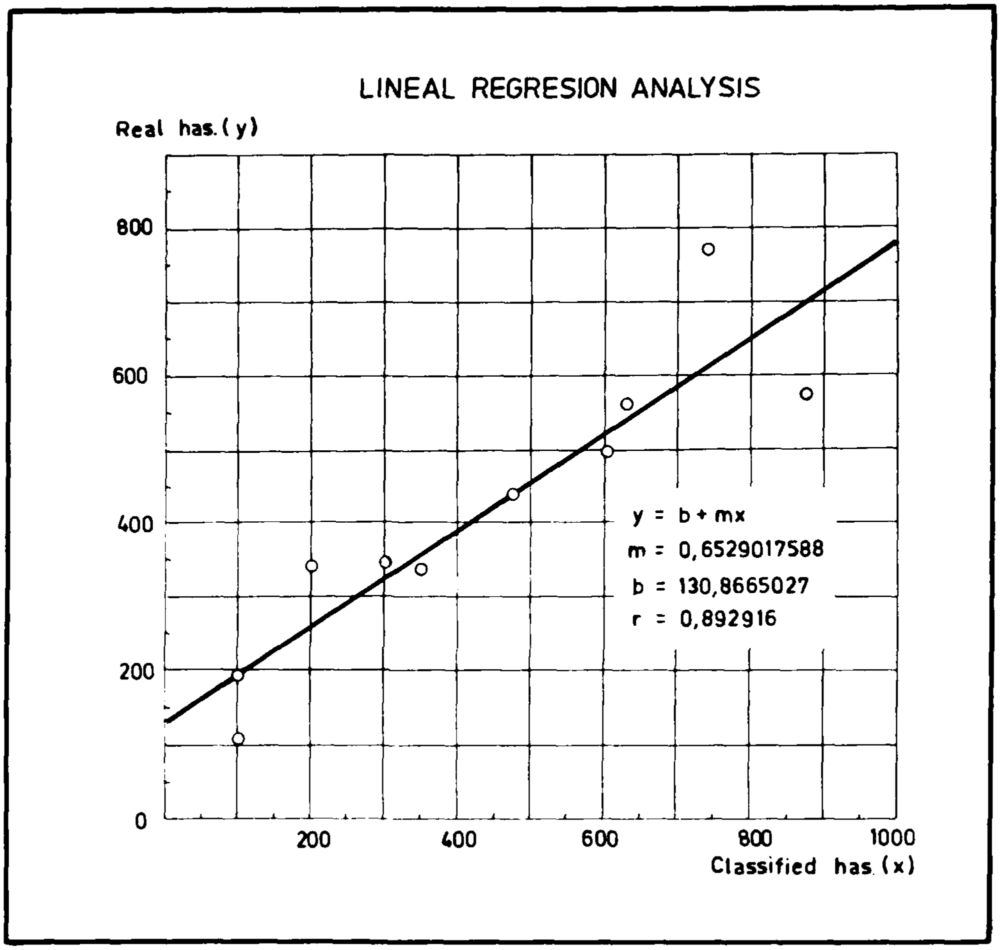
LINEAL REGRESION ANALYSIS
Real has. (y)
800
600
400
200
0
200
400
600
800
1000
Classified has. (x)
y = b + mx
m = 0,6529017588
b = 130,8665027
r = 0,892916

Fig. N° 4

LANDSAT-RELATED STUDY FOR THE MALI LAND USE INVENTORY IN WEST AFRICA*

C.S. Bingham, S. Bouaré and D. Thom

Tippetts-Abbett-McCarthy-Stratton
New York, N.Y., USA (Bingham and Thom)

Ministry of Rural Development of
the Government of the Republic of Mali (S. Bouaré)

ABSTRACT

This paper discusses the mapping and analysis of existing land use and population distribution within the framework of an integrated resource inventory and evaluation--the Mali Land Use Project. Discussion of legend development illustrates the problems of classifying, at the scale of 1:500,000, land uses associated with traditional production systems. The mapsheet of Mopti and its environs is used to portray how differing resource characteristics have contributed to contrasts in population density and patterns of human exploitation.

1. BACKGROUND

Mali's National Institute of Zootechnical, Forestry and Hydrobiological Research of the Ministry in Charge of Rural Development is implementing the Mali Land Use project with funding from the U.S. Agency for International Development and technical assistance from the French Fund for Aid and Cooperation. The firm of Tippetts-Abbett-McCarthy-Stratton (TAMS) and its subcontractors, the Environmental Research Institute of Michigan (ERIM) and American Ag International, have supplied technical consulting services.

Mali depends upon its agricultural and rangeland resources for subsistence and the bulk of its employment and exports, but has lacked a comprehensive and consistent data base to help identify, select and plan their development. The project provides an integrated summary of resource information in the Mali Land and Water Resources Atlas, accompanied by a technical report. The Atlas uses consistent classification schemes and legends; its maps and overlays are presented all at the same scale. Coupled with the establishment of a natural resources data bank in Bamako and a training component, the project lays the foundation to guide development of Mali's natural resources.

The project area covers 582,800 square kilometers, all of Mali south of the Niger River and a limited area to the north as illustrated next.

*Presented at the Seventeenth International Symposium on Remote Sensing of Environment, Ann Arbor, Michigan, May 9-13, 1983.

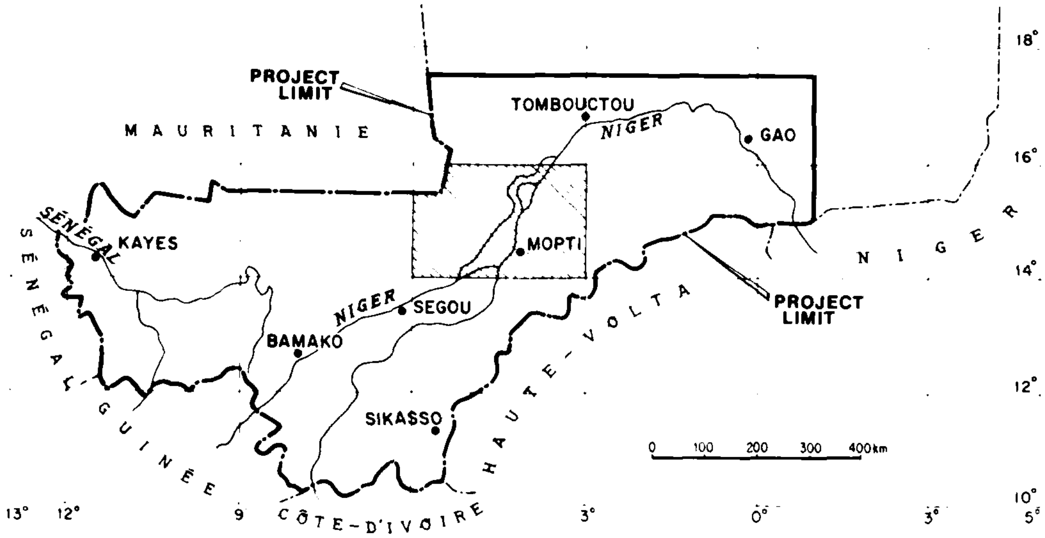

Figure 1. Mali Land Use Project Area

The study relied upon Landsat images and field work to cover this area, in two and a half years. Sixty-five Landsat false color images, geometrically corrected to conform to 1° x 1° topographic maps of the Institut Geographique National at the scale of 1:200,000 were produced from computer compatible tapes obtained from the EROS Data Center. 1/ These images served as the medium to delineate preliminary resource units and record field interpretations. Reconnaissance surveys, extensive ground truthing and analysis of aerial photography permitted verification of image interpretations and, based on similarity of signatures, interpolation for inaccessible and remote areas. Color images at the scale of 1:500,000 facilitated the transfer of information from the 1:200,000 field sheets to the base maps used for publication, black and white imagery mosaics produced from Band 7 and corresponding to IGN topographic maps at the scale of 1:500,000.

The resource inventory includes maps of soil/vegetation units containing soil taxonomic units, classified according to the U.S. soil classification system, and keyed to vegetation descriptions. Water resource maps illustrate precipitation, groundwater resources and surface water characteristics. Maps of existing land use were prepared with transparent thematic overlays of population distribution. The technical report describes these themes as well as crop yields, range productivity, agricultural and grazing practices, agroclimatology, economic characteristics of the agriculture and livestock sectors and land tenure.

The analysis of resource potential focuses on suitability of lands for crops and range at differing levels of technological input. Transparent

---

1/ The Environmental Research Institute of Michigan provided all image products.

overlays portray: (1) soil or land capability based upon the USDA's Land Capability Classification, adapted to suit Mali's environmental conditions; and (2) zones with potential for irrigation and/or groundwater exploitation and precipitation constraints. In addition to resource plans, subsequent steps made possible by this data base include: long-term monitoring of soils and vegetation sampling sites; pilot plans to demonstrate application of various analytical techniques; and transfer of resource information to a geographic information system.

This paper focuses on the mapping and legends for population and land use and the interpretation of the Mopti mapsheet, one of the eleven produced in the Atlas.

2. METHODOLOGY: POPULATION AND LAND USE

2.1 LAND USE MAPPING AND LEGEND

Differing colors, tones, textures, spatial arrangement and other visual clues on the Landsat imagery, dating largely from November and December 1975 and 1976, were the basis for preliminary delineation of mapping units. Interpreters' familiarity with the landscape and repetitive patterns permitted classification of the units according to a preliminary legend. Extensive field checking by ground and air was undertaken to verify the image interpretation. When necessary, the mapping unit was reclassified and adjustments were made to the preliminary legend to produce the final legend. Population maps provided a cross-check on imagery interpretation of agricultural density and topographic maps helped to identify roads and landforms. Cattle routes were traced with the aid of imagery and secondary sources.

Three issues arose in land use mapping and legend development. First, a land use map derived from satellite imagery depends upon the interpretation of land cover, but land cover is not always synonymous with land use. Second, Mali's production systems tend to be a subsistence level, non-commercialized, complex of associated activities. Exclusive, homogeneous categories of land use do not generally exist, aside from areas of very low rainfall where only livestock raising is possible and development projects of irrigated agriculture. Thus, a classification system either is messy or distorts reality. Third, the small map scale of 1:500,000 exacerbates the problems of showing a composite of land uses and of formulating a classification. Therefore, a fractional code using alpha-numerical symbols was devised to portray the multiple features of each mapping unit in the following format:

Land Use Type/Site	Distribution/Density
Crops	Livestock

<u>Land use types</u> are divided into three major categories which roughly correspond to three principal climate zones of Mali: livestock raising, including both nomadic and transhumant types of pastoralism, above the 400 mm isohyet; an agro-pastoral zone where both pastoralism and agriculture occur in different degrees; and below the 700 mm isohyet, a dominantly agricultural zone, associated with sedentary livestock raising. Where agriculture occurs, cultivation is classed as rainfed or irrigated. Four modes of irrigation are distinguished: natural flooding or submersion for crops such as rice; partially controlled flooding; total or modern water control; and recessional (décrue) flood irrigation in which crops, sown after floodwaters fall, benefit from residual moisture in the ground.

<u>Site</u> identifies utilization according to physiographic characteristics for agriculture and vegetation for pastoralism. On the imagery, cleared or cultivated areas, including recent fallow, have a white/yellowish color; they can follow river valleys, appear between dunes, or in other ways systematically relate to landform. In pastoral zones, localization of the land use

with respect to vegetation as well as physiography proved to be the relevant descriptors.

Distribution refers to the pattern of cleared or cultivated land within the unit or the physiographic site. For example, on the imagery, cultivation of stream valleys can appear as a continuous band, or discontinuous, as beads strung out along a valley. Modern irrigated agriculture, typically intense, occurs in a continuous pattern. A dispersed pattern refers to relatively large, scattered patches of cultivation.

Density, ranked in four categories, refers to the proportion of the mapping unit that is cleared or cultivated, as estimated from the images.

Crops grown and livestock raised are noted on the maps in order of their importance, based on the field investigations and secondary sources.

The complete legend is shown below in Table I.

TABLE I. LAND USE LEGEND

LAND USE TYPE

100	PASTORAL	300	AGRICULTURAL
110	Pastoral Production	310	Mixed Agriculture
		311	Rainfed Cultivation
200	AGRO-PASTORAL	312	Irrigated Cultivation
210	Pastoralism Dominant		
211	Rainfed Cultivation	400	BUSH PASTURELAND
212	Irrigated Cultivation		
220	Agriculture Dominant	500	UNUSED
221	Rainfed Cultivation		
222	Irrigated Cultivation		

Mode of Irrigation

a	Natural Submersion Flooding, Depressions	c	Total Water Control
b	Controlled Flooding	d	Flood Recession

SITE (LOCATION)

1.00	CULTIVATION	1.60	Lacustrine Zone
1.10	Plain	1.70	Dunes
1.11	Depression	1.71	Interdune
1.12	Levee	1.72	Interdune and on dunes
1.13	Other	1.73	Old worn dunes
1.20	Flood Plain		
1.21	Alluvial terrace	2.00	LIVESTOCK RAISING
1.22	Depression	2.01	Brousse tigrée (Tiger bushland)
1.30	Valley	2.02	Dunes/Interdune
1.31	Depression, valley bottom	2.03	Sandy plain
1.32	Pediment	2.04	Swampland
1.33	Valley terrace	2.05	Denuded Zone (reg)
1.40	Hills	2.06	Denuded Zone (transhumance route)
1.41	Summit	2.07	Depression in valleys & wadis
1.42	Slope	2.08	Bourgoutières
1.43	Summit & slope	2.09	Dry lakes
1.50	Delta	2.10	Pasture on hills or plateaus
1.51	Inactive delta	2.11	Mixed zone
1.52	Active delta		

DISTRIBUTION

1. Continuous 2. Discontinuous 3. Dispersed

DENSITY

1. 0-10% of mapping unit cleared or cultivated
2. 11-30% cleared or cultivated
3. 31-60% cleared or cultivated
4. > 60% cleared or cultivated

CROPS AND LIVESTOCK

Crops*		Livestock
Mi - Millet	Ct - Cotton	b - cattle
So - Sorghum	Se - Sesame	o - sheep
N - Niébé (cow peas)	D - Dah (Jamaica sorrel)	c - goats
Ms - Maize	T - Tobacco	ca - camels
Rz - Rice	Fo - Fonio (Foxglove)	p - hogs
B - Wheat	Tu - Tubers	
Pt - Bambara peas	Cl - Calabash	
A - Peanuts	Ma - Vegetable Gardening	
P - Plantains	V - Orchards	
Cs - Sugar Cane	Th - Tea	

*Some crops have no common English equivalents. Abbreviations are based on French crop names.

OTHER

Classified Forest and National Parks (Blue)

Existing Irrigated Perimeters over 50 ha I

Generalized Transhumance Route ⟶

2.2 POPULATION MAPPING AND LEGEND

The 1976 Census of Mali, listing the populations of over 10,000 villages and nomadic tribes by arrondissement (smallest administrative unit), provided data for mapping. IGN topographic maps at the scale of 1:500,000 served as working maps upon which villages were located along with the notation of their size. Because all villages did not appear on IGN maps and because spelling discrepancies impeded identification or several villages bore the same or very similar names, census takers' enumeration maps were obtained in order to match names with locations by correlating features common to both maps. Neither census takers' maps nor arrondissement limits were available for parts of the northern study area; therefore, approximate limits were established by plotting locations of known places; population groups, mostly nomadic, were then mapped in the arrondissement of enumeration.

The legend, shown in Figure 2, is based on the following criteria. First, representation of actual settlements rather than density by area was chosen to avoid loss of detail and to illustrate settlement with respect to landform, administrative centers and water sources. Second, the service criteria of government agencies were examined to see if cut-off points for services would provide appropriate breaks for population size classes. Third, the distribution of settlement sizes, along with the service criteria, resulted in the selection of ten size classes, represented by circles proportional

to population class, with the exception of Bamako, the only example in the largest class. Its population size (six times greater than the next largest place) rendered proportional representation awkward. Fourth, legibility dictated the choice of open circles on a transparent overlay to permit use of the overlay with the land use base map and with other thematic maps. The mapping scale proved adequate to show all settlements, proportionally, by using a 2 mm diameter circle for the smallest class. Preliminary mapping of the Mopti mapsheet, with the highest settlement concentration, demonstrated that arbitrary reduction of the smallest circle size to 1 mm made a more legible map. Lastly, to assist in the identification of surroundings, the maps carry symbols and place names denoting the chief places of Mali's administrative districts (7 regions, 46 cercles and 281 arrondissements). Because of the problems in mapping some population groups, e.g., nomads, they are shown symbolically inside a box, placed in the arrondissement of enumeration, to indicate ambiguous location.

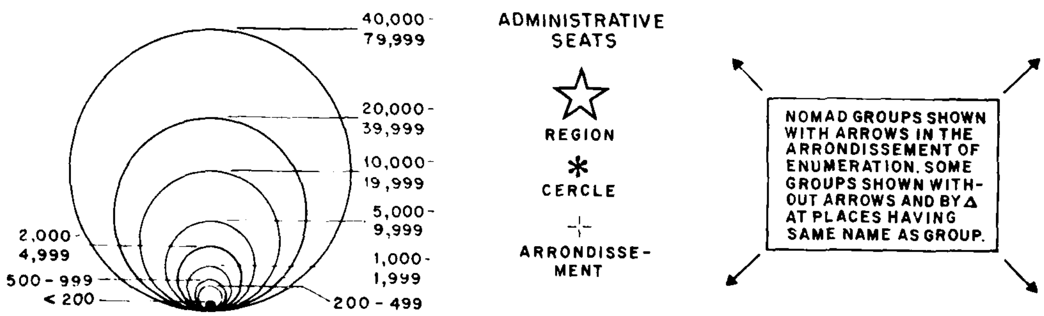

Figure 2. Population Legend

Final maps were derived by applying the circle legend to transparent overlays placed atop the working maps. Village locations were adjusted to compensate for differences between the IGN paper map and the black and white mosaic, thereby achieving proper village placement with respect to topography. Prior to placement of names, a list of all variant spellings (IGN, Census, official ordinance, other sources) was prepared and criteria adopted to ensure consistent spelling of place names.

3. ANALYSIS OF LAND USE AND POPULATION: MOPTI MAPSHEET

The mapsheet of Mopti and its environs mostly covers Mali's Fifth Region (Mopti) and small parts of other administrative regions. The mapsheet not only presents sharp contrasts in population distribution and land use types, but contains some of the most productive and densely populated zones of Mali. Physiographic differences and the interspersing of different ethnic groups have resulted in a variety of production systems that influence land use and population distribution. Physiographic conditions, at a very gross level, appear to be the principal determinant of production systems and, in turn, land use. Ethnic group tradition also influences the type of production system, since particular ethnic groups in Mali tend to be associated with

particular modes of life, e.g., pastoralism or agriculture. [2] The physiographic regions are used as the organizing framework for this discussion of population and land use. The major physiographic regions include the Séno-Gondo Plain, the Bandiagara Plateau, the Inland Delta and the Lakes Region.

3.1 SENO-GONDO PLAIN

The Séno-Gondo Plain, located in the southeast corner of the Mopti map, is populated by the Dogon, a people confined to the Bandiagara Plateau prior to the colonial period, and the Peul. With the end of interethnic hostilities during the colonial period and in response to needs for more land, the Dogon have moved east onto the plain where they practice rainfed agriculture. The Peul, in this milieu, engage in transhumant pastoralism (fixed villages from which herders take livestock on seasonal itineraries according to available pasturage) and some agriculture. Cultivation is practiced between the dunes and on the worn dunes which comprise the plain. Density of cultivation and population is low immediately adjacent to the plateau's escarpment. Cultivation becomes denser (31 to 60% of the mapping unit) to the east; population densities are also relatively high, ranging from 20 to 40 persons per square kilometer, and the distribution of settlements is relatively homogeneous over this part of the plain. Bush-fallowing practices result in fallow periods of five to eight years followed by cultivation for four to six years. Millet is the dominant subsistence crop; sorghum, niébé, dah, peanuts, fonio and sesame are grown as secondary crops. Farmers mostly grow two or more crops in the same field at the same time and often rotate crops over a four-year period in a sequence including millet, sorghum and dah the first year, followed by millet, dah and niébé the second year, with a change to peanuts or fonio the third and fourth years. Although the traditional land tenure system of the Peul and Dogon does not permit the land's alienation (disposal of property rights), selling of land in this area, while not common, is a notable exception to rural custom.

3.2 BANDIAGARA PLATEAU

Despite the rocky, shallow soils of the Bandiagara Plateau (west of the plain), the Dogon cultivate valley floors and slopes of valleys where streams flow off the escarpment. The concentration of cultivation, villages and population is along the edge of the escarpment. Population densities in Sangha and Douro are respectively 60 to 90 persons per square kilometer where relatively small villages are suspended like acrobats in rocky cliffs. The lack of soils and especially water, along with social changes, have not only stimulated outmigration but resulted in relatively intense management of limited space and resources. From east to west of the cliff's edge, population densities diminish from 30 to 40 persons per square kilometer to as low as 10 to 15, in a pattern of scattered villages larger (more than 350 persons) than those on the cliff. Because cultivation is limited to the stream slopes and valleys, density of cultivation is low--10 percent or less of a land use unit. Millet and sorghum are the dominant food crops, with intercropping of niébé and dah. The Dogon are noted farmers and produce a wide variety of vegetables, particularly onions, and rice by constructing small dams and diverting water. This traditional, small-scale irrigation is not mappable at a scale of 1:500,000. At the northern edge of the plateau, pastoral land use typifies a largely uninhabited zone (about 5 persons per square kilometer), used mostly by Peul and Dogon to graze livestock.

---

[2] Ethnic identity has historical origins and reflects ancestry, language, physical traits and/or a way of life. Some people change their ethnic identity when they change their occupation, e.g., from pastoralists to fishermen. Likewise, some groups lose their language and change their occupation, but maintain their ethnicity according to their origins. See Gallais (1962).

3.3 INLAND DELTA

The Inland Delta is or used to be inundated by the Niger River's annual flood. Flood waters, which cannot be accommodated in the main channel, spread out over a vast plain to create the Live or Active Delta. The flooding continues north, channeled by tributaries along extensive linear dunes into what is known as the Lakes Region (Lacustrine Zone). To the east and especially to the west of the Active Delta stretches a broad sedimentary plain, formerly inundated, and known as the Dead or Inactive Delta.

The Active Delta encompasses the area south of Lake Débo and Lake Korientzé, bounded on the east and south by the main channel of the Niger River. The western boundary is less well defined; several kilometers to the west of the Diaka, it parallels that stream channel extending from the Niger River at Diafarabé to Lake Débo. The agro-pastoral production systems of the delta are in rhythm with the annual advance and retreat of flood waters. Near Mopti, flooding begins in July and by August has inundated the Active Delta's plain. In January flood waters have receded and lush, deep pastures called bourgou (characterized by *Echinochloa stagnina*) remain.

In the interior of the inundated delta, land use units are classified as pastoral or as agro-pastoral with pastoralism dominant. Transhumant herds of the Peul and of nomadic groups converge on the bourgou pastures and follow the retreat of the flood waters north. (The calendar, order of entry and use rights are based on the Code of the Dina established by Sékou Amadou in the nineteenth century to sedentarize the Peul and permit the co-existence of agriculture and pastoralism.) With the onset of the rainy season, herders lead the bulk of the herds out of the delta to escape its unhealthy conditions and to graze on the rainy season pasture in the Sahel. In October-November herds return to the periphery of the Active Delta to a waiting zone and then begin the cycle again. Small herds of milk cows, remain in villages and others, composed of young animals not fit for the transhumance, make shorter treks. The large bourgou pastures are generally devoid of permanent settlement or sparsely settled by Peul groups; also uninhabited are the lowest parts of the delta where only rare knolls appear.

The margins of the Active Delta favor more intense occupation. Land use of the west margin is agro-pastoralism with pastoralism dominant and some irrigated agriculture, particularly rice, using natural flooding or simple dams. Planted at the rainy season's onset, rice is harvested in the flood season. Cultivation is dispersed or discontinuous and not dense (10% or less of the mapping unit), except in an area extending along the Diaka (11-30%). Population density ranges from about 10 to 20 persons per square kilometer, but settlements are especially concentrated along the length of the Diaka distributary and other such branches from the Niger. The eastern margin of the Active Delta is characterized by a similar type of agro-pastoralism and near Mopti by modern, controlled rice irrigation in the *casiers* of a rice development project. Population density varies between 25 and 40 persons per square kilometer near Mopti and to the north, but to the south is about 15 persons per square kilometer. Mopti, the third largest city in Mali, is a port and center of commerce as well as the administrative center of the Region. Although the population of the Active Delta is dominantly Peul pastoralists and Rimaïbé (former slaves of the Peul) cultivators, Bambara and Marka agricultralists and especially Bozo fishermen also exploit its multiple resources. The expansion of rice cultivation at the expense of pasture land and increased numbers of livestock using the delta have created resource conflicts and altered the traditional system of exchanges and of land rights.

The Inactive Delta stretches mainly to the west of the Active Delta, but there are small areas to the northeast and southeast. Sand dunes, worn dunes, sandy plains, bush pastureland and areas of sparse vegetation are typical; overall lack of water is the determining factor of land use and population

distribution. Pastoralism prevails to the north. Toward the south, land use units are agro-pastoral with pastoralism dominant and rainfed cultivation. Agriculture is dispersed and 10 percent or less of a land use unit is cultivated, generally for millet, sorghum, peanuts, and niébé and, in some units, fonio, dah, corn, vegetables and pois de terre. In the area as a whole, population density is low, generally about 5 persons per square kilometer or less, but characterized by clusters of villages, often surrounding administrative seats, and a relatively high proportion of large (more than 1,000 inhabitants) villages. In the northern pastoral units, Peul are dominant with some Bambara and, in the southern units of rainfed cultivation, the reverse is the case. Lands of the Office du Niger are located on the Inactive Delta, in the mapsheet's southwest corner. This large irrigation scheme dates from the 1930's; the total control of water, through a system of canals distributing water from a dam on the Niger, has permitted rice paddy cultivation. Population, mostly immigrants to the Office, is relatively dense, 25 or more persons per square kilometer.

3.4 LAKES REGION

This region occupies much of the northern part of the Mopti mapsheet. Characterized by lakes, pools and elongated dunes, its higher local relief prevents complete inundation by Niger flood waters which flow along established channels into pools and lakes. Relative uniformity of its physical characteristics has resulted in a relatively uniform type of land use and homogeneous population distribution. Agro-pastoralism with irrigated agriculture dominant is widespread. Both natural flood and recessional irrigation are practiced. Cultivation is dispersed and of low density (0-10% of each mapping unit). Crops are diverse and include millet, sorghum, rice, cow peas, corn, wheat, tubers and vegetables. Near the larger lakes where the Active Delta meets the Lakes Region are also vast bourgou pastures where pastoralism rather than agriculture is dominant. The agricultural production system is dependent upon the cycle of the annual flood, but is somewhat more precarious than to the south in the Active Delta due to lower rainfall. Population density varies between about 15 and 25 persons per square kilometer. Rather evenly spaced villages with less than 500 inhabitants are punctuated by a few larger villages and towns, mostly administrative seats. The population is diverse: Peul and some Tamachek, and sedentary, cultivator groups of Bambara, Sonrai, Iklan (Bellah) and Rimaïbé.

4. CONCLUSIONS

From the perspective of methodology, the analysis reveals that Landsat imagery at the scales utilized is a convenient starting tool but is not sufficient in itself to show the complexity of the land use pattern which ground checks and field interviews reveal. For population mapping, it serves as a reference tool. Although one could establish a statistical correlation between population concentration and cultivation density, the variation in cropping patterns in Mali would lead to many distortions. The development of a land use legend appropriate to traditional production systems results in many overlapping and mixed categories; specialization in types of crops or livestock is often a matter of subtleties, rather than sharp contrasts.

Population distribution and the pattern of existing land use offer clues about the effectiveness and the level of resource exploitation. In general, the Mopti mapsheet illustrates that population concentration and uses of land are highly dependent upon environmental conditions and that, given the level of available technology, the most hospitable and environmentally favorable resources are most exploited. The isolated Dogon in the Bandiagara Plateau are a noteworthy historical exception. Availability of water seems to be the controlling physiographic factor; soils maps are not yet available to test the hypothesis that the best soils (in terms of productivity) or those most easily tilled with hand implements are the most exploited. For this area, voids of

population appear not to be explained by geographically specific disease as is the case in other parts of Mali where onchocerciasis is present in river valleys. While population concentration in the Mopti mapsheet is superficially related to available infrastructure, it also appears that the infrastructure has followed rather than caused the population concentrations. As additional project information becomes available, population density can be calculated by soil-vegetation unit and soil characteristics can be ranked or quantified. Use of multiple regression techniques would permit the more sophisticated testing of hypotheses related to soil characteristics (depth, available moisture, slope, etc.).

With the growing application of technologically sophisticated methods of acquiring information about the earth, extensive areas can be evaluated and compared. The inventory and evaluation of biological and physical characteristics permit a more rational examination of development options. Certain cautions are in order, however, for traditional production systems like those of Mali. New levels of technology and/or new types of use are likely to disturb old balances between population and resources and to have repercussions on land holdings and rights (land traditionally cannot be alienated from the family ancestry in Mali) and social-political relationships. For example, the extension of irrigated rice cultivation in the delta occurs at the expense of pastoral use, requires the redefinition of property rights and alters social relationships among ethnic groups. The analysis of land use and population helps to raise important questions, particularly when evaluation of development potential runs counter to existing use. Many factors may have acted in the past to prevent such a use from occurring--disease, ethnic tradition, historical events, or the adaptive strategy of interdependent relationships characterized by mixed rather than specialized uses. Land use and settlement are thus reflections of complex and interrelated production systems. In this sense, the inventory and evaluation of population and land use guide the formulation of other critical questions. Development planning depends, then, not only on finding physically suitable locations, but also on uncovering the possible constraints to successful change.

5. REFERENCES

Gallais, Jean. "La signification du groupe ethnique au Mali." L'Homme Mai et Aout 1962, pp. 1-129.

Mali, Ministry of Rural Development, Projet Inventaire des Ressources Terrestres (PIRT). Bamako, Mali, 1982. Maps, images and documentation available in PIRT Documentation Center in Bamako, Mali. Atlas of Land and Water Resources, prepared by TAMS, NYC, NY. (Prior to July 1982, the project was under the National Directorate of Water and Forests of the Ministry of Livestock, Water and Forests.)

LANDSAT DATA
APPLIED TO THE STUDY OF BIOPHYSICAL LAND COVER
OF THE FRENCH NATIONAL PARKS

M. Lenco

Ministere de l'Environment
Neuilly Sur Seine, France

Y. Heymann
L. Rivard

Societe Francaise d'Etudes
et de Recherches Economiques et Statistiques
Montrouge, France

W. Tyler

Environmental Research Institute of Michigan
Ann Arbor, Michigan

SUMMARY

The French national parks located in mountain areas lay in extended zones, difficult of access, upon which homogeneous data about biophysical land cover and vegetation are not numerous. These data are useful to spot and abserve: on the one hand, protected areas or areas to be protected and on the other hand, cultivated areas or zones planned to, belonging to the parks peripheral zone.

Landsat data provide numerical and cartographical information at the 1:100,000 scale which is specific and well fit to the study of the natural spaced encountered in the national parks.

It is the reason why the following studies have been undertaken from 1979 to 1981 on the five French parks located in mountain by the Environment Ministry joint to the parks authorities in order to collect a common bunch of homogeneous and concise data about the whole territory of the national parks.

- Production by ERIM of enhanced false colour images (geometric corrections, contrast stretching, edge enhancement, boundaries digitizing) at the 1:100,000 scale from 4, 5, and 7 Landsat channels as such periods as beginning of summer, and beginning of automn in the parks in which versants are not too steep and shadow effect not too strong.

- Ecological zoning of the parks territory executed by a specialized interpreter using the existing maps and an aerial photograph sample of the last available coverage.

- Biophysical classification of land cover into 10 to 20 categories for each park means of photointerpretation assisted by the parks authorities providing a classification in ten categories common to all the parks.

- Manual measurement of the surface of each land cover category on the central and peripheral areas by means of a points grid.

In order to improve the information accuracy on vegetation quality, the band ratioing: Channel 7 - channel 5/channel 7 + channel 5 strongly correlated to green biomass has been undertaken for certain parks.

The determination of classes of vegetation index is realized through ground data from test sites selected according to previous studies.

The results are given in surface for each class corresponding to the different vegetation categories both for the central and peripheral zones and are mapped into 24 classes in color at the 1:100,000 scale by ERIM.

This methodology was prefered to that of supervised categorization because it is quite fit to the type of information needed, it is not expensive and allows the interpreter to take into account the structural and textural features as well as the characteristics of shape and nearness which are still badly dealt with in available software.

On the other hand, enhanced false colour images permit to the staff of the parks to get well acquainted with radiometric Landsat data and are a good communication tool.

A restored image has been produced for one park as a trial and appeared to be of greater interest for the photointerpreter than the classical enhanced false colour images.

EVALUATION OF CROP YIELD FORECASTING TECHNIQUES BASED ON SATELLITE INFORMATION

Cecilia Espos

Comision Nacional de ıvestigaciones Espaciales
Buenos Aires, Argentina

Ana M. Ravelo
Andres C. Ravelo

Consejo Nacional de Investigaciones Cientificas y Tecnicas
Buenos Aires, Argentina

SUMMARY

The capability of a space-based platofrm to provide information on grain production for major crops grown in the "Pampa" humeda" of Argentina has been one of the driving forces behind CNIE's Landsat program. During the last 10 years, several techniques were developed to use satellite information in assessing crop yields. Different indicators of crop status have been proposed in the literature (stress-degree days, radiance ratios, leaf-area index, etc.). Crop conditions have been correlated with temperature differential between the plant canopy and the air temperatures over critical crop growth stages. Grain yield was correlated to various ratios of the red and near-infrared radiances. Weighted differences of the infrared and visible channels of Landsat data were related to growing vegetation. Those techniques showing the highest potential for crop yield assessment were selected for testing and evaluation. Reflected radiances measured by Landsat, corn yields from experimental sites in Rojas (Buenos Aires) and daily meterological data for the 1978/79, 1979/80, and 1980/81 crop growing seasons are being used in the testing procedure. Additional information on crop moisture conditions during the experiment are being obtained by computing a daily soil moisture budget and agroclimatic indices. Results from this study will allow the choice of one or more corn forecasting techniques suitable for operational purposes.

CONSTRUCTION, INTERPRETATION AND COMPARISON OF THERMAL INERTIA IMAGES OBTAINED FROM AIRBORNE DATA IN A HUMID AND IN AN ARID ENVIRONMENT

F. Bonn
R. Brochu

Universite de Sherbrooke
Sherbrooke, Quebec, Canada

E. Ezra

University of California
Santa Barbara, California

M. Bernier

Canada Centre for Remote Sensing
Ottawa, Ontario, Canada

SUMMARY

In order to assess thermal properties of the environment such as soil moisture, leaf moisture, proximity of subsurface watertables and porosity, thermal inertia images have been generated from day and night aircraft remote sensing measurements (visible, near IR and thermal IR) in an agricultural area of Quebec and in an irrigated desert in California.

The algorithms used were similar to those developed for the Heat Capacity Mapping Mission satellite, but with a spatial resolution of 4m in Quebec and 10m in California. In both cases, image generation needed geometric corrections and spectral weighting factors to estimate albedo, and geometric corrections to estimate temperature difference.

The analysis of the California image, supplemented by extensive ground measurements, shows a good relation between thermal inertia and moisture properties in the upper 50 cm of soil, over bare soil conditions.

The Quebec image, under different crops and forest covers, showed no significant relation between soil moisture and thermal inertia. However, thermal inertia appeared to be correlated with heigth of vegetation and total water-content of the soil/vegetation system.

This comparison raises a discussion about the applicability of thermal inertia mapping to different climatic environments, and the limitations of thermal IR for soil moisture studies when the hydric conditions are close to field capacity.

SPOT SIMULATIONS IN BANGLADESH

J-C. FAVARD

CENTRE NATIONAL D'ETUDES SPATIALES "CNES"

TOULOUSE - FRANCE

and

M.U. CHAUDHURY

SPACE RESEARCH AND REMOTE SENSING ORGANIZATION "SPARRSO"

DACCA - BANGLADESH

I - INTRODUCTION

As part of a contract between the Société Européenne de Propulsion (SEP) and the Space Research and Remote Sensing Organization (SPARRSO) aiming at the implantation of a SPOT receiving ground station in Bangladesh, an airborne remote sensing experiment was carried out in January 82. Its purpose was to allow the generation of Spot-simulated data over a set of given areas.

The interpretation of the data collected was focused on three main topics i.e.rice, coastal areas, cane-sugar.

During the campaign seven zones were covered with the aircraft flying at an altitude of either 3 500 m (11 500 ft) or 7 000 m (23 000 ft). Data from the Daedalus scanner (visible and near infrared bands) were recorded while infrared color photographs were taken. Daedalus data were collected in order to generate radiometric Spot simulations while the photographs are necessary for the geometric simulations.

The geometric approach is aimed at simulating SPOT parameters wich affect the geometrical quality of the images collected by the satellite. These parameters include satellite position and attitude, earth rotation and sphericity, instrument geometry, type of projection and stereoscopy effect. The radiometric approach is aimed at simulating SPOT parameters which affect radiometry (spectral band, the line of sight, local time, the satellite track orientation ...).

This paper deals with the first results gained from the interpretation of the data collected from the scanner over one of the study areas, namely the "Hail Haor" area which is located south of Syhlet.

II - BACKGROUND INFORMATION ON THE STUDY AREA

II.1. - Generalities

The area under study covers Hail Haor, Balishira hillsand Satgaon hills. These are located approximately between the latitudes 24° 18' N to 24° 26' N and longitudes 91° 34' E to 91° 50' E in the southern part of the eastern district of Sylhet, Bangladesh.

The area drains into Meghna river which is one of the three major river systems of Bangladesh - the other two being Bhrahmaputra and the Ganges systems. The climate of the area is sub-tropical with a year round growing season for the crop and is characterized by a monsoon season of extremely heavy rain and a dry winter season during which soil moisture is too insufficient for a satisfactory harvesting. The Hail Haor proper, is a saucer-shaped depression covering a synclinal basin bounded by north-south oriented anticlinal ridges of 50' to 300' high. The eastern anticline constitutes the Balishira hills which goes up to 250' and where the tropical semi-evergreen forest of western Bhannugach is located . Surrounding these forests, there are tea gardens and pine apple orchards. In the west Bhanugath forest reserve, there are artificial plantations of teak and other tropical trees dating back as early as 1927. The anticline in the west constitutes the Satgaon hills which goes up to the elevation of 300'. This hill range also have tropical forest vegetation and plantations. Growth of the forests is less luxuriant in this hill than in Balishira hills and the earliest forest plantation is dating back to 1947. There are tea gardens and pine apple oarchards also in this hill range.

The haor basin is blanketted by recent alluvium and the hills bounding the basin are occupied by sedimentary rocks ranging from Miocene to Pleistocene age. The Hail Haor alluvium consists of two categories : the high land alluvium occupies the area above the normal flood level and consists of light grey clay, silty clay, yellow and brown sand and is slightly consolidated at places. The surface cover of this formation is homesteads, kitchen gardens, orchards around villages etc .. The low land alluvium is distributed in the flood level plan, occupying river bed, natural levee, swamp areas etc. It is mainly light grey silt and fine sand. The surface cover is agricultural lands, fallow lands, meadow lands and homesteads above haor, ponds, etc. The sedimentary rocks is the central part of eastern hills are geologically know locally as Tipum sandstones and consist mainly of sandstone with occasional alterations of siltstone and silty shale. The sandstone is brownish to grey and thick bedded to massive. The silt stone and silty shale are light grey to grey. The surface cover is mainly forest. The sandstone formations in the entire western hills as well as the flanks of the eastern hills are locally know geologically as Dhupitila formation and consists of mainly yellow and brown coloured massive sandstone and thinly bedded and banded and lens type claystone. Surface cover is forest land, tea gardens, horticulture, deforested lands etc . In the hill tops and elevated grounds red to reddish brown clay with dominantly ferruginous concretionary modules, pillets, and bands locally known geologically as Modhupur clay occurs. The surface cover is scrubs fallow land, homesteads etc.

II.2. - Climate

The climate of the study area is tropical and humid, with three district seasons : a warm summer (March through May), a rainy monsoon (June through October) and a cool winter (November through February). Mean annual temperature range from 62'F to 83'F. Relation humidity remains quite high round the year with a minimum of 74 % in March and a maximum of about 90 % in December. Mean annual rainfall in the study area is quite heavy and varies from 2 500 mm to 2750 mm. Distribution of rainfall is in general unfavourable to agricultural production. During the monsoon season it is so excessive as to cause flooding (5 months from May through September), and in the other months (7 months from October to April) of the year it is insufficient for growing crops.

II.3. - Hydrology

There are in all 352 charas or streams which drain into Hail haor from the adjoining hills covering a water shed area of about 240 sq. miles. The Langla river comming from the north and formed by the joint flow of tow bigger streams. Udna and Bilash, constitute the main tributory to the Hail Haor. The natural outlet of the Hail Haor is the Gopla river. It flows in a northerly direction from the Hail Haor and eventually drains into Meghna river. A common prevailing saying depicts more or less the whole picture of Hail haor which runs as follows :

Hail Haor is a Gara (depression).
In which fall three hundred and fifty two charas (Streamlets).
Gopla is the only Khara (outlet).

Many of the streamlets and streams which once flowed into the Hail Haor have dried out.

The number of existing prominent streams are about 43, out of which 21 are from eastern hills, 2 from southern hills and 20 from the western hills. The beds of all these streams are very shallow due to accumulation of sand comming down from upper reaches of the hills. Excessive rainfall in the watershed also causes flush flood bringing in with the flow sand to be desposited over the standing crops and in the main body of the haor.

The water surface area of Hail Haor varies for about 6000 acres to 20,000 acres depending on the seasons. The lowest being in April-May and the highest at the end of the peak of the monsoon in August-September. The volume of water in the Hail haor was estimated from ground truth data collected during January-February, 1982 at about 9.35 ft. (G.T.S.) over 5829 acres feet. The depth of the water area varied from zero to 3.50 feet during the ground truth mission, but during the peak monsoon it varies from 10-15 feet. As Langla and the Copla flow through the western side of the haor and have their own depth, their flow channels constitute the deeper areas of the Hail Haor. It is the deeper channel as well as other deeper areas where the "Dhal" fishing technique is widely used in the months of February-April. The local fisherman put branches of trees in the deep water areas, then surround these with floating bamboo and put water hyacinth and other floating weeds within the blockade.These blockades are rectangular or square in shape and are called "Dhal". Fish take shelter in the blockades where water is deep and cool. These "Dhals" are then surrounded by fishing nets to catch fish almost every forthnight starting from the month of February till April. These "Dhals" are seen in regularly shaped rectangular blocks both in Aerial Photographs and the SPOT simulated data.

II.4. - Landuse

The study area has three main land types viz hilly land, agriculatural land, and haor land. In the hilly land the existing landuse are :

a) - Forestry

- . semi-evergreen forests
- . artificial plantations

b) - Horticulture

- . pineapple gardens
- . citrus and other fruit trees

c) - Tea gardens

- . old tea crop with overhead shade
- . young tea crops

d) - Bushes

- . sun grass (thatch grass)
- . bamboo
- . cleared areas

e) - Homesteads

- . tea estate factories & compounds
- . residential homes

II.4.1. - Agricultural land

In the agriculture land which covers the area from the foot-hills to the fringe of the haor when fully flooded, the landuse are :

a) - Double-cropped area - These are the areas which are never flooded and where through natural

water supply two agricultural crops such as Aus (rice planted during March-April and havested during July-August - both broad cast or transplanted) and Aman (rice planted during monsoon and harvested in November or December - both broadcast or transplanted) can be grown. These are the areas, which remains mostly fallow during the dry season.

b) - Villages - homesteads, yards, kitchen gardens and village groves fall within this category.

c) - Ponds - Large number of ponds which are used for drinking and washing purpose as well as family or community fisheries.

II.4.2. - Haor area

The lowest area is the Haor area which can be divided into the following categories :

a) - Single croped area - These are areas where only one crop can be planted as the areas go under water after the planting season and surfaces when the crops are mature. The water then receeds quite far and the irrigation becomes difficult. These areas grow deep water Aman crops and are suitable for IRRI (high yielding varieties of rice developed by International Rice Research Institute) varieties of rice cultivation or for growing Boro (rice planted during winter and harvested during April to June) with irrigation facilities developed.

b) - Boro areas - These are areas at the fringe of the haor and also along the beets (small, lakes, swamps or body of year round standing water) in the haors. These are the areas when Boro rice or Braus (paddy planted in the late Boro season and harvested in the Aus season) are grown.

c) - Grassland : These are large areas in the main haor which go under water during monsoon. During this period tall grass grow in the area and are cut by boats for stall feeding. These are comparatively higher areas and when the water receeds, these land are quite away from the water fringe. As a result no agricultural effort is made through irrigation. These are used as pasture land by cattle from nearby villages, as well as from far flung areas.

d) - water area : This is the lowest area. Here water remains permenently during all season. This area may again be divided into a few different categories viz :

- clear water areas: these are areas where no vegetation, either rooted or floating can be seen.
- water areas with thick lotus and lilies : these are permanent water areas, but the clear water surface is not always visible from above, as leaves of lotus and lilies float on the water surface.
- grass areas : areas where aquatic grass and reeds grow. Here water surface can be seen from above, but from the side the area looks lile green meadows.

It is interesting to note that water hyacinth grow gregariously and moves over the water surface with wind. As a result these could be seen in different areas of the lake at different seasons. The permanent water body in the haor therefore gives different spectral look in different times of the year and also in different years.

III - RESULTS

Several processings were carried out on the SPOT simulations data and false colour pictures generated. The following features could then be noted.

a) - The lake

- "Dhals" are clearly visible even when their overall size is smaller than the satellite's ground resolution due to a processing which enhances the constrasts locally. However the "Dhals"situated in the channel leading to the lake are less visible since they are even smaller and closer to the banks.The best band to locate these rafts is the near infrared one (S3 for SPOT).

- Several areas can be identified within the lake due to differences in the aquatic vegetation and in their coverage

- There is a close relationship between the colour of the water and the bathymetry.

- In spite of their small width (a few meters) the different channels leading to the lake are clearly visible and could be mapped. However one does not see the actual channels but rather the vegetation on their banks. Here again, local optimisation of the radiometries enhanced their features.

b) - Land use

January is not the best moment of the year to investigate the rice crops since "boro" (winter rice) has just been or has not been planted yet while summer rice has been havested. However the boro growing areas are clearly visible Eastward of the lake. Slight variations radiometrywise in the near infrared band over this area might be due to different planting times. Rice is most probably planted earlier in the North East than in the South. In the North West of the lake, boro planted areas mapping seems much more difficult and data collected in February or March appear to be necessary for such a study.

Tea gardens are clearly visible thanks to their geometrical features (textural parameters). Several plantations gave different radiometric responses. This proved to be due - after ground truthing - to the fact that they correspond to : either young plantations or less dense plantations.

Sorting out this two particular cases is rather difficult since radiometry is influence by the canopy coverage and the two phenomena have the same influence on this parameter.

Finally villages are quite visible as well.

IV - CONCLUSION

As part of this program, studies are to be carried out over the coastal areas by Bangladeshis and French experts. No classifications have been done yet.

The results exposed in this paper are the very first gained from studies which are to be carried on in Bangladesh on an interactive image processing system.

HAIL HAOR

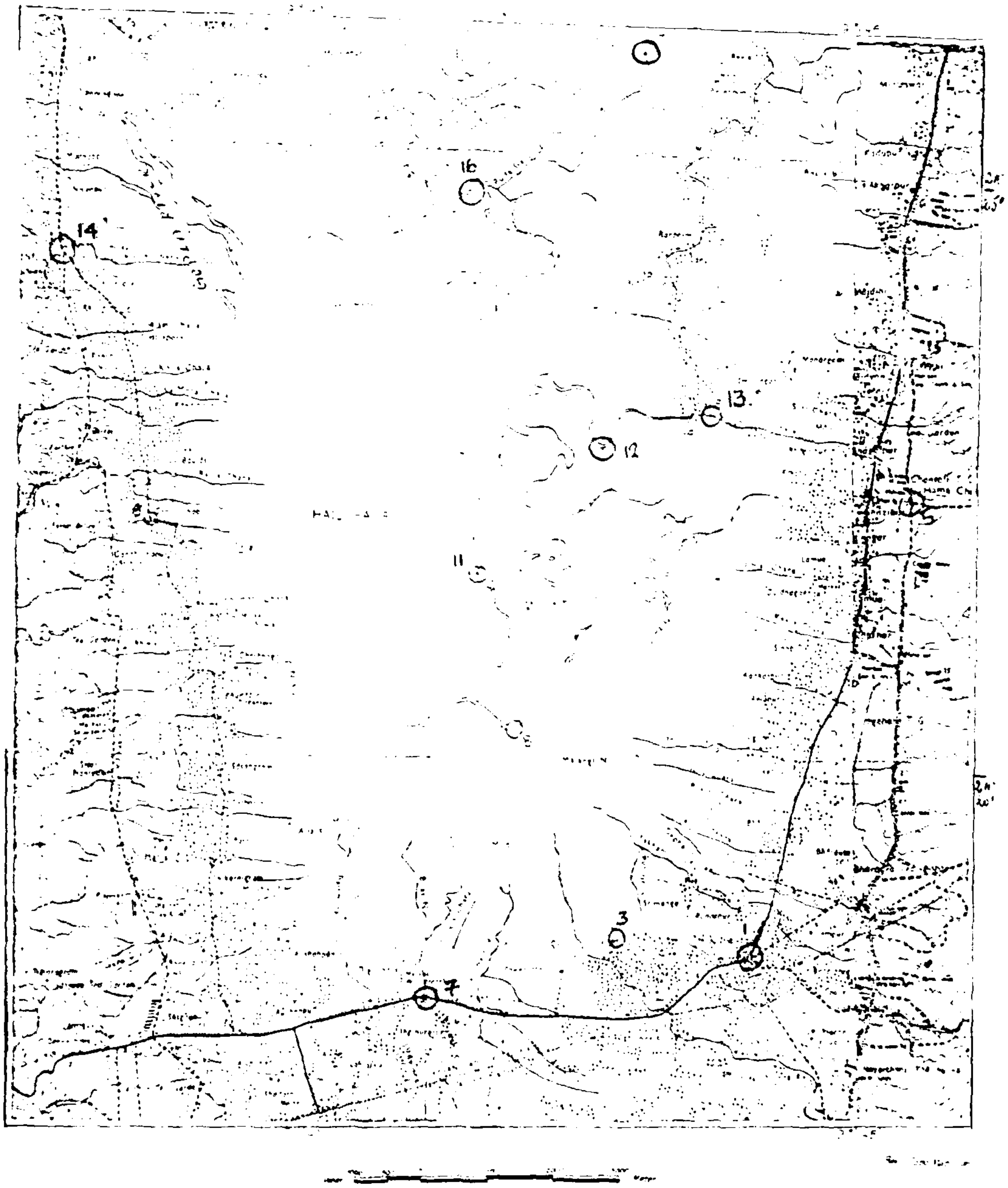

6

IMAGE REGISTRATION BY SEQUENTIAL TESTS OF HYPOTHESES: GAUSSIAN AND BINOMIAL TECHNIQUES*

N.D.A. Mascarenhas and J.A.G. Pereira

Instituto de Pesquisas Espaciais - INPE
Conselho Nacional de Desenvolvimento Científico e Tecnológico - CNPq
Caixa Postal 515, 12200 - São José dos Campos - SP, Brasil

ABSTRACT

The problem of translational image registration has received considerable attention in the area of image processing and recognition as applied to remote sensing. The main methods that have been proposed are based either on correlation techniques or on algorithms of the type SSDA (Sequential Similarity Detection Algorithm), where the error between the two images is accumulated and a threshold sequence is selected, such that the rejection of a candidate position can be done at an early stage. This paper proposes a new approach to image registration problems, based on the theory of sequential test of hypotheses. This leads to the development of two different methods: the first one is based on the Gaussian assumption and uses the fact that the variance of the error between two images to be registered tend to be low on the registration point. The second uses binary images derived from the original ones. The statistical model for the resulting accumulated error is a binomial distribution and the registration position is characterized by a low probability of the binary error being one. In both methods two sequences of thresholds are employed: one leading to the rejection of the point and the other one to the eventual acceptance of it. Experimental results whith both methods are presented. They include registration of a Landsat image against noisy versions of it, of different channels of the same multispectral image, as well as matching of segments of two images taken by the satellite at different dates. Both techniques required a modest amount of computacional effort. The binomial test was found to be the most succesful of the methods in the last two applications.

*Presented at the Seventeenth International Symposium on Remote Sensing of Environment, Ann Arbor, Michigan, May 9-13, 1983.

AD-A134 719 PAPERS SELECTED FOR PRESENTATION AT THE INTERNATIONAL SYMPOSIUM ON REMOTE..(U) ENVIRONMENTAL RESEARCH INST OF MICHIGAN ANN ARBOR . JUN 82

UNCLASSIFIED F/G 14/5 NL

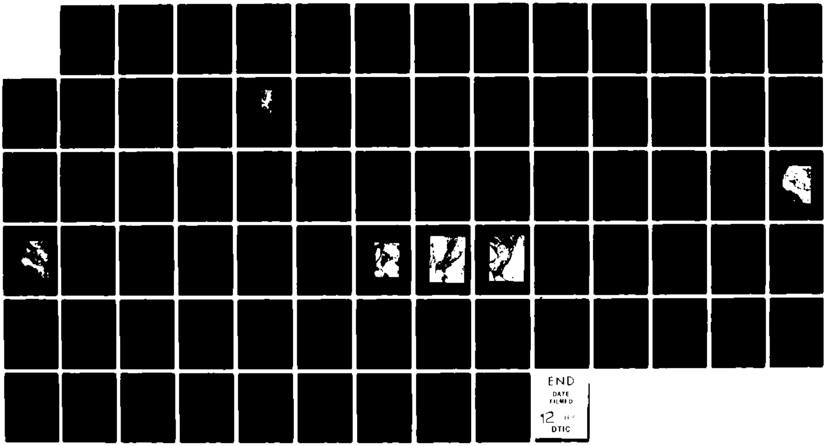

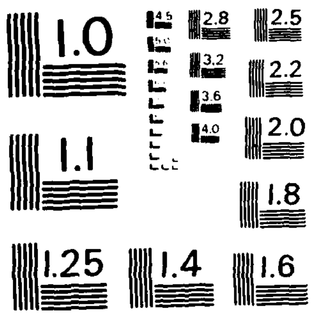
1.0
4.5
2.8
2.5
3.2
2.2
3.6
4.0
2.0
1.1
1.8
1.25
1.4
1.6

1. INTRODUCTION

In remote sensing of earth resources, it is frequently necessary to characterize a scene by taking images at different times or at varying wavelengths with several types of sensors. In all these cases, the position of the sensor can vary from one situation to another, and there is a need to establish a correspondence between different images, in the sense of being able to superimpose both images in the best possible way.

If the images do not differ in scale, rotation or projection, the problem to be solved is basically a translational one. Even when more severe distortions are involved, one of the steps in geometrically correcting one image with respect to the other consists in performing a translational registration of small areas involving well determined features (ground control points).

The main techniques that have been developed so far for solving the image registration problem can be divided into two approaches: correlation techniques and sequential similarity detection (S.S.D.A.) algorithms.

Correlation techniques have been studied extensively. In general, they face the problem of computational costs in performing the normalized correlation for every candidate position and that of the ill defined maximum at the registration point.

S.S.D.A. algorithms were introduced by Barnea and Silverman (1), and they attempt to reduce the number of necessary computations by accumulating the error between the two images and truncating it at an early stage. Hence, only at points near or at registration, the computation is performed at its full precision. Two types of threshold have been introduced by those authors: a) the constant threshold, and b) the monotonically increasing threshold. In both cases, there remains the problem of appropriately selecting the threshold level.

Several authors have worked on sequential techniques for registration. Besides the work of Barnea and Silverman, one could mention the work of Vanderburg and Rosenfeld (2) on hierarchical search in two stages, Rosenfeld (3) on window search optimization sequence, Ramapriyan (4) on sequential search at several levels, and Wong and Hall (5, 6) also an hierarchical technique.

This paper proposes a new approach to image registration problems, based on the sequential tests of hypotheses (S.T.H.) theory. It leads to the development of two different methods: the first based on a Gaussian model for images, and the second applied to binary images.

2. SEQUENTIAL TESTS OF HYPOTHESES

The theory of sequential tests of hypotheses was developed initially by Wald (7), who introduced the sequential probability ratio test.

In order to briefly review the ideas involved in this test (the reader is referred to the original work by Wald (7), or to chapter [illegible] of Hancock and Wintz's book (8) for more details), let f(x, [illegible]) be the probability density function of the random variable being observed. Let H_0 be the hypothesis that [illegible] and H_1 the hypothesis that [illegible]. Successive observations on x are labelled by x_1, x_2, ... and one could define the likelihood ratio

$$\lambda(X_n) = \frac{f(x_1, x_2, \ldots, x_n | \cdot)}{f(x_1, x_2, \ldots, x_n | \cdot)} = \frac{f_{1n}}{f_{n}} \qquad (1)$$

The sequential probabilistic ratio test is defined as follows: two constants A and B (B A) are defined. At each stage of the experiment, the ratio f_{1n} f_{n} is calculated.

$$\text{If} \quad B \quad \frac{f_{n}}{f_{n}} \quad A, \qquad (2)$$

the experiment continues with an additional observation.

$$\text{If} \quad \frac{f_{n}}{f_{n}} \quad A, \qquad (3)$$

the process finishes with the rejection of H (acceptance of H).

$$\text{If} \quad \frac{f_{n}}{f_{n}} \quad B, \qquad (4)$$

the process finishes with the acceptance of H. The constants A and B are chosen in such a way that the error probabilities and (= probability of rejecting H when it is true, and = probability of accepting H when it is false) be specified. It can be shown (see Hancock and Wintz (8) pg. 91) that the following relations are valid.

$$A \quad \frac{1 -}{} , \qquad (5)$$

$$B \quad \frac{}{1 -} . \qquad (6)$$

3. IMAGE REGISTRATION USING THE GAUSSIAN MODEL

3.1 THE MATHEMATICAL MODEL

The problem of translational image registration may be part of a more general problem of precisely registering two images that may differ substantially from each other from the geometrical point of view. However, one can imagine that small segments of the two images, that are approximately in coincidence with each other, would present small variations in scale and orientation. This situation is simulated in this work by the addition of Gaussian noise to one or both images. This Gaussian noise will be white, with zero mean, and independent of the signals, and also independent from each other in the two images. Furthermore, it will be assumed that the two images will be normally distributed. Besides its mathematical tractability, this assumption has received considerable support in most of the literature dealing with remote sensing imagery, notably from Landsat satellites. From these assumptions, it follows that the distribution of the noisy image will be

also Gaussian, with mean equal to the mean of the original image and variance given by the sum of the variances of the image and the noise; that is,

$$V_I = V_S + V_N, \tag{7}$$

where V_S is the variance of the original scene and V_N is the variance of the noise.

The proposed idea is to test the variance of the difference of the two images for each reference position, which would be given by

$$V_D^{i,j} = V_{I_i} + V_{I_j} = 2 V_S + V_{N_i} + V_{N_j}, \tag{8}$$

outside the registration point, and by

$$\hat{V}_D^{i,j} = V_{N_i} + V_{N_j},$$

at the registration point, since it is assumed that the original scene is the same and only the noises associated with each image would be, in general, noncorrelated and with different variances.

A sequential probability ratio test with error probabilities α and β can be performed to test the hypothesis that $\sigma = \sigma_0$ against the alternative H_1 that $\sigma = \sigma_1$.

Set $x_1, x_2, \ldots$ be sucessive observations of x, that represent the difference between two pixels in the two images. It can easily be shown that the inequalities represented by eqs. (3) and (4) are represented in this case by:

$$\sum_{i=1}^{n} x_i^2 \le \frac{2 \log \frac{\beta}{1-\alpha} + nS}{D} = A_n \tag{9}$$

and

$$\sum_{i=1}^{n} x_i^2 \ge \frac{2 \log \frac{1-\beta}{\alpha} + nS}{D} = R_n . \tag{10}$$

A graphical representation of the three zones is presented in Fig. 1, where

$$h_0 = \frac{2 \log \frac{1-\alpha}{\beta}}{D}, \tag{11}$$

$$h_1 = \frac{2 \log \frac{1-\beta}{\alpha}}{D}, \tag{12}$$

and the slope of the straight lines is given by S/D.

3.2 IMPLEMENTATION OF THE GAUSSIAN ALGORITHM

In order to implement and test the algorithm, a Landsat image from the Paraiba Valley in São Paulo State, Brazil, was used, and a 512 X 512 segment was extracted and from now on referred as the "image".

From this original image two families of images were generated, by addition of white Gaussian noise with signal to noise ratio (SNR) of 10:1, 5:1, 2:1, and 1:1. Observe that the noise from one family is noncorrelated with the noise from the other.

The search area was selected as a segment of 80 X 80 pixels, and the windows were taken with the size of 32 X 32 pixels. The processing time on a Burroughs B6800 computer varied between 50 and 90 seconds.

Several combinations of images from both families were tested. The images from each family were also registered with the original image, without noise. The results for the same registration point can be observed in tables I and II where, in the case of more than one accepted point, they are described by the number of pixels that separate them from the true registration point. On the first table, the mean (which was subtracted from the image) and variance of the image were estimated over the search area; on the second table, those parameters were estimated over the whole image. The tests that used the second parameter estimation procedure always presented a substantial increase in the number of accepted points.

It can be observed that, for SNR down to 5:1, the point accepted with the least *number of tests is the true registration point. In the case of* greater amount of noise, the accepted points are around the true registration point, except for a few cases. An arithmetic mean on the x and y coordinates of the largest connected region led always to the true registration, with an error always not greater than one pixel (in most cases, even less than half a pixel).

Figure 2 displays the distribution of the variance of the difference between two images with SNR = 5:1, over a search area of 50 X 50 pixels, centered on the registration point. The figure has been inverted for better *visualization, so the central registration peak represents* the lowest variance.

Attempts were made to register different channels from the same image. The attempts were successful between channels 4 and 5, and 6 and 7. This can be explained in term of the image histograms, that exhibit a much greater similarity between the successfully registered channels.

The multitemporal registration was also tested, involving two images taken six months apart over the Paraíba Valley. A positive result was obtained on channel 4 using both the original (non noisy) images as well as the magnitude of their gradient.

4. IMAGE REGISTRATION USING THE BINARY MODEL

4.1 MATHEMATICAL FORMULATION

Binary images are frequently found in practice, for example as a result *of a thresholding operation.* According to *Muntenau* (9), who evaluated the S.S.D.A. algorithm as applied to binary images, it should be expected that p (the probability of the absolute value of the binary error being one) be approximately .5 far from the registration and approach zero close to the registration position. Experimental measurements were also made, in this work, by thresholding the original and noisy images around their mean values. These results confirmed the fact that, far from registration, the value p = .5

is very reasonable, indenpendently of the noise level, while the value of p at registration is, in general, between .1 and .3, its value being dependent upon the noise level and the variance of the original scene. If a random samping is performed on the window, the binary error accumulated absolute value can clearly be modelled by a binomial random variable. A sequential test of hypotheses can then be formulated to search for the registration point in the following manner: the hypothesis H_0 that the value of p (average of the iriginal Benouilli distribution) is low (say .1, for example) is t ted against the hypothesis H_1 that this value is .5.

By calling

$$A = \log \frac{p_1}{p_0} , \tag{13}$$

and

$$B = \log \frac{1-p_0}{1-p_1} , \tag{14}$$

the inequalities (3) and (4) can be given by

$$d_n \quad \frac{\log \frac{1-}{}}{A+B} + n \frac{B}{A+B} \quad A_n \tag{15}$$

and

$$d_n \quad \frac{\log \frac{1-}{}}{A+B} + n \frac{B}{A+B} = R_n \tag{16}$$

respectively

Figure 1 can also be used to visualize the acceptance zones of p_1 (misregistration), acceptance of p_0 (registration) or continuation of the test. The initial points of the straight lines are now given by

$$h \quad \frac{\log \frac{1-}{}}{A+B} \tag{17}$$

and

$$h \quad \frac{\log \frac{1-}{}}{A+B} \tag{18}$$

and the slope of the straight lines is given by $\frac{B}{A+B}$

4.2 IMPLEMENTATION OF THE BINOMIAL ALGORITHM

The binomial algorithm described above was implemented on the same images as the Gaussian case, in order to provide a performance comparison.

Values for p between .05 and .2 led consistently to the correct registration point. Results are summarized on Tables III and IV. They show that the binomial test seems to be more robust in the sense of always accepting the correct registration point, with the fewest number of tests. The binomial test was found to allow registration between any two channels of the same multispectral image. Farthermore, multitemporal registration was successfully implemented on the four Landsat channels, using both the original images and the magnitude of the gradient, as is observed on Table V. The display of the (inverted) variation of the frequency of occurrence of 1's over a search area of 50 X 50 pixels for multitemporal registration is in Figure 3. The processing time is about the same as the Gaussian method.

5. CONCLUSIONS

The framework of sequential tests of hypotheses (S.T.H.) provided a formal basis for defining the image translation registration problem. Both the Gaussian and binomial models were tested and preliminary results with a specific Landsat frame were evaluated. They included registration of an image against noisy versions of it, of different channels and of images taken six months apart.

6. REFERENCES

(1) Barnea, D.I. and Silverman, H.F., "A Class of Algorithms for Fast Digital Image Registration", IEEE Trans. Comput., vol. C-12, pp. 179-186, Feb. 1972.

(2) Vanderbrug, G.J. and Rosenfeld, A., "Two-Stage Template Matching", IEEE Trans. Comput., vol. C-26, pp. 384-393, April 1977.

(3) Rosenfeld, A. "Ordered Search Techniques in Template Matching", Proc. IEEE, vol. 60, pp. 242-244, Feb. 1972.

(4) Ramapriyan, H.K., "A multilevel Approach to Sequential Detection of Pictorial Features", IEEE Trans. Comput. vol. C-25, pp. 66-78, Jan. 1976.

(5) Wong, R.Y. and Hall, E., "Sequential Hierarchical Scene Matching", IEEE Trans. Comput., Vol. C-27, pp. 359-366, April 1978.

(6) Wong, R.Y. and Hall, E., "Performance Comparison of Scene Matching Techniques", IEEE Trans. Pattern Analysis & Mach. Intel., vol. PAMI 1, pp. 325-330, July 1979.

(7) Wald, A. "Sequential Analysis", John Wiley & Sons Inc., New York, 1947.

(8) Hancock, J.C., Wintz, P.A. "Signal Detection Theory", McGraw Hill Book Co., New York, 1966.

(9) Muntenau, C. "Evaluation of the Sequential Similarity Detection Algorithm Applied to Binary Images", Pattern Recognition, vol. 13, Number 2, pp. 167-175, 1981.

SNR	ACCEPTED		NONDECIDED	
10 : 1	0	0		
10 : 1	0	0		
5 : 1	0	0		
	+2	+1		
	+1	0		
	−1	−1		
5 : 1	0	0		
	−1	−1		
	−1	0		
2 : 1	+2	−2		
	−1	−1		
	0	0		
	0	−1		
	−7	−8		
	−3	−1		
	−1	0		
	+1	0		
	0	−4		
	+1	+1		
	+1	+2		
	−1	−2		
2 : 1	0	0		
	−3	0		
	0	−1		
	+1	+1		
	−1	−1		
	+1	0		
	0	+1		

SNR	ACCEPTED		NONDECIDED	
1 : 1	−1	−1	+1	+2
	−18	−11	−1	+1
	0	−1		
	+1	−1		
	0	0		
	−2	0		
	−1	0		
	+1	0		
	+1	+1		
	0	+1		
	0	−2		
	−1	−2		
	−2	−1		
1 : 1	−1	−1	+15	−12
	0	−1	+14	−13
	0	0		
	−2	−1		
	−1	0		
	0	+1		
	+1	+1		
	+1	0		
	−2	−2		

Table 1. Accepted and nondecided points; Gaussian test; one of the images is noise-free; variance measured on search area; [illegible] 10[illegible]

SNR	ACCEPTED		NONDECIDED
10:1, 10:1	+1	+16	
	0	0	
	+2	+1	
	+1	0	
	-1	0	
	+2	+3	
	0	-1	
	0	-6	
	0	-2	
	+1	-2	
	+1	-1	
	-1	-1	
	+1	+1	
	-2	-2	

Table II. Accepted points; Gaussian test; images with noncorrelated noises; variance measured on global image; [illegible] = 10[illegible]

SNR	ACCEPTED	
[illegible]/10:1	0	0
[illegible]/5:1	0	0
[illegible]/2:1	0	0
	-1	0
[illegible]/1:1	0	0
	+1	0
	-1	-2
	-1	-1
	0	-1
[illegible]10:1	0	0
[illegible]5:1	0	0
[illegible]2:1	+1	0
	0	0
10:1/10:1	0	0
10:1/5:1	0	0
5:1/5:1	0	0
	-1	0

Table III. Accepted points; binomial test; noisy images; [illegible] = 10[illegible]

CHANNELS	ACCEPTED	
4 and 5	0	0
	1	2
	-1	-2
	0	1
4 and 6	0	0
	0	1
	0	2
	-1	0
4 and 7	0	0
	0	1
	0	2
5 and 6	0	0
5 and 7	0	0
6 and 7	0	0
	0	1
	-1	-2
	-1	-3
	0	-1
	0	2

Table IV. Accepted points; binomial test; channels from the same multispectral image; [illegible] = 10[illegible]

CHANNELS	REGISTRATION			
	ORIGINAL		GRADIENT	
4	0	0	0	0
5	0	0	0	0
	0	+1		
6	0	0	0	0
	0	-1	0	-1
	0	+1		
7	0	-1	0	0
	0	0	0	-1
	0	+1		

Table V. Multitemporal registration; binomial test; p =.1, p =.5 for original images; p =.15, p =.5 for the magnitude of the gradient; [illegible] = [illegible] = 10[illegible]

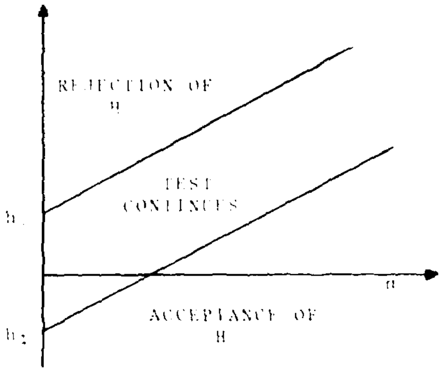

Figure 1. Regions defining the sequential probability ratio test for Gaussian and binomial distributions.

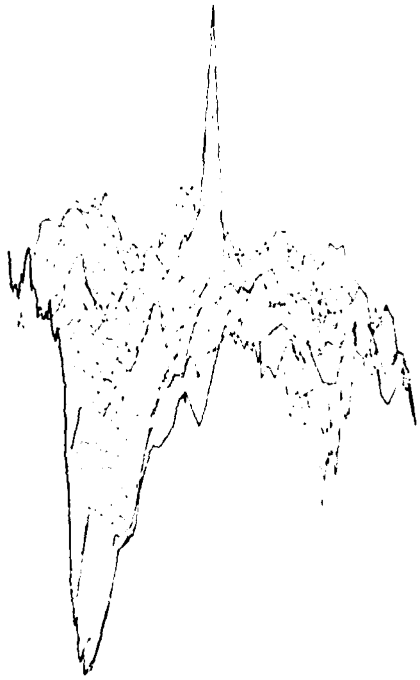

Figure 2. Distribution of the variance (inverted).

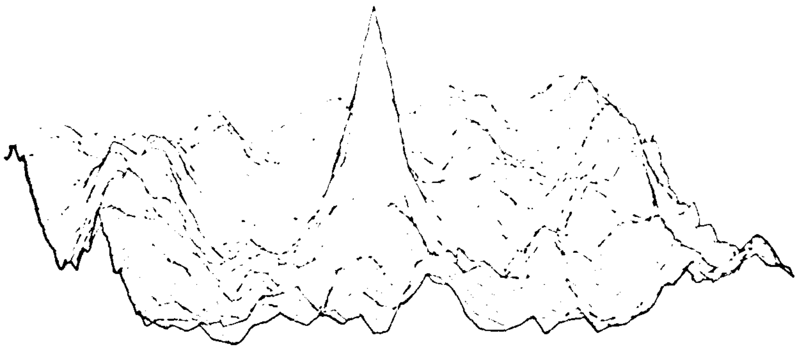

Figure 3. Distribution of the frequency of occurrence of 1's (inverted).

CHESAPEAKE BAY PLUME STUDY (SUPERFLUX) RELATIVE TO THE BIOLOGY OF THE CONTIGUOUS SHELF, FISHERY RESEARCH AND MONITORING

James P. Thomas

National Marine Fisheries Service
Northeast Fisheries Center
Sandy Hook Laboratory
Highlands, New Jersey 07732

ABSTRACT

A study was initiated in 1980 to study the influence of the Chesapeake Bay plume on the contiguous shelf using both in situ and remote sensing techniques. The combined use of in situ and remotely sensed data has enabled us to define the area of the continental shelf that is influenced by the Chesapeake Bay plume. Water emanating from the Bay contained biostimulants, contaminants and other materials as well as increased biomass and biological activity, and a different assemblage of phytoplankton. Remote sensing added to our ability to understand the complex and dynamic plume and adjacent shelf area by 1) providing synoptic and detailed information for the surface field in which in situ measurements were made, and 2) directing surface ships to key areas to maximize their sampling ability. Surface ships provided information concerning 1) the vertical structure of the water column, and 2) variables not directly relatable to those measured by remote sensors.

INTRODUCTION

A study was initiated in 1980 to delineate the role of remote sensing in Federal programs concerned with the monitoring and assessment of the effects of pollution on marine resources. Sponsored jointly by the Northeast Fisheries Center of the National Oceanic and Atmospheric Administration and the Langley Research Center of the National Aeronautics and Space Administration, the study -- called SUPERFLUX -- concentrated on the use of airborne remote sensors to study the impact of estuarine outflows on shelf ecosystems. The Chesapeake Bay plume and offshore waters were selected as the site for a series of prototype experiments (Figure 1), and a number of state agencies and universities participated in the study. Three interactive aircraft-boat experiments (March, June and October 1980) focused on techniques to characterize the spatial extent, variability and biological and chemical properties of the plume and adjacent shelf waters[1]. Seven different remote sensors were used during the course of these experiments (Table 1). This paper reviews some of the findings of the SUPERFLUX program relative to the biology of the contiguous shelf, fishery research and monitoring.

Definition of the Chesapeake Bay Plume

In terms of the biology of the contiguous shelf, fishery research and monitoring we would like to know where the Chesapeake Bay plume goes offshore, how it behaves, what it carries, what it deposits and what its effects are on the biota. We have been interested in defining such an area for long term monitoring and for planning an initial strategy for combatting catastrophic spills of toxic substances and other such occurrences. Boicourt[2] examined the plume area from February 1971 to August 1972, and determined

that the major influence of the Chesapeake Bay plume was southward from the mouth of the Bay along the Virginia coast.

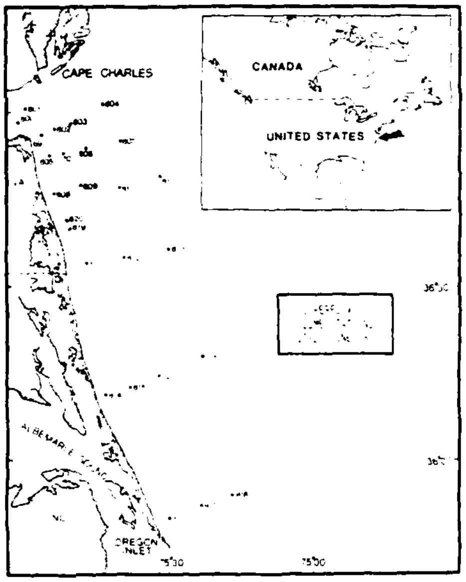

Figure 1. Sample locations

Table I. Remote sensors used during SUPERFLUX.

SENSORS	OPERATIONAL RANGE	OPERATIONAL WAVELENGTHS	VARIABLE MEASURED
Active Fluorosensors			
[illegible]	Visible	[illegible]	Chlorophyll Turbidity Phytoplankton color groups
[illegible]	Visible	[illegible]	all Fluorescing compounds Turbidity Chlorophyll
[illegible]			
[illegible]	Visible & Near IR	[illegible]	Turbidity Chlorophyll
[illegible]	Visible & Near IR	[illegible]	Turbidity Particulate Organics Chlorophyll
[illegible]	Visible & Near IR Thermal IR	[illegible]	Turbidity Chlorophyll Temperature
[illegible]			
[illegible]	Microwave	[illegible]	Salinity
[illegible]	Thermal IR	[illegible]	Temperature

Through SUPERFLUX, we demonstrated via remote sensing that a definable area exists over the continental shelf that is influenced over a period of years by the Chesapeake Bay plume. Munday and Fedosh[3] examined the historical satellite data available from LANDSAT since 1972 to define an area influenced by the Chesapeake Bay plume over the contiguous shelf. From the 81 images they examined, covering all seasons of the year, stages of the tide and winds, they defined areas of influence. In general, they found that the plume frequented a relatively well defined area east and south of the Bay mouth, along the Virginia coast (Figure 2). The thickest part of the plume also was found close to the coast (Figure 3).

Figure 2. Areas visited by the plume under different wind conditions. Based on analysis of LANDSAT imagery the numerals represent sector/zone counts as follows: 1: 0-5; 2: 6-10; 3: 11-20; 4: 21-30; 5: 31-40; 6: 41-50.[3]

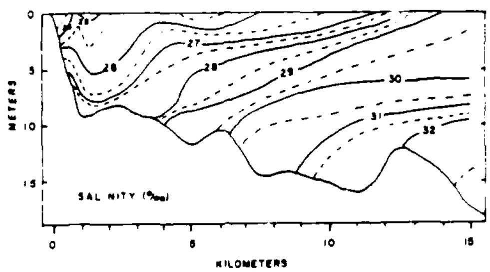

Figure 3. Cross-section of Chesapeake Bay plume salinity off Rudee Inlet on 19 March 1980.[4]

A similar pattern is exhibited in terms of in situ data as indicated by salinity (Figure 4); total suspended material (Figure 4); biostimulants such as the phytoplankton nutrients orthophosphate and ammonium (Figure 5); biomass such as bacterial numbers and chlorophyll a (Figure 6); community structure in terms of phytoplankton assemblages (Figure 7); and ecosystem function such as heterotrophic potential and total plankton respiration (Figure 8). Contaminants such as hydrocarbons associated with total suspended matter, had a similar distribution (Figure 4).

Likewise, remotely sensed data, as evidenced by salinity derived from the L-band microwave radiometer in conjunction with the PRT-5 infrared radiometer (Figure 9); turbidity based on the Ocean Color Scanner (Figure 10); chlorophyll (relative fluorescence) based on the Airborne Oceanographic Lidar (Figure 11); and the Testbed Airborne Multispectral Scanner[14] a' ' phytoplankton community composition derived from an Airborne Lidar Oceanographic Probing Experiment fluorosensor (Figure 12) confirmed a similar distribution of variables. Thus a rather well defined plume or outwelling area from Chesapeake Bay extends over the continental shelf.

The area of influence, however, may contract or expand depending on freshwater discharge from the Bay mouth. During the latter half of 1980, a severe drought caused the plume to contract (Figure 13). Eight years previous Boicourt[2] found a greatly expanded plume caused by excessive rainfall and freshwater runoff following hurricane Agnes (Figure 13).

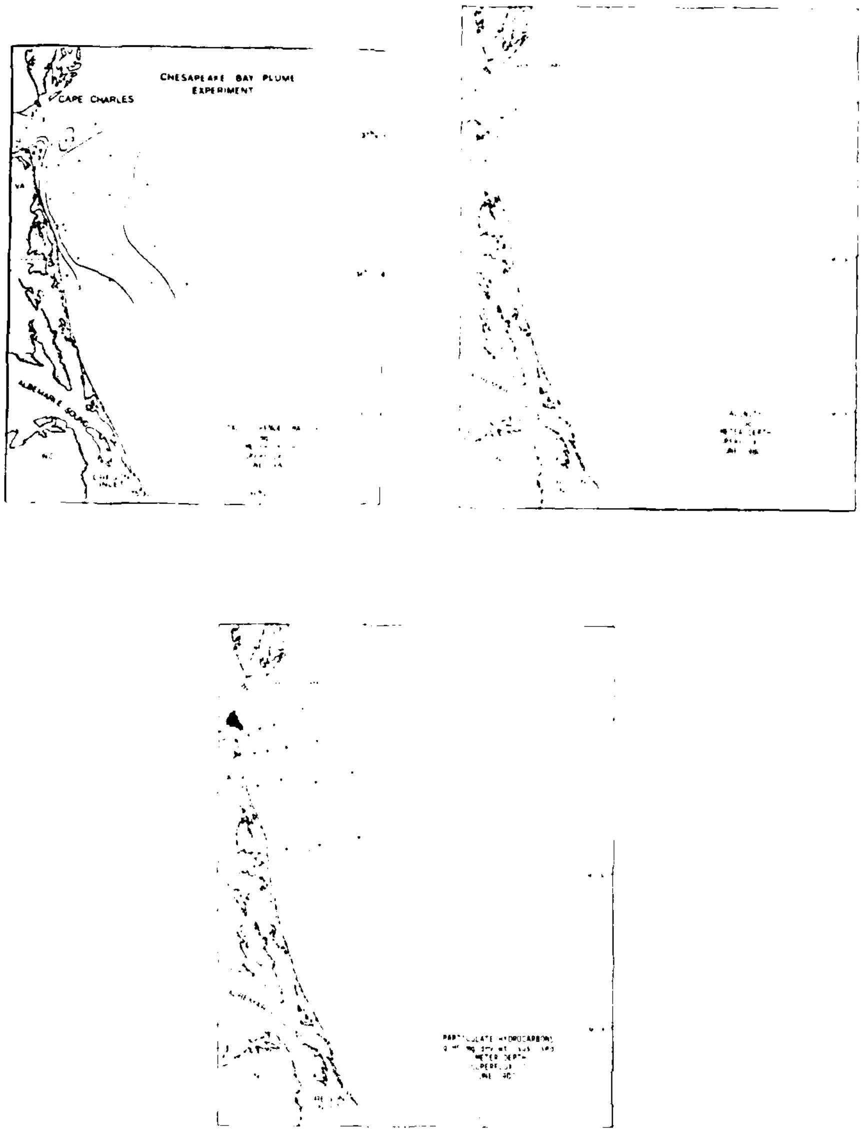

Figure 4. Map illustrating concentration of total suspended matter (mg/l) salinity (o/oo), and hydrocarbon (μg/mg) in surface water (1 m) adjacent to the Chesapeake Bay entrance during June 1980.[6,10,20]

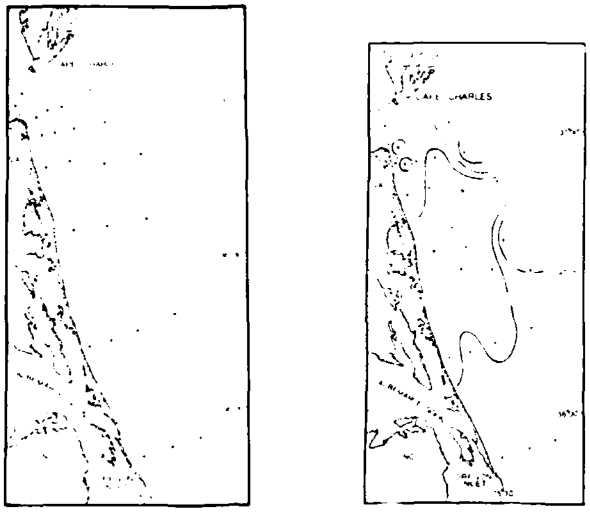

Phosphate (μM). Ammonia (μM).

Figure 5. Distribution of phosphate and ammonia at 1 m in June 1980.[7]

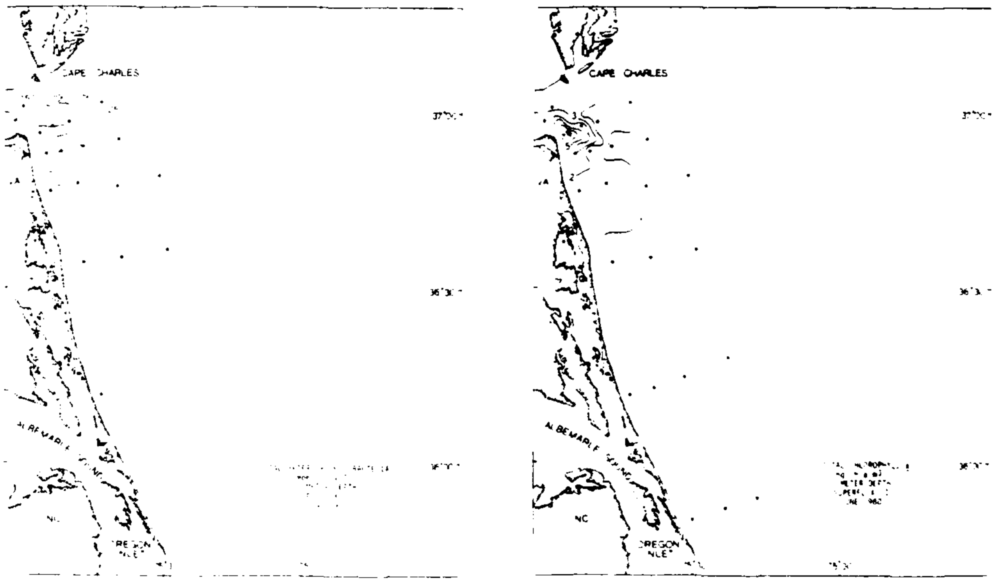

Figure 6. Surface views (1 m) of total heterotrophic bacteria[8] and total chlorophyll a for June 1980.[5]

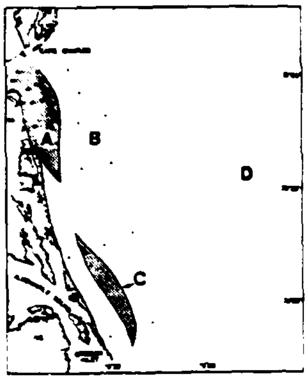

A. *Skeletonema costatum*
Nitzschia pungens
Leptocylindrus danicus
Rhizosolenia delicatula
Chaetoceros sp
Ultraphytoplankton component (<5 microns)
Cylindrotheca closterium

B. *Emiliania huxleyi*
Leptocylindrus danicus
Chaetoceros spp
Nitzschia pungens
Cryptomonas sp.
Gymnodinium sp
Skeletonema costatum

C. *Skeletonema costatum*
Emiliania huxleyi
Leptocylindrus danicus
Rhizosolenia delicatula
Chaetoceros sp
Ultraplankton component (<5 microns)

D. *Emiliania huxleyi*
Syracosphaera pulchra
Rhabdosphaera sp
Rhizosolenia alata
Rhizosolenia styliformis
Rhizosolenia delicatula
Ceratium fusus
Ceratium tripos
Prorocentrum micans
Protoperidinium spp

Figure 7. Phytoplankton assemblages during June 1980.[9]

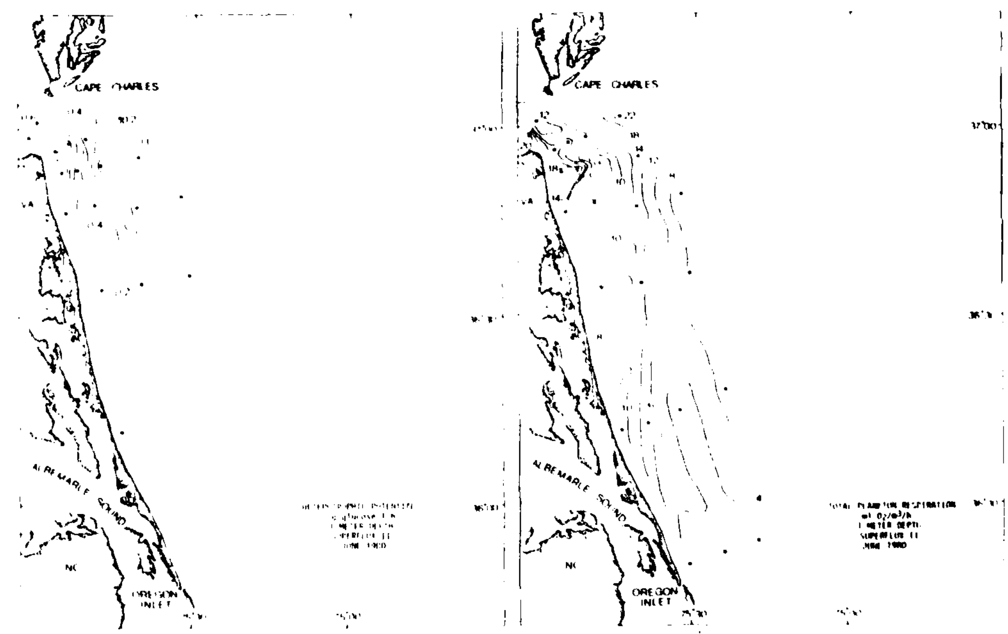

Figure 8. Surface views (1 m) of heterotrophic potential[8] and total plankton respiration[5], 17-27 June 1980.

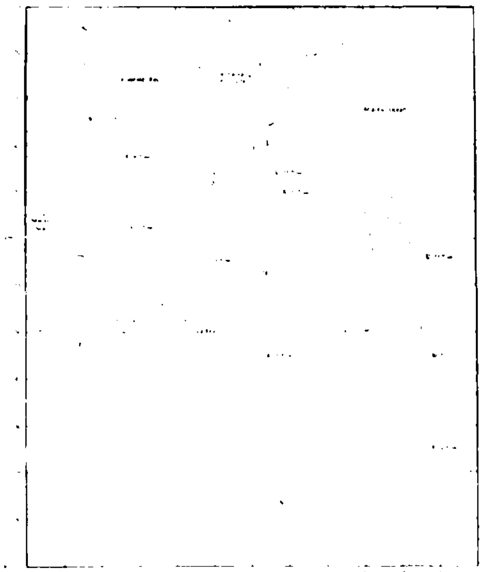

Figure 9a. Remotely sensed salinity map of Chesapeake Bay plume on 23 June 1980 (06:66-08:33 EDT).[11]

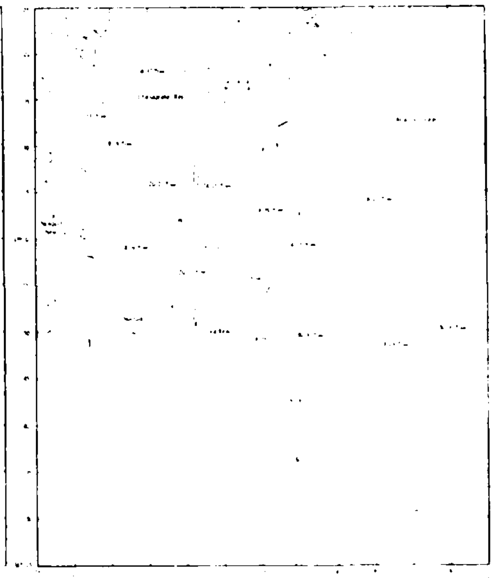

Figure 9b. Remotely sensed salinity map of Chesapeake Bay plume on 25 June 1980 (05:53-08:51 EDT).[11]

Influence of Chesapeake Bay Plume on Contiguous Shelf Ecosystem

The waters emanating from the mouth of Chesapeake Bay exert an influence on the contiguous shelf ecosystem. Some examples of the kinds of influence that the Chesapeake Bay plume has or could have on the shelf system, based on information obtained during the SUPERFLUX experiments, are presented here. We are interested in defining the actual and potential influences of the plume so that with increased understanding our ability to assess and manage the system might be improved.

Flowing out of the Bay with the estuarine water are higher concentrations of total suspended matter (Figure 4) which not only affect light penetration for primary production, but also provide a source of both food and contaminants for particulate feeders, both in the water column and on the seabed. Evidence suggests that particulate material outwelling from the Bay settles to the seabed down the length of the plume (Figure 14).

The Bay also is a source of nutrients for primary producers (Figure 5). These nutrients simulate primary production, resulting in increased biomass, and higher concentrations of phytoplankton and chlorophyll over the area influenced (Figure 6). This increased biomass, plus particulate and dissolved organic material from the estuary, acts as a food source to stimulate and support other trophic levels (Figure 6). Functionally, the response is a biologically more active system in the plume than in adjacent shelf waters. We see this with heterotrophic potential and total plankton respiration (Figure 8), both indicators of rates of utilization and decomposition of organic matter.

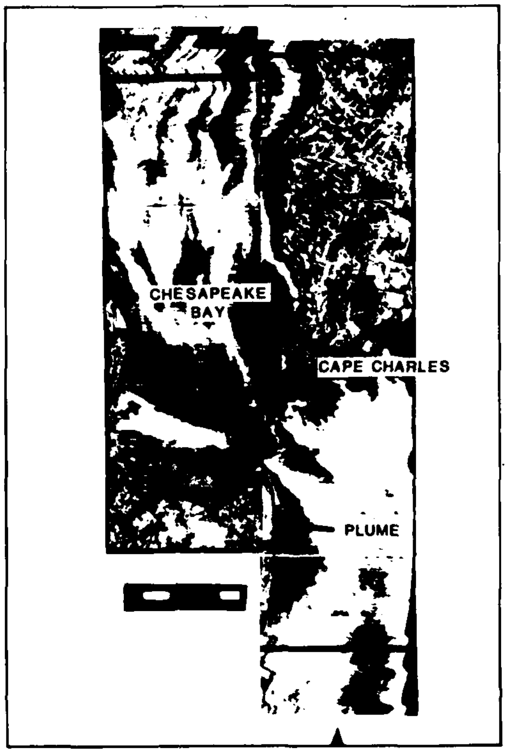

Figure 10. Mosiac of flight lines 1 and 3 of the OCS flown on 20 October 1980.[12]

In terms of community structure the phytoplankton assemblage of the Chesapeake Bay plume is different from surrounding shelf waters (Figure 7 and 12). Thus not only do quantitative and functional differences arise between the plume and the surrounding shelf waters, but also qualitative differences which would affect higher trophic levels through their feeding habits.

Oertel and Wade[10] reported on the characteristics of total suspended matter and associated hydrocarbon concentrations in shelf waters adjacent to Chesapeake Bay. Of particular interest was the fact that there was no congruence in the plumes of total suspended matter, hydrocarbons, and salinity (Figure 4). Each was characteristic of a separate, definable subplume emanating from the Bay mouth. During the June 1980 experiment the total suspended matter subplume was closest to the beach, the hydrocarbon subplume was furthest away, and the salinity subplume was in the middle. Such a distribution, with all flowing from one single bay mouth, suggests different primary sources from within the estuary and the maintenance of the continuity with each of these sources as the materials are carried from the Bay to the shelf. Thus, not only is there stratification or vertical layering and partitioning (between the plume surface waters and the benthos) as suggested earlier in the paper, but also separation of the various stimulating and contaminating influences on a horizontal basis, as demonstrated by Oertel and Wade[10]. This

means that the potential exists for different biological responses to occur in different parts of the outwelled water as well as on the seabed beneath the several subplumes emanating from the Bay mouth. Oertel and Dunstan[17] describe a similar phenomenon for the Georgia estuaries with foam-line fronts forming between the various sources within the estuary and subsequent "uncoupling" at the seaward ends of the plumes offshore. Therefore, this phenomenon is not unique to Chesapeake Bay, but probably is found with most dendritic-patterned estuaries and their offshore plumes.

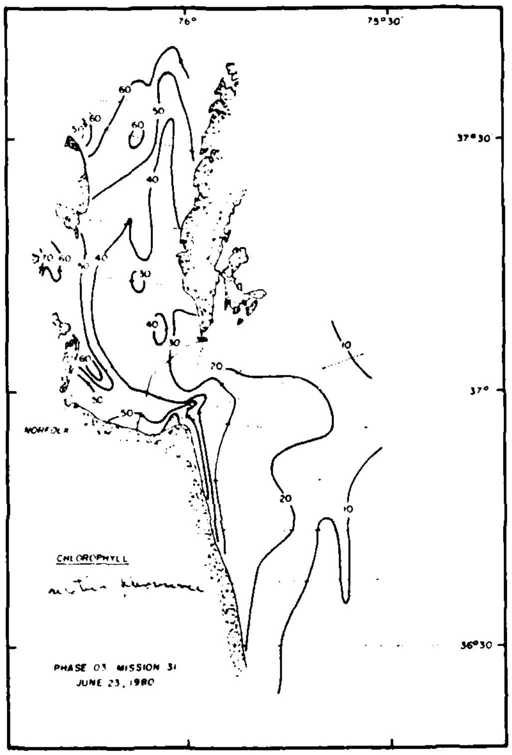

Figure 11. Contoured plots of relative chlorophyll a fluorescence from the AOL flown on 23 June 1980.[13]

Combined Use of In Situ and Remotely Sensed Data

The combined use of *in situ* and remotely sensed data and comparisons between the two provide insight into the potential use of remote sensing in fishery research and monitoring programs such as those described by Pearce[18]. During the June 1980 experiment a salinity plume was defined east and south of the Chesapeake Bay mouth along the Virginia coast based on data collected from a research ship over a period of several days and a number of tidal cycles (Figure 4). The result was a smoothly contoured plume which gave the impression of a discrete tongue of water with a central core emanating from the Bay mouth.

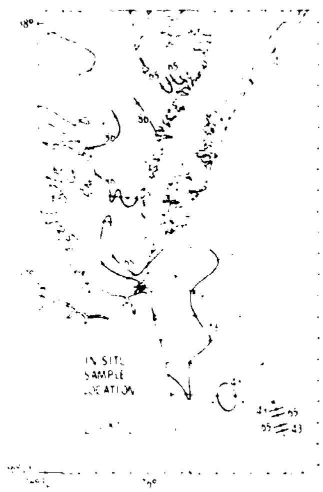

Figure 12. Flight paths and contours from calculations of fluorescence ratios from ALOPE for 23 June 1980 mapping mission. (Numbers on contour lines are fluorescence ratio, R, x 10^2.) The fluorescence ratio (R, x 10^2) varies from about 100 when members of the "golden-brown" color group (Bacillariophyceae and Dinophyceae) are 100 percent of the phytoplankton population, to about 33, when the members of the "green" color group (Chlorophyceae, Euglenophyceae, Prasinophyceae, Eustigmatphyceae, and Xanthophyceae) are 100 percent.[15,16]

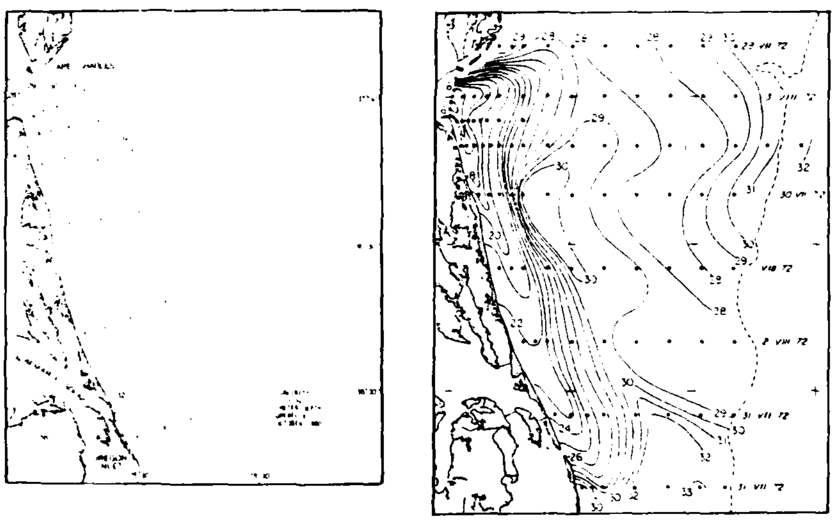

Figure 13. Surface (1 m) salinity distributions (o/oo) for October 1980[1] and July-August 1972.[2]

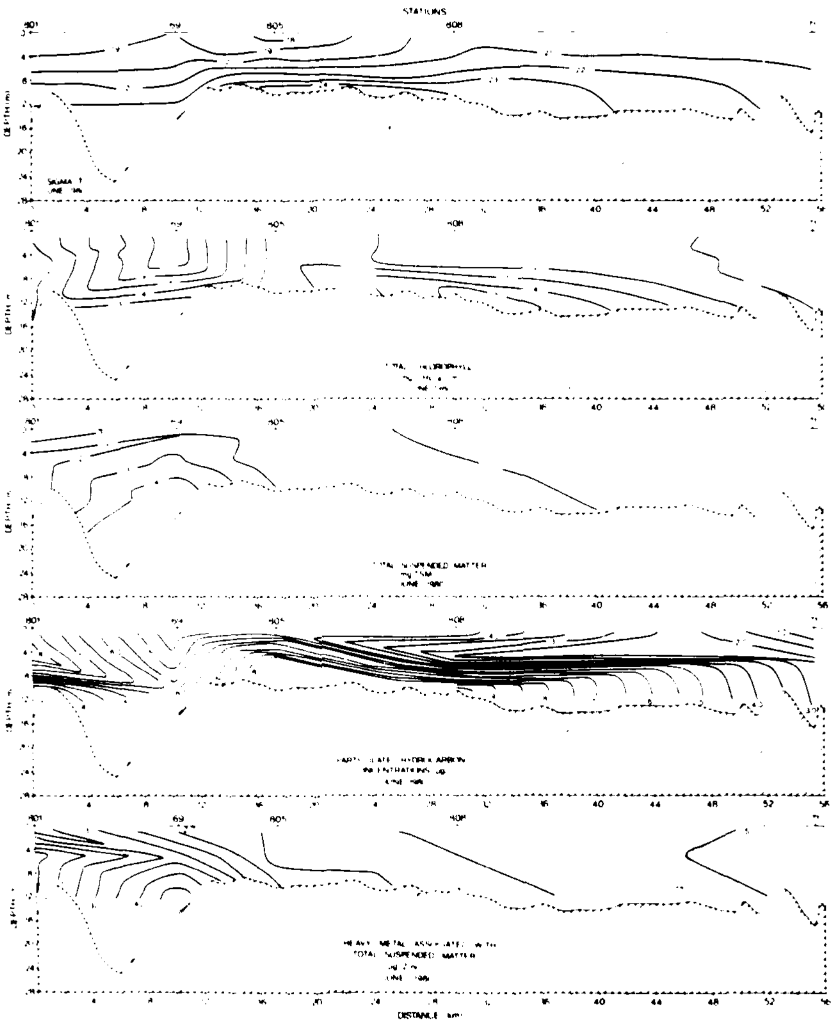

Figure 14. Lengthwise section of the Chesapeake Bay plume for σ_t[5], total chlorophyll a[5], total suspended matter[6], particulate hydrocarbons[20], and heav, metal concentrations[21]. See Figure 1 for station locations.

During this same experiment, but lasting for periods of two hours, instead of several days, an L-band microwave radiometer was flown over the Chesapeake Bay plume area on several different days to map the distribution of surface salinity (Figure 9). These data are nearly synoptic compared with the *in situ* data collected over several days. The contouring is not as smooth and regular, even though the same general pattern is seen in both the *in situ* and remotely sensed data. Notice the change in salinity distribution between

23 June and 25 June. The low salinity water still ranges from the Bay mouth south along the Virginia shore. However, what is particularly interesting is the presence of high salinity water between two tongues of low salinity water exiting southeastward from the Bay mouth (Figure 9b). Isolated pockets of lower or higher salinity water are present. This so called "pocketing", added detail in contouring, and the rather large change in salinity distribution over a period of several days was not in evidence in the more generalized in situ data (Figure 4). This is new information in terms of understanding the dynamics of an estuarine plume. We are unable to obtain this kind of synoptic, repeated and detailed information using a single surface ship! Similar detail is seen in the Ocean Color Scanner (OCS) data (Figure 10). The outline of the plume is not regular; nor is the plume of uniform density.

Additionally, remote sensors have the capability of providing real-time or near real-time output of data sufficiently reduced to be useful in directing operations during the course of an experiment. The OCS data collected by Ohlhorst[12] during June 1980 were transmitted in real-time from the aircraft to a ground station and used to direct operations. The Airborne Oceanographic Lidar[13], the L-band microwave radiometer[11], the PRT-5 infrared radiometer[11], and the Multichannel Ocean Color Scanner[19] all produced data capable of being reduced in near real-time for purposes of directing operations.

A particularly graphic example illustrating the usefulness of airborne remote sensing for defining major regions of the shelf and then directing surface ship sampling was presented by Grew[19]. He used real-time output from a Multichannel Ocean Color Scanner (MOCS) to define the shelf regions and then direct a surface ship to each of the key areas. Approximately 8 to 9 hours prior to the aircraft-directed sampling, the NOAA Ship KELEZ was requested to collect and process surface bucket samples (one every 10 to 15 minutes) for chlorophyll and phaeopigment (for Fo/Fa ratio) from the mouth of Chesapeake Bay east across the shelf to the continental rise. Although processed immediately, the data from these samples were not relayed to aircraft personnel for directing in situ sampling. Once offshore over the continental rise we were asked to proceed back toward the mouth of the Bay along the same line we had just sampled. The difference, however, was that we took many fewer samples and those we did take were at locations selected by airborne MOCS operators on the basis of the real-time output they observed from MOCS.

In our charted data (Figure 15), notice that the cross-shelf profile as defined by both the remotely sensed and the in situ data, are similar. Also that the in situ data derived from the aircraft-directed sampling (Figure 15B) does describe the basic features of the chlorophyll a cross-shelf profile. Thus, a degree of confidence can be had in the remotely sensed data to 1) characterize in real-time the major features of the shelf and slope surface waters, and 2) to direct in situ sampling of these waters. This is particularly relevant to fishery research and monitoring in that the ability to define major type areas in real-time enhances our ability to effectively utilize our ships and personnel.

CONCLUDING REMARKS

In terms of fishery research and monitoring the combined use of in situ and remotely sensed data has enabled us to define, for each experiment as well as over time, the area of the continental shelf that is influenced by the Chesapeake Bay plume. Based on historical as well as present information we know that this area contracts and expands based on freshwater discharge from the Bay mouth and meterological and physical factors affecting the shelf. From SUPERFLUX we know that the waters emanating

from Chesapeake Bay contain biostimulants, contaminants, and other materials as well as increased biomass and biological activity, and structurally different assemblages of organisms. These waters emanating from the Bay are not homogeneous, but rather appear to be a series of discrete subplumes each with its own set of characteristics. We also see evidence to suggest that particulate materials settle from plume waters to the seabed down the length of the plume. Thus, by way of expansion, contraction, changes in direction, and the fractionation or partitioning of materials, the Chesapeake Bay plume exerts greater or lesser, positive and negative influences on the living marine resources of the contiguous shelf.

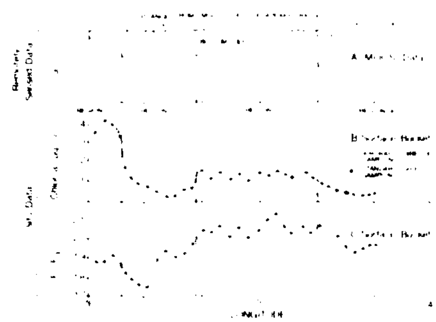

Figure 15. A) Multichannel Ocean Color Scanner (MOCS) data; B) in situ surface chlorophyll a; and C) Fo/Fa ratios along transect from the mouth of Chesapeake Bay across shelf to continental rise and return on 21 October 1980.[19]

From remote sensing we have learned something of the complexity of the Chesapeake Bay plume and adjacent shelf surface waters. Remote sensing of the plume and neighboring shelf waters provided us with more synoptic and more detailed information concerning the distributions of temperature, salinity, turbidity, chlorophyll a, and phytoplankton assemblages in these surface waters than was obtainable using a single surface ship. In certain cases, repeated coverage by remote sensors informed us of some of the dynamic changes that took place over a period of several days. Additionally, sufficiently reduced real-time output from the remote sensors enabled definition of surface water masses over the continental shelf. Such ability to define the various water masses was used to direct in situ sampling of surface waters in near real-time. Thus, remote sensing adds to our ability to understand complex and dynamic areas by 1) providing synoptic and detailed information for the surface field which in situ measurements at isolated locations are being made, and 2) directing surface ships to key areas to maximize their sampling ability.

Surface ships, however, not only provide "sea truth" for the remote sensors, but also examine the vertical structure of the water column and investigate variables not directly relatable to those measured by remote sensors. Thus, it is the flow of information back and forth between remote sensing and in situ sampling that provides the real power to 1) overcome the temporal-spatial problems of in situ sampling, and 2) expand the interpretability of the remotely sensed data to variables not measured directly by the remote sensors.

In future years remote sensing will be used to monitor environmental quality and to assist in managing resources (e.g. directing fishing operations) and habitats (e.g. ecological zoning for development or waste disposal). Finally, because of its perspective vantage point and ability to describe surface flow and transport of materials, remote sensing will be utilized increasingly to respond to catastrophic events and major spills of toxic substances.

REFERENCES

1. Campbell, J. W. and J. P. Thomas (eds.). 1981. Chesapeake Bay Plume Study: Superflux 1980. NASA Conference Publ. 2188 and NOAA/NEMP III 81 ABCDFG 0042. NTIS, Springfield, VA. 522 p.

2. Boicourt, W. C. 1973. The circulation of water on the continental shelf from Chesapeake Bay to Cape Hatteras. Ph.D Thesis, Johns Hopkins University.

3. Munday, J. C. and M. S. Fedosh. 1981. Chesapeake Bay plume dynamics from Landsat. In: Chesapeake Bay Plume Study: Superflux 1980. J. W. Campbell and J. P. Thomas (eds.). NASA Conference Publ. 2188 and NOAA/NEMP III 81 ABCDFG 0042.

4. Ruzecki, E. P. 1981. Temporal and spatial variation of the Chesapeake Bay plume In: Chesapeake Bay Plume Study: Superflux 1980. J. W. Campbell and J. P. Thomas (eds.). NASA Conference Publ. 2188 and NOAA/NEMP III 81 ABCDFG 0042.

5. Robertson, C. N. and J. P. Thomas. 1981. Total plankton respiration in the Chesapeake Bay plume. In: Chesapeake Bay Plume Study: Superflux 1980. J. W. Campbell and J. P. Thomas (eds.). NASA Conference Publ. 2188 and NOAA/NEMP III 81 ABCDFG 0042.

6. Gingerich, K. J. and G. F. Oertel. 1981. Suspended particulate matter in the Chesapeake Bay entrance and adjacent shelf waters. In: Chesapeake Bay Plume Study: Superflux 1980. J. W. Campbell and J. P. Thomas (eds.). NASA Conference Publ. 2188 and NOAA/NEMP III 81 ABCDFG 0042.

7. Wong, G. T. F. and J. F. Todd. 1981. Nutrients in waters on the inner shelf between Cape Charles and Cape Hatteras. In: Chespeake Bay Plume Study: Superflux 1980. J. W. Campbell and J. P. Thomas (eds.). NASA Conference Publ. 2188 and NOAA/NEMP III 81 ABCDFG 0042.

8. Kator, H. I. and P. L. Zubkoff. 1981. Bacterial biomass and heterotrophic potential in the waters of the Chesapeake Bay plume and contiguous shelf. In: Chesapeake Bay Plume Study: Superflux 1980. J. W. Campbell and J. P. Thomas (eds.). NASA Conference Publ. 2188 and NOAA/NEMP III 81 ABCDFG 0042.

9. Marshall, H. G. 1981. Phytoplankton assemblages within the Chesapeake Bay plume and adjacent waters of the continental shelf. In: Chesapeake Bay Plume Study: Superflux 1980. J. W. Campbell and J. P. Thomas (eds.). NASA Conference Publ. 2188 and NOAA/NEMP III 81 ABCDFG 0042.

10. Oertel, G. F. and T. L. Wade. 1981. Characteristics of total suspended matter and associated hydrocarbon concentrations adjacent to the Chesapeake Bay entrance. In: Chesapeake Bay Plume Study: Superflux 1980. J. W. Campbell and J. P. Thomas (eds.). NASA Conference Publ. 2188 and NOAA/NEMP III 81 ABCDFG 0042.

11. Kendall, B. M. 1981. Remote sensing of the Chesapeake Bay plume salinity via microwave radiometry. In: Chesapeake Bay Plume Study: Superflux 1980. J. W. Campbell and J. P. Thomas (eds.). NASA Conference Publ. 2188 and NOAA/NEMP III 81 ABCDFG 0042.

12. Ohlhorst, C. W. 1981. Preliminary analysis of Ocean Color Scanner data from Superflux III. In: Chesapeake Bay Plume Study: Superflux 1980. J. W. Campbell and J. P. Thomas (eds.). NASA Conference Publ. 2188 and NOAA/NEMP III 81 ABCDFG 0042.

13. Hoge, R. E. and R. N. Swift. 1981. Application of the NASA Airborne Oceanographic Lidar to the mapping of chlorophyll and other organic pigments. In: Chesapeake Bay Plume Study: Superflux 1980. J. W. Campbell and J. P. Thomas (eds.). NASA Conference Publ. 2188 and NOAA/NEMP III 81 ABCDFG 0042.

14. Bowker, D. E., C. A. Hardesty, D. A. Jobson and G. S. Bahn. 1981. Analysis of testbed airborne multispectral scanner data from Superflux II. In: Chesapeake Bay Plume Study: Superflux 1980. J. W. Campbell and J. P. Thomas (eds.). NASA Conference Publ. 2188 and NOAA/NEMP III 31 ABCDFG 0042.

15. Jarrett, O., Jr., W. E. Esaias, C. A. Brown, Jr. and E. Brian Pritchard. 1981. Analysis of ALOPE data from Superflux. In: Chesapeake Bay Plume Study: Superflux 1980. J. W. Campbell and J. P. Thomas (eds.). NASA Conference Publ. 2188 and NOAA/NEMP III 81 ABCDFG 0042.

16. Farmer, F. H. 1981. Interpretation of an index of phytoplankton composition calculated from remote airborne fluorsensor data. In: Chesapeake Bay Plume Study: Superflux 1980. J. W. Campbell and J. P. Thomas (eds.). NASA Conference Publ. 2188 and NOAA/NEMP III 81 ABCDFG 0042.

17. Oertel, G. F. and W. M. Dunstan. 1981. Suspended-sediment distribution and certain aspects of phytoplankton production off Georgia, U.S.A. Marine Geol. 40: 171-197.

18. Pearce, J. B. 1981. A marine environmental monitoring and assessment program. In: Chesapeake Bay Plume Study: Superflux 1980. J. W. Campbell and J. P. Thomas (eds.). NASA Conference Publ. 2188 and NOAA/NEMP III 81 ABCDFG 0042.

19. Grew, G. W. 1981. Real-time test of MOCS algorithm during Superflux 1980. In: Chesapeake Bay Plume Study: Superflux 1980. J. W. Campbell and J. P. Thomas (eds.). NASA Conference Publ. 2188 and NOAA/NEMP III 81 ABCDFG 0042.

20. Wade, T. L. and G. F. Oertel. 1981. Concentration of hydrocarbons associated with particles in the shelf waters adjacent to the entrance of Chesapeake Bay. In: Chesapeake Bay Plume Study: Superflux 1980. J. W. Campbell and J. P. Thomas (eds.). NASA Conference Publ. 2188 and NOAA/NEMP III 81 ABCDFG 0042.

21. Harris, R. L. 1980. Metal distributions in suspended sediment in the Chesapeake Bay plume and adjacent Atlantic continental shelf. Northeast Monitoring Program Office, Sandy Hook Laboratory, Highlands, New Jersey, Contract No. NA-80-FA-C-00034.

IMPACTS OF CLIMATE ON VARIATIONS IN SUMMER ICE COVER IN THE CANADIAN ARCTIC

B. DEY

Department of Geology and Geography
Howard University
Washington, D. C. 20059

ABSTRACT

Information regarding variations in the summer ice cover in the Canadian Arctic for 1976 and 1977 was obtained from NOAA and Landsat satellite images. Maps of areal and temporal variations in sea ice cover revealed several interesting features. The retreat rates of the pack ice edge in the western Canadian Arctic, particularly in the Beaufort Sea were faster in 1977 than in 1976. On the other hand, in the eastern Canadian Arctic, particularly, in Baffin Bay the rates of summer ice melt were faster in 1976 compared to 1977.

Three climatic elements, accumulated summer melting degree days, 1000-millibar pressure patterns and 700-millibar height departures were used in this study. The first two climatic elements had a strong impact on ice cover variations. The higher values of accumulated summer melting degree days in the western Canadian Arctic in 1977 as compared to 1976 were related to maximum expansion of open water in the Beaufort Sea. The second most important factor for the vast expansion of open water in the summer of 1977 appeared to be the locations of high and low pressure cells and the resulting southeasterly winds in the southern Beaufort Sea. By contrast, during the 1976 summer season, the southern Beaufort Sea experienced calm conditions or northwesterly winds which kept ice close to the shore.

1. INTRODUCTION

Each summer, the retreat of the pack ice edge and the emergence of open water in the Canadian Arctic plays an important role in the navigation and offshore drilling for gas and oil. Atmospheric circulation patterns are known to be the principal factor in the areal and temporal variations in pack ice edge retreat and expansion of open water (Markham, 1975; Marko, 1975; Rogers, 1978; Walsh and Johnson, 1979a; Dey, 1980a, 1980b). This paper reports on an analysis of the impact of climatic elements on the variations in summer ice cover in the Canadian Arctic during two markedly different but consecutive years: 1976 and 1977.

2. SOURCES OF DATA AND METHODOLOGY

Satellite images particularly of NOAA and Landsat were the main source of sea ice information. Sea ice charts produced by the Ice Climatology and Applications Division, Atmospheric Environment Service (AES), Ottawa were also consulted. Climatic data such as surface temperatures and 1000-millibar constant pressure charts were obtained from the AES, Ottawa. Mean monthly departures of 700-millibar normal height were extracted from the mean monthly 700-millibar charts published in the Monthly Weather Review.

Manual photo interpretation techniques were used to map sea ice conditions in the Canadian Arctic. The techniques and the problems associated with NOAA satellite image interpretation of sea ice cover have been discussed elsewhere (Dey et al., 1979). Mean temperatures above 0°C have been used as base for calculating accumulated summer melting degree days. The 1000-millibar constant pressure charts indicate the locations of high and low pressure cells and the directions of the geostrophic winds. The mean departures of 700-millibar normal heights along 72°N latitude have been drawan for the western hemisphere covering the Canadian Arctic.

The analyses of the variations in summer ice cover in the Canadian Arctic are divided into two parts. The first part, on ice cover and monthly variations, provide a general description based on the analyses of two years of satellite images and sea ice charts. The second part relates three climatic elements (surface temperatures/accumulated summer melting degree days, 1000-millibar atmospheric flow patterns and 700-millibar height departures) with variations of ice cover in the Canadian Arctic for the summer seasons of 1976 and 1977. Finally, the study explains in general terms the impact of climatic elements on summer ice cover variations.

3. VARIATIONS OF SUMMER ICE COVERS: 1976 AND 1977

On 30 June 1976, the retreat of pack ice and the emergence of open water area was small in the southern Beaufort Sea (Fig.1). However, the pack ice retreated northward during the month of July (Fig.2). The open water area extended eastward from the southern Beaufort Sea to the western Amundsen Gulf. The open water area in the southern Beaufort Sea almost remained the same during the months of July and August of 1976, although Amundsen Gulf and part of the southern channels of Queen Elizabeth Archipelago became ice free (Fig.3). However, pack ice significantly retreated from August to September in the Beaufort Sea (Fig.4).

In the eastern sector of the Canadian Arctic, particularly over Baffin Bay and northern Davis Strait, the rates of emergence of open water were faster during the months June through September, 1976 when compared to the rates for the same period over the Beaufort Sea (Figs. 1-4). Baffin Bay and northern Davis Strait became ice free in September, 1976 (Fig.4).

In June 1977, the area of open water was almost the same as it was in June 1976, but the eastern Beaufort Sea adjoining Banks Island was ice free (Fig.1). However, the pack ice significantly retreated towards the north by the end of July 1977 (Fig.2). The area of open water extended over 400 km northward from the coast of Mackenzie Bay. The pack ice in the Beaufort Sea moved further north by the end of August (Fig.3) and continued in September (Fig.4) of 1977.

Over Baffin Bay and northern Davis Strait, the rates of emergence of open water during the summer of 1977 were much slower than that of the summer of 1976 (Figs. 1-4). One significant feature in 1977 was the presence of ice east and northeast of Home Bay by the end of September 1977 (Fig.4).

Figures 1 to 4, indicate both areal and temporal variations of ice cover during the summer months of 1976 and 1977. In the Beaufort Sea, the retreat of pack ice and the expansion of open water were very slow during the months June through August, 1976 when compared with the same period for 1977. However, over Baffin Bay and northern Davis Strait, the rates of emergence of open water during the summer months of 1976 were higher than that of the same period for 1977.

In summary, the summer of 1976 was associated with light ice conditions in Baffin Bay but, heavy ice conditions in the Beaufort Sea, Conversely, the summer of 1977 was associated with light ice conditions in Beaufort Sea but moderate ice conditions in Baffin Bay.

4. IMPACTS OF CLIMATIC ELEMENTS ON SUMMER ICE COVER VARIATIONS

Three climatic elements, surface temperatures/accumulated summer melting degree days, 1000-millibar pressure patterns and 700-millibar height departures for the summers of 1976 and 1977 have been analyzed and related with the variations of sea ice cover during the same period.

4.1 Accumulated Summer Melting Degree Days

The accumulated summer melting degree days, derived from mean temperatures above 0°C are plotted in Figure 5 for four Canadian Arctic stations: Clyde and Cape Dyer in the eastern Canadian Arctic, Sachs Harbour in the western Canadian Arctic and Resolute in the central Canadian Arctic. The most significant features are that, in 1977 summer season, the first occurrance of melting was earlier than in 1976, and the accumulated values of melting degree days were much higher (Fig.5). This was particularly important for Sachs Harbour which is located in the western Canadian Arctic. Note that the areal and temporal variations of sea ice cover in the Beaufort Sea were very significant between the 1976 and 1977 summer seasons.

The climatic station Clyde, located near Home Bay, where sea ice remained at the end of 1977 summer season shows higher values of accumulated summer melting degree days for 1977 than in 1976 (Fig.5). However, the difference of accumulated melting degreee day values were much smaller between 1976 and 1977 when compared with the same period for Sachs Harbour which is located in the western Canadian Arctic.

In summary, strong relationships between accumulated summer melting degree days and sea ice cover variations have been noticed for the Beaufort Sea sector of the Canadian Arctic. However, the relationship was not strong for the Baffin Bay sector of the Canadian Arctic.

4.2 1000-Millibar Pressure Patterns

Though ice cover responds to a single major storm, the areal variations of open water and ice cover at the final day of a month have been satisfactorily related with the mean monthly atmospheric conditions over the Canadian Arctic (Dey, 1980a, 1980b).

The 1000-millibar charts for the months June through August, 1976 (Figs. 6-8) show either calm conditions or northwesterly geostrophic winds (apparent in the pressure gradient and high pressure cells) over the Beaufort Sea. The calm conditions and the northwesterly winds kept sea ice close to the southern coast of the Beaufort Sea (Figs. 1-3). However, in September 1976, the winds were southeasterly (Fig.9) which helped to push pack ice northwestward and as a result more open water emerged in the Beaufort Sea by the end of September 1976 (Fig.4).

During June through August, 1977, the geostrophic winds were southeasterly over the Beaufort Sea (Figs. 6-8) and the winds pushed the pack ice northwest. The southeasterly winds during the months June through August are related to the vast expansion of open water in the Beaufort Sea (Figs. 1-3).

Over Baffin Bay, the geostrophic winds were northwesterly during the months June and August, 1976 (Figs. 6 and 8). The northwesterly winds along with the northwesterly currents (Baffin Island Current) helped to move pack ice from Baffin Bay to Davis Strait and Labrador Sea. On the other hand, during the summer of 1977, the Baffin Bay area remained calm or winds were northeasterly, which caused the pack ice to concentrate northeast of Home Bay.

In summary, the southeasterly winds are related with the vast expansion of open water in the Beaufort Sea. However, the expansion of open water in the Beaufort Sea may be limited during calm conditions, or when the winds are northwesterly. In Baffin Bay, the northwesterly winds are related with the removal of pack ice from Baffin Bay while calm conditions, or northeasterly winds, are related to pack ice concentration northeast of Home Bay.

4.3 700-Millibar Height Departures

Heavy ice conditions in the Beaufort Sea during the summer of 1976 were associated with higher heights than the same period for 1977 (Fig.10) which is considered to be light ice summer

season. Over Baffin Bay, the light ice summer season of 1976 was associated with below normal heights for the months June through August. This is contrary to the previous findings for the 1978 summer season, the year of heavy summer ice conditions in Baffin Bay, which was associated with below normal heights for the months June through August (Dey, 1980c). Walsh and Johnson (1979b) also found that heavy ice conditions in eastern Canadian waters were associated with below normal 700-millibar heights in the Greenland-Baffin Bay area.

In summary, the 700-millibar height departures could not be satisfactorily related with the ice conditions, particularly over the Baffin Bay sector of the Canadian Arctic.

5. CONCLUSIONS

These analyses of two years summer seasons data indicate that the climatic elements of 1000-millibar atmospheric flow patterns (particularly the positions of pressure cells and resultant winds) and the surface temperatures (accumulated summer melting degree days) have significant impacts on variations of sea ice cover, especially over the Beaufort Sea sector of the Canadian Arctic. These efforts support earlier findings (Dey, 1980a, 1980b). The southeasterly winds move pack ice from the southeastern Beaufort Sea northward into the Arctic Ocean, whereas the northwesterly flow keeps pack ice close to the coast of southern Beaufort Sea. The prevailing winds, southeasterly or northwesterly, resulting from the locations of high and low pressure cells cause advection of warm air masses from the southeast or cold air masses from the northwest thereby increasing or decreasing air temperatures/accumulated summer melting degree days, particularly over the Beaufort Sea sector of the Canadian Arctic. Over the eastern Canadian Arctic, particularly over Baffin Bay, the northwesterly winds and high values of accumulated summer melting degree days appeared to cause light ice conditions for the summer of 1976.

Among the three climatic elements (accumulated summer melting degree days, 1000-millibar pressure patterns and 700-millibar height departures) considered in this study, the first two have a strong impact on sea ice variations. The results of this study are preliminary because only two years data sets have been used in these analyses.

6. REFERENCES

Dey, B. 1980a: Variations of August ice cover in the Beaufort Sea and related weather conditions, Bulletin of the American Meteorological Society, Vol. 61, pp. 213-217.

_____. 1980b: Ice cover and related atmospheric conditions in Arctic Canada during the summer of 1978, Monthly Weather Review, Vol. 108, pp. 2092-2097.

_____. 1980c: Seasonal and annual variations in ice cover in Baffin Bay and northern Davis Strait, Canadian Geographer, Vol. 24, pp. 368-384.

_____, H. Moore and A. F. Gregory. 1979: Monitoring and mapping sea-ice breakup and freezeup of Arctic Canada from satellite images, Arctic and Alpine Research, Vol. 11, pp. 229-242.

Markham, W. E. 1975: Ice Climatology of the Beaufort Sea,, Canada Department of Environment, Victoria, B. C., Beaufort Sea Technical Report 26, 87p.

Marko, J. 1975: Satellite Observations of the Beaufort Sea Ice, Canada Department of Environment, Victoria, B. C., Beaufort Sea Technical Report 34, 137p.

Rogers, J. C. 1978: Meteorological factors affecting interannual variability of summer time ice extent in the Beaufort Sea, Monthly Weather Review, Vol. 106, pp. 890-897.

Walsh, J. E. and C. M. Johnson. 1979a: The analysis of Arctic sea ice fluctuations, Journal of Physical Oceanography, Vol. 9, pp. 580-591.

_____. 1979b: Interannual atmospheric variability and associated fluctuations in the Arctic ice extent, Journal of Geophysical Research, Vol. 84, pp. 6915-6928.

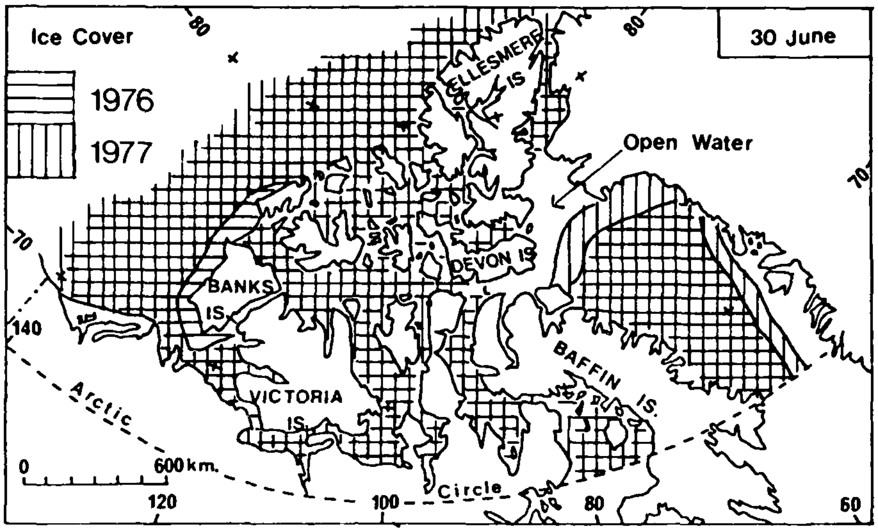

Fig. 1. Ice cover and open water in the Canadian Arctic on 30 June, 1976 and 1977.

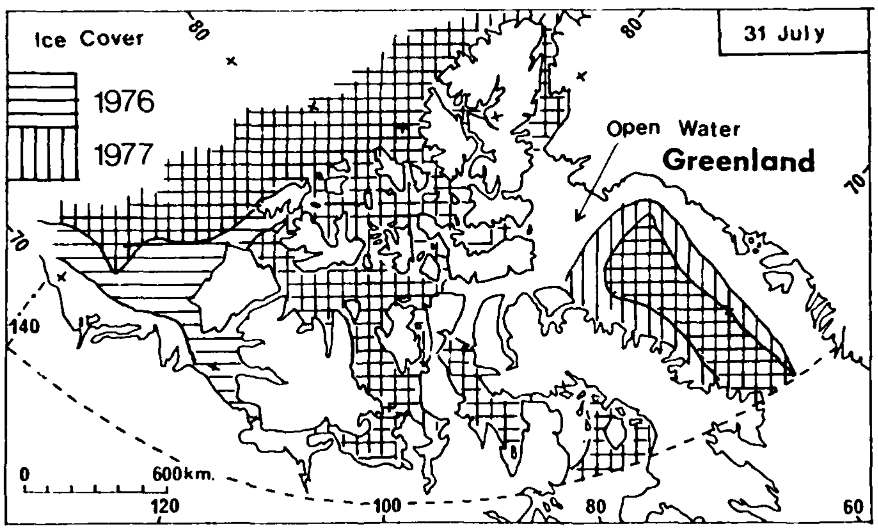

Fig. 2. Ice cover and open water in the Canadian Arctic on 31 July, 1976 and 1977.

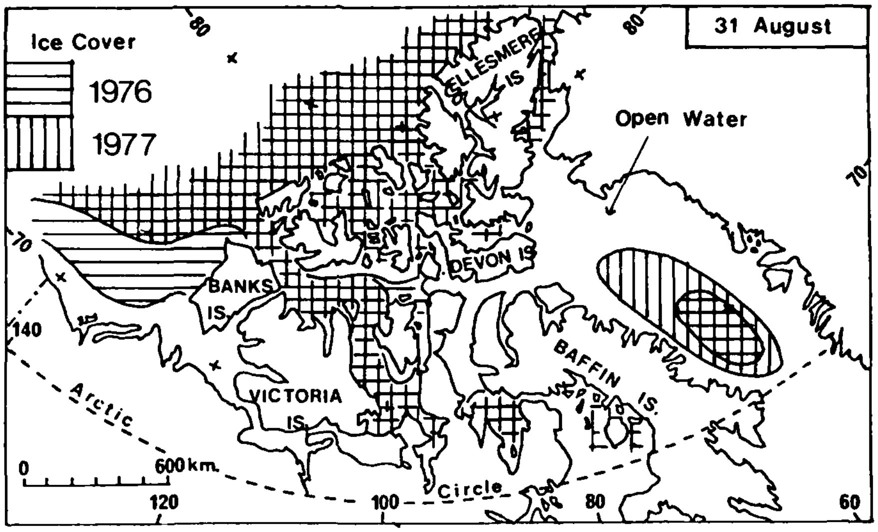

Fig. 3. Ice cover and open water in the Canadian Arctic on 31 August, 1976 and 1977.

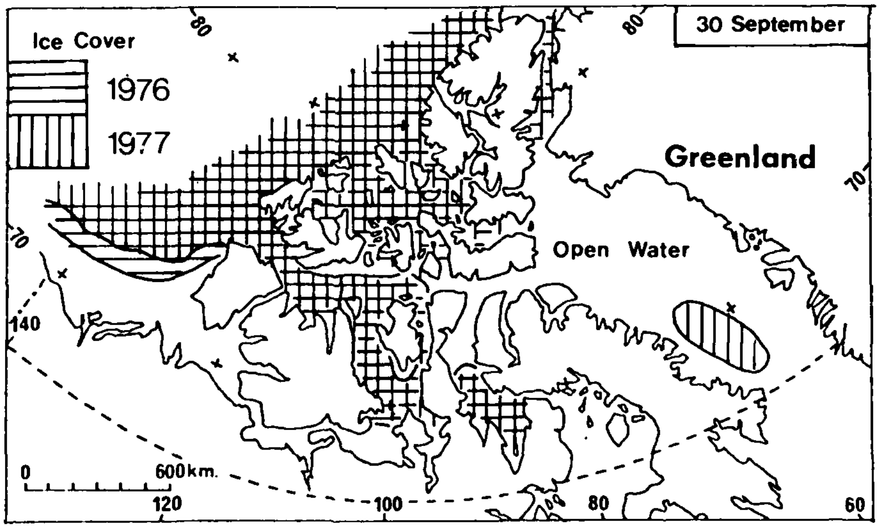

Fig. 4. Ice cover and open water in the Canadian Arctic on 30 September, 1976 and 1977.

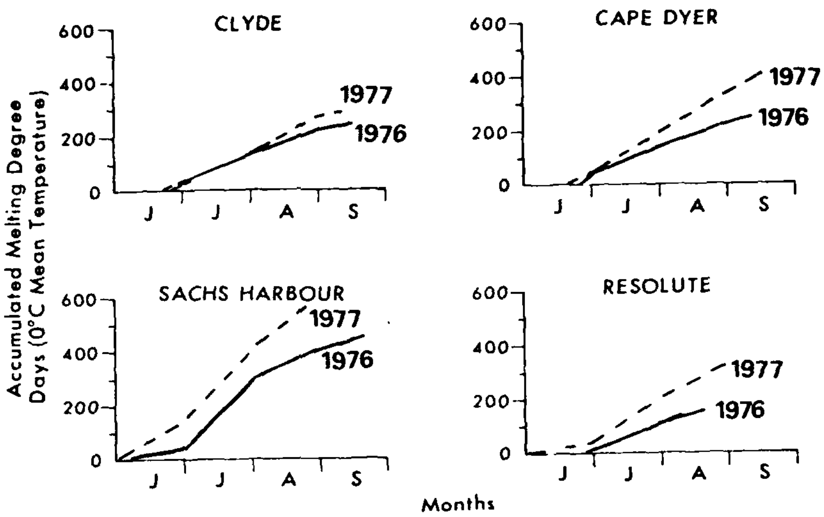

Fig. 5. Accumulated summer melting degree days for the stations Clyde, Cape Dyer, Sachs Harbour and Resolute during 1976 and 1977 summer seasons.

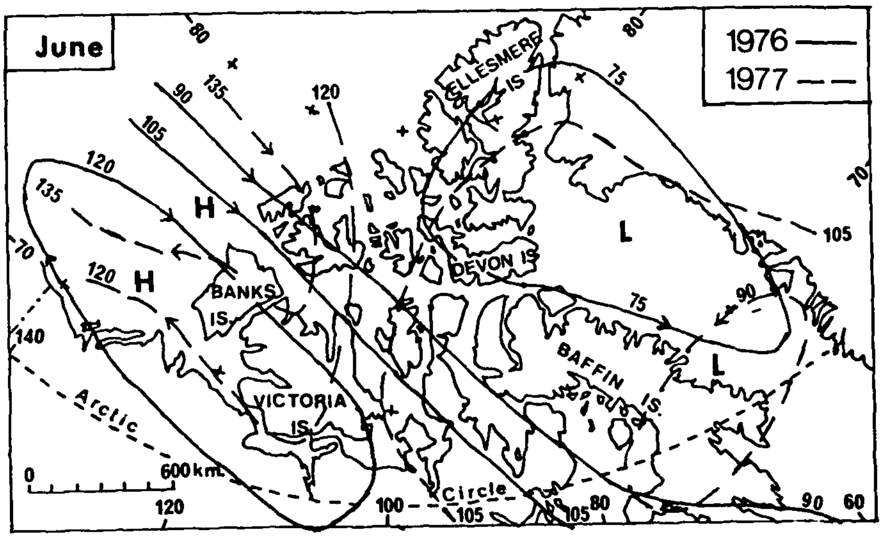

Fig. 6. 1000-millibar map for the month of June 1976 and 1977, showing north-westerly winds over Beaufort Sea in 1976 and southeasterly winds over the same region in 1977.

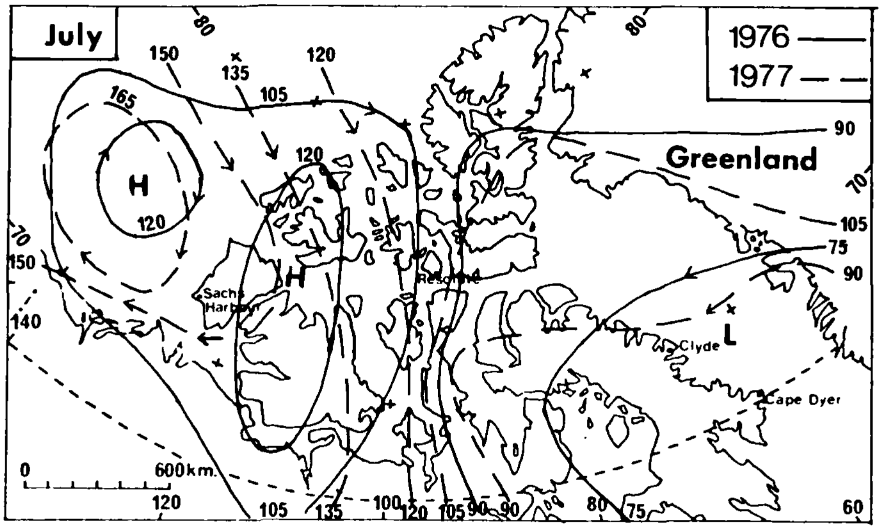

Fig. 7. 1000-millibar map for the month of July 1976 and 1977, showing calm conditions over the Beaufort Sea in 1976 and southeasterly winds over the same region in 1977.

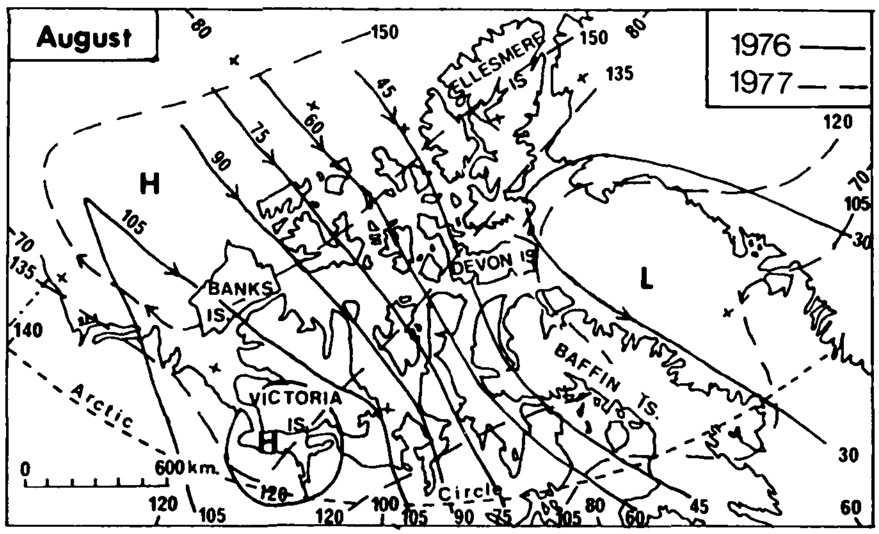

Fig. 8. 1000-millibar map for the month of August 1976 and 1977, showing north-westerly winds over Beaufort Sea in 1976 and southeasterly winds over the same region in 1977.

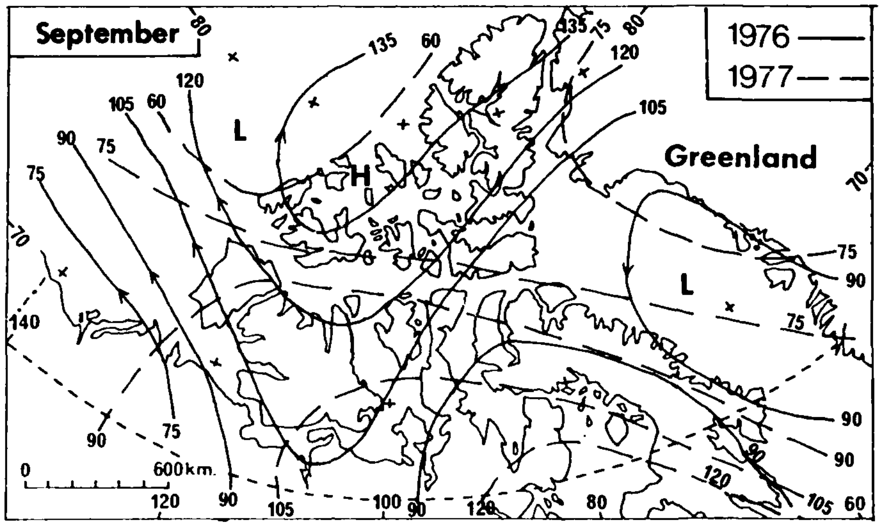

Fig. 9. 1000-millibar map for the month of September 1976 and 1977, showing southeasterly winds over Beaufort Sea in 1976.

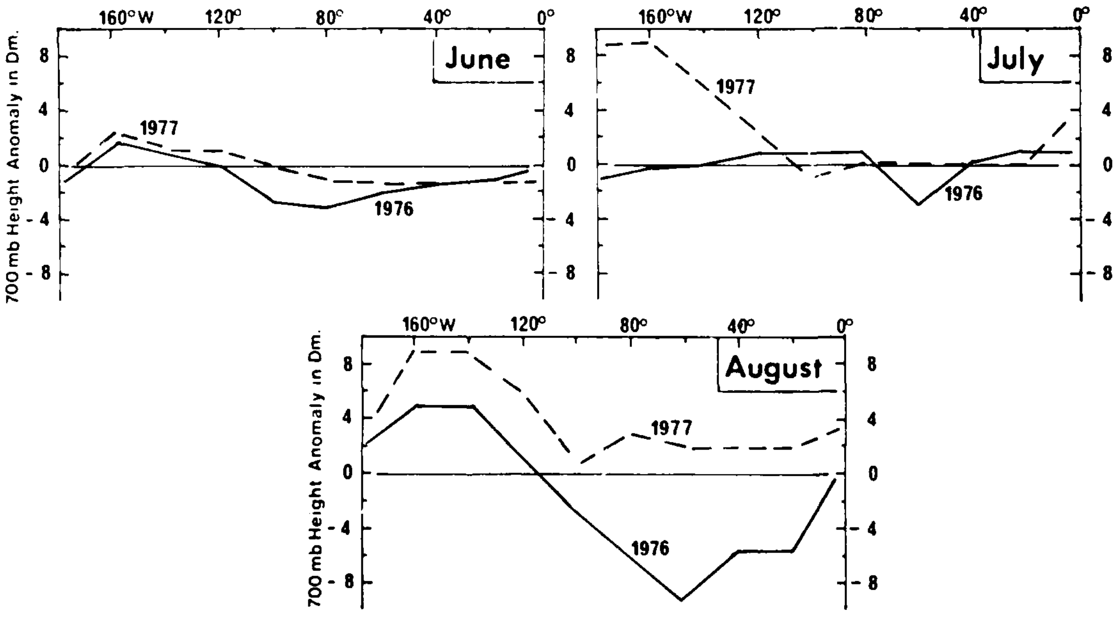

Fig. 10. Mean departure of 700-millibar normal height in decameters along 72°N latitude for June, July and August, 1976 and 1977.

VEGETATION ASSESSMENT OF THE NORTHERN ARABIAN SHIELD FOR GROUND-WATER EXPLORATION USING EDGE-ENHANCED MSS IMAGES*

Graydon Lennis Berlin

Saudi Arabian National Center for Science and Technology (at)
U.S. Geological Survey
2255 North Gemini Drive
Flagstaff, Arizona 86001, USA

Mohamed A. Tarabzouni
Zaki M. Munshi

Saudi Arabian National Center for Science and Technology
P.O. Box 6086
Riyadh, Saudi Arabia

ABSTRACT

Landsat-3 Multispectral Scanner (MSS) digital image data of the Ha'il region of northern Saudi Arabia were subjected to edge-enhancement processing with multiple original data add-back options to highlight small stands of phreatophytic vegetation--an important ground-water indicator. On the basis of a rating detectability scheme for 16 vegetation targets, an edge-enhanced MSS 4, 5, 7 image with 30 percent add-back contained the highest level of vegetation detail. The primary reason for this was that diminution in original data add-back reduced radiometric or albedo masking effects.

1. INTRODUCTION

The discovery of new ground-water reserves in the Arabian Shield of Saudi Arabia is becoming increasingly important as the need for water accelerates and the quality of much of the known recoverable water deteriorates. The objective of this study was to determine the usefulness of edge-enhanced Landsat-3 Multispectral Scanner (MSS) color composite images (bands 4, 5, and 7) for highlighting vegetation known to be, or behaving as, phreatophytes in the Ha'il region of northern Saudi Arabia. The edge-enhancement algorithm incorporated a 5 X 5 pixel window with 100, 50, and 30 percent original data add-back options. For comparative assessments, unenhanced and contrast-stretched color composite MSS images were also evaluated.

Phreatophytic vegetation, with its potentially deep rooting system, draws moisture from the water table under natural conditions throughout the year (Robinson, 1958). Meinzer (1927) notes that phreatophytes

> ...are without question of great practical value as indicators of the occurrence of ground water in arid regions. They give evidence which supplements that furnished by the topography and geology and which is more specific as to the precise localities where the water occurs near the surface. They can not properly be ignored or relegated to casual consideration in any ground-water survey of a desert region.

*Presented at the Seventeenth International Symposium on Remote Sensing of Environment, Ann Arbor, Michigan, May 9-13, 1983.

The thesis for this study was that if the MSS detected natural vegetation during the dry season the flora would be vigorous, abundant, and most likely phreatophytic. These vegetal characteristics could in turn indicate shallow ground water, for it is generally agreed that phreatophytes become scattered and less vigorous as the depth to the water table increases. To reduce potential false identifications between phreatophytes and ephemerals, an MSS scene generated on 29 June 1979 was selected for computer processing to increase the probabililty that the rain-dependent ephemeral plants would be unable to survive the dry summer conditions. For a summer scene, it was assumed that a comparatively lush phreatophyte pattern would contrast sharply with immediately adjacent desert areas which typically support only a sparse growth of xerophytic vegetation.

2. DESCRIPTION OF THE STUDY AREA

The study area lies in the northern part of the Arabian Shield in Ha'il Province (center coordinates--27° N., 42° E.). The region is underlain by an assemblage of Proterozoic plutonic, metavolcanic, and metasedimentary rocks. In several places these basement rocks have been intruded by numerous rhyolite and diabase dikes. Basaltic cinder cones, tuff rings, and lava flows of Pleistocene(?) age are found in the eastern part of the region (Harrat Hutaymah basalt field, Figure 1). A relatively thin veneer of Quaternary surficial deposits covers much of the area; these deposits include wadi sediments, eolian and playa deposits, and poorly-sorted pediment materials (Dodge, 1979). The terrain is moderately rugged, and local relief exceeds 350 m. The drainage system is comprised of numerous ephemeral wadis which drain from three primary catchment highlands--Jabal Aja, Jabal Salma, and Jebel ar Rumman (Figure 1). The most important water-yielding formations are unconsolidated alluvial deposits, typically less than 30-m deep.

The region is in the "arid bioclimatic zone" which is characterized by a precipitation/potential evapotranspiration ratio (P/Etp) of between 0.03 and 0.2 (UNESCO, 1977). For the period 1970-1979, precipitation at Ha'il (Figure 1) averaged 120 mm per year with 87 percent of the rainfall occurring between November and April. Measurable precipitation (0.8 mm) occurred only once between June and September for this 10-year period. Total annual evaporation at Ha'il for the period 1971-1975 averaged 4,268 mm.

Vegetation types indicating abundant soil moisture or near-surface ground water in the test region include the following species.

1. Acacia raddiana (Talah), a glycophyte, is confined almost exclusively to wadi banks. These spiny trees have long vertical roots (tamarix type) which may reach a permanent supply of water (Zohary, 1962). Talah is browsed by goats, sheep, and camels when small, and exclusively by camels when mature. The cutting of Acacia trees is now forbidden in the Kingdom.

2. Phoenix dactylifera (date palm) is a true phreatophyte and as the "old Arab says, 'The date palm, queen of trees, must have her feet in running water and her head in the burning sky'." (Furr et al., 1952; Moustafa et al., 1978). Date palms can live without irrigation if the water table is 1.5-2.0 m below the surface; if deeper, they will survive but will not fruit (Muirhead, 1961).

3. Haloxylon salicornicum (Al Ramith) is a deep-rooting, evergreen perennial shrub (30-70 cm high) with green succulent terete branches (Migahid, 1978). Al Ramith may develop along the fringes of playas and in larger wadis before the onset of high salinity (Adams et al., 1978). It is browsed by sheep and goats and is used as a ground-water indicator if the plants are large and lush during the dry season.

4. Zygophyllum decumbens (Harm') is a low-lying perennial shrub with prostrate branches (Migahid, 1978). Although not browsed as extensively as Al Ramith, sheep are often fed Harm' one day prior to slaughtering because of the extremely high water content of the leaves.

5. Citrullus colocynthis (Hanthal) is a perennial herbaceous plant with long trailing branches; the pulp of the fruit is an official drastic cathartic (Migahid, 1978). Eyre (1963) describes the bewilderment of encountering this plant in the Sahara:

> This plant...has long, soft shoots bearing large, broad leaves which it retains throughout the whole of the summer...On encountering this plant in the midst of its xeromorphic neighbours one would almost be prepared to accept the postulate that it is protected from excessive transpiration in some unknown, almost magical way; it does not seem feasible that such a plant could remain firm and unwilted throughout the savage heat of the Saharan day. In fact it is able to do so only because of its unbelievably efficient and extensive rooting system which taps the water-table permanently and supplies water to the stems and leaves sufficiently rapidly to offset the enormous transpiration rate.

Nomadic pastoralism is common throughout the region. Farming is restricted to oases where ground water is readily available. Ha'il is the region's only urban center (Figure 1); its 1980 population was estimated to be 150,000 (Tarabzouni, 1981).

3. EDGE-ENHANCED IMAGES

The MSS data were first computer processed through the EROS Data Center's EDIPS (EROS Digital Image Processing System) routine. The EDIPS processing "menu" followed four steps (Short, 1982):

1. Radiometric correction of data to adjust for satellite and sensor anomalies;

2. Geometrical correction and resampling of data to Hotine Oblique Mercator projection...;

3. Compensation for atmospheric scatter (haze removal);

4. Display and analysis of the distribution of brightness values (DN's) leading to mapping of image grey levels to preassigned film density levels via logarithmic (nonlinear) tables.

At the U.S. Geological Survey's Image Processing Facility (IPF) in Flagstaff, Arizona, the MSS 4, 5, 7 formatted data (i.e., data bases) were then subjected to edge-enhancement processing. This type of digital processing was used because of its potential for enhancing high-frequency information (i.e., rapid changes in brightness intensity over a short spatial dimension)--in this case accentuating the local contrast between small areal concentrations of natural vegetation and the surrounding desert environment.

The IPF edge-enhancement algorithm is expressed as

$$DN_o = K\ (1-X) + DN_i\ (1+X) - A$$

where:
- DN_o = Output digital number
- K = Constant to keep all values positive; default = 127 (median of the output range for 8-bit data)
- X = Fraction of input digital number (DN_i) to be added back to the high-frequency component
- A = Local average or low-frequency component for a neighborhood or window centered around a central pixel

An image processed in this manner contains radiometric (albedo) low-frequency information (i.e., gradual brightness changes over a relatively large number of pixels) and exaggerated local contrast or high-frequency spatial information.

Varying the X parameter in this equation enables the analyst to control the amount of original data (DN_i) that is added back to the high-frequency component. Such an option makes it possible to reduce the dynamic range between light and dark image areas in direct proportion to diminutions in X. This can permit greater recognizability of high-frequency targets because low-frequency albedo masking effects are reduced. For this study, 30, 50, and 100 percent DN_i add-back options were used. Color composite images (bands 4, 5, 7) incorporating 30 and 100 percent DN_i add-back are shown in Figures 1 and 2.

A 5 X 5 pixel window was used in the edge-enhancement algorithm. This pixel size was selected by a quantitative method that uses the standard deviation of the horizontal first difference of MSS band 7 (Chavez and Bauer, 1982). Additionally, window shape was made equidimensional to ensure that all image directions were weighted equally (Berlin and Chavez, 1983). Each output image was contrast stretched to utilize the full 8-bit range (0-255) of the IPF system.

In addition to the three edge-enhanced color composite images, an MSS 4, 5, 7 standard (unenhanced) EDIPS image and an MSS 4, 5, 7 image incorporating contrast stretches were produced for comparative vegetation assessments (Table 1).

4. INTERPRETATION PROCEDURES AND RESULTS

As a means of assessing the quality of natural vegetation detail portrayed on the images, 16 sites were selected as ground-control targets to establish a detectability rating scheme. Field surveys conducted in September 1980, March 1981, and September 1982 indicated the sites supported vegetation known to be, or behaving as, phreatophytes. The density of cover ranged from 36 to 73 percent. Vegetation types associated with each site are presented below.

Site No.	Environment	Vegetation
1	wadi	*Zygophyllum decumbens*
2	wadi	*Acacia raddiana, Haloxylon salicornicum*
3	fracture	*Phoenix dactylifera*
4	fracture	*Phoenix dactylifera*
5	wadi	*Acacia raddiana*
6	playa	*Haloxylon salicornicum*
7	fracture	*Acacia raddiana, Haloxylon salicornicum*
8	wadi	*Haloxylon salicornicum*
9	playa	*Haloxylon salicornicum*

10	playa	*Haloxylon salicornicum, Citrullus colocynthis*
11	playa	*Haloxylon salicornicum*
12	wadi	*Haloxylon salicornicum*
13	playa	*Haloxylon salicornicum, Citrullus colocynthis*
14	playa	*Haloxylon salicornicum*
15	playa	*Haloxylon salicornicum*
16	wadi	*Acacia raddiana, Haloxylon salicornicum*

Each vegetation anomaly was subjectively rated on the following image detectability scale: 0 = not detectable, 1 = poor expression, 2 = good expression, and 3 = excellent expression. The ratings were determined by interpreting 1:1,000,000-scale color transparencies with an 8-X magnifying lens. A light table with fluorescent lighting was used for viewing the transparencies.

MSS image scoring results for the 16 vegetation sites are presented in Tables 1 and 2. Table 1 presents cumulative scores, and a summary tabulation of the overall value of each image is given in Table 2. This table contains the number and percentages of not detectable, poor, good, and excellent ratings for each image.

The principal findings of the image comparisons are as follows:

1. The three images incorporating edge enhancement contained the highest level of vegetation detail; the unenhanced and contrast stretched only images received significantly lower scores (Tables 1 and 2). This substantiates the thesis that isolated stands of natural vegetation in a desert environment represent high-frequency spatial targets and that their recognizability can be improved by edge-enhancement processing.

2. Several targets were either undetectable or poorly defined on the standard (unenhanced) FDIPS image, and it is possible that several of the vegetal stands rated as poor could have been overlooked if there had been no ground control (Table 2). Although this product is provided routinely by the EROS Data Center, a user without access to a digital image processing system should consider ordering, by special request, FDIPS images that incorporate edge enhancement and contrast stretches for studies of a similar nature.

3. Of the three edge-enhanced composite images, the one with 30 percent DN_i add-back received the highest scores (Tables 1 and 2). Vegetation features were more easily identified in originally dark image areas because albedo masking was dramatically reduced in this image.

5. CONCLUSIONS

The findings of this study indicate that edge-enhanced, contrast-stretched images display vegetation detail not discernable on standard film and contrast-stretched only MSS images. Furthermore, correct use of the DN_i add-back option maximized the display of several vegetation targets. Because this pilot study showed such promising results, the data will be presented to personnel in the Ministry of Agriculture and Water, Kingdom of Saudi Arabia, for a proposed geophysical and/or test well exploration program for several of the anomalous vegetation sites. In addition, we propose to expand the image processing program to MSS scenes covering more remote areas of the Arabian Shield where conventional exploration programs are in the planning stages.

6. REFERENCES

Adams, R., M. Adams, A. Willens, and A. Willens, 1978, Dry Lands: Man and Plants, The Architectural Press, London, 152 p.

Berlin, G. L. and P. S. Chavez, Jr., 1983, Structural evaluation of the eastern Grand Canyon region, Arizona, using Landsat-3 RBV/MSS standard and digitally enhanced images, in International Symposium on Remote Sensing of Environment, 2nd Thematic Conference, Remote Sensing for Exploration Geology, Environmental Research Institute of Michigan, Ann Arbor, in press.

Chavez, P., Jr. and B. Bauer, 1982, An automatic optimum kernel-size selection technique for edge enhancement, Remote Sensing of Environment, v. 12, pp. 23-38.

Dodge, F. C. W., 1979, The Uyaijah Structure, Kingdom of Saudi Arabia, Geological Survey Professional Paper 774-F, U.S. Govt. Printing Office, Washington, D.C., 17 p.

Eyre, S. R., 1963, Vegetation and Soils, A World Picture, Aldine Pub. Co., Chicago, 324 p.

Furr, J. R., F. Currlin, and W. W. Armstrong, 1952, Effects of water shortage during ripening and nitrogen fertilization on yield and quality of Khadrawy dates, Date Grower's Inst. Report, v. 29, pp. 10-12.

Meinzer, O. E., 1927, Plants as Indicators of Ground Water, Geological Survey Water-Supply Paper 577, U.S. Govt. Printing Office, Washington, D.C., 95 p.

Migahid, A. M., 1978, Flora of Saudi Arabia, 2nd ed., revised, Riyadh University Press, Riyadh, Saudi Arabia, 2 vols., 940 p.

Moustafa, S., F. Hussein, and S. Elkahtany, 1978, Yield, fruit quality and ripening of "Sukkari" dates irrigated at different intervals, Proc. Saudi Arabian Biol. Soc., v. 2, pp. 7-15.

Muirhead, D., 1961, Palms, D. S. King, Globe, Arizona, 140 p.

Robinson, T. W., 1958, Phreatophytes, Geological Survey Water-Supply Paper 1423, U.S. Govt. Printing Office, Washington, D.C., 84 p.

Sho[illegible] N. M., 1982, The Landsat Tutorial Workbook, NASA Reference Pub. 1078, U.S. [illegible]t. Printing Office, Washington, D.C., 553 p.

Tarabzouni, M. A., 1981, Computer-Enhanced Landsat Images for Ground Water Exploration in the Northern Arabian Shield, Unpublished Ph.D. Dissertation, University of Tennessee, Knoxville, 279 p.

UNESCO, 1977, World Distribution of Arid Regions, United Nations, Paris, map scale 1:25,000,000.

Zohary, M., 1962, Plant Life of Palestine, Ronald Press, New York, 262 p.

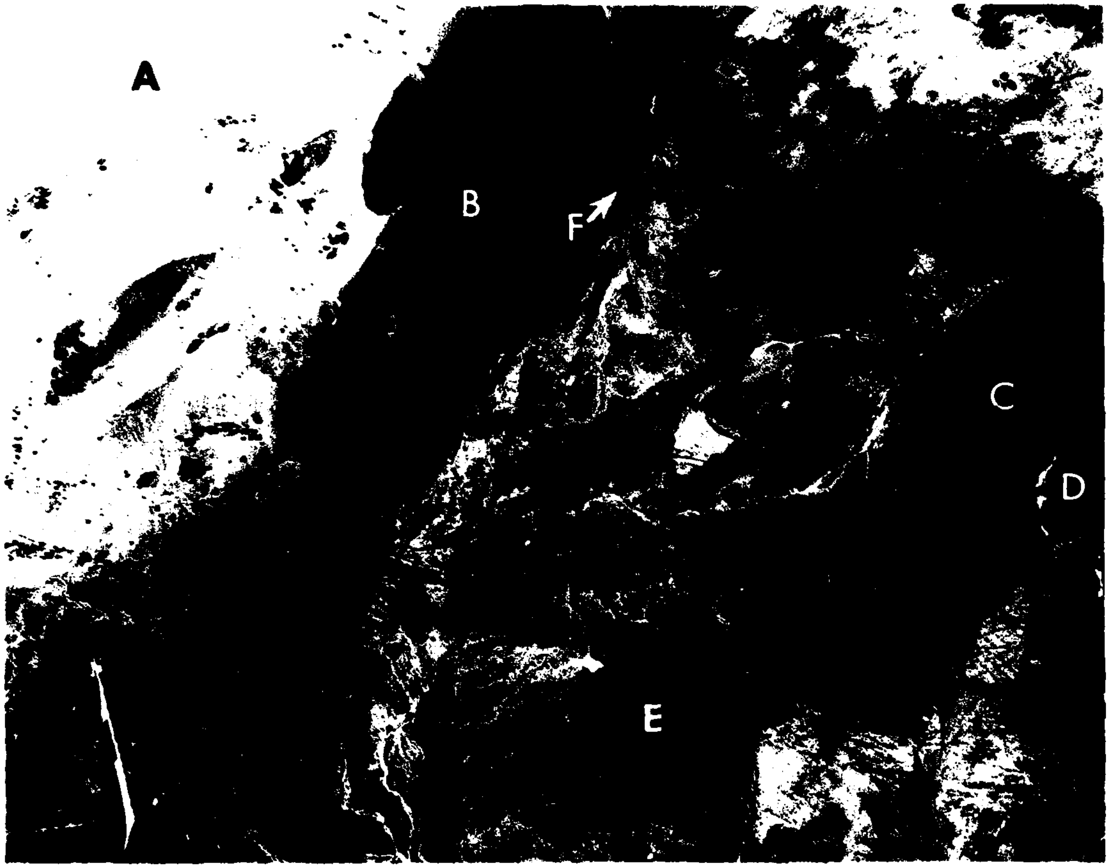

Figure 1. Portion of an MSS band 4, 5, 7 image incorporating edge enhancement with 30 percent original data add-back of the Ha'il region, Saudi Arabia. Annotated features include: (A) the An Nafud sand sea, (B) Jabal Aja, (C) Jabal Salma, (D) the Harrat Hutayma basalt field, (E) Jebel ar Rumman, and (F) the city of Ha'il. Sixteen vegetation targets from this region were selected as ground control for establishing an MSS-based detectability scheme.

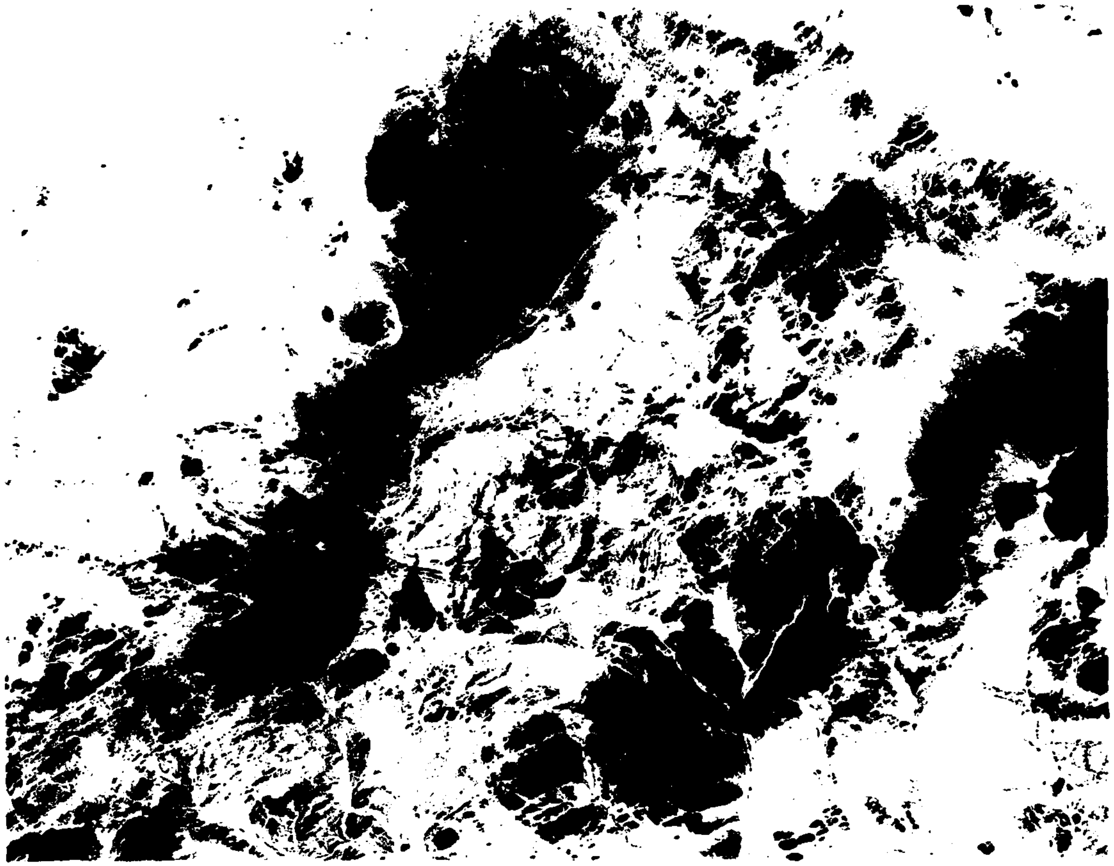

Figure 2. Portion of an MSS band 4, 5, 7 image incorporating edge enhancement with 100 percent original data add-back of the Ha'il region, Saudi Arabia.

Table 1

MSS Images Interpreted for Vegetation Detail and Cumulative Detectability Scores for 16 Vegetation Targets, Ha'il Region, Saudi Arabia

MSS 4, 5, 7 Color Composite Images[1]	Cumulative Detectability Score[2]
1. Edge Enhanced; 5 X 5 Pixel Window, 30% Add-Back	39
2. Edge Enhanced; 5 X 5 Pixel Window, 50% Add-Back	35
3. Edge Enhanced; 5 X 5 Pixel Window, 100% Add-Back	33
4. Linear Contrast Stretched	26
5. Standard Film (Unenhanced)	15

[1]Images 1-3 incorporate linear contrast stretches.
[2]Vegetation targets were rated on a detectability score of 0 = not detectable, 1 = poor expression, 2 = good expression, 3 = excellent expression.

Table 2

MSS Image Detectability Scoring Summary for 16 Vegetation Targets, Ha'il Region, Saudi Arabia

	Image 1	Image 2	Image 3	Image 4	Image 5
No. & (%) of 0 Ratings	0 (-)	0 (-)	0 (-)	1 (6)	5 (31)
No. & (%) of 1 Ratings	2 (13)	3 (19)	4 (25)	7 (44)	7 (44)
No. & (%) of 2 Ratings	5 (31)	7 (44)	7 (44)	5 (31)	4 (25)
No. & (%) of 3 Ratings	9 (56)	6 (38)	5 (31)	3 (19)	0 (-)
No. of Determinations	16	16	16	14	11

DEVELOPMENT OF OPERATIONAL SNOWMELT FORECASTING MODEL FOR VERY LARGE WATERSHEDS IN HIMALAYAS

A.S. Ramamoorthi & P. Subba Rao

National Remote Sensing Agency, Secunderabad-500 003, INDIA

ABSTRACT

During the summer months some of the major multipurpose reservoirs in North India critically depend on the snowmelt runoff for power generation, irrigation and drinking watersupply. Snow-covered watersheds of perennial rivers of India are very large varying from about 2000 sq.miles to about 15,000 sq.miles. They are situated at very high altitudes above 8,000 feet. They are not easily accessible and are hazardous; therefore practically no data is available about the snowfall conditions, temperatures etc. The snow depths vary very widely from a few inches to many feet within short distances. Determining water equivalent is a very formidable task considering the heterogeneous nature of the snow-cover in Himalayas.

If the expected seasonal or fortnightly runoff could be forecast well in time before the onset of snowmelt season, it would be of immense value to water resources project managers to plan in advance the operation of the reservoirs for achieving optimum utilisation of the scarce summer flows. This paper describes in detail the development of a model that has been evolved for the data-scarce very large watersheds in himalayas, with snow cover area (SCA) derived from NOAA imageries as the main input, and used successfully for predicting the snowmelt flows of river Sutlej in the years 1980 and 1981.

INTRODUCTION

India is a vast country the seventh largest country in the world, bounded in the north by the great mountain zone of Himalayas extending over a distance of 2400 kms with depths varying from 240 to 320 kms. India has many large rivers. The rivers originating from Himalayas, like the Indus river system, Ganga and its tributaries, and Brahmaputra are perennial as they are fed both by snowmelt runoff and monsoon rainfall ru[illegible], whereas the rivers

of Peninsular India have flows only during rainy season. To support its millions of people, increase in agricultural and power production is a prime national necessity, and water is the most important input to agriculture and hydropower generation in the country.

Snow is the solid form of water. The precipitation of snow occurs as part of nature's hydrologic cycle. Large quantity of fresh water lies in the form of snow, ice and glaciers in the Himalayas. The snow occurs at an average elevation of over 2,500 metres approximately in India. Snow starts accumulating from the beginning of the winter season and the snow-melt begins in March-April, the maximum being generally in June. Because the snow areas are extensive and are situated at great heights, mostly inaccessible and hazardous, not many snow surveys nor regular collection of data on snow depth, density, etc. by conventional surface and or aerial means have been done hitherto in the Himalayan watersheds. During the summer months some of the major multipurpose reservoirs in North India critically depend on the snow-melt runoff for power generation, irrigation and drinking water-supply. If the runoff during the snow-melt season could be predicted in the beginning of April, it would be of immense value to water resources project managers to plan in advance the operation of the reservoirs for achieving optimum utilisation of the scarce summer flows. With the advent of satellite remote sensing technology, it has now become possible to obtain information about snow covered areas and predict seasonal snowmelt flow within reasonable level of accuracy.

SNOWMELT RUNOFF FORECASTING MODELS IN USE

In USA mostly and in Europe considerable amount of work has been done since 1974 for simulating the snowmelt yields. A NASA Applications Systems Verification and Transfer (ASVT) project on the Operational Applications of Satellite Snow-Cover Observations was begun in 1975 and completed in 1979 in cooperation with nine operational water management agencies. Both Landsat and NOAA satellite data were supplied to these agencies for use in improving snowmelt runoff forecasts.

For the watersheds of Wind River Range, Wyoming, U.S.A. significant relationship between snowcovered area (SCA) derived from LANDSAT imageries and snowmelt runoff was obtained (Rango, 1975, James Foster 1979). However it was concluded that not enough years of data yet existed in order to provide a narrow confidence interval around the forecast volume, when forecasting seasonal flow for a new year was attempted. In the Martinec-Rango Model originally applied on small European mountainous basins and subsequently tested in basins of 75 to 200 sq. miles in Wyoming, the input was SCA from LANDSAT plus ground based temperature and precipitation data on a daily basis. The daily runoff amounts were simulated and seasonal volumes were totalled. Several minor modifications were made to the Martinec-Rango model by Shafer. B.A.. et al (1981) to better approximate the hydrologic conditions, and applied to both Conejos watershed (282 sq.miles) and South Fork Rio Grande Watershed (216 sq.miles)Colorado U.S.A. The simulation model is stated to have performed remarkably well except in one out of seven years. The model's ability to be scaled up and applied on watersheds in excess of 1,000 sq.miles was envisaged and the model was proposed to be adopted in a predictive mode in an operational time frame from 1980. In the King's River Snowmelt Model applied to 1560 sq. miles of watershed (Sierra Nevada, USA) by Hannaford J.F (1979), the input data is LANDSAT imagery (supplemented by NOAA imagery where interpolation was necessary for daily data), the daily temperature, daily precipitation and snowpack water content. The daily snowmelt runoff was successfully simulated and it was concluded that SCA can be used as a parameter in defining the magnitude and timing of snowmelt with an adequate degree of accuracy for operational analysis.

It would thus be seen that the models developed in U.S.A. are mostly simulation models with the following inputs: snow covered area (SCA) derived from Landsat and NOAA imageries, daily precipitation and temperature data from standard climatological stations. They have been developed in respect of watersheds of about 75 sq. miles to 1560 sq. miles which have a very good network of hydrometerological stations and reliable information about the snowfall characteristics; these models are being tested and improved for adoption in an operational mode for forecasting purposes.

DEVELOPMENT OF MODEL FOR SNOWMELT FORECASTING FOR VERY LARGE WATERSHEDS IN HIMALAYAS

Compared to those in USA the snow covered watersheds of perennial rivers of India are very large varying from about 2000 sq.miles to about 15,000 sq. miles. They are situated at very high altitudes above 8,000 feet; some of the world's highest peaks of about 20,000 feet and above are found in the Himalayan ranges. They are not easily accessible and are hazardous; therefore practically no data is available about the snowfall conditions, temperatures etc. The snow depths vary very widely from a few inches to many feet within short distances and hence depth measurements have no meaningful use. The density of snow may vary from as low a value as 0.01 to as much as 0.5. Determining water equivalent is a very formidable task considering the heterogeneous nature of the snowcover in Himalayas. Consequently under these circumstances, SCA which can be fairly accurately determined from satellite imageries obviously becomes the main parameter on which snowmelt runoff simulation and forecasting have to be made in India.

Snow has a high reflectance. In the NOAA visible channel and LANDSAT MSS-5 band, snow can be easily identified because of the strong contrast between snow-covered and snow-free areas. But considerable skill and experience is required in delineating snow from clouds, especially in mountainous catchments, since both snow and clouds have high reflectance.

The Landsat provides data at 18 day intervals and this is a major constraint in snow studies of watersheds in Himalayas where snowfall conditions abruptly change at short intervals. Hence NOAA data which is received daily at the NRSA Earth Station near Hyderabad, India, though of coarser resolution than LANDSAT, obviously is more useful in developing snowmelt models. Further although the snow-covered watersheds of interest to India are very large in extent they are covered in one single date NOAA imagery itself; this is not so the case if LANDSAT imageries have to be used. Hence in the forecasting model which is the first of its kind that has been developed in India for a very large snowcover area of about 15,000 sq. miles of Sutlej river watershed and tested in the years 1980 and 1981, the percentage of snow covered area determined from judiciously selected NOAA satellite imageries have been used.

FORECASTING SEASONAL SNOWMELT RUNOFF OF SUTLEJ RIVER CATCHMENT IN HIMALAYAS

The Sutlej river rises in the Tibetan region of the Himalayas at an altitude of over 16,000 feet, close to the Rakas-Manasarovar lakes and flows at high altitudes. For considerable distance it flows through hilly rugged terrain in India before entering plains. Quite a large part of its hilly watershed is covered with glaciers and snow. There are no major abstractions from the river flow upstream of Bhakra reservoir across Sutlej.

From NOAA pictures (of April) of the years 1975 to 1978 the percentage of SCA of Sutlej river watershed above Bhakra reservoir during these years were determined using Zoom Transferscope and planimeter. A preliminary regression model was developed using these percentages of SCA and the total snowmelt runoff that occurred during the season April to June in the same years. This model was used to predict the snowmelt runoff of 1980. All the NOAA imageries received during the winter period January to March 1980 were examined and the areal extent of snow cover on the days of very heavy snowfall was delineated. Using the regression model the total snow-melt runoff that could be expected was predicted. At the end of June 1980 it was found that the difference between the forecast quantity and that which actually occurred was nine per cent.

The forecasting model was improved in the light of the experience of 1980 and the revised model was used for predicting the 1981 snowmelt runoff of Sutlej. From the daily NOAA imageries of January to March 1981, the imageries of heavy snowfall were selected for determining the SCA to be adopted for forecasting. At the end of the snowmelt season, it was noted that the runoff as predicted and which was informed to the user agency in the first week of April 1981, was only five per cent more than that which actually occurred in 1981. Thus the forecasting model was used in operational mode.

REFERENCES

Applications Systems Verification and Transfer Project Reports on Operational Applications of Satellite Snow-cover Observ tions.

B.A. Shafer, E.E. Jones and D.M. Frick: Snowmelt runoff simulation using the Martinec-Rango Model on the South Fork Rio Grande and Conejos River in Colorado.

Jack:F. Hannaford: Application of satellite imagery to hydrologic modelling snow-melt runoff in the Southern Sierra Nevada.

PLATE No I

SNOW COVER IN HIMALAYAS

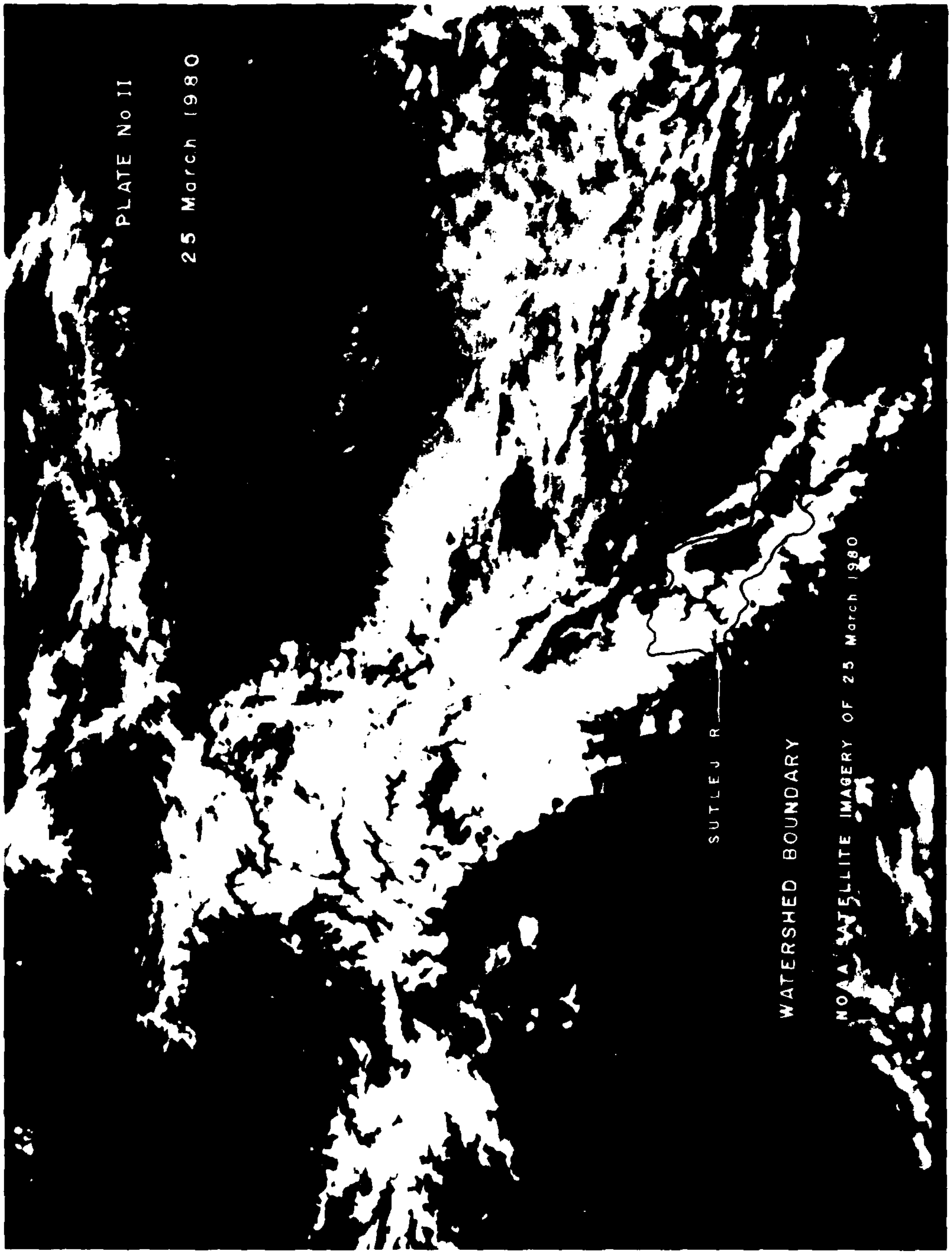
PLATE No II
25 March 1980
SUTLEJ R
WATERSHED BOUNDARY
NOAA SATELLITE IMAGERY OF 25 March 1980

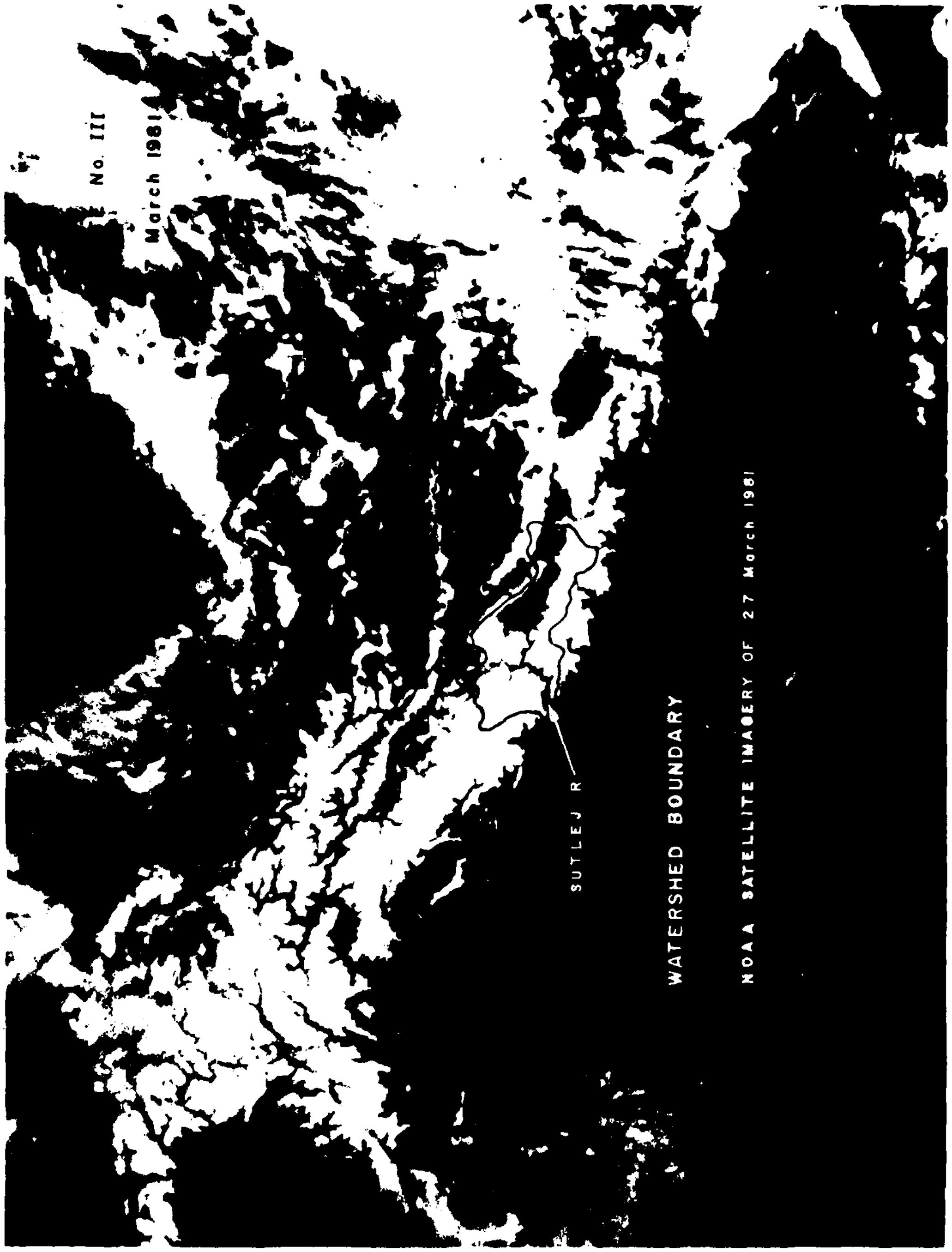
No. III
March 1981
SUTLEJ R
WATERSHED BOUNDARY
NOAA SATELLITE IMAGERY OF 27 March 1981

PLATE No. IV

HYDROGRAPH SHOWING SNOWMELT RUNOFF (Year 1981)
FROM SUTLEJ RIVER BASIN
INTO BHAKRA RESERVOIR

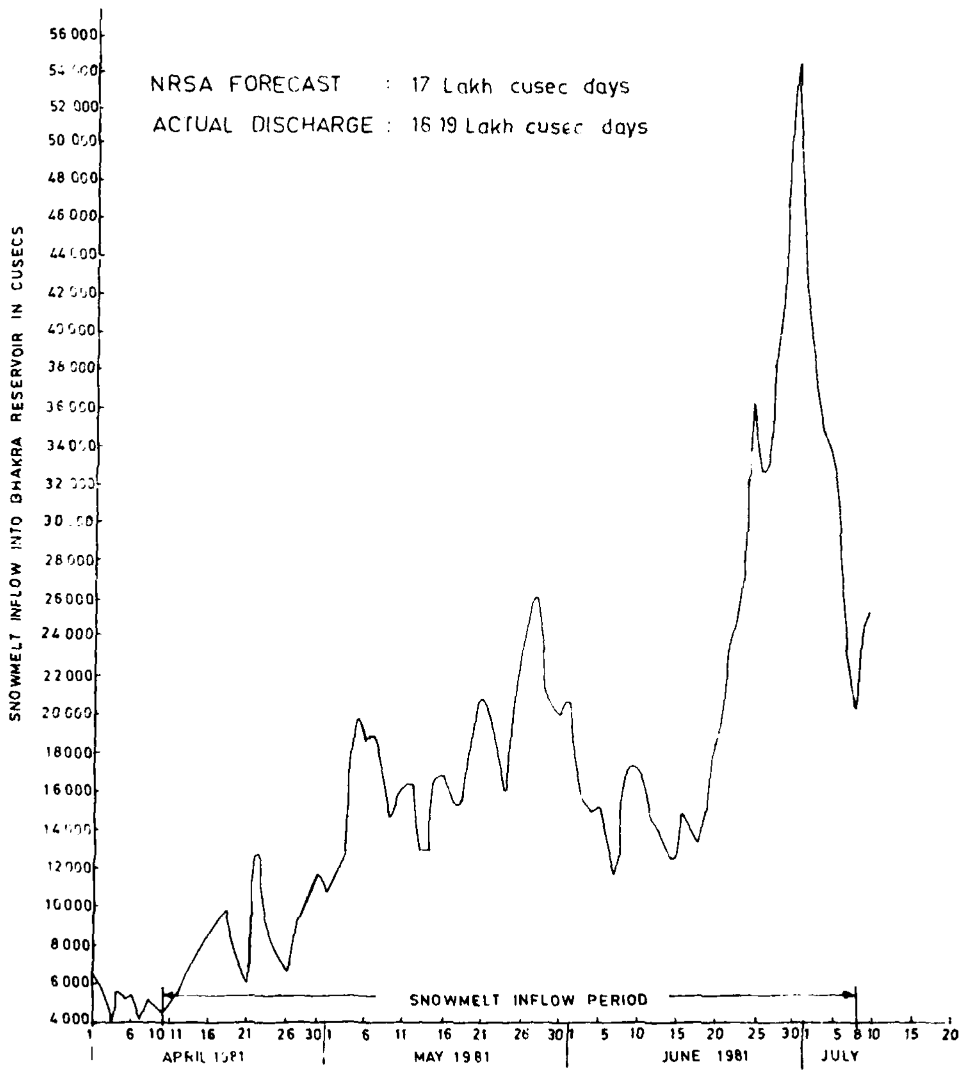

THE IMPACT OF THE DIFFERENT CLIMATIC ELEMENTS ON THE SUB-REGION OF THE "DEPRESSED" CHACO

Jesus Maria Gardiol
Gloria Christina Pujol
Silvia Simonelli
Gustavo Ruben Talamoni

Servicio Meteorologico Nacional
Buenos Aires, Argentina

SUMMARY

The sub-region of the "depressed" Chaco, a typical exponent of seasonal variability, is a major study source with reference to the impact occurred in this zone by a determined weather system.

From a statistical data it is practicable to determine or corroborate the existence of two seasons: one being the dry winter season and another one the summer season in which daily rainfall values may go beyond to those of winter time. This contrast has a special interest for climatologists and meteorologists from the viewpoint of the inference of the effects produced, on the area, by the different meteorological systems and, as far as the length of the forecasting period of the said effects is concerned.

For that purpose a research from conventional meteorological satellite photographs was initiated by using them in its first stage in order to:

(1) Characterize meteorological systems with a greater influence on the zone.
(2) Make correlations with the field measuring.
(3) Assessment in situ of the main effects.
(4) Make a geological and geomorphological characterization of the sub-region; once this stage is performed Landsat image requirement is made, on the 7 infrared bands in order to:

  (a) Study, in mesoscale, the development of a given meteorological system.
  (b) Adjust items b and c for a better understanding of the impact.

From the analysis of the above, it emerged, first of all, the possibility of demarcating the areas more affected by maxima rainfalls and its range period and, this should be the only circumstance for altering the water balance.

This goal leads us to analyze the phenomenon behavior, in a subsequent way, by means of Landsat satellite image interpretation.

And as a final goal which is now in development, water balance is attempted to be explained and, once the necessary correlations are made, it should be taken as a field data for the diagnosis of the change and different crop rotation feasibleness of the above mentioned sub-region.

SPOT AND REMOTE SENSING PROJECTS IN LATIN AMERICAN COUNTRIES

C. Veillas

Centre National d'Etudes Spatiales
Paris, France

SUMMARY

Latin American countries have been involved in space remote sensing for several years. Two Landsat receiving stations are operational and the user's community is organized.

The next generation of compatible Land Observation Satellite System Landsat-D (1982) and SPOT (1984) will offer the opportunity to provide deversified services to Latin American users in the mid 80's.

The first SPOT Land Observation Satellite System, SPOT 1, will be launched by the European Araine Launcher in June 1984.

The launch of SPOT 2, decided by the French Government in October 1981, could take place as early as 1985. Furthermore, it is considered that two or three more satellites could be launched between 1988 and 1994 in order to ensure the continuity of the service over a ten to twelve year period because this condition is essential for developing operational use of remote sensing in most fields of applications.

A subsidiary of the French Space Agency, CNES, the SPOT Image corporation is responsible for promoting and marketing SPOT products on a worldwide basis. The decision to set up this corporation (CNES along with its partners of the G.D.T.A.) was taken in October 1981 by the French Government.

CNES being the manager of the SPOT system encourages direct reception of the data by receiving stations in Latin American countries. Some of them already expressed their interest to do so.

CNES has undertaken with its partners of the G.D.T.A a large simulation program over France since 1979, a campaign was carried out over Africa and Southeast Asia last year and in Ja-uary 1982. Simulations are in progress with some Latin American countries. CNES and GDTA have been participating in educative programs in Latin America and will pursue next year.

As for the simulation and educative programs undertaken with countries in Africa, Southeast Asia, Latin America, CNES is willing to extend such programs in cooperation with other countries, as a preparatory exercise toward an efficient use of the real data from space when they become available.

SPECTRAL STUDY OF THE MAJOR CROPS IN TAIWAN WITH A DUAL-LOOK GROUND-BASED RADIOMETER SYSTEM

Quocheng Sung

National Central University
Chungli, Taiwan, China

SUMMARY

Paddy rice is the major crop of Taiwan. How to use remote sensing techniques in monitoring the growth condition and predicting the yield of paddy rice in nation-wide scale is one of the major thrusts to be fulfilled by the local remote sensing group. Several pilot projects have demonstrated the potential of remote sensing technique in the field of resource inventory. About 88% accuracy of acreage estimation of rice paddies has been achieved by automated analysis of Landsat imagery with some ground-truth data. More and more workers have come to realize that ground-based in situ remote sensing studies are needed to better understand the basic relationship between natural materials and reflectance of radiance and will substantialize the usage of Landsat data. The aerial photography and terrestrial photography were both applied to the spectral study of the paddy rice and sugar-cane. The in situ spectral reflectance data were also collected by sequentially measuring the target and the standard plate using only one radiometer. Variations of reflectance data within groups are often found greater than those between groups due to the atmospheric fluctuation. This kind of error can be possibly reduced by simultaneously measuring radiance and irradiance with two intercalibrated radiometers. However, the analog recording system of simultaneous measurements can be costly and time-consuming in the process of the collected data

A low-cost, dual-look, ground-based radiometer system is then designed to meet the requirement of simultaneous measurements of the spectral data. A single-board microcomputer, Rockwell AIM 65, facilitated with a thermal printer, a character display and a full-size keyboard, is used to control the recording of two Exotech four band radiometers and provides the basic capabilities of statistical manipulation and calibration of the measurements. Two multiplexers were used to select correct channel and appropriate gain according to the atmospheric conditions. The selected input signal was then digitally converted by an eight-bit A/D converter. The conversion time of the commercially available A/D converter ranges from a few micro-seconds to a few milli-seconds. The atmospheric fluctuation is presumably ignored in the order of milli-seconds and the "almost" simultaneous measurements can thus be achieved.

In the field operation, the system is powered by a portable generator. Two radiometers were properly mounted on the top of a five-meter high tripod, with one looking upward and the other looking vertically toward the target. The one which measures irradiance is fitted with a cosine receptor and the other with an apertured receptor. The two instruments are read "almost" at the same time and the ratio of the irradiance and the reflected radiance is calculated immediately. An intensive field test has shown that the variations of the spectral data due to the atmospheric fluctuation can be reduced substantially using this system, and the field operation of the system is greatly time-saving.

An one-year project was then initiated to study the spectral characteristics of the major crops in Taiwan at this fiscal year. Four major types of paddy rice were transplanted under the same conditions at one of the experimental

fields in central Taiwan. The system is used to monitor the daily changes of spectral reflectance of each crop type. The first crop season begins at February and the second ends at early November. Field measurements of the four crop types were recently completed. The statistical work of the collected data is being processed and the results will be available at the end of the year. A better understanding of the spectral charncteristics of paddy rice can be expected with the intensive in situ measurements using the dual-look radiometer system.

AUTOMATIC INTERPRETATION OF MSS-LANDSAT DATA APPLIED TO COAL REFUSE SITE STUDIES IN SOUTHERN SANTA CATARINA STATE, BRAZIL*

H. J. H. Kux
D. de M. Valeriano

Instituto de Pesquisas Espaciais - INPE
Conselho Nacional de Desenvolvimento Científico e Tecnológico - CNPq
C.P. 515 - São José dos Campos - SP - Brasil

ABSTRACT

The coal mining district from southeastern Santa Catarina State is considered one of the most polluted areas of Brazil. This study presents the preliminary results on the application of MSS-LANDSAT digital data to monitor the coal refuse areas and its environmental consequences in this region.

1. INTRODUCTION

The utilization of MSS-LANDSAT data to monitor the coal-mining and reclamation activities has got a strong impetus in the U.S.A., during the last decennium, partly due to a detailed and severe environmental legislation: the Surface Mining Control and Reclamation Act.

Since then a great amount of information has been gathered on the use of digitized LANDSAT data to inventory areas affected by coal mining (e.g. Alexander et alii (1975); Hughes et alii (1975); Wobber et alii (1975); Fish (1977); Russell (1977); Anderson & Tanner (1978); Mamula (1978); Bayne & Lawrence (1979)). Besides that, a great effort has been done on studies over coal mining areas using multi-channel airborne scanners, thus permitting a better understanding of the spectral characteristics of the targets to be mapped with satellite data (e.g. Spisz (1978), Tanner (1979), Spisz & Dooley (1980) and Irons et alii (1980)).

In the coal mining areas of southern Brazil (States of Santa Catarina and Rio Grande do Sul) systematic studies to monitor the mining activities and the collateral environmental degradation, using MSS-LANDSAT data, have not yet been undertaken. Within this perspective the "Projeto Carvão", which is being developed at INPE, aims to adapt and to apply remote sensing techniques to studies on the environmental problems derived from the mining activities at the Southern Santa Catarina Coal Basin and adjoining areas. Taking into account that the pyrite-rich coal refuses which cover a large terrain extension in this region, can be considered as the main pollution sources in this area, the objective of this study is to map the coal refuse sites in the two most affected areas. The first one (Fig. 1) is part of the elder mining area, encompassing the cities of Criciúma (110.660 inhabitants, *1980), Cocal (6500 inh., 1980) and Siderópolis (12.400 inh., 1980). The second one, located between the cities of Tubarão (75.500 inh., 1980) and Laguna (39.600 inh., 1980), at the lower section of the rio Tubarão, is a coastal plain where a lagoonal-estuarine ecosystem is being severely damaged by the very acid drainage running down from refuses and slurries, pertaining to a nearby installed coal-washing

---

*Presented at the Seventeenth International Symposium on Remote Sensing of Environment, Ann Arbor, Michigan, May 9-13, 1983.

*Figures on population obtained from IBGE (non-published).

facility and to a thermoelectrical power plant. In the second area it is also tried a first approach to map the visible extent of the pollution effect by the identification of the acid stressed vegetation along the drainage from the main coal refuse deposit.

2. GEOGRAPHICAL SETTING OF THE POLLUTION PROBLEMS

Both study areas have a high population density, especially the municipality of Criciúma (405 inhab./km², 1980). Within the last 12 years the population from this city grew at a rate of 5% p.a., and it is expected to grow even faster in the coming years, when several heavy industries will be installed in its surroundings. This intense urbanization process is partly due to closing of older, unproductive mines, partly to emigration from rural areas, caused by low productivity of the annual cultures in small farms, hilly terrain, leaching and erosion of soils, etc. Because of severe river pollution, the drinking water supply for Criciúma comes from the foothills of the "Serra Geral", by pipeline, some 60 km to the west of the city. Water shortages are already frequent during the dry season (from May to August). After Cardoso et alii (1981), a total amount of 110.000 m³/day of liquid spills with pH values between 2 and 3, with sulphate contents of 7000 miligrams/liter and iron contents of 2000 miligrams/liter are expelled from the mines and coke ovens. Together with the liquid spills an intensive leaching of the fine materials (silts and clays) occurs at the refuse piles, causing siltation problems in the rivers draining the mining area.

Due to a high content of impurities, such as ashes, the coal from the Southern Santa Catarina Coal Basin has to pass through a long beneficiation process, which can be summarized as follows (Lenz, 1977): the material coming out of the mine, the so-called "run of mine" (ROM), passes through a preliminary washing procedure, and is divided, by density, in two fractions. The first comprehends a variable volume of pyrite-bearing refuses (with up to 20% of pyrite) and losses, corresponding to 70% of the total ROM volume. The second, with an average ash content of 28%, called "pre-washed coal" (PWC), is transported by railroad to the Central Coal Washing Unit at Capivari, near the city of Tubarão. After crushing and washing it is separated in two equivalent portions: the first consisting of metallurgic coal (with 18,5% ashes and 1,8% sulphur), and the second of boiler coal (with 40% ashes and around 5% sulphur), which is burned at a nearby located thermo electrical power plant. The values cited are averages valid for the best betuminous coal seam in S. Catarina: locally the figures for refuses, ashes and sulphur can be higher. Part of the pyrite-rich refuses originated during the beneficiation process, (250.000 tons/year of pyrite residues with 44% S) are used at a sulfuric acid plant, located in the coal harbour of Imbituba (Putzer, 1977).

During the preliminary washing procedure mentioned above, the sulphur contained within the pyrite (FeS_2) undergoes several changes in the presence of water and air (Barton, 1978), namely:

$$2FeS_2 + 2H_2O + 7O_2 \rightarrow 2FeSO_4 + 2H_2SO_4 \qquad (1)$$

$$4FeSO_4 + 2H_2SO_4 + O_2 \rightarrow 2Fe_2(SO_4)_3 + 2H_2O \qquad (2)$$

$$Fe_2(SO_4)_3 + 6H_2O \rightarrow 2Fe(OH)_3 + 3H_2SO_4 \qquad (3)$$

$$FeS_2 + 14Fe^{3+} + 8H_2O \rightarrow 15Fe^{2+} + 2SO_4^{2-} + 16H^+ \qquad (4)$$

In equation (1) the sulfate ion is originated by an oxidation of iron disulfide; in equation (2) ferrous iron becomes non-hydrosoluble ferric iron. When the concentration of sulphuric acid decreases in water, ferric iron is hydrolyzed to ferric hydroxide (equation 3), which origins a red-yellowish coloration within the acid rivers. Another reaction of pyrite with water is its oxidation by ferric iron (equation 4). Accordingly to the same author the longer interruption or ceasing of mining activities can increase these acid

producing reactions if the water is no longer drained or pumped. This situation is very often found in the area around Criciúma. Another type of refuse from the coal mining activity, the "sterile spoils", are the overburden material, originated at open pit mines, which prevail around and north of Siderópolis, where the coal beds are localized very close to soil surface. Its polluting potential is much lower than the pyrite-rich spoils, since the latter contribute almost only with fine sediments to silting in the drainage from the area.

The second area under study mentioned, the coastal plain at the lower Rio Tubarão, presents several lagoons, conected by narrow channels with the open sea. The prevailing vegetation is an association of low and high marshes, partially drained for rice paddies and pastureland. The coal refuses and slurries from the Coal Washing Unit and thermoelectrical power plant are deposited at one of the upper edges of this ecossystem. The resultant very acid drainage pours into the lagoons destroying a great portion of the fishing grounds for shrimp and fish. It should be emphasized that the fishing activity is the feeding basis for over 2000 fishermen families living around these lagoons. An undesired consequence of the destruction of the fish grounds has been a massive proliferation of mosquitos, hence impeding cattle--breeding in that area.

Considering the brazilian National Coal Plan (Ramos, 1982) a reliable forecast, it is expected, at 1985, a total annual production of 17 million tons of PWC. The Southern S. Catarina Coal Basin, will certainly participate with at least two-thirds of this amount, namely with around 12 million annual tons of PWC. This production will correspond to at least 24 mil./tons of refuses and slurries with imprevisible consequences for the environment and men.

3. MATERIALS

- Color infrared (C.I.R.) aerial photographs from August, 1978, at the scale of 1:45.000.

- Coal refuse charts compiled by the E.C.P. (Engenheiros Consultores & Projetistas) staff.

- MSS-LANDSAT's CCT, row path annotation 178/32 from April 24, 1978.

- General Electric Company's Multispectral Image Analyser Image-100 (I-100).

4. METHODS

In the following two sections the pre-processing procedure will be briefly described:

4.1 ATMOSPHERIC EFFECTS CORRECTION

In order to minimize the atmospheric effects of backscattering from sun radiation and target reflection of diffuse sky radiation, the following procedures were developed, after a personal communication with R. P. Lyon:

- An area of the edge of the basaltic plateau in Santa Catarina State, where deep valleys occur, therefore featuring extended relief shadows, was enlarged to a scale of 1:100,000 at the display of the I-100.

- Using the "cluster synthetizer" algorithm (General Electric Comp.,1975), those pixels whose channel 7 values ranged from 0 to 1 in a 255 resolution, were alarmed and designated to one of the I-100 themes.

- This theme was used as a sample in a "single-cell parameter extraction" algorithm (General Electric Comp., 1975), and the mean values of these

pixels for each other channel were subtracted from the whole frame.

4.2 RADIOMETRIC CORRECTION

In order to eliminate the striping effects derived from different responses of the MSS-LANDSAT sensors from the same band, a routine procedure based on a local operator was applied to the frame.

The operator compares the local average of a line with the local average of the anterior line and if the difference is greater than a given threshold, this difference is added to the point of the current line. In order to avoid error propagation, another threshold is input to the system, which establishes a limit to be added to each point (Dutra et alii, unpublished).

4.3 GROUND TRUTH ANALYSIS

The ground truth available for the Criciúma area was a series of coal spoil area charts. The following classes from these charts were used in this study:

sterile spoil
- active
- abandoned and unvegetated
- abandoned and vegetated

pyrite-rich spoils
- active
- abandoned and unvegetated
- abandoned and vegetated

For the Tubarão area, C.I.R. photographs were available. Through visual interpretation, 21 land-use/land cover classes could be identified and were classified into a hierarchical system (Anderson et alii, 1976). The level I from this system is presented below:

I - coal related areas
II - urban areas
III - agricultural areas
IV - wetlands
V - forestlands
VI - barelands
VII - water

4.4 AUTOMATIC ANALYSIS OF MSS-LANDSAT CCT

The first approach to both study areas was an unsupervised classification aiming at the stratification on the areas into spectrally alike classes. This is done by a cluster algorithm, the "Média K" algorithm (Dutra et alii, unpublished).

The cluster algorithm implemented at INPE's I-100 starts counting the number of pixels occupying each cell in a four-channels space. Then it orders these cells decreasingly according to the number of pixels within the cells.

The first k cells will be the k starting centers of the algorithm. It calculates the euclidean distances between these centers and the rest of the cells. With a nearest neighbor routine, it attributes each cell to one of the centers. The mean values of each channel for each population will be the new centers, and the interaction is repeated. A minimum number of cells is given in order to a population be considered as one. This procedure stops when it achieves a given number of interactions or when the distance between the new center and the last one is below a given threshold. The mean vector and the covariance matrix of the populations enter into a "maximum likelihood" algorithm (Velasco et alii, 1979) in order to classify the whole frame.

Considering that the objectives for the two study areas were different, so were the procedures used for each one.

In the Criciúma area, the aim was to identify and to locate only the coal related areas. So these areas were sampled and the pixels obtained were used for the unsupervised classifications with six centers. On the other hand, the objective in the Tubarão area was to identify acid stressed vegetation as well as healthy vegetation and coal related areas. Therefore, to use the entire scene as a sample would be the best procedure. But this cannot be done at INPE's I-100 because of physical restraints of the system. To solve this problem, the resolutions of channels 5 and 7 of MSS-LANDSAT were reduced to 64 levels and the whole scene with only these two channels was input to the unsupervised classification with 8 centers.

Both classifications were not satisfactory. Errors (commissions and omissions) were presented in all classes. The next step was to subdivide the unsupervised classes into specific classes using the C.I.R. aerial photographs or the refuse deposit charts as ground truth, and the unsupervised classification for sample orientation in a supervised procedure,(Lyon & Prelat, 1978).

The 8 classes of the Tubarão area were divided into 18 classes corresponding to most of the level II classes identified in the aerial photographs. The 6 classes of the Criciúma area were reorganized according to the 6 classes found in the coal refuse area charts.

The supervised classification for both areas was based on a "maximum likelihood decision system" algorithm (Velasco et alii, 1979).

The visual impression of the classification of the Tubarão area into 18 classes was much too confusing, with *an excessive fragmentation* of the scene. The discrimination of the acid stressed vegetation from other land cover classes was not possible.

The study in the Tubarão area then turned to a land use/land cover classification where the following 8 classes were well identified:

- coal related areas
- urban areas
- high marshes
- low marshes
- agricultural areas
- plowed lands
- forestlands
- water

In the Criciúma area, the six coal refuse classes were aggregated into two, and new land use classes were identified. The final classification was fairly good, featuring the following classes:

- pyrite-rich spoil areas
- sterile spoil areas
- urban residential areas
- industrial areas
- water bodies

5. DISCUSSION OF RESULTS

The identification of acid stressed vegetation in the Tubarão area was not feasible, probably because of the date of the satellite overpass (April), just at the end of the wet season in the region. So, both acid stressed marshes and acid stressed pastures were identical to the corresponding healthy vegetation.

The results from the Criciúma area met better the objectives of this study. The bare coal refuse areas were well identified and localized with a fairly good internal classification. The urban land use classes, identified in order to help the localization of the spoil areas, presented also a good accuracy (figure 2).

The class "industrial areas" identified most of the large industries of Criciúma as well as the ceramic plant near Cocal.

The class "urban area" had a good performance in Criciúma, including the small villages (Metropolitana, Rio Maina,etc.) spreading chaotically towards the northwestern mining axis. The city of Siderópolis was well identified and few comission errors were noted over abandoned surface mines.

The class corresponding to water bodies is present only within the spoil areas. In the strip mine areas it is the location of the abandoned trenches, which became artificial, channel-like acid water impoundments. The presence of water in pyrite-rich spoil areas indicates sometimes traces of abandoned slurry ponds.

The combined distribution of the two refuse classes gives a good description of the large spoil areas both in shape and localization. Coal refuse areas as small as 3 ha were at least located. The larger ones were located with their actual shape and size.

The internal classification of the coal refuse areas set a compromise: if we better the classification of the sterile spoils, we would incur into commission errors on the pyrite-rich spoil areas and vice-versa. There are many causes for this similarity among the two refuse classes, namely:

- there is some coal mixed in the sterile spoils originated from non--economic coal layers;

- there is also coal along the haul roads within the sterile refuse area;

- the darkening effect of the shadows caused by the sterile refuse piles;

- the spontaneous combustion of the pyrite-rich spoil areas leaving on the surface the inert part of the coal, which resembles to the sterile spoils.

In spite of these constraints, the classification of the spoil areas showed the following results:

1 - The "sterile refuse" class described well the strip mine near Siderópolis. Omissions occured on the naturally reclaimed areas covered with grasses and shrubs and on the artificially reclaimed areas covered by *Eucalyptus*. This class is also present in the pyrite-rich spoil areas, generally occupying the periphery of the refuse area.

2 - The pyrite-rich spoil areas were well represented by its corresponding class, except for the borders where the sterile refuse class predominates, possibly due to the smoothing characteristic of the radiometric correction procedure.

6. CONCLUSIONS

As a first step towards the utilization of MSS-LANDSAT digital data to monitor coal mine refuse sites in Brazil, the objectives of this study were fully achieved.

The results demonstrate that the discrimination of refuse sites against the background is feasible and this product will be useful in a change--detection survey.

The confusion among the two coal refuse classes can be solved by detailed studies over each one of the large refuse sites, in order to categorize the main classes present in these areas. Actually, this will be the next step of the project running, to be developed on two strip mines: one abandoned and the other active, and on a pyrite-rich spoil area, still to be chosen.

The identification of vegetation stressed by acid mine drainage probably will be possible by a multi-date approach. This will certainly better describe the combined effect of seasonality of vegetation and the variations of the pH values according to the specific hydrologic features of the region.

ACKNOWLEDGEMENTS

The authors are indebted to Mr. Nilton Rodrigues, Mr. Joaquim Arantes de Bem and Mr. Adhyles Bortot, all from FATMA (the Santa Catarina State Environmental Protection Agency) for their generous supports during field work in southern Santa Catarina. Mr. Ronaldo G. Couto from ECP - Consulting Engineers, kindly delivered non-published maps on coal refuse areas. Prof. Dr. H. Putzer, from the German Geol. Survey, permitted the publication of figure 1.

REFERENCES

ALEXANDER, S.S.; DEIN, J.; GOLD, D.P. (1973) The use of ERTS-1 MSS data for mapping stripmining and acid mine drainage in Pennsylvania - Symposium on significant results obtained from the ERTS-1, NASA, SP-327, pp. 569-575.

ANDERSON, A.T.; SCHULTZ, D.; BUCHMAN, N.; NOCK, H.M. (1977) LANDSAT imagery for surface mine inventory.Phot. Eng. & Rem. Sens. V:43, pp. 1027-1036.

ANDERSON, J.E.; TANNER, C.E. (1978) Remote monitoring of coal strip mine rehabilitation. U.S. Environmental Protection Agency - Las Vegas N.V.

ANDERSON, J.R.; HARDY, E.E.; ROACH, J.T.; WITNER, R.E. (1976) A land use and land cover classification system for use with remote sensor data. U.S. Geologic Survey, Washington D.C., (paper nº 964).

BARTON, P. (1978) The acid mine drainage. In: NRIAGU, J.O. (Ed) Sulfur in the Environment, Part II: Ecological Impacts. pp. 313-358. John Wiley & Sons, Inc.

BAYNES, J.N.; LAWRENCE, H. (1979) Application of Satellite data to surface mine monitoring in selected counties of South Carolina. Bureau of Mines, U.S. Deptº Interior.

DUTRA, L.V.; MOREIRA, J.C.; Ii; F.A.M. (unpublished) Manual de usuários dos sistemas de tratamentos de imagens digitais. INPE, São José dos Campos.

FISH, B.R. (1977) A feasibility analysis of the employment of satellite imagery to monitor and inspect surface mining operations in western Kentucky. V.1. NASA, Goddard Space Flight Center, Greenbelt, MD.

GENERAL ELECTRIC COMP. (1975) Image-100 user manual. Daytona Beach, FLA.

HUGHES, T.H.; DILLION, A.C.; WHITE, J.R.; DRUMMOND, S.E.; HOOKS, W.G. (1975) Assessment of praticality of remote sensing techniques for a study of the effects of strip mining in Alabama. Univ. of Alabama.

IRONS, J.R.; LACHOWSKI, H.; PETERSON, C. (1980) Remote Sensing of surface mines: a comparative study of sensor system. Proc. 14th. Intern. Symp. on Rem. Sens. of Envir. V.11, pp. 1041-1053, San José, Costa Rica.

LENZ, R. (1977) Uma avaliação geológica e econômica das potencialidades carbo níferas dos Estados de São Paulo, Paraná e Santa Catarina (Norte, Centro e Sul) com propostas detalhadas para futuras prospecções, tomos I - V. Relatório Inédito DNPM, Brasília.

LYON, R.J.P.; PRELAT, A. (1978) Application of the Stanford Remote Sensing Laboratory (STANSORT) system in monitoring the surface coal mines using LANDSAT digital data. Stanford Univ. Cal.

MAMULA, N. (1978) Remote Sensing methods for monitoring surface coal mining in the northern great Plains. U.S. Geol. Survey Jour. Research, V.6 (2), pp. 149-160.

PUTZER, H. (1977) Die Brasilianischen Steinkohlen-Lagerstätten und ihre optimalen nutzungsmöglichkeiten. Geol. Jb. D23, S.3-18. Hannover.

RAMOS, B.W. (1982) Carvão: Situação e Perspectivas. Rev. Ciências da Terra. Nº 2, pp. 47-49.

RUSSELL, O.R. (1977) Application of LANDSAT-2 data to the implementation and enforcement of the Pennsylvania surface mining conservation and reclamation act - NASA, Goddard Space Flight Center, Greenbelt, M.D.

SPISZ, E.W. (1978) Application of multispectral scanner data to the study of an abandoned surface coal mine. NASA Tech. Memorandum 78912.

SPISZ, E.W. & DOOLEY, J.T. (1980) Assessment of Satellite and aircraft multispectral scanner data for strip-mine monitoring. NASA Tech. Memorandum 79268.

VELASCO, F.R.D.; PRADO, L.O.C.; SOUZA, R.C.M. (1979) Sistema MAXVER (Manual do Usuário). INPE, São José dos Campos.

WOBBER, F.J.; RUSSELL, O.R.; DEELY, D.J. (1975) Multiscale aerial and orbital techniques for management of coal-mined lands. Photogrammetria. V.31 (4), pp. 117-133.

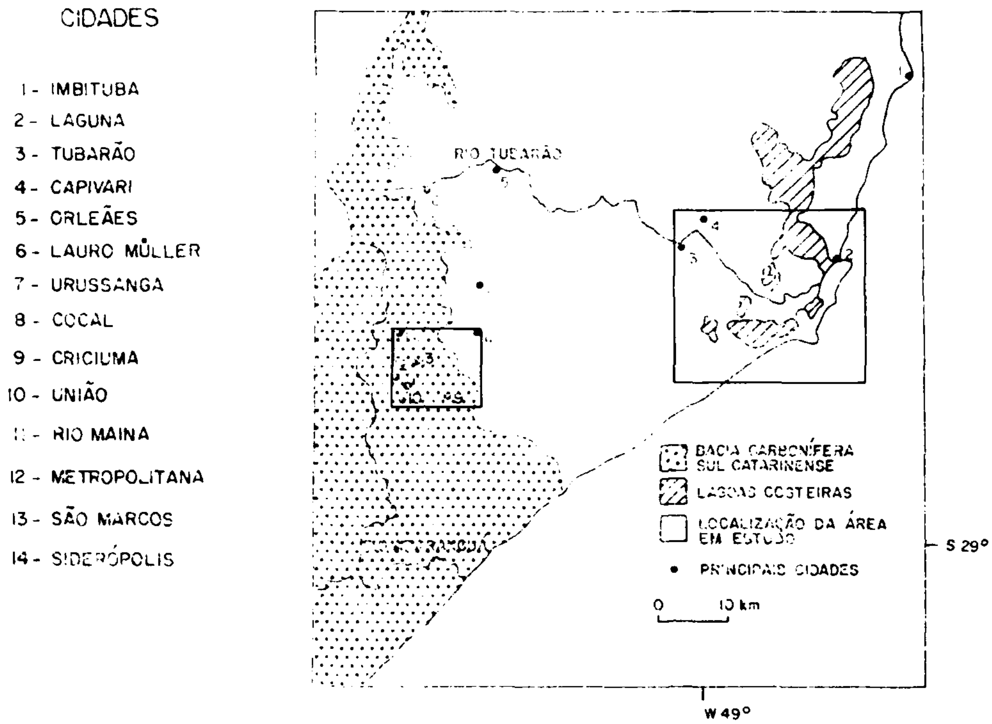

Figure 1 - Location of the study area.

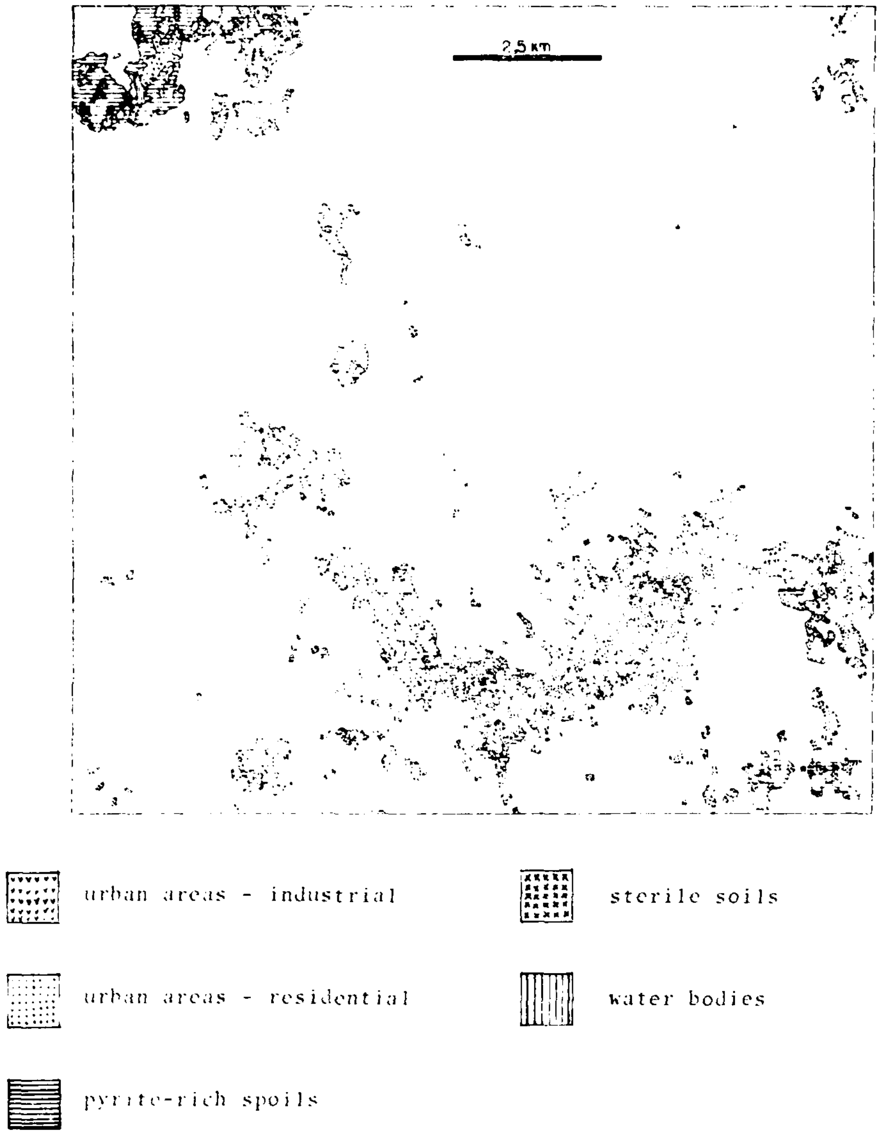

Figure 2 - Thematic classification, Criciúma area.

MULTIDISCIPLINARY STUDIES IN DEL NEUQUEN PROVINCE, ARGENTINA

J.A. Ferrer
N.J. Onesti

Consejo Federal de Inversiones
Buenos Aires, Argentina

SUMMARY

Upon request of the Government of the Province of del Neuquen, the Consejo Federal de Inversiones - through the Project and Studies Division, started in 1978 several studies and actions tending to identify and give priority to areas apt for agriculture and livestock exploitation. The studies cover the 16 political departments of the province with a total surface of 94,708 km^2.

According to its surface, the province is considered the four in importance within the Patagonia region and the thirteenth within the total territory of the Argentine Republic.

The climate in del Neuquen can be divided in two areas, east and west, with an intermediate variable zone. The east is a desertic area with very little rain and the west is quite rainy and cold, therefore, the relief altitude decreases from west and east and the central and western geological complexity is simplified in the eastern plateau.

The province of del Neuquen, due to its natural characteristic, offers the possibility of developing several irrigation works. However, to date, the existing potential has not been systematically nor rationally investigated, nor have the different possibilities been evaluated.

On account of this, the Consejo Federal de Inversiones has prepared a program of studies, which in general terms includes the following points:

I. Climate

Most of the information is obtained from the National Meteorological Service. This information is statistic and graphics are provided in order to point out elements and principal facts of climate.

II. Superficial Hydric Resource:

Hydrology: recopilation, analysis and processing of the existing information in order to delimit irrigated and potentially irrigateable areas.

Availability of water per area in study: the hydric resources will be calculated and delimited as per information available.

III. Soil

Regional study: the background to be employed are either scarce and certain or quite general.

The primary and secondary information of the separation obtained from the aereal and satellital conventional analysis is processed.

Irrigational studies in the basins of Colorado and del Neuquen rivers: a larger amount of information can be obtained from this than from the regional studies with a larger amount of original information obtained in camp.

IV. Social and Economic Aspects:

- Analysis of spatial order: is used to know the relations which are established between different geographical spaces in the province.
- Social analysis of population centers: the cities next to the areas to be irrigated and their principal characteristics are studied.
- Economic analysis of preselected areas: the economic and campaign studies will allow to distinguish the activity centers next to the areas.
- Social and economic provincial regionalization and insertion in preselected areas: analysis and characterization of particular and differential aptitudes of the areas in order to evaluate their possibilities of insertion to the actual provincial social and economical organization.

V. Expeditive appreciation of necessary works in order to capture, conduct and provide defence in the basins of the Colorado and Neuquen rivers. The available information is analyzed for each area establishing probable demands for irrigation, drainage and works.

VI. Explicit rules in order to give priority to irrigation areas: will be elaborated by provincial functionaries and technicians for different areas.

VII. Priority of areas selected: the identified areas will be made based on natural resources as well as social and economic rules.

For the different studies, the use of Landsat images (El, 2, and 3; MSS sensor, bands 4, 5, and 7, black and white, composed false color) has allowed, together with an exhaustive analysis of existing conventional aereal photographs, to separate each one of the areas in units of landscapes using patron elements as relief, topographic differences of elevations, evidences of erosion processes, sediments, etc.

Working scales are 1:50,000; 1:100,000 and 1:500,000; and principal representation scales are 1:50,000; 1:500,000; 1:1,000,000 and 1:2,000,000.

Finally, the different study disciplines and excellent photographic definition helps to draw limits and allows for economy observations and efficiency of necessary camp works.

AD P002035

ANALYSIS OF MULTI-DATE LANDSAT-GEOPIC FOR MAPPING VINAL (Prosopis ruscifolia) AND ITS TEMPORAL EXPANSION

Carlos M. Viola Binaghi, Alberto B. Viola, and Eduardo G. Viola
Aeroterra S.A., Buenos Aires, Argentina

and

William G. Brooner
Earth Satellite Corporation, Chevy Chase, Maryland, USA

ABSTRACT

Rapid proliferation of Vinal, a tree found in the Gran Chaco region of Argentina, impacts both the economy and ecology of Formosa Province. Landsat-GEOPIC digital imagery, combined with effective ground sampling surveys, provided new information on the occurrence and distribution of Vinal in a cost and time effective manner. Changes in extent and distribution of Vinal over a 6,822 km^2 study area were analyzed using 1975 and 1980 Landsat data and digital change analyses in the EarthSat GEOPIC Interact system. Results indicate a seven to ten percent annual area increase of Vinal. Landsat GEOPIC processing was used to generate images and distribution (land cover) and change analysis maps at 1:100,000 scale.

I. INTRODUCTION

Vinal (*Prosopis ruscifolia*) is a tree found in the Gran Chaco region of northern Argentina. It commonly grows to approximately 7 to 9 metres in height, with breast height diameters (bhd) between 15 and 25 cm in its mature form (20 years of age). Dispersed trees may have up to 45 bhd. Vinal grows rapidly, and at 3 to 5 years of age it may achieve heights of 3 to 5 metres. An important characteristic is the presence of sharp thorns of up to 15 cm in length.

Vinal is considered an invader species, aggressively colonizing different environments, and is often found in association with diverse vegetation types. Massive colonization of Vinal over extensive areas has created serious problems for pasture and range management, loss of pastures, and contributed to soil erosion through replacement of other natural vegetation cover types.

The invasion of Vinal has been aggravated since 1935 due to interactions of natural as well as cultural factors, including land clearing for cultivation, pastures, and roads, drainage of esteros (shallow, marshy depressions), irrational use of fire, periodic flood inundations, etc. As a result, there are presently areas with densities of Vinal as high as 2,000 to 3,000 plants per hectare. The explosive diffusion of Vinal has impacted large areas in the Argentina provinces of Formosa and Chaco, as well as Santiago del Estero and Salta.

In recent years (particularly the past decade), numerous studies and field experiment station investigations have addressed problems associated with Vinal control of expansion. New areas of research have been identified as well as solutions, particularly in terms of

alternative control techniques. A continuing problem is the rapid proliferation of this aggressive species which impacts both the economy and ecology of Formosa Province.

The present study focused on demonstrating applications of Landsat and other remotely sensed data to the mapping of Vinal and its temporal dynamics. The investigations, conducted in 1980 and 1981, were without precedent, represent a unique application of Landsat and which successfully met many of the original project objectives.

2. OBJECTIVES

The present study was designed to investigate and demonstrate the application of digitally processed Landsat data (using the GEOPIC™ system), complemented by aerial reconnaissance and ground surveys, for mapping the distribution of Vinal, its occurrence in different ecosystems, and its temporal dynamics. The study was conducted in a 7,500 km^2 project area located in Patino and Pirane Departments of Formosa Province (Argentina). Specific objectives included analyses to:

a. Stratify areas occupied by Vinal from other principal forest species.
b. Stratify associations of Vinal and other classes of _Prosopis_ species.
c. Detect areas of instability or potential invasion by Vinal.
d. Assess changes and rates of expansion by Vinal over a 5-year period.
e. Develop and transfer methodologies and techniques applicable to other forest inventories in Formosa Province.

3. STUDY AREA

The study area is contained on Landsat images for WRS Path 243/Row 078, and lies approximately 180 km northwest of the city of Formosa. Settlement is concentrated in and around several towns and colonies and along road networks, and population density within the study area is low.

Several rivers and streams cross the study area, trending in a southeasterly direction. Between the rivers and streams, the terrain has very minor relief, undulating on the order of only a couple of metres or less, and characterized by poor drainage. Much of the land is seasonally wet; marshes occupy extensive areas known as "esteros" which are shallow depressions (commonly from 0.5 metre to no more than 1 metre in depth) with internal drainage. Standing water levels within esteros varies seasonally, and in some years surficial water occurs throughout the year. In periods of excessive water, the esteros will overflow and drain across adjacent areas.

The majority of the study area is covered by natural forests and grasslands of several principal types and associations. Much of the area is grazed by cattle, a significant economic activity in the Province. Settlements and roads occur in higher, and hence, drier sites and are typically surrounded by concentrations of cultivation activity.

Simplistic descriptions of land cover in the project area include High Forest and Low Forest (both open and closed canopies), and non-forested areas, principally grass covered marshes (esteros), pastures (both natural and artificial), and cultivated areas. The location and distribution of each type is closely related to soils and correlated to the microphysiography of the region.

4. CHARACTERISTICS OF VINAL DISTRIBUTION

Some believe that Vinal invaded only grass covered areas until the past 30-40 years, at which time settlers began agricultural developments leading to the present landscape patterns. During this latter period, Vinal distribution has extended to additional sites and includes associations with other _Prosopis Spp._ which do not have similar aggressive invader characteristics.

When forest cover is cleared, such as for road construction, pasture development, etc., Vinal is typically the first species to colonize sites which do not have well established woody vegetative cover. Its aggressive character allows it to become established quickly, and to grow in the absence of competition in the form of a small shrub, reaching 1-2 metres height in only one to two years. Left without eradicative control efforts, it will become a woody tree reaching 3-4 metres height in 15-20 years, and in some instances as much as 7-9 metres height.

Vinal will also typically border the esteros, invading herbaceous environments above the waterline, but will not tolerate inundation. During drier years, Vinal may occupy large portions of esteros, but the tree will d e and recede to slightly higher sites when surficial water returns.

One hypothesis holds that esteros are gradually becoming more shallow. When Vinal and other species (principally herbaceous) die due to inundation, plant materials deposited on the estero floor gradually build the organic soil base. Over time, the estero becomes more shallow and the surface area extends outward.

Vinal seeds are transported to new sites by several mechanisms whereby it may further expand its occupancy. Seed pods and young leaves are eaten by cattle which browse on low forest trees; cattle, however, cannot digest the seeds which are expurged through the animal's digestive system and deposited to organic sites. Seeds are also transported by water, both the fluctuations of water levels within esteros and through rapid sheet runoff during periods of intense precipitation (which may typically exceed 150 mm/hour).

Soil type appears to not be an important factor for the establishment and growth of Vinal (although soil formation processes resultant from extant landscape morphology influences distribution of other forest associations). Vinal appears to be able to establish itself and thrive on any soil, limited only by inundation of water. In fact, flooding of Vinal sites for a period of six months is considered to be one of the effective control mechanisms resulting from research conducted in recent years.

5. SELECTION AND PREPARATION OF LANDSAT DATA

Two Landsat scenes for WRS Path 243/Row 078 were selected and acquired for use in the Vinal analysis: 1) Image No. 20142-13090, 13 June 1975; 2) Image No. 22086-78115, 8 October 1980.

The most recent scene (8 October 1980) was acquired by the Argentinean earth receiving station (CNIE). This scene was processed in EarthSat's GEOPIC system in November 1980 and used in the reconnaissance field surveys during December 1980. In addition, the spectral classification analyses were applied to the 8 October 1980 scene.

The 13 June 1975 scene was acquired at NASA's Goddard Space Flight Center. It also was processed in EarthSat's GEOPIC system in January 1981 and was used in the temporal change analyses conducted in February 1981.

The GEOPIC system is a digital image processing system which by definition utilizes only Landsat CCT's. The image corrections and enhancements applied in the GEOPIC process are state-of-the-art for commercially available digital image products worldwide. While most of the image products used in the study were at 1:100,000 scale, GEOPIC color prints were also prepared at 1:60,000 scale for successful use as field survey working materials.

Previous Landsat investigations and applications in Formosa Province used only the bulk Landsat photographic image products. The Vinal project was the first application of digital Landsat image processing in Formosa Province, and it utilized GEOPIC processed data exclusively. Further, the CCT generated by CNIE for the 8 October 1980 Landsat scene was the first CNIE scene to be digitally processed outside of CNIE.

6. FIELD SURVEYS

Reconnaissance field surveys were conducted in December 1980. The objectives of these surveys were to acquire field observations of Vinal, correlate these observations with features presented on the Landsat GEOPIC imagery, and acquire field documentation of Vinal characteristics and distribution.

Provincial personnel participated in all aspects of the field surveys. The objectives were efficiently and satisfactorily met, due largely to preparations and support provided by Provincial personnel.

Terrestrial surveys enabled observation of most ecological systems, landscapes and land uses contained on the Landsat GEOPIC image, and included areas where Vinal was extensive and dominant, areas where Vinal was observed in various associations, and areas where Vinal was not observed.

The terrestrial field surveys were severely hampered by extensive flooding resulting from extreme rainfall throughout Formosa Province in preceding weeks. The flooding complicated making detailed correlations between field observations and the Landsat GEOPIC imagery. The Landsat scene was acquired 8 October 1980, following a period with little precipitation for several months. As a result, for example, water levels in esteros, when imaged, were low. In mid-December, following extensive rains and inundations, water levels in the esteros were abnormally high, and the surface area exceeded normal limits as well as those indicated on the Landsat images. Most pastures and many cultivated fields were under water. Nevertheless, due to the resolution and clarity of the Landsat GEOPIC image (at 1:100,000 and 1:60,000 scales) it was consistently possible to identify ground position to image location throughout areas visited in the study area.

In addition, several aerial reconnaissance overflights of the study area were conducted. These observations confirmed further the extensive flooding and landscape inundation which hampered ground travel. They provided effective overview to the project area and facilitated Landsat GEOPIC comparisons. The Landsat image, in fact, was used for inflight navigation and documentation when over the Vinal study area.

Both terrestrial and oblique aerial photographs were acquired to document observations of Vinal and related landscape features. These photographs included scenes for use "ground truth" in subsequent Landsat analyses, and multispectral photos for subsequent analyses of the spectral characteristics of Vinal and associated land cover features.

7. APPLICATION OF METEOROLOGICAL DATA TO THE LANDSAT ANALYSIS

The Gran Chaco region is situated in a humid subtropical mesothermal forest climate which is constantly moist and which may receive rainfall all through the year. Climate in the study area is an important environmental characteristic, particularly precipitation which is highly variable both in frequency and intensity and impacts management of the region's natural resources.

Although the average annual precipitation in the project area is slightly less than one metre, it is evident that averages are of rather limited value when data are examined over a period of a number of years.

In addition, evaporation rates are high, exceeding precipitation throughout the Chaco region resulting in an annual net deficit water budget in a region which experiences excessive water during portion of the year.

Daily precipitation records were analyzed for short periods (90 days) prior to each Landsat scene data to understand the landscape conditions, viz a viz surface water extant at each time period. This is noted because the meteorological conditions preceding the field work created landscape conditions significantly different than those imaged on the two temporal Landsat scenes.

8. SPECTRAL CHARACTERISTICS OF VINAL

One purpose in acquiring field photography was to provide data for analysis of spectral characteristics of Vinal and associated land cover features. The approach was very simplistic, and was not intended for quantitative spectrometric analysis. Rather, using analytical spectral density measurements, of ground and aerial photographs provided qualitative and comparative data for the Vinal project area.

Measurements were made using MacBeth TD-504 and RD-519 densitometers on ektachrome, ektochrome infrared, Tri-X (47B, 58 and 25 Wratten filters), and Black-and-White Infrared (89B filter) film type for six categories of land cover:

- Vinal associations bordering esteros
- Mixed estero vegetation
- Low forest with high associated Vinal density
- Low closed forest
- High forest
- Water

Multiple measurements were made and averaged; variations between measurements are attributed primarily to atmosphere (varying distances between camera and target), varying density of vegetation (introducing ground and other "noise" into the sample measurements), and varying moisture conditions extant in the study area at the time of field surveys.

9. LANDSAT MULTISPECTRAL CLASSIFICATION

One of the objectives of the Vinal project was to investigate the application of Landsat multispectral classification for analyzing the occurrence and distribution of Vinal and other land cover types. The Landsat multispectral classification was applied to the 8 October 1980 scene, using the EarthSat Interact System.

The multispectral classification procedures used a unique approach involving combined supervised and non-supervised techniques to "map" nine (9) categories of land cover in an area of approximately 294,400 hectares. The categories represent land cover and can generally be related to ecological environments of the project area. The results were presented both cartographically in a color classification image at 1:100,000 scale, and in tabular format as summarized in Table I.

TABLE I. Land Cover Classification Results

Category	Hectares	% Total
Cultivation, Urban Areas, etc.	16,265	6.5
Estero-type Vegetation	26,885	9.1
Young Vinal	41,415	14.4
Vinal/Low Forest	58,295	19.8
Low Open Forest	29,760	10.1
Low Closed Forest	33,340	11.3
High Forest	75,685	25.8
Water	5,335	1.8
Unclassified	3,420	1.2
	294,400	100.0

10. ESTIMATED DISTRIBUTION OF VINAL

An attempt was made to estimate the occurrence of Vinal in the 294,400 hectare study area of Landsat classification.

Such estimates require certain assumptions of the percentage of each category representing Vinal as opposed to other vegetation species or land cover types. The assumptions were derived from carefully prepared definitions for each of the nine

categories contained on the land cover classification map, and which were generated through field experience and corollary data.

The estimated percent of Vinal area for each land cover category is shown in Table II, along with the resulting tabulation estimate that Vinal occupies approximately 82,270 hectares, or 28 percent, of the classified image area in October 1980.

TABLE II. Estimated Occurrence of Vinal

Category	Estimated % Vinal	Hectares Total	Hectares Vinal
Cultivation, Urban, etc.	0	19,265	0
Estero-type Vegetation	10	26,885	2,688
Vinal	90	42,415	38,173
Vinal/Low Forest	50	58,295	29,148
Low Open Forest	30	29,760	8,928
Low Closed Forest	10	33,340	3,334
High Forest	0	75,685	0
Water	0	5,335	0
Unclassified	0	3,420	0
		294,400	82,271

This estimate has been supported by Provincial personnel envolved in related Vinal programs. It may be refined through additional work involving, in particular, field surveys designed to better define the characteristics and occurrence of Vinal in each of the existing Landsat classification land cover categories.

Only in areas where Vinal is extensive and is the dominant land cover type is it possible to identify the plants using Landsat imagery, whose resolution is 0.4 hectares. Individual trees cannot be detected nor identified. Further, mixtures of different species will create a composite reflectance value within the 0.4 hectar resolution area. Hence, it is possible to classify and map Vinal in some of the environments in which it occurs, e.g., bordering esteros, but in other areas the ecological unit or land cover category rather than individual or dominant species is classified and mapped. The resulting Landsat GEOPIC classification image is a realistic description and "map" of the imaged landscape.

11. LANDSAT TEMPORAL CHANGE ANALYSIS

A final objective of the Vinal project was to examine multi-date Landsat imagery, and to apply GEOPIC system techniques to the detection and analysis of changes in the spatial distribution of Vinal. This analysis was performed using Landsat scenes acquired on 8 October 1980 and 13 June 1975.

Although this analysis ultimately achieved useful results, it was frustrated by a variety of problems ranging from different computer tape formats (EROS vs. CNIE), different geometrical characteristics, different seasons and hence, environmental conditions, etc.

The Landsat change analysis was performed in an area of approximately 6,882 km^2, using techniques which differenced MSS 5/7 ratios of each scene. Three (3) categories were generated in both image (cartographic) and tabular format:

	%	Area (has)
• Areas where vegetation increased between 1975 and 1980, which commonly corresponded to increases in Vinal.	14.2	97,724.4

•	Areas where vegetation decreased between 1975 and 1980, which are generally in esteros and cultivated areas and are interpreted to be residual effects of images acquired in different seasons.	16.5	113,553
•	Areas of no significant change between 1975 and 1980.	69.3	476,922.6

The first category includes changes in Vinal area, as well as esteros. It correlates closely with the Estero and Vinal categories of the land cover classification where Vinal is the dominant low forest type and is often of young age as indicated by shrub form. In an analysis of the Temporal Change, it was estimated that approximately 50 percent of the first category represents Vinal or potential Vinal sites. This results in an increase in Vinal of over 9,000 hectares per year with an annual area increase rate of between 7 and 10 percent.

12. ADDITIONAL RESULTS

In addition to the findings and results presented above, the following are summarized from the Landsat investigations:

- It is possible to differentiate and stratify Vinal occupied areas from other principal species in some but not all ecosystems. It is possible to differentiate and stratify ecosystems, and Vinal occurrence may be estimated when its probable density in each ecosystem is known.
- It does not appear possible to differentiate associations of Vinal and Algarrobo (also Prosopis Spp.) using Landsat except in those areas where distinction may be made on ecological environments and supported by field data.
- Areas of instability or potential for invasion of aggressive woody plants may be identified by surrogate means of associated land cover, correlated with ground observations. These include grass covered areas bordering esteros, along roads and in pastures, as well as areas of low forest with open canopies (which are also typically grazed).
- The Landsat GEOPIC image displays pixel reflectance values whose patterns correlate well with forest inventory maps. Hence, Landsat can be very useful in a Forest Inventory of Formosa Province in the initial stages of delineating land cover types. Subsequent field surveys, sampling including photointerpretation, and Landsat GEOPIC/Interact system classification may be used to identify land cover types. A suitable scale for this work is 1:100,000.

13. CONCLUSIONS

While the rapid proliferation of Vinal continues to impact both the economy and ecology of Formosa Province, the reported Landsat investigations represent original and unique applications. Objectives were successfully met, and new areas of research were identified.

A combination of existing published information, effective ground sampling techniques, remote sensing systems, and state-of-the-art digital image processing and analysis techniques have provided new and additional information on the occurrence and distribution of Vinal in a cost-effective and time-effective manner. Such information is essential to resource development planning in Formosa Province.

Many completed studies of Vinal have been significant in their findings and results. They can certainly be considered successful, but our measures of success in the present

research investigations must account for the rapid improvements in technology and technique over only a few years. To be successful this year or next, approaches and techniques must stay abreast of the rapid technology improvements.

The success of a resource inventory, such as the Vinal investigations, and a resource development program using remotely sensed data requires a variety of professional skills and experience if the program is to result in useful information for planning and management. It is our belief that the principal skills and professional experience required lie in three areas: resource inventory and mapping; resource development planning and management; and remote sensing technologies. The Vinal investigation team, including Earth Satellite Corporation (USA), Aeroterra S.A. (Argentina), the Subsecretary of Natural Resources and Ecology (Formosa Province), and the National Commission on Vinal (Ministry of Interior), completely and expertly met these requirements.

AUTHOR INDEX

END

DATE
FILMED

12-83

DTIC